PROPRIOSPINAL NEURONS: ESSENTIAL ELEMENTS IN LOCOMOTION, AUTONOMIC FUNCTION AND PLASTICITY AFTER SPINAL CORD INJURY AND DISEASE

EDITED BY: Katinka Stecina, Kristine C. Cowley, Claire Francesca Meehan, Michelle Maria Rank and Michael A. Lane

PUBLISHED IN: Frontiers in Cellular Neuroscience and Frontiers in Systems Neuroscience

frontiers Research Topics

frontiers

ISSN 1664-8714
ISBN 978-2-88966-916-5
DOI 10.3389/978-2-88966-916-5

About Frontiers

Frontiers is more than just an open-access publisher of scholarly articles: it is a pioneering approach to the world of academia, radically improving the way scholarly research is managed. The grand vision of Frontiers is a world where all people have an equal opportunity to seek, share and generate knowledge. Frontiers provides immediate and permanent online open access to all its publications, but this alone is not enough to realize our grand goals.

Frontiers Journal Series

The Frontiers Journal Series is a multi-tier and interdisciplinary set of open-access, online journals, promising a paradigm shift from the current review, selection and dissemination processes in academic publishing. All Frontiers journals are driven by researchers for researchers; therefore, they constitute a service to the scholarly community. At the same time, the Frontiers Journal Series operates on a revolutionary invention, the tiered publishing system, initially addressing specific communities of scholars, and gradually climbing up to broader public understanding, thus serving the interests of the lay society, too.

Dedication to Quality

Each Frontiers article is a landmark of the highest quality, thanks to genuinely collaborative interactions between authors and review editors, who include some of the world's best academicians. Research must be certified by peers before entering a stream of knowledge that may eventually reach the public - and shape society; therefore, Frontiers only applies the most rigorous and unbiased reviews.
Frontiers revolutionizes research publishing by freely delivering the most outstanding research, evaluated with no bias from both the academic and social point of view. By applying the most advanced information technologies, Frontiers is catapulting scholarly publishing into a new generation.

What are Frontiers Research Topics?

Frontiers Research Topics are very popular trademarks of the Frontiers Journals Series: they are collections of at least ten articles, all centered on a particular subject. With their unique mix of varied contributions from Original Research to Review Articles, Frontiers Research Topics unify the most influential researchers, the latest key findings and historical advances in a hot research area! Find out more on how to host your own Frontiers Research Topic or contribute to one as an author by contacting the Frontiers Editorial Office: frontiersin.org/about/contact

PROPRIOSPINAL NEURONS: ESSENTIAL ELEMENTS IN LOCOMOTION, AUTONOMIC FUNCTION AND PLASTICITY AFTER SPINAL CORD INJURY AND DISEASE

Topic Editors:
Katinka Stecina, University of Manitoba, Canada
Kristine C. Cowley, University of Manitoba, Canada
Claire Francesca Meehan, University of Copenhagen, Denmark
Michelle Maria Rank, The University of Melbourne, Australia
Michael A. Lane, Drexel University, United States

Citation: Stecina, K., Cowley, K. C., Meehan, C. F., Rank, M. M., Lane, M. A., eds. (2021). Propriospinal Neurons: Essential Elements in Locomotion, Autonomic Function and Plasticity after Spinal Cord Injury and Disease. Lausanne: Frontiers Media SA. doi: 10.3389/978-2-88966-916-5

Table of Contents

04 ***Editorial: Propriospinal Neurons: Essential Elements in Locomotion, Autonomic Function and Plasticity After Spinal Cord Injury and Disease***
Kristine C. Cowley, Michael A. Lane, Claire F. Meehan, Michelle M. Rank and Katinka Stecina

07 ***The Mechanistic Basis for Successful Spinal Cord Stimulation to Generate Steady Motor Outputs***
Amr A. Mahrous, Mohamed H. Mousa and Sherif M. Elbasiouny

23 ***Changes in Activity of Spinal Postural Networks at Different Time Points After Spinalization***
Pavel V. Zelenin, Vladimir F. Lyalka, Grigori N. Orlovsky and Tatiana G. Deliagina

42 ***Mapping Connectivity Amongst Interneuronal Components of the Locomotor CPG***
Farhia Haque and Simon Gosgnach

50 ***Flexor and Extensor Ankle Afferents Broadly Innervate Locomotor Spinal Shox2 Neurons and Induce Similar Effects in Neonatal Mice***
Erik Z. Li, D. Leonardo Garcia-Ramirez and Kimberly J. Dougherty

68 ***Intraspinal Plasticity Associated With the Development of Autonomic Dysreflexia After Complete Spinal Cord Injury***
Felicia M. Michael, Samir P. Patel and Alexander G. Rabchevsky

78 ***Propriospinal Neurons: Essential Elements of Locomotor Control in the Intact and Possibly the Injured Spinal Cord***
Alex M. Laliberte, Sara Goltash, Nicolas R. Lalonde and Tuan Vu Bui

94 ***Spinal V3 Interneurons and Left–Right Coordination in Mammalian Locomotion***
Simon M. Danner, Han Zhang, Natalia A. Shevtsova, Joanna Borowska-Fielding, Dylan Deska-Gauthier, Ilya A. Rybak and Ying Zhang

117 ***Novel Activity Detection Algorithm to Characterize Spontaneous Stepping During Multimodal Spinal Neuromodulation After Mid-Thoracic Spinal Cord Injury in Rats***
Raymond Chia, Hui Zhong, Bryce Vissel, V. Reggie Edgerton and Parag Gad

129 ***Biphasic Effect of Buspirone on the H-Reflex in Acute Spinal Decerebrated Mice***
Yann Develle and Hugues Leblond

139 ***Role of Propriospinal Neurons in Control of Respiratory Muscles and Recovery of Breathing Following Injury***
Victoria N. Jensen, Warren J. Alilain and Steven A. Crone

150 ***Music Restores Propriospinal Excitation During Stroke Locomotion***
Iseline Peyre, Berthe Hanna-Boutros, Alexandra Lackmy-Vallee, Claire Kemlin, Eléonore Bayen, Pascale Pradat-Diehl and Véronique Marchand-Pauvert

163 ***Critical Components for Spontaneous Activity and Rhythm Generation in Spinal Cord Circuits in Culture***
Samuel Buntschu, Anne Tscherter, Martina Heidemann and Jürg Streit

frontiers in Cellular Neuroscience

EDITORIAL
published: 20 May 2021
doi: 10.3389/fncel.2021.695424

Editorial: Propriospinal Neurons: Essential Elements in Locomotion, Autonomic Function and Plasticity After Spinal Cord Injury and Disease

Kristine C. Cowley[1,2†], *Michael A. Lane*[3,4†], *Claire F. Meehan*[5†], *Michelle M. Rank*[6†] *and Katinka Stecina*[1,2*†]

[1] Department of Physiology and Pathophysiology, University of Manitoba, Winnipeg, MB, Canada, [2] Spinal Cord Research Centre, Max Rady College of Medicine, University of Manitoba, Winnipeg, MB, Canada, [3] Department of Neurobiology and Anatomy, College of Medicine, Drexel University, Philadelphia, PA, United States, [4] Marion Murray Spinal Cord Research Centre, Drexel University, Philadelphia, PA, United States, [5] Department of Neuroscience, Faculty of Health Sciences, University of Copenhagen, Copenhagen, Denmark, [6] Department of Anatomy and Physiology, The University of Melbourne, Parkville, VIC, Australia

Keywords: propriospinal, neuron, respiration, locomotion, autonomic function, motor control, central pattern generator

Editorial on the Research Topic

Propriospinal Neurons: Essential Elements in Locomotion, Autonomic Function and Plasticity After Spinal Cord Injury and Disease

OPEN ACCESS

Edited and reviewed by:
Enrico Cherubini, European Brain Research Institute, Italy

***Correspondence:**
Katinka Stecina
katinka.stecina@umanitoba.ca

†These authors have contributed equally to this work

Specialty section:
This article was submitted to Cellular Neurophysiology, a section of the journal Frontiers in Cellular Neuroscience

Received: *15 April 2021*
Accepted: *19 April 2021*
Published: *20 May 2021*

Citation:
Cowley KC, Lane MA, Meehan CF, Rank MM and Stecina K (2021) Editorial: Propriospinal Neurons: Essential Elements in Locomotion, Autonomic Function and Plasticity After Spinal Cord Injury and Disease. Front. Cell. Neurosci. 15:695424. doi: 10.3389/fncel.2021.695424

Propriospinal, the combination of a Latin expression for "one's own" and the word spinal, refers to neurons with somas and axons terminating within the extent of the spinal cord. Propriospinal neurons (PSNs) are contained entirely within the spinal cord and may have short segmental or multi-segment projections. Seminal research on PSNs lead by Lundberg (1979) first identified separate populations of PSNs: with either short- (1–3 spinal segments) (Jankowska et al., 1974, 1983; Edgley and Jankowska, 1987) or long-distance projections (spanning several spinal segments) (Jankowska et al., 1974). A well-recognized example of the latter are the cervical PSNs directly coordinating forelimb-hindlimb function (Alstermark et al., 1979). This early research underpins the more modern discoveries detailing the functional properties of anatomically distinct PSN populations. This series of articles uses the broadest definition of PSNs with an emphasis on operational capacity in order to highlight the full integrative capacity of PSNs. In fact, the complex integration capabilities of all PSN subpopulations were recognized in early research stages. Experiments using decerebrate cat preparations allowed for the simultaneous examination of inputs from multiple brain regions (Illert and Lundberg, 1978) and from peripheral sources to PSNs, thus highlighting the core integration functions of PSNs. While significant advances have been gained in research capabilities since this early work, the theme of integration has remained as a stronghold.

Propriospinal neurons can convey descending commands (Cowley et al., 2008) and participate in the integration of these commands with afferent sensory feedback from the periphery. They also serve to mediate and coordinate rhythmic motor output involving multiple joints, with corresponding neurons spanning several spinal segments. Discrete networks of PSNs constitute essential building blocks of the central pattern generators for respiration, locomotion and autonomic functions. Three in depth review articles in this collection revisit decades of research to provide a new perspective on the current understanding of the role of PSNs in these research fields. Laliberte et al. provide a broad-spectrum analysis of evidence that PSNs are not only acting as essential elements of locomotor control circuits in the intact spinal cord, but also play a significant role after spinal cord injury.

Respiratory PSNs have been described in the spinal cord of many species as discussed by Jensen et al. and these PSN populations contribute to the recovery of breathing after spinal cord injury. An excellent overview on how plasticity of PSNs is associated with the recovery of autonomic function is given by Michael et al. in relation to complete spinal injury and autonomic dysreflexia.

Given the complexity of PSNs and their diverse functional capabilities, how might we dissect these propriospinal circuits? Developmental markers to identify or manipulate specific classes of propriospinal neurons offer valuable tools to investigate spinal circuits. While knowledge about PSN-motoneuron connectivity has advanced substantially with the help of molecular, genetic, anatomical, and electrophysiological research techniques; mapping the landscape of spinal interneuronal connectivity has lagged behind. Experimental approaches addressing this gap are offered by Haque and Gosgnach.

The analysis of locomotor circuits has especially benefited from developmental genetics. In this collection, three genetically defined populations, the so-called V3, Shox2, and Hb9 interneurons have been examined by Danner et al. Here they make innovative use of murine optogenetic approaches and combine these results with large-scale computational modeling studies to show that V3 commissural neurons provide mutual excitation to separate populations of neurons involved in left-right extensor activity. The experiments by Li et al. show that Shox2 neurons are interposed in multiple sensory pathways. Furthermore, these Shox2 neurons, receiving input from low threshold proprioceptive flexor and extensor nerves, can activate or inhibit both the rhythm and patterning layers of the locomotor central pattern generator. Buntschu et al. combined patch-clamp and array recordings to investigate Hb9 interneurons in spinal cord cultures. Their findings described key ion channels that contribute to spontaneous intrinsic and repetitive spiking and thereby to the generation of network bursts.

Develle and Leblond examine the pharmacological manipulations of hindlimb reflexes within hours after spinal injury. Unexpected biphasic effects on PSNs of segmental reflex loops were identified by applying serotonin receptor agonists known to trigger stepping in mice after complete spinal transections.

Combinatorial strategies targeting PSN networks to promote recovery after spinal cord injury were addressed in two studies. A study by Mahrous et al. utilized combined stimulation of sensory and motor inputs (electrically or pharmacologically) that lead to more stable motor output than sensory or motor stimulation alone. The experiment by Chia et al. evaluated spontaneous stepping freely performed by rats. The methods and algorithms developed by this work provide exciting possibilities for examining the PSN contribution to free movement in the home-cage environment.

In addition to locomotion, postural reflexes are also dependent on PSNs. Zelenin et al. showed that PSNs undergo rapid changes within days of spinalization that allows for the restoration of normal activity levels in spinal interneurons, and a slow recovery over months that restores motoneurone excitability. Postural responses, however, fail to be reinstated and poor sensory-motor coordination of timing remains.

Peyre et al. investigated the effects of listening to music, albeit arrhythmic music, on walking in stroke survivors. They showed that a knee excitation reflex evoked by pre-tibial flexor stimulation after a stroke was significantly larger during walking without sound than when listening to music. This suggests that arrhythmic music listening modulates propriospinal excitability during post-stroke walking; likely representing brainstem modulation of PSN activity. In other words, music may be useful to "retrain" sensory-motor coordination via PSN networks after a neural injury in humans.

In summary, the articles brought together in this special edition highlight fundamental work on PSNs and the networks contributing to motor and autonomic functions, and do so from a broad perspective, reflecting the diverse role of PSNs. The review papers in this collection reinforce the critical role of sensory input in the recruitment of PSNs as well as in directing the output of PSN networks. An additional important finding reflected in the original research papers is that PSNs play a prominent and essential role in both hindlimb and forelimb coordination and respiratory muscle activity—in both health and disease. The research collected here reminds us that little is currently understood about the role of PSNs in autonomic functions under normal or abnormal conditions. This special collection of research is both fascinating and exciting, and overall suggests that it is finally time to shift the paradigm on PSNs. Rather than viewing PSNs as a uniform neuronal network with limited functional impact, it is now clear that they are in fact a diverse population of neurons. PSNs are critical components of a variety of networks with important functional roles beyond mere limb coordination.

AUTHOR CONTRIBUTIONS

All authors listed have made a substantial, direct and intellectual contribution to the work, and approved it for publication.

REFERENCES

Alstermark, B., Lundberg, A., Norrsell, U., and Sybirska, E. (1979). Role of C3-C4 propriospinal neurones in forelimb movements in the cat. *Acta Physiol. Scand.* 105, 24A. doi: 10.1111/j.1748-1716.2006.01655.x

Cowley, K. C., Zaporozhets, E., and Schmidt, B. J. (2008). Propriospinal neurons are sufficient for bulbospinal transmission of the locomotor command signal in the neonatal rat spinal cord. *J. Physiol.* 586, 1623–1635. doi: 10.1113/jphysiol.2007.148361

Edgley, S. A., and Jankowska, E. (1987). Propriospinal neurones in the middle lumbar segments of the cat spinal cord interposed in reflex pathways from group II muscle afferents to hind-limb motoneurones. *J. Physiol.* 320:70P.

Illert, M., and Lundberg, A. (1978). Collateral connections to the lateral reticular nucleus from cervical propriospinal neurones projecting to forelimb motoneurones in the cat. *Neurosci. Let.* 7, 167–172. doi: 10.1016/0304-3940(78)90162-3

Jankowska, E., Lundberg, A., Roberts, W. J., and Stuart, D. (1974). A long propriospinal system with direct effect on motoneurones and on interneurones in the cat lumbosacral cord. *Exp. Brain Res.* 21, 169–194. doi: 10.1007/BF00234388

Jankowska, E., Lundberg, A., and Stuart, D. (1983). Propriospinal control of interneurons in spinal reflex pathways from tendon organs in the cat. *Brain Res.* 261, 317–320. doi: 10.1016/0006-8993(83)90636-4

Lundberg, A. (1979). "Integration in a propriospinal motor centre controlling the forelimb in the cat," in *Integration in the Nervous System,* eds H. Asanuma and V. J. Wilson (Tokyo: IGAKU-SHOIN), 47–65.

Conflict of Interest: The authors declare that the research was conducted in the absence of any commercial or financial relationships that could be construed as a potential conflict of interest.

frontiers in Cellular Neuroscience

ORIGINAL RESEARCH
published: 09 August 2019
doi: 10.3389/fncel.2019.00359

The Mechanistic Basis for Successful Spinal Cord Stimulation to Generate Steady Motor Outputs

*Amr A. Mahrous[1,2], Mohamed H. Mousa[3] and Sherif M. Elbasiouny[1,3]**

[1] Department of Neuroscience, Cell Biology, and Physiology, Boonshoft School of Medicine and College of Science and Mathematics, Wright State University, Dayton, OH, United States, [2] Department of Physiology, Feinberg School of Medicine, Northwestern University, Chicago, IL, United States, [3] Department of Biomedical, Industrial, and Human Factors Engineering, College of Engineering and Computer Science, Wright State University, Dayton, OH, United States

Electrical stimulation of the spinal cord is a promising rehabilitation intervention to restore/augment motor function after spinal cord injury (SCI). Combining sensory feedback with stimulation of remaining motor circuits has been shown to be a prerequisite for the functional improvement of SCI patients. However, little is known about the cellular mechanisms potentially underlying this functional benefit in the injured spinal cord. Here, we combine computer simulations with an isolated whole-tissue adult mouse spinal cord preparation to examine synaptic, cellular, and system potentials measured from single motoneurons and ventral roots. The stimulation protocol included separate and combined activation of the sensory inputs (evoked by dorsal root stimulation) and motor inputs (evoked by stimulation of spinal cord tissue) at different frequencies, intensities, and neuromodulatory states. Our data show that, while sensory inputs exhibit short-term depression in response to a train of stimulation, motor inputs exhibit short-term facilitation. However, the concurrent activation of both inputs elicits a stronger and steadier motor output. This effect is enhanced by the application of pharmacological neuromodulators. Furthermore, sensorimotor excitatory postsynaptic potentials (EPSPs) summate sublinearly (i.e., their combination produces an excitatory potential smaller than the sum of the excitatory potentials they would individually produce). However, ventral root compound action potentials (CoAPs) summate supralinearly generating much higher outputs. Computer simulations revealed that the contrasting summation and disproportionality in plasticity between the excitatory postsynaptic potentials (EPSPs) and CoAPs result from the motoneuronal firing threshold acting as an amplitude-selective filter. Together, these results provide the mechanistic basis for the cellular processes contributing to the generation of steady motor outputs using spinal stimulation. This data has great potential to guide the design of more effective stimulation protocols in SCI patients.

Keywords: spinal motoneurons, electrical stimulation, spinal cord injury, motor output, use-dependent adaptation, sensorimotor integration

OPEN ACCESS

Edited by:
Michelle Maria Rank,
The University of Melbourne, Australia

Reviewed by:
Jürg Streit,
University of Bern, Switzerland
Marie-Pascale Cote,
Drexel University, United States

***Correspondence:**
Sherif M. Elbasiouny
sherif.elbasiouny@wright.edu

Specialty section:
This article was submitted to Cellular Neurophysiology, a section of the journal Frontiers in Cellular Neuroscience

Received: *16 April 2019*
Accepted: *23 July 2019*
Published: *09 August 2019*

Citation:
Mahrous AA, Mousa MH and Elbasiouny SM (2019) The Mechanistic Basis for Successful Spinal Cord Stimulation to Generate Steady Motor Outputs. Front. Cell. Neurosci. 13:359. doi: 10.3389/fncel.2019.00359

INTRODUCTION

Electrical stimulation of the spinal cord is currently showing promise for motor rehabilitation after spinal cord injury (SCI). With electrical stimulation, patients showed improved trunk control, standing, stepping, and urogenital function (Carhart et al., 2004; Harkema et al., 2011; Gerasimenko et al., 2015; Angeli et al., 2018). Notably, patients with complete SCI were able to stand and step with minimal assistance only when trains of electrical stimulation activating intrinsic motor pathways and circuits in the transected spinal cord was provided (Harkema et al., 2011; Gerasimenko et al., 2015; Angeli et al., 2018; Wagner et al., 2018). In these studies, SCI patients could not step or stand without electrical stimulation – even with manual facilitation or after several training sessions. This indicates the necessity of the electrically evoked motor potentials to the generation of these functional benefits. Importantly, electrical stimulation was not effective unless it included proprioceptive feedback generated from muscle length changes and load-bearing during stepping and standing, indicating that sensorimotor integration mediates these effects.

To investigate the effects of electrical stimulation after SCI at the synaptic, cellular, and system levels, we used electrophysiological recordings and computer simulations to study the plasticity, integration, and neuromodulation of electrically evoked sensory and motor synaptic potentials in an isolated spinal cord preparation. Specifically, our goals were to: (1) Identify the characteristics of electrically triggered sensory and motor synaptic potentials generated in motoneurons (synaptic level), (2) understand how electrically triggered sensory and motor synaptic potentials integrate within the motoneuron (cellular level), and (3) examine the transformation of electrically triggered sensorimotor potentials into a motor output at the ventral roots (system level), which determines the muscle force.

Motor behaviors are determined by how different synaptic inputs to motoneurons are integrated to produce the firing patterns of spinal motoneurons, and by how these individual motoneuron outputs are integrated into system output (muscle force). In the spinal cord, three excitatory sources determine the firing pattern of motoneurons: Descending motor commands from supraspinal structures (referred to as '*motor inputs*'), segmental sensory inputs from the periphery (referred to as '*sensory inputs*'), and local interneuronal inputs within the spinal cord (Carp and Wolpaw, 2010). Both the sensory and descending motor fibers form mono- and/or oligo-synaptic connections with motoneurons in the spinal cord (Eccles, 1946; Brown and Fyffe, 1981; Riddle et al., 2009; Liang et al., 2014; Witham et al., 2016). Therefore, the generation of an appropriate motor output for a given motor task is determined by the integration of sensory and motor inputs in the spinal cord and their ability to further engage local premotor interneurons (sensorimotor integration) (Rossignol et al., 2006; Kim et al., 2017).

As premotor interneurons fire repetitively, their synapses on motoneurons undergo typical short-term plasticity alterations (i.e., short-term facilitation or depression). Such plasticity is common to all neurons in the nervous system (Zucker and Regehr, 2002; Regehr, 2012). With successive electrical stimuli, some synaptic inputs to the target motoneuron become progressively smaller (i.e., synaptic depression), whereas others become progressively larger (i.e., synaptic facilitation). These forms of plasticity can be potentially regulated by the level of monoaminergic neuromodulators in the spinal cord. Neuromodulators such as serotonin and noradrenaline have powerful effects on the dynamics of synapses, and can even convert short-term synaptic depression to facilitation (Bevan and Parker, 2004; Barriere et al., 2008; Zhao et al., 2011; Nadim and Bucher, 2014). Presynaptically, Ca^{2+} influx and vesicular release probability are targets for neuromodulators (Logsdon et al., 2006; Higley and Sabatini, 2010). Postsynaptic neuromodulation, on the other hand, can be achieved through controlling ionic conductances on the dendrites that amplify or suppress synaptic currents (Lee and Heckman, 2000; Heckman et al., 2004; Sun et al., 2005; Miles et al., 2007). Recent studies show that electrical stimulation of either dorsal root sensory inputs or local motor inputs to motoneurons results in variable forms of short-term plasticity (Barriere et al., 2008; Jiang et al., 2015). It is currently unknown how these forms of plasticity change in presence of monoaminergic neuromodulation. Nonetheless, these variable sensory and motor inputs integrate during normal movements and thus are needed after SCI in order to generate steady motor outputs.

We therefore hypothesized that combined electrical stimulation of sensory and motor inputs in the transected spinal cord yields higher and more stable motor output than that generated by either input separately. To test this hypothesis, we used a whole-tissue *ex vivo* spinal cord preparation from adult mice to study the synaptic, cellular, and system effects evoked by electrical stimulation at different amplitudes (1.5× and 10× threshold), frequencies (25 and 50 Hz), and neuromodulatory states (in presence or absence of a noradrenergic agonist). The synaptic (i.e., excitatory postsynaptic potentials, EPSPs), cellular (i.e., motoneuron action potentials, APs), and system (ventral roots compound APs, coAPs) responses were simultaneously recorded during stimulation. Stimulation protocols included the sensory input ('S' condition, via dorsal roots), motor input ('M' condition, via descending tracts), or both ('S&M' condition, via dorsal roots and descending tracts). Our results show (1) EPSPs and coAPs of the S input exhibited progressive depression, (2) EPSPs and coAPs of the M input exhibited progressive facilitation, and (3) their combined effect (S&M) generated higher EPSP and coAP amplitudes with steady profiles. This combined enhancement was magnified at higher neuromodulatory states. Additionally, while the sensory and motor EPSPs exhibited sublinear summation, coAPs exhibited supralinear summation. Computer simulations of our experimental data showed that the differing summation of sensory and motor inputs at the cellular and system levels is because the motoneurons' firing threshold acts as an amplitude-selective filter. This transforms small EPSP amplitude changes into large coAP amplitude responses. The simulations also demonstrated that the integrated S&M EPSPs maintained motoneuron membrane potential above the firing threshold longer. This generated steady motor output with successive stimuli, which could not be achieved by either input separately.

In sum, these data provide mechanistic insights into how and why combining sensory feedback with motor stimulation evokes strong muscle contractions and stable motor function in patients with SCI. These results can be leveraged into improved stimulation protocols, leading to improved restoration of movement and independence for SCI patients.

MATERIALS AND METHODS

Animals

The fifty three male mice (B6SJL, Jackson laboratory, Bar Harbor, ME) were used in this study, 30–200 days old. The sacrocaudal spinal cord was surgically transected and isolated, maintained *in vitro*, and used to record single motoneuron behavior as well as ventral root response. This part of the adult spinal cord can be reliably maintained *in vitro* for several hours (Bennett et al., 2001; Jiang and Heckman, 2006). All surgical and experimental procedures in this study were carried out in accordance with the recommendations of Wright State University Animal Care and Use Committee. The protocol was approved by the Wright State University Animal Care and Use Committee.

Ex vivo Whole Tissue Spinal Cord Preparation

The procedures for surgical isolation of the sacrocaudal spinal cord has been previously described (Mahrous and Elbasiouny, 2017). Briefly, the animal was first deeply anesthetized using urethane ($\geq$ 0.18 g/100 g, injected intraperitoneally). When the animal no longer responded to toe pinching, it was placed in a dissection dish and supplied with carbogen (95% O_2/5% CO_2) through a face mask. The spinal cord was exposed by means of dorsal laminectomy and longitudinal incision of the dura mater. The cord was transected around L4 segment and the caudal part with the attached roots was transferred to a dissection dish full of oxygenated modified artificial cerebrospinal fluid (mACSF, see below). The ventral and dorsal roots were separated and the cord was transected at the lumbosacral enlargement (L6). The cord was then pinned with the ventral side upward in a recording chamber and perfused with oxygenated normal artificial cerebrospinal fluid (nACSF, see below) at a rate of 2.5–3 ml/min. The dorsal and ventral roots were mounted on bipolar wire electrodes and covered with petroleum jelly to prevent drying. All experiments were performed at room temperature ($\sim$21°C).

Electrophysiological Recordings

Ventral Root Recording

Ventral roots were connected to a differential amplifier (Kinetic Software, GA) with 1000× gain and 300 Hz – 3 KHz bandwidth filter. We performed most of our recordings at the S4 segments where the responses were most stable and highest in amplitude (see below in 'sensory and motor inputs'). During the first 30–40 min in the recording chamber, the ventral root response to dorsal root stimulation steadily increased in amplitude. Hence, the cord was allowed to recover for nearly 1 h before any recordings were started. The ventral root responses to trains of electrical stimulation were quantified as the peak-to-peak measurements of its compound action potentials (CoAPs).

Single Motoneuron Recordings

Using sharp intracellular glass microelectrodes, single motoneurons were recorded in the isolated whole tissue. These glass electrodes were pulled using a micropipette puller (P97, Sutter instruments, CA), and filled with 3M potassium acetate and 100 mM KCl and had a resistance of 25–40 MΩ. The microelectrodes were advanced into the ventral horn using a micro-positioner (2660, Kopf instruments, CA). Motoneurons were identified by antidromic stimulation of the ventral root and were accepted for recording when the resting membrane potential was below −60 mV and the antidromic spike was $\geq$ 60 mV. The Na^+ channel blocker, QX-314 (50–100 mM), was used in the internal electrode solution to inhibit action potential generation, so that the exact amplitude of the synaptic potentials can be determined. The amplitudes of synaptic potentials during a train of stimulation were measured as the voltage change at the peak of the EPSP relative to the baseline resting membrane potential before the stimulation train. Intracellular recordings were performed using an Axoclamp 2B amplifier (Molecular Devices, CA) running in bridge or discontinuous current clamp (DCC) mode and low-pass filtered at 3 kHz.

The outputs of both the intracellular and extracellular amplifiers were digitized using Power 1401-3 data acquisition interface (CED, United Kingdom) at 10–20 kHz. Data were acquired into a computer controlled by Spike2 software (version 8.06, CED) and stored for offline analysis.

Sensory and Motor Inputs

Sensory Inputs

The sensory inputs (S) were induced by electrical stimulation of the dorsal roots. Dorsal roots were connected through bipolar wire electrodes (**Figure 1**, electrode 'A') to a stimulator (Isoflex, AMPI), and stimulated with 0.1 ms pulses at either 1.5 or 10 times threshold (1.5×T or 10×T). The threshold for dorsal root stimulation was defined as the smallest amount of current delivered to the dorsal root to produce a minimal response (compound action potential, coAP) in the ventral roots, and ranged from 1.5 to 6 μA. In some experiments, another bipolar electrode was placed on the dorsal root more proximally to record the root potential. The response to dorsal root stimulation was most consistent and stable at the lower sacral as well as the caudal ventral roots (S3 to Co2).

Motor Inputs

The motor inputs (M) were induced by electrical stimulation of the spinal cord tissue (**Figure 1**, electrode 'D'). A concentric bipolar electrode (0.125 mm stainless steel contact diameter insulated by Teflon from a stainless steel tube 0.2 ID/0.35 OD) was placed on the ventral surface close to the midline at the L6 segment (Jiang et al., 2015). Brief electrical pulses (0.1 ms) were delivered through the concentric electrode at 1.5×T or 10×T. The threshold was defined as the smallest amount of current,

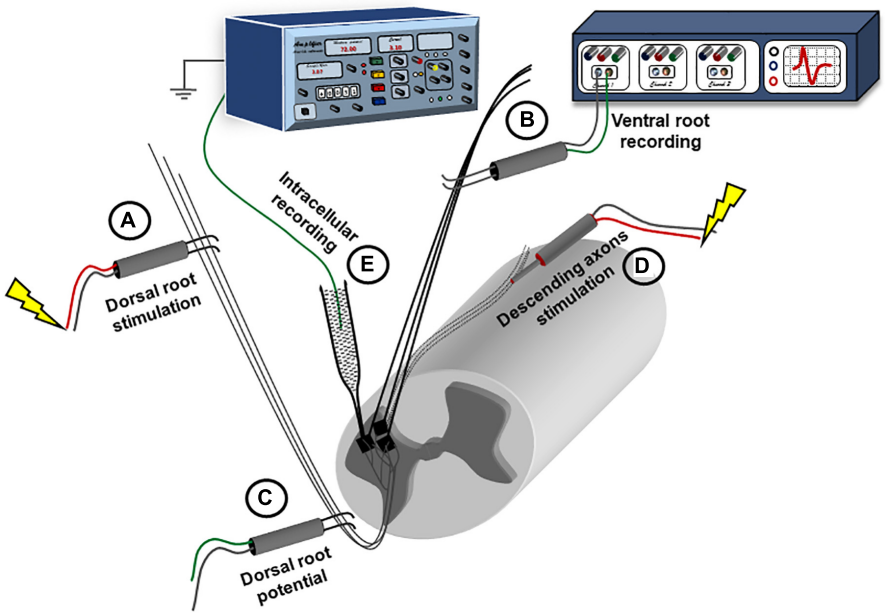

FIGURE 1 | Experimental setup for recording synaptic responses to sensory and descending stimulation. The spinal cord is placed ventral side up in a perfusion chamber. Ventral and dorsal roots are mounted on bipolar wire electrodes above the solution level, and covered with petroleum jelly. The dorsal roots **(A)** are connected to a stimulator; while the ventral roots **(B)** are connected to a multichannel extracellular amplifier for recording. Another extracellular recording electrode is placed on the dorsal root **(C)** more proximally and connected to the extracellular amplifier to record the dorsal root volley. A concentric electrode **(D)** is placed on the ventral side to stimulate the descending axons. Intracellular recording is performed using sharp electrodes **(E)** advanced through the ventral surface.

delivered through the concentric electrode, which produces a response in the ipsilateral ventral roots, and ranged from 100 to 200 μA. The largest response to motor stimulation was at the S1 segment and the smallest was at the caudal segments. Therefore, we conducted our recordings at S4 where the responses to both sensory and motor inputs were stable.

The response to each synaptic input was recorded separately, and then both pathways were stimulated simultaneously to study integration. To induce a higher neuromodulatory state, the α_1-adrenergic receptor agonist, methoxamine (10 μM), was added to the recording solution. After 10 min of continuous exposure, the electrical stimulation paradigm was repeated.

Effective Synaptic Currents

To measure the effective synaptic currents generated by the sensory and motor inputs in **Figure 7**, we modified the methodology described in Heckman and Binder (1988). We used the voltage change at the fifth pulse as the steady state input in our protocol. The protocol was repeated with different values of injected current through the intracellular microelectrode. The relationship established between the injected current and the voltage change was then used to estimate the effective synaptic currents, and the slopes were compared to test if the synaptic inputs changed the input resistance of the cell.

Physiological Solutions

Normal Artificial Cerebrospinal Fluid

The nACSF was formed of the following (in mM): 128 NaCl, 3 KCl, 1.5 $MgSO_4$, 1 NaH_2PO_4, 2.5 $CaCl_2$, 22 $NaHCO_3$, and 12 glucose. The osmolarity of the solution was ∼295 mOsm, and the pH was 7.35–7.4 when aerated with carbogen (95% O_2 and 5% CO_2).

Modified Artificial Cerebrospinal Fluid

The mACSF contained the following (in mM): 118 NaCl, 3 KCl, 1.3 $MgSO_4$, 5 $MgCl_2$, 1.4 NaH_2PO_4, 1.5 $CaCl_2$, 24 $NaHCO_3$, and 25 glucose. This high Mg^{2+}/low Ca^{2+} solution decreases the activity in the cord during dissection. The osmolarity of the solution was ∼310 mOsm, and the pH was 7.35–7.4 when aerated with carbogen (95% O_2 and 5% CO_2).

Drugs and Chemicals

N-(2,6-Dimethylphenylcarbamoylmethyl) triethyl ammonium bromide (QX-314), a membrane-impermeable blocker of the voltage-gated Na^+ channels; strychnine (STR), a blocker of the glycine receptors; picrotoxin (PTX), a blocker of the $GABA_A$ receptors; methoxamine, an agonist of the alpha-1 adrenergic receptors. All of the drugs were purchased from Sigma (St. Louis, MO, United States), and all of the chemical components of the physiological solutions were purchased from Thermo Fisher Scientific (Waltham, MA, United States).

Computational Models

Computer Model of the Motor Pool

To simulate the response of spinal motoneurons to electrically evoked sensory and motor inputs, we employed a multiscale, high-fidelity computer model of the alpha-motoneuron pool, which is described in full detail in Jiang et al. (2015). This

model is based on 3D reconstructed motoneuron anatomy data and bridges the synaptic, cellular, and system scales. Motoneurons with reconstructed morphologies, as opposed to simplified computer models of motoneurons, were employed because the simplification of dendritic morphology has been shown to generate large errors in simulating motoneuron firing behaviors and active properties (Elbasiouny, 2014). The motor pool model consisted of 50 cells and was implemented using the NEURON simulation environment (Hines and Carnevale, 1997). The model of individual cells was based on that developed for alpha motoneurons by Elbasiouny et al. (2005), which incorporated realistic alpha motoneuron morphology, realistic dendritic distribution of synaptic inputs, and somatic and dendritic active conductances. This cell model was used because it has been highly optimized to reproduce multiple electrophysiological datasets of spinal motoneurons obtained under different recording conditions (current- and voltage-clamp, motoneuron activation via synaptic inputs and current injection) (Elbasiouny et al., 2005, 2006). The somatic active conductances included the fast Na^+ and delayed rectified K^+ channels (which mediate the AP spike), and the Ca^{2+}-activated K^+ channels and N-type Ca^{2+} channels (which mediate the afterhyperpolarization, AHP). The dendritic active conductances included the low voltage-activated L-type Ca^{2+} channels (which mediate Ca^{2+} persistent inward current, Ca^{2+} PIC). The passive and active properties of the Elbasiouny et al. (2005) model were varied to match the electrical properties of sacral motoneurons of different types (i.e., slow, fatigue-resistant, and fast-fatigable types) in order to more accurately represent the motoneuron pool.

Each individual motoneuron cell model was driven by two sources of synapses: sensory and motor synapses. The distribution of excitatory and inhibitory sensory and motor synapses was uniform on the motoneuron dendrites and their conductances were the same across all cells in the pool. This assumption is supported by the equal synaptic input limb motoneurons receive from inhibitory Renshaw and Ia-reciprocal inhibitions and the small variability in amplitude of inputs motoneurons receive from excitatory Ia-afferents and vestibulospinal input (Powers and Binder, 2001). Following the methodology of Jiang et al. (2015), the excitatory and inhibitory conductances of the sensory and motor synapses were calculated from the experimental data and adjusted in order to reproduce our ventral root recordings before and after administration of STR and PTX (**Table 1** shows the synaptic conductances for the sensory and motor inputs). To simulate the effects of electrical stimulation of the sensory and/or motor inputs, the sensory and motor synapses were activated synchronously and repeatedly at frequencies comparable to the stimulation frequencies tested in our experiments (i.e., 25 and 50 Hz). Accordingly, the synaptic conductances in the model accounted for the strength of the synapses on motoneurons and the probability of neurotransmitter release at that stimulation frequency. Following the methodology of Jiang et al. (2015), the model also incorporated the depolarization in membrane potential between pulses for the sensory and motor inputs.

To mimic our EPSP recordings in presence of QX-314 in the micropipette, we measured EPSPs in simulations when Na^+ channels were blocked.

Driving Force Simulations

To investigate the effects of changing the driving force on synaptic integration (**Figure 8**), we used an FR cell from the pool model to run these simulations. In these simulations, the somatic voltage-gated conductances were removed from the model to isolate the synaptic effects. The sensory and motor synapses were distributed uniformly over the dendrites (**Figure 8A**). The onset and time to peak for each synapse were matched to the experimental data (**Table 2**) for the sensory and motor inputs. The synapses were activated using a single pulse, and the maximum conductances for each synapse were weighted based on the relative amplitudes of the first response generated by each input at 1.5×T intensity in the experimental data. All model parameters were kept unchanged during each run except for the reversal potential of the synapses, which was varied to change the driving force (resting membrane potential kept at −70 mV). Sensory and motor synaptic responses in our preparation were eliminated by DNQX (blocker of AMPARs, not shown) indicating that these synapses are glutamatergic. Therefore, sensory and motor synapses were given the same equilibrium potential during each run.

Statistical Analysis

The statistical analyses were performed using GraphPad Prism software (La Jolla, CA, Version 7.01). Repeated-measures one-way ANOVA was used to test changes in the amplitude of coAPs and EPSPs at different stimulation pulses to a specific pathway (i.e., sensory, motor, or sensorimotor). When the response at each pulse was compared between two different pathways, or before and after drug treatment, a repeated-measures two-way ANOVA

TABLE 1 | Synaptic conductances of the sensory and motor inputs in the simulations.

Pulse #	Synaptic conductances (μS)			
	Sensory input		Motor input	
	Excitatory	Inhibitory	Excitatory	Inhibitory
P1	0.016	0.014	0.009	0.0022
P2	0.00976	0.0063	0.00954	0.0022
P3	0.0096	0.00588	0.009504	0.00187
P4	0.0104	0.00868	0.00954	0.00242
P5	0.01008	0.00868	0.009765	0.00308

TABLE 2 | Different timing parameters for the synaptic potentials of the sensory and motor inputs.

Time parameters (Mean ± *SD*, milliseconds)	Sensory input	Motor input	Number, *p*-value
Delay from trigger	1.97 ± 0.54	1.85 ± 0.32	$N = 11$, $p = 0.46$
Time to peak (T_{Peak})	1.69 ± 0.58	2.14 ± 0.59	$N = 11$, $p = 0.04$
Half decay time ($T_{1/2}$)	4.3 ± 1.86	5.71 ± 1.78	$N = 11$, $p = 0.01$

was used. For *post hoc* analyses, Tukey test was used with two-way ANOVA and Dunnett test was used with one-way ANOVA. *T*-test was used to compare the delay, time to peak, and decay time of EPSPs of different pathways. A *p*-value of < 0.05 was considered significant for all tests.

RESULTS

In this study, the whole-tissue adult sacrocaudal spinal cord was used to study the plasticity, integration, and neuromodulation of electrically evoked sensory and motor synaptic inputs generated in spinal motoneurons. The sensory input was activated by electrical stimulation of the ipsilateral dorsal roots, which generates a response that contains a prominent monosynaptic component, presumably from the Ia muscle afferents. On the other hand, the motor input was activated via surface electrical stimulation of the ventrolateral funiculus of the rostral end of the sacrocaudal preparation. This stimulation activates local interneurons in addition to the remaining axons of descending tracts, primarily the lateral vestibulospinal tract (LVST, see section "Discussion" for more details). The synaptic, cellular, and system responses to electrical stimulation were recorded as EPSPs and somatic APs measured from single motoneurons using intracellular sharp electrodes and coAPs measured from the ventral roots using extracellular wire electrodes, respectively (**Figure 1**).

Short trains of electrical stimuli (five pulses) of low intensity (1.5×T, T is threshold of each pathway) or high intensity (10×T) at physiological frequencies (25 Hz or 50 Hz) were delivered to either the dorsal roots (sensory input, S), the remaining descending axons (motor input, M), or both simultaneously (sensorimotor input, S&M). Threshold was determined separately for the S and M inputs, and was identified as the minimum stimulation intensity needed to activate that particular pathway to evoke the smallest observable response in the ventral roots.

Electrically Evoked Sensory Inputs Exhibit Depression With a Train of Stimulation

Electrical stimulation of the dorsal roots (S input), at both intensities (1.5×T and 10×T) and frequencies (25 Hz and 50 Hz), generated coAPs in the ventral roots that became progressively smaller with successive pulses of stimulation (**Figure 2A**, top panel). This pattern was consistent among different roots and different animals at intensities of 1.5×T (red bars labeled 'S' in **Figure 4A**, and **Supplementary Figure 1A**) and 10×T (red bars labeled 'S' in **Figure 5A**, and **Supplementary Figure 2A**); $n = 15$, repeated-measures one-way ANOVA, $p < 0.0001$ for all intensity/frequency combinations.

When sensory synaptic responses were recorded intracellularly in single motoneurons, the cells initially fired action potentials, but later failed with subsequent pulses (**Figure 2A**, middle panel). To measure the amplitude of sensory EPSPs, QX-314 (a blocker of the voltage-gated Na^+ channels) was added to the internal microelectrode solution in order to block cell spiking (**Figure 2A**, bottom panel). Similar to coAPs, sensory EPSPs exhibited progressive depression in response to a train of stimulation to the dorsal root at the tested frequencies and intensities (red bars of **Figures 4B**, **5B** and **Supplementary Figures 1B, 2B**, $n = 12$/each, repeated-measures one-way ANOVA, $p \leq 0.005$ for all intensity/frequency combinations). This gradual depression occurred in spite of the membrane depolarization (1 ± 0.17 mV at 1.5×T and 1.76 ± 0.3 mV at 10×T) during the pulse train (**Figure 2A** bottom panel and **Supplementary Figure 3A**). Importantly, the depression seen in the coAPs' amplitude was much more pronounced compared to the depression seen in EPSPs (in **Figure 4** and **Supplementary Figure 1**, compare red bars labeled 'S' in A and B of the same figure). For instance, by the 5th pulse of stimulation, the amplitude of coAPs was reduced on average by 95%, whereas the amplitude of corresponding EPSPs was reduced on average by only 33%. This indicates a disproportion between the cellular (EPSP data) and system (coAP data) plasticity in the sensory input to motoneurons.

Plasticity of the Sensory Inputs Is Partially Due to Short-Term Synaptic Depression

The depression seen in the response to sensory inputs could result from one or more of several factors: (1) sensory axons fail to fire at the stimulation frequencies used, (2) activation of polysynaptic inhibitory pathways in the cord affects later pulses than earlier ones, and/or (3) depression of synaptic transmission caused by depletion of vesicular neurotransmitter release at the terminal. The following experiments aimed to separate and quantify these factors.

First, to test if the observed depression is due to the failure of sensory axons in conducting APs at the stimulating frequencies, we used a recording electrode on the dorsal root (labeled 'C' in **Figure 1**) to record the dorsal root potential, which has a magnitude proportional to the number of stimulated sensory axons. Repeated-measures one-way ANOVA showed that dorsal root potentials at all pulses were not different when stimulated at 1.5×T (**Figure 3A**, $n = 12$, $p = 0.3$) or 10×T (**Figure 3B**, $n = 12$, $p = 0.7$). This indicates that similar number of sensory axons were consistently stimulated and recruited by each of the five pulses. Therefore, the depression observed in sensory coAPs and EPSPs is not due to failure of stimulation. Interestingly, when the stimulation intensity was increased to 100×T, no further increase in the dorsal root potential amplitude was seen relative to 10×T, indicating that 10×T recruited the maximum number of sensory axons.

Second, to test the contribution of inhibitory pathways to the measured sensory depression, strychnine and picrotoxin (selective blockers of glycine and GABA) were administered to block inhibitory synaptic transmission. In presence of strychnine and picrotoxin, the sensory input showed less depression (**Figure 3C**, $n = 8$, repeated-measures two-way ANOVA, $p < 0.001$). For instance, the amplitude of coAPs in the 4th and 5th pulses (when polysynaptic pathways have

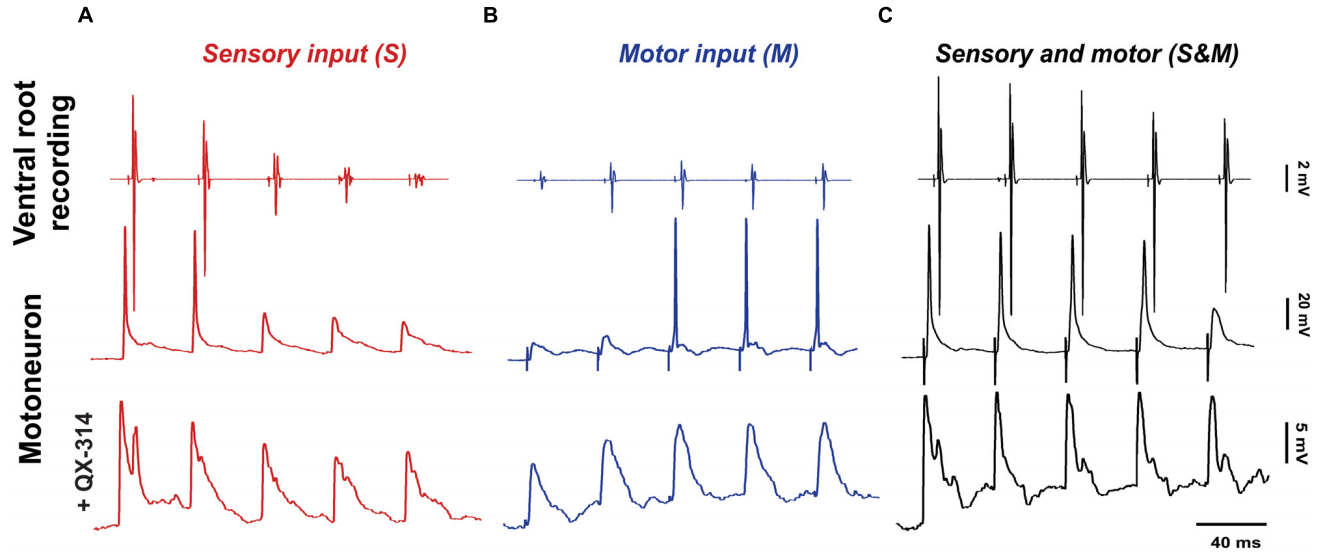

FIGURE 2 | Adapting sensory and motor inputs generate a steady motor output. The response to electrical stimulation (5 pulses at 25 Hz) of the dorsal roots (**A**, red), descending axons (**B**, blue) or both of them simultaneously (**C**, black). The top panel shows compound action potentials (coAPs) recorded in the ventral roots, while the middle and bottom panels show spikes and synaptic potentials (EPSPs) in single motoneurons with or without the Na^+ channel blocker QX-314 in the internal electrode solution, respectively.

been stimulated more relative to the early pulses) was reduced by 37–42% after administration of strychnine and picrotoxin, as opposed to 80–90% depression before their administration (**Figure 3C**, $p < 0.01$). These data indicate that about 50–60% of the sensory depression is mediated by activation of polysynaptic inhibitory pathways. Thus, the remaining decline can be attributed to use-dependent depression at the presynaptic terminals.

Electrically Evoked Motor Inputs Exhibit Facilitation With a Train of Stimulation

To activate the motor input, electrical stimulation was delivered to the ventral surface of the spinal cord below the lumbosacral enlargement next to the midline. A similar protocol of 5-pulse trains at intensities of 1.5×T or 10×T and frequencies of 25 or 50 Hz was used. Electrical stimulation evoked coAPs in the ventral roots that gradually increased in amplitude (**Figure 2B**, top panel). Again, this pattern was consistent among different roots and different animals at intensities of 1.5×T ('M' labeled bars in **Figure 4A** and **Supplementary Figure 1A**) and 10×T (blue bars labeled 'M' in **Figure 5A** and **Supplementary Figure 2A**); $n = 15$/each, repeated-measures one-way ANOVA, $p < 0.01$ for all intensity/frequency combinations.

In single motoneurons, motor EPSPs evoked by a train of stimulation gradually increased in amplitude, which sometimes resulted in generation of action potentials with the later pulses (**Figure 2B**, middle panel). When action potentials were blocked by QX-314 in the microelectrode (**Figure 2B**, bottom panel), motor EPSPs showed similar patterns of facilitation at the tested frequencies and intensities (blue bars labeled 'M' in **Figures 4B**, **5B** and **Supplementary Figures 1B, 2B**, $n = 12$/each, repeated-measures one-way ANOVA, $p \leq 0.008$ for all intensity/frequency combinations). The membrane potential of motoneurons exhibited consistent progressive depolarization during motor stimulation (**Figure 2B** and **Supplementary Figure 3**) which contributes to the facilitation of the synaptic potentials.

The degree of motor facilitation was more profound in the coAPs compared to EPSP synaptic potentials (in **Figure 4** and **Supplementary Figure 1**, compare blue bars labeled 'M' in A and B of the same figure). The coAPs at the second to the fifth pulse increased by more than 110%, compared to only a 34% increase in the EPSPs' amplitudes. This indicates disproportionality between the cellular and system plasticity, similar to that observed in the sensory input.

Contrasting Summation of Electrically Evoked Synaptic Effects Between the Synaptic and System Levels

The data above show that electrically evoked sensory and motor inputs to motoneurons have different synaptic plasticity patterns in response to a train of electrical stimuli. We then investigated the characteristics (amplitude and profile) of the motor output generated from concurrent activation of both inputs (S&M). When dorsal roots and descending fibers were stimulated simultaneously, the S&M coAPs at the ventral roots exhibited less adaptation and had higher amplitudes than those generated from either input separately (**Figure 2C**, top panel). This pattern was consistent among different roots and different animals at intensities of 1.5×T (black bars labeled 'S&M' in **Figure 4A** and **Supplementary Figure 1A**) and 10×T (black bars labeled 'S&M' in **Figure 5A**

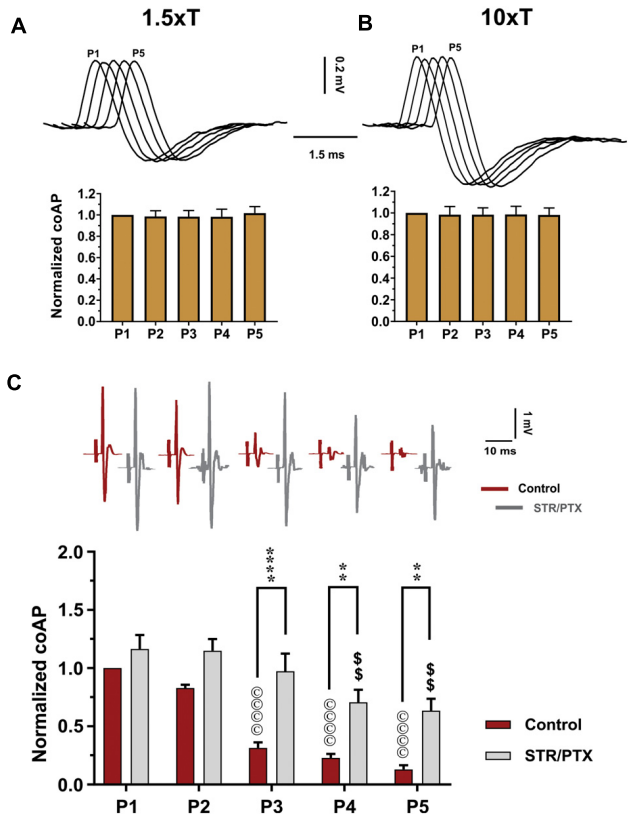

FIGURE 3 | Depression of the sensory inputs is partially due to activation of inhibitory pathways, not stimulation failure. The dorsal root potentials recorded in response to electrical stimulation of the roots' distal end at 1.5×T **(A)** and 10×T **(B)** do not show any adaptation. Top: Example dorsal root potentials recorded in the same dorsal root at different intensities. Bottom: Summary of responses from multiple experiments. The root potentials were normalized to the amplitude of the first response in each experiment. Data show no stimulation failure during a 5-pulse train at 25 HZ (n = 12, repeated-measures one-way ANOVA, p = 0.29 and p = 0.66, respectively – error bars represent *SD*). **(C)** CoAPs recorded in the ventral roots exhibit gradual depression in response to a train of stimulation to the dorsal root. This depression is partially alleviated when synaptic inhibition is blocked by strychnine (STR) and picrotoxin (PTX; n = 8, repeated-measures two-way ANOVA, p = 0.0001). Top: Example coAPs recorded under normal conditions (black trace) and in presence of synaptic inhibition blockers in the same ventral root (gray trace). Bottom: summary of coAPs' amplitudes in presence and absence of STR/PTX. The coAps were normalized to the amplitude at the 1st pulse under control conditions. *The symbol '©' denotes significant difference from control P1 response, and '$' denotes significant difference from P1 response in presence of STR/PTX.*

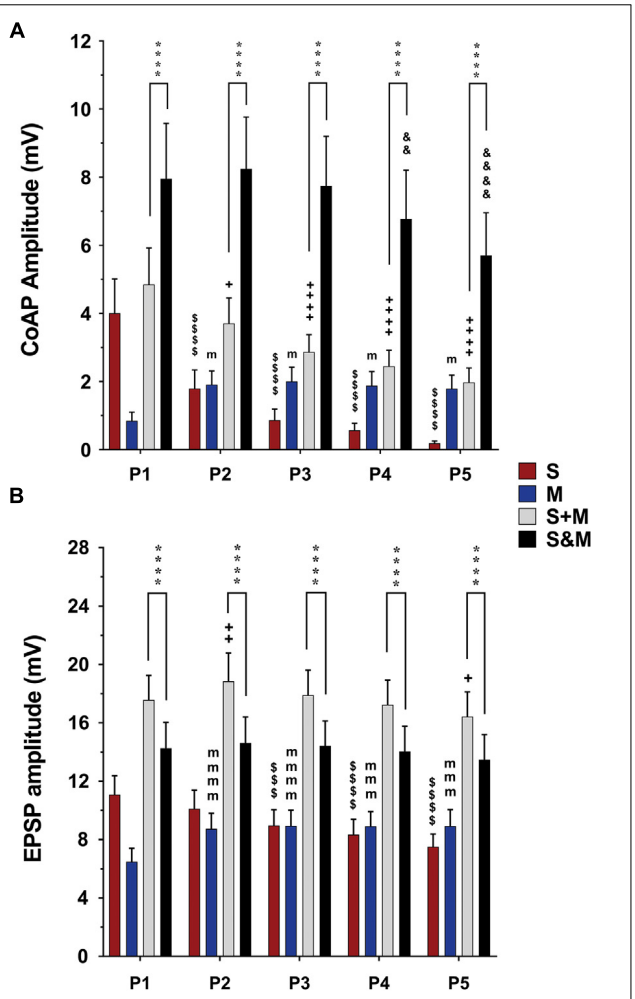

FIGURE 4 | Summary of the responses to individual and integrated sensory and motor inputs at 1.5×T/25 Hz stimulation. Summary of responses in the ventral roots **(A)** and single motoneurons **(B)** to 5-pulse electrical stimulation (P1–P5) at a frequency of 25 Hz delivered to the dorsal roots (sensory inputs, '*S*'), descending fibers (motor inputs, '*M*'), or both (sensorimotor integrated inputs, '*S&M*'). **(A)** In the ventral roots, coAPs generated by the sensory inputs exhibit depression while those generated by the motor inputs (M) exhibit facilitation. When compared to the linear summation of the two inputs (S + M), the simultaneous activation of the two inputs (S&M) results in a steadier motor output, and supralinear summation of the coAPs (S&M > S + M), n = 15. **(B)** At the cellular level, the EPSPs generated by each individual pathway follow the same adaptation pattern as the coAP, though less dramatically. The integration of the two inputs results in non-adapting synaptic potentials, and sublinear summation of the EPSPs (S + M > S&M), n = 12. Data represented as the mean ± SEM. Repeated-measures one-way ANOVA was used to study the pattern of adaptation of each input. Repeated-measures two-way ANOVA was used to test the type of integration (S&M vs. S + M). The symbol '$' denotes significant difference from S P1, 'm' denotes significant difference from the M P1, ' + ' denotes significant difference from S + M P1, '&' denotes significant difference from S&M P1, and '*' denotes significant difference between S&M and S + M.

and **Supplementary Figure 2A**). For instance, there was no change in S&M amplitudes between the first three pulses (**Figure 4A**). Relative to the 1st pulse response, the 4th and 5th S&M pulses showed an average decline of only 15 and 28%, respectively, compared to an 86 and 95% decrease in the S coAPs; to a 122 and 111% increase in the M coAPs; and to the linear summation of individual S and M inputs (termed 'S + M'), which showed a 50 and 59% decrease in the coAPs. This shows that simultaneous activation of S&M inputs generated steadier coAPs with a train of stimulation.

At the synaptic level, the S&M EPSPs also exhibited a non-adapting pattern: Their amplitudes did not change at any pulse

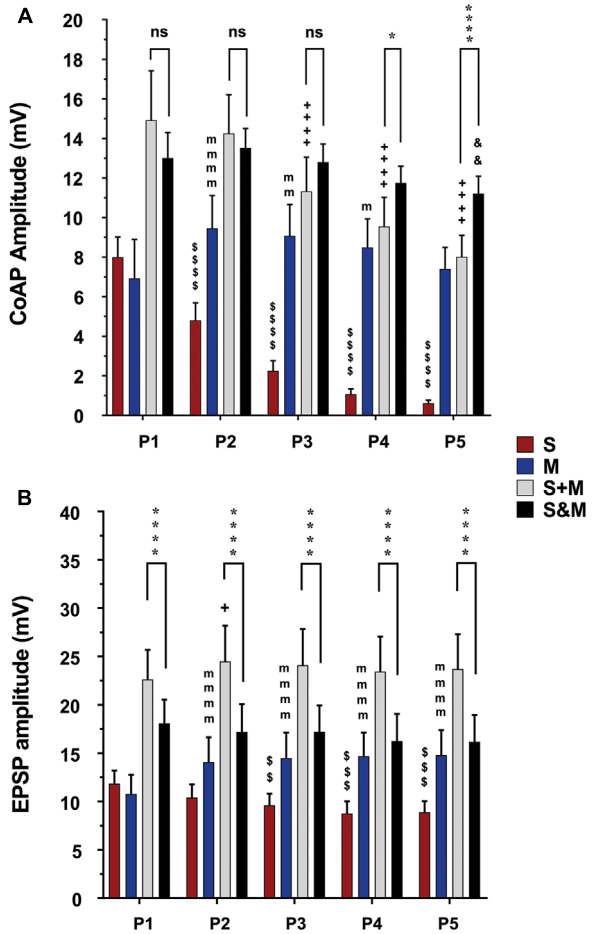

FIGURE 5 | Summary of the responses to individual and integrated sensory and motor inputs at 10×T/25Hz stimulation. Summary of responses to 10×T/25 Hz electrical stimulation of the sensory and descending pathways (The layout is similar to **Figure 4**). **(A)** In the ventral roots, the responses follow the same adaptation patterns as the lower stimulation intensity. The integration of the two inputs results in a steadier motor output and linear summation of the coAPs, except at P4 and P5, where it becomes supralinear (S&M ≥ S + M), $n = 15$. **(B)** In motoneurons, integration of the two inputs results in non-adapting synaptic potentials (S&M) and sublinear summation (S + M > S&M), $n = 12$. Data representation, statistical analysis, and significance symbols are the same as in **Figure 4**.

for 1.5×T and 10×T intensities [**Figure 2C**, bottom panel and black bars labeled 'S&M' in **Figure 4B** ($p = 0.38$) and **Supplementary Figure 1B** ($p = 0.44$) for 1.5×T and **Figure 5B** ($p = 0.54$) and **Supplementary Figure 2B** ($p = 0.77$) for 10×T]. This is different from the separate sensory or motor EPSPs, which each exhibited about a one-third decrease or increase, respectively, by the 5th pulse. This non-adapting pattern is likely because the facilitation generated from the motor input balances the depression generated from the sensory input, leading to steady EPSPs. This is also evident in the changes of the baseline membrane potential during stimulation. The progressive depolarization of the membrane during stimulation seems to be mainly driven by the motor pathway (**Figure 2C** and **Supplementary Figure 3**). Collectively, the data indicate that combining sensory and motor inputs generates a steadier motor output at the system level.

To quantify the integration of inputs, we compared the amplitudes of coAPs resulting from simultaneous stimulation of both pathways (referred to as 'S&M') to the linear sum of amplitudes of separate S and M coAPs (referred to as 'S + M'). At the system level, the amplitudes of S&M coAPs were significantly larger than those of S + M coAPs at all five pulses at 1.5×T ($n = 15$, repeated-measures two-way ANOVA, $p < 0.001$), indicating supralinear summation of the responses at the system level (**Figure 4A** and **Supplementary Figure 1A**). With 10×T stimulation, supralinear summation was observed only at the last two pulses at 25 Hz (**Figure 5A**), but not at 50 Hz (**Supplementary Figure 2A**). At the synaptic level, S&M EPSPs summation pattern, on the other hand, was totally opposite – in which EPSPs exhibited sublinear summation (**Figure 4B**, S&M < S + M, $n = 12$, $p = 0.003$). These data indicate a discrepancy in input summation between the synaptic and system levels. Importantly, at all the tested stimulation frequencies/intensities, simultaneous activation of both inputs (S&M) evoked stronger and more stable motor output than the linear summation of individual inputs (S + M). Together, combining sensory and motor inputs generates higher as well as steadier motor output at the synaptic and system levels.

To this point, our results show that: (1) The S input exhibits depression at the synaptic (EPSP data) and system (coAP data) levels; (2) the M input exhibits facilitation at the synaptic and system levels; (3) there is a disproportion in the magnitude of induced plasticity between the synaptic and system levels for both inputs, in that plasticity is more profound at the system level than at the synaptic level; (4) simultaneous activation of both inputs (S&M condition) generates a stronger and steadier (i.e., less adaptive) responses at the synaptic and system levels; and (5) there is a discrepancy in summation of S and M inputs between the synaptic and system levels, in that EPSPs summate sublinearly, whereas coAPs summate supralinearly.

Computer Simulations to Examine the Discrepancy in Summation and Disproportionality in Plasticity Between the Synaptic and System Levels

Our experimental data revealed that sensorimotor inputs (S&M) always summate supralinearly at the system level (**Figures 4A**, **5A**) but always summate sublinearly at the synaptic level (**Figures 4B**, **5B**). Additionally, the magnitude of depression in the sensory input (or the magnitude of facilitation in the motor input) was more pronounced at the system level than at the cellular level (compare **Figures 4A**, **5A** to **Figures 4B**, **5B**, respectively). To examine this discrepancy in summation and disproportion in plasticity of sensory and motor inputs between the synaptic and system levels, we employed a multi-scale high-fidelity computational model of the spinal motor pool to investigate the process of transformation of synaptic inputs into cell firing. We tested the hypothesis that the

motoneuron firing threshold acts as an amplitude-selective filter, resulting in the summation discrepancy and plasticity disproportionality phenomena.

We used the computational model of the spinal motor pool published in Jiang et al. (2015) to simulate our experimental recordings on the activation of the motoneuron pool (50 cells in the pool model) with 5 pulses at 1.5×T, via the sensory, motor, or both inputs. Two sets of synapses were uniformly distributed over the dendrites of each cell in the pool model: One set of synapses was used to represent the sensory input to each cell and another to represent the motor input to each cell. The synaptic conductances of each input were adjusted to simulate the amplitudes of coAPs and EPSPs as generated from the separate stimulation of the sensory or motor input at 25 Hz (**Table 1** shows the synaptic conductances for the sensory and motor inputs). The increases in membrane potential observed experimentally between pulses for the sensory and motor inputs were also incorporated in the model. In that way, the model reproduced the amplitude and profile of depression in coAPs and EPSPs of the sensory input (compare the 1st bars in **Figures 4A,B** to the 1st bars in **Figures 6A,B**, respectively), reproduced the amplitude and profile of facilitation in coAPs and EPSPs of the motor input (compare the 2nd bars in **Figures 4A,B** to the 2nd bars in **Figures 6A,B**, respectively), as well as reproduced the depolarization in membrane potential between pulses. Importantly, when both inputs were simultaneously activated, the pool model replicated all features of the S&M experimental recordings. Specifically, the model replicated the steady, non-adapting profile of coAPs and EPSPs of the S&M condition (compare the 4th bars in **Figures 4A,B** to the 4th bars in **Figures 6A,B**, respectively). The model also replicated the supralinear summation of S&M coAPs relative to S + M (compare the 3rd and 4th bars in **Figure 6A**), as well as replicated the sublinear summation of S&M EPSPs relative to S + M (compare the 3rd and 4th bars in **Figure 6B**). Additionally, the model simulated the increasing difference between the S + M and S&M coAPs over the 5 pulses (compare the differences between the 3rd and 4th bars over the 5 pulses in **Figure 6A** to those in **Figure 4A**), as well as simulated the relatively constant difference between the S + M and S&M EPSPs at all 5 pulses (compare the differences between the 3rd and 4th bars over the 5 pulses in **Figure 6B** to those in **Figure 4B**). In sum, the pool model has accurately simulated the discrepancy in summation and disproportionality in plasticity of S&M inputs observed experimentally between the synaptic and system levels. We focused next on explaining these two phenomena using the computational model.

To test our hypothesis on the effect of the motoneuron firing threshold, we varied the firing threshold of individual motoneurons in the pool model to different levels while measuring the amplitudes of the resulting S&M coAPs and EPSPs. Each level was compared to the amplitudes from separate inputs at that level (**Figure 6C**, the horizontal dotted line represents linear summation, S + M). Importantly, when the motoneuron firing threshold was depolarized, the magnitude of the coAP supralinear summation increased proportionally at all pulses (compare the difference between the horizontal dotted line and the first 4 bars over the five pulses in **Figure 6C**). However, the magnitude of the EPSP sublinear summation was similar at all threshold levels (compare the difference between the horizontal dotted line and the last bar over the five pulses in **Figure 6C**). In other words, EPSPs always summate sublinearly and independently from the cell firing threshold (see next section for more explanation), whereas the coAP summation depends on the firing threshold: the more depolarized the firing threshold, the larger the supralinear summation. It is striking that small depolarizing shifts in the firing threshold (on the order of 0.5 mV) resulted in such large summation differences (**Figure 6C**). This variation in the coAP summation, but fixed EPSPs summation causes the

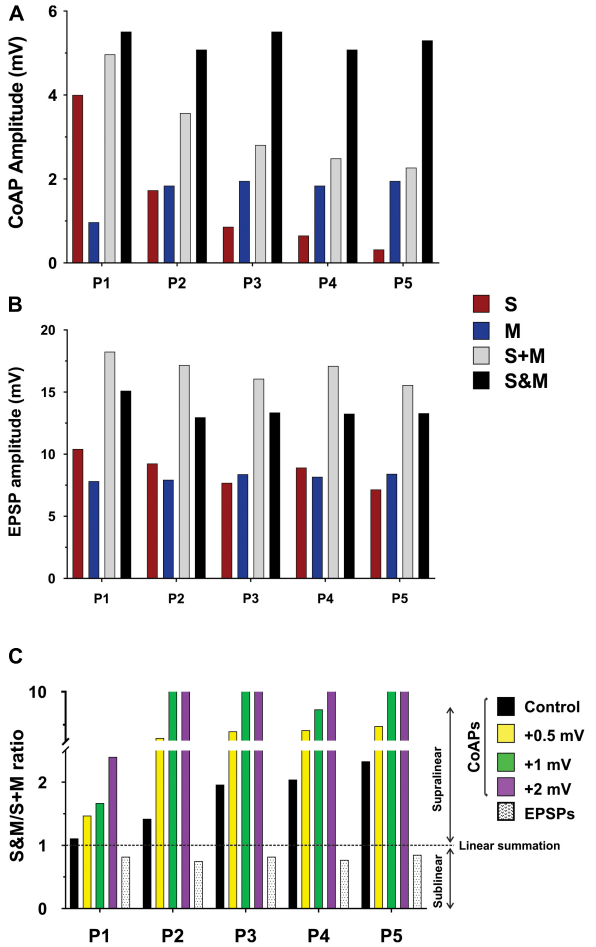

FIGURE 6 | Computational model showing the effect of changing the firing threshold of individual motoneurons on the summation of sensory and motor inputs. Data obtained from a computational model of a motor pool (50 cells) which is stimulated using two separate uniformly-distributed synaptic inputs, and generates an output analogous to the experimental data. **(A)** The output of the motor pool (compare to **Figure 4A**). **(B)** The EPSP profile in a motoneuron (compare to **Figure 4B**). **(C)** The S&M/S + M response ratio of the pool output is dramatically increased by minor shifts of the cells' firing threshold to more depolarized potentials. The summation of the EPSPs was sublinear and its magnitude was similar at all firing threshold levels, thus we show it at one level here.

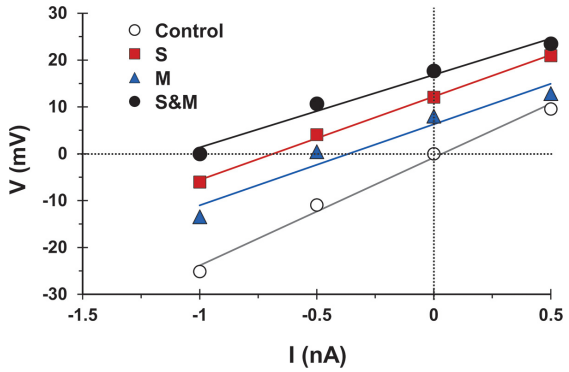

FIGURE 7 | The activation of sensory and/or motor inputs does not cause a significant change in motoneuron conductance. Voltage measurements versus injected current for a motoneuron in response to injected current alone (open circles), and injected current combined with sensory input activation (S, squares), motor input activation (M, triangles), or combined sensorimotor input (S&M, filled circles). The solid lines indicate the best linear fit to the data points. Effective synaptic current for any of the synaptic inputs is equal in magnitude, but opposite in sign to the injected current at which V (injected + synaptic) = 0. The slopes of the fit lines are not different (Linear regression, $p = 0.2$) indicating that the activation of the synapses did not significantly change the cell input conductance, $n = 4$.

disproportionality in plasticity observed between the synaptic and system levels.

Sublinear Summation of Electrically Evoked EPSPs Is Due to Changes in Driving Force

At all the tested frequencies and intensities, the summation of the sensorimotor EPSPs was sublinear. This effect could result from: (1) an increase in the effective cell conductance, and/or (2) a decrease in the driving force of the synaptic current. The following set of experiments and simulations examined these potential mechanisms.

First, to test whether synaptic activation changed the motoneuron input conductance, we followed the method of Binder and Powers (1999) and measured the voltage response to injected current alone or combined with synaptic activation. We then compared the slope of the best linear fit of the voltage responses generated by injected current and synaptic activation ('S' condition, 'M' condition, or 'S&M' condition in **Figure 7**) to that of the injected current alone ('control' condition in **Figure 7**). Because the slope of the control line is determined by the cell input conductance, any change in the slope upon synaptic activation would indicate a change in the cell conductance (Binder and Powers, 1999). Because the slopes of the S, M, and S&M lines were not different from that of control ($n = 4$), this indicated that these synaptic inputs did not alter the cell input conductance and, therefore, did not contribute to the sublinear integration of sensory and motor EPSPs.

Second, to investigate the effect of changing the driving force of the synapse, we measured different characteristics of the EPSPs as described in **Figure 8A**. The EPSPs generated from the S and M inputs had similar delays ($p = 0.46$, paired t-test), indicating that these EPSPs reached the motoneuron soma synchronously. However, the EPSPs generated by the M input took longer to reach their peak amplitude ($p = 0.04$, paired t-test) and longer to decay ($p = 0.01$, paired t-test) than those of the S input (experimental data summarized in **Table 2**). To test the effect of changing the synapse driving force on EPSPs summation, we simulated our EPSPs experimental recordings. Specifically, we incorporated the experimental data on S and M EPSPs (In **Table 2**) into one of the motoneurons in the computational pool model (**Figure 8A**, see methods for details). Also, the equilibrium potential of the synapses on that model cell was varied in order to test the effect of changing the synapse driving force on the difference between the integrated (S&M) EPSPs and the linear sum of individual (S + M) EPSPs (**Figure 8B**). As the driving force increased, the magnitude of sublinearity increased, and the gain of the relationship was determined by the conductances of the synapses (compare the gray and black traces in **Figure 8B**). Thus, strong synapses (i.e., large-amplitude EPSPs) would summate sublinearly more than weak synapses (i.e., small-amplitude EPSPs).

Taken together, the data show that sublinear summation of sensory and motor EPSPs at the synaptic level is caused by changes in local driving force, and not by increased input conductance of the cell.

Effect of the Neuromodulatory State on Adaptation and Integration of Electrically Evoked Potentials

The level of neuromodulation sets the excitability level of both presynaptic and postsynaptic neurons in the spinal network and thus affects patterns of synaptic plasticity (Barriere et al., 2008; Nadim and Bucher, 2014). The *ex vivo* spinal cord preparation used in this study represents a relatively low neuromodulatory state (i.e., low excitability level) due to the absence of the neuromodulation normally provided via serotoninergic and noradrenergic descending inputs. It resembles, however, the clinical situation of complete SCI.

Recent studies show that pharmacological neuromodulation improves the response to electrical stimulation after SCI in *in vivo* rodent studies (Courtine et al., 2009) as well as human clinical studies (Gerasimenko et al., 2015). To study the effect of enhanced neuromodulatory state on sensorimotor integration in the spinal cord, 10 μM of methoxamine, an α_1-adrenergic receptor agonist, was applied (Lee and Heckman, 1999) and the ventral root coAPs at 10×T/25 Hz were recorded (**Figure 9**, $n = 6$). Using repeated measures two-way ANOVA, and Tukey *post hoc* test, the response at each pulse after adding methoxamine was compared to its corresponding one before treatment. Importantly, addition of methoxamine enhanced the coAP responses to the sensory ($p < 0.001$) and motor ($p = 0.007$) inputs. The S&M EPSPs became much larger in presence of methoxamine (**Figure 9B**), generating steadier coAPs that became larger at the last two pulses ($p = 0.03$).

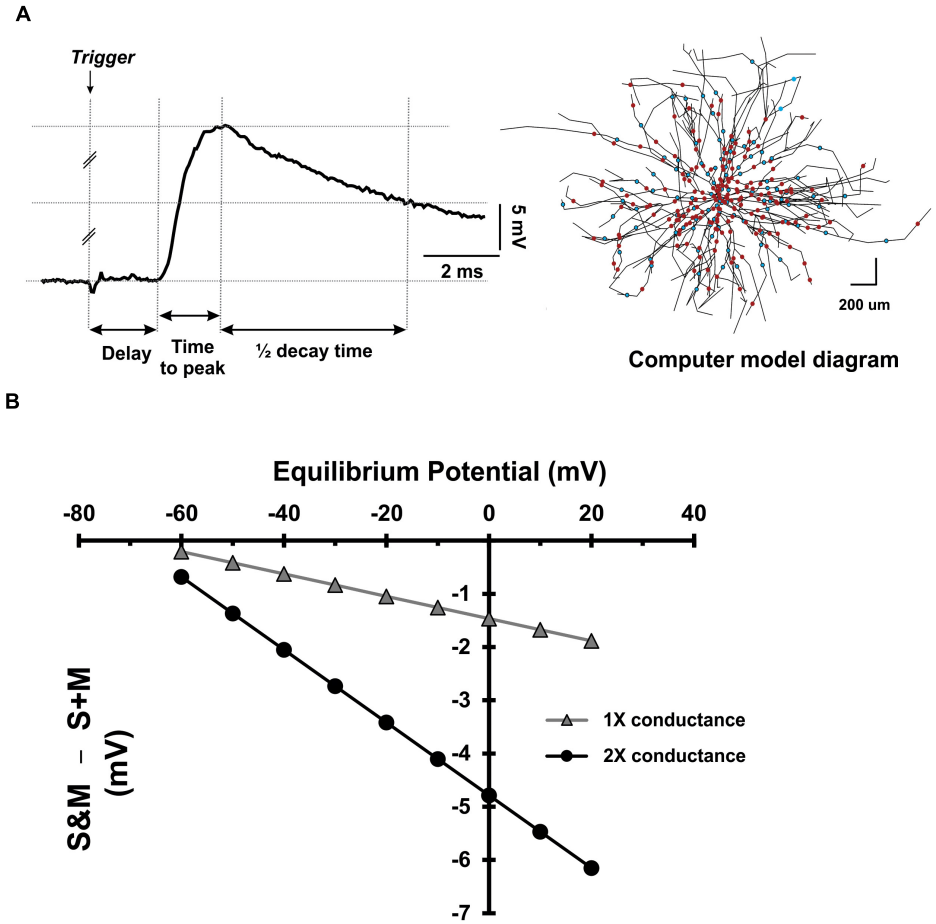

FIGURE 8 | Dependence of EPSP summation on driving force. **(A)** *Left*: Measurement of different parameters of sensory and motor EPSPs to be used in a computer model. *Right*: a diagram of the motoneuron model used to investigate the effect of the driving force on sensory and motor EPSPs' integration. The cell has detailed anatomy and generates sensory and motor EPSPs with the same parameters as experimental data. The dots indicate the location of the uniformly distributed synapses on the soma and dendrites (red for sensory synapses and blue for motor synapses). **(B)** The deviation of EPSP summation from linearity plotted as a function of the synapses' equilibrium potential. Data collected using the model motoneuron in panel **(A)**.

Interestingly, methoxamine also prolonged the decay of EPSPs (compare the falling phases of the EPSPs before and after methoxamine in **Figure 9B**, $n = 7$), leading to elevated membrane depolarization between EPSPs, which facilitated their summation. These results explain how pharmacological neuromodulation of the spinal motoneuron networks enhances the electrically evoked motor activity observed in animals and humans (Courtine et al., 2009; Gerasimenko et al., 2015). This also supports our conclusions on the mechanism of generating steadier and stronger motor outputs.

DISCUSSION

The current study provides comprehensive investigation of the plasticity, integration, and neuromodulation of electrically evoked sensorimotor inputs in spinal motoneurons, and the resultant motor output in absence of supraspinal inputs. Using electrophysiological recordings and computer simulations, we show that integration of electrically evoked sensory and motor inputs, despite having different plasticity patterns, help generate a stronger and steadier motor output, which is more readily achievable at higher neuromodulatory states. Our data revealed, for the first time, contrasting types of summation between the synaptic and system levels. In motoneurons, sensory and motor EPSPs undergo sublinear summation due to reduction in the driving force of the sensory and motor synaptic currents during their concurrent activation. Nonetheless, the amplitude of the generated sensorimotor EPSPs are large enough to maintain the motoneuronal membrane potential above the firing threshold; thereby increasing the number of motoneurons recruited by each stimulus in the train. This leads to two functional outcomes: The coAPs evoked by motoneurons at the ventral roots, compared to those generated by either input separately, become larger and steadier in amplitude throughout the stimulation train. This leads to a stronger and more stable spinal motor output. Accordingly, these results provide, for the first time, mechanistic explanation for the cellular processes contributing

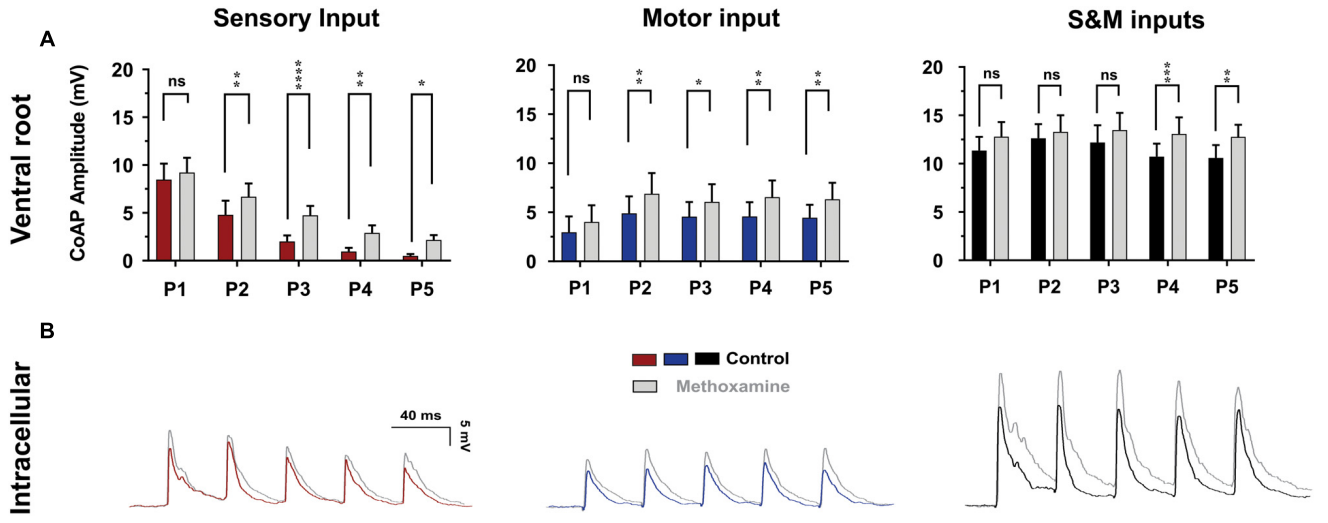

FIGURE 9 | The effect of methoxamine on plasticity and integration of sensorimotor inputs. **(A)** The effect of methoxamine (10 μM) on the ventral root response to 10×T/25 Hz stimulation, showing separate and combined sensory and motor inputs. Methoxamine enhanced the response to both the sensory and motor inputs, and helped generate a more stable motor output. Data represented as the mean ± SEM. Repeated-measures two-way ANOVA was used to test the effect of methoxamine on each type of synaptic inputs, $n = 6$. **(B)** The application of methoxamine (10 μM) to the bath solution increases the amplitude and slows down the decay of the synaptic potentials, $n = 7$. The recording microelectrode contained QX-314 to prevent spiking.

to the functional motor improvement observed in subjects with complete SCI when electrical stimulation is delivered. Additionally, these data could potentially guide and/or refine the design of more effective stimulation protocols in patients with SCI, ultimately improving the restoration of motor control and patient independence.

Short-Term Plasticity of Sensory and Motor Inputs

Repeated activation of synapses can result in either gradual increase or decrease in the resulting synaptic current in the postsynaptic cell. This phenomenon is known as use-dependent (or short-term) plasticity, which is a hallmark of synaptic transmission in the nervous system (Zucker and Regehr, 2002; Fioravante and Regehr, 2011). This form of synaptic plasticity is caused by changes in the Ca^{2+} dynamics and the probabilistic vesicular release at the presynaptic terminal (Neher and Sakaba, 2008; Regehr, 2012). We characterized the short-term changes in synaptic activity of the electrically triggered sensory and motor inputs to spinal motoneurons at physiological frequencies. The excitatory potentials generated in motoneurons by electrical stimulation of the dorsal roots (the sensory input) are dominated by the monosynaptic glutamatergic connections of the Ia afferents (Pinco and Lev-Tov, 1993; Jiang et al., 2015). A train of stimulation to the dorsal roots results in gradual depression of the evoked response. These results agree with published data that showed a similar pattern for sensory inputs *in vitro* (Lev-Tov and Pinco, 1992; Barriere et al., 2008; Jiang et al., 2017). This depression was only partially relieved when we blocked synaptic inhibition, and it persisted when polysynaptic transmission is blocked by mephenesin (Lev-Tov and Pinco, 1992). This indicates a role for reduced transmitter release from vesicles in short-term depression. Reduced vesicular release is commonly seen in synapses with high initial release probability (Alabi and Tsien, 2012), evident by the large-amplitude of the 1st EPSP in a train of stimuli. In agreement with this explanation, the plasticity pattern of this Ia afferent-motoneuron synapse was reversed to facilitation by lowering the extracellular calcium (Pinco and Lev-Tov, 1993). With low Ca^{2+}, the 1st EPSP of the train becomes smaller and the subsequent ones are progressively larger, due to build-up of Ca^{2+} in the synaptic terminals.

The motor inputs were activated by stimulation of the local motor circuits and remaining descending axons in the ventral funiculus of the sacral cord. Only a few descending tracts reach the sacral cord, including the LVST (Gossard et al., 1996; Liang et al., 2014). Fibers of the LVST originate in the lateral vestibular nucleus and travel the entire length of the spinal cord, where they synapse mainly onto ipsilateral ventral horn neurons in the mouse, rat, and cat (Gossard et al., 1996; Kuze et al., 1999; Bacskai et al., 2002; Liang et al., 2014). A few other descending tracts originating in the oral pontine reticular nucleus (PnO), and gigantocellular reticular nucleus (Gi) have also been traced down to the sacral cord of the mouse (Liang et al., 2015, 2016). However, the Gi fibers project bilaterally in the spinal cord (Liang et al., 2016) and the PnO sends only a small number of fibers to the lower segments of the spinal cord (Liang et al., 2015). Because we usually observed strong ipsilateral response to descending stimulation, we posit that the response is generated primarily by activation of the LVST fibers in addition to local interneurons.

The synaptic potentials and effective synaptic currents generated by the motor input were generally smaller than those generated by the sensory input. This is in agreement with studies

of cat motoneurons which showed that cells with high input resistance have smaller effective synaptic currents from the LVST than from Ia afferents (Binder et al., 2000). The motor input EPSPs had a similar delay to the sensory response, but with longer time-to-peak and half-decay time. This could be the result of fusion of multiple EPSPs, as the response has a pronounced polysynaptic component (Jiang et al., 2015). Alternatively, the synapses might be located more distally on the motoneuron dendrites (Magee, 2000; Spruston, 2008). The slow decay of the inputs increases the chance for integration, which would be more influential when other synaptic inputs have different onset.

Upon successive stimulation of the descending inputs, motor EPSPs showed facilitation, resulting in gradual enhancement of coAPs in the ventral roots. Interestingly, the membrane potential between EPSPs at different pulses was depolarized, and sometimes remained elevated for few seconds after the train. The facilitation of the descending response, thus, could be due to: (1) short-term synaptic facilitation (STF), caused by gradual accumulation of Ca^{2+} in the synaptic terminals, or (2) increased background network excitation resulting from summation of asynchronous EPSPs (Jiang et al., 2015), or a combination of both.

Of note, with either input, the ventral root coAPs show larger changes than the EPSPs recorded in single motoneurons (discussed below). When the two inputs are combined, two features of the resulting sensorimotor response are notable. First, opposite summation styles between the EPSPs (synaptic level) and coAPs (system level) is observed: sublinear summation of EPSPs vs. supralinear summation of coAPs. Second, the motor output of the integrated sensorimotor inputs is larger and steadier (i.e., without adaptation during stimulation) than the individual responses.

Contrasting Summation Between the Synaptic and System Levels

Sublinear summation of EPSPs has been reported in different neuronal types (Wolf et al., 1998; Magee, 2000). In cat motoneurons, summation of EPSPs is slightly but significantly sublinear (Binder and Powers, 1999; Powers and Binder, 2000). This effect could be due to increased cell conductance upon activation of synaptic ion channels, a decrease in the driving force of the synaptic current, or both. Our measurements of the sensory and motor EPSPs at different holding currents showed no change in the slope of the current/voltage relationship of the cell, indicating no change in the total cell conductance. To test the effect of the driving force, we used a computational model of a single motoneuron to study the integration of synaptic potentials with characteristics incorporated from our experimental data. Two findings are notable from these simulations: (1) Summation of the sensory and motor EPSPs is always sublinear, and the degree of sublinearity is proportional to the driving force, and (2) sublinearity increases when the synaptic conductance is increased (i.e., summation of large-amplitude EPSPs would be more sublinear than that of small-amplitude EPSPs). In fact, sublinearity in our experimental data at 10×T is more pronounced than that at 1.5×T, confirming this trend.

Despite this sublinear summation of EPSP amplitudes at the synaptic level, the increased amplitude of the integrated S&M EPSPs is large enough to maintain the motoneuron membrane potential above the firing threshold. Thus, the probability of the motoneuron firing APs by electrical stimuli becomes much higher than the sum of the probability of each separate input (i.e., supralinear summation). In other words, the motoneuronal firing threshold filters out subthreshold sublinearly summating synaptic events, and only converts probabilistic supra-threshold EPSPs into system events, effectively acting as an amplitude-selective filter separating the synaptic and system levels. This explains the mismatch in summation and plasticity between EPSPs and coAPs observed in the present study. This also explains the effectiveness of including proprioceptive sensory feedback to induce stepping and standing in patients with complete SCI via spinal cord stimulation (Harkema et al., 2011; Angeli et al., 2018): The S&M combination and amplitude-selection-filter effect enhanced the probability of supra-threshold EPSPs generation. This study demonstrates the significant impact the motoneuronal firing threshold has on the transformation of electrically evoked synaptic potentials into motor system output. The simulations showed that minor shifts in the firing threshold (in the order of 0.5 mV) would have drastic effects on the generated motor output.

Effects of the Neuromodulatory State

In this study, we examined the effect of neuromodulation on short-term synaptic plasticity of the sensory and motor inputs to spinal motoneurons. Methoxamine, the α_1-adrenergic receptor agonist, has been shown to increase the excitability of the spinal motor networks (Lee and Heckman, 1999; Gabbay and Lev-Tov, 2004; Rank et al., 2011; Mahrous and Elbasiouny, 2018). In our data, methoxamine-induced neuromodulatory state resulted in less sensory depression, more descending facilitation, and even more stable integrated output. This provides the mechanism behind the enhancement of the effect of spinal stimulation when combined with pharmacological neuromodulation (Ichiyama et al., 2008; Courtine et al., 2009; Duru et al., 2015; Gerasimenko et al., 2015).

This study mechanistically highlights the role of sensorimotor integration in generating steady motor outputs. Our data could explain the need to combine spinal cord electrical stimulation with peripheral sensory feedback (generated during motor training) to successfully induce stepping and standing in patients with complete SCI. In addition, our results support that this effect could be boosted by pharmacological neuromodulators. The data also suggest that dorsal root stimulation might be combined with spinal cord stimulation to improve the clinical outcome in patients who failed to independently stand and step with epidural stimulation alone. Taken together, the mechanistic understanding provided by these results is expected to guide the field in designing more refined and effective electrical stimulation interventions, with the ultimate goal of maximizing restored movement, quality of life, and independence in SCI patients.

DATA AVAILABILITY

All datasets generated for this study are included in the manuscript and/or the **Supplementary Files**.

ETHICS STATEMENT

This study was carried out in accordance with the recommendations of Wright State University Animal Care and Use Committee. The protocol was approved by the Wright State University Animal Care and Use Committee.

AUTHOR CONTRIBUTIONS

AM and SE conceived the presented idea, discussed the results, and verified the analytical methods. AM planned and carried out the experimental work, and drafted the manuscript. MM and SE developed the computer models and performed the computer simulations. AM, MH, and SE edited and approved the final manuscript.

FUNDING

Funding for this work was provided to SE by: (1) the U.S. National Institute of Health – National Institute of Neurological Disorders and Stroke (NIH-NINDS) grant # NS091836, and (2) the National Academy of Sciences (NAS) and the United States Agency for International Development (USAID). Any opinions, findings, conclusions, or recommendations expressed in this article are those of the authors alone, and do not necessarily reflect the views of USAID or NAS.

SUPPLEMENTARY MATERIAL

The Supplementary Material for this article can be found online at: https://www.frontiersin.org/articles/10.3389/fncel.2019.00359/full#supplementary-material

REFERENCES

Alabi, A. A., and Tsien, R. W. (2012). Synaptic vesicle pools and dynamics. *Cold Spring Harb. Perspect. Biol.* 4:a013680. doi: 10.1101/cshperspect.a013680

Angeli, C. A., Boakye, M., Morton, R. A., Vogt, J., Benton, K., Chen, Y., et al. (2018). Recovery of over-ground walking after chronic motor complete spinal cord injury. *N. Engl. J. Med.* 379, 1244–1250. doi: 10.1056/NEJMoa1803588

Bacskai, T., Szekely, G., and Matesz, C. (2002). Ascending and descending projections of the lateral vestibular nucleus in the rat. *Acta Biol. Hung.* 53, 7–21. doi: 10.1556/abiol.53.2002.1-2.3

Barriere, G., Tartas, M., Cazalets, J. R., and Bertrand, S. S. (2008). Interplay between neuromodulator-induced switching of short-term plasticity at sensorimotor synapses in the neonatal rat spinal cord. *J. Physiol.* 586, 1903–1920. doi: 10.1113/jphysiol.2008.150706

Bennett, D. J., Li, Y., and Siu, M. (2001). Plateau potentials in sacrocaudal motoneurons of chronic spinal rats, recorded in vitro. *J. Neurophysiol.* 86, 1955–1971. doi: 10.1152/jn.2001.86.4.1955

Bevan, S., and Parker, D. (2004). Metaplastic facilitation and ultrastructural changes in synaptic properties are associated with long-term modulation of the lamprey locomotor network. *J. Neurosci.* 24, 9458–9468. doi: 10.1523/jneurosci.3391-04.2004

Binder, M. D., Hamm, T. M., and Maltenfort, M. G. (2000). "Comparison of effective synaptic currents generated in spinal motoneurons by activating different input systems," in *Biomechanics and Neural Control of Posture and Movement*, eds J. M. Winters and P. E. Crago (New York, NY: Springer), 74–82. doi: 10.1007/978-1-4612-2104-3_4

Binder, M. D., and Powers, R. K. (1999). Synaptic integration in spinal motoneurones. *J. Physiol. Paris* 93, 71–79. doi: 10.1016/s0928-4257(99)80137-5

Brown, A. G., and Fyffe, R. E. (1981). Direct observations on the contacts made between ia afferent fibres and alpha-motoneurones in the cat's lumbosacral spinal cord. *J. Physiol.* 313, 121–140. doi: 10.1113/jphysiol.1981.sp013654

Carhart, M. R., He, J., Herman, R., D'luzansky, S., and Willis, W. T. (2004). Epidural spinal-cord stimulation facilitates recovery of functional walking following incomplete spinal-cord injury. *IEEE Trans. Neural. Syst. Rehabil. Eng.* 12, 32–42. doi: 10.1109/tnsre.2003.822763

Carp, J. S., and Wolpaw, J. R. (2010). "Motor neurons and spinal control of movement," in *Encyclopedia of Life Sciences*, ed. D. J. Perkel (Chichester: John Wiley & Sons, Ltd.).

Courtine, G., Gerasimenko, Y., Van Den Brand, R., Yew, A., Musienko, P., Zhong, H., et al. (2009). Transformation of nonfunctional spinal circuits into functional states after the loss of brain input. *Nat. Neurosci.* 12, 1333–1342. doi: 10.1038/nn.2401

Duru, P. O., Tillakaratne, N. J., Kim, J. A., Zhong, H., Stauber, S. M., Pham, T. T., et al. (2015). Spinal neuronal activation during locomotor-like activity enabled by epidural stimulation and 5-hydroxytryptamine agonists in spinal rats. *J. Neurosci. Res.* 93, 1229–1239. doi: 10.1002/jnr.23579

Eccles, J. C. (1946). Synaptic potentials of motoneurones. *J. Neurophysiol.* 9, 87–120. doi: 10.1152/jn.1946.9.2.87

Elbasiouny, S. M. (2014). Development of modified cable models to simulate accurate neuronal active behaviors. *J. Appl. Physiol. (1985)* 117, 1243–1261. doi: 10.1152/japplphysiol.00496.2014

Elbasiouny, S. M., Bennett, D. J., and Mushahwar, V. K. (2005). Simulation of dendritic cav1.3 channels in cat Lumbar motoneurons: spatial distribution. *J. Neurophysiol.* 94, 3961–3974. doi: 10.1152/jn.00391.2005

Elbasiouny, S. M., Bennett, D. J., and Mushahwar, V. K. (2006). Simulation of Ca2+ persistent inward currents in spinal motoneurones: mode of activation and integration of synaptic inputs. *J. Physiol.* 570, 355–374. doi: 10.1113/jphysiol.2005.099119

Fioravante, D., and Regehr, W. G. (2011). Short-term forms of presynaptic plasticity. *Curr. Opin. Neurobiol.* 21, 269–274. doi: 10.1016/j.conb.2011.02.003

Gabbay, H., and Lev-Tov, A. (2004). Alpha-1 adrenoceptor agonists generate a "fast" NMDA receptor-independent motor rhythm in the neonatal rat spinal cord. *J. Neurophysiol.* 92, 997–1010. doi: 10.1152/jn.00205.2004

Gerasimenko, Y. P., Lu, D. C., Modaber, M., Zdunowski, S., Gad, P., Sayenko, D. G., et al. (2015). Noninvasive reactivation of motor descending control after paralysis. *J. Neurotrauma* 32, 1968–1980. doi: 10.1089/neu.2015.4008

Gossard, J. P., Floeter, M. K., Degtyarenko, A. M., Simon, E. S., and Burke, R. E. (1996). Disynaptic vestibulospinal and reticulospinal excitation in cat lumbosacral motoneurons: modulation during fictive locomotion. *Exp. Brain Res.* 109, 277–288.

Harkema, S., Gerasimenko, Y., Hodes, J., Burdick, J., Angeli, C., Chen, Y., et al. (2011). Effect of epidural stimulation of the lumbosacral spinal cord on voluntary movement, standing, and assisted stepping after motor complete paraplegia: a case study. *Lancet* 377, 1938–1947. doi: 10.1016/S0140-6736(11)60547-3

Heckman, C. J., and Binder, M. D. (1988). Analysis of effective synaptic currents generated by homonymous Ia afferent fibers in motoneurons of the cat. *J. Neurophysiol.* 60, 1946–1966. doi: 10.1152/jn.1988.60.6.1946

Heckman, C. J., Kuo, J. J., and Johnson, M. D. (2004). Synaptic integration in motoneurons with hyper-excitable dendrites. *Can. J. Physiol. Pharmacol.* 82, 549–555. doi: 10.1139/y04-046

Higley, M. J., and Sabatini, B. L. (2010). Competitive regulation of synaptic Ca2+ influx by D2 dopamine and A2A adenosine receptors. *Nat. Neurosci.* 13, 958–966. doi: 10.1038/nn.2592

Hines, M., and Carnevale, T. (1997). The NEURON simulation environment. *Neural Comput.* 9, 1179–1209. doi: 10.1162/neco.1997.9.6.1179

Ichiyama, R. M., Courtine, G., Gerasimenko, Y. P., Yang, G. J., Van Den Brand, R., Lavrov, I. A., et al. (2008). Step training reinforces specific spinal locomotor circuitry in adult spinal rats. *J. Neurosci.* 28, 7370–7375. doi: 10.1523/JNEUROSCI.1881-08.2008

Jiang, M. C., Adimula, A., Birch, D., and Heckman, C. J. (2017). Hyperexcitability in synaptic and firing activities of spinal motoneurons in an adult mouse model of amyotrophic lateral sclerosis. *Neuroscience* 362, 33–46. doi: 10.1016/j.neuroscience.2017.08.041

Jiang, M. C., Elbasiouny, S. M., Collins, W. F. III, and Heckman, C. J. (2015). The transformation of synaptic to system plasticity in motor output from the sacral cord of the adult mouse. *J. Neurophysiol.* 114, 1987–2004. doi: 10.1152/jn.00337.2015

Jiang, M. C., and Heckman, C. J. (2006). In vitro sacral cord preparation and motoneuron recording from adult mice. *J. Neurosci. Methods* 156, 31–36. doi: 10.1016/j.jneumeth.2006.02.002

Kim, L. H., Sharma, S., Sharples, S. A., Mayr, K. A., Kwok, C. H. T., and Whelan, P. J. (2017). Integration of descending command systems for the generation of context-specific locomotor behaviors. *Front. Neurosci.* 11:581. doi: 10.3389/fnins.2017.00581

Kuze, B., Matsuyama, K., Matsui, T., Miyata, H., and Mori, S. (1999). Segment-specific branching patterns of single vestibulospinal tract axons arising from the lateral vestibular nucleus in the cat: a PHA-L tracing study. *J. Comp. Neurol.* 414, 80–96. doi: 10.1002/(sici)1096-9861(19991108)414:1<80::aid-cne7>3.0.co;2-e

Lee, R. H., and Heckman, C. J. (1999). Enhancement of bistability in spinal motoneurons in vivo by the noradrenergic alpha1 agonist methoxamine. *J. Neurophysiol.* 81, 2164–2174. doi: 10.1152/jn.1999.81.5.2164

Lee, R. H., and Heckman, C. J. (2000). Adjustable amplification of synaptic input in the dendrites of spinal motoneurons in vivo. *J. Neurosci.* 20, 6734–6740. doi: 10.1523/jneurosci.20-17-06734.2000

Lev-Tov, A., and Pinco, M. (1992). In vitro studies of prolonged synaptic depression in the neonatal rat spinal cord. *J. Physiol.* 447, 149–169. doi: 10.1113/jphysiol.1992.sp018996

Liang, H., Bacskai, T., Watson, C., and Paxinos, G. (2014). Projections from the lateral vestibular nucleus to the spinal cord in the mouse. *Brain Struct. Funct.* 219, 805–815. doi: 10.1007/s00429-013-0536-4

Liang, H., Watson, C., and Paxinos, G. (2015). Projections from the oral pontine reticular nucleus to the spinal cord of the mouse. *Neurosci. Lett.* 584, 113–118. doi: 10.1016/j.neulet.2014.10.025

Liang, H., Watson, C., and Paxinos, G. (2016). Terminations of reticulospinal fibers originating from the gigantocellular reticular formation in the mouse spinal cord. *Brain Struct. Funct.* 221, 1623–1633. doi: 10.1007/s00429-015-0993-z

Logsdon, S., Johnstone, A. F., Viele, K., and Cooper, R. L. (2006). Regulation of synaptic vesicles pools within motor nerve terminals during short-term facilitation and neuromodulation. *J. Appl. Physiol. (1985)* 100, 662–671. doi: 10.1152/japplphysiol.00580.2005

Magee, J. C. (2000). Dendritic integration of excitatory synaptic input. *Nat. Rev. Neurosci.* 1, 181–190. doi: 10.1038/35044552

Mahrous, A. A., and Elbasiouny, S. M. (2017). SK channel inhibition mediates the initiation and amplitude modulation of synchronized burst firing in the spinal cord. *J. Neurophysiol.* 118, 161–175. doi: 10.1152/jn.00929.2016

Mahrous, A. A., and Elbasiouny, S. M. (2018). Modulation of SK channels regulates locomotor alternating bursting activity in the functionally-mature spinal cord. *Channels (Austin)* 12, 9–14. doi: 10.1080/19336950.2017.1389825

Miles, G. B., Hartley, R., Todd, A. J., and Brownstone, R. M. (2007). Spinal cholinergic interneurons regulate the excitability of motoneurons during locomotion. *Proc. Natl. Acad. Sci. U.S.A.* 104, 2448–2453. doi: 10.1073/pnas.0611134104

Nadim, F., and Bucher, D. (2014). Neuromodulation of neurons and synapses. *Curr. Opin. Neurobiol.* 29, 48–56. doi: 10.1016/j.conb.2014.05.003

Neher, E., and Sakaba, T. (2008). Multiple roles of calcium ions in the regulation of neurotransmitter release. *Neuron* 59, 861–872. doi: 10.1016/j.neuron.2008.08.019

Pinco, M., and Lev-Tov, A. (1993). Modulation of monosynaptic excitation in the neonatal rat spinal cord. *J. Neurophysiol.* 70, 1151–1158. doi: 10.1152/jn.1993.70.3.1151

Powers, R. K., and Binder, M. D. (2000). Summation of effective synaptic currents and firing rate modulation in cat spinal motoneurons. *J. Neurophysiol.* 83, 483–500. doi: 10.1152/jn.2000.83.1.483

Powers, R. K., and Binder, M. D. (2001). Input-output functions of mammalian motoneurons. *Rev. Physiol. Biochem. Pharmacol.* 143, 137–263. doi: 10.1007/bfb0115594

Rank, M. M., Murray, K. C., Stephens, M. J., D'amico, J., Gorassini, M. A., and Bennett, D. J. (2011). Adrenergic receptors modulate motoneuron excitability, sensory synaptic transmission and muscle spasms after chronic spinal cord injury. *J. Neurophysiol.* 105, 410–422. doi: 10.1152/jn.00775.2010

Regehr, W. G. (2012). Short-term presynaptic plasticity. *Cold Spring Harb. Perspect. Biol.* 4:a005702. doi: 10.1101/cshperspect.a005702

Riddle, C. N., Edgley, S. A., and Baker, S. N. (2009). Direct and indirect connections with upper limb motoneurons from the primate reticulospinal tract. *J. Neurosci.* 29, 4993–4999. doi: 10.1523/JNEUROSCI.3720-08.2009

Rossignol, S., Dubuc, R., and Gossard, J. P. (2006). Dynamic sensorimotor interactions in locomotion. *Physiol. Rev.* 86, 89–154. doi: 10.1152/physrev.00028.2005

Spruston, N. (2008). Pyramidal neurons: dendritic structure and synaptic integration. *Nat. Rev. Neurosci.* 9, 206–221. doi: 10.1038/nrn2286

Sun, X., Zhao, Y., and Wolf, M. E. (2005). Dopamine receptor stimulation modulates AMPA receptor synaptic insertion in prefrontal cortex neurons. *J. Neurosci.* 25, 7342–7351. doi: 10.1523/jneurosci.4603-04.2005

Wagner, F. B., Mignardot, J. B., Le Goff-Mignardot, C. G., Demesmaeker, R., Komi, S., Capogrosso, M., et al. (2018). Targeted neurotechnology restores walking in humans with spinal cord injury. *Nature* 563, 65–71. doi: 10.1038/s41586-018-0649-2

Witham, C. L., Fisher, K. M., Edgley, S. A., and Baker, S. N. (2016). Corticospinal inputs to primate motoneurons innervating the forelimb from two divisions of primary motor cortex and area 3a. *J. Neurosci.* 36, 2605–2616. doi: 10.1523/JNEUROSCI.4055-15.2016

Wolf, E., Zhao, F. Y., and Roberts, A. (1998). Non-linear summation of excitatory synaptic inputs to small neurones: a case study in spinal motoneurones of the young *Xenopus* tadpole. *J. Physiol.* 511(Pt 3), 871–886. doi: 10.1111/j.1469-7793.1998.871bg.x

Zhao, S., Sheibanie, A. F., Oh, M., Rabbah, P., and Nadim, F. (2011). Peptide neuromodulation of synaptic dynamics in an oscillatory network. *J. Neurosci.* 31, 13991–14004. doi: 10.1523/JNEUROSCI.3624-11.2011

Zucker, R. S., and Regehr, W. G. (2002). Short-term synaptic plasticity. *Annu. Rev. Physiol.* 64, 355–405.

Conflict of Interest Statement: The authors declare that the research was conducted in the absence of any commercial or financial relationships that could be construed as a potential conflict of interest.

frontiers in Cellular Neuroscience

ORIGINAL RESEARCH
published: 21 August 2019
doi: 10.3389/fncel.2019.00387

Changes in Activity of Spinal Postural Networks at Different Time Points After Spinalization

*Pavel V. Zelenin, Vladimir F. Lyalka, Grigori N. Orlovsky and Tatiana G. Deliagina**

Department of Neuroscience, Karolinska Institute, Stockholm, Sweden

Postural limb reflexes (PLRs) are an essential component of postural corrections. Spinalization leads to disappearance of postural functions (including PLRs). After spinalization, spastic, incorrectly phased motor responses to postural perturbations containing oscillatory EMG bursting gradually develop, suggesting plastic changes in the spinal postural networks. Here, to reveal these plastic changes, rabbits at 3, 7, and 30 days after spinalization at T12 were decerebrated, and responses of spinal interneurons from L5 along with hindlimb muscles EMG responses to postural sensory stimuli, causing PLRs in subjects with intact spinal cord (control), were characterized. Like in control and after acute spinalization, at each of three studied time points after spinalization, neurons responding to postural sensory stimuli were found. Proportion of such neurons during 1st month after spinalization did not reach the control level, and was similar to that observed after acute spinalization. In contrast, their activity (which was significantly decreased after acute spinalization) reached the control value at 3 days after spinalization and remained close to this level during the following month. However, the processing of postural sensory signals, which was severely distorted after acute spinalization, did not recover by 30 days after injury. In addition, we found a significant enhancement of the oscillatory activity in a proportion of the examined neurons, which could contribute to generation of oscillatory EMG bursting. Motor responses to postural stimuli (which were almost absent after acute spinalization) re-appeared at 3 days after spinalization, although they were very weak, irregular, and a half of them was incorrectly phased in relation to postural stimuli. Proportion of correct and incorrect motor responses remained almost the same during the following month, but their amplitude gradually increased. Thus, spinalization triggers two processes of plastic changes in the spinal postural networks: rapid (taking days) restoration of normal activity level in spinal interneurons, and slow (taking months) recovery of motoneuronal excitability. Most likely, recovery of interneuronal activity underlies re-appearance of motor responses to postural stimuli. However, absence of recovery of normal processing of postural sensory signals and enhancement of oscillatory activity of neurons result in abnormal PLRs and loss of postural functions.

Keywords: spinal cord injury, balance control, postural reflexes, spinal neurons, spinal networks, spasticity

OPEN ACCESS

Edited by:
Katinka Stecina,
University of Manitoba, Canada

Reviewed by:
Tuan Vu Bui,
University of Ottawa, Canada
Grzegorz Hess,
Jagiellonian University, Poland

***Correspondence:**
Tatiana G. Deliagina
Tatiana.Deliagina@ki.se

Specialty section:
This article was submitted to Cellular Neurophysiology, a section of the journal Frontiers in Cellular Neuroscience

Received: *15 May 2019*
Accepted: *06 August 2019*
Published: *21 August 2019*

Citation:
Zelenin PV, Lyalka VF, Orlovsky GN and Deliagina TG (2019) Changes in Activity of Spinal Postural Networks at Different Time Points After Spinalization. Front. Cell. Neurosci. 13:387. doi: 10.3389/fncel.2019.00387

INTRODUCTION

Animals and humans maintain the basic body posture due to the activity of the postural control system. Normal operation of this system is important for standing, for keeping balance during locomotion (Horak and Macpherson, 1996; Macpherson et al., 1997a; Orlovsky et al., 1999), as well as for providing postural support for voluntary movements (Massion and Dufosse, 1988). In terrestrial quadrupeds, the postural system responsible for maintenance of the dorsal-side-up trunk orientation is driven mainly by sensory signals from limb mechanoreceptors (Inglis and Macpherson, 1995; Horak and Macpherson, 1996; Deliagina et al., 2000, 2006, 2012; Beloozerova et al., 2003; Stapley and Drew, 2009). It was demonstrated that this system consists of two relatively independent sub-systems controlling orientation of the anterior and posterior parts of the body in the transverse plane, respectively (Beloozerova et al., 2003; Deliagina et al., 2006).

Earlier, in decerebrate rabbits, we characterized postural limb reflexes (PLRs), which in intact animals significantly contribute to postural corrections generated in response to perturbation of the body posture during standing (Musienko et al., 2008, 2010; Deliagina et al., 2012), as well as to keeping balance during walking (Musienko et al., 2014). We demonstrated that though the spinal cord contains neuronal networks generating EMG pattern of PLRs, efficacy of spinal PLRs is low, and thus, contribution of supraspinal signals is important for generation of functional PLRs (Musienko et al., 2010; Deliagina et al., 2014). Two groups of spinal interneurons (F-neurons and E-neurons) contributing to generation of PLRs have been revealed (Hsu et al., 2012; Zelenin et al., 2015). Since PLRs cause a change in activity of limb extensors, and during PLRs F- and E-neurons were activated in-phase and in anti-phase with extensors, it was suggested that some of them are pre-motor interneurons exciting and inhibiting extensor motoneurons, respectively (Zelenin et al., 2015).

Spinalization results in dramatic impairment of the postural system and postural functions practically do not recover with time (Macpherson et al., 1997b; Macpherson and Fung, 1999; Rossignol et al., 1999, 2002; Barbeau et al., 2002; Lyalka et al., 2011; Chvatal et al., 2013). Immediate effect of spinalization is spinal shock, characterized by muscular hypotonus, and absence of most spinal reflexes (Ashby and Verrier, 1975; Brown, 1994; Ditunno et al., 2004). Spinal networks, deprived of supraspinal influences, undergo considerable spontaneous changes over time (Frigon and Rossignol, 2006; Roy and Edgerton, 2012; D'Amico et al., 2014), which result in gradual development of spasticity, characterized by abnormal reflex responses, clonus, spasms and hypertonus (Brown, 1994; Young, 1994; Hultborn, 2003; Hyngstrom et al., 2008; Frigon et al., 2011; Johnson et al., 2013, 2017). In postural functions, spasticity is manifested as incorrect motor responses to posture-related sensory signals and oscillatory EMG activity in limb muscles (Lyalka et al., 2011). The aim of the present study was to reveal the changes in spinal postural networks underlying the development of spasticity.

Recently, we characterized the starting point for development of spasticity that is the state of spinal postural networks in the spinal shock condition (just after acute spinalization) (Zelenin et al., 2013, 2016a). We found a significant decrease in activity of F- and E-neurons, changes in the distribution of F and E-neurons in the spinal gray matter, as well as distortions in processing of posture-related sensory information. It was also demonstrated that acute spinalization causes a decrease in the excitability of spinal motoneurons (Barnes et al., 1962; Walmsley and Tracey, 1983; Johnson et al., 2013). These distortions in operation of postural networks lead to the loss of postural functions observed in subjects in the spinal shock condition.

Here, to reveal plastic changes in spinal postural networks underlying the development of spasticity, rabbits at 3, 7, and 30 days after spinalization at T12 were decerebrated, and responses of spinal interneurons from L5 to stimulation that evoked PLRs in subjects with intact spinal cord, were recorded. The results were compared with control data from animals with intact spinal cord, as well as with data obtained after acute spinalization in our previous studies (Zelenin et al., 2013, 2015, 2016a).

Short accounts of some parts of this study has been published as abstracts (Deliagina et al., 2015; Lyalka et al., 2017).

MATERIALS AND METHODS

Experiments were carried out on 16 adult male New Zealand rabbits (weighing 2.5–3.0 kg). All experiments were conducted in accordance with NIH guidelines and were approved by the local ethical committee (Norra Djurförsöksetiska Nämnd) in Stockholm. The data for F-, E-, and non-modulated neurons obtained in experiments were compared with the control data and with data obtained after acute spinalization taken from the database of our earlier studies. The experimental subjects, as well as all methods used in the control study (except for spinalization, Zelenin et al., 2015) and in the study devoted to acute spinalization (Zelenin et al., 2016a) were similar to those used in the present study. The control data for F-, E-, and non-modulated neurons, as well as data devoted to effect of acute spinalization on F-, E-, and non-modulated neurons have been published earlier (Zelenin et al., 2015, 2016a, respectively).

Surgical Procedures

Each rabbit was subjected to two operations. The first surgery was performed under Hypnorm-midazolam anesthesia, using aseptic procedures. The level of anesthesia was controlled by applying pressure to a paw (to detect limb withdrawal), and by examining the size and reactivity of pupils. In 13 rabbits during first surgery a laminectomy at the T11–T12 level was done, and the dura in the rostral part of the T12 segment was opened. Then, a complete transection of the spinal cord was done under the dissecting microscope by means of a small scalpel. Later, the incision was closed in anatomic layers.

In 3 ($N = 5$), 7 ($N = 3$), and 30 ($N = 5$) days after spinalization, rabbits were taken to acute experiment. For induction of anesthesia, the animal was injected with propofol (average dose, 10 mg/kg, administrated intravenously). Afterward, it was continued on isoflurane (1.5–2.5%) delivered in O_2. The trachea was cannulated and laminectomy at L5 (exposing the spinal cord for recording of neurons) was performed. To insert the

recording microelectrode, small holes (∼1 mm^2) were made in the dura mater at L5. Bipolar EMG electrodes were inserted bilaterally into two representative extensors: gastrocnemius lateralis (ankle extensor) and vastus lateralis (knee extensor). The rabbit was decerebrated at the precollicular-postmammillary level (Musienko et al., 2008), and then, the anesthesia was discontinued. The rectal temperature and mean blood pressure of the decerebrate preparation during the experiment were kept, respectively, at 37–38°C and at greater than 90 mmHg. Collection of data began 1.5–2 h after decerebration.

In three rabbits during the first surgery chronic implantation of bipolar EMG electrodes was perform bilaterally into *m. gastrocnemius lateralis* (Gast, ankle extensor) and *m. vastus lateralis* (Vast, knee extensor) by using the method described earlier (Lyalka et al., 2011). After complete recovery from the surgery (in 3–4 days), postural responses of the rabbit to tilts were recorded (see below). Then a second surgical operation (that is spinalization at T12 level) was performed. At 3, 7, and 30 days after spinalization, the animal was subjected to tests on the tilting platform.

Animal Care

After surgery each animal was individually caged and had access to food (dry rabbit food, hay, and carrots) and water. The bottom of the cage was covered by absorbing soft tissue. The animals were monitored attentively. Every 12 h for 48 h after surgery, the rabbits received an analgesic (Temgesic, 0.01 mg/kg sc). In addition, Rimadyl (4 mg/kg sc) was given before surgery and 2 days after surgery to reduce inflammation. The first 2 days after spinalization the animals received 25 ml of Ringer solution (sc) twice a day. In spinal animals the bladder was expressed manually a few times daily, as well as the hindquarters were inspected and cleaned if necessary.

Experimental Designs

The design for acute experiments (**Figure 1A**) was similar to that described earlier (Musienko et al., 2010; Hsu et al., 2012; Zelenin et al., 2013, 2015). Shortly, the head and spine were fixed, the hindlimbs with configuration similar to that in intact standing rabbit (Beloozerova et al., 2003) were placed on the horizontal platform while the forelimbs were hung in a hammock. The whole platform or its left and right part separately, could be tilted to the left and to the right around the medial axis (**Figures 1B–D**) with the amplitude ±20°. The platform tilts caused flexion/extension movements at the hindlimb joints and almost vertical displacements of the limb distal point with magnitude ∼5 cm. A trapezoidal time trajectory of the platform tilt causing trapezoid trajectory of foot displacement was used. The duration of the rotation from the right to the left or from the left to the right was ∼1 s and each tilted position was maintained during ∼3–4 s. The angle of the platform tilt was monitored by a mechanical sensor, and after scaling, represented the vertical foot position (**Figures 1E**, **2A,B**). In decerebrate rabbits with intact spinal cord, sensory signals from hindlimbs caused by the platform tilts evoked PLRs: activation of extensors in the flexing limb leading to an increase in its contact force and inactivation of extensors in the extending limb resulting in a decrease in its contact force (Musienko et al., 2010).

Postural test of intact rabbits freely standing on a tilting platform have been described earlier (Deliagina et al., 2000; Beloozerova et al., 2003; Lyalka et al., 2009, 2011). The test did not require a specific training of the animals. In short, the rabbit was placed on two horizontal platforms (one platform supported the forelimbs and another one – the hindlimbs, **Figure 1H**). The platform supporting the hindlimbs could be tilted in the transverse plane of the animal (angle α, **Figures 1H,J**). The amplitude and trapezoidal time trajectory of tilting were the same as in experiments on decerebrate rabbits. In intact rabbits the tilt of the platform supporting the hindquarters evoked corrective hindlimb movements stabilizing the dorsal-side-up orientation of the caudal part of the trunk (**Figure 1J**; Beloozerova et al., 2003), while in spinal rabbits the corrective movements were absent and the trunk followed the platform movement (**Figure 1K**; Lyalka et al., 2011). During postural test EMGs from selected hindlimb muscles were recorded along with the tilt angle of the platform.

Recordings and Data Analysis

Spinal neurons were recorded extracellularly in L5 by varnish-insulated tungsten electrodes (75 μm shaft diameter, 4–7 MΩ impedance; FHC, Bowdoin, ME, United States). We had intention to record spinal interneurons from different areas of the gray matter, therefore the motor nuclei area (indicated by the dotted line in **Figures 3A,B**) was avoided. Location of recorded neurons was marked on the L5 cross section map by using their lateral and vertical coordinates (Shek et al., 1986; Hsu et al., 2012; Zelenin et al., 2013).

Neuronal activity, EMGs and signals from the mechanical sensors were amplified, digitized (with a sampling frequency of 30, 5, and 1 kHz, respectively) and recorded on a computer. EMGs were rectified and smoothed with the time constant, 100 ms. We used the data acquisition and analysis Power1401/Spike2 system (Cambridge Electronic Design, Cambridge, United Kingdom), which also allowed to perform spike-sorting based on the waveform-matching algorithm (vertical template width 10–20%; maximal vertical scaling to match 0%; minimal percentage of points matching the template 75%). Only neurons with stable spike shape were used for analysis.

Since in the majority of neurons the phase of modulation was determined by the tilt-related sensory input from the ipsilateral limb (Hsu et al., 2012; Zelenin et al., 2015), the activity of each neuron in the movement cycle of the ipsilateral limb was characterized. First, the raster of activity of the neuron in sequential cycles was obtained (**Figure 1F**). Second, each cycle was divided into 12 bins taking as the cycle onset the onset of the limb flexion. Bins 1–2 and 7–8 corresponded to flexion and extension of the limb, respectively, while bins 3–6 and 9–12, to maintenance of the flexed and extend position, respectively (**Figure 1G**). Then, the spike frequency in each bin was averaged over the identical bins in all cycles and the phase histogram of activity of the neuron was generated (**Figure 1G**). The mean frequency in bins 1–6 and in bins 7–12 (corresponding to flexion and extension of the ipsilateral limb, respectively) were calculated

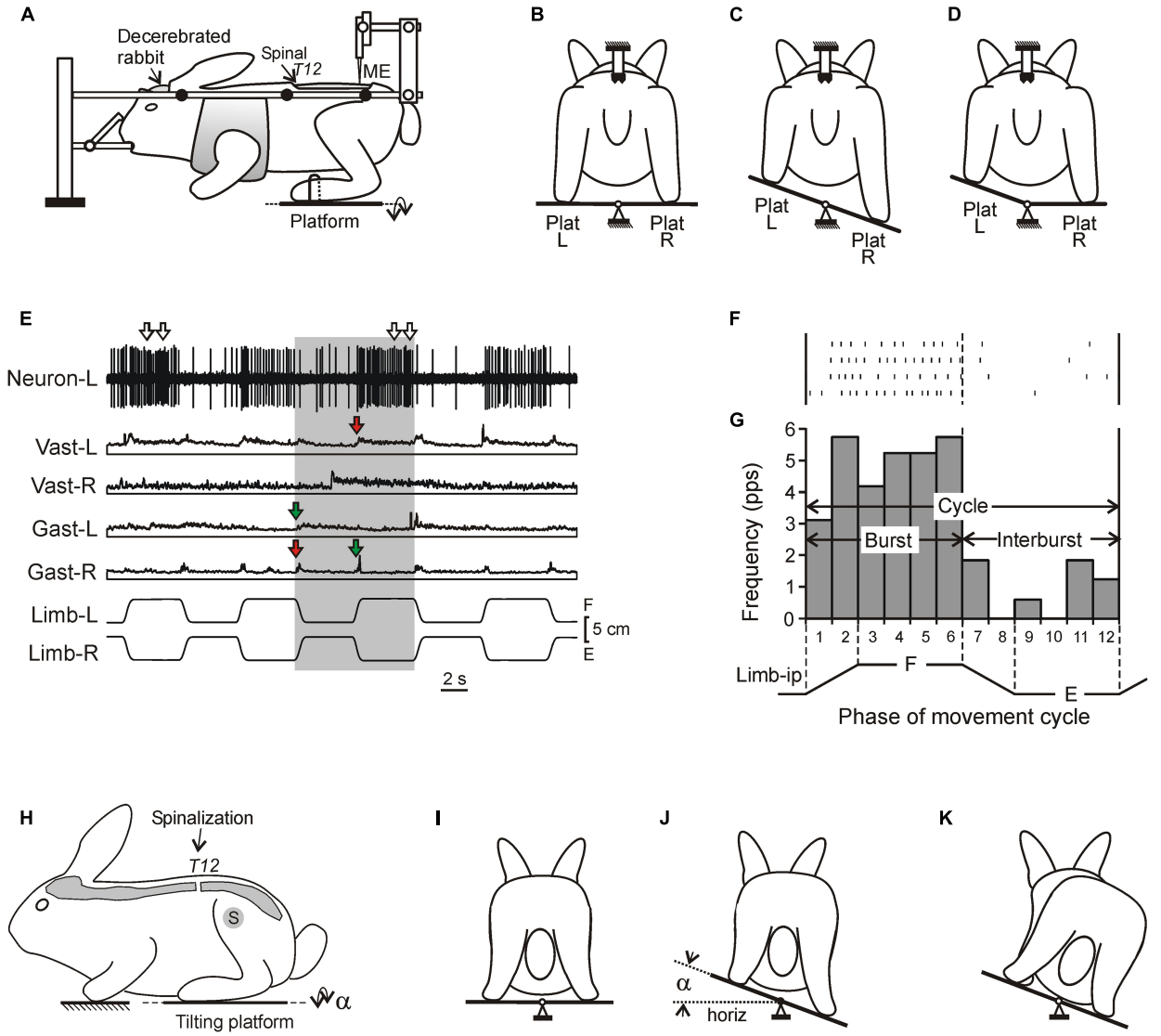

FIGURE 1 | Experimental designs. **(A–D)** A design for acute experiments. The chronic spinalized at T12 level rabbit was decerebrated and fixed in a rigid frame [points of fixation are indicated by black circles in **(A)**]. The whole platform **(C)** or its left or right part [Plat L and Plat R in **(D)**] could be periodically tilted, causing flexion–extension movements [F and E in **(E)**, respectively] of the two limbs (in anti-phase) or one of them, respectively. These movements were monitored by mechanical sensors (Limb-L and Limb-R, respectively). Activity of spinal neurons from L5 was recorded by means of the microelectrode [ME in **(A)**]. **(E)** Responses of a neuron from the left side of the spinal cord (Neuron-L) and electromyographic (EMG) responses in the left and right *m. gastrocnemius lateralis* (Gast-L and Gast-R, respectively) and m. *vastus lateralis* (Vast-L and Vast-R, respectively) to flexion/extension anti-phase movements of the hindlimbs in the rabbit on day 7 after spinalization. Red and green arrows indicate, respectively, residual correctly and incorrectly phased (in relation to the platform tilts), responses in Vast and Gast muscles. White arrows indicate oscillatory bursts in neuronal response. **(F,G)** A raster of responses of the neuron shown in **(E)** in four sequential movement cycles of the ipsilateral limb and a histogram of its spike activity in different phases (1–12) of the cycle of movement (F, flexion; E, extension) of the ipsilateral limb (Limb-ip). The neuron was activated with flexion of the ipsilateral limb (F-neuron). The halves of the cycle with higher (F, bins 1–6) and lower (E, bins 7–12) neuronal activity were designated as "burst" and "interburst" periods, respectively. **(H–K)** Testing of postural reactions to tilts. The animal was standing on two platforms, one under the forelimbs and one under the hindlimbs. Platform under the hindlimbs could be tilted in the transverse plane (α is the platform tilt angle). The sagittal plane of the animal was aligned with the axis of platform rotation. **(J)** Normal postural reaction to tilt in intact rabbit. **(K)** Absence of postural reaction to tilt in spinal rabbit.

and compared. The larger value was termed the burst frequency (F_{BURST}), while the smaller – the interburst frequency (F_{INTER}) (**Figure 1G**). A neuron with statistically significant difference between its burst frequency and interburst frequency (two-tailed Student's *t*-test, $P < 0.05$) was considered as modulated by tilts. In addition, the mean cycle frequency [$F_{CYCLE} = (F_{INTER} + F_{BURST})/2$] and the depth of modulation ($M = F_{BURST} - F_{INTER}$) were calculated.

To reveal changes in the activity of local neuronal populations in different areas of the gray matter at different time points after spinalization, "heatmaps" for the mean frequency and the depth of modulation in control as well as at each of four time points

after spinalization were generated (**Supplementary Figure S1**). To calculate a value of the parameter in a point with coordinates (x,y) on the heatmap, values of the parameter for the neurons recorded in close proximity to this point were used. Depending on the distance d from recording point to the point (x,y), these values were weighted [Gaussian weighting $w(d) = exp(-d^2/D^2)$ with the spatial constant D = 0.4 mm]. To reveal changes in the parameter, subtraction of the heatmap for control from the corresponding heatmap for a particular time point after spinalization was performed (**Figure 5**).

To characterize changes in motoneuronal activity (excitability) at different time points after spinalization, the mean value of EMG amplitude was determined during tilts and normalized to the amplitude observed in the same animal before spinalization.

As it was shown earlier (Lyalka et al., 2011) and confirmed in the present study, after spinalization, tilt of the platform evoked EMG bursts, which could be superimposed upon ordinary responses of the muscles. To clarify whether interneurons contribute to generation of these EMG oscillations, the oscillatory activity of F- and E-neurons, as well as non-modulated neurons in control and at different time points after spinalization, was compared. We found that the spiking activity of recorded neurons included not only ordinary responses to tilts, which may contain the dynamic component (higher frequency discharge during tilt) and/or the static component (firing with a constant or slowly decreasing frequency during maintenance of the tilt angle), but sometimes also oscillatory activity (irregular spike bursts with durations approximately 0.25–1 s) superimposed on the ordinary activity. Since it is difficult to discriminate between the burst of activity representing the dynamic component of the response to tilt and the oscillatory burst, to characterize quantitatively the oscillatory component of neuronal activity, we analyzed neuronal activity only during periods when the tilt angle was maintained constant (the plateau phases of tilts). For each plateau we converted the spike sequence into the instantaneous frequency, $f(t)$, and smoothened it with the sliding averaging (time constant 0.25 s). Then using the built-in software functions, we estimated the ordinary neuronal activity with the best linear fit, $f_{OR}(t)$, and calculated the oscillatory component, $f_{OS}(t)$, as $f_{OS}(t) = f(t) - f_{OR}(t)$. Then we calculated the square root average of $f_{OS}(t)$, which reflects the absolute amplitude of oscillatory firing, as well as squared ratio of the square root averages of $f_{OS}(t)$ to $f(t)$, which reflects the power of oscillations. The later shows how large were the oscillations compared to the instantaneous frequency, $f(t)$. Values of the absolute amplitude of oscillatory firing, as well as values of the power of oscillations obtained in a neuron were then averaged separately for tilts to the right and tilts to the left.

All quantitative data in this study were presented as mean ± SEM. To test the statistical significance of difference between means, two-tailed Student's t-test ($P < 0.05$) was used. To estimate the statistical significance of the effects of spinalization on the proportion of F-, E-, and non-modulated neurons, we used Pearson's χ^2 test ($P < 0.05$).

In a proportion of the examined neurons, peripheral receptive fields were studied. To reveal receptive fields, palpation of hindlimb muscle bellies, light brushing of the hairs, pinching the skin by fingers were used. In cases, when a cutaneous input was revealed, the responses from the underlying muscles were ignored.

Histological Procedures

To verify positions of recording sites on the cross-section of the spinal cord, at the end of each experiment we made reference electrolytic lesions in L5. The piece of the spinal cord containing these lesions as well as the piece with the site of spinalization were fixed with 10% formalin solution, frozen and cut to sections of 30 μm thickness. The sections were stained with Cresyl violet. Locations of recording sites were verified in relation to the reference lesions. Examination of sections from the areas of spinalization has shown that the transection of the spinal cord was complete in all rabbits.

RESULTS

Motor Responses to Tilts at Different Time Points After Spinalization

We found that well-coordinated EMG pattern of PLRs observed in decerebrate rabbits with intact spinal cord (activation of extensors in the flexing limb, as well as inactivation of extensors in the extending limb; Musienko et al., 2008, 2010), was absent after spinalization at each of studied time points (**Figures 1E**, **2A,B**). Responses of individual muscles to tilts were poorly coordinated. Each muscle could have four types of activity, as well as spontaneously switch between them: (i) correct response (activation during the ipsi-hindlimb flexion, indicated by red arrows in **Figures 1E**, **2A,B**); (ii) incorrect response (activation during the contra-limb flexion, indicated by green arrows in **Figures 1E**, **2A,B**); (iii) correct/incorrect response (response to both ipsi- and contra-hindlimb flexion); and (iv) no response to tilt. In addition, on day 30 after spinalization, tilt could evoke the repetitive EMG bursts in some muscles superimposed on the ordinary EMG responses (**Figure 2B**). The amplitude of EMG responses, which was very small on day 3 after spinalization (**Figure 2A**), gradually increased (**Figures 1E**, **2B**).

As seen in **Figure 2C**, before spinalization (Control) the overwhelming majority of the EMG responses to tilts were correct, while after acute spinalization (Acute) the responses were absent in 81% of cases and very weak residual responses were observed in 19% of cases (and only 8% of them were correct). However, already on day 3 after spinalization, EMG responses were observed in about 60% of cases and there were no substantial changes in the percent of EMG responses on day 7 and 30. Nevertheless, the percentage of correct responses was low (10% on day 3 and 27% on day 30). Acute spinalization produced a dramatic decrease (to 3.5% of the level observed in the same decerebrate rabbits before spinalization) in the amplitude of EMGs in extensor muscles (Gast and Vast).

To assess excitability of motoneurons (reflected in EMG amplitude), as well as to compare changes of EMG responses to tilts in decerebrate rabbits and in the rabbits with intact brain taking place over time after spinalization, three rabbits with

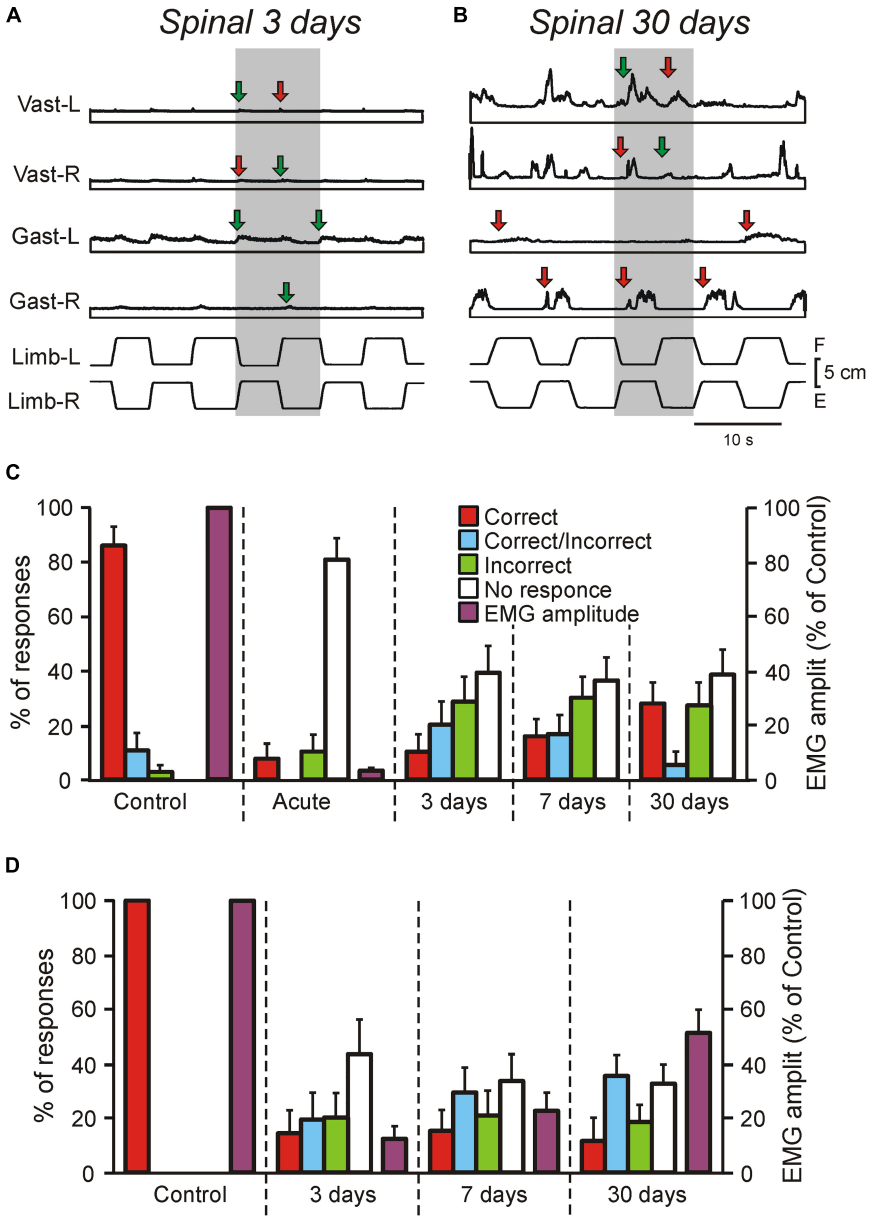

FIGURE 2 | Motor responses of rabbits and decerebrate preparations to tilts in control and at different time points after spinalization. **(A–C)** EMG responses to the whole platform tilts in the rabbit decerebrated on day 3 after spinalization **(A)** and in the rabbit decerebrated on day 30 after spinalization. The EMGs of the following muscles are presented: left (L) and right (R) vastus (Vast), and gastrocnemius (Gast). Red and green arrows in **(A,B)** indicate onsets of correct and incorrect responses, respectively. **(C)** Proportion of different types of EMG responses to the whole platform tilts in Vast and Gast recorded in decerebrate rabbits with intact spinal cord (Control, $N = 5$, $n = 50$), after acute spinalization (Acute, $N = 5$, $n = 50$), at 3 days ($N = 3$, $n = 18$), 7 days ($N = 3$, $n = 24$), and 30 days ($N = 6$, $n = 34$) after spinalization, as well as their amplitude in control and after acute spinalization ($N = 3$, $n = 18$). Correct, activation with ipsi-limb flexion; Incorrect, activation with contra-limb flexion; Correct/Incorrect, activation with both movements; No response, no EMG response to tilt. **(D)** Proportion of different types of EMG responses to the whole platform tilts in Vast and Gast recorded in the same rabbits before spinalization, at 3, 7, and 30 days after spinalization, as well as their amplitude ($N = 3$, $n = 37$, 39, and 40, respectively). Correct, activation with ipsilateral tilt; Incorrect, activation with contralateral tilt; Correct/Incorrect, activation with both ipsi- and contra-tilts; No response, no EMG response to tilt.

chronically implanted EMG electrodes were tested on the tilting platform before and on 3rd, 7th, and 30th day after spinalization (see section "Materials and Methods," **Figures 1H–K**). Their postural reactions were similar to those described in our previous studies (Beloozerova et al., 2003; Lyalka et al., 2009, 2011). Before spinalization, rabbits maintained balance when the platform under their hindlimbs was tilted (**Figure 1J**). The stereotypic postural responses included extension of the hindlimb (due to activation of its extensor muscles) on the side moving downward, and flexion of the hindlimb (due to reduction in

activity of its extensors) on the opposite side. These reciprocal flexion/extension movements of the hindlimbs displaced the caudal part of the trunk in the transverse plane, in the direction opposite to the platform tilt, thus reducing its deviation from dorsal-side-up position.

After spinalization, a well-coordinated EMG pattern observed in intact animals was transformed into weak and poorly coordinated activity of individual muscles. As in decerebrate spinal rabbits, each extensor muscle could spontaneously switch between four types of activity: (i) correct response (activation during the ipsilateral tilt), (ii) incorrect response (activation during the contralateral tilt), (iii) correct/incorrect response (response to both ipsilateral and contralateral tilts), and (iv) no response to tilt. In addition, as in decerebrate rabbits, tilts often evoked repetitive EMG bursts superimposed on the response to tilt.

We found that as in decerebrate rabbits, in chronic spinal rabbits EMG responses were observed in about 60% of cases on day 3 after spinalization and there were no substantial changes in the percent of responses on day 7 and 30 (**Figure 2D**). Like in decerebrate rabbits, at each time point after spinalization, the minority (about 15%) of responses were correct. The EMG amplitude (which constituted only about 13% of control on day 3 after spinalization) gradually increased over time and reached about 50% of control on day 30. Thus, the level of activity in motoneurons did not return to control level 1 month after spinalization. Due to disintegration of the EMG pattern and a decrease in the response magnitude, at each of three time points after spinalization, corrective hindlimb movements were absent and the body followed the platform movement (**Figure 1K**).

Spinal Neurons at Different Time Points After Spinalization

Proportion of Different Types of Neurons

In rabbits decerebrated 3 (N = 5), 7 (N = 3), and 30 (N = 5) days after spinalization at T12, 275, 235, and 265 neurons, respectively, were recorded during passive flexion/extension limb movements caused by periodical tilts of the whole platform. They were considered as putative interneurons, since the majority of these neurons were recorded outside the motor nuclei area (**Figures 3A,B**, dotted line).

To reveal the changes in spinal postural networks taking place during the 1st month after spinalization, the data obtained in the present study, were compared to data from our previous studies obtained on decerebrate rabbits with intact spinal cord (control data, Zelenin et al., 2015) and on decerebrate rabbits after acute spinalization (Zelenin et al., 2016a). In those studies a large samples of neurons (n = 499 and n = 370, respectively) were analyzed. As in control and after acute spinalization, F-, E-, and non-modulated neurons were found in all rabbits on 3rd, 7th, and 30th day after spinalization. Like in control and after acute spinalization, F-, E-, and non-modulated neurons were distributed over the gray matter and intermixed (**Figures 3A,B**).

We found that at each of the studied time points after spinalization the relative number of F-neurons was significantly smaller than that in control population (χ^2 test, $P < 0.0001$, $P < 0.05$, and $P < 0.0001$, respectively, after acute spinalization, at day 3, 7, and 30 after spinalization; **Figure 3C**). By contrast, the relative number of non-modulated neurons after acute spinalization, as well as at 3, 7, and 30 days after spinalization, was significantly larger than that in control (χ^2 test, $P < 0.0001$ at each of four time points; **Figure 3C**). The relative number of E-neurons after spinalization was rather similar to that in control population, though a small but significant decrease was observed at 3 and 7 days after spinalization (χ^2 test, $P < 0.001$ and $P < 0.05$, respectively; **Figure 3C**).

Activity of Neurons

F-Neurons

After acute spinalization the main parameters of activity [the mean frequency (**Figure 4A**), the depth of modulation (**Figure 4B**) and the burst frequency (**Figure 4C**)] exhibited a significant decrease, as compared to those in control, in F-neurons located in zone 3. However, already at 3 days after spinalization these parameters reached the control value and remained close to this level at 7 and 30 days (**Figures 4A–C**). Caused by acute spinalization changes in values of the main parameters of activity of F-neurons located in zones 1 and 2 were insignificant (**Figures 4A–D**). However, at 30 days after spinalization, F-neurons located in zone 1 exhibited almost 50% decrease in the value of the depth of modulation (9.1 $\pm$ 1.3 pps vs. 17.1 $\pm$ 1.5 pps in control). It was caused by a significant decrease in the value of their mean burst frequency (14.0 $\pm$ 1.6 pps vs. 20.8 $\pm$ 1.5 pps in control (**Figure 4C**). In addition, F-neurons located in zone 2 exhibited a significant decrease (as compared with control) in the mean value of the interburst frequency at 3 and 7 days after spinalization (**Figure 4D**). However, it returned to the control level at day 30.

To delineate more precisely the areas of the gray matter containing populations of neurons exhibiting a significant change in activity at different time points after spinalization as compared with control, heatmaps (see section "Materials and Methods") for the mean frequency (**Supplementary Figures S1A–F**) and the depth of modulation (**Supplementary Figures S1F–J**) were used.

Acute spinalization caused a significant reduction (by 2–6 pps) in the mean frequency of neuronal populations located in the ventral half of zone 2 and the medial part of zone 3 (delineated by solid and hatched lines for p = 0.01 and p = 0.05, respectively, on subtraction Control from Acute in **Figure 5A**). All differences in activity of local populations of neurons, observed in 3, 7, and 30 days after spinalization (except for the difference in a small area in the dorsal horn at day 3, **Figure 5B**), were insignificant as compared with control. Thus, in general, the control value of the mean frequency was restored at 3 days after spinalization and remained at control level during the following 27 days.

Acute spinalization led to a significant decrease in the depth of modulation of the F-neurons located in the ventro-medial part of the ventral horn (**Figure 5E**). At 3 and 7 days after spinalization, small differences in the depth of modulation of neuronal populations located in different areas of the gray matter, as compared with control were insignificant. Thus, in general, the control value of the depth of modulation was restored at 3 days after spinalization and remained at control level during the

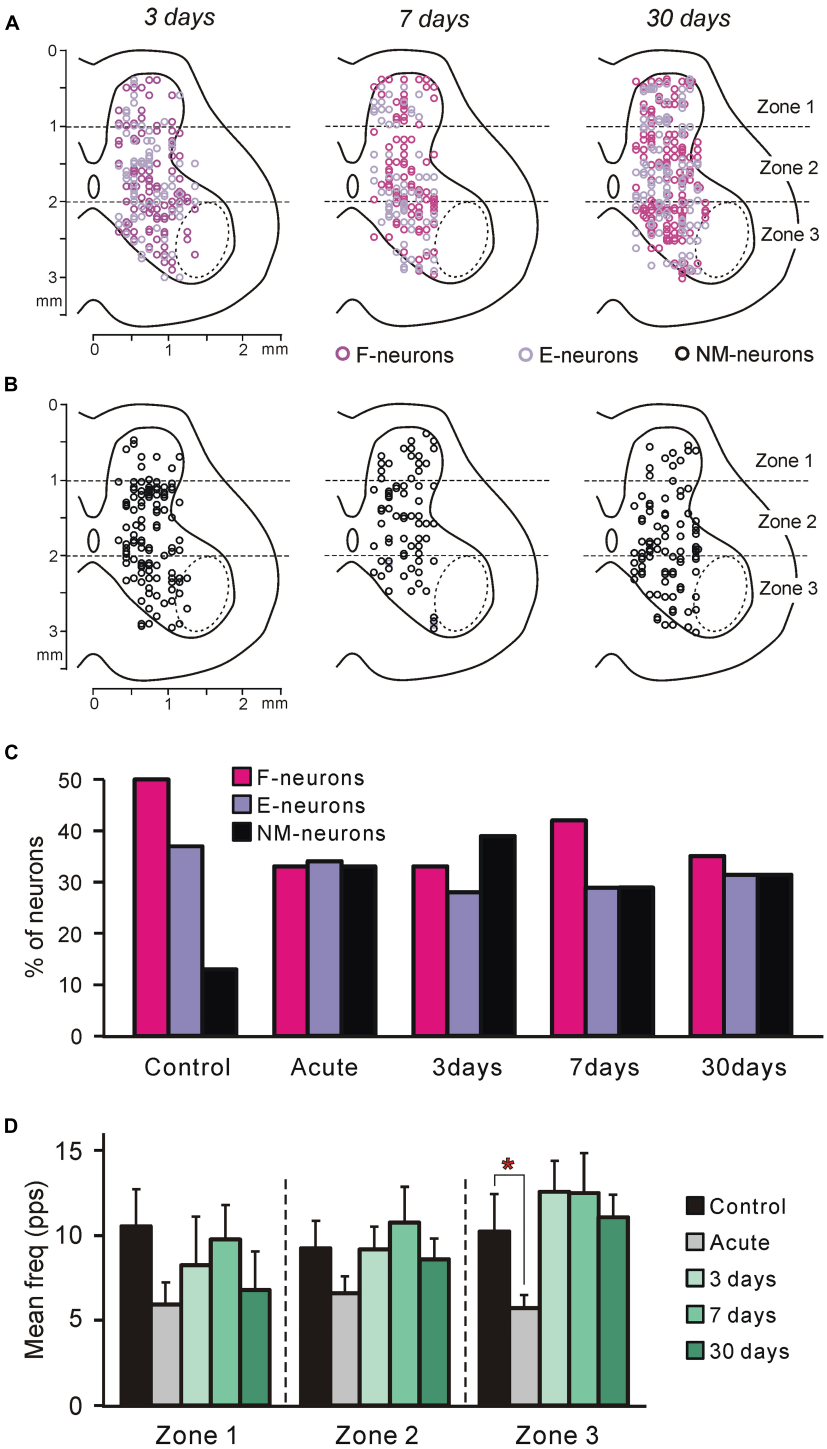

FIGURE 3 | Neurons recorded at different time points after spinalization. **(A,B)** Position of all F- and E-neurons **(A)**, as well as all non-modulated neurons **(B)** on the cross-section of the spinal cord recorded on 3rd, 7th, and 30th day after spinalization. **(C)** Relative number of F-, E-, and non-modulated neurons in control and at different time points after spinalization. The number of F-, E-, and non-modulated neurons, respectively, was n = 249, 186, and 64 in control, n = 122, 127, and 121 after acute spinalization, n = 91, 76, and 108 on day 3, n = 98, 68, and 69 on day 7, and n = 93, 86, and 86 on day 30 after spinalization. **(D)** Activity of non-modulated spinal neurons in control and at different time points after spinalization. The mean and SEM. values of the mean frequency of non-modulated neurons recorded in control, after acute spinalization (Acute), as well as at 3, 7, and 30 days after spinalization are shown for sub-populations of non-modulated neurons located in different zones (1–3) of the gray matter. The numbers of non-modulated neurons recorded in zones 1–3 in control and after acute spinalization were n = 14, 27, 23 and n = 18, 44, 59, respectively. The numbers of non-modulated neurons recorded in zones 1–3 in spinal rabbits on 3rd, 7th, and 30th day after spinalization were n = 9, 60, 39, n = 17, 32, 20, and n = 11, 38, 37, respectively. Indication of significance level: $^*p < 0.05$.

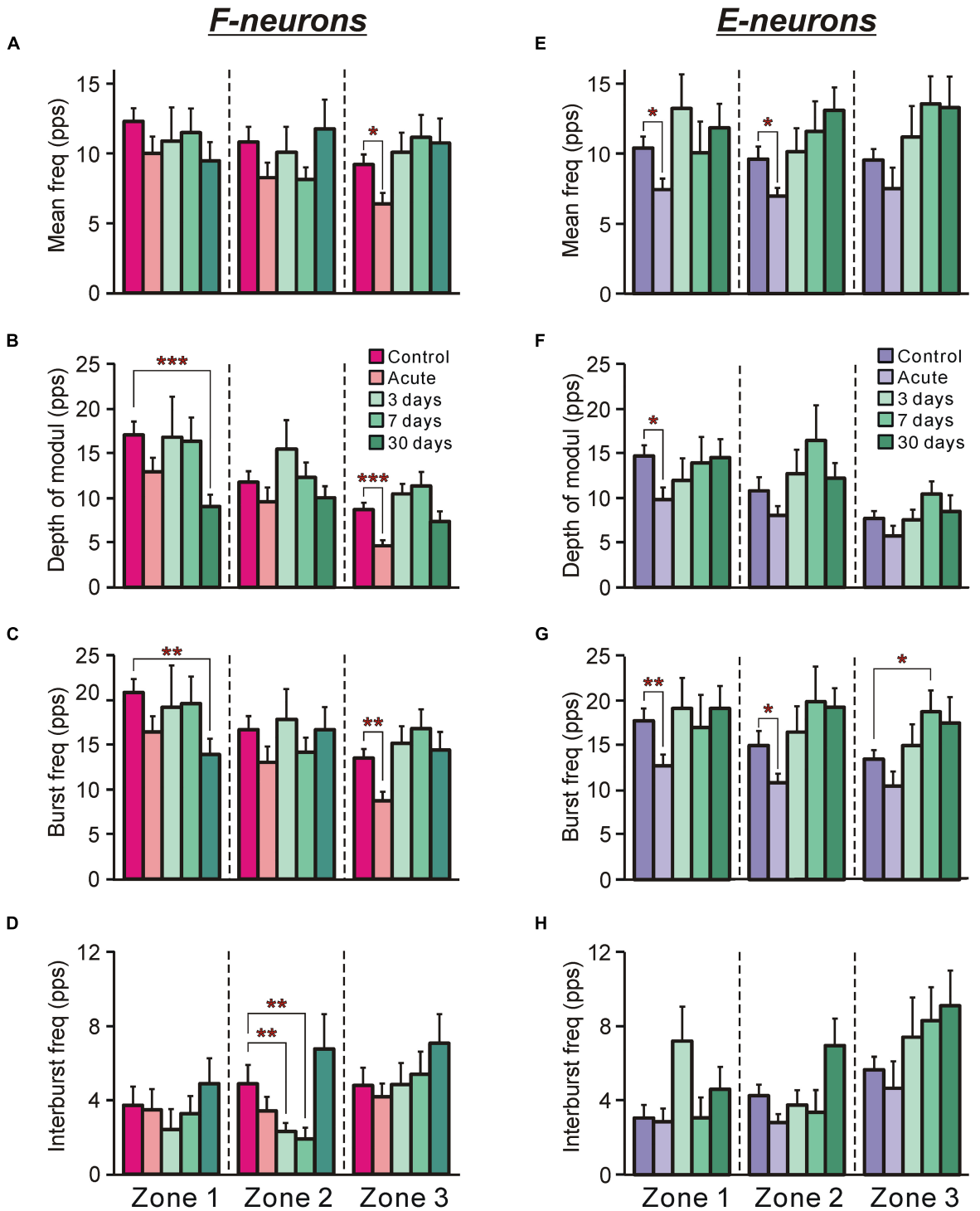

FIGURE 4 | The activity of F-neurons and E-neurons during tilts of the whole platform in control and at different time points after spinalization. The mean and SEM. values of different characteristics of the activity [the mean frequency **(A,E)**, the depth of modulation **(B,F)**, the burst frequency **(C,G)**, and the interburst frequency **(D,H)**] of F-neurons **(A–D)** and E-neurons **(E–H)** in control (Control), after acute spinalization (Acute), and on 3rd, 7th, and 30th days after spinalization (3, 7, and 30 days, respectively). These values are shown for sub-populations of F- and E-neurons located in different zones (1–3) of the gray matter (**Figures 3A,B**). The numbers of F-neurons recorded in zones 1, 2, 3 in control were $n = 62, 94, 93$, after acute spinalization – $n = 30, 49, 43$, on 3 day – $n = 15, 36, 40$, on 7th day – $n = 24, 38, 36$, on 30th day – $n = 21, 39, 33$. The numbers of E-neurons recorded in zones 1, 2, 3 in control were $n = 49, 63, 74$, after acute spinalization – $n = 30, 78, 19$, on 3 day – $n = 12, 37, 27$, on 7th day – $n = 17, 18, 33$, on 30th day – $n = 20, 35, 28$. Indication of significance level: $^{*}p < 0.05$, $^{**}p < 0.01$, and $^{***}p < 0.001$.

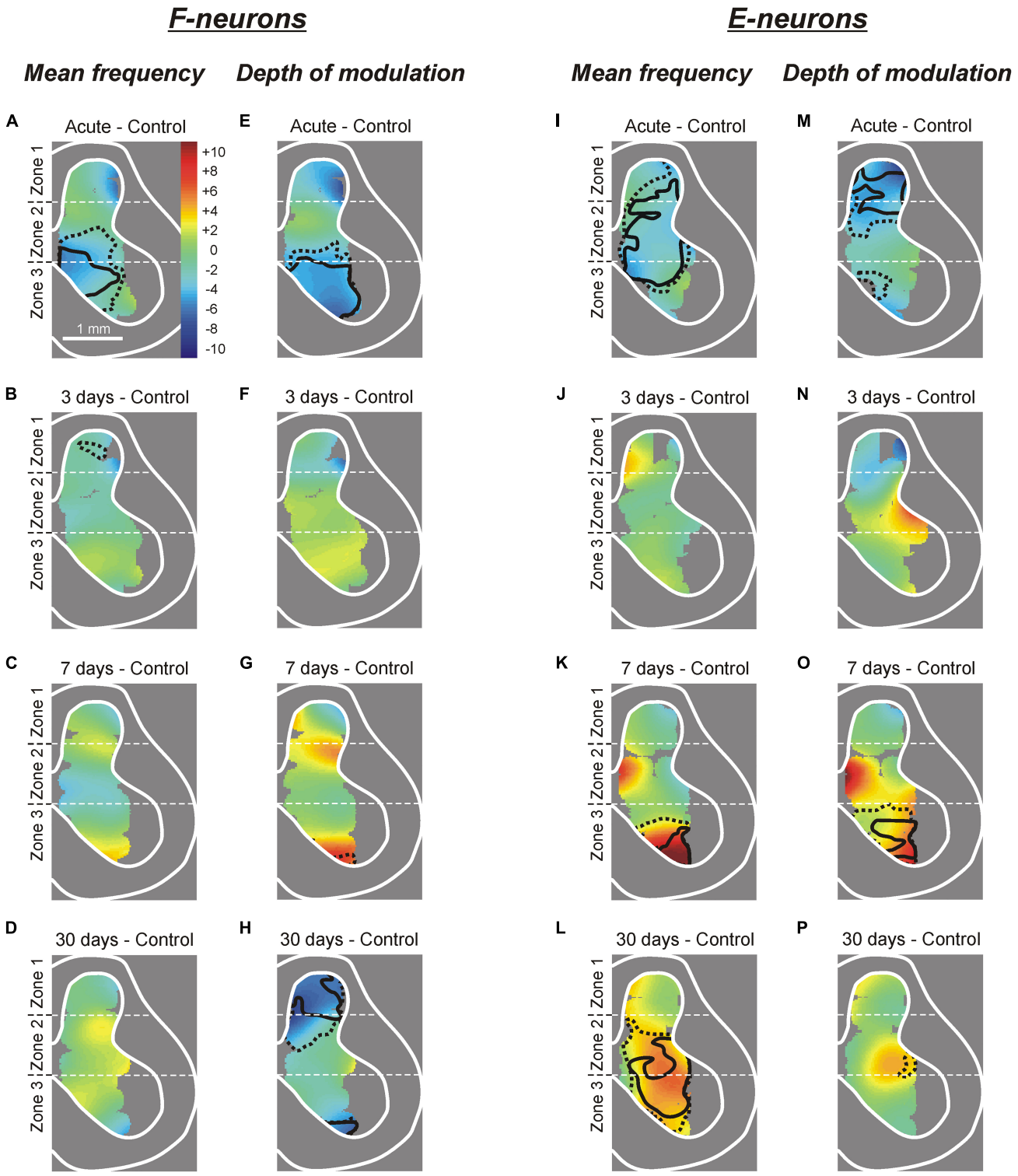

FIGURE 5 | Changes in the mean frequency and in the depth of modulation of local populations of F- and E-neurons at different time points after spinalization. The difference between the averaged distribution of the mean frequency **(A–D,I–L)** and of the depth of modulation **(E–H,M–P)** of F-neurons **(A–H)** and E-neurons **(I–P)** on the cross-section of the spinal cord at a particular time point after spinalization and the corresponding distribution in control (subtraction of Control from corresponding spinal). Averaged distributions of the mean frequency and depth of modulation for F- and E-neurons in control, after acute spinalization, as well as on 3rd, 7th, and 30th day after spinalization are presented as heatmaps in **Supplementary Figure S1**.

following 4 days. However, at 30 days after spinalization we found a significant reduction in the depth of modulation of neuronal populations located in the dorsal horn and in the most ventral part of the zone 3 (**Figure 5H**).

E-Neurons

After acute spinalization the decrease in most parameters of activity was statistically significant in populations of E-neurons located in zones 1 and 2 (**Figures 4E–H**). We found that at 3 days after spinalization the values of all parameters of activity in zone 1 and zone 2 populations of E-neurons returned to the control level, and did not differ from control level at 7 and 30 days after spinalization (**Figures 4E–H**). In contrast to F-neurons, after acute spinalization the main parameters of activity of E-neurons located in zone 3 did not differ from those in control. They also were similar to control at 3, 7, and 30 days after spinalization (except for the mean burst frequency at day 7 that was significantly higher than in control, **Figure 4G**).

Acute spinalization evoked a significant reduction in the mean frequency of E-neurons located in the dorsal part of the ventral horn, in the intermediate area and in the ventro-lateral part of the dorsal horn (**Figure 5I**), while the depth of modulation was significantly reduced in the population located in the dorsal horn (**Figure 5M**). Like in F-neurons, at 3 days after spinalization both parameters of activity in populations of E-neurons located in different parts of the gray matter (including those which exhibited a significant reduction of these parameters after acute spinalization) did not differ significantly from control (**Figures 5J,N**). While at 7 days after spinalization both the mean frequency and the depth of modulation in populations of F-neurons located in different parts of the gray matter did not differ significantly from control (**Figures 5C,G**, respectively), in populations of E-neurons some significant dynamic changes in activity were observed. Thus, at 7 days after spinalization, both the mean frequency and the depth of modulation in the population of E-neurons located in ventral half of the ventral horn significantly exceeded the control level (**Figures 5K,O**, respectively). At 30 days after spinalization, the area of the gray matter containing populations of E-neurons exhibiting the mean frequency significantly higher than that in control expanded and occupied almost whole zone 3 and ventral three quarters of zone 2 (**Figure 5L**). By contrast, the depth of modulation significantly increased (as compared with control) in populations of E-neurons located in the ventral part of zone 3 at 7 days after spinalization (**Figure 5O**), returned to control level at 30 days after spinalization (**Figure 5P**).

Non-modulated neurons

After acute spinalization, a significant decrease in the mean frequency was observed in population of non-modulated neurons located in zone 3 (**Figure 3D**). At 3 days after spinalization it returned to control level and was similar to control at 7 and 30 days after spinalization (**Figure 3D**). After acute spinalization as well as at 3, 7, and 30 days after spinalization, the mean frequency of non-modulated neurons located in zones 1 and 2 did not differ significantly from that in control.

Thus, we found that activity of F-neurons located in the ventral horn, and E-neurons located in the dorsal horn, which was significantly decreased after acute spinalization, returned to control level at day 3 after spinalization. By contrast, F-neurons located in the dorsal horn and E-neurons located in the ventral horn, which activity was not affected by acute spinalization, exhibited significant changes in activity at later time points after spinalization (e.g., in F-neurons, a significant decrease in the mean burst frequency and depth of modulation was observed at day 30 after spinalization, while in E-neurons, a significant increase in the mean cycle frequency and depth of modulation was found at day 7 after spinalization).

Processing of Tilt-Related Sensory Information

Modulation of neuronal activity caused by tilts is determined by somatosensory inputs from limbs. To characterize the changes in the processing of tilt-related sensory information at different time points after spinalization, in animals at 3rd, 7th, and 30th day after spinalization, respectively, in 133, 147, and 157 neurons, in addition to responses to the whole platform tilts, we recorded responses to tilts of the right and left part of the platform (**Figure 1D**). The results were compared to control and to those obtained after acute spinalization.

Sources of Modulation of F- and E-Neurons

Tilts of either the right or left part of the platform, allowed to reveal the sources of tilt-related sensory input to individual neurons. As in control (Zelenin et al., 2015) and after acute spinalization (Zelenin et al., 2016a), in animals at 3rd, 7th, and 30th day after spinalization, four types of neurons were found. Type 1 and Type 2 neurons received tilt-related sensory input from ipsilateral limb only and from contralateral limb only, respectively (**Supplementary Figures S2A–F**, respectively). By contrast, Type 3 and Type 4 neurons received sensory inputs from both hindlimbs. However, Type 3 neurons were activated by ipsilateral limb flexion and contralateral limb extension, or ipsilateral limb extension and contralateral limb flexion (**Supplementary Figures S2G–I**), while Type 4, by flexion of each of hindlimbs (**Supplementary Figures S2J–L**), or by extension of each of hindlimbs.

We found that at each time point after spinalization about twofold increase in relative number of both Type 1 F-neurons (**Figure 6A**) and Type 1 E-neurons (**Figure 6B**) was observed. They constituted 73% of F-neurons after acute spinalization, and 75, 64, and 73% at 3, 7, and 30 days after spinalization, respectively, vs. 43% in control, and 78% of E-neurons after acute spinalization, and 75, 77, and 65% at 3, 7, and 30 days after spinalization, respectively, vs. 32% in control. Correspondingly, the proportion of neurons with input from the contralateral hindlimb (Types 2–4), decreased (after acute spinalization, at 3, 7, and 30 days after spinalization, respectively, 28, 25, 36, and 27% of F-neurons vs. 57% in control, and 22, 26, 23, and 35% of E-neurons vs. 68% in control). These changes in proportions of Type 1 neurons and Types 2–4 neurons were significant both for F- and E-groups (χ^2 test, $P < 0.0001$, except for F-neurons

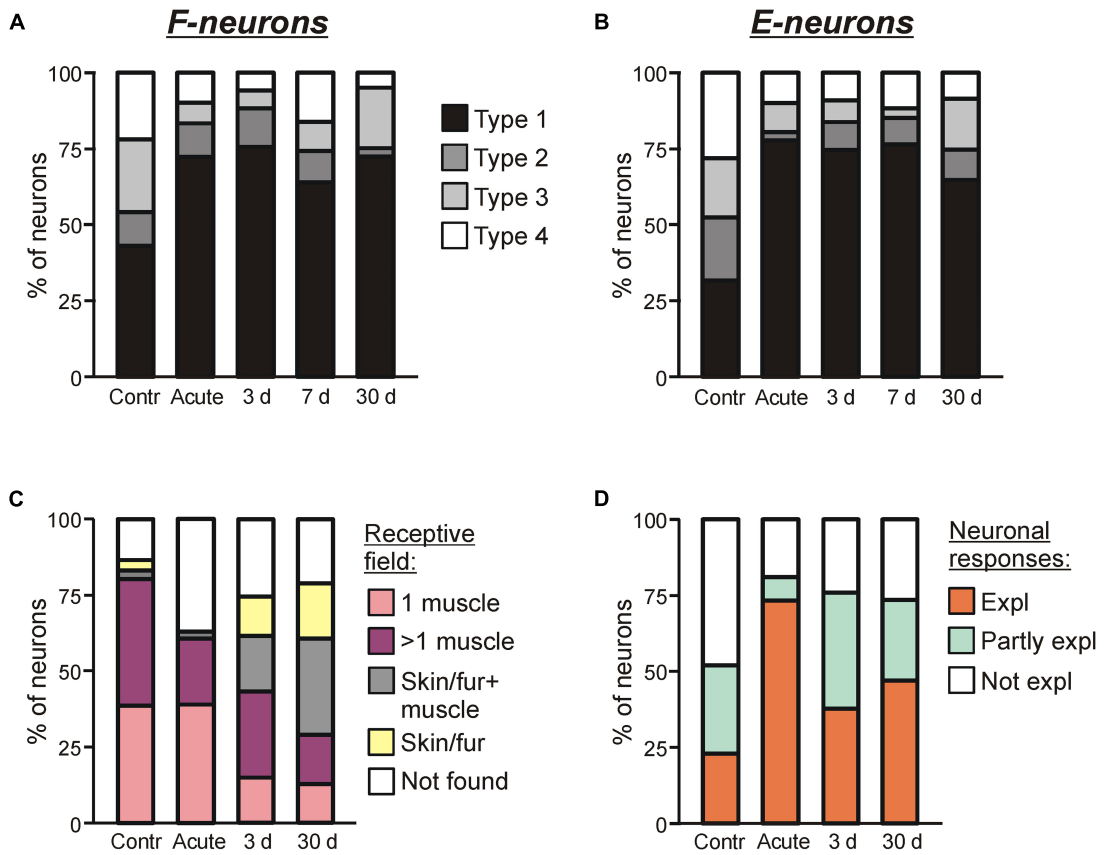

FIGURE 6 | Sources of modulation and receptive fields of F- and E-neurons in control and at different time points after spinalization. Percentage of F-neurons **(A)** and E-neurons **(B)** receiving different combinations of tilt-related somatosensory inputs from the limbs (Types 1–4) in control (*Contr*), after acute spinalization (*Acute*) and on 3rd day (3 days), 7th day (7 days), 30th day (30 days) after spinalization. See text for explanation. **(C)** Proportion of neurons receiving sensory inputs from different sources, i.e., from receptors of only one muscle (*1 muscle*), from receptors of more than one muscle (*>1 muscle*), from cutaneous and muscle receptors (*Skin/fur + muscle*), from cutaneous receptors only (*Skin/fur*), and with no receptive field found (*Not found*) in control, after acute spinalization, on 3rd and 30th day after spinalization. See text for explanation. **(D)** Proportion of neurons in which response to tilts could be completely explained (*Expl*), partly explained (*Partly expl*) and could not be explained (*Not expl*) by input from their receptive field, in control, after acute spinalization, on 3rd and 30th day after spinalization.

on 7th day after spinalization, which had lower significance level, $P = 0.001$).

Efficacy of Sensory Inputs to F- and E-Neurons From Different Limbs

The efficacy of sensory input from a particular limb to the neuron is reflected in its activity modulation depth caused by the tilts of the platform under the limb. In control, the depth of modulation averaged over F-neurons located in each of three zones was much larger during tilts of the ipsilateral platform (**Figure 7A**) than during tilts of the contralateral platform (**Figure 7B**). In both cases, in F-neurons located in each of three zones of the gray matter (except for zone 1 in case of contralateral platform tilt) a similar tendency in the changes of this parameter was observed. The value of the depth of modulation, which was substantially decreased after acute spinalization, returned to control level on 3rd day and was maintained on this level on 7th day after spinalization. However, on 30th day after spinalization it was substantially reduced as compared with control and had value similar to that observed after acute spinalization (**Figures 7A,B**).

In contrast to F-neurons, in control, the depth of modulation averaged over E-neurons located in each of three zones was similar during tilts of the ipsilateral platform and during tilts of the contralateral platform (compare corresponding values in **Figures 7C,D**). The acute spinalization caused a dramatic reduction (almost to zero) of the depth of modulation caused by tilts of the contralateral limb and it remained almost at the same level on 3rd, 7th, and 30th day after spinalization (**Figure 7D**). By contrast, the depth of modulation of averaged over E-neurons located in each of three zones caused by tilts of the ipsilateral limb was not affected by acute spinalization and did not differ significantly from control level on 3rd, 7th, and 30th day after spinalization (**Figure 7C**).

Relation Between Responses to Tilts and Receptive Fields of Neurons

On 3rd and 30th day after spinalization, somatosensory receptive fields were found, respectively, in 98 out of 131 and 108 out of 137 tested modulated neurons. The proportion of such neurons at each of these two time points after spinalization was slightly

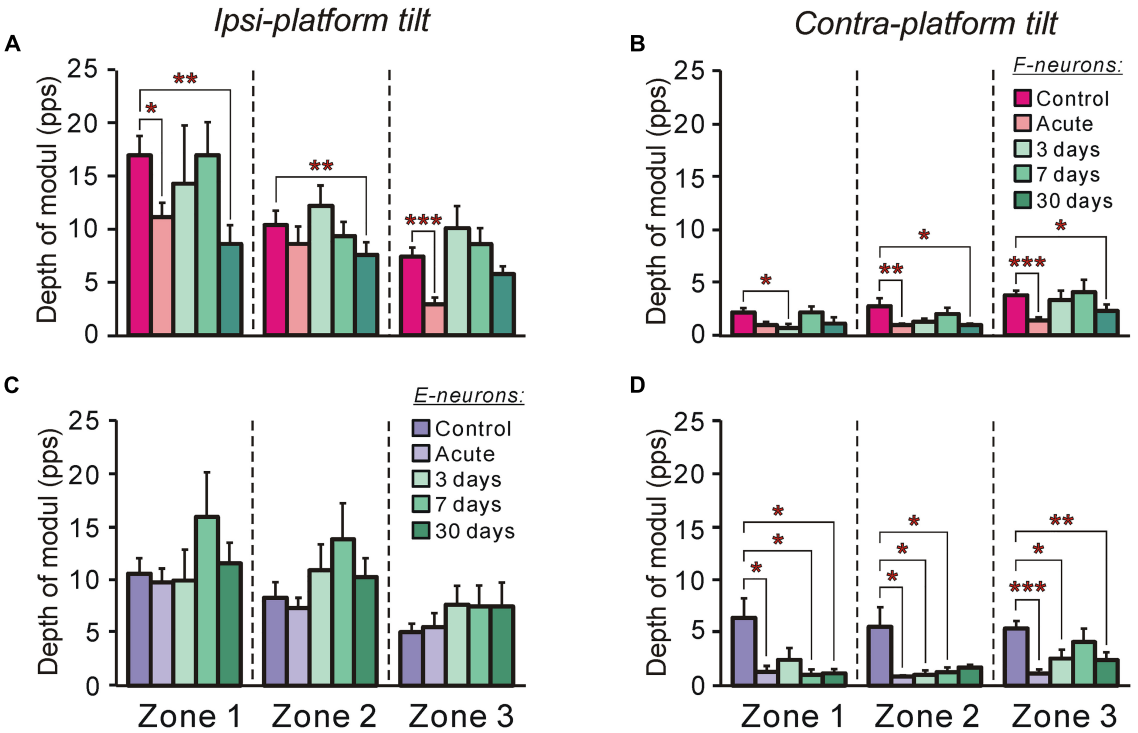

FIGURE 7 | The efficacy of tilt-related sensory inputs from the ipsilateral and contralateral limbs to F- and to E-neurons in control and at different time points after spinalization. **(A,B)** The mean and SEM. values of the depth of modulation of F-neurons recorded in control, after acute spinalization and on 3rd day, 7th day, and 30th day after spinalization during tilts of the ipsilateral **(A)** and contralateral **(B)** limbs. The numbers of F-neurons from zones 1, 2, 3 subjected to these tests were: in control animals – n = 42, 62, 71, respectively; in animals after acute spinalization – n = 28, 41, 33, respectively; in animals on 3rd day after spinalization – n = 12, 24, 31, respectively; in animals on 7th day after spinalization – n = 23, 32, 31, respectively; in animals on 30th day after spinalization – n = 18, 35, 31, respectively. **(C,D)** The mean and SEM. values of the depth of modulation of E-neurons recorded in control, after acute spinalization and on 3rd day, 7th day, and 30th day after spinalization during tilts of the ipsilateral **(C)** and contralateral **(D)** limbs. The numbers of E-neurons from zones 1, 2, 3 subjected to these tests were: in control animals – n = 32, 45, 55, respectively; in animals after acute spinalization – n = 25, 67, 17, respectively; in animals on 3rd day after spinalization – n = 8, 34, 24, respectively; in animals on 7th day after spinalization – n = 16, 16, 29, respectively; in animals on 30th day after spinalization – n = 20, 30, 23, respectively. Designations are the same as in **Figure 4**. Indication of significance level: *$p < 0.05$, **$p < 0.01$, and ***$p < 0.001$.

smaller than that in control, but slightly higher than that after acute spinalization (75% on 3rd day and 79% on 30th day vs. 86% in control and 63% after acute spinalization; χ^2 test, $p = 0.02$, and $p = 0.002$) (**Figure 6C**).

The relative numbers of neurons with different types of receptive fields observed on 3rd and 30th days after spinalization differed from those observed in control and after acute spinalization (**Figure 6C**). Thus, in control and after acute spinalization, the majority of neurons (81 and 61%, respectively) had "deep" receptive fields (i.e., the neurons responded to palpation of muscles only), while neurons responding to stimulation of fur or/and skin constituted the minority (6 and 2%, respectively). In contrast, on 3rd and 30th day after spinalization, neurons with "deep" receptor fields represented the minority (57 out of 131, 43%, and 29 out of 137, 40%, respectively), while substantial number of neurons responded to stimulation of fur or/and skin (41 out of 131, 31% and 68 out of 137, 50%). On 3rd and 30th day after spinalization, more than a twofold decrease in the percentage of neurons with deep receptive fields from one muscle as compared with those observed in control and after acute spinalization was revealed (respectively, 15 and 13% vs. 39% in control and 39% after acute spinalization; χ^2 test, $p < 0.0001$). Also, on 3rd and 30th day after spinalization, a significant decrease in the proportion of neurons in which receptive fields were not found as compared with that after acute spinalization was observed (respectively, 25 and 21% vs. 37%; χ^2 test, $p = 0.02$, and $p = 0.002$).

For 42 and 34 modulated neurons with deep receptive fields recorded on 3rd and 30th day after spinalization, sensory signals from the receptive field of a neuron presumably caused by tilts were compared with responses of this neuron to tilts. It has been suggested that the tilt of the platform activates load and stretch receptors in flexors and extensors of extending and flexing limb, respectively. We found that on 3rd and 30th day after spinalization, in 38 and 47% of neurons, respectively, the response to tilts could be explained by sensory inputs from the receptive field (*Expl* in **Figure 6D**, 3 and 30 days, respectively), while in 24 and 26% of neurons, respectively, it could not be explained (*Not expl* in **Figure 6D**, 3 and 30 days, respectively). Finally, 38% of neurons recorded on 3rd day after spinalization and 27% of neurons recorded on 30th day after spinalization had sensory inputs that could explain responses to tilts as

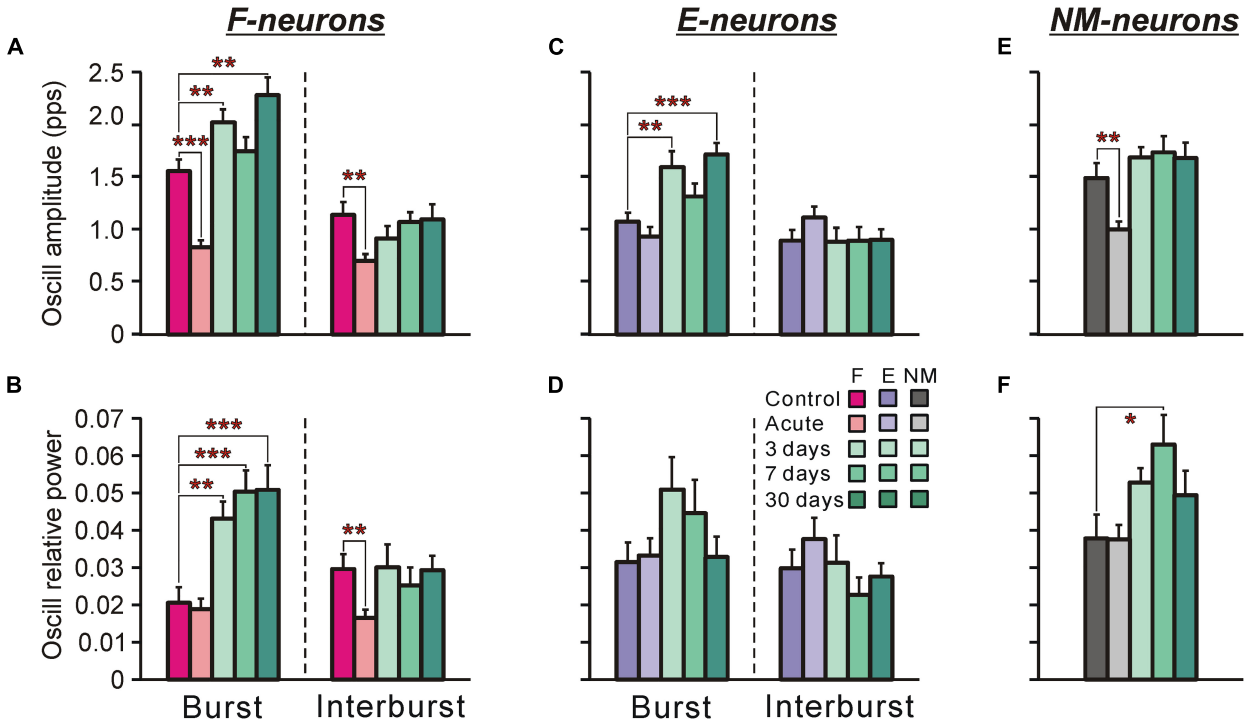

FIGURE 8 | Oscillatory component in activity of F-, E-, and non-modulated neurons during tilts of the whole platform in control and at different time points after spinalization. The mean and SE values of the amplitude of the oscillatory component of activity **(A,C,E)** and the relative power of the oscillatory componet **(B,D,F)** of F-neurons **(A,B)**, E-neurons **(C,D)**, and non-modulated (NM) neurons **(E,F)** in control (*Control*), after acute spinalization (*Acute*), and on 3rd, 7th, and 30th days after spinalization (3, 7, and 30 days, respectively). Designations and numbers of neurons are the same as in **Figure 4**. Indication of significance level: $*p < 0.05$, $**p < 0.01$, and $***p < 0.001$.

well as mismatching inputs, e.g., excitatory inputs from the antagonistic muscles of one limb (*Partly expl* in **Figure 6D**, 3 and 30 days, respectively). As seen in **Figure 6D**, on 3rd and 30th day after spinalization, almost twofold decrease in the proportion of neurons in which input from the receptive field could explain the response to tilts, and almost fivefold increase in the proportion of neurons in which response could be partly explained by input from the receptive field as compared to that after acute spinalization were observed (could explain responses: 38% on 3rd day and 27% on 30th day vs. 73% after acute spinalization; could partly explain responses: 38% on 3rd days and 27% on 30th day vs. 8% after acute spinalization). As compared to control, almost twofold decrease in the proportion of neurons, in which response could not be explained by input from the receptive field, observed after acute spinalization was maintained on 3rd and 30th day after spinalization (18% after acute spinalization, 24% on 3rd day, and 26% of the 30th day vs. 48% in control).

Thus, we found severe distortions (as compared with control) in processing of tilt-related sensory signals at each of four time points after spinalization. They were manifested in a change in the source of modulation of F-and E-neurons, in some changes in the efficacy of tilt-related sensory inputs from limbs to these neurons as well as in changes of their receptive fields.

Oscillatory Activity of Neurons

As it was mentioned above, at later time points after spinalization, tilting often evoked EMG bursts in the hindlimb muscles, which could be superimposed on the ordinary EMG responses (**Figure 2B**). Bursting (that we term here "oscillatory activity") caused by tilts was also often observed in activity of recorded neurons (indicated with white arrows in **Figure 1E**). To characterize this activity quantitatively, we used two parameters: the absolute amplitude of oscillatory activity, and the relative power of the oscillatory signal (see section "Materials and Methods" for details).

Figures 8A–F show the means ± SEM values of the absolute amplitude of oscillatory activity (**Figures 8A,C,E**) and the relative power of the oscillatory signal (**Figures 8B,D,F**) for F-neurons (**Figures 8A,B**) and E-neurons (**Figures 8C,D**) calculated separately for the burst and interburst phases of the tilt cycle, as well as for non-modulated neurons (**Figures 8E,F**). As one can see, some oscillatory activity was exhibited by neurons even in control. Acute spinalization either did not change this activity or resulted in its decrease, which could be seen in a significant reduction of the amplitude of oscillations in F-neurons and in non-modulated neurons (**Figures 8A,E**, respectively). Since the ordinary responses to tilts were also weakened after acute spinalization, the relative power of oscillatory activity remained the same as in control except for the interbursts in

F-neurons (**Figure 8B**). At 3 days after spinalization an increase in the oscillatory activity of all three groups of neurons was observed. The amplitude of oscillations became significantly higher than in control during bursts of F- and E-neurons, while during interburst phases it returned to the control level (**Figures 8A,C**). In non-modulated neurons, the amplitude of oscillations also returned to the control level on day 3 after spinalization (**Figure 8E**). In general, on day 7 as well as on day 30, the amplitude of oscillations in each of three groups of neurons was similar to that observed on day 3.

We found also that in F-neurons, more than twofold increase in the relative power of oscillations during bursts was observed (**Figure 8B**) from day 3 after spinalization, suggesting that the oscillatory activity constituted substantially larger part of the entire signal, as compared with control. In E-neurons and non-modulated neurons, the average increase in the relative power was not statistically significant, except for the non-modulated neurons at 7 days after spinalization (**Figures 8D,F**).

To conclude, we found a dramatic increase in oscillatory activity of F-neurons in spinal animals, which could contribute to generation of EMG bursting.

DISCUSSION

In the present study, we characterized the activity of spinal interneurons of postural networks, and the processing of posture-related sensory signals at three time points after spinalization in rabbits. Comparison of these data with the data obtained in our earlier studies on rabbits with intact spinal cord (control; Zelenin et al., 2015) and on rabbits after acute spinalization (Zelenin et al., 2013, 2016a) allowed us to characterize the changes in the spinal postural networks taking place over time after spinalization and underlying development of spasticity.

As in control and after acute spinalization, on day 3, day 7, and day 30 after spinalization we found three groups of neurons (F-neurons, E-neurons, and non-modulated neurons).

It was demonstrated with the method of reversible spinalization (Zelenin et al., 2013), that disappearance of supraspinal drive did not change the phase of modulation in most F- and E-neurons (though caused a significant decrease in their activity), while some of modulated neurons became non-modulated or completely inactivated. It was suggested that F- and E-neurons recorded after acute spinalization are elements of spinal postural networks (Musienko et al., 2010) contributing to generation of PLRs in animals with intact spinal cord (Zelenin et al., 2016a). Since the relative number of F-, E-, and non-modulated neurons revealed on day 3, 7, and 30 after spinalization was similar to that observed after acute spinalization, one can assume that the majority of F- and E-neurons recorded at these time points after spinalization are elements of the same network that generates PLRs in animals with intact spinal cord.

After spinalization, the relative number of F-neurons significantly decreased, while the number of non-modulated neurons increased as compared with control. The increase in the number of non-modulated neurons could be explained by the fact that a part of neurons modulated before spinalization, after spinalization became non-modulated, while the decrease in the number of F-neurons – by a predominance of F-neurons in the population of modulated neurons completely inactivated by spinalization (Zelenin et al., 2013).

We found that as in subjects with intact spinal cord, at each time point after spinalization F- and E-neurons were evenly distributed across the gray matter and intermixed. This could be explain by the fact that interneurons with inputs from group I and group II afferents from the limbs muscles (which transmit tilt-related sensory signals causing modulation of F- and E- neurons) were found in each of three zones of the gray matter (Bannatyne et al., 2003, 2006, 2009; Jankowska and Edgley, 2010). However, elimination of supraspinal drive caused by acute spinalization affected significantly only specific populations of F- and E-neurons (F-neurons within zone 3 and E-neurons within zones 1 and 2) (Zelenin et al., 2016a). Interneurons with inputs from group I and II afferents and from rubrospinal, reticulospinal and vestibulospinal systems were revealed in laminae VII (located in zones 2 and 3) and laminae VIII (located in Zone 3) (Bannatyne et al., 2003, 2009; Jankowska and Edgley, 2010). Thus, probably the main reason for the decrease in activity of E-neurons in zone 2 and F-neurons in zone 3 is the loss of supraspinal inputs. However, the reason for the significant decrease in activity of E-neurons located in zone 1 is not clear, since revealed in this zone interneurons with input from group II muscle afferents receive corticospinal drive (Bannatyne et al., 2006; Jankowska and Edgley, 2010) which is inactive in decerebrate subject. As the majority of almost completely inactivated by reversible spinalization neurons were F-neurons located in zone 3 (Zelenin et al., 2013), it was suggested that inactivation of premotor F-neurons located in zone 3 substantially contribute to disappearance of PLRs at acute stage of spinal cord injury (Zelenin et al., 2013, 2016a,b). Such pre-motor interneurons with supraspinal inputs and with inputs from group I and II afferents were found in zone 3 (Cavallari et al., 1987; Jankowska et al., 2005, 2009; Bannatyne et al., 2006, 2009; Jankowska, 2008; Stecina et al., 2008; Jankowska and Edgley, 2010; Gosgnach et al., 2017).

Surprisingly, we found that all activity parameters of spinal neurons (mean frequency, burst and interburst frequency, as well as depth of modulation), which were significantly reduced after acute spinalization, returned to the control level already on day 3 after spinalization. This rapid increase in activity of F- and E-neurons could be caused by different factors: by spontaneous increase in excitability of spinal interneurons after deprivation of supraspinal influences, by an increase in efficacy of sensory input from limb mechanoreceptors, by an increase in the strength of sensory input (e.g., due to spontaneous increase of excitability of deprived of supraspinal influences gamma-motoneurons leading to an increase in signals from muscle spindles). At the same time point (day 3 after spinalization when activity of F- and E-neurons reached the control level), we found a substantial increase in relative number of residual EMG responses to tilts as compared with

that observed after acute spinalization. One can suggest that this increase was caused by restoration of excitability level of spinal interneurons. However, on day 3 EMG responses to tilts in hindlimb extensors were very weak and EMG amplitude constituted only about 12% of control, suggesting that excitability level of motoneurons at this time point remained very low. We found that with time EMG amplitude gradually increased and reached about 50% of control at day 30 after spinalization. Dramatic reduction in excitability level of motoneurons caused by spinalization (primarily due to the loss of persistent inward currents; Conway et al., 1988; Crone et al., 1988; Hounsgaard et al., 1988) and its slow rate of recovery over time was reported earlier (Johnson et al., 2013). Thus, one can conclude that spinalization triggers two processes: fast recovery of excitability level of interneurons (taking days) and slow recovery of excitability level of motoneurons (taking months).

At later time points after spinalization, we found significant changes in some activity parameters of populations of F- and E-neurons located in areas of the gray matter, which were not affected by acute spinalization. This result reflects continuous plastic changes in spinal postural networks taking place with time after spinalization. Most likely, a significant decrease in the depth of modulation of F-neurons located in the dorsal horn on day 30 after spinalization was caused by a significant decrease in the efficacy of sensory input from the ipsilateral limb, while a significant increase in the mean frequency of E-neurons in the ventral horn as well as in intermedial area of the gray matter – by an increase in their excitability level. The reasons for these changes as well as why these changes did not cause any significant changes in motor responses to tilts are not clear.

One of the reasons for abnormal reflex responsiveness characteristic for spasticity is distortions in the processing of sensory information (Frigon and Rossignol, 2006; D'Amico et al., 2014). We found that the processing of tilt-related sensory signals, which was severely distorted after acute spinalization did not recover during following month. Thus, contribution of tilt-related sensory inputs from the ipsilateral and contralateral limbs to modulation of F- and E-neurons did not reach control level within 1 month after spinalization. As after acute spinalization, at each of time points we found an almost twofold decrease in the relative number of neurons with a contribution of input from the contralateral limb (Types 2–4). Most likely, commissural interneurons transmitting signals from the contralateral limb were inactivated by acute spinalization and their excitability level did not reach control level during 1 month of observation. Such commissural neurons, with sensory input from the limb, and inputs from supraspinal structures, have been described (Jankowska, 2008). Recently, contribution of inhibitory V0 commissural interneurons to generation of postural corrections caused by tilts has been demonstrated (Vemula et al., 2018). In addition, we found significant changes in efficacy of tilt-related sensory inputs from ipsilateral and contralateral limb to specific populations of F-neurons taking place at different time points after spinalization. This result is in line with numerous evidences suggesting spontaneous plastic changes in spinal pathways mediating sensory signals from muscle and cutaneous receptors taking place with time after spinalization (Frigon and Rossignol, 2006; D'Amico et al., 2014; Johnson et al., 2017).

Besides the changed relative contribution of sensory inputs from the ipsilateral and contralateral limbs, we observed dramatically modified receptive fields of F- and E-neurons with increased (up to 60% vs. 7% in control and 4% after acute spinalization) relative number of neurons activated from skin/fur receptors. This new sensory input can contribute to recovery of activity value of spinal interneurons after spinalization. Abnormal expansion of receptor fields of motoneurons in spinal subjects was reported earlier (Hyngstrom et al., 2008; Frigon et al., 2011; Johnson et al., 2013).

It was shown that in chronic spinal rabbits, tilts often evoked repetitive EMG bursts superimposed on the ordinary EMG responses (Lyalka et al., 2011). Such EMG bursts (but generated at higher frequencies and termed clonus) are the symptom observed in spinal cord injured patients, and presumably caused by the central generating mechanisms in response to somatosensory signals (Beres-Jones et al., 2003). In rabbits, a gradual increase in oscillatory EMG activity during 1st month after spinalization was reported (Lyalka et al., 2011). It was suggested that this is due to enhancement of excitability in the spinal rhythm-generating networks. In the present study, we found a significant enhancement of the oscillatory activity in F-neurons from day 3 after spinalization, which can contribute to generation of EMG bursting. A gradual increase in EMG bursting during the 1st month after spinalization most likely reflects a slow gradual increase in the excitability level of motoneurons.

One of the symptoms characteristics for chronic spinal subjects is spasms of long duration appeared spontaneously or caused by unspecific sensory stimuli (Brown, 1994; Young, 1994; Hultborn, 2003). Multiple mechanisms underlying generation of spasms were suggested including changes in biophysical properties of motor neurons (Eken et al., 1989; Kiehn and Eken, 1998; Bennett et al., 1999; Li and Bennett, 2003; Li et al., 2004; Murray et al., 2010), reduced presynaptic inhibition of afferents (Faist et al., 1994; Xia and Rymer, 2005), changes in inhibition efficacy (Pierrot-Deseilligny et al., 1979; Shefner et al., 1992; Crone et al., 1994, 2004; Kapitza et al., 2012). A recent study suggests a major role of excitatory (glutamatergic) interneurons in triggering and sustaining the spasms (Bellardita et al., 2017), and in particular, a critical role of V3 interneurons for their initiation (Lin et al., 2019). In the present study, the mechanism underlying generation of spasms was not analyzed, since repetitive sensory stimulation caused by platform tilts abolished spasms.

To conclude, in the present study the activity of spinal neurons of postural networks at different time points after spinalization in mammals have been characterized for the first time. The obtained results suggest that spinalization triggers two processes of plastic changes of postural networks. First, a rapid (taking

days) process of recovery of the normal general activity level in spinal interneurons (though with oscillatory activity stronger than in control), which underlies appearance of residual motor responses to posture-related stimuli containing EMG bursting. Second, a slow (taking months) process of recovery of the motoneuronal excitability leading to gradual increase of EMG amplitude of these responses. However, absence of recovery of normal processing of postural sensory signals results in abnormal PLRs and loss of postural functions.

DATA AVAILABILITY

The datasets generated for this study are available on request to the corresponding author.

ETHICS STATEMENT

Animal Subjects: the animal study was reviewed and approved by Norra Djurförsöksetiska Nämnden in Stockholm.

AUTHOR CONTRIBUTIONS

TD and GO designed the experiments. PZ, VL, and TD performed the experiments and analyzed the data. All authors participated in the writing and reviewing of the manuscript.

FUNDING

This work was supported by grants from the NIH (R01 NS-064964), Swedish Research Council (No. 11554 and No. 2017-02944), and Gösta Fraenckels Foundation to TD, as well as by grant from the Swedish Research Council (No. 21076) to PZ.

SUPPLEMENTARY MATERIAL

The Supplementary Material for this article can be found online at: https://www.frontiersin.org/articles/10.3389/fncel.2019.00387/full#supplementary-material

REFERENCES

Ashby, P., and Verrier, M. (1975). Neurophysiological changes following spinal cord lesions in man. *Can. J. Neural. Sci.* 2, 91–100. doi: 10.1017/s0317167100020060

Bannatyne, B. A., Edgley, S. A., Hammar, I., Jankowska, E., and Maxwell, D. J. (2003). Networks of inhibitory and excitatory commissural interneurons mediating crossed reticulospinal actions. *Eur. J. Neurosci.* 18, 2273–2284. doi: 10.1046/j.1460-9568.2003.02973.x

Bannatyne, B. A., Edgley, S. A., Hammar, I., Stecina, K., Jankowska, E., and Maxwell, D. J. (2006). Different projections of excitatory and inhibitory dorsal horn interneurons relaying information from group II muscle afferents in the cat spinal cord. *J. Neurosci.* 26, 2871–2880. doi: 10.1523/jneurosci.5172-05.2006

Bannatyne, B. A., Liu, T. T., Hammar, I., Stecina, K., Jankowska, E., and Maxwell, D. J. (2009). Excitatory and inhibitory intermediate zone interneurons in pathways from feline group I and II afferents: differences in axonal projections and input. *J. Physiol.* 587, 379–399. doi: 10.1113/jphysiol.2008.159129

Barbeau, H., Fung, J., Leroux, A., and Ladouceur, M. (2002). A review of the adaptability and recovery of locomotion after spinal cord injury. *Prog. Brain Res.* 137, 9–25. doi: 10.1016/s0079-6123(02)37004-3

Barnes, C. D., Joynt, R. J., and Schottelius, B. A. (1962). Motoneuron resting potentials in spinal shock. *Am. J. Physiol.* 203, 1113–1116. doi: 10.1152/ajplegacy.1962.203.6.1113

Bellardita, C., Caggiano, V., Leiras, R., Caldeira, V., Fuchs, A., Bouvier, J., et al. (2017). Spatiotemporal correlation of spinal network dynamics underlying spasms in chronic spinalized mice. *eLife* 6:e23011. doi: 10.7554/eLife.23011

Beloozerova, I. N., Zelenin, P. V., Popova, L. B., Orlovsky, G. N., Grillner, S., and Deliagina, T. G. (2003). Postural control in the rabbit maintaining balance on the tilting platform. *J. Neurophysiol.* 90, 3783–3793. doi: 10.1152/jn.00590.2003

Bennett, D. J., Gorassini, M., Fouad, K., Sanelli, L., Han, Y., and Cheng, J. (1999). Spasticity in rats with sacral spinal cord injury. *J. Neurotrauma* 16, 69–84. doi: 10.1089/neu.1999.16.69

Beres-Jones, J. A., Johnson, T. D., and Harkema, S. J. (2003). Clonus after human spinal cord injury cannot be attributed solely to recurrent muscle-tendon stretch. *Exp. Brain Res.* 149, 222–236. doi: 10.1007/s00221-002-1349-5

Brown, P. (1994). Pathophysiology of spasticity. *J. Neurol. Neurosurg. Psychiatry* 57, 773–777.

Cavallari, P., Edgley, S. A., and Jankowska, E. (1987). Post-synaptic actions of mid-lumbar interneurons on motoneurons of hind-limb muscles in the cat. *J. Physiol.* 389, 675–689. doi: 10.1113/jphysiol.1987.sp016677

Chvatal, S. A., Macpherson, J. M., Torres-Oviedo, G., and Ting, L. H. (2013). Absence of postural muscle synergies for balance after spinal cord transection. *J. Neurophysiol.* 110, 1301–1310. doi: 10.1152/jn.00038.2013

Conway, B. A., Hultborn, H., Kiehn, O., and Mintz, I. (1988). Plateau potentials in α-motoneurones induced by intravenous injection of L-DOPA and clonidine in the spinal cat. *J. Physiol.* 405, 369–384. doi: 10.1113/jphysiol.1988.sp017337

Crone, C., Hultborn, H., Kiehn, O., Mazieres, L., and Wigström, H. (1988). Maintained changes in motoneuronal excitability by short-lasting synaptic inputs in the decerebrate cat. *J. Physiol.* 405, 321–343. doi: 10.1113/jphysiol.1988.sp017335

Crone, C., Nielsen, J., Petersen, N., Ballegaard, M., and Hultborn, H. (1994). Disynaptic reciprocal inhibition of ankle extensors in spastic patients. *Brain* 117 (Pt 5), 1161–1168. doi: 10.1093/brain/117.5.1161

Crone, C., Petersen, N. T., Nielsen, J. E., Hansen, N. L., and Nielsen, J. B. (2004). Reciprocal inhibition and corticospinal transmission in the arm and leg in patients with autosomal dominant pure spastic paraparesis (ADPSP). *Brain* 127, 2693–2702. doi: 10.1093/brain/awh319

D'Amico, J. M., Condliffe, E. G., Martins, K. J., Bennett, D. J., and Gorassini, M. A. (2014). Recovery of neuronal and network excitability after spinal cord injury and implications for spasticity. *Front. Integr. Neurosci.* 8:36. doi: 10.3389/fnint.2014.00036

Deliagina, T. G., Beloozerova, I. N., Orlovsky, G. N., and Zelenin, P. V. (2014). Contribution of supraspinal systems to generation of automatic postural responses. *Front. Integr. Neurosci.* 8:76. doi: 10.3389/fnint.2014.00076

Deliagina, T. G., Beloozerova, I. N., Popova, L. B., Sirota, M. G., Swadlow, H., Grant, G., et al. (2000). Role of different sensory inputs for maintenance of body posture in sitting rat and rabbit. *Motor Control* 4, 439–452. doi: 10.1123/mcj.4.4.439

Deliagina, T. G., Sirota, M. G., Zelenin, P. V., Orlovsky, G. N., and Beloozerova, I. N. (2006). Interlimb postural coordination in the standing cat. *J. Physiol.* 573, 211–224. doi: 10.1113/jphysiol.2006.104893

Deliagina, T. G., Zelenin, P. V., Lyalka, V. F., Hsu, L.-J., and Orlovsky, G. N. (2015). Changes in activity of spinal postural networks at different time points after spinalization. *Soc. Neurosci. Abstr.* 214.04.

Deliagina, T. G., Zelenin, P. V., and Orlovsky, G. N. (2012). Physiological and circuit mechanisms of postural control. *Curr. Opin. Neurobiol.* 22, 646–652. doi: 10.1016/j.conb.2012.03.002

Ditunno, J. F., Little, J. W., Tessler, A., and Burns, A. S. (2004). Spinal shock revised: a four-phase model. *Spinal Cord* 42, 383–395. doi: 10.1038/sj.sc.3101603

Eken, T., Hultborn, H., and Kiehn, O. (1989). Possible functions of transmitter-controlled plateau potentials in alpha motoneurones. *Prog. Brain Res.* 80, 257–267. doi: 10.1016/s0079-6123(08)62219-0

Faist, M., Mazevet, D., Dietz, V., and Pierrot-Deseilligny, E. (1994). A quantitative assessment of presynaptic inhibition of Ia afferents in spastics. Differences in hemiplegics and paraplegics. *Brain* 117 (Pt 6), 1449–1455. doi: 10.1093/brain/117.6.1449

Frigon, A., Johnson, M. D., and Heckman, C. J. (2011). Altered activation patterns by triceps surae stretch reflex pathways in acute and chronic spinal cord injury. *J. Neurophysiol.* 106, 1669–1678. doi: 10.1152/jn.00504.2011

Frigon, A., and Rossignol, S. (2006). Functional plasticity following spinal cord lesions. *Prog. Brain Res.* 157, 231–260.

Gosgnach, S., Bikoff, J. B., Dougherty, K. J., El Manira, A., Lanuza, G. M., and Zhang, Y. (2017). Delineating the diversity of spinal interneurons in locomotor circuits. *J. Neurosci.* 37, 10835–10841. doi: 10.1523/JNEUROSCI.1829-17.2017

Horak, F., and Macpherson, J. (1996). "Postural orientation and equilibrium," in *Handbook of Physiology. Exercise: Regulation and Integration of Multiple Systems*, eds J. Shepard and L. Rowell (New York, NY: Oxford University Press), 255–292.

Hounsgaard, J., Hultborn, H., Jespersen, B., and Kiehn, O. (1988). Bistability of α-motoneurones in the decerebrate cat and in the acute spinal cat after intravenous 5-hydroxytryptophan. *J. Physiol.* 405, 345–367. doi: 10.1113/jphysiol.1988.sp017336

Hsu, L.-J., Zelenin, P. V., Orlovsky, G. N., and Deliagina, T. G. (2012). Effects of galvanic vestibular stimulation on postural limb reflexes and neurons of spinal postural network. *J. Neurophysiol.* 108, 300–313. doi: 10.1152/jn.00041.2012

Hultborn, H. (2003). Changes in neuronal properties and spinal reflexes during development of spasticity following spinal cord lesions and stroke: studies in animal models and patients. *J. Rehab. Med.* 41(Suppl. 41), 46–55. doi: 10.1080/16501960310010142

Hyngstrom, A., Johnson, M., Schuster, J., and Heckman, C. J. (2008). Movement-related receptive fields of spinal motoneurones with active dendrites. *J. Physiol.* 586, 1581–1593. doi: 10.1113/jphysiol.2007.149146

Inglis, J. T., and Macpherson, J. M. (1995). Bilateral labyrinthectomy in the cat: effects on the postural response to translation. *J. Neurophysiol.* 73, 1181–1191. doi: 10.1152/jn.1995.73.3.1181

Jankowska, E. (2008). Spinal interneuronal networks in the cat: elementary components. *Brain Res. Rev.* 57, 46–55. doi: 10.1016/j.brainresrev.2007.06.022

Jankowska, E., Bannatyne, B. A., Stecina, K., Hammar, I., Cabaj, A., and Maxwell, D. J. (2009). Commissural interneurons with input from group I and II muscle afferents in feline lumbar segments: neurotransmitters, projections and target cells. *J Physiol.* 587, 401–418. doi: 10.1113/jphysiol.2008.159236

Jankowska, E., and Edgley, S. A. (2010). Functional subdivision of feline spinal interneurons in reflex pathways from group 1b and II muscle afferents; an update. *Eur J Neurosci* 32, 881–893. doi: 10.1111/j.1460-9568.2010.07354.x

Jankowska, E., Edgley, S. A., Krutki, P., and Hammar, I. (2005). Functional differentiation and organization of feline midlumbar commissural interneurons. *J. Physiol.* 565, 645–658. doi: 10.1113/jphysiol.2005.083014

Johnson, M. D., Frigon, A., Hurteau, M. F., Cain, C., and Heckman, C. J. (2017). Reflex wind-up in early chronic spinal injury: plasticity of motor outputs. *J. Neurophysiol.* 117, 2065–2074. doi: 10.1152/jn.00981.2016

Johnson, M. D., Kajtaz, E., Cain, C. M., and Heckman, C. J. (2013). Motoneuron intrinsic properties, but not their receptive fields recover in chronic spinal injury. *J. Neurosci.* 27, 18806–18813. doi: 10.1523/jneurosci.2609-13.2013

Kapitza, S., Zörner, B., Weinmann, O., Bolliger, M., Filli, L., Dietz, V., et al. (2012). Tail spasms in rat spinal cord injury: changes in interneuronal connectivity. *Exp. Neurol.* 236, 179–189. doi: 10.1016/j.expneurol.2012.04.023

Kiehn, O., and Eken, T. (1998). Functional role of plateau potentials in vertebrate motor neurons. *Curr. Opin. Neurobiol.* 8, 746–752. doi: 10.1016/s0959-4388(98)80117-7

Li, Y., and Bennett, D. J. (2003). Persistent sodium and calcium currents cause plateau potentials in motoneurons of chronic spinal rats. *J. Neurophysiol.* 90, 857–869. doi: 10.1152/jn.00236.2003

Li, Y., Gorassini, M. A., and Bennett, D. J. (2004). Role of persistent sodium and calcium currents in motoneuron firing and spasticity in chronic spinal rats. *J. Neurophysiol.* 91, 767–783. doi: 10.1152/jn.00788.2003

Lin, S., Li, Y., Lucas-Osma, A. M., Hari, K., Stephens, M. J., Singla, R., et al. (2019). Locomotor-related V3 interneurons initiate and coordinate muscles spasms after spinal cord injury. *J. Neurophysiol.* 121, 1352–1367. doi: 10.1152/jn.00776.2018

Lyalka, V. F., Hsu, L.-J., Karayannidou, A., Zelenin, P. V., Orlovsky, G. N., and Deliagina, T. G. (2011). Facilitation of postural limb reflexes in spinal rabbits by serotonergic agonist administration, epidural electrocal stimulation, and postural training. *J. Neurophysiol.* 106, 1341–1354. doi: 10.1152/jn.00115.2011

Lyalka, V. F., Orlovsky, G. N., and Deliagina, T. G. (2009). Impairment of postural control in rabbits with extensive spinal cord lesions. *J. Neurophysiol.* 101, 1932–1940. doi: 10.1152/jn.00009.2008

Lyalka, V. F., Zelenin, P. V., Hsu, L.-J., Orlovsky, G. N., and Deliagina, T. G. (2017). "Changes in activity of spinal postural networks at different time points after spinalization," in *Proceedings of the 2nd Nordic Neuroscience Meeting*, Stockholm, 112.

Macpherson, J. M., Deliagina, T. G., and Orlovsky, G. N. (1997a). "Control of body orientation and equilibrium in vertebrates," in *Neurons, Networks, and Motor Behaviour*, eds A. I. Selverston, P. S. G. Stein, S. Grillner, and D. G. Stuart (Cambridge, MA: MIT Press), 257–267.

Macpherson, J. M., Fung, J., and Jacob, R. (1997b). "Postural orientation,equilibrium, and the spinal cord," in *Neuronal Regeneration, Reorganization, and Repair, Advances in Neurology*, Vol. 72, ed. F. J. Seil (Philadelphia, PA: Lippincott Williams & Wilkins), 227–232.

Macpherson, J. M., and Fung, J. (1999). Weight support and balance during perturbed stance in the chronic spinal cat. *J. Neurophysiol.* 82, 3066–3081. doi: 10.1152/jn.1999.82.6.3066

Massion, L., and Dufosse, M. (1988). Coordination between posture and movement: why and how? *News Physiol. Sci.* 3, 88–93. doi: 10.1152/physiologyonline.1988.3.3.88

Murray, K. C., Nakae, A., Stephens, M. J., Rank, M., D'Amico, J., Harvey, P. J., et al. (2010). Recovery of motoneuron and locomotor function after spinal cord injury depends on constitutive activity in 5-HT2C receptors. *Nat. Med.* 16, 694–700. doi: 10.1038/nm.2160

Musienko, P. E., Deliagina, T. G., Gerasimenko, Y. P., Orlovsky, G. N., and Zelenin, P. V. (2014). Limb and trunk mechanisms for balance control during locomotion in quadrupeds. *J. Neurosci.* 34, 5704–5716. doi: 10.1523/JNEUROSCI.4663-13.2014

Musienko, P. E., Zelenin, P. V., Lyalka, V. F., Orlovsky, G. N., and Deliagina, T. G. (2008). Postural performance in decerebrated rabbit. *Behav. Brain Res.* 190, 124–134. doi: 10.1016/j.bbr.2008.02.011

Musienko, P. E., Zelenin, P. V., Orlovsky, G. N., and Deliagina, T. G. (2010). Facilitation of postural limb reflexes with epidural stimulation in spinal rabbits. *J. Neurophysiol.* 103, 1080–1092. doi: 10.1152/jn.00575.2009

Orlovsky, G. N., Deliagina, T. G., and Grillner, S. (1999). *Neuronal Control of Locomotion. From Mollusc to Man*. Oxford: Oxford University Press.

Pierrot-Deseilligny, E., Katz, R., and Morin, C. (1979). Evidence of Ib inhibition in human subjects. *Brain Res.* 166, 176–179. doi: 10.1016/0006-8993(79)90660-7

Rossignol, S., Bouyer, L., Barthelemy, D., Langlet, C., and Leblond, H. (2002). Recovery of locomotion in the cat following spinal cord lesions. *Brain Res. Rev.* 40, 257–266. doi: 10.1016/s0165-0173(02)00208-4

Rossignol, S., Drew, T., Brustein, E., and Jiang, W. (1999). "Locomotor performance and adaptation after partial or complete spinal cord lesions in the cat," in *Peripheral and Spinal Mechanisms in the Neural Control of Movement*, ed. M. D. Binder (Amsterdam: Elsevier), 349–365. doi: 10.1016/s0079-6123(08)62870-8

Roy, R. R., and Edgerton, V. R. (2012). Neurobiological perspective of spasticity as occurs after a spinal cord injury. *Exp. Neurol.* 235, 116–122. doi: 10.1016/j.expneurol.2012.01.017

Shefner, J. M., Berman, S. A., Sarkarati, M., and Young, R. R. (1992). Recurrent inhibition is increased in patients with spinal cord injury. *Neurology* 42, 2162–2168.

Shek, J. W., Wen, G. Y., and Wisniewski, H. M. (1986). *Atlas of the Rabbit Brain and Spinal Cord*. New York, NY: Karger.

Stapley, P., and Drew, T. (2009). The pontomedullary reticular formation contributes to the compensatory postural responses observed following removal of the support surface in the standing cat. *J. Neurophysiol.* 101, 1334–1350. doi: 10.1152/jn.91013.2008

Stecina, K., Slawinska, U., and Jankowska, E. (2008). Ipsilateral actions from the feline red nucleus on hindlimb motoneurones. *J. Physiol.* 586, 5865–5884. doi: 10.1113/jphysiol.2008.163998

Vemula, M. D. G., Lyalka, V. F., Talpalar, A. E., Kiehn, O., Deliagina, T. G., and Zelenin, P. V. (2018). Role of V0 commissural interneurons in control of basic motor behaviors. *Soc. Neurosci. Abstr.* 151.01.

Walmsley, B., and Tracey, D. J. (1983). The effect of transection and cool block of the spinal cord on synaptic transmission between 1a afferents and motoneurons. *Neuroscience* 9, 445–451. doi: 10.1016/0306-4522(83)90307-x

Xia, R., and Rymer, W. Z. (2005). Reflex reciprocal facilitation of antagonist muscles in spinal cord injury. *Spinal Cord* 43, 14–21. doi: 10.1038/sj.sc.3101656

Young, R. R. (1994). Spasticity: a review. *Neurology* 44, 12–20.

Zelenin, P. V., Hsu, L.-J., Lyalka, V. F., Orlovsky, G. N., and Deliagina, T. G. (2015). Putative spinal interneurons mediating postural limb reflexes provide a basis for postural control in different planes. *Eur. J. Neurosci.* 41, 168–181. doi: 10.1111/ejn.12780

Zelenin, P. V., Lyalka, V. F., Hsu, L.-J., Orlovsky, G. N., and Deliagina, T. G. (2013). Effects of reversible spinalization on individual spinal neurons. *J. Neurosci.* 33, 18987–18998. doi: 10.1523/JNEUROSCI.2394-13.2013

Zelenin, P. V., Lyalka, V. F., Hsu, L.-J., Orlovsky, G. N., and Deliagina, T. G. (2016a). Effects of acute spinalization on neurons of postural networks. *Sci. Rep.* 6:27372. doi: 10.1038/srep27372

Zelenin, P. V., Lyalka, V. F., Orlovsky, G. N., and Deliagina, T. G. (2016b). Effect of acute lateral hemisection of the spinal cord on spinal neurons of postural networks. *Neuroscience* 339, 235–253. doi: 10.1016/j.neuroscience.2016.09.043

Conflict of Interest Statement: The authors declare that the research was conducted in the absence of any commercial or financial relationships that could be construed as a potential conflict of interest.

frontiers in Cellular Neuroscience

PERSPECTIVE
published: 04 October 2019
doi: 10.3389/fncel.2019.00443

Mapping Connectivity Amongst Interneuronal Components of the Locomotor CPG

Farhia Haque[1] *and Simon Gosgnach*[1,2]*

[1] Neuroscience and Mental Health Institute, University of Alberta, Edmonton, AB, Canada, [2] Department of Physiology, Faculty of Medicine & Dentistry, University of Alberta, Edmonton, AB, Canada

The basic rhythmic activity characteristic of locomotion in mammals is generated by a neural network, located in the spinal cord, known as the locomotor central pattern generator (CPG). Although a great deal of effort has gone into the study of this neural circuit over the past century, identification and characterization of its component interneurons has proven to be challenging, largely due to their location and distribution. Recent work incorporating a molecular approach has provided a great deal of insight into the genetic identity of interneurons that make up this neural circuit, as well as the specific roles that they play during stepping. Despite this progress we still know relatively little regarding the manner in which these neuronal populations are interconnected. In this article we review the interneuronal populations shown to be involved in locomotor activity, briefly summarize their specific function, and focus on experimental work that provides insight into their synaptic connectivity. Finally, we discuss how recently developed viral approaches can potentially be incorporated to provide further insight into the network structure of this neural circuit.

Keywords: locomotion, central pattern generator, interneuron, synapse, connectivity

OPEN ACCESS

Edited by:
Katinka Stecina,
University of Manitoba, Canada

Reviewed by:
Simon M. Danner,
Drexel University, United States
Tuan Vu Bui,
University of Ottawa, Canada

***Correspondence:**
Simon Gosgnach
gosgnach@ualberta.ca

Specialty section:
This article was submitted to Cellular Neurophysiology, a section of the journal Frontiers in Cellular Neuroscience

Received: *31 May 2019*
Accepted: *18 September 2019*
Published: *04 October 2019*

Citation:
Haque F and Gosgnach S (2019) Mapping Connectivity Amongst Interneuronal Components of the Locomotor CPG. Front. Cell. Neurosci. 13:443. doi: 10.3389/fncel.2019.00443

INTRODUCTION

When broken down into its individual movements, the act of walking is an alarmingly complex activity which requires the precise contraction of numerous muscles on either side of the body, while cortical and sensory information is continuously processed and integrated in order to generate seamless, fluid movement. While in the intact animal, locomotor activity is initiated by descending input, the basic alternation that is characteristic of mammalian locomotion is generated by a neural circuit that is located in the spinal cord known as the locomotor central pattern generator (CPG- reviewed in Kiehn, 2016). Once activated, this neural circuit is independently able to generate long lasting locomotor activity and, remarkably, is also able to modulate its output to account for complex sensory information (Forssberg, 1979; Quevedo et al., 2005; Rossignol et al., 2006).

Although the mammalian locomotor CPG was discovered more than a century ago (Brown, 1911), progress toward identifying the interneuronal components of this neural network has been relatively slow. Recent advances in molecular genetic, anatomical tracing, and imaging techniques have generated a substantial amount of new information regarding components of the mammalian locomotor CPG. At the spinal level, a molecular approach has been used to divide

the developing neural tube of the embryonic mouse into ten distinct "parent" populations of interneurons (dI1-dI6, V0-V3) based on transcription factor expression (Goulding and Lamar, 2000; Goulding, 2009; Arber, 2012; Lu et al., 2015). Subsequent characterization of each population has resulted in the identification of a number of distinct subpopulations within each "parent" population based on downstream transcription factor expression (Catela et al., 2015; Gosgnach et al., 2017; Ziskind-Conhaim and Hochman, 2017; Cote et al., 2018; Bikoff, 2019). Since transcription factor expression dictates neuronal characteristics such as cell fate, channel composition, axonal projection pattern, and neurotransmitter phenotype, it was originally postulated that populations of neurons with a similar genetic background would have similar characteristics, and a similar function during locomotor activity. Studies performed over the past 15 years have characterized each of the genetically-defined neuronal populations that settle in the spinal cord, and defined their function during locomotor activity (reviewed in Grossmann et al., 2010; Kiehn, 2016; Deska-Gauthier and Zhang, 2019). Based on this work we can now identify the specific populations that are responsible for such key functions as left-right (Lanuza et al., 2004; Talpalar et al., 2013), and flexor-extensor (Zhang et al., 2014; Britz et al., 2015) coordination.

Despite this progress we still know very little regarding the manner in which these populations are interconnected to one another in order to produce locomotor activity. This is essential information if we are to gain a better understanding of the structure and mechanism of function of the locomotor CPG. In this article we will discuss the current state of knowledge regarding the synaptic connectivity of each population that has been shown to be involved in locomotor activity. Although computational modeling has been used to predict synaptic connectivity amongst many of these populations (Rybak et al., 2015; Shevtsova et al., 2015; Danner et al., 2016, 2017; Shevtsova and Rybak, 2016) we will not discuss this work here, we will simply provide a comprehensive summary of the findings of anatomical tracing and electrophysiological experiments that have probed connectivity amongst neuronal components of the locomotor CPG situated in the lumbar spinal cord. Finally, we will present new data which identifies the upstream synaptic partners of WT1-expressing interneurons, and discuss recently developed viral approaches that can be utilized to provide insight into the connectivity of interneuronal populations that comprise the locomotor CPG and generate key information regarding the network structure of this neural circuit.

V0 INTERNEURONS

The V0 population can be divided up into a dorsal subpopulation ($V0_D$) which expresses the transcription factor Dbx1 postmitotically, and a ventral population ($V0_V$) that expresses Evx1 in addition to Dbx1 (Moran-Rivard et al., 2001; Pierani et al., 2001). Both the $V0_D$ and $V0_V$ subsets are intermingled in lamina VIII of the postnatal spinal cord.

Initial studies into the function of the V0 population during locomotor activity indicated that these cells are crucial for appropriate alternation of contralateral motoneurons during stepping (Lanuza et al., 2004). A subsequent study considered the specific role of the $V0_D$ and $V0_V$ subpopulations independently, and demonstrated that the dorsal subset is inhibitory and responsible for coordinating left-right alternation at slow locomotor speeds, while the ventral subset is excitatory and responsible for this function when locomotor speed increases (Talpalar et al., 2013; Bellardita and Kiehn, 2015).

The specific connectivity responsible for this speed-dependent control of left-right alternation during locomotion has not been demonstrated. Investigations into the axonal projection pattern of V0 neurons located in the lumbar spinal cord indicated that greater than 90% of the axons from both $V0_D$ and $V0_V$ cells project to the contralateral spinal cord and, after crossing the midline, project up to four segments in the rostral direction (Moran-Rivard et al., 2001; Pierani et al., 2001). $V0_V$ neurons in the cervical spinal cord have been shown to project long descending commissural axons which terminate on neurons in the lumbar segments (Ruder et al., 2016). Retrograde transynaptic tracing with pseudorabies virus, which expresses GFP in all infected cells (i.e., PRV-152- Kerman et al., 2003), demonstrated that the V0 neurons in the lumbar segments contact contralateral motoneurons (Lanuza et al., 2004), although it is essential to keep in mind that V0 cells may synapse onto additional cell types since it is not possible to identify downstream synaptic partners other than motoneurons using this experimental approach, nor is it possible to determine the proportion of V0 neurons that contact motoneurons.

Additional analysis of the genetic lineage of the V0 population has indicated that the Evx1-expressing $V0_V$ subpopulation contains a small number of cells (5% of the entire V0 population) that express the transcription factor Pitx2, are cholinergic, project axons both ipsilaterally and contralaterally, and make contact onto motoneurons as well as unidentified interneurons in the dorsal and intermediate nucleus of the spinal cord (Zagoraiou et al., 2009). These neurons are referred to as the $V0_C$ subset and, based on functional deficits which are apparent in their absence, they have been hypothesized to modulate motoneuronal activity in a task dependent manner during stepping (Zagoraiou et al., 2009).

V1 INTERNEURONS

The V1 neurons are overwhelmingly inhibitory and primarily located in lamina VII/IX of the spinal cord (Saueressig et al., 1999). The Renshaw cells, a functionally defined population which receives input from motoneurons and inhibits Ia inhibitory interneurons (IaINs) and motoneurons (Renshaw, 1941; Eccles et al., 1954), as well as the Ia INs, which receive input from muscle afferents and Renshaw cells and inhibit motoneurons (Mendell and Henneman, 1971), are each derived from this cell population (Alvarez et al., 2005; Stam et al., 2012). Outside of these two subsets, which together comprise 22% of the entire population, V1 neurons exhibit a tremendous amount of diversity. Recent work demonstrated that a minimum of 19 genetically distinct "clades" of V1 neurons, each with a unique

physiological signature and distribution in the ventral spinal cord (Bikoff et al., 2016; Gabitto et al., 2016).

Given the diversity inherent within this population it is not surprising that a number of functions have been attributed to the V1 neurons. Ablation or silencing of the entire V1 population results in a drastic slowing of the locomotor rhythm (Gosgnach et al., 2006), while ablation of both the V1 and V2b neurons results in aberrant ipsilateral flexor-extensor alternation, and indicates that these two populations work together to coordinate the activity of ipsilateral motoneurons during stepping (Zhang et al., 2014). These latter results match up well with anatomical data showing that V1 neurons preferentially synapse on flexor motoneurons (Britz et al., 2015) while V2b neurons primarily contact extensor motoneurons. In addition, to contacting motoneurons, terminals from V1 neurons can also be found in close proximity to unidentified interneurons in lamina VII as well as the deep dorsal horn (Alvarez et al., 2005).

Given the molecular and physiological diversity displayed by this population it is essential to keep in mind that inhibition or deletion of the entire V1 population results in loss of function of multiple "clades," each of which likely possess a more discreet function during stepping, and the locomotor phenotypes observed when the entire population is silenced or ablated may be a consequence of the removal of several, functionally heterogeneous subtypes.

V2 INTERNEURONS

The V2 population can be divided up into the V2a subset, which are excitatory and express the transcription factor Chx10, as well as the inhibitory V2b subset which express GATA2/3 (Lundfald et al., 2007; Peng et al., 2007). While both subsets of V2 neurons are primarily located in laminae VII-X of the ventral spinal cord postnatally, there is a subtle variation in their distribution with the V2a cells evenly distributed throughout laminae VII, VIII, and X, while the V2b cells are clustered in lamina X and lamina IX (Lundfald et al., 2007). Both the V2a and V2b neurons located in the lumbar spinal cord project their axons exclusively to the ipsilateral side of the spinal cord before terminating within two segments in the rostral and caudal directions (Lundfald et al., 2007). Consistent with their aforementioned role in coordinating flexor-extensor alternation during locomotion, the V2b neurons preferentially contact extensor (rather than flexor) motoneurons, and synaptic terminals from this subset have also been found on members of the $V0_C$ population as well as unidentified neurons in lamina VII/VIII (Zhang et al., 2014). In addition, subsequent study of the V2a (Ruder et al., 2016) and V2b (Flynn et al., 2017) populations located in the cervical spinal cord demonstrated that both subtypes are involved regulating hindlimb locomotor activity via long descending ipsilateral connections to neurons located in the lumbar spinal cord.

Surprisingly, given their strictly ipsilateral axonal projection pattern, the V2a neurons were shown to be involved in coordinating left-right alternation during locomotor activity (Crone et al., 2008). This was hypothesized to be mediated by excitation of commissural interneurons which were shown to receive input from the V2a population (Crone et al., 2008). While the genetic background of a significant portion of these commissural neurons is unknown, the finding that a subset belong to the Evx1-expressing $V0_V$ interneurons is consistent with later work indicating that the V2a neurons are dispensable for slow locomotor activity but required for left-right alternation as the frequency of stepping increases (Crone et al., 2009). While there is no direct experimental evidence indicating that V2a neurons excite ipsilateral motoneurons, this connectivity has been predicted since the burst amplitude of motor axons varies during locomotor activity when Chx10 neurons are absent (Dougherty and Kiehn, 2010).

V3 INTERNEURONS

The V3 interneurons express the transcription factor Sim1 (Briscoe et al., 1999), and are spread through the dorsal, intermediate, and ventral spinal cord at birth (Zhang et al., 2008). Recent electrophysiological characterization of this population has demonstrated that V3 cells in each of these regions possesses unique electrophysiological characteristics (Borowska et al., 2013, 2015). Overall, 97% of V3 neurons project commissural axons (Blacklaws et al., 2015), and investigation of their neurotransmitter phenotype indicated that this population is exclusively excitatory (Zhang et al., 2008).

Regarding their specific synaptic partners, injection of the retrograde transsynaptic tracer PRV-152 into the hindlimb musculature of mice indicated that at least a subset of V3 cells contact motoneurons, with approximately 90% of the V3 cells with this projection pattern contacting motoneurons on the contralateral side of the spinal cord. As previously discussed, tracing with PRV-152 does not enable the specific proportion of the population that contacts motoneurons to be determined, and we know that V3 neurons also contact IaINs, Renshaw cells, as well as V2b cells and other, unidentified, commissural neurons (Zhang et al., 2008). Recent work incorporating an electrophysiological approach demonstrated that some of these commissural neurons which receive input from the V3 neurons may also belong to the V3 population themselves. Photostimulation of ventromedially located V3 cells was shown to activate other neighboring V3 cells as well as those in the ventrolateral spinal cord, while photostimulation of ventrolaterally located V3 cells was shown to excite ipsilateral motoneurons (Chopek et al., 2018). Many of the ventromedially and ventrolaterally located V3 neurons were also shown to have a contralaterally projecting axonal branch, however the specific termination point, and functional impact of this branch is unknown (Chopek et al., 2018). At this point the specific role of each subpopulation of V3 cells during locomotion is unclear. All functional studies have been carried out in the absence of the entire V3 population which has led to non-specific locomotor deficits such as a lack of robustness and regularity, indicative of a population that may have a number of functionally diverse subsets (Zhang et al., 2008). A more complete picture of the role of V3 neurons during locomotor activity will be apparent

once each subsets of this population has been identified and investigated individually.

dI6 INTERNEURONS

dI6 neurons express the transcription factors WT1 or DMRT3 at postmitotic time points (Goulding, 2009), and settle in lamina VII/VIII of the postnatal spinal cord (Dyck et al., 2012; Griener et al., 2017). The DMRT3 subset of dI6 neurons is an inhibitory population (Perry et al., 2019) which projects axons to both ipsilateral and contralateral targets. Retrograde tracing with PRV-152 demonstrated that the DMRT3 neurons project to motoneurons on either side of the spinal cord (Andersson et al., 2012) but again, given the nature of these experiments, the proportion of the DMRT3 population with this projection pattern is unknown. Recent work has also identified axon terminals from DMRT3-expressing neurons in close proximity to Renshaw cells as well as cholinergic neurons (possibly $V0_C$ interneurons) located near the central canal (Perry et al., 2019). This population has been predicted to play a critical role during locomotion based on data indicating that they are rhythmically active during stepping (Perry et al., 2019), as well as defects observed in left-right alternation in their absence (Andersson et al., 2012).

Like the DMRT3-expressing subset of dI6 cells, the WT1+ neurons are inhibitory. Work carried out in my laboratory has demonstrated that this subset extends commissural axons (Haque et al., 2018), however they do not make monosynaptic contact onto motoneurons. Synaptic terminals of WT1+ neurons were observed in close proximity to commissural neurons in the intermediate spinal cord, specifically members of the DMRT3+ and Evx1+ populations (Haque et al., 2018). All WT1-expressing neurons recorded during fictive locomotion were rhythmically-active and their importance during locomotion was confirmed by experiments which demonstrated left-right coordination defects were apparent when this subpopulation is silenced (Haque et al., 2018). Based on their connectivity as well as the locomotor phenotype in their absence we postulated that they work together with the V0 and DMRT3 populations to regulate left-right alternation during stepping (Haque et al., 2018).

Further support for this hypothesis comes from recent work from our laboratory in which we incorporated a viral approach to investigate the upstream synaptic partners of WT1-expressing neurons. All procedures for these experiments were performed on mice in accordance with the Canadian Council on Animal Welfare and approved by the Animal Welfare Committee at the University of Alberta. For these experiments four 3–5 days old $WT1^{Cre}$ mice of either sex were anesthetized with isoflurane, and once surgical plane was reached a small incision was made directly over the L3 segment, a laminectomy was performed at this segment, and 100–200 nL of the Cre-dependent, retrograde, transsynaptic virus Introvert Pseudorabies virus (i.e., Introvert-PRV, kind gift Dr. Jeffrey Friedman, HHMI, Rockefeller Univ.) was microinjected directly into the ventral aspect of the third lumbar spinal segment (i.e., L3). This virus has been shown to infect, and express GFP, in Cre expressing cells at the injection site between 15 and 20 h after injection, before traveling to all monosynaptically connected upstream synaptic partners 26–30 h after injection (Pomeranz et al., 2017). At the appropriate time after injection animals were anesthetized and perfused with 4% paraformaldehyde (PFA). The entire CNS was dissected out, and tissue was post fixed (24 h in 4% PFA), cryoprotected in 30% sucrose, and frozen in preparation for cryosectioning. Inspection of sections cut 20 h after injection and stained with antibodies to GFP (to identify cells that took up the virus) and WT1 revealed that 87% of GFP- expressing neurons were WT1+ (**Figure 1A**) confirming that this virus preferentially infects Cre expressing neurons.

To determine the identity of the spinal neurons that synapse onto WT1-expressing cells sections cut from spinal cords harvested 30 h post injection were stained with antibodies against Evx1, En1, Chx10, and Dmrt3 in order to label $V0_V$, V1, V2a, and a subset of the dI6 interneuronal populations, respectively. A mean of 5.4 ± 3.9 (SD) GFP+ (i.e., viral infected)

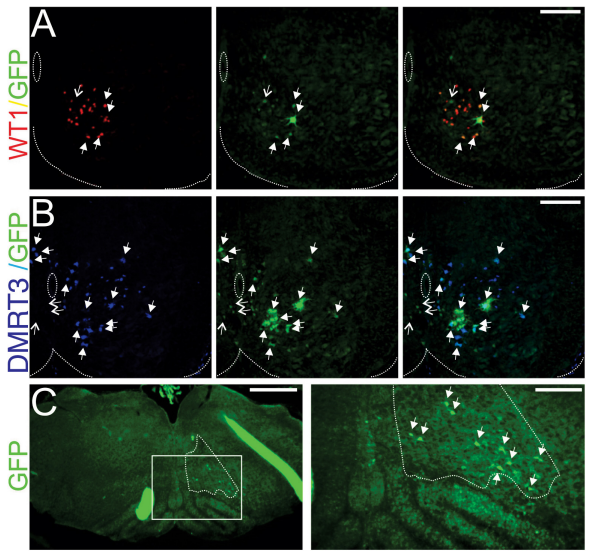

FIGURE 1 | WT1-expressing neurons in the lumbar spinal cord receive monosynaptic input from DMRT3+ cells and well as the reticular formation. **(A)** 20 μm section cut from the third lumbar (L3) spinal segment of a $WT1^{Cre}$ mouse 20 h after Introvert-PRV injection reveals that the majority of cells taking up the virus (green cells, GFP+) express WT1 (red cells). Filled arrows indicate infected cells that are WT1+, open arrows indicate those that are WT1−. **(B)** 20 μm section cut from the L2 spinal segment 30 h after microinjection of Introvert-PRV into the L3 segment illustrates that the some DMRT3+ neurons (blue) are infected (green) and thus monosynaptically connect to WT1-expressing neurons. Filled arrows indicate infected cells that are DMRT3+ and open arrows those that are DMRT3-. In panels **(A,B)** dashed lines indicate the central canal and the ventral extent of the spinal cord, scale Bars = 100 μm. **(C)** Section cut from the brainstem 30 h after injection of Introvert PRV into the L3 segment reveal that cells within the reticular nucleus gigantocellularis (region surrounded by dashes, determined by consultation with the Allen Brain Atlas) are infected (green cells indicated by arrows in panel to the right) and thus contact WT1 neurons in the lumbar spinal cord. Panel to the right is a magnification of boxed region in the left panel. Scale bar in the left panel = 500 μm, in the right panel 200 μm.

cells per 20 μm hemi-section (n = 5) were found throughout the lower thoracic to lumbar (T10-L5) segments of the spinal cord. We found no co-labeling with En1 or Chx10- expressing neurons, and only one viral infected cell that expressed Evx1 (i.e., a $V0_V$ neuron), however 95.9% of viral infected cells were DMRT3+ (**Figure 1B**), indicating that much of the input to WT1-expressing neurons at the spinal level comes from this closely related cell population.

Interestingly, inspection of serial brainstem sections from these same mice after Introvert PRV was injected into the lumbar spinal cord indicated that 4.2 ± 2.1 (SD) viral infected cells could be found in the ventral aspect of the reticular nucleus gigantocellularis (n = 3 mice, **Figure 1C**), a brainstem region housing glutamatergic neurons involved in generating high speed locomotor activity (Capelli et al., 2017), as well as glycinergic neurons that result in the cessation of stepping (Bouvier et al., 2015). Although we were not able to determine whether excitatory or inhibitory neurons within this region contact the WT1-expressing population, our data does raise the possibility that the reticular nucleus may provide ongoing modulation of the activity of interneuronal components of this neural network, circuitry that would be functionally relevant when quadrupedal animals switch between gaits from walking to trotting to galloping.

INTERNEURONAL POPULATIONS POTENTIALLY INVOLVED IN LOCOMOTOR RHYTHM GENERATION

The transcription factor Shox2 is expressed in a subset of V2a neurons as well as other, Chx10 negative interneurons. These Shox2+/Chx10− neurons have recently been shown to be excitatory, and possess many properties of locomotor rhythm generating neurons (Dougherty et al., 2013). As a whole (i.e., no distinction could be made between Chx10+ and Chx10- subsets), Shox2-expressing neurons project toward ipsilateral targets including other Shox2+ interneurons, motoneurons, as well as unidentified commissural interneurons (Dougherty et al., 2013). Interestingly in depth analysis of the projection pattern of Shox2 neurons that were Chx10+ and Chx10- indicates that each subset only projects to other members belonging to the same subtype and there is no connectivity between Chx10+ and Chx10- Shox2+ neurons (Ha and Dougherty, 2018).

Another population of interneurons located in close proximity to the Shox2+ population is marked by postnatal expression of Hb9 (Hinckley et al., 2005). Members of this small population of excitatory interneurons, project to one another via chemical and electrical synapses as well as onto ipsilateral motoneurons (Hinckley and Zisnind-Conhaim, 2006; Wilson et al., 2007), and they have also been implicated in locomotor rhythm generation (Brownstone and Wilson, 2008; Hinckley et al., 2010; Caldeira et al., 2017), although their involvement has been debated (see Kwan et al., 2009).

DISCUSSION

We are now approaching 20 years since the first published work incorporating a molecular genetic approach to identify, and functionally characterize, interneuronal components of the locomotor CPG. While this approach has resulted in a tremendous amount of new data, we still know little regarding the manner in which these populations interact with one another. This information is required if we hope to understand how this neural circuit operates, and devise therapies targeted at restoring function after spinal cord injury.

Thus far a number of studies have used approaches such as the retrograde transynaptic transport of PRV-152 to identify interneuronal populations that contact hindlimb motoneurons, however relatively little connectivity between the genetically-defined interneuronal populations has been revealed. While it is certainly valuable to identify last order interneurons that project to hindlimb motoneurons, it is essential to keep in mind that these experiments do not indicate exclusivity, and that these last order interneurons are also likely to project to other interneuronal populations. In fact, each of the studies that have incorporated an anterograde approach to investigate the distribution of axon terminals of an interneuronal population

TABLE 1 | Axonal projection pattern and identified synaptic targets for each of the genetically-defined interneuronal populations located in the ventral spinal cord postnatally that have been identified to participate in locomotor activity.

Population	Subset	Transmitter	Axonal projection	Synaptic targets
V0	$V0_D$	Inhibitory	Contralateral	Contralateral motoneurons
	$V0_V$	Excitatory	Contralateral	
	$V0_C$	Excitatory	Ipsi/contralateral	ipsi/contralateral motoneurons, unidentified lamina VIII and dorsal horn interneurons
V1	RC	Inhibitory	Ipsilateral	Motoneurons, IaINs
	IaIN	Inhibitory	Ipsilateral	Motoneurons
	V1	Inhibitory	Ipsilateral	Flexor motoneurons, unidentified ventral interneurons
V2	V2a	Excitatory	Ipsilateral	$V0_V$ and unidentified commissural interneurons
	V2b	Inhibitory	Ipsilateral	Extensor motoneurons, V0c INs, unidentified neurons in lamina VII and VIII
V3		Excitatory	Ipsi/contralateral	Ipsi/contralateral motoneurons, Renshaw cells, IaINs, ipsilateral V3 interneurons as well as unidentified ipsilateral and contralateral targets.
dI6	DMRT3	Inhibitory	Ipsi/contralateral	Ipsilateral and contralateral motoneurons
	WT1	Inhibitory	Ipsi/contralateral	DMRT3 + dI6 cells and V0v interneurons

has led to the identification of input to multiple regions, or onto multiple cell types, within the spinal cord (see **Table 1**). Given the vast diversity within each parent population these findings are not surprising. While this makes studies into the connectivity of the locomotor CPG more technically demanding, recent progress in the development of viral approaches (reviewed in Luo et al., 2018) is beginning to provide the tools required to reveal the manner in which these genetically-defined interneuronal populations are activated and interconnected. As more discrete subsets of interneurons are identified within each parent population, these techniques are likely to become increasingly valuable for deciphering connectivity amongst them.

DATA AVAILABILITY STATEMENT

The datasets generated for this study are available on request to the corresponding author.

ETHICS STATEMENT

The animal study was reviewed and approved by IACUC-University of Alberta.

AUTHOR CONTRIBUTIONS

Both authors listed have made a substantial, direct and intellectual contribution to the work, and approved it for publication.

FUNDING

This research was funded by Canadian Institutes of Health Research Grant (MOP 86470), and the generous support of the Stollery Children's Hospital Foundation through the Women and Children's Health Research Institute.

ACKNOWLEDGMENTS

Dr. Wei Zhang provided technical assistance. Drs. Jeffrey Friedman (HHMI/Rockefeller University, NY), Thomas Jessell (HHMI/Columbia University, NY), and Jay Bikoff (St. Jude Children's Hospital, Memphis, TN) provided reagents used in this study.

REFERENCES

Alvarez, F. J., Jonas, P. C., Sapir, T., Hartley, R., Berrocal, M. C., and Geiman, E. J. (2005). Postnatal phenotype and localization of spinal cord V1 derived interneurons. *J. Comp. Neurol.* 493, 177–192. doi: 10.1002/cne.20711

Andersson, L. S., Larhammar, M., Memic, F., Wootz, H., Schwochow, D., and Rubin, C. J. (2012). Mutations in DMRT3 affect locomotion in horses and spinal circuit function in mice. *Nature* 488, 642–646. doi: 10.1038/nature11399

Arber, S. (2012). Motor circuits in action: specification, connectivity, and function. *Neuron* 74, 975–989. doi: 10.1016/j.neuron.2012.05.011

Bellardita, C., and Kiehn, O. (2015). Phenotypic characterization of speed-associated gait changes in mice reveals modular organization of locomotor networks. *Curr. Biol.* 25, 1426–1436. doi: 10.1016/j.cub.2015.04.005

Bikoff, J. B. (2019). Interneuron diversity and function in the spinal motor system. *Curr. Opin. Physiol.* 8, 36–43. doi: 10.1016/j.cophys.2018.12.013

Bikoff, J. B., Gabitto, M. I., Rivard, A. F., Drobac, E., Machado, T. A., and Miri, A. (2016). Spinal inhibitory interneuron diversity delineates variant motor microcircuits. *Cell* 165, 207–219. doi: 10.1016/j.cell.2016.01.027

Blacklaws, J., Deska-Gauthier, D., Jones, C. T., Petracca, Y. L., Liu, M., and Zhang, H. (2015). Sim1 is required for the migration and axonal projections of V3 interneurons in the developing mouse spinal cord. *Dev. Neurobiol.* 75, 1003–1017. doi: 10.1002/dneu.22266

Borowska, J., Jones, C. T., Deska-Gauthier, D., and Zhang, Y. (2015). V3 interneuron subpopulations in the mouse spinal cord undergo distinctive postnatal maturation processes. *Neuroscience.* 295, 221–228. doi: 10.1016/j.neuroscience.2015.03.024

Borowska, J., Jones, C. T., Zhang, H., Blacklaws, J., Goulding, M., and Zhang, Y. (2013). Functional subpopulations of V3 interneurons in the mature mouse spinal cord. *J. Neurosci.* 33, 18553–18565. doi: 10.1523/JNEUROSCI.2005-13.2013

Bouvier, J., Caggiano, V., Leiras, R., Caldeira, V., Bellardita, C., Balueva, K., et al. (2015). Descending command neurons in the brainstem that halt locomotion. *Cell* 163, 1191–1203. doi: 10.1016/j.cell.2015.10.074

Briscoe, J., Sussel, L., Serup, P., Hartigan-, O., Connor, D., Jessell, T. M., et al. (1999). Homeobox gene Nkx2.2 and specification of neuronal identity by graded Sonic hedgehog signalling. *Nature* 398, 622–627. doi: 10.1038/19315

Britz, O., Zhang, J., Grossmann, K. S., Dyck, J., Kim, J. C., and Dymecki, S. (2015). A genetically defined asymmetry underlies the inhibitory control of flexor-extensor locomotor movements. *eLife* 4:e04718.

Brown, T. G. (1911). The intrinsic factors in the act of progression in mammals. *Proc. R. Soc. B* 84, 308–319. doi: 10.1098/rspb.1911.0077

Brownstone, R. M., and Wilson, J. M. (2008). Strategies for delineating spinal locomotor rhythm-generating networks and the possible role of Hb9 interneurones in rhythmogenesis. *Brain Res. Rev.* 57, 64–76. doi: 10.1016/j.brainresrev.2007.06.025

Caldeira, V., Dougherty, K. J., Borgius, L., and Kiehn, O. (2017). Spinal Hb9:Cre-derived excitatory interneurons contribute to rhythm generation in the mouse. *Sci. Rep.* 7:41369. doi: 10.1038/srep41369

Capelli, P., Pivetta, C., Soledad Esposito, M., and Arber, S. (2017). Locomotor speed control circuits in the caudal brainstem. *Nature* 551, 373–377. doi: 10.1038/nature24064

Catela, C., Shin, M. M., and Dasen, J. S. (2015). Assembly and function of spinal circuits for motor control. *Annu. Rev. Cell Devel Biol.* 31, 669–698. doi: 10.1146/annurev-cellbio-100814-125155

Chopek, J. W., Nascimento, F., Beato, M., Brownstone, R. M., and Zhang, Y. (2018). Sub-populations of spinal V3 interneurons form focal modules of layered pre-motor microcircuits. *Cell Rep.* 25, 146–156. doi: 10.1016/j.celrep.2018.08.095

Cote, M.-P., Murray, L. M., and Knikou, M. (2018). Spinal control of locomotion: individual neurons, their circuits and functions. *Front. Physiol.* 25:784. doi: 10.3389/fphys.2018.00784

Crone, S. A., Quinlan, K. A., Zagoraiou, L., Droho, S., Restrepo, C. E., and Lundfald, L. (2008). Genetic ablation of V2a ipsilateral interneurons disrupts left-right locomotor coordination in mammalian spinal cord. *Neuron* 60, 70–83. doi: 10.1016/j.neuron.2008.08.009

Crone, S. A., Zhong, G., Harris-Warrick, R., and Sharma, K. (2009). In mice lacking V2a interneurons, gait depends on speed of locomotion. *J. Neurosci.* 29, 7098–7109. doi: 10.1523/JNEUROSCI.1206-09.2009

Danner, S. M., Shevtsova, N. A., Frigon, A., and Rybak, I. A. (2017). Computational modeling of spinal circuits controlling limb coordination and gaits in quadrupeds. *eLife* 6:e31050. doi: 10.7554/eLife.31050

Danner, S. M., Wilshin, S. D., Shevtsova, N. A., and Rybak, I. A. (2016). Central control of interlimb coordination and speed dependent gait expression in quadrupeds. *J. Physiol.* 594, 6947–6967. doi: 10.1113/JP272787

Deska-Gauthier, D., and Zhang, Y. (2019). The functional diversity of spinal interneurons and locomotor control. *Curr. Opin. Physiol.* 8, 99–108. doi: 10.1016/j.cophys.2019.01.005

Dougherty, K. J., and Kiehn, O. (2010). Functional organization of V2a-related locomotor circuits in the rodent spinal cord. *Ann. N. Y. Acad. Sci.* 1198, 85–93. doi: 10.1111/j.1749-6632.2010.05502.x

Dougherty, K. J., Zagoraiou, L., Satoh, D., Rozani, I., Doobar, S., and Arber, S. (2013). Locomotor rhythm generation linked to the output of spinal shox2 excitatory interneurons. *Neuron* 80, 920–933. doi: 10.1016/j.neuron.2013.08.015

Dyck, J., Lanuza, G. M., and Gosgnach, S. (2012). Functional characterization of dI6 interneurons in the neonatal mouse spinal cord. *J. Neurophysiol.* 107, 3256–3266. doi: 10.1152/jn.01132.2011

Eccles, J. C., Fatt, P., and Koketsu, K. (1954). Cholinergic and inhibitory synapses in a pathway from motor-axon collaterals to motoneurones. *J. Physiol.* 126, 524–562. doi: 10.1113/jphysiol.1954.sp005226

Flynn, J. R., Conn, V. L., Boyle, K. A., Hughes, D. I., Watanabe, M., and Velasquez, T. (2017). Anatomical and molecular properties of long descending propriospinal neurons in mice. *Front. Neuroanat.* 11:5. doi: 10.3389/fnana.2017.00005

Forssberg, H. (1979). Stumbling corrective reaction: a phase-dependent compensatory reaction during locomotion. *J. Neurophysiol.* 42, 936–953. doi: 10.1152/jn.1979.42.4.936

Gabitto, M. I., Pakman, A., Bikoff, J. B., Abbott, L. F., Jessell, T. M., and Paninski, L. (2016). Bayesian sparse regression analysis documents the diversity of spinal inhibitory interneurons. *Cell* 65, 220–233. doi: 10.1016/j.cell.2016.01.026

Gosgnach, S., Bikoff, J. B., Dougherty, K. J., El Manira, A., Lanuza, G. M., and Zhang, Y. (2017). Delineating the diversity of spinal interneurons in locomotor circuits. *J. Neurosci.* 37, 10835–10841. doi: 10.1523/JNEUROSCI.1829-17.2017

Gosgnach, S., Lanuza, G. M., Butt, S. J., Saueressig, H., Zhang, Y., and Velasquez, T. (2006). V1 spinal neurons regulate the speed of vertebrate locomotor outputs. *Nature* 440, 215–219. doi: 10.1038/nature04545

Goulding, M. (2009). Circuits controlling vertebrate locomotion: moving in a new direction. *Nat. Rev. Neurosci.* 10, 507–518. doi: 10.1038/nrn2608

Goulding, M., and Lamar, E. (2000). Neuronal patterning: making stripes in the spinal cord. *Curt Biol.* 10, 565–568.

Griener, A., Zhang, W., Kao, H., Haque, F., and Gosgnach, S. (2017). Anatomical and electrophysiological characterization of a population of dI6 interneurons in the neonatal mouse spinal cord. *Neuroscience* 362, 47–59. doi: 10.1016/j.neuroscience.2017.08.031

Grossmann, K. S., Giraudin, A., Britz, O., Zhang, J., and Goulding, M. (2010). Genetic dissection of rhythmic motor networks in mice. *Prog. Brain Res.* 187, 19–37. doi: 10.1016/B978-0-444-53613-6.00002-2

Ha, N. T., and Dougherty, K. J. (2018). Spinal Shox2 interneuron interconnectivity related to function and development. *eLife* 7:e42519. doi: 10.7554/eLife.42519

Haque, F., Rancic, V., Zhang, W., Clugston, R., Ballanyi, K., and Gosgnach, S. (2018). WT1-Expressing interneurons regulate left-right alternation during mammalian locomotor activity. *J. Neurosci.* 38, 5666–5676. doi: 10.1523/JNEUROSCI.0328-18.2018

Hinckley, C. A., Hartley, R., Wu, L., Todd, A., and Ziskind-Conhaim, L. (2005). Locomotor-like rhythms in a genetically distinct cluster of interneurons in the mammalian spinal cord. *J. Neurophysiol.* 93, 1439–1449. doi: 10.1152/jn.00647.2004

Hinckley, C. A., Wiesner, E. P., Mentis, G. Z., Titus, D. J., and Ziskind-Conhaim, L. (2010). Sensory modulation of locomotor-like membrane oscillations in Hb9-expressing interneurons. *J. Neurophysiol.* 103, 3407–3423. doi: 10.1152/jn.00996.2009

Hinckley, C. A., and Zisnind-Conhaim, L. (2006). Electrical coupling between locomotor-related excitatory interneurons in the mammalian spinal cord. *J. Neurosci.* 26, 8477–8483. doi: 10.1523/jneurosci.0395-06.2006

Kerman, I. A., Enquist, L. W., Watson, S. J., and Yates, B. J. (2003). Brainstem substrates of sympatho-motor circuitry identified using trans-synaptic tracing with pseudorabies virus recombinants. *J. Neurosci.* 23, 4657–4666. doi: 10.1523/jneurosci.23-11-04657.2003

Kiehn, O. (2016). Decoding the organization of spinal circuits that control locomotion. *Nat. Rev. Neurosci.* 17, 224–238. doi: 10.1038/nrn.2016.9

Kwan, A. C., Dietz, S. B., Webb, W. W., and Harris-Warrick, R. M. (2009). Activity of Hb9 interneurons during fictive locomotion in mouse spinal cord. *J. Neurosci.* 29, 11601–11613. doi: 10.1523/JNEUROSCI.1612-09.2009

Lanuza, G. M., Gosgnach, S., Pierani, A., Jessell, T. M., and Goulding, M. (2004). Genetic identification of spinal interneurons that coordinate left-right locomotor activity necessary for walking movements. *Neuron* 42, 375–386. doi: 10.1016/s0896-6273(04)00249-1

Lu, D. C., Niu, T., and Alaynick, W. A. (2015). Molecular and cellular development of spinal cord locomotor circuitry. *Front. Mol. Neurosci.* 8:25. doi: 10.3389/fnmol.2015.00025

Lundfald, L., Restrepo, C. E., Butt, S. J., Peng, C. Y., Droho, S., and Endo, T. (2007). Phenotype of V2-derived interneurons and their relationship to the axon guidance molecule EphA4 in the developing mouse spinal cord. *Eur. J. Neurosci.* 26, 2989–3002. doi: 10.1111/j.1460-9568.2007.05906.x

Luo, L., Callaway, E. M., and Svoboda, K. (2018). Genetic dissection of neural circuits: a decade of progress. *Neuron* 98, 256–281. doi: 10.1016/j.neuron.2018.03.040

Mendell, L. M., and Henneman, E. (1971). Terminals of single Ia fibers: location, density, and distribution within a pool of 300 homonymous motoneurons. *J. Neurophysiol.* 34, 171–187. doi: 10.1152/jn.1971.34.1.171

Moran-Rivard, L., Kagawa, T., Saueressig, H., Gross, M. K., Burrill, J., and Goulding, M. (2001). Evx1 is a postmitotic determinant of v0 interneuron identity in the spinal cord. *Neuron* 29, 385–399. doi: 10.1016/s0896-6273(01)00213-6

Peng, C. Y., Yajima, H., Burns, C. E., Zon, L. I., Sisodia, S. S., Pfaff, S. L., et al. (2007). Notch and MAML signaling drives Scl-dependent interneuron diversity in the spinal cord. *Neuron* 53, 813–827. doi: 10.1016/j.neuron.2007.02.019

Perry, S., Larhammar, M., Vieillard, J., Nagaraja, C., Hilscher, M. M., and Tafreshiha, A. (2019). Characterization of Dmrt3-derived neurons suggest a role within locomotor circuits. *J. Neurosci.* 39, 1771–1782. doi: 10.1523/JNEUROSCI.0326-18.2018

Pierani, A., Moran-Rivard, L., Sunshine, M. J., Littman, D. R., Goulding, M., and Jessell, T. M. (2001). Control of interneuron fate in the developing spinal cord by the progenitor homeodomain protein Dbx1. *Neuron* 29, 367–384. doi: 10.1016/s0896-6273(01)00212-4

Pomeranz, L. E., Ekstrand, M. I., Latcha, K. N., Smith, G. A., Enquist, L. W., and Friedman, J. M. (2017). Gene expression profiling with Cre-conditional pseudorabies virus reveals a subset of midbrain neurons that participate in reward circuitry. *J. Neurosci.* 37, 4128–4144. doi: 10.1523/JNEUROSCI.3193-16.2017

Quevedo, J., Stecina, K., Gosgnach, S., and McCrea, D. A. (2005). Stumbling corrective reaction during fictive locomotion in the cat. *J. Neurophysiol.* 94, 2045–2052. doi: 10.1152/jn.00175.2005

Renshaw, B. (1941). Influence of discharge of motoneurons upon excitation of neighboring motoneurons. *J. Neurophysiol.* 4, 167–183. doi: 10.1152/jn.1941.4.2.167

Rossignol, S., Dubuc, R., and Gossard, J. P. (2006). Dynamic sensorimotor interactions in locomotion. *Physiol. Rev.* 86, 89–154. doi: 10.1152/physrev.00028.2005

Ruder, L., Takeoka, A., and Arber, S. (2016). Long-distance descending spinal neurons ensure quadrupedal locomotor stability. *Neuron* 92, 1063–1078. doi: 10.1016/j.neuron.2016.10.032

Rybak, I. A., Dougherty, K. J., and Shevtsova, N. A. (2015). Organization of the mammalian locomotor cpg: review of computational model and circuit architectures based on genetically identified spinal interneurons(1,2,3). *eNeuro* 2:ENEURO.0069-15.2015. doi: 10.1523/ENEURO.0069-15.2015

Saueressig, H., Burrill, J., and Goulding, M. (1999). Engrailed-1 and netrin-1 regulate axon pathfinding by association interneurons that project to motor neurons. *Development* 126, 4201–4212.

Shevtsova, N. A., and Rybak, I. A. (2016). Organization of flexor-extensor interactions in the mammalian spinal cord: insights from computational modelling. *J. Physiol.* 594, 6117–6131. doi: 10.1113/JP272437

Shevtsova, N. A., Talpalar, A. E., Markin, S. N., Harris-Warrick, R. M., Kiehn, O., and Rybak, I. A. (2015). Organization of left-right coordination of neuronal activity in the mammalian spinal cord: insights from computational modelling. *J. Physiol.* 593, 2403–2426. doi: 10.1113/JP270121

Stam, F. J., Hendricks, T. J., Zhang, J., Geiman, E. J., Francius, C., and Labosky, P. A. (2012). Renshaw cell interneuron specialization is controlled by a temporally restricted transcription factor program. *Development* 139, 179–190. doi: 10.1242/dev.071134

Talpalar, A. E., Bouvier, J., Borgius, L., Fortin, G., Pierani, A., and Kiehn, O. (2013). Dual-mode operation of neuronal networks involved in left-right alternation. *Nature* 500, 85–88. doi: 10.1038/nature12286

Wilson, J. M., Cowan, A. I., and Brownstone, R. M. (2007). Heterogeneous electrotonic coupling and synchronization of rhythmic bursting activity in mouse Hb9 interneurons. *J. Neurophys.* 98, 2370–2381. doi: 10.1152/jn.00338.2007

Zagoraiou, L., Akay, T., Martin, J. F., Brownstone, R. M., Jessell, T. M., and Miles, G. B. (2009). A cluster of cholinergic premotor interneurons modulates mouse locomotor activity. *Neuron* 64, 645–662. doi: 10.1016/j.neuron.2009.10.017

Zhang, J., Lanuza, G. M., Britz, O., Wang, Z., Siembab, V. C., and Zhang, Y. (2014). V1 and v2b interneurons secure the alternating flexor-extensor motor activity mice require for limbed locomotion. *Neuron* 82, 138–150. doi: 10.1016/j.neuron.2014.02.013

Zhang, Y., Narayan, S., Geiman, E., Lanuza, G. M., Velasquez, T., and Shanks, B. (2008). V3 spinal neurons establish a robust and balanced locomotor rhythm during walking. *Neuron* 60, 84–96. doi: 10.1016/j.neuron.2008.09.027

Ziskind-Conhaim, L., and Hochman, S. (2017). Diversity of molecularly defined spinal interneurons engaged in mammalian locomotor pattern generation. *J Neurophysiol.* 118, 2956–2974. doi: 10.1152/jn.00322.2017 doi: 10.1152/jn.00322.2017

Conflict of Interest: The authors declare that the research was conducted in the absence of any commercial or financial relationships that could be construed as a potential conflict of interest.

frontiers in Cellular Neuroscience

ORIGINAL RESEARCH
published: 09 October 2019
doi: 10.3389/fncel.2019.00452

Flexor and Extensor Ankle Afferents Broadly Innervate Locomotor Spinal Shox2 Neurons and Induce Similar Effects in Neonatal Mice

*Erik Z. Li, D. Leonardo Garcia-Ramirez and Kimberly J. Dougherty**

Department of Neurobiology and Anatomy, Drexel University College of Medicine, Philadelphia, PA, United States

Central pattern generators (CPGs) in the thoracolumbar spinal cord generate the basic hindlimb locomotor pattern. The locomotor CPG integrates descending commands and sensory information from the periphery to activate, modulate and halt the rhythmic program. General CPG function and response to sensory perturbations are well described in cat and rat models. In mouse, roles for many genetically identified spinal interneurons have been inferred from locomotor alterations following population deletion or modulation. However, the organization of afferent input to specific genetically identified populations of spinal CPG interneurons in mouse remains comparatively less resolved. Here, we focused on a population of CPG neurons marked by the transcription factor Shox2. To directly test integration of afferent signaling by Shox2 neurons, sensory afferents were stimulated during patch clamp recordings of Shox2 neurons in isolated spinal cord preparations from neonatal mice. Shox2 neurons broadly displayed afferent-evoked currents at multiple segmental levels, particularly from caudal dorsal roots innervating distal hindlimb joints. As dorsal root stimulation may activate both flexor- and extensor-related afferents, preparations preserving peripheral nerves were used to provide more specific activation of ankle afferents. We found that both flexor- and extensor-related afferent stimulation were likely to evoke similar currents in a given Shox2 neuron, as assessed by response polarity, latency, duration and amplitude. It has been proposed that Shox2 neurons can be divided into neurons which contribute to rhythm generation and neurons that are premotor by the absence and presence of the V2a marker Chx10, respectively. Response to afferent stimulation did not differ based on Chx10 expression. Although currents evoked in response to flexor and extensor afferent activation did not follow expected functional antagonism, they were consistent with the observation that stimulation of flexor- and extensor-related afferents both reset the phase of ongoing fictive locomotion to flexion in neonatal mice. Together, the data suggest that Shox2 neurons are interposed in multiple sensory pathways and low threshold proprioceptive input reinforces sensory perturbation of ongoing locomotion by similarly activating or inhibiting both the rhythm and patterning layers of the CPG.

Keywords: locomotion, central pattern generator, spinal cord, interneuron, sensory input

OPEN ACCESS

Edited by:
Claire Francesca Meehan, University of Copenhagen, Denmark

Reviewed by:
Simon Arthur Sharples, University of St Andrews, United Kingdom
Hans Hultborn, University of Copenhagen, Denmark

***Correspondence:**
Kimberly J. Dougherty
kjd86@drexel.edu

Specialty section:
This article was submitted to Cellular Neurophysiology, a section of the journal Frontiers in Cellular Neuroscience

Received: *06 August 2019*
Accepted: *20 September 2019*
Published: *09 October 2019*

Citation:
Li EZ, Garcia-Ramirez DL and Dougherty KJ (2019) Flexor and Extensor Ankle Afferents Broadly Innervate Locomotor Spinal Shox2 Neurons and Induce Similar Effects in Neonatal Mice. Front. Cell. Neurosci. 13:452. doi: 10.3389/fncel.2019.00452

INTRODUCTION

Locomotion is an essential part of the behavioral repertoire of many animals for seeking resources or escaping danger and is frequently accomplished by means of a repetitive motor pattern. In humans and other vertebrates, neural circuits in the spinal cord known as locomotor central pattern generators (CPGs) are capable of generating this basic motor pattern. In humans, these circuits are localized in the thoracolumbar spinal cord and an analogous region exists for hindlimb locomotion in quadrupedal animals such as cats and rodents. Although CPG circuits can independently generate the basic rhythm and alternating motor pattern, descending control from supraspinal structures and ascending sensory inputs from proprioceptors and cutaneous afferents are normally integrated to enable skilled and automated movements (Goulding, 2009; Kiehn, 2016). Understanding CPG circuit organization and sensory modulation of the circuit may be essential to develop strategies for locomotor recovery in several pathologies including spinal cord injury, stroke and multiple sclerosis.

Sensory afferents play an important role in the generation and modulation of context-appropriate shifts in locomotor stance/swing timing and muscle force. Experiments in cats and rats have allowed very fine partitioning of sensorimotor function during locomotion and resulted in significant advances in understanding CPG control (McCrea, 2001; Rossignol et al., 2006). For example, spinally transected cats can adapt locomotor frequency to match treadmill speed and this behavior is abolished following dorsal root transection (Andersson et al., 1978; Grillner and Rossignol, 1978). In a similar fashion, sinusoidal movements of the hip can entrain ongoing locomotor-like nerve outputs in an animal model treated with a neuromuscular blocker (Andersson and Grillner, 1983). Throughout the stance phase, input from ankle extensors also provide speed-dependent enhancement of force generation in hindlimb extensor muscles (Duysens and Pearson, 1980; Conway et al., 1987; Gossard et al., 1994; Guertin et al., 1995; Mayer et al., 2018).

In addition to relatively long-lasting sensory inputs, locomotor generation is also sensitive to acute sensory signals. Brief electrical stimulation of ankle extensors in the cat terminates ongoing flexor activity and initiates extensor activity (Conway et al., 1987). In the normal transition of stance to swing, hip angle at swing onset is relatively constant across a range of locomotor tasks (Lam and Pearson, 2001; McVea et al., 2005). Furthermore, acute stretch of hindlimb flexor muscles at the hip and ankle can also initiate a new flexor phase (Perreault et al., 1995; Hiebert et al., 1996; Stecina et al., 2005). Additionally, activation of the foot cutaneous afferents evokes a stumbling corrective response to avoid an obstacle (Prochazka et al., 1978; Wand et al., 1980; Mayer and Akay, 2018).

The ability of sensory signals to entrain and perturb locomotion strongly implies that sensory afferents have access to CPG circuit elements, likely through multiple distinct and possibly overlapping pathways. In the cat and rat models, these effects are well established, but it has been difficult to determine the CPG neuronal elements which receive and integrate sensory information, partly because no clear anatomic nuclei can reliably identify such interneurons. Similarly, computational models based on the cat and rat experimental results are limited in the data available to directly identify classes of spinal neurons comprising the CPG (Brown, 1911; Pearson and Duysens, 1976; Grillner, 1981; McCrea, 2001; Rybak et al., 2006a,b; Guertin, 2009). Sensory modulation of locomotor activity is also known to occur in the mouse, but the effects are less fully described (Hinckley et al., 2010; Akay et al., 2014; Takeoka et al., 2014). However, by leveraging transgenic tools available in the mouse model, many neuronal populations with locomotor functions have been identified and a putative circuit architecture has been proposed (for review see Rybak et al., 2015). Data from the cat and rat and from the mouse are therefore complementary in that sensory effects are well-described in the cat and rat but circuit elements are difficult to identify, and vice-versa in the mouse. Therefore, understanding the mechanisms by which sensory information is conveyed to CPG neurons in the mouse will not only provide novel information regarding CPG circuit organization and connectivity, but will also provide an important link between these two bodies of literature.

Sensory perturbations which have strong locomotor effects are likely to be mediated by neurons which participate in the generation of locomotor rhythm. Although a marker which can reliably and specifically label all such neurons remains elusive, specific genetically identified populations of neurons are thought to comprise subsets of the rhythm-generating (RG) kernel (Brownstone and Wilson, 2008; Dougherty and Ha, 2019). Here, we focus on neurons identified by the transcription factor Shox2, a subset of which have been proposed to play a role in locomotor rhythm generation (Dougherty et al., 2013).

The goals of this study were to determine how proprioceptive afferent information reaches Shox2 neurons and affects fictive locomotion in mouse. We demonstrate that Shox2 neurons receive broad innervation from sensory afferents in the quiescent state, likely mediated by a minimally disynaptic pathway. Based on effects seen in the cat and rat, we hypothesized that low-threshold input from ankle extensor and flexor afferents would induce opposing effects in Shox2 neurons. Instead, we found that most Shox2 neurons receive similar postsynaptic currents following both ankle extensor stimulation and ankle flexor stimulation which were predominantly inhibitory and could be long duration. Shox2 neurons are known to overlap with the V2a population and more specific labeling of RG neurons can be accomplished by specifically targeting non-V2a Shox2 neurons ($Shox2^{RG}$). The V2a Shox2 subpopulation ($Shox2^{PF}$) is thought to be enriched for downstream interneurons which recruit motor neurons, a function that has been referred to as pattern forming (PF) (Rybak et al., 2006a,b, 2015). $Shox2^{PF}$ neurons which responded to ankle afferent stimulation were preferentially situated in rostral lumbar segments, but the response patterns otherwise did not differ between $Shox2^{RG}$ and $Shox2^{PF}$ neurons. This corresponded with the finding that both ankle flexor and extensor afferent stimulation reset ongoing fictive locomotion by activating flexor motor pools. Taken together, this suggests that low threshold proprioceptive input may reach rhythm and

patterning layers similarly, thereby reinforcing the sensory effect on locomotion at both levels.

MATERIALS AND METHODS

All experimental procedures were approved by the Institutional Animal Care and Use Committee at Drexel University and followed the guidelines of the National Institutes of Health for laboratory animal welfare. Experiments were performed using Shox2::Cre (Dougherty et al., 2013); Rosa26-flox-Stop-flox-tdTomato (Ai9 from Jax Mice, #007909, Madisen et al., 2010) or in Shox2::Cre;Ai9;Chx10eGFP (also called Vsx2-eGFP, MMRRC, 011391-UCD, Gong et al., 2003) transgenic mice.

Spinal Cord Preparations

Spinal cords preparations were isolated from postnatal day (P)1 to P4 mice. Briefly, mice were decapitated and eviscerated, after which the vertebral bodies were removed to expose the spinal cord. The spinal cord and attached dorsal root ganglia (DRG) were then removed in ice cold dissecting solution. Spinal cord preparations were isolated in a dissecting solution bubbled with 95% O_2/5% CO_2 (carbogen) containing in mM: 111 NaCl, 3 KCl, 11 glucose, 25 $NaHCO_3$, 3.7 $MgSO_4$, 1.1 $KH2PO_4$, and 0.25 $CaCl_2$.

Peripheral Nerve Dissection

In some experiments, the dissection was extended to include hindlimb peripheral nerves. Care was taken during removal of the vertebral bodies to avoid damaging spinal nerves. Hindlimb muscles were removed to expose the sciatic nerve and its branches, which were then dissected free. In mice, there is strain-specific variation in lumbar spinal cord anatomy (Rigaud et al., 2008). Spinal roots from the third and fourth lumbar levels are the primary contributions to the sciatic nerve in the mice used for this study.

Accessing Shox2 Neurons

In order to visualize Shox2 neurons for whole cell patch clamp, it was necessary to create a tissue window. To prevent compression of the cord, spinal meninges were first carefully removed or split over incision sites. In experiments using a ventral horn-removed preparation, a section of ventral horn was removed (L2-S2) using a surgical microknife (5.0 mm cutting edge, 15.0 cutting angle, Fine Science Tools #10315-12) to gain visual access to spinal interneurons for patch clamp. For experiments using a hemisect preparation, a unilateral section of spinal cord (L2-S2) was removed. Following isolation, spinal cords were transferred to room temperature (RT) artificial cerebral spinal fluid (ACSF) recording solution containing in mM: 111 NaCl, 3 KCl, 11 glucose, 25 $NaHCO_3$, 1.3 $MgSO_4$, 1.1 KH_2PO_4, and 2.5 $CaCl_2$. Cords were incubated in carbogen-bubbled ACSF for a minimum of 30 min prior to recording.

Preparations From Older Mice

In subsets of some experiments, mice aged P5–P14 were used. Mice <P8 were dissected using the procedures described above. Mice P8 and older were first anesthetized with isoflurane prior to decapitation and spinal cords were isolated using an alternative glycerol-based dissecting solution bubbled with carbogen and containing in mM: 3 KCl, 11 glucose, 25 $NaHCO_3$, 1.3 $MgSO_4$, 1.1 KH_2PO_4, 2.5 $CaCl_2$, 222 glycerol. Following isolation, these cords were incubated in carbogen-bubbled recording ACSF at 37°C for 30 min and then allowed to equilibrate to RT for 30 min prior to recording.

Electrophysiology

Patch Clamp

Shox2 neurons were recorded in ACSF and visually identified at 63× on an Olympus BX51WI microscope with LED illumination (X-Cite) by red fluorescence (Semrock Brightline CY3-4040C). In cords from Shox2::cre;Ai9;Chx10eGFP mice, Shox2 neurons were further specified by the V2a-specific marker Chx10 into the Chx10-negative $Shox2^{RG}$ or the Chx10-positive $Shox2^{PF}$ based on green fluorescence (Semrock Brightline FITC-3540C). Intracellular electrodes were pulled to 5–8 MΩ using a Sutter P-1000 and filled with intracellular solution containing in mM: 128 K-gluconate, 10 HEPES, 0.0001 $CaCl_2$, 1 glucose, 4 NaCl, 5 ATP, and 0.3 GTP. Cells were recorded in whole-cell configuration from the soma using a Multiclamp 700B and digitized at 10–20 kHz with an Axon Digidata 1550A connected to a PC tower running Clampex.

Afferent Stimulation and Spinal Root Recordings

During recordings of Shox2 neurons, dorsal roots or peripheral nerves were stimulated with tight-fitting glass suction electrodes to activate afferent sensory pathways. Ventral roots were cut free proximal to the spinal nerve to prevent transmission of antidromic axon potentials in efferent motor pathways. Dorsal root and peripheral nerves were stimulated using 50 μs square pulses with a 10 s interstimulus interval to reduce effects of short-term synaptic plasticity. Pulse waveforms were generated by either an Axon Digidata 1550A or an AMPI Master-9 pulse stimulator connected to an optical stimulus isolator. In some experiments, afferent volleys in dorsal roots or ventral root reflexes were also recorded. Signals were amplified 1000× and bandpass filtered from 10 Hz to 1 kHz using a model MA 102 amplifier (custom built in the workshop of the Zoological Institute, University of Cologne, Germany), then digitized at 100 kHz with an Axon Digidata 1550A connected to a PC. Where reported, stimulus threshold (1 × T) for afferent volley or ventral root reflex was defined as the minimum current respectively necessary to reliably evoke dorsal root or ventral root responses in 10/10 trials.

Postsynaptic Current Analysis

Post-stimulation currents recorded in Shox2 neurons were categorized as stimulation-evoked if the response was present in at least 8 out of 10 stimulation trials. Current components were identified as inhibitory or excitatory based on reversal potential (inhibitory < -35 mV, excitatory > -5 mV). Current properties including latency, peak amplitude and duration were measured using Clampfit 10 (Molecular Devices). Latency was measured as

the difference between the time that the current exceeded pre-stimulus baseline levels and the time of stimulation. Jitter was defined as the standard deviation in the latency of the earliest current components. Amplitude is reported and analyzed as absolute value. Where data is presented using box and whisker plots, the boxplot labels median, 1st quartile and 3rd quartile, with whiskers extending to 1.5× the interquartile range beyond the 1st and 3rd quartiles.

Measurement of Cell Location

Many genetically labeled interneuron populations show differences in function or connectivity that is dependent on cellular position. In this study, cellular position was measured and reported as segmental level, mediolateral position and dorsoventral position. Distances were measured from images captured at 10× immediately following cell recordings and before removing the patch electrode. These measurements were then normalized according to the following procedures. The center point of the dorsal root at the entry zone is designated as segment number and Shox2 segmental level is normalized such that the distance between each dorsal root entry zone center point is 1. Mediolateral position is reported as the distance between the cell and the midsagittal plane divided by distance between the lateral tissue border and the midsagittal plane, resulting in a normalized value from 0 (medial) to 1 (lateral). Similarly, dorsoventral position is reported as the distance between the cell and the dorsal tissue border divided by the distance between the dorsal and ventral tissue borders, resulting in a normalized value from 0 (dorsal) to 1 (ventral).

Locomotor Experiments

Spinal cords were prepared from P1–P3 mice with attached peripheral nerves. Fictive locomotion was evoked with 7 μM *N*-methyl-D-aspartate (NMDA) and 8 μM serotonin (5-HT). Cords were allowed to equilibrate with the locomotor cocktail for at least 15 min prior to recording. Flexor- and extensor-related locomotor activity were respectively recorded from L1 and L4 ventral roots using tight-fitting glass suction electrodes and digitized at 10 kHz. Locomotor burst envelopes were generated by rectifying and low-pass filtering at 0.25–0.55 Hz. Locally-weighted scatterplot smoothing (LOWESS) with a 3–60 s window was used to generate a locally adaptive signal threshold for burst onset and offset. For perturbation experiments, trains of electrical stimulation (4–6 pulses, 50 μs pulse duration, 20 Hz) were delivered to peripheral nerves in 100 s intervals. In these preparations, ventral roots were transected proximal to the spinal nerve to prevent antidromic transmission along motor fibers.

Statistical Tests and Reporting

Univariate descriptive statistics were reported as mean ± standard deviation and range unless otherwise specified. Statistical tests were performed using the R 3.6.0 software package with a criterion $\alpha < 0.05$ for significance. All statistical tests were performed on raw values even when plotted on log-axes for visualization. Categorical data was analyzed using Chi-squared tests, with Yate's continuity correction used for 2 × 2 contingency tables. For comparisons between groups of continuous variables, normality was first tested using the Shapiro–Wilk test and homogeneity of variances (homoscedasticity) was tested using the Fligner-Killeen test of homogeneity of variances. For two groups, comparisons of normally-distributed data were performed using Welch's unequal variance *t*-tests. For more than two groups, comparisons of normally-distributed data were performed with one-way ANOVA for homoscedastic data and Welch's unequal variances ANOVA for heteroscedastic data. *Post hoc* comparisons following non-parametric ANOVAs were performed with Tukey's honest significant differences test. Comparisons of non-normal data were performed with the Wilcoxon rank sum test (Mann–Whitney *U* Test) for two groups or Kruskal–Wallis rank sum test (parametric ANOVA) for more than two groups. When applied to heteroscedastic data, parametric tests were interpreted as tests of stochastic dominance rather than location. *Post hoc* comparisons following Kruskal–Wallis rank sum tests were performed using Dunn's test corrected for multiple comparisons using the Holm–Bonferroni method (Dinno, 2015).

RESULTS

Shox2 Neurons Receive Input From Sensory Afferent Pathways

Sensory inputs may have either local or distant effects on spinal circuits. Ankle afferents, in particular, have been shown to influence activity at hip and knee joints (Duysens and Pearson, 1980; Angel et al., 1996). We therefore first investigated the distribution of Shox2 neurons receiving sensory input from different segmental regions by determining whether Shox2 neurons received postsynaptic currents in the quiescent state following afferent stimulation at rostral and caudal lumbar levels. Shox2 neurons are located in the intermediate and ventral regions of the spinal cord which is fortuitous for various reduced preparations to visually access these neurons for whole cell patch clamp recordings. For these experiments, the most ventral part of the spinal cord was removed from isolated spinal cords prepared from P1–P14 mice, allowing fluorescently labeled Shox2 neurons to be visualized for whole-cell patch clamp recordings (**Figure 1A**). Rostral (L1 or L2) and caudal lumbar (L4 or L5) dorsal roots were stimulated while Shox2 neurons were monitored with whole cell recordings.

Recorded postsynaptic currents were considered to be stimulation evoked if they were present in at least 8 out of 10 trials (**Figure 1B**). Nearly all Shox2 neurons displayed postsynaptic currents in response to L4/L5 DR stimulation (95%, 21/22 from 12 mice). Currents were also observed in Shox2 neurons following L1/L2 DR stimulation, albeit less often (42%, 8/19 from 9 mice; **Figure 1C**). Threshold for L4/L5-evoked response in Shox2 neurons (39.81 ± 22.60 μA, range 15.00–100.00 μA) was lower than for L1/L2-evoked responses (124.38 ± 93.33 μA, range 60.00–350.0 μA) (Wilcoxon rank sum test, $W = 160.5$, $p = 0.0002$, data not shown). Evoked currents recorded in Shox2 neurons often had more than one component and could be divided into those containing purely excitatory components, purely inhibitory components, or both

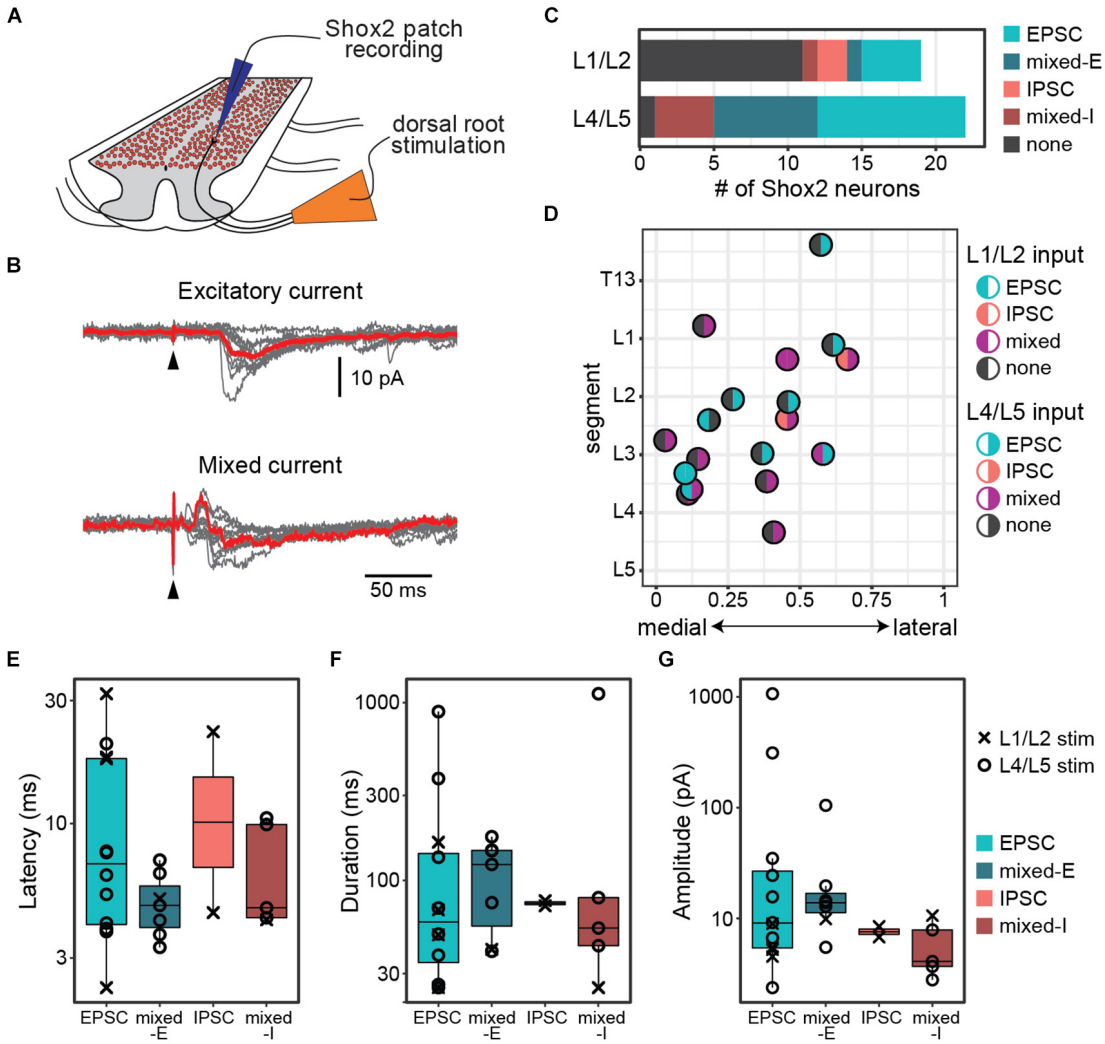

FIGURE 1 | Postsynaptic currents are detected in Shox2 neurons following dorsal root stimulation. **(A)** Cartoon of experimental setup for the ventral horn-removed experiments. Dorsal roots were stimulated while recording from Shox2 neurons (red) in lumbar segments of cords isolated from Shox2::cre;Rosa26-lsl-tdTomato mice. **(B)** Postsynaptic currents were recorded in Shox2 neurons in response to stimulation of rostral (L1 or L2) and/or caudal (L4 or L5) lumbar dorsal roots. Evoked currents in Shox2 neurons were only excitatory (EPSC), only inhibitory (IPSC), or mixed with shortest latency components that were excitatory (mixed-E) or inhibitory (mixed-I). Top: example showing excitatory current. Gray traces show 10 individual trials and red trace shows average. Black triangle indicates stimulation artifact. Bottom: example showing mixed-I current. **(C)** Number of recorded Shox2 neurons displaying postsynaptic currents in response to stimulation of dorsal L1/L2 (8/19) and L4/L5 roots (21/22). **(D)** Responses of Shox2 neurons in which both L1/L2 and L4/L5 stimulation were tested are plotted according to lumbar level and mediolateral position. The color of each point is based on response (EPSC in teal, IPSC in pink, mixed in purple, and gray for no response) following L1/L2 (left half) and L4/L5 (right half) stimulation. The center point of the dorsal root at the entry zone is designated as segment number. **(E–G)** Latency, duration, and amplitude were characterized for each response to L1/L2 (x) and L4/L5 (o) stimulation and plotted on log scale for better visualization of points.

(mixed responses). Mixed responses could be further divided into those with shortest latency components that were excitatory (mixed-E) or inhibitory (mixed-I). L1/L2 stimulation elicited a mix of all response types in the Shox2 neurons with observed evoked currents. Shox2 neurons displayed EPSCs or mixed currents following L4/5 stimulation, but not currents composed solely of IPSCs. However, when considering only Shox2 neurons in which a postsynaptic current was observed, no difference was detected in the distribution of these response subtypes when comparing L1/L2 and L4/L5 dorsal root stimulation (χ^2 = 6.31, df = 3, p = 0.10). In a subset of Shox2 neurons (18/23), the response to both L1/L2 and L4/L5 DR stimulation was tested (**Figure 1D**). No association was observed between current presence/absence following L1/L2 and following L4/L5 DR stimulation (χ^2 = 0.055, df = 1, p = 0.81). Currents evoked in Shox2 neurons following L1/L2 and L4/L5 dorsal root stimulation had similar proportions of current response types (χ^2 = 6.31, df = 3, p = 0.097). We were also unable to detect any segmental variation in Shox2 neuron response presence for L1/L2 stimulation (Kolmogorov–Smirnov test, segmental level of neurons receiving or not receiving currents following L1/L2 stimulation: D = 0.18, p = 0.98)

or L4/L5 stimulation (all but 1 tested neuron responded to L4/L5 stimulation).

To better understand the effects of afferent stimulation on Shox2 neurons, we characterized the response latency, duration and amplitude (**Figures 1E–G**). Most (85.7%, 18/21) Shox2 neurons which responded to L4/L5 stimulation responded to currents at strengths of 50 μA, so responses were characterized at this strength to reduce the possibility of activating high-threshold nerve fibers. Neurons responding to L1/L2 typically required much stronger dorsal root stimulation, so currents resulting from L1/L2 stimulation were characterized close to the threshold to observe a current response (<20 pA above threshold). Overall, response latencies were 8.65 ± 7.37 ms (range 2.3–31.9 ms) from the stimulation, suggesting that sensory stimulation can access Shox2 neurons through multiple pathways with differing numbers of interposed interneurons. No difference in latency distribution was observed between responses with an initial excitatory or inhibitory component (Kolmogorov–Smirnov test, $D = 0.42$, $p = 0.90$), nor could we detect a difference in latency between different response types (Kruskal–Wallis rank sum test, $\chi^2 = 2.34$, df = 3, $p = 0.505$). Since inhibitory and excitatory responses showed no difference in response latency, it is likely that most inputs to Shox2 neurons are not monosynaptic. Response durations (159.0 ± 261.64 ms, range 24.97–1120.0 ms), here considered as the total duration of the multicomponent input, and postsynaptic current peak amplitudes (66.21 ± 213.02 pA, range 2.38–1066.66 pA) were highly variable and similarly showed no difference between different response subtypes (Kruskal–Wallis rank sum test, duration: $\chi^2 = 1.01$, df = 3, $p = 0.80$; amplitude: $\chi^2 = 5.52$, df = 3, $p = 0.14$). Further, there were no significant differences between L1/2 and L4/5 evoked EPSCs in Shox2 neurons for any measure described (Wilcoxon rank sum test, latency: $W = 22$, $p = 0.37$; duration: $W = 13.5$, $p = 0.73$; amplitude: $W = 27$, $p = 0.073$). In summary, we observe that Shox2 neurons across the lumbar segmental and mediolateral extent of the cord respond robustly to L4/L5 stimulation, likely through a heterogeneous set of sensory processing pathways.

Stimulation of Both Common Peroneal and Tibial Nerves Induce Postsynaptic Currents in Shox2 Neurons

In the lumbar region of the spinal cord, ventral root activity from the rostral and caudal levels has been found to correspond respectively to flexor and extensor motor activity in the hindlimb. However, a single ventral or dorsal root innervates multiple muscle groups that can span several joints and may include both flexors and extensors (Vejsada and Hník, 1980; Peyronnard and Charron, 1983). Dorsal root stimulation at any lumbar level is likely to activate both flexor- and extensor-related proprioceptive pathways simultaneously. Therefore, evoked currents measured in Shox2 neurons in response to dorsal root stimulation could result from activation of pathways that are flexor-related, extensor-related or both.

To address this issue, we modified our ventral horn-removed preparation to include preserved hindlimb peripheral nerves and isolated common peroneal (CPn) and tibial nerves (Tn) to provide more specific activation of flexor- and extensor-related proprioceptors around the ankle joint (**Figure 2A**). For these experiments, neonatal mice ≤ P7 were utilized. The CPn suction electrode was attached at the level of the fibular neck to activate flexor-related afferents. The Tn suction electrode was attached proximal to the nerve branches innervating the medial and lateral gastrocnemius (extensor) muscles. Stimulation threshold for currents evoked in Shox2 neurons was found to be 60.2 ± 48.4 μA for CPn and 70.0 ± 54.3 μA for Tn. Therefore, presence and properties of evoked currents were characterized from 100 to 150 μA stimulation, which was sufficient to evoke reliable responses in most Shox2 neurons receiving input from either nerve.

Postsynaptic currents were detected in 46% (12/26 from 12 mice) of tested Shox2 neurons following CPn stimulation and 18% (5/27 from 13 mice) following Tn stimulation. Currents could be divided into excitatory, inhibitory or mixed responses as described above. The proportion of response types was not significantly different between responses to CPn and Tn stimulation ($\chi^2 = 4.69$, df = 3, $p = 0.20$; **Figure 2B**). As only 4 responses were mixed, these were not subdivided into mixed-E and mixed-I populations for further analyses.

In 96% (26/27 from 13 mice) of recorded neurons, both Tn and CPn stimulation were tested (**Figure 2C**). Presence or absence of currents evoked in response to CPn stimulation was not found to be associated with Tn evoked current presence ($\chi^2 = 1.42$, df = 1, $p = 0.23$). Shox2 neurons located throughout the lumbar cord responded to both CPn and Tn stimulation (**Figure 2C**). No differences were detected in the segmental distribution of Shox2 neurons on the basis of CPn stimulation response or Tn stimulation response presence (Kolmogorov–Smirnov test, segmental level of neurons receiving or not receiving currents following CPn stimulation: $D = 0.20$, p-value = 0.90; following Tn stimulation: $D = 0.37$, $p = 0.50$). Further, there were no apparent differences in medial-lateral distribution. 15% (4/26) of Shox2 neurons displayed postsynaptic currents in response to both CPn and Tn stimulation. In these neurons, 75% (3/4) of neurons showed concordance in current type following CPn and Tn stimulation, but these included excitatory, inhibitory and mixed current response types (**Figure 2C**). In the fourth neuron, CPn and Tn stimulation both induced early excitatory postsynaptic currents, but there was also a longer latency inhibitory current (mixed-E) following Tn stimulation.

We also characterized the latency, duration, and amplitude of these evoked currents (**Figures 2D–F**). Overall latencies were 14.46 ± 5.52 ms (range 7.51–26.47 ms). No significant differences in latency or duration were detected between excitatory, inhibitory or mixed response types (Kruskal–Wallis rank sum test, latency: $\chi^2 = 2.29$, df = 2, $p = 0.32$; duration: $\chi^2 = 1.0392$, df = 2, $p = 0.59$). Primary afferents fibers are glutamatergic, so inhibitory postsynaptic currents measured in Shox2 neurons are mediated by minimally disynaptic pathways.

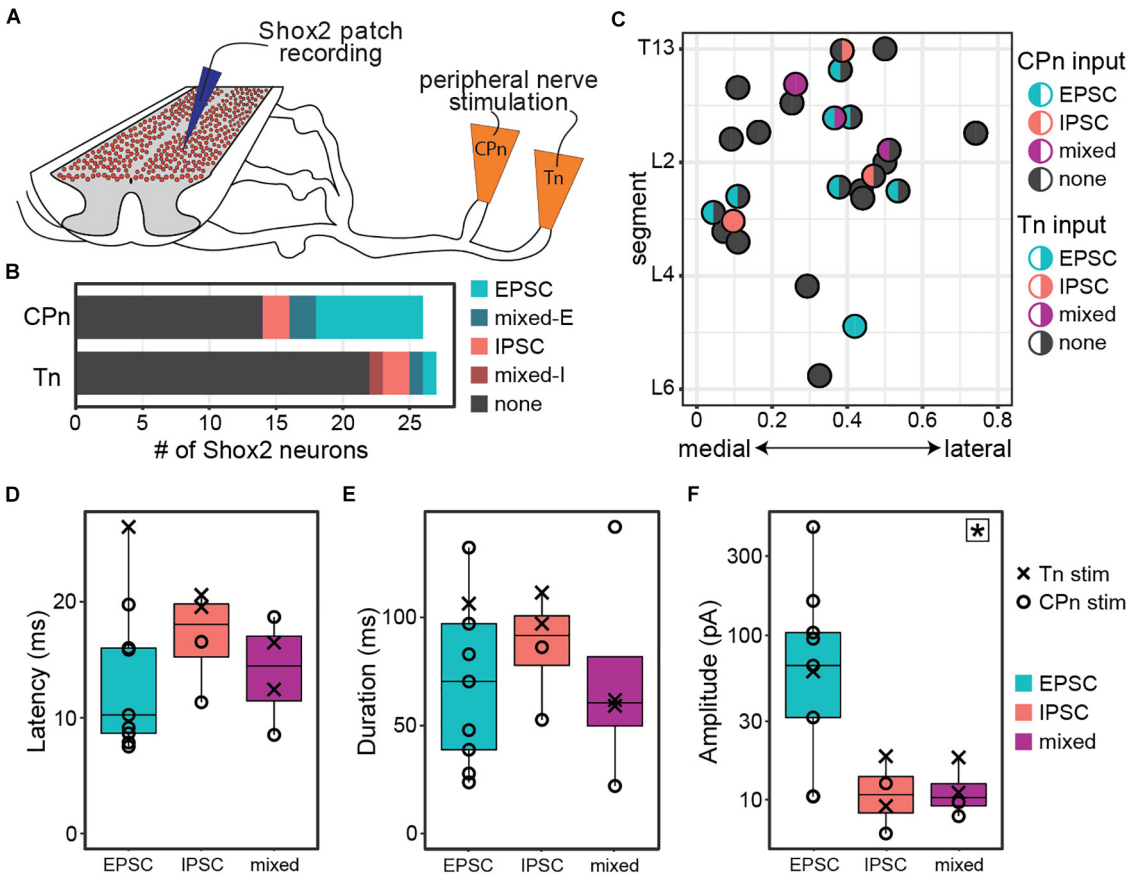

FIGURE 2 | Both common peroneal and tibial nerve stimulation can induce postsynaptic currents in Shox2 neurons. **(A)** Cartoon of ventral horn-removed spinal cord preparation with intact sciatic nerve branches for stimulation of common peroneal (CPn) and tibial nerves (Tn). **(B)** The proportion of excitatory, inhibitory, mixed-E, and mixed-I currents detected in Shox2 neurons following CPn stimulation and following Tn stimulation. **(C)** Shox2 neurons recorded during stimulation of both CPn and Tn are plotted according to anatomical position and color-coded based on response type. Segment number corresponds to the center point of the dorsal root at the entry zone. Shox2 neurons displaying postsynaptic currents to CPn and Tn stimulation were observed throughout the lumbar cord. **(D–F)** Latency, duration and amplitude plotted for each response subtype. Mixed-E and mixed-I responses were pooled into a single mixed subtype. Latency and duration did not significantly differ between evoked excitatory, inhibitory or mixed currents, whereas peak amplitude differed significantly between current types ($p = 0.027$, indicated by star in upper right corner). *Post hoc* testing did not detect significant pairwise comparisons when corrected for multiple comparisons (see text for details). Amplitude plotted on log scale for clarity.

As excitatory and inhibitory response latencies are comparable, we therefore suggest that both excitatory and inhibitory responses are primarily mediated by minimally disynaptic pathways. However, we observed a subset of cells with excitatory currents (5/9) with latencies shorter than the earliest inhibitory responses observed (**Figure 2D**, <11.34 ms); thus we cannot rule out the possibility of monosynaptic excitatory connections between primary afferents and Shox2 neurons. Current amplitudes differed between excitatory, inhibitory and mixed currents, but *post hoc* testing was unable to identify which currents differed in pairwise comparisons when corrected for multiple comparisons (Kruskal–Wallis rank sum test, $\chi^2 = 7.26$, df = 2, $p = 0.027$; *post hoc* Dunn's test, EPSC-IPSC: $p = 0.088$, EPSC-Mixed: $p = 0.059$, IPSC-Mixed: $p = 1.0$). Larger EPSC amplitudes may be expected, given that both resting membrane potential and the holding potential for measurements (−50 mV) are near the chloride reversal potential. Taken together, only subsets of Shox2 neurons in this preparation receive input from CPn and/or Tn. CPn input was observed more frequently and the observed postsynaptic currents are predominantly excitatory.

Input From Ankle Afferents to Shox2 Neurons Involved in Rhythm Generation and Pattern Formation Is Heterogenous but Primarily Inhibitory in the Hemisect Preparation

CPG circuits consist of neuronal elements spread across several lamina and many of these elements are likely removed in the ventral horn-removed preparation (Kiehn and Butt, 2003). However, each lateral half of the lumbar cord is thought to contain a CPG circuit for the ipsilateral hindlimb (Whelan et al., 2000; Frigon et al., 2013; Rybak et al., 2015). In order to preserve ventral horn CPG elements and to record motor activity

via the ventral roots, we switched to a hemisect preparation, again in mice ≤ P7 (**Figure 3A**). In this preparation, afferent volleys and ventral root reflexes (VRR) can be observed following peripheral nerve stimulation (**Figures 3B,C**). VRR threshold was defined as the lowest stimulation amplitude in which a deflection in the root recording was consistently observed. As the deflection at threshold is very small and comparatively long-lasting, it may correspond to a subthreshold depolarization of the motor neuron pool. As stimulus intensity is increased, we observe a progressive increase in afferent fiber and motor neuron recruitment. In a subset of preparations, we recorded either the afferent volley or VRR following Tn stimulation and quantified the threshold. Afferent volley threshold (25.29 ± 9.52 μA, range 12–40 μA) was not significantly different from VRR threshold (22.64 ± 9.90 μA, range 11–40 μA) but it should be noted that the volley and reflex were not recorded in the same preparation in most cases (**Figure 3D**). In 3 preparations, both afferent volley and VRR were measured from the same preparation. In these animals, the afferent volley threshold is lower than the VRR threshold.

To target low threshold sensory afferents and avoid activating nociceptive C-fibers, stimulation was delivered at 2 times threshold (×T) for a VRR (Kiehn et al., 1992; Talpalar et al., 2011; Bui et al., 2013). Threshold for VRR was similar between CPn (21 ± 10.2 μA, range 9–45 μA) and Tn (21.9 ± 11.8 μA, range 10–43 μA) (Wilcoxon rank sum test, $W = 99.5$, $p = 0.96$, data not shown). Postsynaptic currents were measured from Shox2 neurons and included in analysis if a postsynaptic current was observed in response to nerve stimulation in at least 80% of trials. The majority (85.5%, 65/76 from 17 mice) of evoked currents occurred in 100% of experimental trials. Most neurons showed responses that were multicomponent. Shox2 neurons were recorded in voltage clamp configuration at membrane potentials from −80 to 10 mV to better isolate excitatory and inhibitory components (**Figure 4A**). As before, responses were categorized into EPSC, IPSC, mixed-E and mixed-I categories. For most cases of mixed responses, the excitatory and inhibitory components came in a fixed order in response to each stimulus.

In order to more specifically target Shox2 neurons proposed to be involved in rhythm generation and premotor neurons involved in pattern formation, experiments in the hemisect preparation were performed in Shox2cre;R26-lsl-tdTomato;Chx10GFP mice so that recorded neurons could be classified as putative $Shox2^{RG}$ ($tomato^{+}GFP^{-}$) or $Shox2^{PF}$ ($tomato^{+}GFP^{+}$) based on fluorescent protein expression. 61% (24/39 from 17 mice) of $Shox2^{RG}$ and 48.0% (12/25 from 10 mice) of $Shox2^{PF}$ neurons responded to CPn stimulation (**Figure 4B**). 67.5% (27/40) of $Shox2^{RG}$ and 52.0% (13/25) of $Shox2^{PF}$ neurons responded to Tn stimulation. No significant difference was detected between the proportion of $Shox2^{RG}$ and $Shox2^{PF}$ neurons which responded to CPn ($\chi^2 = 0.65$, df = 1, $p = 0.42$) or Tn stimulation ($\chi^2 = 0.98$, df = 1, $p = 0.32$). In the hemisect preparation, unlike the ventral horn-removed preparation, the overall proportions of Shox2 neurons responding to CPn and Tn stimulations were similar (CPn: 56.25%, 36/64 neurons; Tn: 61.5%, 40/65; $\chi^2 = 0.19$, df = 1, $p = 0.67$).

Unlike the data from the ventral horn-removed preparations, most recorded responses were inhibitory (**Figure 4B**). Of the 76 postsynaptic currents measured in $Shox2^{RG}$ and $Shox2^{PF}$ neurons following peripheral nerve stimulation, 14.5% (11/76) were EPSCs, 10.5% (8/76) were mixed-E, 64.5% (49/76) were IPSCs and 10.5% (8/76) were mixed-I. After grouping responses based on $Shox2^{RG}$/$Shox2^{PF}$ and stimulation site, no significant differences were detected in the proportion of response types received ($\chi^2 = 9.01$, df = 9, p-value = 0.44). In some neurons,

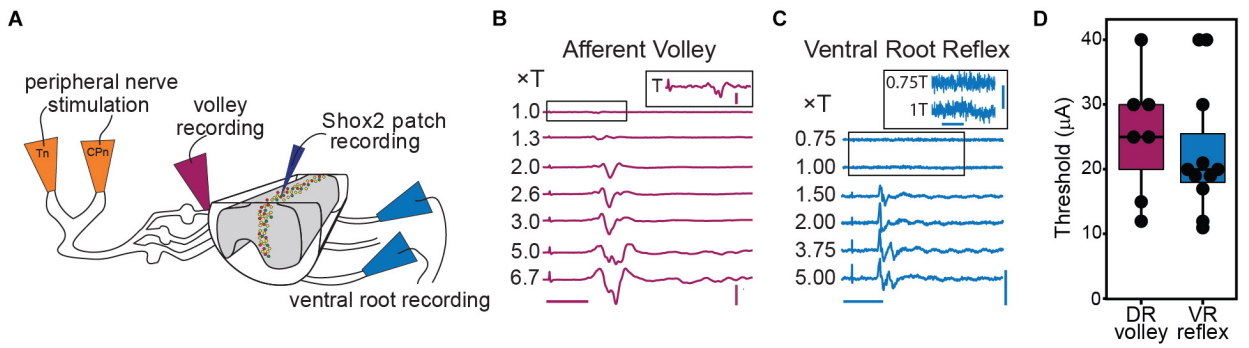

FIGURE 3 | Graded afferent stimulation in the lumbar-hemisected isolated spinal cord preparation. **(A)** Cartoon of hemisected isolated cord preparation from Shox2::cre;Rosa26-lsl-tdTomato;Chx10GFP mice ($Shox2^{RG}$ $Shox2^{+}Chx10^{-}$) neurons are red and $Shox2^{PF}$ ($Shox2^{+}Chx10^{+}$) neurons are yellow. **(B)** Examples of afferent volley recorded from L4 DR following Tn stimulation. The inset shows the boxed region of the 1.0 × T stimulation on a larger scale for clarity. The deflection on the far left of each trace is the stimulus artifact. Horizontal scale bar is 20 ms. Vertical scale bar is 0.8 mV for main figure and 0.08 mV for inset. **(C)** L4 ventral root reflexes recorded during stimulation of Tn at different stimulation intensities. Threshold was defined as the minimum current necessary to detect a response in the L4 ventral root following CPn or Tn stimulation. The boxed regions of 0.75 and 1.0 × T are shown on a different scale in the inset for clarity. The deflection seen at 1T was small yet consistent. Horizontal scale bars are 20 ms. Vertical scale bar is 0.1 mV for main figure and 0.01 mV for inset. **(D)** Stimulation intensities at threshold for afferent volley and ventral root reflexes following Tn stimulation are plotted. In most preparations, either afferent volley or ventral root reflexes were recorded, but not both.

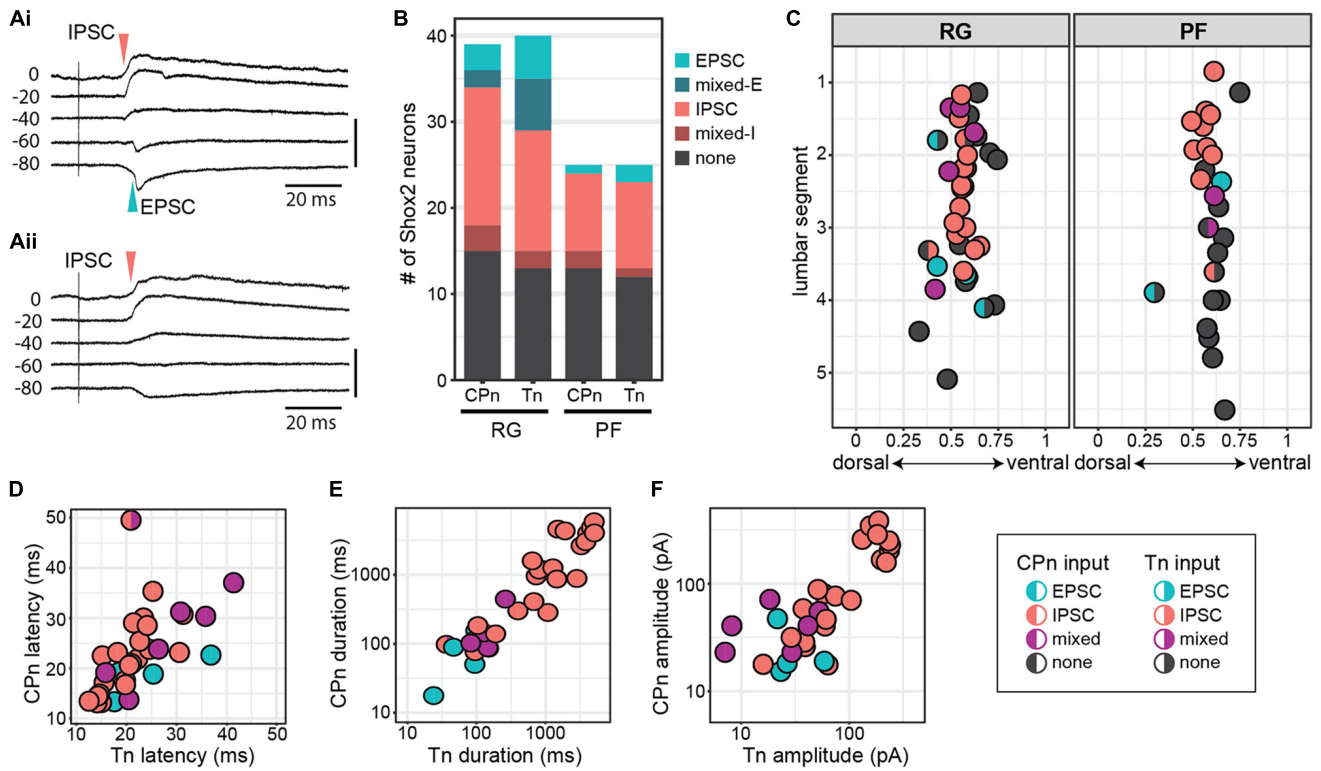

FIGURE 4 | Shox2 neurons which respond to CPn and Tn stimulation respond similarly to both. **(A)** Example traces showing intracellular currents measured from two Shox2 neurons at various membrane holding potentials following Tn stimulation at 2 × T. **(Ai)** A mixed-E response showing inhibitory outward currents (red arrow, upward deflection) followed by excitatory inward currents (green arrow, downward deflection). **(Aii)** A response showing only inhibitory currents with a reversal potential near –60 mV. **(B)** Postsynaptic current types detected in Shox2^{RG} and Shox2^{PF} neurons following stimulation of CPn and Tn. **(C)** Shox2^{RG} and Shox2^{PF} neurons at multiple segmental levels receive postsynaptic currents following CPn and Tn stimulation. Shox2 neurons responding to CPn were significantly more likely to respond to Tn as well (χ^2 = 31.99, df = 1, p = 1.55e-08). Dual responding Shox2 neurons showed a significant association between responses (EPSC, IPSC, mixed) following CPn and Tn stimulation (χ^2 = 60.06, df = 4, p = 2.82e-12), with IPSCs being most common. Data shown as a plot with neuronal position. **(D–F)** In neurons which received postsynaptic currents following CPn and Tn stimulation, response latency, duration and amplitude were positively correlated between CPn and Tn response (linear regression, latency: adjusted R^2 = 0.32, slope = 0.50, t = 4.00, p = 0.0004; duration: adjusted R^2 = 0.77, slope = 0.83, t = 10.35, p = 1.41e-11; amplitude: adjusted R^2 = 0.68, slope = 0.61, t = 8.35, p = 1.95e-09). Duration and amplitude plotted on log scale for clarity.

stimulation at 5 × T was also tested. In these neurons, the earliest current components typically did not shift from inhibitory to excitatory or vice-versa (data not shown).

Shox2 Neurons That Respond to Tn and CPn Respond Similarly to Both

Although it is predicted that CPG neurons receive synaptic input directly or indirectly from sensory afferents, the organization of those inputs onto CPG neurons is less clear. For example, it is unknown whether distinct populations of CPG neurons receive synaptic input from different sensory groups (i.e., flexor/extensor), or whether a subset of CPG neurons integrate input from multiple sensory afferents. In a subset of recorded Shox2 neurons (63/68, 92.6%), we were able to test evoked responses to both CPn and Tn stimulation. We observed postsynaptic currents in response to both CPn and Tn in 52.4% (33/63) of neurons (dual responders), to CPn only in 3.2% (2/63) of neurons, to Tn only in 9.5% (6/63) of neurons and to neither in 34.9% (22/63) of neurons. Shox2 neurons responding to CPn were significantly more likely to respond to Tn as well (χ^2 = 31.99, df = 1, p = 1.55e-08; **Figure 4C**).

Interestingly, 97.0% (32/33) of Shox2 dual responders displayed the same type of postsynaptic current (EPSC, IPSC, mixed) following stimulation of either peripheral nerve and this association was statistically significant (χ^2 = 60.06, df = 4, p = 2.82e-12). This concordance was present in both Shox2^{RG} neurons and Shox2^{PF} neurons. Rostral (above the L3 segment) Shox2^{PF} neurons were more likely to receive CPn or Tn input than caudal (L3 segment and below) Shox2^{PF} neurons (χ^2 = 5.03, df = 1, p = 0.025). In contrast, Shox2^{RG} neurons receiving CPn and Tn input did not appear to show a rostrocaudal bias (χ^2 = 0.41, df = 1, p = 0.52). In addition to response type, we also observed a positive correlation between CPn and Tn latency (23.07 ± 7.90 ms, range 12.57–49.89 ms), duration (1321.89 ± 1687.49 ms, range 15.13–5853.43 ms) and

amplitude (85.68 ± 87.65 pA, range 7.09–383.21 pA) in Shox2 dual responders (linear regression, latency: adjusted R^2 = 0.32, slope = 0.50, t = 4.00, p = 0.0004; duration: adjusted R^2 = 0.77, slope = 0.83, t = 10.35, p = 1.41e-11; amplitude: adjusted R^2 = 0.68, slope = 0.61, t = 8.35, p = 1.95e-09; **Figures 4D–F**). Considered together, these results suggest that Shox2 neurons integrate sensory information from flexor-related and extensor-related ankle afferents.

Input From Ankle Afferents to Shox2 Neurons Is Also Minimally Disynaptic in the Hemisect Preparation

Because response latencies in Shox2 neurons were variable in all preparations used, we conducted a more thorough analysis of response latency in the hemisect preparation to better understand the organization of CPG neuron sensory modulation. Response latencies were highly variable (12.5–49.9 ms) and no difference in latency distribution was detected when the data was separated by whether the earliest response was excitatory or inhibitory (Kolmogorov–Smirnov test, D = 0.14, p = 0.93; **Figure 5A**). The earliest latencies of both excitatory (23.72 ± 8.22 ms, range 13.34–41.36 ms) and inhibitory (22.85 ± 7.85 ms, range 12.57–49.89 ms) postsynaptic currents were similar, suggesting that the connections from CPn and Tn nerves to Shox2 neurons are not monosynaptic. No difference in distribution of postsynaptic current latencies was detected between Shox2^{RG} (24.2 ± 8.59 ms, range 13.13–49.89 ms) and Shox2^{PF} neurons (20.73 ± 5.73 ms, range 12.57–36.83 ms) (Kolmogorov–Smirnov test, D = 0.23, p = 0.25).

For comparison, we also measured the latency of afferent volleys measured at the L4 entry zone and latency of the L4 VRR relative to the onset of stimulation (**Figure 5B**). As with the measurement of stimulus threshold, it should be noted that the volley and reflex were not recorded in the same preparation in most cases. Because afferent volley latencies (13.04 ± 5.44 ms, range 6.14–23.49 ms) and VRR latencies (20.05 ± 10.64 ms, range 6.70–41.10 ms) were comparable to postsynaptic current latencies, it is difficult to be certain that CPn and Tn input to Shox2 neurons is not monosynaptic based on latency alone. Response jitter has been used as an additional criterion to identify monosynaptic postsynaptic events (Bui et al., 2013; Pujala et al., 2016). We therefore measured the standard deviation of postsynaptic current latency in 10 stimulation trials for each neuron (**Figures 5Ci,ii**). In some neurons, the earliest postsynaptic components were not reliable, thus resulting in higher reported jitter value (**Figure 5Ciii**). Unsurprisingly, a positive relationship was seen between latency and jitter (linear regression, slope = 0.24, t = 7.24, df = 74, p = 3.56e-10; **Figure 5D**). Jitter for inhibitory responses was 2.65 ± 2.31 ms (range 0.11–8.86 ms); excitatory responses, 2.06 ± 3.44 ms (range 0.11–12.02 ms); mixed-E responses, 3.89 ± 4.60 ms (range 0.15–11.27 ms); and mixed-I responses, 3.47 ± 3.61 ms (range 0.45–10.29 ms). The lower range of jitter for excitatory responses is similar to the lower range of jitter for inhibitory responses, further suggesting that afferent-evoked excitatory currents measured in Shox2 neurons are not monosynaptic. As latency post-stimulation may also be affected by differences in preparations due to age, myelination, conduction pathway length and fluctuations in room temperature, data were also analyzed after normalizing latency by subtracting VRR latency; however, this did not substantially change the results (data not shown). We therefore suggest that both excitatory and inhibitory currents are consistent with a minimally disynaptic pathway from CPn and Tn afferents to Shox2 neurons.

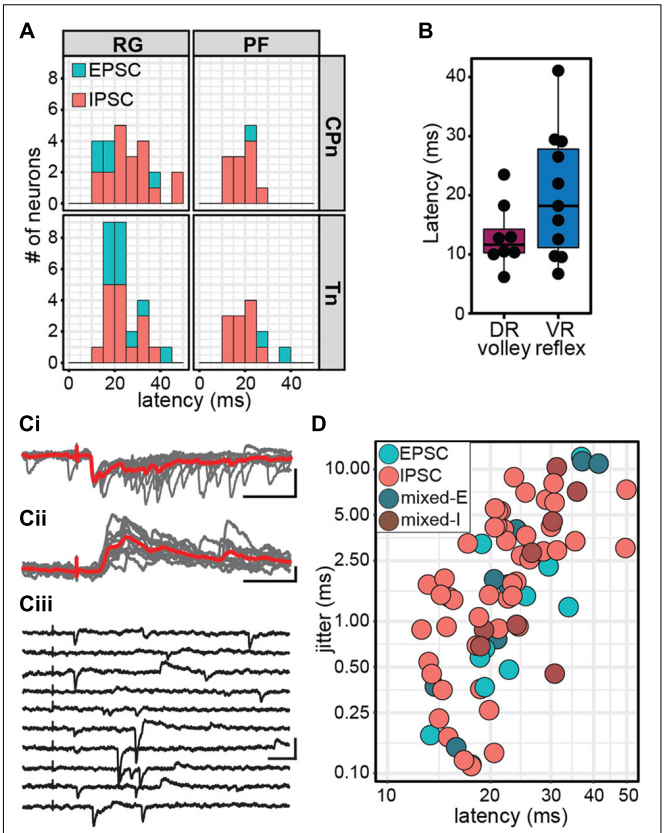

FIGURE 5 | Stimulation of ankle afferents induce postsynaptic currents in Shox2 neurons via a minimally disynaptic pathway in the hemisect preparation. **(A)** Latency distribution of early postsynaptic currents in Shox2^{RG} and Shox2^{PF} neurons following CPn and Tn stimulation. Responses are coded according to polarity of the earliest response component. Inhibitory responses occurred at approximately the same latency as the earliest excitatory responses measured. **(B)** Latencies for dorsal root (DR) volley and ventral root (VR) reflexes were similarly varied. Ventral root reflex latencies spanned nearly the entire range of latencies of evoked currents in Shox2 neurons. **(C)** Example traces showing different Shox2 neurons at different latencies and jitter. Vertical scale bars are 20 pA and horizontal are 50 ms. **(Ci)** Low latency, low jitter excitatory response. Gray traces are 10 individual trials superimposed and red trace is average. **(Cii)** Medium latency, medium jitter inhibitory response. **(Ciii)** High latency, high jitter response showing occasional failures of the earliest component. Jitter is calculated from all sweeps in which any response is seen, resulting in large measured jitter values. **(D)** Latency and jitter of the earliest component of postsynaptic currents observed following CPn and Tn stimulation, color-coded by response subtype. Points plotted on log scale for clarity. A positive relationship was seen between latency and jitter (linear regression, adjusted R^2 = 0.41, t = 7.24, p = 3.56e-10).

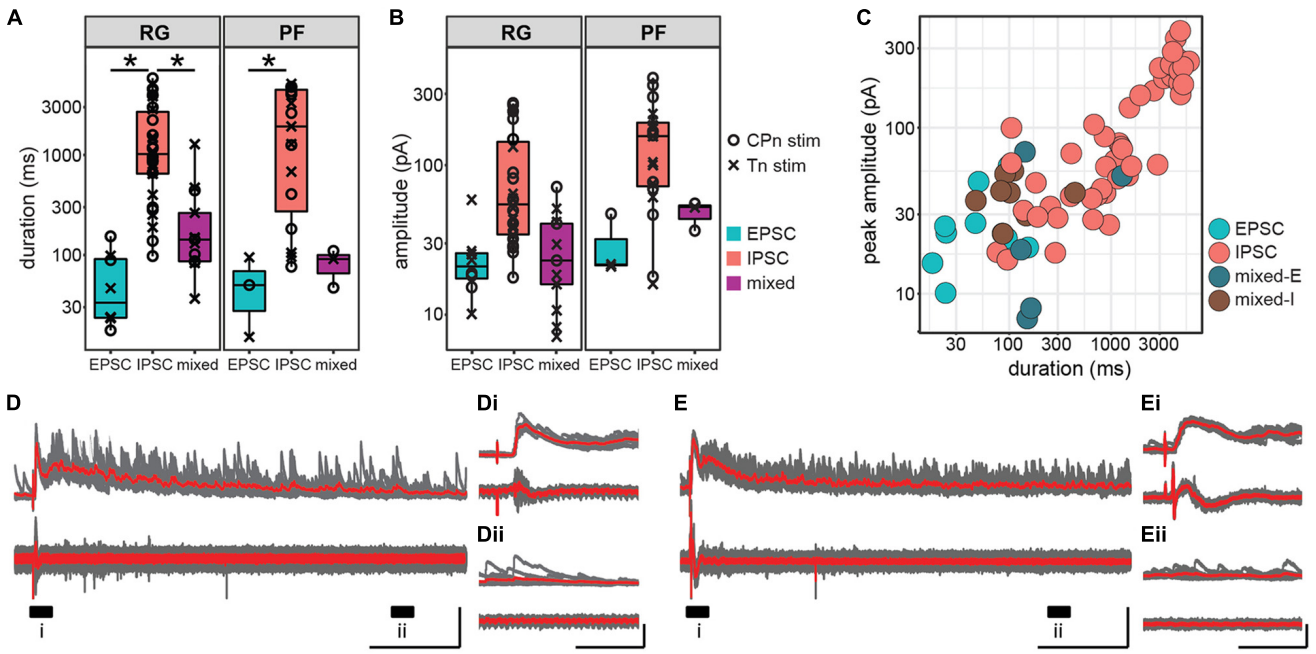

FIGURE 6 | Inhibitory postsynaptic currents in response to ankle afferent stimulation are larger and persist for longer than excitatory postsynaptic currents. **(A)** Duration of postsynaptic currents measured in the hemisect preparation, plotted on log scale for clarity. Current duration was greater for inhibitory responses than for excitatory responses in both the Shox2^{RG} population and the Shox2^{PF} population ($p < 0.05$). **(B)** Absolute peak amplitude of postsynaptic currents, plotted on log scale for clarity. Amplitude for excitatory current components was measured near the inhibitory reversal potential (–50 to –65 mV) and for inhibitory current components near the excitatory reversal potential (0 mV). **(C)** Peak amplitude and duration of postsynaptic currents in individual Shox2 neurons plotted on a log-log scale. Peak amplitude and response duration are positively correlated (linear regression, adjusted $R^2 = 0.81$, slope = 0.047, $t = 17.84$, df = 74, $p = 1.60e\text{-}28$). **(D,E)** Example traces showing large, long duration inhibitory response to afferent stimulation. Shox2 neuron recording is at the top and ventral root recording at the bottom. Ten individual trials (gray) are overlaid with the average of the trials in red. Labeled regions (i, ii) are expanded in insets **(Di,Dii,Ei,Eii)**. In these neurons a low-jitter initial response is followed by a prolonged period in which inhibitory currents continue to be received by Shox2 neurons. Vertical scale bars are 200 pA for intracellular recordings and 0.1 mV for extracellular root recordings. Horizontal scale bars are 1000 ms in **(D,E)** and 100 ms in insets.

Response Duration and Amplitude Are Greater in Inhibitory Responses Than Excitatory Responses in the Hemisect Preparation

In addition to latency and jitter of the early response, we also characterized the duration and peak amplitude of the entire response. Response duration was significantly higher in Shox2 neurons receiving inhibitory inputs (1962.44 ± 1798.97 ms, range 76.16–5853.43 ms) than in Shox2 neurons receiving excitatory (57.75 ± 44.98 ms, range 15.13–153.49 ms) or mixed input (229.30 ± 308.28 ms, range 36.60–1282.00 ms) (Kruskal–Wallis rank sum test, $\chi^2 = 38.7$, df = 2, $p = 3.97e\text{-}9$; *post hoc* Dunn's test, EPSC-IPSC: $p = 1.82e\text{-}7$, EPSC-Mixed: $p = 0.116$, IPSC-Mixed: $p = 6.99e\text{-}5$). Differences in duration were also detected when Shox2^{RG} and Shox2^{PF} populations were analyzed separately (**Figure 6A**). In order to better isolate inhibitory and excitatory current components in pure and mixed responses, amplitudes were respectively measured near the excitatory and inhibitory reversal potentials and reported here as absolute values. Inhibitory amplitudes were 116.32 ± 95.63 pA (range 16.00–383.21 pA), excitatory amplitudes were 26.07 ± 14.33 pA (range 10.11–58.79 pA) and mixed amplitudes were 32.82 ± 18.92 pA (range 7.09–71.44 pA) When comparing Shox2^{RG} and Shox2^{PF} neurons, no significant difference in amplitude was detected for excitatory and mixed currents (excitatory: Wilcoxon rank sum test, $W = 9$, $p = 0.63$; mixed: Welch's unequal variances *t*-test, $t = 2.37$, df = 5.9, $p = 0.056$). Inhibitory currents observed in Shox2^{PF} neurons (150.0 ± 104.6 pA, range 16.0–383.2 pA) were statistically likely to have greater amplitude than those observed in Shox2^{RG} neurons (95.0 ± 84.4 pA, range 17.6–258.8 pA) (Wilcoxon rank sum test, $W = 186$, $p = 0.042$, $n1 = 19$, $n2 = 30$) (**Figure 6B**). A positive association was observed between response duration and amplitude (linear regression, adjusted $R^2 = 0.81$, slope = 0.047, $t = 17.84$, df = 74, $p = 1.60e\text{-}28$; **Figure 6C**). Interestingly, in some neurons we observed sustained current activity, sometimes over 5 s after the initial stimulation. All of these responses were inhibitory and occurred with similar frequency following CPn stimulation and Tn stimulation. In the representative traces shown in **Figures 6D,E**, an initial large, consistent response can be observed followed by a prolonged period (>1 s) over which many inhibitory currents are seen with variable timing. These results suggest recurrent activation of a circuit with inhibitory synapses on some Shox2 neurons following single pulse stimulation of sensory afferents.

Both CPn and Tn Stimulation Evoke Flexor-Biased Locomotor Perturbations in P1-3 Mice

It may be surprising that stimulation of CPn and Tn nerves which innervate antagonist muscles both produce similar effects in Shox2 neurons. In many animal models, flexor and extensor afferents generally evoke opposing effects on ongoing locomotion (McCrea, 2001; Rossignol et al., 2006). However, it has been shown that the development of this phenotype does not occur until P4 in the rat and it is possible that a similar developmental switch occurs in the mouse (Iizuka et al., 1997; Hinckley et al., 2010). We therefore applied brief trains of stimulation (50 μs, 20 Hz, 4–6 pulses) during drug-evoked fictive locomotion in whole cord preparations from P1 to P3 mice with attached peripheral nerves (n = 7 mice). Stimulation strength was set to 2 × T for VRR for each nerve, measured before locomotor drugs were applied. Ventral root activity was monitored using suction electrodes attached to the flexor-biased L1 VR and the extensor-biased L4 VR. Stimulation was delivered at a regular interval, typically 100 s, which was unrelated to locomotor phase. Therefore, stimulation could occur in any part of the locomotor cycle. Trials where the stimuli occurred during the flexor-related burst period were considered separately from those that occurred during the interburst period. To quantify the effects of CPn and Tn stimulation during ongoing locomotion, we analyzed the cycle period and duty cycle of the flexor-biased ventral root following stimulation either during the flexor-related burst or the interburst period which includes the extensor-related burst. Each cycle was defined as the flexor burst and following interburst period, so stimulation during the burst occurred in the earlier portion of the cycle and stimulation during the interburst period occurred in the later portion of the cycle. As flexor bursts typically occupied less than half of the cycle and stimulations were delivered at 100 s intervals, fewer trials in which stimulation occurred during a burst were available for analysis. Stimulation trials were only considered if the standard deviation of the three cycles preceding stimulation was less than 50% of the mean cycle period. For each animal and condition, cycle periods were averaged and an animal was only considered if the standard deviation of the three averaged cycles preceding stimulation was less than 10% of the mean cycle period.

Both CPn (**Figure 7A**) and Tn (**Figure 7B**) stimulation induced the onset of a new flexor burst and truncated an ongoing extensor burst when applied during the flexor interburst period. Following stimulation, the evoked flexor burst was typically longer than previous flexor bursts and often greater in amplitude. These excitatory effects could sometimes be seen for several cycles. In many cases, a concomitant decrease in amplitude was seen in the extensor bursts following stimulation. This resulted in statistically significant changes in cycle period (**Figure 7C**). Following CPn stimulation, we observed a reduction of cycle period in the perturbed burst, corresponding to a truncation of the interburst period in 7/7 preparations (Kruskal–Wallis rank sum test, χ^2 = 26.6, df = 6, p = 0.00017). Typically, we also observed an increase of cycle period in the following cycle corresponding to a longer flexor burst. In one preparation, we instead observed a reduction of cycle period in the two cycles following perturbation, corresponding to an increased locomotor frequency. Following Tn stimulation, the evoked flexor burst sometimes appeared immediately and sometimes after a short delay. In both cases, we observed similar reductions in cycle period for the perturbed cycle and increase in cycle period in the cycle after Tn stimulation in 5/7 cords (Kruskal–Wallis rank sum test, χ^2 = 19.575, df = 6, p = 0.0033, n = 7 preparations). When stimulation was applied during the burst, significant differences in cycle period were observed following CPn stimulation, but not Tn stimulation (Kruskal–Wallis rank sum test, CPn: χ^2 = 13.4,

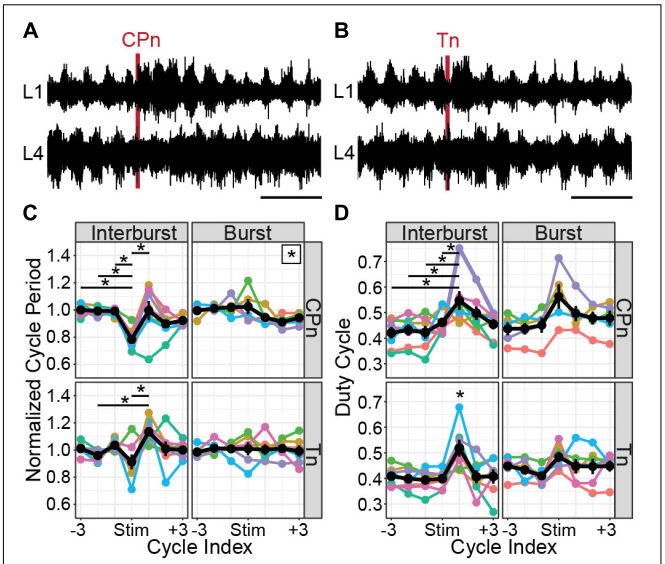

FIGURE 7 | CPn and Tn stimulation trains both induce flexor-biased resetting of drug-evoked fictive locomotion in cords from P1 to P3 mice. **(A)** Representative example of CPn stimulation (50 μs, 20 Hz, 6 pulses) applied during the flexor interburst period of drug-induced locomotion. Top trace shows recording from L1 VR and bottom trace from L4 VR, corresponding to flexor and extensor motor output respectively. Following CPn stimulation (red line), there is truncation of the ongoing extensor burst and initiation of a new flexor burst. **(B)** Representative example of Tn stimulation applied during the flexor interburst period. Following Tn stimulation (red line), there is truncation of the ongoing extensor burst and initiation of a new flexor burst. In some cases, but not always, there is a short delay preceding the flexor burst initiation. **(C)** Normalized cycle period measured from L1 VR recordings before, during and after CPn and Tn stimulation delivered during either the flexor interburst period or burst. Cycles are defined as starting with the flexor burst. Colors correspond to different spinal cord preparations and the black line shows the mean and standard error. When stimulation was delivered during the interburst period, both CPn and Tn stimulation typically reduced the cycle period of the ongoing cycle by truncating the interburst period and increased the cycle period of the subsequent cycle containing the evoked flexor burst. Stars indicate significant pairwise comparison ($p < 0.05$). A star in the upper right corner of the plot indicates significant omnibus test without significant post-hoc comparisons. **(D)** Duty cycle measured from L1 VR recordings before, during and after CPn and Tn stimulation during either the flexor interburst period or burst. Colors correspond to different spinal cord preparations and the black line shows the mean and standard error. Increase in duty cycle for the cycle following stimulation during the interburst period corresponds to an increased burst duration for the evoked flexor burst. A star directly above a point indicates significant pairwise comparisons ($p < 0.05$) with every other point.

df = 6, $p = 0.037$, $n = 5$ preparations; Tn: $\chi^2 = 1.65$, df = 6, $p = 0.95$, $n = 6$ preparations). However, *post hoc* testing with corrections for multiple comparisons for changes in cycle period following CPn stimulation during the flexor burst did not show any significant pairwise comparisons.

Increases in cycle period can result from prolongation of either the burst or interburst period. We therefore also quantified the duty cycle, defined as the L1 burst duration divided by the cycle period. When stimulation was applied during the interburst period, we again observed significant differences in duty cycle for both CPn and Tn stimulation (**Figure 7D**). Specifically, there was an increase in the duty cycle for the cycle following stimulation, corresponding to the stimulation-evoked flexor burst that was typically longer in duration [CPn: Kruskal–Wallis rank sum test, $\chi^2 = 14.3$, df = 6, $p = 0.027$, $n = 7$ preparations; Tn: one-way ANOVA, $F(6,42) = 3.98$, $p = 0.0030$, $n = 7$ preparations]. When stimulation was applied during the flexor burst, no statistically significant change in duty cycle was observed [CPn: one-way ANOVA, $F(6,28) = 2.05$, $p = 0.091$, $n = 5$ preparations; Tn: Kruskal–Wallis rank sum test, $\chi^2 = 6.3$, df = 6, $p = 0.39$, $n = 6$ preparations].

Taken together, these results demonstrate that flexor and extensor-related ankle afferents both induce flexor-biased resetting of ongoing locomotion in P1–P3 mice. Resetting behavior is more consistent across mice following CPn stimulation than following Tn stimulation and it is possible that this behavior may be different in older mice.

DISCUSSION

Our experiments were designed to provide insight into the sensory modulation of CPG neurons. We focused on Shox2 neurons, which can be separated into neurons with roles in rhythm generation ($Shox2^{RG}$) and pattern formation ($Shox2^{PF}$). Spinal cord preparations were isolated from neonatal mice and sensory afferents were activated via electrical stimulation of either dorsal root or peripheral nerve while recording from Shox2 neurons. The key findings of our study are that Shox2 neurons with both identities broadly receive postsynaptic currents following afferent stimulation in the quiescent state. In these experiments, Shox2 neurons which responded to activation of flexor and extensor sensory afferents tended to display similar currents to both. Furthermore, we show that in a large subset of medially located Shox2 neurons, the postsynaptic current characteristics following CPn and Tn stimulation were highly associated.

Sensory Afferent Stimulation Produces Heterogenous Effects on Shox2 Neurons

In all three preparations used in this study, activation of sensory afferents induced postsynaptic currents that were consistent and robust across multiple trials, but which were highly variable between different neurons. We observed EPSCs, IPSCs, mixed responses and non-responders in all preparations with no clear spatial organization and which did not differ according to stimulation site or $Shox2^{RG}$/$Shox2^{PF}$ identity. Recorded postsynaptic currents also occurred with a range of latencies and durations, and with differing numbers of synaptic components.

There are multiple possible explanations for this heterogeneity. Firstly, Shox2 neurons are known to be heterogeneous in many ways. Although deletion experiments have defined locomotor roles for $Shox2^{RG}$ and $Shox2^{PF}$ neurons, it is not clear that every Shox2 neuron is truly part of the CPG. Indeed, although most Shox2 neurons are rhythmically active during pharmacologically evoked fictive locomotion, slightly less than a third of Shox2 neurons are not (Dougherty et al., 2013). Furthermore, rhythmically active Shox2 neurons consist of both flexor- and extensor-aligned pools with no known genetic or electrophysiological marker. Connectivity experiments were performed in the quiescent state and therefore we were unable to identify whether the recorded neurons were flexor-aligned, extensor-aligned or non-rhythmic. Thus, one possible explanation for the mixture of responses seen is that flexor-aligned, extensor-aligned and non-rhythmic Shox2 neurons show stereotypical response patterns which appear heterogeneous in the undifferentiated population.

Another possibility is that the response of CPG neurons to sensory stimulation is strongly modulated by locomotor context. For example, Ib afferents from extensor muscles are known to inhibit extensor motor neurons in the quiescent context via a disynaptic pathway but to activate extensor motor neurons during locomotion (Gossard et al., 1994). Therefore, it is possible that Shox2 neurons may receive functionally different inputs from sensory afferents in a state-dependent manner. Although these studies cannot directly address this possibility, it is known that repetitive sensory stimulation can evoke locomotor-like rhythms, presumably via a pathway synapsing on rhythm-generating circuits. Additionally, activation of CPG circuitry is more reliant on afferent pathways following spinal cord injury (Takeoka et al., 2014; Takeoka and Arber, 2019). Therefore, it is likely that at least some sensory afferents can access rhythm-generating neurons in a functionally relevant manner even in the quiescent state. Specifically, our observation that Shox2 neurons receive afferent input from multiple sensory pathways with differing polarities and latencies in the quiescent state is consistent with the possibility that context-specific inhibitory gating alone could produce powerful and flexible modulation of sensory effects on locomotion.

Finally, the electrical stimulation used in these experiments is relatively non-specific. In particular, dorsal root stimulation will activate many afferent pathways including proprioceptive inputs from flexor, extensor and bifunctional muscles as well as cutaneous afferents. In order to more specifically activate flexor- and extensor-related afferents, we stimulated CPn and Tn respectively. However, CPn and Tn also both contain a mix of proprioceptive and mechanoreceptive afferents. CPn is a hindlimb nerve which innervates muscles and skin of the lateral and anterior compartment of the leg, as well as skin of the foot dorsum and some intrinsic foot muscles. Tn is a hindlimb nerve which innervates the muscles and skin of the posterior compartment of the leg as well as the foot plantar surface and some intrinsic foot muscles. We were primarily interested in

understanding proprioceptive input in our experiments and so limited our stimulation to 2 × T for VRR (Kiehn et al., 1992; Talpalar et al., 2011; Bui et al., 2013). However, low strength electrical stimulation will activate fibers from both muscle spindles (Type Ia and II) and Golgi tendon organs (Type Ib), as well as low threshold mechanoreceptors. Thus, it is possible that non-specific activation of different sensory modalities could have evoked the flexor-biased effects that we observed following Tn stimulation. In the cat, enhancement of extensor muscle activity from activation of ankle extensor proprioceptors is Ib dependent and the effect of spindle activation on locomotor phase timing is minimal (Conway et al., 1987). Activation of many cutaneous hindlimb afferents can induce resetting to flexion. However, the foot pad which is innervated by Tn has been shown to have phase-dependent effects during locomotion, enhancing extensors during stance and flexors during swing (Duysens and Pearson, 1976; Duysens, 1977). This phase-dependent pattern is different from the flexor-biased effects we observed, which were strongest during the extensor burst. Therefore, the effects observed in this study are unlikely to result solely from non-specific activation of sensory fiber types.

Taken together, the results suggest that although Shox2 neurons are highly responsive to afferent stimuli, the synaptic pathways interposed between sensory afferents and Shox2 neurons are complex, overlapping and may involve differing numbers and differing populations of interposed neurons.

Similar Postsynaptic Currents Are Observed Following Both CPn and Tn Stimulation in Shox2 Neurons

Although there was large variability between Shox2 neurons in the effect of sensory afferent stimulation, we nevertheless observed an interesting and consistent pattern in neurons which responded to stimulation of both CPn and Tn. As assessed by presence, polarity, duration and amplitude, postsynaptic currents seen in Shox2 neurons were highly similar following CPn and Tn stimulation in the hemisect preparation. In contrast, many other studies have highlighted the opposing roles of flexor- and extensor-specified afferents on ongoing locomotion (Conway et al., 1987; Guertin et al., 1995; Hiebert et al., 1996; McCrea, 2001; Stecina et al., 2005; Rossignol et al., 2006). As mentioned above, one possible explanation for this discrepancy is that alterations in sensory processing are known to occur during locomotion in a state- and phase-dependent manner and Shox2 behavior was assayed in the quiescent state for these studies. Thus it is possible that if these experiments were repeated in a locomotor context, differential modulation of CPn- and Tn-related postsynaptic currents in Shox2 neurons may result in response patterns more closely aligned with flexor-extensor antagonism. These context-specific changes could result from either central modulation of CPG interneurons or through direct modulation of afferent pathways through mechanisms such as primary afferent depolarization (Forssberg et al., 1975; Andersson et al., 1978; García-Ramírez et al., 2014; Goulding et al., 2014). Another possible explanation for this discrepancy is that these experiments utilized neonatal mice, while the effects of proprioceptive input have been best characterized in the adult animal models. Indeed, in the rat, a developmental switch has been shown to occur at around P4 (Iizuka et al., 1997). Prior to this switch, low-intensity quadriceps nerve stimulation results in flexor burst prolongation whereas during P4–P6 the same stimulation induces flexor burst truncation. Sensory perturbation of locomotion in the mouse model is less well-characterized, but flexor-biased resetting phenotypes have also been reported following stimulation of the predominantly extensor-related L5 dorsal root in young mice (Hinckley et al., 2010). Consistent with this, we demonstrate that trains of either CPn and Tn stimulation both result in a flexor-biased resetting pattern in P1-P3 mice. Although the majority of data collected from the hemisect preparations with peripheral nerve dissections were from mice <P4, the data includes 5 neurons from a P7 mouse, of which 3 were $Shox2^{RG}$ and 2 were $Shox2^{PF}$. Among these neurons, all responded to both CPn and Tn similarly (4 inhibitory and 1 mixed). This may be due to later maturation of sensory locomotor modulation in mice versus rat, differential modulation of sensory pathways between the quiescent and locomotor context (Rossignol et al., 2006), or simply persistence of neonatal connectivity patterns in some neurons at P7 that would be expected to gradually switch with age. Additionally, electrical coupling between Shox2 neurons is prevalent at least to P17 (Ha and Dougherty, 2018). It is possible that gap junctional coupling is leading to the detection of indirect inputs that would not be observed if tested following the decline of electrical connections (Marder et al., 2017). Further exploration of developmental changes in sensory pathways synapsing on CPG elements could provide important insights into locomotor learning and circuit plasticity.

In the ventral horn-removed preparations, these results were less robust but similar. Of the 4 Shox2 neurons in the ventral horn-removed peripheral nerve preparation which responded to both CPn and Tn stimulation, 3 Shox2 neurons showed the same response polarity following both stimulation types and the fourth neuron received excitatory current with CPn stimulation and mixed-E currents with Tn stimulation. It is not clear why the Tn response rate was relatively lower in the ventral horn-removed peripheral nerve preparation than the hemisect preparation, but may suggest a difference specific to the medial-most population accessible for patch clamp in the hemisect preparation or a difference in dorsal-ventral distribution of neurons interposed in the CPn and Tn processing pathways.

Similarly, in the ventral horn-removed dorsal root preparation, a small number of neurons responded to both L2 and L5 stimulation, none of which displayed the fully opposing EPSC-IPSC phenotype although many unsurprisingly displayed mixed currents. Postsynaptic currents in Shox2 neurons were more likely to be observed following L5 than L2 stimulation. Both hip afferents and ankle afferents should have strong access to the rhythm-generating circuitry as both have been shown to be able to modulate step timing and entrain ongoing locomotion (Duysens and Pearson, 1980; Conway et al., 1987; Gossard et al., 1994; Guertin et al., 1995; Perreault et al., 1995; Lam and Pearson, 2001; McVea et al., 2005). Therefore,

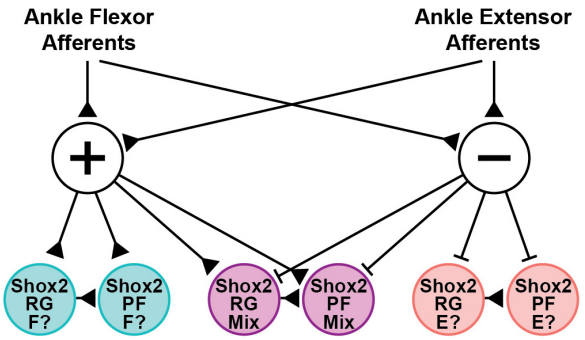

FIGURE 8 | Hypothesized structure of afferent pathways synapsing on Shox2 neurons in the neonate. Ankle flexor-related afferents from the CPn and extensor-related afferents from the Tn synapse on both excitatory (+) and inhibitory (–) interneuron populations. The interposed excitatory interneurons subsequently synapse on three sets of Shox2^{RG} and Shox2^{PF} populations that receive excitatory, inhibitory or mixed inputs. Pathways are depicted disynaptically but may be oligosynaptic. This connectivity structure is proposed on the basis of data collected in the quiescent context, but is consistent with the observed flexor-biased modulation of ongoing locomotion at P1-P3 by activation of CPn and Tn afferents. Together, this suggests that the Shox2 population receiving excitatory inputs (teal) may be flexor-related (F?), while the Shox2 population receiving inhibitory inputs (pink) may be extensor-related (E?). Developmental changes in connectivity either by pruning or by context-dependent activation of gating circuits are expected to occur at the level of the interposed interneurons. Production of connectivity structures in which flexor- and extensor-related Shox2 neurons receive excitatory inputs from homonymous afferents and inhibitory inputs from antagonist afferents, as suggested by studies in the rat and cat, can be more easily explained by pruning or gating if the interposed neurons targeted by CPn and Tn afferents are distinct from one another (not depicted).

these results may possibly reflect a differential role for Shox2 neurons in the integration of information from hip and ankle afferents. Shox2^{RG} neurons are known to comprise only a subset of the locomotor rhythm-generating kernel, as deletion of all Shox2 neurons results in slowed locomotion but does not fully eliminate it. Therefore, another neuronal population in the CPG may more strongly integrate information from hip-related afferents.

Shox2 neurons are proposed to contribute to both the RG and PF layers of the CPG (Dougherty et al., 2013; Rybak et al., 2015). In the hemisect preparation, we identified Chx10-negative Shox2^{RG} and Chx10-positive Shox2^{PF} neurons. Both Shox2^{RG} and Shox2^{PF} neurons responded at similar rates and showed similar patterns of response characteristics. This is consistent with previous experimental data and modeling studies which have predicted that afferent feedback should have access to neurons serving both RG and PF roles (Grillner, 1981; Burke et al., 2001; Rossignol et al., 2006; McCrea and Rybak, 2007). Additionally, both Shox2^{RG} and Shox2^{PF} neurons are known to contribute to flexor- and extensor-aligned populations during locomotion. Therefore, the Shox2 neurons recorded in these experiments should represent a heterogeneous population with some neurons being flexor-aligned and others extensor-aligned. Because both CPn and Tn stimulation during locomotion induced flexor-biased resetting, we would therefore expect neurons that are inhibited to be extensor-aligned and neurons which are excited to be flexor-aligned so long as excitatory/inhibitory response patterns in the quiescent state are predictive of postsynaptic currents in the locomotor state (**Figure 8**). Flexor-biased Shox2 neurons have previously been reported to comprise the majority of Shox2 neurons, which corresponds with the primarily excitatory currents seen in the ventral horn removed dorsal root and peripheral nerve preparations. However, in the hemisect preparation, most currents are inhibitory. The reasons for this are unclear, but differences in afferent connectivity between the medially located subpopulation of Shox2 neurons that are accessible in the hemisect preparation and the mediolaterally dispersed neurons accessible in the ventral horn-removed preparations may suggest mediolateral patterning of Shox2 neuron function and identity. In this study, we were unable to detect mediolateral connectivity differences within data collected using the ventral horn-removed preparations; however, in a previous study using retrograde viral tracing, the distribution of Shox2 neurons which synapsed on ankle extensor motor neurons extended further medially in comparison to Shox2 neurons which synapsed on ankle flexor motor neurons (Dougherty et al., 2013).

Long-Lasting Inhibitory Responses Were Observed in a Subset of Shox2 Neurons Recorded From the Hemisect Preparation

In a subset of Shox2 neurons in the hemisect preparation, we also identified a long-lasting inhibitory circuit that synapses on these neurons. This subpopulation is comprised of both Shox2^{RG} neurons and Shox2^{PF} neurons. In these neurons, postsynaptic currents were recorded with durations of up to several seconds, suggesting activation of a recurrently activated circuit which can provided sustained inhibitory currents to Shox2 neurons. It is unclear why these currents were detected only in the hemisect preparation, but two explanations seem plausible. Firstly, the neurons that are accessible in the hemisect preparation are very medial and so this circuit may be spatially organized such that medial neurons are more likely to be activated. Secondly, it is possible that this recurrent circuit is located at least partially in the ventral portion of the cord and therefore is damaged or removed in the ventral horn-removed dorsal root and peripheral nerve preparations. Long-lasting inhibitory effects following peripheral nerve stimulation have previously been reported (Rudneva and Slivko, 2000). It is possible that similar mechanisms and common neuronal substrates are involved in responses observed here. As prolonged trains of dorsal root stimulation can induce locomotion *in vitro*, it is possible that one role for these long-lasting inhibitory currents in response to single pulse stimulation is to prevent inadvertent inappropriate activation of locomotor circuits. Furthermore, as such currents are detected in only a subpopulation of Shox2^{RG} and Shox2^{PF} neurons, it is possible that they may serve to bias the initial CPG state, thus priming the CPG circuitry to produce initial motor activity that is appropriate to the

current hindlimb position and load. Another possibility is that these currents may act to modulate circuit excitability. Descending and central modulation of multiple CPG circuit elements and sensory pathways in state and phase-dependent manners are known to be important for the appropriate control of locomotion, and proprioceptive inputs may act similarly (Rossignol et al., 2006; Humphreys and Whelan, 2012; Kim et al., 2017). Modeling experiments have further suggested that neuronal activation level is a critical parameter in the generation of rhythmic activity and that intrinsically rhythmic populations may undergo qualitative shifts from non-active to bursting and then to tonic activity (Shevtsova et al., 2015; Ausborn et al., 2018). Thus, prolonged inhibitory currents may serve to modulate excitatory state during either the initiation or maintenance of locomotor rhythm generation (Nadim et al., 2011). Finally, in computational models of single element oscillators, inhibitory inputs have been shown to have stronger and more reliable effects on phase resetting than do excitatory inputs (Oprisan et al., 2003; Maran et al., 2008). Therefore, these strong inhibitory currents may be important for resetting if they persist in the locomotor state. Based on our data, we are unable to distinguish between which of the above possibilities are more likely, but future experiments will focus on these questions.

DATA AVAILABILITY STATEMENT

The datasets generated for this study are available on request to the corresponding author.

ETHICS STATEMENT

The animal study was reviewed and approved by the Drexel University Institutional Animal Care and Use Committee.

AUTHOR CONTRIBUTIONS

EL and KD conceptualized the study, analyzed the data, and drafted the manuscript. EL, DG-R, and KD designed the experiments. DG-R and EL developed the spinal cord preparations. EL performed the experiments. All authors read, edited, and approved the final manuscript.

FUNDING

This work was supported by NIH NINDS R01 NS095366 and R01 NS104194 (KD), NIH NINDS F30 NS110199, and the Drexel University Dean's Fellowship for Excellence in Collaborative or Themed Research (EL).

ACKNOWLEDGMENTS

The authors are grateful to Lihua Yao for technical assistance and Ilya Rybak, Simon Giszter, Ngoc Ha, and Nicholas Stachowski for discussions and comments on the manuscript.

REFERENCES

Akay, T., Tourtellotte, W. G., Arber, S., and Jessell, T. M. (2014). Degradation of mouse locomotor pattern in the absence of proprioceptive sensory feedback. *Proc. Natl. Acad. Sci. U.S.A.* 111, 16877–16882. doi: 10.1073/pnas.1419045111

Andersson, O., Forssberg, H., Grillner, S., and Lindquist, M. (1978). Phasic gain control of the transmission in cutaneous reflex pathways to motoneurones during 'fictive' locomotion. *Brain Res.* 149, 503–507. doi: 10.1016/0006-8993(78)90493-6

Andersson, O., and Grillner, S. (1983). Peripheral control of the cat's step cycle. *Acta Physiol. Scand.* 118, 229–239. doi: 10.1111/j.1748-1716.1983.tb07267.x

Angel, M. J., Guertin, P., Jiménez, T., and McCrea, D. A. (1996). Group I extensor afferents evoke disynaptic EPSPs in cat hindlimb extensor motorneurones during fictive locomotion. *J. Physiol.* 494, 851–861. doi: 10.1113/jphysiol.1996.sp021538

Ausborn, J., Koizumi, H., Barnett, W. H., John, T. T., Zhang, R., Molkov, Y. I., et al. (2018). Organization of the core respiratory network: insights from optogenetic and modeling studies. *PLoS Comput. Biol.* 14:e1006148. doi: 10.1371/journal.pcbi.1006148

Brown, T. G. (1911). The intrinsic factors in the act of progression in the mammal. *Proc. R. Soc. Lond. B.* 84, 308–319. doi: 10.1098/rspb.1911.0077

Brownstone, R. M., and Wilson, J. M. (2008). Strategies for delineating spinal locomotor rhythm-generating networks and the possible role of Hb9 interneurones in rhythmogenesis. *Brain Res. Rev.* 57, 64–76. doi: 10.1016/j.brainresrev.2007.06.025

Bui, T. V., Akay, T., Loubani, O., Hnasko, T. S., Jessell, T. M., and Brownstone, R. M. (2013). Circuits for grasping: spinal dI3 interneurons mediate cutaneous control of motor behavior. *Neuron* 78, 191–204. doi: 10.1016/j.neuron.2013.02.007

Burke, R. E., Degtyarenko, A. M., and Simon, E. S. (2001). Patterns of locomotor drive to motoneurons and last-order interneurons: clues to the structure of the CPG. *J. Neurophysiol.* 86, 447–462. doi: 10.1152/jn.2001.86.1.447

Conway, B. A., Hultborn, H., and Kiehn, O. (1987). Proprioceptive input resets central locomotor rhythm in the spinal cat. *Exp. Brain Res.* 68, 643–656. doi: 10.1007/BF00249807

Dinno, A. (2015). Nonparametric pairwise multiple comparisons in independent groups using Dunn's test. *Stata J.* 15, 292–300. doi: 10.1177/1536867x1501500117

Dougherty, K. J., and Ha, N. T. (2019). The rhythm section: an update on spinal interneurons setting the beat for mammalian locomotion. *Curr. Opin. Physiol.* 8, 84–93. doi: 10.1016/j.cophys.2019.01.004

Dougherty, K. J., Zagoraiou, L., Satoh, D., Rozani, I., Doobar, S., Arber, S., et al. (2013). Locomotor rhythm generation linked to the output of spinal Shox2 excitatory interneurons. *Neuron* 80, 920–933. doi: 10.1016/j.neuron.2013.08.015

Duysens, J. (1977). Reflex control of locomotion as revealed by stimulation of cutaneous afferents in spontaneously walking premammillary cats. *J. Neurophysiol.* 40, 737–751. doi: 10.1152/jn.1977.40.4.737

Duysens, J., and Pearson, K. G. (1976). The role of cutaneous afferents from the distal hindlimb in the regulation of the step cycle of thalamic cats. *Exp. Brain Res.* 24, 245–255. doi: 10.1007/BF00235013

Duysens, J., and Pearson, K. G. (1980). Inhibition of flexor burst generation by loading ankle extensor muscles in walking cats. *Brain Res.* 187, 321–332. doi: 10.1016/0006-8993(80)90206-1

Forssberg, H., Grillner, S., and Rossignol, S. (1975). Phase dependent reflex reversal during walking in chronic spinal cats. *Brain Res.* 85, 103–107. doi: 10.1016/0006-8993(75)91013-6

Frigon, A., Hurteau, M.-F., Thibaudier, Y., Leblond, H., Telonio, A., and D'Angelo, G. (2013). Split-belt walking alters the relationship between locomotor phases and cycle duration across speeds in intact and chronic spinalized adult cats. *J. Neurosci.* 33, 8559–8566. doi: 10.1523/JNEUROSCI.3931-12.2013

García-Ramírez, D. L., Calvo, J. R., Hochman, S., and Quevedo, J. N. (2014). Serotonin, dopamine and noradrenaline adjust actions of myelinated afferents via modulation of presynaptic inhibition in the mouse spinal cord. *PLoS One* 9:e89999. doi: 10.1371/journal.pone.0089999

Gong, S., Zheng, C., Doughty, M. L., Losos, K., Didkovsky, N., Schambra, U. B., et al. (2003). A gene expression atlas of the central nervous system based on bacterial artificial chromosomes. *Nature* 425, 917–925. doi: 10.1038/nature02033

Gossard, J.-P., Brownstone, R. M., Barajon, I., and Hultborn, H. (1994). Transmission in a locomotor-related group Ib pathway from hindlimb extensor muscles in the cat. *Exp. Brain Res.* 98, 213–228. doi: 10.1007/BF00228410

Goulding, M. (2009). Circuits controlling vertebrate locomotion: moving in a new direction. *Nat. Rev. Neurosci.* 10, 507–518. doi: 10.1038/nrn2608

Goulding, M., Bourane, S., Garcia-Campmany, L., Dalet, A., and Koch, S. (2014). Inhibition downunder: an update from the spinal cord. *Curr. Opin. Neurobiol.* 26, 161–166. doi: 10.1016/j.conb.2014.03.006

Grillner, S. (1981). "Control of locomotion in bipeds, tetrapods, and fish," in *Handbook of Physiology, Section I: The Nervous System*, Vol. 2, *Motor Control*, ed. V. B. Brooks (Bethesda, MD: American Physiological Society), 1179–1236. doi: 10.1002/cphy.cp010226

Grillner, S., and Rossignol, S. (1978). On the initiation of the swing phase of locomotion in chronic spinal cats. *Brain Res.* 146, 269–277. doi: 10.1016/0006-8993(78)90973-3

Guertin, P., Angel, M. J., Perreault, M. C., and McCrea, D. A. (1995). Ankle extensor group I afferents excite extensors throughout the hindlimb during fictive locomotion in the cat. *J. Physiol.* 487, 197–209. doi: 10.1113/jphysiol.1995.sp020871

Guertin, P. A. (2009). The mammalian central pattern generator for locomotion. *Brain Res. Rev.* 62, 45–56. doi: 10.1016/j.brainresrev.2009.08.002

Ha, N. T., and Dougherty, K. J. (2018). Spinal Shox2 interneuron interconnectivity related to function and development. *eLife* 7:e42519. doi: 10.7554/eLife.42519

Hiebert, G. W., Whelan, P. J., Prochazka, A., and Pearson, K. G. (1996). Contribution of hind limb flexor muscle afferents to the timing of phase transitions in the cat step cycle. *J. Neurophysiol.* 75, 1126–1137. doi: 10.1152/jn.1996.75.3.1126

Hinckley, C. A., Wiesner, E. P., Mentis, G. Z., Titus, D. J., and Ziskind-Conhaim, L. (2010). Sensory modulation of locomotor-like membrane oscillations in Hb9-expressing interneurons. *J. Neurophysiol.* 103, 3407–3423. doi: 10.1152/jn.00996.2009

Humphreys, J. M., and Whelan, P. J. (2012). Dopamine exerts activation-dependent modulation of spinal locomotor circuits in the neonatal mouse. *J. Neurophysiol.* 108, 3370–3381. doi: 10.1152/jn.00482.2012

Iizuka, M., Kiehn, O., and Kudo, N. (1997). Development in neonatal rats of the sensory resetting of the locomotor rhythm induced by NMDA and 5-HT. *Exp. Brain Res.* 114, 193–204. doi: 10.1007/PL00005628

Kiehn, O. (2016). Decoding the organization of spinal circuits that control locomotion. *Nat. Rev. Neurosci.* 17, 224–238. doi: 10.1038/nrn.2016.9

Kiehn, O., and Butt, S. J. B. (2003). Physiological, anatomical and genetic identification of CPG neurons in the developing mammalian spinal cord. *Prog. Neurobiol.* 70, 347–361. doi: 10.1016/S0301-0082(03)00091-1

Kiehn, O., Iizuka, M., and Kudo, N. (1992). Resetting from low threshold afferents of N-methyl-d-aspartate-induced locomotor rhythm in the isolated spinal cord-hindlimb preparation from newborn rats. *Neurosci. Lett.* 148, 43–46. doi: 10.1016/0304-3940(92)90800-M

Kim, L. H., Sharma, S., Sharples, S. A., Mayr, K. A., Kwok, C. H. T., and Whelan, P. J. (2017). Integration of descending command systems for the generation of context-specific locomotor behaviors. *Front. Neurosci.* 11:581. doi: 10.3389/fnins.2017.00581

Lam, T., and Pearson, K. G. (2001). Proprioceptive modulation of hip flexor activity during the swing phase of locomotion in decerebrate cats. *J. Neurophysiol.* 86, 1321–1332. doi: 10.1152/jn.2001.86.3.1321

Madisen, L., Zwingman, T. A., Sunkin, S. M., Oh, S. W., Zariwala, H. A., Gu, H., et al. (2010). A robust and high-throughput Cre reporting and characterization system for the whole mouse brain. *Nat. Neurosci.* 13, 133–140. doi: 10.1038/nn.2467

Maran, S. K., Sieling, F. H., Prinz, A. A., and Canavier, C. C. (2008). Predicting excitatory phase resetting curves in bursting neurons. *BMC Neurosci.* 9:134. doi: 10.1186/1471-2202-9-S1-P134

Marder, E., Gutierrez, G. J., and Nusbaum, M. P. (2017). Complicating connectomes: electrical coupling creates parallel pathways and degenerate circuit mechanisms. *Dev. Neurobiol.* 77, 597–609. doi: 10.1002/dneu.22410

Mayer, W. P., and Akay, T. (2018). Stumbling corrective reaction elicited by mechanical and electrical stimulation of the saphenous nerve in walking mice. *J. Exp. Biol.* 221:jeb178095. doi: 10.1242/jeb.178095

Mayer, W. P., Murray, A. J., Brenner-Morton, S., Jessell, T. M., Tourtellotte, W. G., and Akay, T. (2018). Role of muscle spindle feedback in regulating muscle activity strength during walking at different speed in mice. *J. Neurophysiol.* 120, 2484–2497. doi: 10.1152/jn.00250.2018

McCrea, D. A. (2001). Spinal circuitry of sensorimotor control of locomotion. *J. Physiol.* 533, 41–50. doi: 10.1111/j.1469-7793.2001.0041b.x

McCrea, D. A., and Rybak, I. A. (2007). Modeling the mammalian locomotor CPG: insights from mistakes and perturbations. *Prog. Brain Res.* 165, 235–253. doi: 10.1016/S0079-6123(06)65015-2

McVea, D. A., Donelan, J. M., Tachibana, A., and Pearson, K. G. (2005). A role for hip position in initiating the swing-to-stance transition in walking cats. *J. Neurophysiol.* 94, 3497–3508. doi: 10.1152/jn.00511.2005

Nadim, F., Zhao, S., Zhou, L., and Bose, A. (2011). Inhibitory feedback promotes stability in an oscillatory network. *J. Neural Eng.* 8:065001. doi: 10.1088/1741-2560/8/6/065001

Oprisan, S. A., Thirumalai, V., and Canavier, C. C. (2003). Dynamics from a time series: can we extract the phase resetting curve from a time series? *Biophys. J.* 84, 2919–2928. doi: 10.1016/s0006-3495(03)70019-8

Pearson, K. G., and Duysens, J. (1976). "Function of segmental reflexes in the control of stepping in cockroaches and cats," in *Neural Control of Locomotion Advances in Behavioral Biology*, eds R. M. Herman, S. Grillner, P. S. G. Stein, and D. G. Stuart, (Boston, MA: Springer), 519–537. doi: 10.1007/978-1-4757-0964-3_21

Perreault, M. C., Angel, M. J., Guertin, P., and McCrea, D. A. (1995). Effects of stimulation of hindlimb flexor group II afferents during fictive locomotion in the cat. *J. Physiol.* 487, 211–220. doi: 10.1113/jphysiol.1995.sp020872

Peyronnard, J. M., and Charron, L. (1983). Motoneuronal and motor axonal innervation in the rat hindlimb: a comparative study using horseradish peroxidase. *Exp. Brain Res.* 50, 125–132. doi: 10.1007/BF00238239

Prochazka, A., Sontag, K. H., and Wand, P. (1978). Motor reactions to perturbations of gait: proprioceptive and somesthetic involvement. *Neurosci. Lett.* 7, 35–39. doi: 10.1016/0304-3940(78)90109-x

Pujala, A., Blivis, D., and O'Donovan, M. J. (2016). Interactions between dorsal and ventral root stimulation on the generation of locomotor-like activity in the neonatal mouse spinal cord. *eNeuro* 3:ENEURO.0101-16.2016. doi: 10.1523/ENEURO.0101-16.2016

Rigaud, M., Gemes, G., Barabas, M.-E., Chernoff, D. I., Abram, S. E., Stucky, C. L., et al. (2008). Species and strain differences in rodent sciatic nerve anatomy: implications for studies of neuropathic pain. *Pain* 136, 188–201. doi: 10.1016/j.pain.2008.01.016

Rossignol, S., Dubuc, R., and Gossard, J.-P. (2006). Dynamic sensorimotor interactions in locomotion. *Physiol. Rev.* 86, 89–154. doi: 10.1152/physrev.00028.2005

Rudneva, V. N., and Slivko, ÉI. (2000). Long-lasting H-reflex inhibition evoked by stimulation of a nerve to the antagonist muscles and vibrational stimulation of the muscle receptors in humans. *Neurophysiology* 32, 34–37. doi: 10.1007/BF02515166

Rybak, I. A., Dougherty, K. J., and Shevtsova, N. A. (2015). Organization of the mammalian locomotor CPG: review of computational model and circuit architectures based on genetically identified spinal interneurons. *eNeuro* 2:ENEURO.0069-15.2015. doi: 10.1523/ENEURO.0069-15.2015

Rybak, I. A., Shevtsova, N. A., Lafreniere-Roula, M., and McCrea, D. A. (2006a). Modelling spinal circuitry involved in locomotor pattern generation: insights from deletions during fictive locomotion. *J. Physiol.* 577, 617–639. doi: 10.1113/jphysiol.2006.118703

Rybak, I. A., Stecina, K., Shevtsova, N. A., and McCrea, D. A. (2006b). Modelling spinal circuitry involved in locomotor pattern generation: insights from the effects of afferent stimulation. *J. Physiol.* 577, 641–658. doi: 10.1113/jphysiol.2006.118711

Shevtsova, N. A., Talpalar, A. E., Markin, S. N., Harris-Warrick, R. M., Kiehn, O., and Rybak, I. A. (2015). Organization of left-right coordination of neuronal activity in the mammalian spinal cord: insights from computational modelling. *J. Physiol.* 593, 2403–2426. doi: 10.1113/JP270121

Stecina, K., Quevedo, J., and McCrea, D. A. (2005). Parallel reflex pathways from flexor muscle afferents evoking resetting and flexion enhancement during fictive locomotion and scratch in the cat. *J. Physiol.* 569, 275–290. doi: 10.1113/jphysiol.2005.095505

Takeoka, A., and Arber, S. (2019). Functional local proprioceptive feedback circuits initiate and maintain locomotor recovery after spinal cord injury. *Cell Rep.* 27, 71.e3–85.e3. doi: 10.1016/j.celrep.2019.03.010

Takeoka, A., Vollenweider, I., Courtine, G., and Arber, S. (2014). Muscle spindle feedback directs locomotor recovery and circuit reorganization after spinal cord injury. *Cell* 159, 1626–1639. doi: 10.1016/j.cell.2014.11.019

Talpalar, A. E., Endo, T., Löw, P., Borgius, L., Hägglund, M., Dougherty, K. J., et al. (2011). Identification of minimal neuronal networks involved in flexor-extensor alternation in the mammalian spinal cord. *Neuron* 71, 1071–1084. doi: 10.1016/j.neuron.2011.07.011

Vejsada, R., and Hník, P. (1980). Radicular innervation of hindlimb muscles of the rat. *Physiol. Bohemoslov.* 29, 385–392.

Wand, P., Prochazka, A., and Sontag, K. H. (1980). Neuromuscular responses to gait perturbations in freely moving cats. *Exp. Brain Res.* 38, 109–114. doi: 10.1007/bf00237937

Whelan, P., Bonnot, A., and O'Donovan, M. J. (2000). Properties of rhythmic activity generated by the isolated spinal cord of the neonatal mouse. *J. Neurophysiol.* 84, 2821–2833. doi: 10.1152/jn.2000.84.6.2821

Conflict of Interest: The authors declare that the research was conducted in the absence of any commercial or financial relationships that could be construed as a potential conflict of interest.

frontiers in Cellular Neuroscience

REVIEW
published: 08 November 2019
doi: 10.3389/fncel.2019.00505

Intraspinal Plasticity Associated With the Development of Autonomic Dysreflexia After Complete Spinal Cord Injury

*Felicia M. Michael, Samir P. Patel and Alexander G. Rabchevsky**

Department of Physiology, Spinal Cord and Brain Injury Research Center, University of Kentucky, Lexington, KY, United States

Traumatic spinal cord injury (SCI) leads to disruption of sensory, motor and autonomic function, and triggers structural, physiological and biochemical changes that cause reorganization of existing circuits that affect functional recovery. Propriospinal neurons (PN) appear to be very plastic within the inhibitory microenvironment of the injured spinal cord by forming compensatory circuits that aid in relaying information across the lesion site and, thus, are being investigated for their potential to promote locomotor recovery after experimental SCI. Yet the role of PN plasticity in autonomic dysfunction is not well characterized, notably, the disruption of supraspinal modulatory signals to spinal sympathetic neurons after SCI at the sixth thoracic spinal segment or above resulting in autonomic dysreflexia (AD). This condition is characterized by unmodulated sympathetic reflexes triggering sporadic hypertension associated with baroreflex mediated bradycardia in response to noxious yet unperceived stimuli below the injury to reduce blood pressure. AD is frequently triggered by pelvic visceral distension (bowel and bladder), and there are documented structural relationships between injury-induced sprouting of pelvic visceral afferent C-fibers. Their excitation of lumbosacral PN, in turn, sprout and relay noxious visceral sensory stimuli to rostral disinhibited thoracic sympathetic preganglionic neurons (SPN) that manifest hypertension. Herein, we review evidence for maladaptive plasticity of PN in neural circuits mediating heightened sympathetic reflexes after complete high thoracic SCI that manifest cardiovascular dysfunction, as well as contemporary research methodologies being employed to unveil the precise contribution of PN plasticity to the pathophysiology underlying AD development.

Keywords: propriospinal, interneuron, sympathetic preganglionic neurons, cardiovascular dysfunction, hypertension

OPEN ACCESS

Edited by:
Michelle Maria Rank,
The University of Melbourne, Australia

Reviewed by:
Tuan Vu Bui,
University of Ottawa, Canada
Shaoping Hou,
Drexel University, United States
James W. Grau,
Texas A&M University, United States

****Correspondence:***
Alexander G. Rabchevsky
agrab@uky.edu

Received: *26 August 2019*
Accepted: *28 October 2019*
Published: *08 November 2019*

Citation:
Michael FM, Patel SP and Rabchevsky AG (2019) Intraspinal Plasticity Associated With the Development of Autonomic Dysreflexia After Complete Spinal Cord Injury. Front. Cell. Neurosci. 13:505. doi: 10.3389/fncel.2019.00505

INTRODUCTION

Propriospinal neurons (PN) have intraspinal origins and project to interneurons in other spinal cord segments as reported in electrophysiological and tract-tracing studies in feline and rodent models (Alstermark et al., 1981; Chung and Coggeshall, 1983; Skinner et al., 1989; Jankowska, 1992; Flynn et al., 2011). They mediate information relayed between afferent and efferent fibers and, thus, aid in the interaction and integration of different spinal circuits. PN are highly versatile as their function depends on all the spinal circuits with which they are integrated, like motor function associated with central pattern generators (CPG; Ballion et al., 2001; Jordan and Schmidt, 2002) or with circuits relaying painful stimuli to supraspinal centers (Szentagothai, 1964). Thus, PN plays critical roles in transmitting information pertaining to motor, sensory and autonomic function (Jankowska, 1992; Conta and Stelzner, 2004). While we present evidence on the role of PN plasticity for motor recovery after spinal cord injury (SCI), herein we review factors influencing autonomic dysfunction and the contribution of PN plasticity towards this pathophysiology; and how such maladaptive plasticity might be targeted.

PN ROLE IN MOTOR CONTROL AFTER SPINAL CORD INJURY

PN exhibit a high level of neuroplasticity in humans with complete high cervical (C) SCI, in which transcutaneous electrical stimulation of lower limb nerves evoke motor responses in distal forearms (Calancie, 1991). Since such interlimb responses are absent in uninjured or partially injured SCI individuals, and there is a time-dependent decrease in the latency of upper limb muscle responses to electrical stimulation of peripheral nerves in the lower limb, this signifies an increase in regenerative sprouting below the injury to strengthen pre-existing synapses (Calancie et al., 1996). Electrophysiological recordings in cats with lesions at cervical spinal levels C5–C6 show that PN in the C3-C4 region integrate with the severed supraspinal tracts such as corticospinal, rubrospinal, reticulospinal and tectospinal tracts and relay information to distal motor neurons below the injury (Illert et al., 1977). PN mediate both excitatory and inhibitory postsynaptic potentials from corticospinal tracts to distal motor neurons after their transection at C5/C6 in cats (Alstermark et al., 1984). Primate studies have shown that following unilateral corticospinal tract transection in which C3-C4 PN remains intact, the lost grasping reflex is restored within 15 days (Sasaki et al., 2004; Alstermark et al., 2011). This indicates that PN contributes to voluntary motor function *via* disynaptic or polysynaptic pathways constituting corticospinal or reticulospinal tracts that are relayed *via* PN onto motor neurons. Similarly, a trisynaptic cortico-reticulospinal pathway has been reported in rats (Alstermark and Pettersson, 2014), wherein grasping reflex is controlled by both cortico-reticulospinal tract and polysynaptic connections in the spinal cord.

The CPG circuits are responsible for controlling rhythmic motor functions like walking, swimming, crawling, respiration, etc. As observed in isolated spinal cord preparations from neonatal rats subjected to chemical and electrical stimulation, the locomotor CPG is reported to modulate inter-limb coordination and stepping reflex mediated by PN, such that fictive motor responses occurred in phase opposition, similar to walking gait in adult rats (Ballion et al., 2001; Juvin et al., 2005; Zaporozhets et al., 2006). PN project both short and long tracts and their functions vary depending on their location, axonal length, and the direction of the signal relay. Tract tracing studies in uninjured rats using cholera toxin beta injections at L1/L2 in the ventral horn have documented the distribution of short-range PN both ipsilateral and contralateral within the lumbar enlargement (Liu et al., 2010). Similarly, labeling of neurons in the L2-L4 dorsal horns of rats using Phaseolus vulgaris leucoagglutinin and biotinylated dextran (BDA) tracers to differentiate between lateral and medial axonal projections show that the lateral fibers project along the entire length of the spinal cord whereas the medial fibers have shorter projections (Petkó and Antal, 2000). Long-range PN can be classified based on the direction of their axonal projections as ascending or descending, and long descending tracts create links between cervical and lumbar circuits involved in locomotor coordination (Brockett et al., 2013). Moreover, following mid-thoracic dorsal hemisection in rats, new circuits are formed between corticospinal tract axons and PN in the cervical spinal cord whose long tracts eventually connect with lumbar motor neurons (Bareyre et al., 2004).

Short-range PN are reported to be involved in forelimb grasping reflex and hindlimb motor coordination, among other functions, depending on their location in cervical vs. lumbar enlargements (Kostyuk et al., 1971; Alstermark and Kümmel, 1986; Gerasimenko et al., 2002). PN have an innate ability for *de novo* sprouting across the lesion in a feline midsagittal spinal transection model, despite their proximity to the axonal inhibitory protein, chondroitin sulfate proteoglycan (Fenrich et al., 2007; Fenrich and Rose, 2009). In addition to laminae VI and VII, lamina X of upper lumbar (L1/L2) spinal gray matter is considered as one of the presumptive sites for hindlimb CPG interneurons (Kjaerulff and Kiehn, 1996; Magnuson et al., 2005; Beaumont et al., 2006; Reed et al., 2006), and therapeutic preservation of such PN after upper lumbar contusion SCI is correlated with improved locomotor recovery (Patel et al., 2012). Application of N-methyl-D-aspartate (NMDA) between two opposite staggered thoracic spinal cord hemisections abolishes restored spontaneous hind limb functional recovery, suggesting ablation of sprouting PN prevents the formation of newly formed detour circuits after SCI; but the precise contribution of PN to functional recovery has yet to be characterized (Courtine et al., 2008). Using this injury model, Fouad et al. (2010) showed that constitutive activity of serotonergic (5-HT2c) receptors is required to elicit both spasticity as well as spontaneous locomotion *via* PN plasticity.

Injured PN axons respond positively to the presence of specific growth factors in mice with spinal hemisection

(Anderson et al., 2018) and, therefore, PN plasticity is being targeted for its potential to elicit motor recovery after SCI. Accordingly, viral vectors have been used to label specific PN to delineate their roles in forelimb and hindlimb motor circuits in both naïve and mid-thoracic (T9) spinal contused rats (Sheikh et al., 2018). Specifically, highly efficient retrograde gene-transfer (HiRet) lentiviral Tet-On inducible expression vectors have been used to selectively label PN from specific locomotor circuits at C6-T1 or L1-L4. Notably, following T10 contusion SCI, there is a reduction in PN labeling in the T7 spinal cord compared to C3-C4 levels. Such viral vectors may be applied similarly to selectively target PN to activate or silence them to unveil their roles in motor recovery.

AUTONOMIC DYSFUNCTION AFTER SPINAL CORD INJURY

Loss of Supraspinal Control

Profound autonomic dysfunction occurs after an SCI interrupts bulbospinal projections to sympathetic preganglionic neurons (SPN) in the thoracolumbar intermediolateral cell column (IML), which results in the loss of sympathetic modulation from the caudal and rostral ventrolateral medulla (CVLM and RVLM; Finestone and Teasell, 1993). Typically, the higher and more complete the injury, the direr the autonomic consequences as disconnection of SPN from bulbospinal neurons affects the regulation of sympathetic cardiovascular responses (Lehmann et al., 1987). Autonomic dysreflexia (AD) is an often debilitating condition characterized by erratic episodes of severe hypertension associated with or without bradycardia that occurs in patients with complete or incomplete SCI above T5/T6 levels (Karlsson, 1999). The incidence rate of this condition ranges between 20% and 70% in patients suffering from chronic SCI (Snow et al., 1978; Braddom and Rocco, 1991), and symptoms of AD include severe headaches, facial flushing, sweating, shivering, anxiety, piloerection, nausea, changes in vision, nasal congestion, et cetera (Kewalramani, 1980). Patients may also experience arrhythmias, atrial fibrillation, and paroxysmal hypertension (Ekland et al., 2008; Lee and Joo, 2017). Distension of pelvic viscera due to impacted bowel or full bladder is the most common trigger for AD, though other triggers can include ingrown nails and pressure sores (Snow et al., 1978; Harati, 1997; Krassioukov et al., 2003). Consequently, a massive increase in afferent signals reach the spinal cord and trigger a strong sympathetic response resulting in vasoconstriction below the injury (**Figure 1**).

Normally, supraspinal sympathetic regulation starts at the medullary neurons within the RVLM which project onto the SPN (Moon et al., 2002; Hou et al., 2013a). Axons of the SPN depolarize postganglionic neurons within prevertebral sympathetic ganglia that innervate target organs that are countered by the parasympathetic innervation by the vagus nerve (Strack et al., 1988). Baroreflex controls blood pressure *via* baroreceptors present in the heart and blood vessels that monitor and relay the rise/fall in pressure to the nucleus tractus solitarius (NTS) in the brainstem that then modulates the sympathetic response, accordingly. Supraspinal denervation results in the sudden depletion of descending excitatory signals resulting in a 50–70% loss of innervation to SPN (Llewellyn-Smith and Weaver, 2001). This, in turn, strengthens the existing spinal excitatory synapses and promotes reorganization of spinal circuits (Krassioukov and Weaver, 1996; Cassam et al., 1997). Notably, the severity of experimental AD in mice is correlated with the level of serotonergic inputs in the spinal cord that innervate the IML (Cormier et al., 2010), and grafting of neural stem cells derived from embryonic brainstem into T4 spinal transection sites in rats reduced the severity of experimentally induced AD (Hou et al., 2013b). These findings indicate that improving serotonergic connections between the brainstem and regions of IML below the lesion may aid in alleviating severity of AD. However, whether serotonergic innervation improves PN function or modulates SPN directly is uncertain.

Importantly, AD events are accompanied by adrenal hyperactivity with the level of adrenaline and noradrenaline increasing after SCI in humans and rodents that exhibit AD (Chiou-Tan et al., 1998; Leman et al., 2000; Teasell et al., 2000; Karlsson, 2006). SPN that innervate the adrenal gland show increased expression in the immediate early gene c-Fos after experimentally induced AD, a marker for cellular activity (Leman and Sequeira, 2002). It is posited that the alpha-adrenoceptors in blood vessels become hyper-responsive due to reduced presynaptic noradrenaline re-uptake or as a consequence of sympathetic dysfunction (Teasell et al., 2000). This hypersensitivity may also occur as a response to sympathetic mediated vasoconstriction in cutaneous blood vessels (Stjernberg, 1986). While adrenergic hypersensitivity is a noted contributing factor peripherally, we focus on the role of intraspinal plasticity in AD development.

Synaptic Reorganization of SPN

The SPN neurons in the IML responsible for sympathetic activity extending from T1 to L2 spinal segments and SCI-induced changes in SPN phenotype are thought to influence the development of AD (Pyner and Coote, 1994; Krassioukov and Weaver, 1995b). SPN located in the IML sends sympathetic signals to the postganglionic neurons, which in turn relay the information to the target organs like heart, blood vessels, kidney, adrenal gland, etc. (**Figure 1**). In humans with complete SCI, the somal size of the SPN distal to the injury is reduced by almost half at 2 weeks after injury, but similar to normal sizes at longer time points (years; Krassioukov et al., 1999). Following high thoracic (T3) spinal cord transection in rats, dendritic morphologies of SPN show severe atrophy by the first week below the injury (Weaver et al., 1997; Klimaschewski, 2001) with cells closer to the transection site more severely affected than those more distal. While SPN recovers regular morphology after 2 weeks, they also show increased sensitivity to peripheral and visceral stimuli (Krenz and Weaver, 1998a). The increased expression of growth-associated proteins like GAP-43 and synaptophysin (pre-synaptic markers) distal to a T4-T5 transection site a week after injury in rats infers that new intraspinal circuits form in the IML

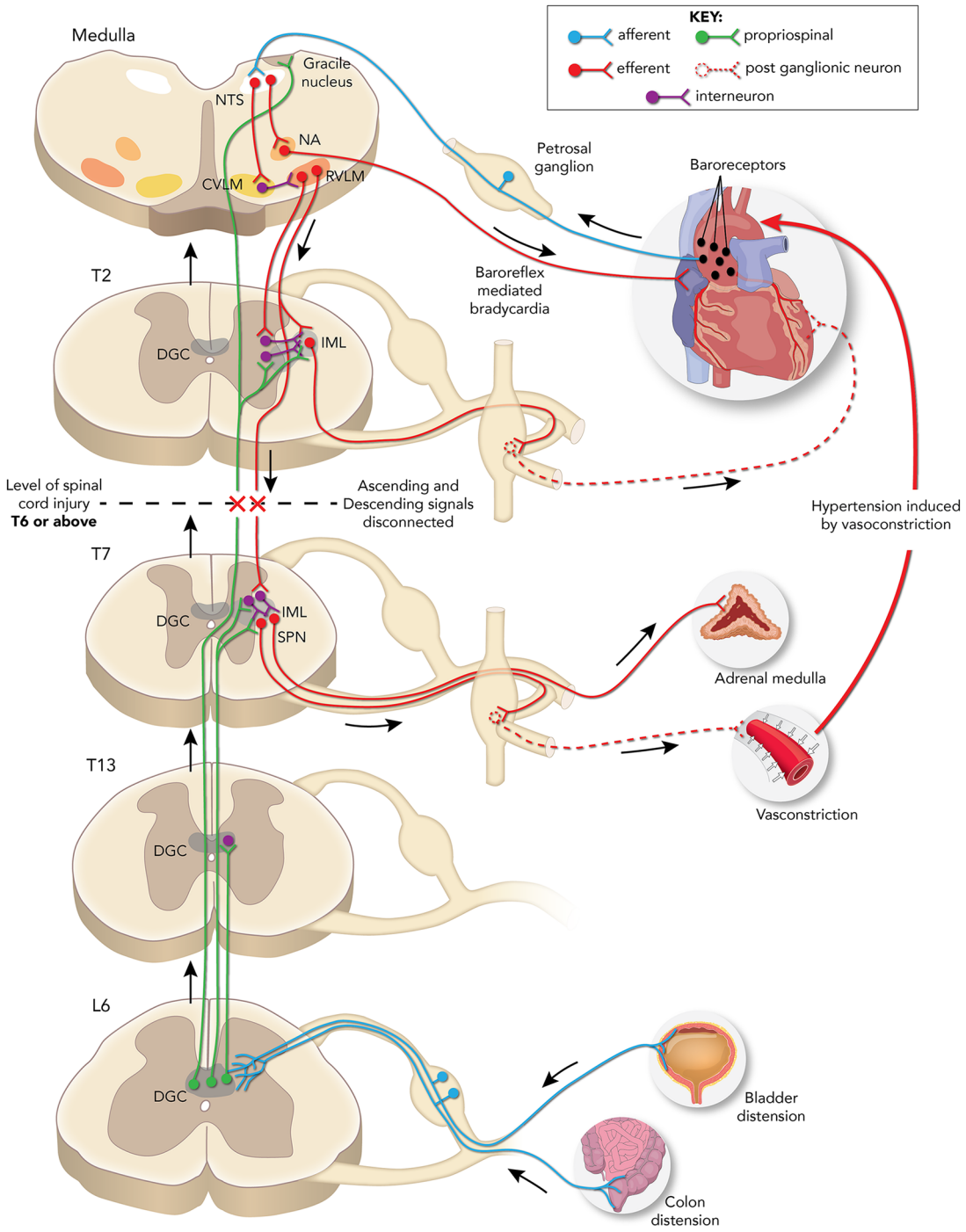

FIGURE 1 | Schematic representation of neuronal pathways disrupted/rerouted by complete spinal cord injury (SCI) above the sixth thoracic (T6) spinal level associated with the development of autonomic dysreflexia (AD) evoked by noxious pelvic visceral distension. Sensory afferent fibers (blue) from the distended bladder or colon transmit noxious stimuli to short and/or long projection propriospinal neurons (PN; green) present in the dorsal gray commissure (DGC) at corresponding spinal levels. These PN then relay the signal rostrally to activate sympathetic preganglionic neurons (SPN) present in the thoracolumbar intermediolateral cell column (IML) directly or *via* interneurons to trigger adrenal hyperactivity, peripheral vasoconstriction, and consequent hypertension. The change in pressure is sensed by baroreceptors (black dots) in the aortic arch which relay the information *via* the nucleus tractus solitarius (NTS) in the medulla to the nucleus ambiguous (NA) that elicits: (1) a parasympathetic bradycardic response and/or; (2) concomitant neuromodulation *via* caudal and rostral ventrolateral medulla (CVLM and RVLM) projections to the IML directly or *via* interneurons to maintain normal blood pressure. After T6 SCI, the decentralized SPN elicits uninhibited vasoconstriction and hypertension, while the NA signals baroreflex mediated bradycardia. The lack of supraspinal regulation of SPN below the injury site maintains the hypertensive response until the noxious stimuli are removed, and maladaptive plasticity of both primary afferent fibers and PN are associated with the development of AD.

after transection (Krassioukov and Weaver, 1996; Weaver et al., 1997). Such reorganization alters the nature of the input to SPN as noted by Llewellyn-Smith and Weaver (2001), who showed that glutamatergic inputs to SPN decreases whereas GABAergic inputs increase during this 2-weeks reorganization period.

Maladaptive Plasticity of Nociceptive Afferents

Whether PN plasticity can be harnessed to improve both motor function while abrogating the development of AD is uncertain, based primarily on the overwhelming evidence that maladaptive neuroplasticity after SCI contributes to several pathological sequelae such as AD, cardiac arrhythmias, neuropathic pain, spasticity, bowel, bladder and sexual dysfunction (Collins et al., 2006; Mathias, 2006; Nout et al., 2006; de Groat and Yoshimura, 2006). In various animal models, both corticospinal and intraspinal circuits are reorganized following SCI (Tandon et al., 2009; Ghosh et al., 2010; Asboth et al., 2018), and such sudden increases in neuronal sprouting without suitable axon guidance cues and supraspinal modulation leads to an imbalance of inhibitory and excitatory signaling (see Brown and Weaver, 2012).

Complete T4 SCI in rats elicits afferent fiber sprouting into lower spinal levels that persist chronically (Krassioukov and Weaver, 1995a). Afferent fibers include Aβ, Aδ, and C-fibers, with calcitonin gene-related peptide (CGRP) expressed in all three types (McCarthy and Lawson, 1990; Lawson et al., 1993, 1996; Krenz and Weaver, 1998b; Wong et al., 2000; Marsh and Weaver, 2004). Maladaptive plasticity mediating pain and autonomic dysfunction has been attributed to an increased intraspinal sprouting of both CGRP immunoreactive nociceptive afferent C-fibers into the dorsal horns below the site of SCI (Christensen and Hulsebosch, 1997; Krenz et al., 1999), as well as increased serotonergic fiber densities rostral to the injury (Oatway et al., 2005). Altered glutamatergic signaling after SCI contributes to abnormally increased activity in spinal sympathetic reflex circuits (Maiorov et al., 1997), and Krenz and Weaver (1998b) reported that hyperreflexia observed after injury was due to due sprouting of unmyelinated C-fibers to increase afferent fiber input onto interneurons. While the primary contributing factors for the development of AD after injury are thought to be maladaptive sprouting of afferent fibers and PN, their individual contributions to this syndrome remain uncertain.

For example, the prevention of C-fiber sprouting using intrathecal nerve growth factor (NGF) neutralizing antibody or trkA-IgG fusion protein in T4 spinal transected rats decreases CGRP-fiber density in association with reduced AD symptoms in experimental rats undergoing experimental colorectal distension (CRD; Christensen and Hulsebosch, 1997; Krenz et al., 1999; Marsh et al., 2002; Weaver et al., 2006). Moreover, complete T4 transection significantly increases sprouting of C-fibers innervating the distal colon into the lumbosacral spinal cord (Hou et al., 2009), and over-expression of NGF using viral vectors injected into the lumbosacral dorsal horn increases the severity of AD in response to CRD (Cameron et al., 2006). On the contrary, while viral over-expression of semaphorin 3a, a chemorepulsive factor for C-fibers, reduces the severity of CRD induced hypertension in parallel to reduced sprouting of nociceptive visceral afferent C-fibers into the spinal cord, it does not completely abolish the pathology. Alternatively, increased CGRP+ fiber sprouting following complete T4 spinal transection does not accompany the development of AD in some strains of mice (Jacob et al., 2003), which points to an underappreciated role played by PN plasticity in manifesting AD.

AUTONOMIC PN

Autonomic PN are pre-sympathetic as they innervate the SPN to control their level of excitation (Gebber and McCall, 1976), but the role of PN in eliciting sympathetic control is highly underappreciated. Supraspinal centers play critical roles in sympathetic regulation when compared to interneurons, but when this control is lost due to pathological conditions like SCI, then the PN take over sympathetic regulation by directly acting on the SPN to evoke responses (Schramm, 2006). The primary afferent fibers that carry the signal to the spinal cord are not directly linked to the SPN, they communicate with the SPN primarily *via* interneurons that may be excitatory or inhibitory in nature depending on the type and location of the stimuli (Chau et al., 2000). PN with sympathetic function predominantly present in the dorsal horn of cats were identified electrophysiologically by Gebber and McCall (1976) by cross-correlating PN spikes with signals in sympathetic nerves, and all signals with low inter-spike intervals (<20) were inferred to be from sympathetic PN.

BDA anterograde tracer injected into the central gray matter at rat L6-S2 spinal levels shows that ascending PN extend projections up to cervical levels through lamina X, and retrograde labeling using wheat germ agglutinin-horseradish peroxidase show projections to laminae VII and VIII at lumbar and thoracic levels indicating the anatomical locations of ascending PN (Matsushita, 1998; Petkó and Antal, 2000). Similarly, when Phaseolus vulgaris leucoagglutinin tracer is injected in lamina X of the lumbosacral cord, PN projection axons in the dorsal column and ventrolateral funiculus at the cervical level are labeled (Wang et al., 1999). Transynaptic retrograde tracing with pseudorabies virus injected into the adrenal gland, kidney, and stellate ganglion label PN in lamina VII and X extending from T4–T13, T11–T13 and C1–C4 spinal levels, respectively (Strack et al., 1989; Jansen et al., 1995; Tang et al., 2004). Moreover, a population of GABAergic interneurons innervating SPN has also been identified in the spinal central autonomic area (Deuchars et al., 2005), also termed the dorsal gray commissure (DGC, lamina X). Importantly, bladder distension in rats with spinal transection activates afferent fibers to increase the number of c-Fos-immunoreactive neurons in the DGC/lamina X and lateral dorsal horn of the L6/S1 segments (Vizzard, 2000), indicating that lumbosacral PN disconnected from supraspinal control are activated *de novo* by visceral stimuli following SCI.

Plasticity of Autonomic PN After SCI

Ascending PN plasticity is believed to contribute to the development of AD. These neurons relay visceral sensory

information towards the SPN in the thoracic cord (Rabchevsky, 2006; Schramm, 2006). Functional plasticity of PN comprising spinal sympathetic circuits after SCI in the rat was reported by Krassioukov et al. (2002) investigating sympathetically-correlated interneuron responses to applied stimuli below the injury hours (acute) or 1 month (chronic) following T3 transection. It was found that only in the chronic stage of injury, interneurons' electrical activities were cross-correlated with renal sympathetic nerve activities during CRD and skin pinching caudal to the injury. This study showed that plasticity occurs within somatosensory PN that modulate sympathetic activity in the weeks after injury and that peripheral stimulation in chronic SCI rats activates more interneurons compared to acute SCI animals.

Accordingly, BDA tracers injected into the lumbosacral cord following T4 transection show more labeling of ascending lumbosacral PN fibers that originate at the DGC and terminate proximal to Fluorogold-labeled thoracic SPN (Hou et al., 2008). The visceral sensory afferent fibers terminate at the DGC and the signal is relayed up towards the target regions *via* intraspinal projection neurons (Pascual et al., 1993; Hosoya et al., 1994; Al-Chaer et al., 1996; Matsushita, 1998; Vizzard et al., 2000). Extended CRD trials performed 2 weeks after T4 SCI increase neuronal activity throughout the lumbosacral DGC, as shown by conspicuously higher numbers of c-Fos positive neurons in comparison to sham controls (Hou et al., 2008). However, it is currently unclear whether ascending DGC neurons modulate SPN activity by directly projecting to the SPN or indirectly *via* interneurons. After SCI, the supraspinal control is lost but the SPN are activated by peripheral afferent stimuli whose signal is relayed *via* ascending PN to trigger a sympathetic response, resulting in hypertension (**Figure 1**; Schramm, 2006).

Excitatory interneuron connectivity with SPN preferentially increases after T3 spinal transection in mice, and repeated CRD induces an increase in these excitatory interneurons co-labeled with vGlut2 (Ueno et al., 2016). This indicates that visceral noxious stimuli trigger excitatory PN sprouting that augments SPN signaling leading to AD. The existence of PN relaying afferent input to SPN may be sufficient to trigger sympathetic responses, and the lack of supraspinal modulatory signals results in uninhibited continuous sympathetic firing leading to hypertensive crises (Rabchevsky, 2006). Thus, plasticity of ascending PN and local sensory afferent fibers augment the noxious input to activate SPN, which in turn triggers a volley of sympathetic discharge and consequent vasoconstriction leading to AD (**Figure 1**).

Techniques for Targeting PN Selectively

Electrophysiology and retrograde tract-tracing are the most common tools used to identify the tracts involved in autonomic function. Although several studies labeling long descending PN and short tract PN exist, it is still highly challenging to specifically target and label ascending propriospinal tracts after injury due to unintended labeling of fibers en passage. Moreover, it is reported that transsynaptic labeling by pseudorabies virus is significantly reduced in the T4 transected spinal cord (Duale et al., 2009), thus limiting the availability of effective tools for tracing the course of these neurons after injury. While selective inhibition of interneurons may aid in understanding and possibly alleviating the development and/or symptoms of AD, silencing interneurons involved in eliciting AD without affecting the interneurons involved in other important functions adds to the complexity when no effective tools exist to specifically identify interneurons. Using contemporary chemogenetic tools designed to silence specific neuronal populations of PN, it may now be possible to target and delineate the role of PN plasticity in the development of AD.

In this regard, Kinoshita et al. (2012) reversibly silenced PN involved in primate forelimb control by infecting the ventral horn of C6-T1 spinal segments in macaque monkeys with HiRet lentiviral vectors that contained enhanced tetanus neurotoxin toxin light chain (eTeNT) and eGFP coding sequences downstream of the tetracycline-responsive element (TRE) sequence. An adeno-associated viral vector containing the Tet-On sequence (AAV-Tet-On) was injected in the intermediate zone of cervical C2-C5 levels prospectively containing the cell soma, and only cells that had been transfected by both vectors were silenced by the Tet-ON reaction with doxycycline. Since PNs extend through these areas, they were predominantly labeled and selectively silenced by these vectors, thus enabling selective and temporal labeling with GFP and simultaneous silencing of the forelimb locomotor circuit encompassing the motor cortex, PN and motor neurons controlling hand movement. In theory, a similar modality may be used to identify the role of PN in rodent SCI models that elicit AD by selectively silencing lumbosacral PN that relay signals from afferent fibers below the lesion to SPN during noxious CRD. Specifically, the GFP tagged Hiret lentiviral vectors can be used to retrogradely label ascending lumbosacral PN innervating the thoracic IML, and by injecting AAV-TetON vectors to transduce PN in the lumbosacral DGC, it would enable selective targeting and silencing of the dual-labeled ascending PN (Eldahan and Rabchevsky, 2018).

CONCLUSION

PN plasticity after traumatic SCI plays a critical role in improving not only spontaneous motor function but also potentially aggravating autonomic dysfunction. In addition to afferent C-fiber sprouting and loss of supraspinal regulation of the IML, maladaptive plasticity of PN below the level of high thoracic SCI appears essential for manifesting chronic autonomic dysfunction. Thus, while selectively promoting PN sprouting might serve as a promising therapeutic target for specific motor functional recovery, it may also be prevented selectively to combat AD development and/or severity, and the advancement of strategies to reversibly silence these interneurons will help further our understanding on their role in AD.

AUTHOR CONTRIBUTIONS

FM wrote the first draft of the manuscript. SP reviewed the manuscript. AR critically evaluated the manuscript and wrote the final revised version. All authors contributing to the manuscript have read and approved the submitted version.

FUNDING

We gratefully acknowledge the support of an endowment from the University of Kentucky, Spinal Cord and Brain Injury Research Center (AGR).

ACKNOWLEDGMENTS

We greatly thank Matt Hazzard and Tom Dolan for their artistic renditions, University of Kentucky, College of Medicine.

REFERENCES

Al-Chaer, E. D., Lawand, N. B., Westlund, K. N., and Willis, W. D. (1996). Visceral nociceptive input into the ventral posterolateral nucleus of the thalamus: a new function for the dorsal column pathway. *J. Neurophysiol.* 76, 2661–2674. doi: 10.1152/jn.1996.76.4.2661

Alstermark, B., and Kümmel, H. (1986). Transneuronal labelling of neurones projecting to forelimb motoneurones in cats performing different movements. *Brain Res.* 376, 387–391. doi: 10.1016/0006-8993(86)90205-2

Alstermark, B., Lindstrom, S., Lundberg, A., and Sybirska, E. (1981). Integration in descending motor pathways controlling the forelimb in the cat: 8. Ascending projection to the lateral reticular nucleus from C3–C4 propriospinal also projecting to forelimb motoneurones. *Exp. Brain Res.* 42, 282–298. doi: 10.1007/bf00237495

Alstermark, B., Lundberg, A., and Sasaki, S. (1984). Integration in descending motor pathways controlling the forelimb in the cat. 12. Interneurones which may mediate descending feed-forward inhibition and feed-back inhibition from the forelimb to C3–C4 propriospinal neurones. *Exp. Brain Res.* 56, 308–322. doi: 10.1007/bf00236286

Alstermark, B., and Pettersson, L. G. (2014). Skilled reaching and grasping in the rat: lacking effect of corticospinal lesion. *Front. Neurol.* 5:103. doi: 10.3389/fneur.2014.00103

Alstermark, B., Pettersson, L. G., Nishimura, Y., Yoshino-Saito, K., Tsuboi, F., Takahashi, M., et al. (2011). Motor command for precision grip in the macaque monkey can be mediated by spinal interneurons. *J. Neurophysiol.* 106, 122–126. doi: 10.1152/jn.00089.2011

Anderson, M. A., O'Shea, T. M., Burda, J. E., Ao, Y., Barlatey, S. L., Bernstein, A. M., et al. (2018). Required growth facilitators propel axon regeneration across complete spinal cord injury. *Nature* 561, 396–400. doi: 10.1038/s41586-018-0467-6

Asboth, L., Friedli, L., Beauparlant, J., Martinez-Gonzalez, C., Anil, S., Rey, E., et al. (2018). Cortico-reticulo-spinal circuit reorganization enables functional recovery after severe spinal cord contusion. *Nat. Neurosci.* 21, 576–588. doi: 10.1038/s41593-018-0093-5

Ballion, B., Morin, D., and Viala, D. (2001). Forelimb locomotor generators and quadrupedal locomotion in the neonatal rat. *Eur. J. Neurosci.* 14, 1727–1738. doi: 10.1046/j.0953-816x.2001.01794.x

Bareyre, F. M., Kerschensteiner, M., Raineteau, O., Mettenleiter, T. C., Weinmann, O., and Schwab, M. E. (2004). The injured spinal cord spontaneously forms a new intraspinal circuit in adult rats. *Nat. Neurosci.* 7, 269–277. doi: 10.1038/nn1195

Beaumont, E., Onifer, S. M., Reed, W. R., and Magnuson, D. S. (2006). Magnetically evoked inter-enlargement response: an assessment of ascending propriospinal fibers following spinal cord injury. *Exp. Neurol.* 201, 428–440. doi: 10.1016/j.expneurol.2006.04.032

Braddom, R. L., and Rocco, J. F. (1991). Autonomic dysreflexia. A survey of current treatment. *Am. J. Phys. Med. Rehabil.* 70, 234–241. doi: 10.1097/00002060-199110000-00002

Brockett, E. G., Seenan, P. G., Bannatyne, B. A., and Maxwell, D. J. (2013). Ascending and descending propriospinal pathways between lumbar and cervical segments in the rat: evidence for a substantial ascending excitatory pathway. *Neuroscience* 240, 83–97. doi: 10.1016/j.neuroscience.2013.02.039

Brown, A., and Weaver, L. C. (2012). The dark side of neuroplasticity. *Exp. Neurol.* 235, 133–141. doi: 10.1016/j.expneurol.2011.11.004

Calancie, B. (1991). Interlimb reflexes following cervical spinal cord injury in man. *Exp. Brain Res.* 85, 458–469. doi: 10.1007/bf00229423

Calancie, B., Lutton, S., and Broton, J. G. (1996). Central nervous system plasticity after spinal cord injury in man: interlimb reflexes and the influence of cutaneous stimulation. *Electroencephalogr. Clin. Neurophysiol.* 101, 304–315. doi: 10.1016/0924-980x(96)95194-2

Cameron, A. A., Smith, G. M., Randall, D. C., Brown, D. R., and Rabchevsky, A. G. (2006). Genetic manipulation of intraspinal plasticity after spinal cord injury alters the severity of autonomic dysreflexia. *J. Neurosci.* 26, 2923–2932. doi: 10.1523/JNEUROSCI.4390-05.2006

Cassam, A. K., Llewellyn-Smith, I. J., and Weaver, L. C. (1997). Catecholamine enzymes and neuropeptides are expressed in fibres and somata in the intermediate gray matter in chronic spinal rats. *Neuroscience* 78, 829–841. doi: 10.1016/s0306-4522(96)00599-4

Chau, D., Johns, D. G., and Schramm, L. P. (2000). Ongoing and stimulus-evoked activity of sympathetically correlated neurons in the intermediate zone and dorsal horn of acutely spinalized rats. *J. Neurophysiol.* 83, 2699–2707. doi: 10.1152/jn.2000.83.5.2699

Chiou-Tan, F. Y., Robertson, C. S., and Chiou, G. C. (1998). Catecholamine assays in a rat model for autonomic dysreflexia. *Arch. Phys. Med. Rehabil.* 79, 402–404. doi: 10.1016/s0003-9993(98)90140-x

Christensen, M. D., and Hulsebosch, C. E. (1997). Spinal cord injury and anti-NGF treatment results in changes in CGRP density and distribution in the dorsal horn in the rat. *Exp. Neurol.* 147, 463–475. doi: 10.1006/exnr.1997.6608

Chung, K., and Coggeshall, R. E. (1983). Propriospinal fibers in the rat. *J. Comp. Neurol.* 217, 47–53. doi: 10.1002/cne.902170105

Collins, H. L., Rodenbaugh, D. W., and DiCarlo, S. E. (2006). Spinal cord injury alters cardiac electrophysiology and increases the susceptibility to ventricular arrhythmias. *Prog. Brain Res.* 152, 275–288. doi: 10.1016/s0079-6123(05)52018-1

Conta, A. C., and Stelzner, D. J. (2004). Differential vulnerability of propriospinal tract neurons to spinal cord contusion injury. *J. Comp. Neurol.* 479, 347–359. doi: 10.1002/cne.20319

Cormier, C. M., Mukhida, K., Walker, G., and Marsh, D. R. (2010). Development of autonomic dysreflexia after spinal cord injury is associated with a lack of serotonergic axons in the intermediolateral cell column. *J. Neurotrauma* 27, 1805–1818. doi: 10.1089/neu.2010.1441

Courtine, G., Song, B., Roy, R. R., Zhong, H., Herrmann, J. E., Ao, Y., et al. (2008). Recovery of supraspinal control of stepping *via* indirect propriospinal relay connections after spinal cord injury. *Nat. Med.* 14, 69–74. doi: 10.1038/nm1682

de Groat, W. C., and Yoshimura, N. (2006). Mechanisms underlying the recovery of lower urinary tract function following spinal cord injury. *Prog. Brain Res.* 152, 59–84. doi: 10.1016/s0079-6123(05)52005-3

Deuchars, S. A., Milligan, C. J., Stornetta, R. L., and Deuchars, J. (2005). GABAergic neurons in the central region of the spinal cord: a novel substrate for sympathetic inhibition. *J. Neurosci.* 25, 1063–1070. doi: 10.1523/JNEUROSCI.3740-04.2005

Duale, H., Hou, S., Derbenev, A. V., Smith, B. N., and Rabchevsky, A. G. (2009). Spinal cord injury reduces the efficacy of pseudorabies virus labeling of sympathetic preganglionic neurons. *J. Neuropathol. Exp. Neurol.* 68, 168–178. doi: 10.1097/nen.0b013e3181967df7

Ekland, M. B., Krassioukov, A. V., McBride, K. E., and Elliott, S. L. (2008). Incidence of autonomic dysreflexia and silent autonomic dysreflexia in men with spinal cord injury undergoing sperm retrieval: implications for clinical practice. *J. Spinal Cord Med.* 31, 33–39. doi: 10.1080/10790268.2008.11753978

Eldahan, K. C., and Rabchevsky, A. G. (2018). Autonomic dysreflexia after spinal cord injury: systemic pathophysiology and methods of management. *Auton. Neurosci.* 209, 59–70. doi: 10.1016/j.autneu.2017.05.002

Fenrich, K. K., and Rose, P. K. (2009). Spinal interneuron axons spontaneously regenerate after spinal cord injury in the adult feline. *J. Neurosci.* 29, 12145–12158. doi: 10.1523/JNEUROSCI.0897-09.2009

Fenrich, K. K., Skelton, N., MacDermid, V. E., Meehan, C. F., Armstrong, S., Neuber-Hess, M. S., et al. (2007). Axonal regeneration and development of de novo axons from distal dendrites of adult feline commissural interneurons after a proximal axotomy. *J. Comp. Neurol.* 502, 1079–1097. doi: 10.1002/cne.21362

Finestone, H. M., and Teasell, R. W. (1993). Autonomic dysreflexia after brainstem tumor resection. A case report. *Am. J. Phys. Med. Rehabil.* 72, 395–397. doi: 10.1097/00002060-199312000-00011

Flynn, J. R., Graham, B. A., Galea, M. P., and Callister, R. J. (2011). The role of propriospinal interneurons in recovery from spinal cord injury. *Neuropharmacology* 60, 809–822. doi: 10.1016/j.neuropharm.2011.01.016

Fouad, K., Rank, M. M., Vavrek, R., Murray, K. C., Sanelli, L., and Bennett, D. J. (2010). Locomotion after spinal cord injury depends on constitutive activity in serotonin receptors. *J. Neurophysiol.* 104, 2975–2984. doi: 10.1152/jn.00499.2010

Gebber, G. L., and McCall, R. B. (1976). Identification and discharge patterns of spinal sympathetic interneurons. *Am. J. Physiol.* 231, 722–733. doi: 10.1152/ajplegacy.1976.231.3.722

Gerasimenko, Y. P., Makarovskii, A. N., and Nikitin, O. A. (2002). Control of locomotor activity in humans and animals in the absence of supraspinal influences. *Neurosci. Behav. Physiol.* 32, 417–423. doi: 10.1023/a:1015836428932

Ghosh, A., Haiss, F., Sydekum, E., Schneider, R., Gullo, M., Wyss, M. T., et al. (2010). Rewiring of hindlimb corticospinal neurons after spinal cord injury. *Nat. Neurosci.* 13, 97–104. doi: 10.1038/nn.2448

Harati, Y. (1997). "Autonomic disorders associated with spinal cord injury," in *Clinical Autonomic Disorders*, 2nd Edn., ed. P. A. Low (Philadelphia, PA: Lippincott-Raven), 455–461.

Hosoya, Y., Nadelhaft, I., Wang, D., and Kohno, K. (1994). Thoracolumbar sympathetic preganglionic neurons in the dorsal commissural nucleus of the male rat: an immunohistochemical study using retrograde labeling of cholera toxin subunit B. *Exp. Brain Res.* 98, 21–30. doi: 10.1007/bf00229105

Hou, S., Duale, H., Cameron, A. A., Abshire, S. M., Lyttle, T. S., and Rabchevsky, A. G. (2008). Plasticity of lumbosacral propriospinal neurons is associated with the development of autonomic dysreflexia after thoracic spinal cord transection. *J. Comp. Neurol.* 509, 382–399. doi: 10.1002/cne.21771

Hou, S., Duale, H., and Rabchevsky, A. G. (2009). Intraspinal sprouting of unmyelinated pelvic afferents after complete spinal cord injury is correlated with autonomic dysreflexia induced by visceral pain. *Neuroscience* 159, 369–379. doi: 10.1016/j.neuroscience.2008.12.022

Hou, S., Lu, P., and Blesch, A. (2013a). Characterization of supraspinal vasomotor pathways and autonomic dysreflexia after spinal cord injury in F344 rats. *Auton. Neurosci.* 176, 54–63. doi: 10.1016/j.autneu.2013.02.001

Hou, S., Tom, V. J., Graham, L., Lu, P., and Blesch, A. (2013b). Partial restoration of cardiovascular function by embryonic neural stem cell grafts after complete spinal cord transection. *J. Neurosci.* 33, 17138–17149. doi: 10.1523/JNEUROSCI.2851-13.2013

Illert, M., Lundberg, A., and Tanaka, R. (1977). Integration in descending motor pathways controlling the forelimb in the cat. 3. Convergence on propriospinal neurones transmitting disynaptic excitation from the corticospinal tract and other descending tracts. *Exp. Brain Res.* 29, 323–346. doi: 10.1007/bf00236174

Jacob, J. E., Gris, P., Fehlings, M. G., Weaver, L. C., and Brown, A. (2003). Autonomic dysreflexia after spinal cord transection or compression in 129Sv, C57BL, and Wallerian degeneration slow mutant mice. *Prog. Brain Res.* 183, 136–146. doi: 10.1016/s0014-4886(03)00161-4

Jankowska, E. (1992). Interneuronal relay in spinal pathways from proprioceptors. *Prog. Neurobiol.* 38, 335–378. doi: 10.1016/0301-0082(92)90024-9

Jansen, A. S., Wessendorf, M. W., and Loewy, A. D. (1995). Transneuronal labeling of CNS neuropeptide and monoamine neurons after pseudorabies virus injections into the stellate ganglion. *Brain Res.* 683, 1–24. doi: 10.1016/0006-8993(95)00276-v

Jordan, L. M., and Schmidt, B. J. (2002). Propriospinal neurons involved in the control of locomotion: potential targets for repair strategies? *Prog. Brain Res.* 137, 125–139. doi: 10.1016/s0079-6123(02)37012-2

Juvin, L., Simmers, J., and Morin, D. (2005). Propriospinal circuitry underlying interlimb coordination in mammalian quadrupedal locomotion. *J. Neurosci.* 25, 6025–6035. doi: 10.1523/JNEUROSCI.0696-05.2005

Karlsson, A. K. (1999). Autonomic dysreflexia. *Spinal Cord* 37, 383–391. doi: 10.1038/sj.sc.3100867

Karlsson, A. K. (2006). Autonomic dysfunction in spinal cord injury: clinical presentation of symptoms and signs. *Prog. Brain Res.* 152, 1–8. doi: 10.1016/s0079-6123(05)52034-x

Kewalramani, L. S. (1980). Autonomic dysreflexia in traumatic myelopathy. *Am. J. Phys. Med.* 59, 1–21.

Kinoshita, M., Matsui, R., Kato, S., Hasegawa, T., Kasahara, H., Isa, K., et al. (2012). Genetic dissection of the circuit for hand dexterity in primates. *Nature* 487, 235–238. doi: 10.1038/nature11206

Kjaerulff, O., and Kiehn, O. (1996). Distribution of networks generating and coordinating locomotor activity in the neonatal rat spinal cord *in vitro*: a lesion study. *J. Neurosci.* 16, 5777–5794. doi: 10.1523/JNEUROSCI.16-18-05777.1996

Klimaschewski, L. (2001). Increased innervation of rat preganglionic sympathetic neurons by substance P containing nerve fibers in response to spinal cord injury. *Neurosci. Lett.* 307, 73–76. doi: 10.1016/s0304-3940(01)01922-x

Kostyuk, P. G., Vasilenko, D. A., and Lang, E. (1971). Propriospinal pathways in the dorsolateral funiculus and their effects on lumbosacral motoneuronal pools. *Brain Res.* 28, 233–249. doi: 10.1016/0006-8993(71)90657-3

Krassioukov, A. V., Bunge, R. P., Pucket, W. R., and Bygrave, M. A. (1999). The changes in human spinal sympathetic preganglionic neurons after spinal cord injury. *Spinal Cord* 37, 6–13. doi: 10.1038/sj.sc.3100718

Krassioukov, A. V., Furlan, J. C., and Fehlings, M. G. (2003). Autonomic dysreflexia in acute spinal cord injury: an under-recognized clinical entity. *J. Neurotrauma* 20, 707–716. doi: 10.1089/089771503767869944

Krassioukov, A. V., and Weaver, L. C. (1995a). Episodic hypertension due to autonomic dysreflexia in acute and chronic spinal cord-injured rats. *Am. J. Physiol.* 268, H2077–H2083. doi: 10.1152/ajpheart.1995.268.5.h2077

Krassioukov, A. V., and Weaver, L. C. (1995b). Reflex and morphological changes in spinal preganglionic neurons after cord injury in rats. *Clin. Exp. Hypertens* 17, 361–373. doi: 10.3109/10641969509087077

Krassioukov, A. V., and Weaver, L. C. (1996). Morphological changes in sympathetic preganglionic neurons after spinal cord injury in rats. *Neuroscience* 70, 211–225. doi: 10.1016/0306-4522(95)00294-s

Krassioukov, A. V., Johns, D. G., and Schramm, L. P. (2002). Sensitivity of sympathetically correlated spinal interneurons, renal sympathetic nerve activity, and arterial pressure to somatic and visceral stimuli after chronic spinal injury. *J. Neurotrauma* 19, 1521–1529. doi: 10.1089/089771502762300193

Krenz, N. R., Meakin, S. O., Krassioukov, A. V., and Weaver, L. C. (1999). Neutralizing intraspinal nerve growth factor blocks autonomic dysreflexia caused by spinal cord injury. *J. Neurosci.* 19, 7405–7414. doi: 10.1523/JNEUROSCI.19-17-07405.1999

Krenz, N. R., and Weaver, L. C. (1998a). Changes in the morphology of sympathetic preganglionic neurons parallel the development of autonomic dysreflexia after spinal cord injury in rats. *Neurosci. Lett.* 243, 61–64. doi: 10.1016/s0304-3940(98)00101-3

Krenz, N. R., and Weaver, L. C. (1998b). Sprouting of primary afferent fibers after spinal cord transection in the rat. *Neuroscience* 85, 443–458. doi: 10.1016/s0306-4522(97)00622-2

Lawson, S. N., McCarthy, P. W., and Prabhakar, E. (1996). Electrophysiological properties of neurones with CGRP-like immunoreactivity in rat dorsal root ganglia. *J. Comp. Neurol.* 365, 355–366. doi: 10.1002/(sici)1096-9861(19960212)365:3<355::aid-cne2>3.3.co;2-s

Lawson, S. N., Perry, M. J., Prabhakar, E., and McCarthy, P. W. (1993). Primary sensory neurones: neurofilament, neuropeptides, and conduction velocity. *Brain Res. Bull.* 30, 239–243. doi: 10.1016/0361-9230(93)90250-f

Lee, E. S., and Joo, M. C. (2017). Prevalence of autonomic dysreflexia in patients with spinal cord injury above T6. *Biomed Res. Int.* 2017, 2027594–2027594. doi: 10.1155/2017/2027594

Lehmann, K. G., Lane, J. G., Piepmeier, J. M., and Batsford, W. P. (1987). Cardiovascular abnormalities accompanying acute spinal cord injury in humans: incidence, time course and severity. *J. Am. Coll. Cardiol.* 10, 46–52. doi: 10.1016/s0735-1097(87)80158-4

Leman, S., Bernet, F., and Sequeira, H. (2000). Autonomic dysreflexia increases plasma adrenaline level in the chronic spinal cord-injured rat. *Neurosci. Lett.* 286, 159–162. doi: 10.1016/s0304-3940(00)01111-3

Leman, S., and Sequeira, H. (2002). Activation of adrenal preganglionic neurons during autonomic dysreflexia in the chronic spinal cord-injured rat. *Auton. Neurosci.* 98, 94–98. doi: 10.1016/s1566-0702(02)00040-1

Liu, T. T., Bannatyne, B. A., and Maxwell, D. J. (2010). Organization and neurochemical properties of intersegmental interneurons in the lumbar enlargement of the adult rat. *Neuroscience* 171, 461–484. doi: 10.1016/j.neuroscience.2010.09.012

Llewellyn-Smith, I. J., and Weaver, L. C. (2001). Changes in synaptic inputs to sympathetic preganglionic neurons after spinal cord injury. *J. Comp. Neurol.* 435, 226–240. doi: 10.1002/cne.1204

Magnuson, D. S., Lovett, R., Coffee, C., Gray, R., Han, Y., Zhang, Y. P., et al. (2005). Functional consequences of lumbar spinal cord contusion injuries in the adult rat. *J. Neurotrauma* 22, 529–543. doi: 10.1089/neu.2005.22.529

Maiorov, D. N., Weaver, L. C., and Krassioukov, A. V. (1997). Relationship between sympathetic activity and arterial pressure in conscious spinal rats. *Am. J. Physiol.* 272, H625–H631. doi: 10.1152/ajpheart.1997.272.2.h625

Marsh, D. R., and Weaver, L. C. (2004). Autonomic dysreflexia, induced by noxious or innocuous stimulation, does not depend on changes in dorsal horn substance p. *Ann. Ital. Chir.* 21, 817–828. doi: 10.1089/089771504126960 5

Marsh, D. R., Wong, S. T., Meakin, S. O., MacDonald, J. I., Hamilton, E. F., and Weaver, L. C. (2002). Neutralizing intraspinal nerve growth factor with a trkA-IgG fusion protein blocks the development of autonomic dysreflexia in a clip-compression model of spinal cord injury. *J. Neurotrauma* 19, 1531–1541. doi: 10.1089/089771502762300201

Mathias, C. J. (2006). Orthostatic hypotension and paroxysmal hypertension in humans with high spinal cord injury. *Prog. Brain Res.* 152, 231–243. doi: 10.1016/s0079-6123(05)52015-6

Matsushita, M. (1998). Ascending propriospinal afferents to area X (substantia grisea centralis) of the spinal cord in the rat. *Exp. Brain Res.* 119, 356–366. doi: 10.1007/s002210050351

McCarthy, P. W., and Lawson, S. N. (1990). Cell type and conduction velocity of rat primary sensory neurons with calcitonin gene-related peptide-like immunoreactivity. *Neuroscience* 34, 623–632. doi: 10.1016/0306-4522(90)90169-5

Moon, E. A., Goodchild, A. K., and Pilowsky, P. M. (2002). Lateralisation of projections from the rostral ventrolateral medulla to sympathetic preganglionic neurons in the rat. *Brain Res.* 929, 181–190. doi: 10.1016/s0006-8993(01)03388-1

Nout, Y. S., Leedy, G. M., Beattie, M. S., and Bresnahan, J. C. (2006). Alterations in eliminative and sexual reflexes after spinal cord injury: defecatory function and development of spasticity in pelvic floor musculature. *Prog. Brain Res.* 152, 359–372. doi: 10.1016/s0079-6123(05)52024-7

Oatway, M. A., Chen, Y., Bruce, J. C., Dekaban, G. A., and Weaver, L. C. (2005). Anti-CD11d integrin antibody treatment restores normal serotonergic projections to the dorsal, intermediate and ventral horns of the injured spinal cord. *J. Neurosci.* 25, 637–647. doi: 10.1523/jneurosci.3960-04.2005

Pascual, J. I., Insausti, R., and Gonzalo, L. M. (1993). Urinary bladder innervation in male rat: termination of primary afferents in the spinal cord as determined by transganglionic transport of WGA-HRP. *J. Urol.* 150, 500–504. doi: 10.1016/s0022-5347(17)35535-0

Patel, S. P., Sullivan, P. G., Lyttle, T. S., Magnuson, D. S. K., and Rabchevsky, A. G. (2012). Acetyl-L-carnitine treatment following spinal cord injury improves mitochondrial function correlated with remarkable tissue sparing and functional recovery. *Neuroscience* 210, 296–307. doi: 10.1016/j.neuroscience.2012.03.006

Petkó, M., and Antal, M. (2000). Propriospinal afferent and efferent connections of the lateral and medial areas of the dorsal horn (laminae I-IV) in the rat lumbar spinal cord. *J. Comp. Neurol.* 422, 312–325. doi: 10.1002/(sici)1096-9861(20000626)422:2<312::aid-cne11>3.0.co;2-a

Pyner, S., and Coote, J. H. (1994). Evidence that sympathetic preganglionic neurones are arranged in target-specific columns in the thoracic spinal cord of the rat. *J. Comp. Neurol.* 342, 15–22. doi: 10.1002/cne.903420103

Rabchevsky, A. G. (2006). Segmental organization of spinal reflexes mediating autonomic dysreflexia after spinal cord injury. *Prog. Brain Res.* 152, 265–274. doi: 10.1016/s0079-6123(05)52017-x

Reed, W. R., Shum-Siu, A., Onifer, S. M., and Magnuson, D. S. (2006). Inter-enlargement pathways in the ventrolateral funiculus of the adult rat spinal cord. *Neuroscience* 142, 1195–1207. doi: 10.1016/j.neuroscience.2006.07.017

Sasaki, S., Isa, T., Pettersson, L. G., Alstermark, B., Naito, K., Yoshimura, K., et al. (2004). Dexterous finger movements in primate without monosynaptic corticomotoneuronal excitation. *J. Neurophysiol.* 92, 3142–3147. doi: 10.1152/jn.00342.2004

Schramm, L. P. (2006). Spinal sympathetic interneurons: their identification and roles after spinal cord injury. *Prog. Brain Res.* 152, 27–37. doi: 10.1016/s0079-6123(05)52002-8

Sheikh, I. S., Keefe, K. M., Sterling, N. A., Junker, I. P., Eneanya, C. I., Liu, Y., et al. (2018). Retrogradely transportable lentivirus tracers for mapping spinal cord locomotor circuits. *Front. Neural Circuits* 12:60. doi: 10.3389/fncir.2018.00060

Skinner, R. D., Nelson, R., Griebel, M., and Garcia-Rill, E. (1989). Ascending projections of long descending propriospinal tract (LDPT) neurons. *Brain Res. Bull.* 22, 253–258. doi: 10.1016/0361-9230(89)90050-6

Snow, J. C., Sideropoulos, H. P., Kripke, B. J., Freed, M. M., Shah, N. K., and Schlesinger, R. M. (1978). Autonomic hyperreflexia during cystoscopy in patients with high spinal cord injuries. *Paraplegia* 15, 327–332. doi: 10.1038/sc.1977.49

Stjernberg, L. (1986). Cutaneous vasomotor sensitivity to noradrenalin in spinal and intact man. *Scand. J. Rehabil. Med.* 18, 127–132.

Strack, A. M., Sawyer, W. B., Marubio, L. M., and Loewy, A. D. (1988). Spinal origin of sympathetic preganglionic neurons in the rat. *Brain Res.* 455, 187–191. doi: 10.1016/0006-8993(88)90132-1

Strack, A. M., Sawyer, W. B., Platt, K. B., and Loewy, A. D. (1989). CNS cell groups regulating the sympathetic outflow to adrenal gland as revealed by transneuronal cell body labeling with pseudorabies virus. *Brain Res.* 491, 274–296. doi: 10.1016/0006-8993(89)90063-2

Szentagothai, J. (1964). Neuronal and synaptic arrangement in the substantia gelatinosa rolandi. *J. Comp. Neurol.* 122, 219–239. doi: 10.1002/cne.901220207

Tandon, S., Kambi, N., Lazar, L., Mohammed, H., and Jain, N. (2009). Large-scale expansion of the face representation in somatosensory areas of the lateral sulcus after spinal cord injuries in monkeys. *J. Neurosci.* 29, 12009–12019. doi: 10.1523/jneurosci.2118-09.2009

Tang, X., Neckel, N. D., and Schramm, L. P. (2004). Spinal interneurons infected by renal injection of pseudorabies virus in the rat. *Brain Res.* 1004, 1–7. doi: 10.1016/j.brainres.2004.01.016

Teasell, R. W., Arnold, J. M., Krassioukov, A., and Delaney, G. A. (2000). Cardiovascular consequences of loss of supraspinal control of the sympathetic nervous system after spinal cord injury. *Arch. Phys. Med. Rehabil.* 81, 506–516. doi: 10.1053/mr.2000.3848

Ueno, M., Ueno-Nakamura, Y., Niehaus, J., Popovich, P. G., and Yoshida, Y. (2016). Silencing spinal interneurons inhibits immune suppressive autonomic reflexes caused by spinal cord injury. *Nat. Neurosci.* 19, 784–787. doi: 10.1038/nn.4289

Vizzard, M. A. (2000). Increased expression of spinal cord Fos protein induced by bladder stimulation after spinal cord injury. *Am. J. Physiol. Regul. Integr. Comp. Physiol.* 279, R295–R305. doi: 10.1152/ajpregu.2000.279.1.r295

Vizzard, M. A., Brisson, M., and De Groat, W. C. (2000). Transneuronal labeling of neurons in the adult rat central nervous system following inoculation of pseudorabies virus into the colon. *Cell Tissue Res.* 299, 9–26. doi: 10.1007/s004419900128

Wang, C. C., Willis, W. D., and Westlund, K. N. (1999). Ascending projections from the area around the spinal cord central canal: a Phaseolus vulgaris leucoagglutinin study in rats. *J. Comp. Neurol.* 415, 341–367. doi: 10.1002/(sici)1096-9861(19991220)415:3<341::aid-cne3>3.0.co;2-7

Weaver, L. C., Cassam, A. K., Krassioukov, A. V., and Llewellyn-Smith, I. J. (1997). Changes in immunoreactivity for growth associated protein-43 suggest reorganization of synapses on spinal sympathetic neurons after cord transection. *Neuroscience* 81, 535–551. doi: 10.1016/s0306-4522(97)00151-6

Weaver, L. C., Marsh, D. R., Gris, D., Brown, A., and Dekaban, G. A. (2006). Autonomic dysreflexia after spinal cord injury: central mechanisms and strategies for prevention. *Prog. Brain Res.* 152, 245–263. doi: 10.1016/s0079-6123(05)52016-8

Wong, S. T., Atkinson, B. A., and Weaver, L. C. (2000). Confocal microscopic analysis reveals sprouting of primary afferent fibres in rat dorsal horn after spinal cord injury. *Neurosci. Lett.* 296, 65–68. doi: 10.1016/s0304-3940(00)01601-3

Zaporozhets, E., Cowley, K. C., and Schmidt, B. J. (2006). Propriospinal neurons contribute to bulbospinal transmission of the locomotor command signal in the neonatal rat spinal cord. *J. Physiol.* 572, 443–458. doi: 10.1113/jphysiol.2005.102376

Conflict of Interest: The authors declare that the research was conducted in the absence of any commercial or financial relationships that could be construed as a potential conflict of interest.

frontiers in Cellular Neuroscience

REVIEW
published: 12 November 2019
doi: 10.3389/fncel.2019.00512

Propriospinal Neurons: Essential Elements of Locomotor Control in the Intact and Possibly the Injured Spinal Cord

*Alex M. Laliberte†, Sara Goltash†, Nicolas R. Lalonde and Tuan Vu Bui**

Department of Biology, Faculty of Science, Brain and Mind Research Institute, University of Ottawa, Ottawa, ON, Canada

Propriospinal interneurons (INs) communicate information over short and long distances within the spinal cord. They act to coordinate different parts of the body by linking motor circuits that control muscles across the forelimbs, trunk, and hindlimbs. Their role in coordinating locomotor circuits near and far may be invaluable to the recovery of locomotor function lost due to injury to the spinal cord where the flow of motor commands from the brain and brainstem to spinal motor circuits is disrupted. The formation and activation of circuits established by spared propriospinal INs may promote the re-emergence of locomotion. In light of progress made in animal models of spinal cord injury (SCI) and in human patients, we discuss the role of propriospinal INs in the intact spinal cord and describe recent studies investigating the assembly and/or activation of propriospinal circuits to promote recovery of locomotion following SCI.

Keywords: propriospinal neurons, spinal locomotor networks, central pattern generators, spinal cord injury, detour circuits

OPEN ACCESS

Edited by:
Michelle Maria Rank,
The University of Melbourne, Australia

Reviewed by:
Andrew Paul Tosolini,
University College London, United Kingdom
Alain Frigon,
Université de Sherbrooke, Canada
Kimberly J. Dougherty,
Drexel University, United States

***Correspondence:**
Tuan Vu Bui
tuan.bui@uottawa.ca

† These authors have contributed equally to this work

Specialty section:
This article was submitted to Cellular Neurophysiology, a section of the journal Frontiers in Cellular Neuroscience

Received: *29 August 2019*
Accepted: *29 October 2019*
Published: *12 November 2019*

Citation:
Laliberte AM, Goltash S, Lalonde NR and Bui TV (2019) Propriospinal Neurons: Essential Elements of Locomotor Control in the Intact and Possibly the Injured Spinal Cord. Front. Cell. Neurosci. 13:512. doi: 10.3389/fncel.2019.00512

INTRODUCTION

Successful locomotion depends upon the precise coordination of multiple muscles across numerous joints and limbs, as well as the simultaneous engagement of multiple trunk and stabilizing muscles (Frigon, 2017). This patterned motor output must be adjusted dynamically at differing speeds and in response to various obstacles and perturbations, requiring the constant integration of sensory information. While the role of supraspinal centers, particularly in relation to the planning, initiation, and modulation of locomotion (Lajoie and Drew, 2007; Capelli et al., 2017; Caggiano et al., 2018; Josset et al., 2018; Oueghlani et al., 2018), should not be discounted, many of the key functions of locomotion are performed by interneuron (IN) networks within the spinal cord. This is particularly evident from experiments utilizing *ex vivo* spinal cord preparations where application of electrical stimulation, light illumination, or a variety of neurotransmitter/pharmacological agonist cocktails have successfully evoked fictive locomotion – sustained rhythmic and appropriately patterned flexor and extensor activity recorded in motor nerves of the spinal cord – in the absence of supraspinal input (Atsuta et al., 1991; Jiang et al., 1999; Whelan et al., 2000; Hägglund et al., 2010). The innate potential of select propriospinal INs, defined as spinal cord INs that originate and terminate within the spinal cord while spanning at least one spinal cord segment, to activate locomotion makes them an attractive therapeutic target for spinal cord injury (SCI) (Flynn et al., 2011). However, an incomplete understanding of their

integration within locomotor systems remains a significant obstacle to the use of propriospinal INs in the therapies seeking to restore lost locomotor function. Emergent genetic and molecular techniques that allow the identification and manipulation of specific propriospinal IN populations have greatly accelerated this research. It is the purpose of this review to summarize and update the current state of knowledge regarding the organization and function of locomotion-associated propriospinal INs in intact and spinal cord lesioned mammals as well as to examine seminal and recent attempts to manipulate propriospinal INs to rescue locomotor function.

PROPRIOSPINAL INTERNEURONS PROPAGATE LOCOMOTOR COMMANDS FROM SUPRASPINAL LOCOMOTOR REGIONS

At first glance, propriospinal INs occupy a conceptually straightforward role in locomotion. Propriospinal INs receive inputs from descending locomotor pathways and propagate received motor commands rostrocaudally to locomotor circuits via short or long, ipsilateral or commissural axons (**Figure 2A**). To fulfill this role, some propriospinal INs project axons that only travel a few segments (short propriospinal), while others project axons that travel many more segments, spanning far enough to connect cervical with lumbar segments (long propriospinal). Short and long propriospinal IN axons can stay within the same side of the body as their cell bodies (**Figure 1**, straight lines), while others cross to the other side (**Figure 1**, lines with arc segments). We include commissural INs for their possible involvement in forming detour circuits following an injury to the spinal cord. Evidence for the role of propriospinal INs in propagating locomotor commands rostrocaudally has been well-established in the mammalian CNS. For example, the application of certain neurotransmitter agonists to only the cervicothoracic spinal cord was found to generate rhythmic hindlimb activity in neonatal rat preparations (Cowley and Schmidt, 1997). Transections at caudal thoracic and rostral lumbar segments also abolished locomotor activity below the caudal lesion site, demonstrating the importance of INs in this region for locomotor output in more caudal lumbar segments (Cowley and Schmidt, 1997). Additional evidence for propriospinal locomotor relays was demonstrated using brainstem stimulation in rat brainstem-spinal cord *in vitro* preparations, where hindlimb locomotor-like activity was observed despite staggered contralateral spinal cord lesions that severed all ipsilateral bulbospinal connections on both sides of the spinal cord (Cowley et al., 2008). These findings suggest that either brainstem locomotor regions have projections to the contralateral spinal cord that decussate at the spinal levels between the hemisections, or that propriospinal INs with contralateral projections propagate locomotor commands from supraspinal centers (e.g., red lines with arc segments in **Figure 1**). The latter explanation that propriospinal networks are integrated into bulbospinal locomotor control appears more likely given (1) the predominance of ipsilaterally projecting axons over contralaterally projecting from brainstem locomotor centers (Stelzner and Cullen, 1991; Liang et al., 2011; Sivertsen et al., 2016) and (2) subsequent physiological experiments which found that blockade of synaptic transmission in cervicothoracic segments (using a variety of strategies: no Ca^{2+}, high Mg^{2+}, CNQX, AP-5) resulted in the abolition of brainstem stimulation-induced lumbar locomotor activity (Zaporozhets et al., 2006).

These studies strongly suggest a role for propriospinal INs in the propagation of locomotor commands, implying that propriospinal INs either innervate or form part of the locomotor

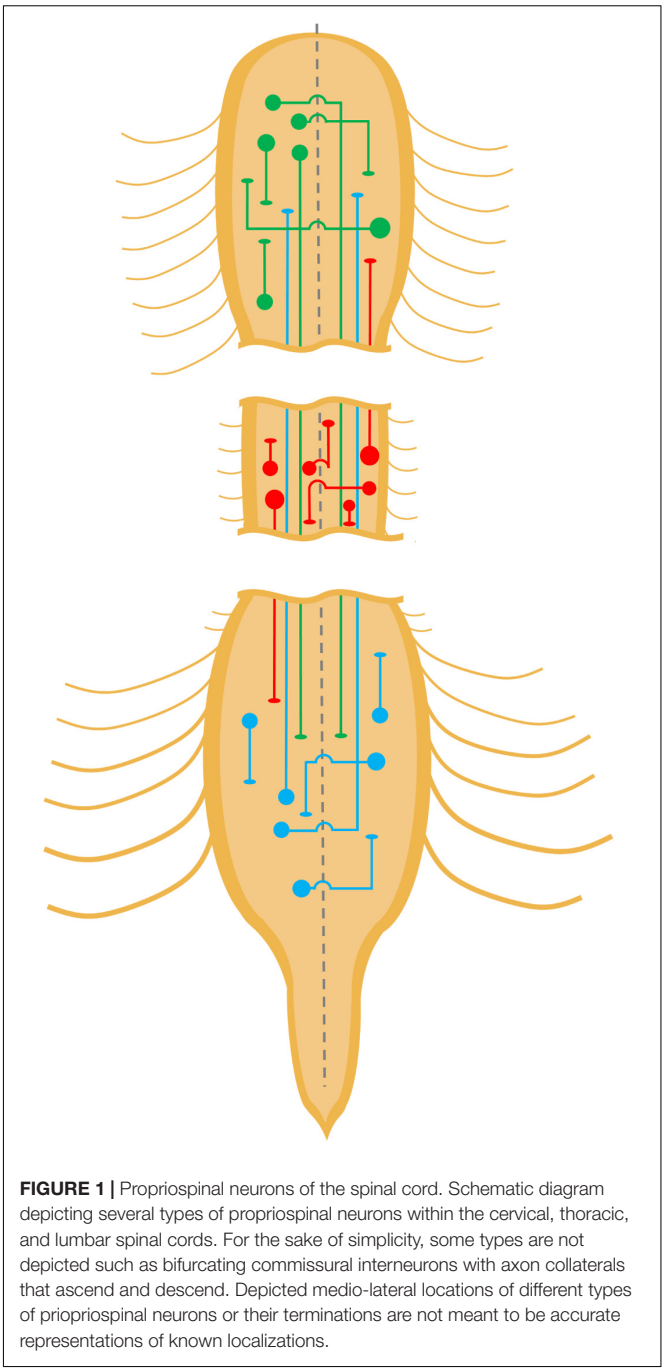

FIGURE 1 | Propriospinal neurons of the spinal cord. Schematic diagram depicting several types of propriospinal neurons within the cervical, thoracic, and lumbar spinal cords. For the sake of simplicity, some types are not depicted such as bifurcating commissural interneurons with axon collaterals that ascend and descend. Depicted medio-lateral locations of different types of propriospinal neurons or their terminations are not meant to be accurate representations of known localizations.

central pattern generator (CPG). Indeed, it has been proposed that the locomotor CPG may be composed of multiple unit CPGs distributed along the length of the spinal cord and across its midline controlling subsets of muscles, in particular, those acting upon particular joints such as the hip, knee, or ankle (Grillner et al., 1976; Kjaerulff and Kiehn, 1996; Wiggin et al., 2012; Gerasimenko et al., 2016; Mantziaris et al., 2017). Short propriospinal neurons (**Figure 1**, short lines, green and blue, straight or with arc segment) may act as relays between non-overlapping unit CPGs within cervical or lumbar segments. Alternatively, short propriospinal INs may be part of unit CPGs if the circuitry for each unit CPG is spread out over several spinal cord segments. In either case, propriospinal connections can propagate locomotor commands from their initial targets to adjacent nodes containing CPG components.

PROPRIOSPINAL INTERNEURONS PERFORM FUNCTIONS OF THE LOCOMOTOR CPG

Ontogenic studies of molecularly defined populations of propriospinal INs have provided ample evidence of the contributions of propriospinal INs to locomotor CPG function. While others have extensively reviewed the developmental origin of INs comprising the locomotor CPG (Gosgnach et al., 2017), this information is critical to understanding the role of propriospinal INs in locomotor function and therefore, a brief overview of this topic is warranted. It should be noted that each of the developmentally defined IN populations are believed to be heterogeneous to varying degrees, potentially containing several distinct subpopulations of INs with different characteristics. As a result, not all of these subpopulations will meet the currently used definition of propriospinal INs. However, at least some portion of the IN populations discussed below appear to be propriospinal based on their reported projection characteristics (reviewed in Lu et al., 2015), and their putative function in locomotion (**Table 1**).

During embryogenesis, the spatiotemporal distribution of signaling molecules such as Wnt, BMP, and Sonic hedgehog, across three spatial axes – rostral–caudal, medial–lateral, and dorsal–ventral – leads to a complex spatiotemporal pattern of transcription factor activation that results in the emergence of a specific set of progenitor pools within the spinal cord (Dasen and Jessell, 2009). In total, there are 13 progenitor pools from which INs and motoneurons will emerge. All dorsal IN populations (dI1–dI6) come from progenitor pools pd1–6 and the late-born pdIL$_A$ and pdIL$_B$. Four ventral IN populations (V0–V3) emerge from the p0–3 pool while the motoneurons arise from the motor domain pMN (reviewed in Lu et al., 2015). The ventrally derived populations have received considerable interest in relation to locomotion, as it has been postulated that they constitute the core elements of the CPG located primarily within the spinal ventral horn (reviewed in Kiehn, 2016). Therefore, many genetic manipulations have targeted these ventral IN populations. Initial experiments with isolated spinal cords observed the conservation of rhythmicity following a sagittal section along the midline of chronically isolated adult cat spinal cords (Kato, 1990). This observation seems to indicate that rhythmogenesis can be generated solely from ipsilaterally projecting neurons within each side of the spinal cord. Therefore, the first ablation studies targeted ipsilaterally projecting INs.

The V1 embryonic population of INs, which are marked by the expression of the engrailed-1 (En1) transcription factor, generates inhibitory neurons that project ipsilaterally (Higashijima et al., 2004; Benito-Gonzalez and Alvarez, 2012). Approximately 30%

TABLE 1 | Overview of major developmentally defined interneuron populations and their proposed role in locomotion.

Interneuron population	Projection characteristics	Neurotransmitter phenotype	Putative function in mammalian locomotion
V0$_V$ (*DBX1+/EVX1+*)	Long and short commissural	Glutamatergic (excitatory)	Coordinates left–right alternation during locomotion. Loss of function particularly affects alternation during higher speed locomotion.
V0$_D$ (*DBX1+/PAX7+*)	Long and short commissural	GABA/glycinergic (inhibitory)	Coordinates left–right alternation during locomotion. Loss of function particularly affects alternation during lower speed locomotion.
V0$_C$ (*DBX1+/EVX1+/PITX2+*)	Short ipsilateral and commissural	Cholinergic (excitatory)	Modulates activity of some motoneuron pools during specific locomotor tasks.
V1 (*EN1+*)	Short and long ipsilateral	GABA/glycinergic (inhibitory)	Coordinate flexor–extensor activity, potentially through the inhibition flexor activity. Include Renshaw and Ia IN populations with well-defined roles in recurrent and reciprocal inhibition of motoneurons.
V2a (*CHX10+*)	Long and short ipsilateral	Glutamatergic (excitatory)	Propagate locomotor commands to commissural interneurons involved with left–right coordination.
V2b (*GATA2/3+*)	Long and short ipsilateral	GABA/glycinergic (inhibitory)	Coordinate flexor–extensor activity, potentially through the inhibition of extensor activity.
V3 (*SIM1+*)	Short commissural and ipsilateral	Glutamatergic (excitatory)	Stabilize locomotor pattern, reducing variability in ipsilateral and contralateral gait.
dI3 (*ISL1+*)	Short ipsilateral	Glutamatergic (excitatory)	Relay cutaneous and proprioceptive information to CPG. Essential for locomotor rehabilitation.
dI4 dIL$_A$ (*Ptf1a+*)	Short ipsilateral Short commissural	GABAergic (inhibitory)	Mediate presynaptic inhibition of sensory terminals onto spinal neurons to gate sensory feedback and ensure smooth execution of movements.
dI6 (*DMRT3+* and/or *WT1+*)	Short commissural and ipsilateral	GABA/glycinergic (inhibitory)	Stabilize locomotor pattern, reducing variability in ipsilateral and contralateral gait.

of En1+ INs become Ia INs or Renshaw cells and form inhibitory synapses onto motoneurons or other Ia INs (Alvarez et al., 2005). As the V1/Ia IN population projects ipsilaterally within the spinal cord, targeted ablation of En1+ INs was expected to result in the loss of flexor–extensor intralimb coordination. Instead, loss of V1 neurons resulted in a loss of high-speed locomotor activity. Indeed, mice lacking V1 INs had lower top speeds on the rotarod test compared to their control mates, and the duration of the step cycle was increased in recordings made from isolated spinal cords (Gosgnach et al., 2006). Subsequent experiments using genetic methods to block synaptic transmission from V1 INs instead of developmental ablation recapitulated this finding (Zhang et al., 2014). While V1 IN silencing alone did not prevent flexor–extensor coordination, V1 IN ablation resulted in a prolonged flexion phase in both neonatal and adult mice, while optogenetic activation of V1s resulted in the suppression of flexor activity (Britz et al., 2015). A recent study provided further confirmation of the role of V1 INs in the regulation of flexor burst duration, and also found evidence that they regulate extensor activity in the absence of commissural input, possibly suggesting a more dynamic role for V1 INs in the generation of biomechanically advantageous flexion/extension asymmetry (Falgairolle and O'Donovan, 2019). Interestingly, the combined inactivation of both V1 IN and a subset of the V2 IN population (V2b) resulted in a total loss of flexor–extensor alternation (Zhang et al., 2014). Parallel examination of V2b INs determined that they inhibit extensor motoneurons in an analogous manner to the V1 INs with flexor motoneurons (Britz et al., 2015). These results appear to support the functional cooperativity of V1 and V2b INs to maintain the appropriate balance of flexor and extensor activity during locomotion.

Another ipsilaterally projecting population of propriospinal INs that has garnered interest in the context of locomotion is the Chx10-expressing V2a subpopulation. Unlike V1 and V2b INs, the V2a INs exclusively provide glutamatergic input in the mouse spinal cord (Al-Mosawie et al., 2007; Lundfald et al., 2007). The zebrafish homolog to the V2a population, identified by its expression of Chx10, is sufficient for generating locomotor rhythm (Ljunggren et al., 2014); however, this role is not entirely conserved in mammals. Optogenetic or synaptic blockade of the Shox2+ INs, some of which belong to the V2a population, perturbed locomotor rhythmogenesis in neonate mice (Dougherty et al., 2013), but ablation of only the Shox2+ V2a INs did not eliminate the mammalian spinal cord's ability to generate rhythm. Surprisingly, V2a IN ablation created deficits in left–right alternation at intermediate to high speeds in adult mice (Crone et al., 2008, 2009), suggesting that the V2a INs, in fact, also innervate commissural INs responsible for left–right coordination.

While rhythmicity is conserved following midsagittal lesioning of the spinal cord, left–right coordination is lost, which is an important element of gait. Cross-talk between contralateral halves of the CPG is a critical feature of the locomotor network, where activity on one side can affect the contralateral locomotor output. This contralateral influence has been demonstrated through work involving split-belt treadmills (left and right limbs can be made to walk at different speeds), where compensatory alterations in phase duration were observed on the contralateral side when the speed was changed unilaterally (Frigon et al., 2013, 2017). Interestingly, this compensation occurs even in spinal cord transected cats, suggesting a propriospinal mechanism (Frigon et al., 2013, 2017). Indeed, the silencing of lumbar propriospinal neurons projecting from L2 to L5 in the adult rat was found to alter left–right coordination independent of speed (Pocratsky et al., 2017). These L2-to-L5 projecting propriospinal neurons consisted of both ipsilaterally projecting and commissural INs.

Commissural INs ensure proper coordination of both sides of the body during locomotion. These neurons may be contacted by V1 and V2a/V2b subtypes, potentially allowing them to coordinate shifts in flexion–extension across the left and right limbs during changes in speed. Commissural INs act by providing an excitatory or inhibitory drive to contralateral motor circuits. Their axons cross the midline at the same level as their cell bodies (Matsuyama et al., 2006) and then can project up and/or down the spinal cord (Eide et al., 1999; Stokke et al., 2002; Quinlan and Kiehn, 2007), even going as far as communicating between the cervical and lumbar segments (English et al., 1985; Matsuyama et al., 2004; Reed et al., 2006; Brockett et al., 2013; Ni et al., 2014; Mitchell et al., 2016; Ruder et al., 2016). One such population is the V0 INs, which are classified by their early expression of the developing brain homeobox 1 (DBX1). There are at least three subtypes of V0 INs: $V0_D$ (delineated by paired box protein 7, PAX7), $V0_V$ (express even-skipped homolog protein 1, EVX1), and $V0_C$, which express paired-like homeobox transcription factor 2 (PITX2) and EVX1 (Moran-Rivard et al., 2001; Zagoraiou et al., 2009; Talpalar et al., 2013). Targeted ablation of DBX1-expressing neurons (all V0 INs) resulted in the loss of left–right alternation, giving way to synchronous hopping behavior at all frequencies of locomotion. Interestingly, selective loss of the $V0_D$s has a more marked effect on coordination at slow locomotor speeds, whereas selective loss of the $V0_V$s leads to loss of coordination at fast locomotor speeds (Talpalar et al., 2013). Unlike the other V0 populations that have clear roles in left–right coordination of locomotion, $V0_c$s modulate motoneuron excitability through direct cholinergic inputs (Zagoraiou et al., 2009). The targeted ablation of the $V0_C$s in adult mice did not have any measurable effect on the locomotor pattern but showed task-dependent modification of specific hindlimb muscle activity during swimming but not during walking (Zagoraiou et al., 2009).

The dI6 INs are another IN subtype involved with left–right coordination. They are marked by expression of either WT1, DMRT3, or Wt1/DMRT3, and form appositions with both ipsilateral and contralateral motoneuron pools (Andersson et al., 2012; Griener et al., 2017). A loss of functional DMRT3 led to an increase of dI6 INs exhibiting a Wt1+ identity and a drastic reduction in commissural projections, causing both the loss of coordination between the left and right CPGs, as well as a loss of coordination of the flexion–extension cycle in mice and horses. This evidence is consistent with the role of crossed inhibition in maintaining left–right alternation – as is the case for $V0_D$ neurons – and also the role of ipsilateral inhibition in flexor–extensor balance (V1 and V2b INs).

One final ventral IN is the Sim1-expressing V3 population, a class of glutamatergic bilaterally projecting INs (Chopek et al., 2018). This population is highly heterogeneous in terms of their connectivity. V3 axons extend contralaterally, where they account for 22% of contacts on motoneurons positive for the excitatory neurotransmitter transporter VGluT2, and 27% of VGluT2 contacts on parvalbumin-positive Ia INs and Renshaw cells (Zhang et al., 2008). Silencing of V3 synaptic transmission using a cell-selective tetanus toxin light chain subunit (TeNT) expression system degraded locomotor pattern by increasing the variation in burst duration and interburst interval. Interestingly, the locomotor output was highly asymmetrical between the right and left flexor, increasing the burst duration of only one of two left–right L2 roots in the neonatal mouse spinal cord (Zhang et al., 2008). This latter finding may point to the involvement of V3 INs in stabilizing left–right alternation during walking. However, a subsequent study identified electrophysiological evidence of distinct V3 subpopulations in the spinal cord and suggested that differential recruitment of these subpopulations may occur during different modes of locomotion (Borowska et al., 2013). The dorsal V3 INs were primarily recruited during running episodes (in contrast to static and swimming conditions) when there is additional sensory feedback associated with greater mechanical loading. It was also found that these dorsal V3 INs received more inputs from sensory afferents than the ventral V3 population. Based on previous morphological examinations of commissural excitatory INs, the authors proposed that this dorsal V3 subpopulation may be responsible for relaying sensory information used to indirectly adjust left–right coordination, while the ventral V3 population presumably synchronizes motor outputs across multiple levels (Borowska et al., 2013). In a related fashion, computational modeling of the locomotor CPG identified V3 INs as a possible mediator of the transition from alternating to synchronous modes of locomotion with increasing speed (from trot to gallop to bound), but empirical evidence of this proposed function is currently lacking (Danner et al., 2017). A recent electrophysiological study uncovered a layered structure within the V3 subpopulation, where a ventromedial population may receive supraspinal locomotor commands while a ventrolateral population may relay these commands to different segments to coordinate several motor pools (Chopek et al., 2018). As such, V3 INs could reflect the dual roles of propriospinal INs to relay locomotor commands and to coordinate multiple components that form unit CPGs.

PROPRIOSPINAL INTERNEURONS COORDINATE FORELIMB AND HINDLIMB LOCOMOTOR NETWORKS

Separate CPGs regulate patterning of forelimb and hindlimb stepping, as evidenced by the ability of cervical and lumbar spinal cord segments to produce rhythmic oscillation independently of each other in the neonatal rat spinal cord (Ballion et al., 2001; Juvin et al., 2005; Gordon et al., 2008). However, the execution of smooth quadrupedal locomotion necessitates the coupling of forelimb and hindlimb motor outputs. This coupling occurs at the spinal cord level, as demonstrated by the coordinated rhythmic coupling of forelimb and hindlimb extensors during fictive locomotion in neonatal rodent isolated spinal cord preparations (Ballion et al., 2001; Juvin et al., 2005, 2012; Gordon et al., 2008). As such, the mechanism of this coupling is thought to occur either through inter-CPG communication via propriospinal INs or the integration of external sensory cues (Juvin et al., 2012). With regard to the former hypothesis, Juvin et al. (2005, 2012) found that the coupling of hindlimb and forelimb rhythm in neonatal rat fictive locomotor preparations was lost when a sucrose block was applied to the thoracic spinal cord, suggesting that direct connections between the CPGs are necessary to maintain coordination. Indeed, the existence of long propriospinal axons connecting these regions had long been hypothesized (Miller et al., 1973), and neuroanatomical evidence confirmed the presence of long ascending propriospinal connections from rostral lumbar spinal cord (**Figure 1**, long blue or upward red lines) to the cervical region along the ventrolateral funiculus (VLF) (Molenaar and Kuypers, 1978; English et al., 1985; Reed et al., 2006), with a majority of these neurons (85%) expressing VGluT2 (Brockett et al., 2013). The highest proportion of these ascending projections were ipsilateral (nine times more frequent than contralateral), and tended to be concentrated in the rostral lumbar segments (Brockett et al., 2013). Lesions to the thoracic VLF in the cat disrupt forelimb–hindlimb coupling (Brustein and Rossignol, 1998), further supporting the notion that these long ascending propriospinal INs maintain inter-CPG coordination. To test whether one CPG could govern the other via these propriospinal connections, Juvin and colleagues performed a midsagittal incision from C1 to T7 and found that left–right alternation was preserved when the connection to the caudal CPG remained, but subsequently disrupted when the caudal spinal cord was bathed in bicuculline and strychnine – GABA and glycine receptor antagonists – to disrupt the caudal locomotor pattern. In contrast, disruption of cervical left–right alternation through the addition of bicuculline and strychnine to the cervical spinal cord bath did not modify the lumbar pattern, suggesting the dominance of ascending propriospinal pathways in the regulation of forelimb/hindlimb coupling in the neonatal rat (Juvin et al., 2005).

While the long ascending propriospinal INs appear to play a major role in forelimb/hindlimb coordination, there is considerable evidence suggesting that long descending propriospinal INs (**Figure 1**, long green or downward red lines) also play a role in interlimb coordination (Matsushita et al., 1979; Skinner et al., 1980; Menétrey et al., 1985; Alstermark et al., 1987; Nathan et al., 1996). Ruder et al. (2016) used lumbar-injected retrograde *canine adenovirus-2* vectors in combination with a cervically injected adeno-associated virus (AAV) expressing the diphtheria toxin receptor, to selectively ablate lumbar-projecting cervical INs upon administration of the diphtheria toxin. Interestingly, they found that selective deletion of these long descending propriospinal INs resulted in the loss of coordination between hindlimbs, particularly at higher speeds (Ruder et al., 2016). More generally, the ablation of these neurons also reduced spontaneous locomotor speed and decreased the duration of locomotor bouts, which

was accompanied or potentially compounded by the postural instability during locomotion that was observed. Examination of the neurotransmitter phenotype and developmental origin of long descending propriospinal INs revealed that those INs with connections to the highly rhythmogenic L2 region (Cazalets et al., 1995) are predominantly excitatory, with relatively minor representation of V2b INs (5.3%), and negligible V1 and V3 IN representation (Flynn et al., 2017). Similarly, Ruder et al. (2016) found a strong representation of excitatory V0 and V2 INs with very few V1, V3, and dI3 INs extending cervicolumbar projections. Even though the importance of forelimb/hindlimb coupling may be amplified in quadrupeds, there is circumstantial evidence that suggests this phenomenon also exists in bipedal animals. Coupling of bipedal arm and leg movements has been observed in upright walking (Dietz, 2002; Zehr et al., 2009, 2016; Frigon, 2017; Pearcey and Zehr, 2019), swimming (Wannier et al., 2001), and crawling (MacLellan et al., 2013) in humans, mirroring the expected behavior of paired oscillators observed in quadrupedal locomotion.

PROPRIOSPINAL INTERNEURONS INTEGRATE SENSORY INFORMATION TO SHAPE LOCOMOTOR OUTPUT

One of the critical features of mammalian locomotion is the integration of proprioceptive and cutaneous sensory information to guide locomotor output. Acute spinalized cats can spontaneously adjust to varying treadmill speed after administration of the noradrenergic agonist clonidine (Forssberg and Grillner, 1973). Other experiments using chronic spinal kittens found that spontaneous adjustment to speed could be performed even when individual limbs were subjected to different speeds using split-belt treadmills, a locomotor program analogous to turning (Forssberg et al., 1980; Frigon et al., 2013). These studies demonstrate the ability of the mammalian CPG to modify its locomotor pattern based on external sensory cues. While some of this can be explained by direct feedback from sensory afferents, integration of multimodal sensory feedback by propriospinal INs and rostrocaudal propagation of this signal may be required to generate complex sensory-induced motor responses involving multiple muscles (Levine et al., 2014). There are several specific phenomena that support this hypothesis. For example, the non-monosynaptic facilitation of motoneuron pools associated with stimulation of several lower limb nerves (common peroneal, posterior tibial, femoral) is thought to be mediated through short propriospinal INs situated rostral to the respective group of motoneurons (Chaix et al., 1997). Whereas long propriospinal INs could underlie the inter-limb modulation of reflexes such as the observations that static contralateral arm extension or flexion in humans produces soleus H-reflex facilitation or attenuation, respectively (Delwaide et al., 1977), while ipsilateral or contralateral sinusoidal arm movements depress soleus H-reflex excitability (Knikou, 2007).

While these findings strongly suggest a role for propriospinal INs in the integration and propagation of sensory feedback during movement, determining the identity and organization of the IN populations responsible is an ongoing endeavor. Several molecularly defined classes of spinal neurons described above have already been shown to receive sensory afferent inputs (e.g., V1, V3 INs). Neurons derived from dorsal progenitor domains are very likely to be involved in sensorimotor integration. For example, motor synergy encoder neurons, characterized by Tcfap2β and Satb1/2 expression, are involved in linking multiple motor pools together, and this muscle coordination seems to require sensory input (Levine et al., 2014). The dorsal IN type 4 (dI4 INs) mediate presynaptic inhibition of sensory terminals onto spinal neurons in order to properly gate sensory feedback to ensure smooth execution of movements in mice (Betley et al., 2009; Fink et al., 2014). Finally, the dorsal IN type 3 (dI3) INs seem another likely candidate for sensorimotor integration at the level of the spinal cord. The largely excitatory dI3 INs receive inputs from low-threshold cutaneous and proprioceptive afferents and extend projections to motoneuron pools within the cervical and lumbar enlargements (Bui et al., 2013, 2016). While no long descending propriospinal axons from cervical dI3 INs to lumbar segments have been found (Ruder et al., 2016), transsynaptic tracing experiments from the mouse quadriceps muscle found that dI3 INs project from adjacent lumbar segments (55% L1–L2, 6% L3, 39% L4–L6) to the flexor motoneuron pool, suggesting a moderately dispersed pattern of short propriospinal connectivity (Stepien et al., 2010). dI3 IN loss-of-function resulted in minor disturbances in locomotor gait in mice (Bui et al., 2016), which may speak to the distributed integration of sensory input among different spinal populations. More strikingly, their silencing attenuates recovery of treadmill stepping following SCI, implicating a specific population of spinal propriospinal INs in the recovery of motor function (Bui et al., 2016). As such, dI3 INs are one of the first populations of molecularly defined propriospinal INs that have been shown to be involved in the recovery of locomotor function following SCI. However, more generally, there is an abundance of literature implicating propriospinal INs in the recovery of locomotion after SCI, a topic that will be explored in depth below.

ROLE OF PROPRIOSPINAL NEURONS IN THE RECOVERY OF LOCOMOTOR FUNCTION

Spinal cord injury can lead to a devastating loss of motor function. The severity of motor function loss depends on the location and nature of the injury, which dictates the degree of disruption of communication between the supraspinal centers controlling movement and spinal motor circuits. By virtue of their role in communicating higher motor commands to spinal circuits, a major focus of spinal cord repair has been the regeneration of descending tracts across the lesion site to restore lost motor input (Tuszynski and Steward, 2012). Accumulating evidence points to propriospinal INs as an additional target for promoting the recovery of locomotor function (Taccola et al., 2018; Loy and Bareyre, 2019). As a consequence of their position within the spinal cord and their

central role in the generation of locomotion, propriospinal INs are well-situated to propagate supraspinal commands to motor systems below the level of injury. Furthermore, the shorter distance required for propriospinal axons to bridge the lesion compared to axons from cortical or brainstem neurons make them a more straightforward target for regenerative approaches. Several changes to neural circuits involving propriospinal INs have been observed that could facilitate the recovery of locomotor function.

Propriospinal INs Receive New Connections From Supraspinal Neurons

New synaptic contacts made by descending tracts onto propriospinal INs following SCI have been repeatedly demonstrated in animal models of SCI. Seminal work by Bareyre et al. (2004) revealed that spontaneous sprouting of axon collaterals from the corticospinal tract (CST), in particular, those contacting propriospinal INs, could promote recovery of locomotion after SCI. After a mid-thoracic dorsal transection of CST axons in rats, lesioned CST axons spontaneously sprouted collaterals into the cervical gray matter where they made new connections with both short and long propriospinal INs. Remarkably, the CST projections onto short propriospinal INs, which did not bridge the lesion site, were lost 12 weeks after injury while the CST contacts made with the long propriospinal INs crossing the lesion site were maintained. In addition, the number of direct contacts between long propriospinal axon terminals and lumbosacral motoneurons was doubled 8 weeks after the dorsal hemisection. The maintenance of these intraspinal pathways from cervical to lumbar segments following the dorsal hemisection was verified by pseudorabies virus tracing and their functionality was supported by EMG signals in the hindlimb evoked by intracortical microstimulation. Similarly, lesioning of the reticulospinal tract (RtST) by a unilateral cervical hemisection in adult rats was shown to increase reticulo-propriospinal contacts from damaged RtST axons (Filli et al., 2014). Since brainstem locomotor pathways such as the RtST are critical in control of locomotion in mammals (Brownstone and Chopek, 2018), the remodeling of reticulospinal pathways involving propriospinal INs may be an important factor in locomotor recovery (Asboth et al., 2018).

Propriospinal INs Form Detours Around Lesions

One reason why descending inputs may be increasing their connections with propriospinal INs after an injury is the ability of these spinal neurons to form circuits, which may be pre-existing or *de novo*, that circumnavigate spinal lesions to provide an alternative flow of motor commands to spared lumbar circuits for locomotion. This hypothesis has been tested, in particular, using the staggered hemisection injury paradigm (Kato et al., 1984; Courtine et al., 2008; May et al., 2017). In these studies, an initial hemisection is made to sever ipsilateral descending pathways on one side of the body (**Figure 2B**). A second hemisection is subsequently made on the other side of the body at a more rostral thoracic segment to disrupt spared descending pathways contralateral to the first hemisection. In some studies, the second hemisection is made immediately or after a delay, the latter to determine whether the earlier hemisection was followed by adaptations to spinal circuits that may lead to spontaneous recovery of stepping function (Courtine et al., 2008; May et al., 2017). When an initial hemisection

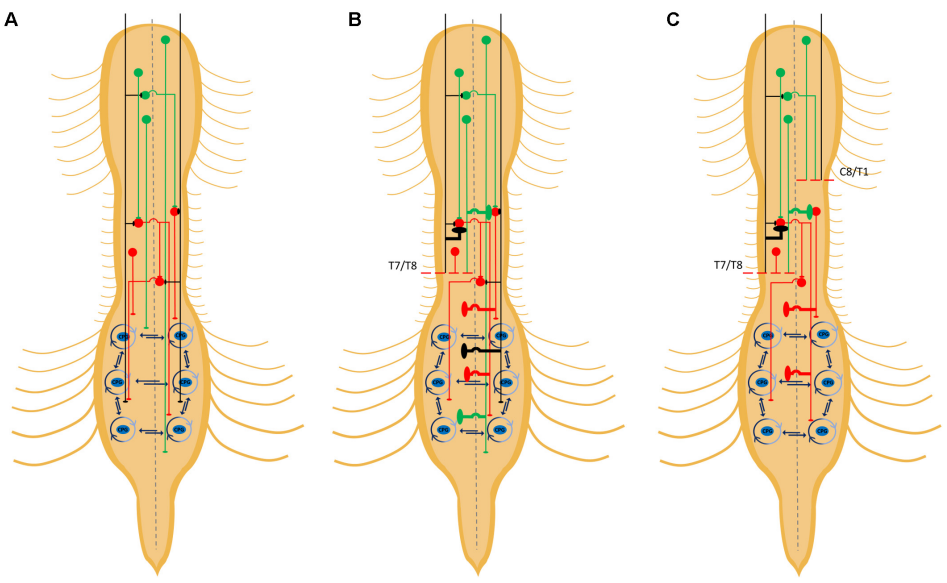

FIGURE 2 | Detour circuits arising from staggered hemisections. Schematic diagram depicting some propriospinal circuits innervating lumbar central pattern generators (CPGs) **(A)**, some possible detour circuits formed after an initial hemisection **(B)**, and spared detour circuits following a second, delayed, contralateral hemisection **(C)**. Collateral sprouting depicted by bold lines. The propriospinal neurons within the lumbar spinal cord are not depicted but would either be connected to, or part of, CPGs. Descending inputs from detour circuits projecting to the lumbar spinal cord can project to lumbar propriospinal neurons and/or lumbar CPGs.

at T12 was followed 10 weeks later by a second contralateral hemisection at T7, greater recovery of locomotor activity was observed compared to animals that received the contralateral hemisections at T7 and T12 simultaneously (Courtine et al., 2008). The improvements in recovery when hemisections were made with a delay as opposed to simultaneously suggests that the initial hemisection promoted remodeling of propriospinal circuits to form detours around this initial hemisection that were not disrupted by the second, delayed, contralateral hemisection (**Figure 2C**). Locomotor recovery following the delayed staggered hemisections was associated with evidence of connectivity between spared lumbar circuits with propriospinal INs in the intervening region between the lesions (T8–T10) while showing virtually no direct connectivity between supraspinal locomotor nuclei and lumbar circuits. Furthermore, an excitotoxic ablation of T8–T10 neurons eliminated any observed spontaneous recovery, supporting the idea that propriospinal INs had formed detours to permit the transmission of descending information to hindlimb CPGs (Courtine et al., 2008).

The possibility of detour circuits formed by propriospinal INs was further strengthened by evidence of increased connectivity between descending RtST tracts and propriospinal INs following a staggered contralateral hemisection protocol where one hemisection at T10 eliminated the ipsilateral RtST and CST followed by an over-hemisection at T7 removing the contralateral RtST and both CSTs (May et al., 2017). The number of RtST contacts onto propriospinal INs was significantly higher if both hemisections were made with a delay, suggesting again that locomotor commands were routed through detour circuits formed by propriospinal INs after the first hemisection.

Propriospinal INs Relay Sensory Feedback to Activate Spinal Locomotor Circuits

The formation of detours around spinal lesions is not possible after complete SCI, and so far, axonal regeneration across lesion sites remains a significant challenge. However, animal models of complete SCI often exhibit some recovery of locomotor function despite a lack of any meaningful regeneration across lesion sites. This recovery is believed to involve plasticity in spinal circuits below the lesion site (Barrière et al., 2008; Rossignol and Frigon, 2011; Martinez et al., 2012) and propriospinal INs are poised to play significant roles in promoting this recovery due to their ability to communicate across spinal segments.

Activation of sensory feedback in the days following complete SCI has repeatedly been shown to be crucial to this recovery of locomotor function (Bouyer and Rossignol, 2003; Lavrov et al., 2008; Sławińska et al., 2012; Takeoka et al., 2014). Propriospinal INs that integrate sensory feedback may be particularly central to promoting locomotor recovery by relaying sensory feedback to the spared CPGs distributed across the lumbar spinal cord. For example, dI3 INs, which integrate cutaneous and proprioceptive inputs, have been shown to be involved in the recovery of locomotor function following complete SCI. dI3 IN loss-of-function significantly depressed the ability to generate sensory stimulus-induced locomotor activity in a reduced spinal cord locomotor preparation and largely eliminated the benefits of treadmill training after SCI (Bui et al., 2016).

With increasing evidence that propriospinal INs may play an invaluable role in promoting recovery of locomotor function, several different approaches have been explored that center on these neurons. We describe these strategies below.

THERAPEUTIC STRATEGIES FOR SCI UTILIZING PROPRIOSPINAL INs

Stimulation of Propriospinal INs to Augment Activity After SCI

Although many neurons and cells die after SCI around the lesion site, some neurons survive the injury but may become dormant, leading to a state where voluntary movements are absent. These neurons may still have the capacity to become excited in response to convergent inputs from spared descending tracts and sensory feedback, but so far, in human SCI patients with sustained loss of movements, this has only been observed when combined with electrical neuromodulation and/or pharmacological interventions (Gerasimenko et al., 2007; Courtine et al., 2009; Harkema et al., 2011; Angeli et al., 2014). Pharmacological strategies aimed at enhancing propriospinal IN activity promote locomotion by facilitating the transmission of motor commands through propriospinal relays, and by increasing the excitability of downstream locomotor networks.

This particular approach stems from experiments using *ex vivo* spinal cord and brainstem–spinal cord preparations, wherein fictive locomotor activity could be induced using a variety of physiological and pharmacological manipulations to achieve a state of increased excitability in the locomotor network. Transient elevations in extracellular potassium or application of neurotransmitter agonists restored locomotor activity elicited by brainstem stimulation following a staggered hemisection paradigm to sever all direct bulbospinal connections in a neonatal brainstem–spinal cord preparation (Zaporozhets et al., 2011), suggesting that dormant propriospinal relays could be activated with the appropriate stimulus. Subsequent testing of neurotransmitter agonists, including serotonin, dopamine, and norepinephrine, successfully induced locomotor activity when applied to thoracic segments in spinal cord preparations with staggered contralateral hemisections at T1/T2 and T9/T10. Glutamatergic agonist NMDA only promoted locomotor activity in this experimental paradigm when applied with serotonin, while acetylcholine did not promote locomotor activity. *In vivo* animal studies have also demonstrated the efficacy of similar pharmacological approaches in promoting locomotor activity following SCI. This was first demonstrated in acutely spinalized cats injected with L-DOPA, where it was observed that stimulation of flexor reflex afferents could elicit ipsilateral flexor and contralateral extensor activity reminiscent of normal locomotor patterning (Jankowska et al., 1967). More recent iterations of this approach have focused on serotonin receptor agonists such as quipazine and 8-OH-DPAT, typically delivered in combination with step training and/or epidural stimulation

to promote locomotor recovery in rodent models of SCI (Fong et al., 2005; Gerasimenko et al., 2007; Ichiyama et al., 2008; Courtine et al., 2009; Cowley et al., 2015; Duru et al., 2015). Epidural stimulation, which is often applied through the use of microelectrode arrays implanted over the lumbosacral cord (Lavrov et al., 2008; Angeli et al., 2018; Capogrosso et al., 2018; Wagner et al., 2018), does not explicitly target propriospinal INs. However, the ability of epidural stimulation to facilitate the production of hindlimb stepping after SCI seems to be a consequence of the recruitment of propriospinal INs along with MNs by the activation of sensory afferents (Capogrosso et al., 2013; Moraud et al., 2016; Formento et al., 2018). Therefore, while these mixed chemical and electrical interventions are not entirely specific to propriospinal INs and are likely to have broader effects on locomotor network excitability, it should be noted that significant locomotor recovery was observed when quipazine was locally injected to target propriospinal relays in staggered hemisection models at T2–T4 and T9–T11 segments (Cowley et al., 2015).

Propriospinal INs in lumbar segments, well below the injury site, may also be targeted for stimulation. For example, silencing dI3 INs has been shown to shunt recovery of stepping following a complete transection (Bui et al., 2016). It follows that stimulating spared dI3 INs in the lumbar spinal cord may be effective in reviving CPG activity in the absence of descending locomotor commands. Stimulation of intact propriospinal INs linked with vertebrate CPG rhythmogenesis such as V2a INs (Crone et al., 2009; Ljunggren et al., 2014), and Shox2+ INs [non-V2a subpopulation (Dougherty et al., 2013)] could also be useful for activating CPGs in the injured spinal cord. Direct stimulation of these populations of propriospinal INs or enhancing their plasticity to promote connectivity with detour circuits could be part of effective therapeutic approaches to restore lost locomotor function.

While these general stimulation approaches hold great promise or have already shown some efficacy in restoring function, a better understanding of the relevant propriospinal IN populations may result in more effective treatment strategies. For example, specific optogenetic stimulation of V3 INs in a mouse model of sacral SCI produces muscle spasms putatively generated by a disinhibited or hyperexcitable locomotor network (Lin et al., 2019). Inhibiting V3 INs was found to reduce the appearance of these muscle spasms; however, subthreshold stimulation of these same neurons also prevented sustained muscle spasms, but would theoretically enable them to be recruited for locomotor functions (Lin et al., 2019). The varied effects of V3 IN manipulation, from detrimental to beneficial, emphasize the need for a better understanding of the contributions of different populations of propriospinal INs to locomotor recovery after SCI.

Disinhibition of Propriospinal IN Activity Following SCI

Enhancing the activity of propriospinal INs, in particular, those involved in bypassing or circumventing a lesion appears to be a promising strategy. However, a recent study suggests that downregulating the excitability of spinal inhibitory INs may enable increased activity in propriospinal circuits, which ultimately leads to improved recovery of locomotor function (Chen et al., 2018). Systemic delivery of CLP290, an agonist of the neuron-specific K^+/Cl^- co-transporter KCC2, improved locomotor recovery in a staggered hemisection paradigm in adult mice. Interestingly, selective expression of KCC2 in GABAergic, but not glutamatergic or cholinergic neurons of the spinal cord, resulted in the sustained recovery of hindlimb stepping. Expressing KCC2 in GABAergic neurons seemed to increase the activity of propriospinal INs between the staggered hemisections, suggesting that generalized increases in activity of spinal circuits involving propriospinal INs may not be effective without concomitantly decreasing the influence of inhibitory neurons gating the flow of descending commands through propriospinal relays.

More generally, locomotor network disinhibition has also been shown to promote locomotor activity following spinal cord transection in cats. Using this experimental model, it was found that untrained cats or those with poor stepping function could be prompted to execute successful stepping after the administration of either glycinergic receptor antagonist strychnine, or $GABA_A$ receptor antagonist bicuculline (Robinson and Goldberger, 1986; Edgerton et al., 1997; de Leon et al., 1999). Interestingly, these strategies to block inhibitory synapses did not yield significant benefit in animals that had previously received step training, suggesting that either a plateau locomotor function had already been reached, or that the step training itself influenced the function of inhibitory synapses in the locomotor network.

Promoting Propriospinal Plasticity Following SCI Through Physical Activity

Physical rehabilitation with treadmill-aid or robotic assistance has been shown to increase recovery of hindlimb stepping beyond the levels of spontaneous recovery (Dietz et al., 1995; Goldshmit et al., 2008; Edgerton and Roy, 2009; Harkema et al., 2011, 2012; Rossignol and Frigon, 2011; Martinez et al., 2012; Angeli et al., 2014; Gill et al., 2018; Wagner et al., 2018). Animal models of SCI provide evidence that this activity-dependent recovery could be associated with changes in connectivity to propriospinal circuits or reorganization of propriospinal circuitry (Theisen et al., 2017). Anatomical tracing experiments (van den Brand et al., 2012) provide evidence that overground training in rats following staggered hemisections at T7 and T10 increases CST projections onto T8/T9 spinal INs that are putative propriospinal INs. Locomotor training has also been shown to partially reverse the loss of cholinergic innervation of motoneurons, putatively from propriospinal cholinergic INs (the $V0_C$ INs, Zagoraiou et al., 2009), following SCI (Skup et al., 2012).

Sensorimotor integration involving propriospinal INs may be modified by step training (Cote, 2004; Knikou and Mummidisetty, 2014). Certainly, proprioceptive feedback activated during locomotor training seems to be essential for the establishment of detour circuits and locomotor recovery (Takeoka et al., 2014). Hindlimb proprioception, in particular, was found to be critical for the guidance of

propriospinal detour circuits following a thoracic hemisection, as hindlimb-targeted ablation of proprioceptive afferents yielded a similarly reduced number of propriospinal connections compared to a more generalized ablation of proprioceptive afferents (Takeoka and Arber, 2019). Interestingly, forelimb activity has been linked to the recovery of hindlimb locomotor control in incomplete SCI (Shah et al., 2013). Training of both forelimbs and hindlimbs of rats with a thoracic hemisection had a greater impact on recovery than training hindlimbs alone (Shah et al., 2013). Quadrupedal step training activated sensory inputs from the forelimbs, which in turn seemed to increase the number of thoracic propriospinal INs rostral to the lesion site that projected to upper lumbar segments. These results and others suggest a complexity in the influence of forelimb and hindlimb sensory activation in promoting plasticity of both descending and ascending propriospinal circuits following SCI (Côté et al., 2012).

While physical rehabilitation seems to promote recovery of hindlimb stepping, levels of recovery have yet to be optimized (Torres-Espín et al., 2018). A number of approaches have been attempted to increase recovery levels further. Recent studies have reported that promoting recovery through electrical and pharmacological stimulation can augment the extent of recovery derived from locomotor training in rodent models of SCI (Asboth et al., 2018). Indeed, the combination of locomotor step training, epidural stimulation, and injection of dopaminergic and serotonergic agonists increased recovery of locomotor activity, including volitional locomotion, after the loss of CST innervation resulting from spinal contusion injury. Neuroanatomical tracing, in combination with optogenetic and/or chemogenetic manipulations, suggests that this recovery results from cortico–reticulo–spinal reorganization that includes increased synaptic contact from the motor cortex to the ventral gigantocellular reticular nuclei, and from the ventral gigantocellular nuclei to putative propriospinal INs (Asboth et al., 2018).

Promoting Axonal Growth Across the Lesion

Propriospinal INs exhibit the capacity to regenerate their axons across lesion sites in the spinal cord. Commissural INs, some of which are likely to be propriospinal, have been shown to form crossing connections across the lesion site following midsagittal spinal sections through their axons (Fenrich et al., 2007; Fenrich and Rose, 2009). Immunostaining and electrophysiology were used to demonstrate that newly formed synapses from these commissural INs were functional and could evoke potentials in contralateral motoneurons. Therefore, at least some propriospinal INs would seem to have the capacity to grow through the inhibitory environment of spinal lesions.

Promoting regrowth of propriospinal INs may be facilitated by overexpression of growth-associated genes or application of neurotrophic factors such as brain-derived neurotrophic factor (BDNF) and NT-3, which have been shown to promote sprouting and rewiring of neurons at the injury site (Bradbury et al., 1999; Hammond et al., 1999). Application of BDNF to the left motor cortex after a thoracic over-hemisection in mice caused collateral sprouting of injured CST axons and formation of contacts with propriospinal INs that was accompanied by functional recovery (Vavrek et al., 2006). In another study, the transduction of the transcription factor Kruppel-like factor 7 (KLF7) by an AAV vector above the injury site after a T10 contusion was shown to promote both descending propriospinal axon plasticity and synapse formation after a T10 contusion in adult mice (Li et al., 2017). KLF7 regulates the expression of a number of genes, including the neurotrophin NGF and its receptor TrkA (Caiazzo et al., 2010). This enhancement of propriospinal plasticity by KLF7 overexpression was associated with significantly improved motor function.

The regenerative capacity of axons of injured propriospinal INs and descending motor axons can be further enhanced by substrates that promote regrowth. For example, peripheral nerve grafts, in combination with the neurotrophin glial cell line-derived neurotrophic factor (GDNF) and the enzyme chondroitinase ABC to degrade inhibitory chondroitin sulfate proteoglycans within lesion scars, promoted the extension of spinal axon processes within and across the graft (Tom et al., 2009). A more recent study suggests that the application of specific growth factors selected to increase the intrinsic capacity of propriospinal INs for axonal growth, to induce the expression of growth-supporting substrate, and to provide guidance cues for regenerating axons, could be sufficient to induce axonal regeneration across a lesion (Anderson et al., 2018). Delivery of osteopontin, insulin-like growth factor 1, ciliary-derived neurotrophic factor, fibroblast growth factor 2, epidermal growth factor, and glial-derived neurotrophic factor through a combination of AAV injections or synthetic hydrogels near and in the lesion site promoted the growth of propriospinal INs through a spinal lesion in both a rat and mouse complete SCI model. While behavioral improvements observed using this strategy were relatively minor, the new propriospinal projections appeared to be capable of conducting action potentials across the lesion site, opening the door to future strategies to improve the integration of these axons into motor circuitry. While these strategies hold promise, the heterogeneity of propriospinal INs (i.e., short versus long-projection), as well as the type and location of the spinal cord lesion are likely to influence the gene-expression and substrate requirements for successful regeneration (Conta and Stelzner, 2004; Swieck et al., 2019).

The identification and application of multiple molecules to coax the regrowth of descending and propriospinal axons across the lesion site and toward spinal locomotor circuits caudal to the lesion site have led to promising results. However, there is still a significant gap between the level of recovered motor function in treated SCI animals and locomotor function in the intact state. A recent study highlights the possibility of promoting propriospinal axon plasticity through the engagement of the components of the motor circuit downstream from descending inputs and propriospinal INs, namely motoneurons and the musculoskeletal system. Motoneurons have extensive dendritic arborizations, some of which even extend beyond the gray matter into the white matter (Rose and Richmond, 1981; Keirstead and Rose, 1983; Tosolini and Morris, 2016). This broad coverage of the

ventral spinal cord could permit motoneurons to have far-ranging influences on regenerating processes after SCI, perhaps through the release of BDNF (Ying et al., 2005; Joseph et al., 2012). While motoneuron dendrites undergo atrophy after SCI (Gazula et al., 2004), the delivery of AAV expressing NT-3 to locomotion-associated motoneurons via transiently demyelinated sciatic nerves after a T10 contusion in mice reduced motoneuron dendrite atrophy. This reduced atrophy was accompanied by an increased presence of descending inputs from spared propriospinal INs onto MNs within the L2–L5 spinal cord levels when compared to non-treated controls and resulted in modest improvements in locomotor behavior (Wang et al., 2018). Interestingly, motoneuron dendrite atrophy after SCI is reduced by exercise (Gazula et al., 2004), further suggesting that combining the application of molecules to increase regenerative properties of propriospinal INs, whether directly or through the influence of other components of the locomotor network, with physical activity could produce greater levels of functional recovery.

Finally, several studies suggest that the benefits of promoting axonal growth of propriospinal axons through growth-stimulating molecules can have unintended consequences. These secondary complications have been illustrated, in particular, for BDNF. AAV delivery of BDNF in rats spinalized at thoracic level improved weight support and treadmill walking over untreated SCI animals (Ziemlińska et al., 2014). However, increased excitability of spinal locomotor circuits eventually resulted in increased clonic movements in BDNF-treated animals over time. This was potentially due to the upregulation of glutamatergic (vGluT2) and GABAergic (GABA, GAD1, and GAD2) transmission in combination with reduced levels of the potassium chloride co-transporter, KCC2, which alters the reversal potential of chloride channels associated with GABA/glycinergic synapses causing them to become depolarizing instead of hyperpolarizing. Similarly, another study reported that BDNF overexpression through viral delivery and/or cell grafts in a cervical hemisection rat model led to spasticity-like symptoms such as clenching of the paws and sustained wrist flexion (Fouad et al., 2013). Motor circuits of the spinal cord are not the only ones that can be modified by BDNF, as viral delivery of BDNF following complete thoracic transection in adult rats promoted stepping function but also increased pain sensitization (Boyce et al., 2012). Therefore, these results emphasize the need for tight regulation of the timing of delivery and the dosage of growth-promoting molecules in order to avoid secondary complications.

Strategies Aiming to Generate New or Replace Lost Propriospinal INs

An alternative approach to modulating the activity of existing propriospinal INs or promoting remodeling of propriospinal circuits would be to replace lost propriospinal INs due to injury (Bonner and Steward, 2015; Courtine and Sofroniew, 2019). Recently, neural stem cell transplantation has gained much attention as a repair mechanism after SCI. Transplantation of neural stem/progenitor cells (NSPC) was shown to promote functional recovery after mild and moderate contusion at the T9 level in mice by reorganizing the circuitry of propriospinal INs (Yokota et al., 2015). Retrograde transsynaptic tracing showed that propriospinal circuits reorganize in both longitudinal and transverse directions, enhancing synaptic integration between the engrafted NSPCs and the host neurons. Recently, human neural stem cell grafts into C7 hemisection lesion sites in non-human primates were shown to extend axons into the caudal spinal cord of the host. These same grafts exhibited evidence of integration with descending tracts from supraspinal motor centers, a feature that was associated with improvements in forelimb function (Rosenzweig et al., 2018). As such, these stem cell interventions provide a promising strategy to generate new propriospinal relays in cases where spared motor circuitry is insufficient to restore meaningful motor function after SCI.

PERSPECTIVES

As demonstrated by the research described herein, propriospinal INs are necessary for the appropriate control of locomotion in the intact state. It is therefore unsurprising that propriospinal INs are also critical to locomotor recovery after SCI, and represent important therapeutic targets for novel SCI treatments. However, given the diversity of propriospinal INs in organization and function as well as the neural dysfunction that can arise from neural plasticity following SCI (Boyce et al., 2012; Beauparlant et al., 2013; Fouad et al., 2013; Ziemlińska et al., 2014), effectively harnessing propriospinal INs will likely require significant advancement in our understanding of how these neurons adapt to SCI, and how different populations work together to support locomotion after a substantial loss of supraspinal input. New methods to non-invasively manipulate propriospinal INs, either regionally using epidural stimulation, or in a population-specific manner using chemogenetic and optogenetic approaches (Asboth et al., 2018; Mondello et al., 2018; Lin et al., 2019), will be critical to develop new therapeutic strategies and to improve our understanding of propriospinal IN function after SCI. Supplemental strategies to improve integration of propriospinal IN relays, such as the transcranial stimulation approach proposed to induce greater CST plasticity to propriospinal INs (Krishnan et al., 2019), or more conventionally, locomotor training paradigms to refine these propriospinal circuits, may also prove to be critical for the optimization of locomotor recovery. In any case, as the knowledge of propriospinal INs and locomotion steadily advances, the future of the field appears bright – with significant challenges and opportunities for discovery on the horizon.

AUTHOR CONTRIBUTIONS

AL, SG, NL, and TB wrote the sections of the manuscript, contributed to the manuscript revision, and read and approved the submitted version. NL and TB designed the figures.

FUNDING

This research was funded by the Natural Sciences and Engineering Research Council (RGPIN-2015-06403), the International Foundation for Research in Paraplegia (P167), and an Ontario Early Researcher Award (ER16-12-214).

ACKNOWLEDGMENTS

We would like to acknowledge the efforts of all researchers who have contributed to advancing our understanding of spinal motor circuits and their repair after injury and apologize to those individuals whose work was not cited due to space limitations or oversight.

REFERENCES

Al-Mosawie, A., Wilson, J. M., and Brownstone, R. M. (2007). Heterogeneity of V2-derived interneurons in the adult mouse spinal cord. *Eur. J. Neurosci.* 26, 3003–3015. doi: 10.1111/j.1460-9568.2007.05907.x

Alstermark, B., Lundberg, A., Pinter, M., and Sasaki, S. (1987). Subpopulations and functions of long C3-C5 propriospinal neurones. *Brain Res.* 404, 395–400. doi: 10.1016/0006-8993(87)91402-08

Alvarez, F. J., Jonas, P. C., Sapir, T., Hartley, R., Berrocal, M. C., Geiman, E. J., et al. (2005). Postnatal phenotype and localization of spinal cord V1 derived interneurons. *J. Comp. Neurol.* 493, 177–192. doi: 10.1002/cne.20711

Anderson, M. A., O'Shea, T. M., Burda, J. E., Ao, Y., Barlatey, S. L., Bernstein, A. M., et al. (2018). Required growth facilitators propel axon regeneration across complete spinal cord injury. *Nature* 561, 396–400. doi: 10.1038/s41586-018-0467-6

Andersson, L. S., Larhammar, M., Memic, F., Wootz, H., Schwochow, D., Rubin, C.-J., et al. (2012). Mutations in DMRT3 affect locomotion in horses and spinal circuit function in mice. *Nature* 488, 642–646. doi: 10.1038/nature11399

Angeli, C. A., Boakye, M., Morton, R. A., Vogt, J., Benton, K., Chen, Y., et al. (2018). Recovery of over-ground walking after chronic motor complete spinal cord injury. *N. Engl. J. Med.* 379, 1244–1250. doi: 10.1056/NEJMoa1803588

Angeli, C. A., Edgerton, V. R., Gerasimenko, Y. P., and Harkema, S. J. (2014). Altering spinal cord excitability enables voluntary movements after chronic complete paralysis in humans. *Brain J. Neurol.* 137, 1394–1409. doi: 10.1093/brain/awu038

Asboth, L., Friedli, L., Beauparlant, J., Martinez-Gonzalez, C., Anil, S., Rey, E., et al. (2018). Cortico-reticulo-spinal circuit reorganization enables functional recovery after severe spinal cord contusion. *Nat. Neurosci.* 21, 576–588. doi: 10.1038/s41593-018-0093-5

Atsuta, Y., Abraham, P., Iwahara, T., Garcia-Rill, E., and Skinner, R. D. (1991). Control of locomotion in vitro: II. Chemical stimulation. *Somatosens. Mot. Res.* 8, 55–63. doi: 10.3109/08990229109144729

Ballion, B., Morin, D., and Viala, D. (2001). Forelimb locomotor generators and quadrupedal locomotion in the neonatal rat. *Eur. J. Neurosci.* 14, 1727–1738. doi: 10.1046/j.0953-816x.2001.01794.x

Bareyre, F. M., Kerschensteiner, M., Raineteau, O., Mettenleiter, T. C., Weinmann, O., and Schwab, M. E. (2004). The injured spinal cord spontaneously forms a new intraspinal circuit in adult rats. *Nat. Neurosci.* 7:269. doi: 10.1038/nn1195

Barrière, G., Leblond, H., Provencher, J., and Rossignol, S. (2008). Prominent role of the spinal central pattern generator in the recovery of locomotion after partial spinal cord injuries. *J. Neurosci.* 28, 3976–3987. doi: 10.1523/JNEUROSCI.5692-07.2008

Beauparlant, J., van den Brand, R., Barraud, Q., Friedli, L., Musienko, P., Dietz, V., et al. (2013). Undirected compensatory plasticity contributes to neuronal dysfunction after severe spinal cord injury. *Brain* 136, 3347–3361. doi: 10.1093/brain/awt204

Benito-Gonzalez, A., and Alvarez, F. J. (2012). Renshaw cells and ia inhibitory interneurons are generated at different times from p1 progenitors and differentiate shortly after exiting the cell cycle. *J. Neurosci.* 32, 1156–1170. doi: 10.1523/JNEUROSCI.3630-12.2012

Betley, J. N., Wright, C. V. E., Kawaguchi, Y., Erdélyi, F., Szabó, G., Jessell, T. M., et al. (2009). Stringent specificity in the construction of a GABAergic presynaptic inhibitory circuit. *Cell* 139, 161–174. doi: 10.1016/j.cell.2009.08.027

Bonner, J. F., and Steward, O. (2015). Repair of spinal cord injury with neuronal relays: from fetal grafts to neural stem cells. *Brain Res.* 1619, 115–123. doi: 10.1016/j.brainres.2015.01.006

Borowska, J., Jones, C. T., Zhang, H., Blacklaws, J., Goulding, M., and Zhang, Y. (2013). Functional subpopulations of V3 interneurons in the mature mouse spinal cord. *J. Neurosci.* 33, 18553–18565. doi: 10.1523/JNEUROSCI.2005-13.2013

Bouyer, L. J. G., and Rossignol, S. (2003). Contribution of cutaneous inputs from the hindpaw to the control of locomotion. II. spinal cats. *J. Neurophysiol.* 90, 3640–3653. doi: 10.1152/jn.00497.2003

Boyce, V. S., Park, J., Gage, F. H., and Mendell, L. M. (2012). Differential effects of brain-derived neurotrophic factor and neurotrophin-3 on hindlimb function in paraplegic rats. *Eur. J. Neurosci.* 35, 221–232. doi: 10.1111/j.1460-9568.2011.07950.x

Bradbury, E. J., Khemani, S., King, V. R., Priestley, J. V., and McMahon, S. B. (1999). NT-3 promotes growth of lesioned adult rat sensory axons ascending in the dorsal columns of the spinal cord. *Eur. J. Neurosci.* 11, 3873–3883. doi: 10.1046/j.1460-9568.1999.00809.x

Britz, O., Zhang, J., Grossmann, K. S., Dyck, J., Kim, J. C., Dymecki, S., et al. (2015). A genetically defined asymmetry underlies the inhibitory control of flexor–extensor locomotor movements. *eLife* 4:e04718. doi: 10.7554/eLife.04718

Brockett, E. G., Seenan, P. G., Bannatyne, B. A., and Maxwell, D. J. (2013). Ascending and descending propriospinal pathways between lumbar and cervical segments in the rat: Evidence for a substantial ascending excitatory pathway. *Neuroscience* 240, 83–97. doi: 10.1016/j.neuroscience.2013.02.039

Brownstone, R. M., and Chopek, J. W. (2018). Reticulospinal systems for tuning motor commands. *Front. Neural Circuits* 12:30. doi: 10.3389/fncir.2018.00030

Brustein, E., and Rossignol, S. (1998). Recovery of locomotion after ventral and ventrolateral spinal lesions in the cat. I. deficits and adaptive mechanisms. *J. Neurophysiol.* 80, 1245–1267. doi: 10.1152/jn.1998.80.3.1245

Bui, T. V., Akay, T., Loubani, O., Hnasko, T. S., Jessell, T. M., and Brownstone, R. M. (2013). Circuits for grasping: spinal dI3 interneurons mediate cutaneous control of motor behavior. *Neuron* 78, 191–204. doi: 10.1016/j.neuron.2013.02.007

Bui, T. V., Stifani, N., Akay, T., and Brownstone, R. M. (2016). Spinal microcircuits comprising dI3 interneurons are necessary for motor functional recovery following spinal cord transection. *eLife* 5:e21715. doi: 10.7554/eLife.21715

Caggiano, V., Leiras, R., Goñi-Erro, H., Masini, D., Bellardita, C., Bouvier, J., et al. (2018). Midbrain circuits that set locomotor speed and gait selection. *Nature* 553, 455–460. doi: 10.1038/nature25448

Caiazzo, M., Colucci-D'Amato, L., Esposito, M. T., Parisi, S., Stifani, S., Ramirez, F., et al. (2010). Transcription factor KLF7 regulates differentiation of neuroectodermal and mesodermal cell lineages. *Exp. Cell Res.* 316, 2365–2376. doi: 10.1016/j.yexcr.2010.05.021

Capelli, P., Pivetta, C., Soledad Esposito, M., and Arber, S. (2017). Locomotor speed control circuits in the caudal brainstem. *Nature* 551, 373–377. doi: 10.1038/nature24064

Capogrosso, M., Wagner, F. B., Gandar, J., Moraud, E. M., Wenger, N., Milekovic, T., et al. (2018). Configuration of electrical spinal cord stimulation through real-time processing of gait kinematics. *Nat. Protoc.* 13, 2031–2061. doi: 10.1038/s41596-018-0030-9

Capogrosso, M., Wenger, N., Raspopovic, S., Musienko, P., Beauparlant, J., Bassi Luciani, L., et al. (2013). A computational model for epidural electrical stimulation of spinal sensorimotor circuits. *J. Neurosci.* 33, 19326–19340. doi: 10.1523/JNEUROSCI.1688-13.2013

Cazalets, J. R., Borde, M., and Clarac, F. (1995). Localization and organization of the central pattern generator for hindlimb locomotion in newborn rat. *J. Neurosci.* 15, 4943–4951. doi: 10.1523/jneurosci.15-07-04943.1995

Chaix, Y., Marque, P., Meunier, S., Pierrot-Deseilligny, E., and Simonetta-Moreau, M. (1997). Further evidence for non-monosynaptic group I excitation of motoneurones in the human lower limb. *Exp. Brain Res.* 115, 35–46. doi: 10.1007/pl00005683

Chen, B., Li, Y., Yu, B., Zhang, Z., Brommer, B., Williams, P. R., et al. (2018). Reactivation of dormant relay pathways in injured spinal cord by KCC2 Manipulations. *Cell* 174, 521–535.e13. doi: 10.1016/j.cell.2018.06.005

Chopek, J. W., Nascimento, F., Beato, M., Brownstone, R. M., and Zhang, Y. (2018). Sub-populations of spinal V3 interneurons form focal modules of layered pre-motor microcircuits. *Cell Rep.* 25, 146–156.e3. doi: 10.1016/j.celrep.2018.08.095

Conta, A. C., and Stelzner, D. J. (2004). Differential vulnerability of propriospinal tract neurons to spinal cord contusion injury. *J. Comp. Neurol.* 479, 347–359. doi: 10.1002/cne.20319

Cote, M.-P. (2004). Step training-dependent plasticity in spinal cutaneous pathways. *J. Neurosci.* 24, 11317–11327. doi: 10.1523/JNEUROSCI.1486-04.2004

Côté, M.-P., Detloff, M. R., Wade, R. J., Lemay, M. A., and Houlé, J. D. (2012). Plasticity in ascending long propriospinal and descending supraspinal pathways in chronic cervical spinal cord injured rats. *Front. Physiol.* 3:330. doi: 10.3389/fphys.2012.00330

Courtine, G., Gerasimenko, Y., van den Brand, R., Yew, A., Musienko, P., Zhong, H., et al. (2009). Transformation of nonfunctional spinal circuits into functional states after the loss of brain input. *Nat. Neurosci.* 12, 1333–1342. doi: 10.1038/nn.2401

Courtine, G., and Sofroniew, M. V. (2019). Spinal cord repair: advances in biology and technology. *Nat. Med.* 25, 898–908. doi: 10.1038/s41591-019-0475-6

Courtine, G., Song, B., Roy, R. R., Zhong, H., Herrmann, J. E., Ao, Y., et al. (2008). Recovery of supraspinal control of stepping via indirect propriospinal relay connections after spinal cord injury. *Nat. Med.* 14, 69–74. doi: 10.1038/nm1682

Cowley, K. C., MacNeil, B. J., Chopek, J. W., Sutherland, S., and Schmidt, B. J. (2015). Neurochemical excitation of thoracic propriospinal neurons improves hindlimb stepping in adult rats with spinal cord lesions. *Exp. Neurol.* 264, 174–187. doi: 10.1016/j.expneurol.2014.12.006

Cowley, K. C., and Schmidt, B. J. (1997). Regional distribution of the locomotor pattern-generating network in the neonatal rat spinal cord. *J. Neurophysiol.* 77, 247–259. doi: 10.1152/jn.1997.77.1.247

Cowley, K. C., Zaporozhets, E., and Schmidt, B. J. (2008). Propriospinal neurons are sufficient for bulbospinal transmission of the locomotor command signal in the neonatal rat spinal cord. *J. Physiol.* 586, 1623–1635. doi: 10.1113/jphysiol.2007.148361

Crone, S. A., Quinlan, K. A., Zagoraiou, L., Droho, S., Restrepo, C. E., Lundfald, L., et al. (2008). Genetic ablation of V2a ipsilateral interneurons disrupts left-right locomotor coordination in mammalian spinal cord. *Neuron* 60, 70–83. doi: 10.1016/j.neuron.2008.08.009

Crone, S. A., Zhong, G., Harris-Warrick, R., and Sharma, K. (2009). In mice lacking v2a interneurons, gait depends on speed of locomotion. *J. Neurosci.* 29, 7098–7109. doi: 10.1523/JNEUROSCI.1206-09.2009

Danner, S. M., Shevtsova, N. A., Frigon, A., and Rybak, I. A. (2017). Computational modeling of spinal circuits controlling limb coordination and gaits in quadrupeds. *eLife* 6:e31050. doi: 10.7554/eLife.31050

Dasen, J. S., and Jessell, T. M. (2009). Hox networks and the origins of motor neuron diversity. *Curr. Top. Dev. Biol.* 88, 169–200. doi: 10.1016/S0070-2153(09)88006-X

de Leon, R. D., Tamaki, H., Hodgson, J. A., Roy, R. R., and Edgerton, V. R. (1999). Hindlimb locomotor and postural training modulates glycinergic inhibition in the spinal cord of the adult spinal cat. *J. Neurophysiol.* 82, 359–369. doi: 10.1152/jn.1999.82.1.359

Delwaide, P. J., Figiel, C., and Richelle, C. (1977). Effects of postural changes of the upper limb on reflex transmission in the lower limb. Cervicolumbar reflex interactions in man. *J. Neurol. Neurosurg. Psychiatry* 40, 616–621. doi: 10.1136/jnnp.40.6.616

Dietz, V. (2002). Do human bipeds use quadrupedal coordination? *Trends Neurosci.* 25, 462–467. doi: 10.1016/s0166-2236(02)02229-4

Dietz, V., Colombo, G., Jensen, L., and Baumgartner, L. (1995). Locomotor capacity of spinal cord in paraplegic patients. *Ann. Neurol.* 37, 574–582. doi: 10.1002/ana.410370506

Dougherty, K. J., Zagoraiou, L., Satoh, D., Rozani, I., Doobar, S., Arber, S., et al. (2013). Locomotor rhythm generation linked to the output of spinal shox2 excitatory interneurons. *Neuron* 80, 920–933. doi: 10.1016/j.neuron.2013.08.015

Duru, P. O., Tillakaratne, N. J. K., Kim, J. A., Zhong, H., Stauber, S. M., Pham, T. T., et al. (2015). Spinal neuronal activation during locomotor-like activity enabled by epidural stimulation and 5-hydroxytryptamine agonists in spinal rats. *J. Neurosci. Res.* 93, 1229–1239. doi: 10.1002/jnr.23579

Edgerton, V. R., de Leon, R. D., Tillakaratne, N., Recktenwald, M. R., Hodgson, J. A., and Roy, R. R. (1997). Use-dependent plasticity in spinal stepping and standing. *Adv. Neurol.* 72, 233–247.

Edgerton, V. R., and Roy, R. R. (2009). Robotic training and spinal cord plasticity. *Brain Res. Bull.* 78, 4–12. doi: 10.1016/j.brainresbull.2008.09.018

Eide, A.-L., Glover, J., Kjaerulff, O., and Kiehn, O. (1999). Characterization of commissural interneurons in the lumbar region of the neonatal rat spinal cord. *J. Comp. Neurol.* 403, 332–345. doi: 10.1002/(SICI)1096-9861(19990118)403

English, A. W., Tigges, J., and Lennard, P. R. (1985). Anatomical organization of long ascending propriospinal neurons in the cat spinal cord. *J. Comp. Neurol.* 240, 349–358. doi: 10.1002/cne.902400403

Falgairolle, M., and O'Donovan, M. J. (2019). V1 interneurons regulate the pattern and frequency of locomotor-like activity in the neonatal mouse spinal cord. *PLoS Biol.* 17:e3000447. doi: 10.1371/journal.pbio.3000447

Fenrich, K. K., and Rose, P. K. (2009). Spinal interneuron axons spontaneously regenerate after spinal cord injury in the adult feline. *J. Neurosci.* 29, 12145–12158. doi: 10.1523/JNEUROSCI.0897-09.2009

Fenrich, K. K., Skelton, N., MacDermid, V. E., Meehan, C. F., Armstrong, S., Neuber-Hess, M. S., et al. (2007). Axonal regeneration and development of de novo axons from distal dendrites of adult feline commissural interneurons after a proximal axotomy. *J. Comp. Neurol.* 502, 1079–1097. doi: 10.1002/cne.21362

Filli, L., Engmann, A. K., Zörner, B., Weinmann, O., Moraitis, T., Gullo, M., et al. (2014). Bridging the gap: a reticulo-propriospinal detour bypassing an incomplete spinal cord injury. *J. Neurosci.* 34, 13399–13410. doi: 10.1523/JNEUROSCI.0701-14.2014

Fink, A. J. P., Croce, K. R., Huang, Z. J., Abbott, L. F., Jessell, T. M., and Azim, E. (2014). Presynaptic inhibition of spinal sensory feedback ensures smooth movement. *Nature* 509, 43–48. doi: 10.1038/nature13276

Flynn, J. R., Conn, V., Boyle, K. A., Hughes, D. I., Watanabe, M., Velasquez, T., et al. (2017). Anatomical and molecular properties of long descending propriospinal neurons in mice. *Front. Neuroanat.* 11:5. doi: 10.3389/fnana.2017.00005

Flynn, J. R., Graham, B. A., Galea, M. P., and Callister, R. J. (2011). The role of propriospinal interneurons in recovery from spinal cord injury. *Neuropharmacology* 60, 809–822. doi: 10.1016/j.neuropharm.2011.01.016

Fong, A. J., Cai, L. L., Otoshi, C. K., Reinkensmeyer, D. J., Burdick, J. W., Roy, R. R., et al. (2005). Spinal cord-transected mice learn to step in response to quipazine treatment and robotic training. *J. Neurosci.* 25, 11738–11747. doi: 10.1523/JNEUROSCI.1523-05.2005

Formento, E., Minassian, K., Wagner, F., Mignardot, J. B., Le Goff-Mignardot, C. G., Rowald, A., et al. (2018). Electrical spinal cord stimulation must preserve proprioception to enable locomotion in humans with spinal cord injury. *Nat. Neurosci.* 21, 1728–1741. doi: 10.1038/s41593-018-0262-6

Forssberg, H., and Grillner, S. (1973). The locomotion of the acute spinal cat injected with clonidine i.v. *Brain Res.* 50, 184–186. doi: 10.1016/0006-8993(73)90606-9

Forssberg, H., Grillner, S., Halbertsma, J., and Rossignol, S. (1980). The locomotion of the low spinal cat. II. Interlimb coordination. *Acta Physiol. Scand.* 108, 283–295. doi: 10.1111/j.1748-1716.1980.tb06534.x

Fouad, K., Bennett, D. J., Vavrek, R., and Blesch, A. (2013). Long-term viral brain-derived neurotrophic factor delivery promotes spasticity in rats with a cervical spinal cord hemisection. *Front. Neurol.* 4:187. doi: 10.3389/fneur.2013.00187

Frigon, A. (2017). The neural control of interlimb coordination during mammalian locomotion. *J. Neurophysiol.* 117, 2224–2241. doi: 10.1152/jn.00978.2016

Frigon, A., Desrochers, E., Thibaudier, Y., Hurteau, M.-F., and Dambreville, C. (2017). Left-right coordination from simple to extreme conditions during split-belt locomotion in the chronic spinal adult cat. *J. Physiol.* 595, 341–361. doi: 10.1113/JP272740

Frigon, A., Hurteau, M.-F., Thibaudier, Y., Leblond, H., Telonio, A., and D'Angelo, G. (2013). Split-belt walking alters the relationship between locomotor phases and cycle duration across speeds in intact and chronic spinalized adult cats. *J. Neurosci.* 33, 8559–8566. doi: 10.1523/JNEUROSCI.3931-12.2013

Gazula, V.-R., Roberts, M., Luzzio, C., Jawad, A. F., and Kalb, R. G. (2004). Effects of limb exercise after spinal cord injury on motor neuron dendrite structure. *J. Comp. Neurol.* 476, 130–145. doi: 10.1002/cne.20204

Gerasimenko, Y., Gad, P., Sayenko, D., McKinney, Z., Gorodnichev, R., Puhov, A., et al. (2016). Integration of sensory, spinal, and volitional descending inputs in regulation of human locomotion. *J. Neurophysiol.* 116, 98–105. doi: 10.1152/jn.00146.2016

Gerasimenko, Y. P., Ichiyama, R. M., Lavrov, I. A., Courtine, G., Cai, L., Zhong, H., et al. (2007). Epidural spinal cord stimulation plus quipazine administration enable stepping in complete spinal adult rats. *J. Neurophysiol.* 98, 2525–2536. doi: 10.1152/jn.00836.2007

Gill, M. L., Grahn, P. J., Calvert, J. S., Linde, M. B., Lavrov, I. A., Strommen, J. A., et al. (2018). Neuromodulation of lumbosacral spinal networks enables independent stepping after complete paraplegia. *Nat. Med.* 24, 1677–1682. doi: 10.1038/s41591-018-0175-7

Goldshmit, Y., Lythgo, N., Galea, M. P., and Turnley, A. M. (2008). Treadmill training after spinal cord hemisection in mice promotes axonal sprouting and synapse formation and improves motor recovery. *J. Neurotrauma* 25, 449–465. doi: 10.1089/neu.2007.0392

Gordon, I. T., Dunbar, M. J., Vanneste, K. J., and Whelan, P. J. (2008). Interaction between developing spinal locomotor networks in the neonatal mouse. *J. Neurophysiol.* 100, 117–128. doi: 10.1152/jn.00829.2007

Gosgnach, S., Bikoff, J. B., Dougherty, K. J., El Manira, A., Lanuza, G. M., and Zhang, Y. (2017). Delineating the diversity of spinal interneurons in locomotor circuits. *J. Neurosci.* 37, 10835–10841. doi: 10.1523/JNEUROSCI.1829-17.2017

Gosgnach, S., Lanuza, G. M., Butt, S. J. B., Saueressig, H., Zhang, Y., Velasquez, T., et al. (2006). V1 spinal neurons regulate the speed of vertebrate locomotor outputs. *Nature* 440, 215–219. doi: 10.1038/nature04545

Griener, A., Zhang, W., Kao, H., Haque, F., and Gosgnach, S. (2017). Anatomical and electrophysiological characterization of a population of dI6 interneurons in the neonatal mouse spinal cord. *Neuroscience* 362, 47–59. doi: 10.1016/j.neuroscience.2017.08.031

Grillner, S., Perret, C., and Zangger, P. (1976). Central generation of locomotion in the spinal dogfish. *Brain Res.* 109, 255–269. doi: 10.1016/0006-8993(76)905291

Hägglund, M., Borgius, L., Dougherty, K. J., and Kiehn, O. (2010). Activation of groups of excitatory neurons in the mammalian spinal cord or hindbrain evokes locomotion. *Nat. Neurosci.* 13, 246–252. doi: 10.1038/nn.2482

Hammond, E. N., Tetzlaff, W., Mestres, P., and Giehl, K. M. (1999). BDNF, but not NT-3, promotes long-term survival of axotomized adult rat corticospinal neurons in vivo. *Neuroreport* 10, 2671–2675. doi: 10.1097/00001756-199908200-00043

Harkema, S., Gerasimenko, Y., Hodes, J., Burdick, J., Angeli, C., Chen, Y., et al. (2011). Effect of epidural stimulation of the lumbosacral spinal cord on voluntary movement, standing, and assisted stepping after motor complete paraplegia: a case study. *Lancet Lond. Engl.* 377, 1938–1947. doi: 10.1016/S0140-6736(11)60547-3

Harkema, S. J., Schmidt-Read, M., Lorenz, D. J., Edgerton, V. R., and Behrman, A. L. (2012). Balance and ambulation improvements in individuals with chronic incomplete spinal cord injury using locomotor training-based rehabilitation. *Arch. Phys. Med. Rehabil.* 93, 1508–1517. doi: 10.1016/j.apmr.2011.01.024

Higashijima, S., Masino, M. A., Mandel, G., and Fetcho, J. R. (2004). Engrailed-1 expression marks a primitive class of inhibitory spinal interneuron. *J. Neurosci.* 24, 5827–5839. doi: 10.1523/JNEUROSCI.5342-03.2004

Ichiyama, R. M., Gerasimenko, Y., Jindrich, D. L., Zhong, H., Roy, R. R., and Edgerton, V. R. (2008). Dose dependence of the 5-HT agonist quipazine in facilitating spinal stepping in the rat with epidural stimulation. *Neurosci. Lett.* 438, 281–285. doi: 10.1016/j.neulet.2008.04.080

Jankowska, E., Jukes, M. G. M., Lund, S., and Lundberg, A. (1967). The effect of dopa on the spinal cord 5. Reciprocal organization of pathways transmitting excitatory action to alpha motoneurones of flexors and extensors. *Acta Physiol. Scand.* 70, 369–388. doi: 10.1111/j.1748-1716.1967.tb03636.x

Jiang, Z., Carlin, K. P., and Brownstone, R. M. (1999). An in vitro functionally mature mouse spinal cord preparation for the study of spinal motor networks. *Brain Res.* 816, 493–499. doi: 10.1016/s0006-8993(98)01199-8

Joseph, M. S., Tillakaratne, N. J. K., and de Leon, R. D. (2012). Treadmill training stimulates brain-derived neurotrophic factor mRNA expression in motor neurons of the lumbar spinal cord in spinally transected rats. *Neuroscience* 224, 135–144. doi: 10.1016/j.neuroscience.2012.08.024

Josset, N., Roussel, M., Lemieux, M., Lafrance-Zoubga, D., Rastqar, A., and Bretzner, F. (2018). Distinct contributions of mesencephalic locomotor region nuclei to locomotor control in the freely behaving mouse. *Curr. Biol.* 28, 884–901.e3. doi: 10.1016/j.cub.2018.02.007

Juvin, L., Gal, J.-P. L., Simmers, J., and Morin, D. (2012). Cervicolumbar coordination in mammalian quadrupedal locomotion: role of spinal thoracic circuitry and limb sensory inputs. *J. Neurosci.* 32, 953–965. doi: 10.1523/JNEUROSCI.4640-11.2012

Juvin, L., Simmers, J., and Morin, D. (2005). Propriospinal circuitry underlying interlimb coordination in mammalian quadrupedal locomotion. *J. Neurosci.* 25, 6025–6035. doi: 10.1523/JNEUROSCI.0696-05.2005

Kato, M. (1990). Chronically isolated lumbar half spinal cord generates locomotor activities in the ipsilateral hindlimb of the cat. *Neurosci. Res.* 9, 22–34. doi: 10.1016/0168-0102(90)90042-d

Kato, M., Murakami, S., Yasuda, K., and Hirayama, H. (1984). Disruption of fore- and hindlimb coordination during overground locomotion in cats with bilateral serial hemisection of the spinal cord. *Neurosci. Res.* 2, 27–47. doi: 10.1016/0168-0102(84)90003-8

Keirstead, S. A., and Rose, P. K. (1983). Dendritic distribution of splenius motoneurons in the cat: comparison of motoneurons innervating different regions of the muscle. *J. Comp. Neurol.* 219, 273–284. doi: 10.1002/cne.902190303

Kiehn, O. (2016). Decoding the organization of spinal circuits that control locomotion. *Nat. Rev. Neurosci.* 17, 224–238. doi: 10.1038/nrn.2016.9

Kjaerulff, O., and Kiehn, O. (1996). Distribution of networks generating and coordinating locomotor activity in the neonatal rat spinal cord in vitro: a lesion study. *J. Neurosci.* 16, 5777–5794.

Knikou, M. (2007). Neural coupling between the upper and lower limbs in humans. *Neurosci. Lett.* 416, 138–143. doi: 10.1016/j.neulet.2007.01.072

Knikou, M., and Mummidisetty, C. K. (2014). Locomotor training improves premotoneuronal control after chronic spinal cord injury. *J. Neurophysiol.* 111, 2264–2275. doi: 10.1152/jn.00871.2013

Krishnan, V. S., Shin, S. S., Belegu, V., Celnik, P., Reimers, M., Smith, K. R., et al. (2019). Multimodal evaluation of TMS - induced somatosensory plasticity and behavioral recovery in rats with contusion spinal cord injury. *Front. Neurosci.* 13:387. doi: 10.3389/fnins.2019.00387

Lajoie, K., and Drew, T. (2007). Lesions of area 5 of the posterior parietal cortex in the cat produce errors in the accuracy of paw placement during visually guided locomotion. *J. Neurophysiol.* 97, 2339–2354. doi: 10.1152/jn.01196.2006

Lavrov, I., Courtine, G., Dy, C. J., van den Brand, R., Fong, A. J., Gerasimenko, Y., et al. (2008). Facilitation of stepping with epidural stimulation in spinal rats: role of sensory input. *J. Neurosci. Off.* 28, 7774–7780. doi: 10.1523/JNEUROSCI.1069-08.2008

Levine, A. J., Hinckley, C. A., Hilde, K. L., Driscoll, S. P., Poon, T. H., Montgomery, J. M., et al. (2014). Identification of a cellular node for motor control pathways. *Nat. Neurosci.* 17, 586–593. doi: 10.1038/nn.3675

Li, W.-Y., Wang, Y., Zhai, F.-G., Sun, P., Cheng, Y.-X., Deng, L.-X., et al. (2017). AAV-KLF7 promotes descending propriospinal neuron axonal plasticity after spinal cord injury. *Neural Plast.* 2017:1621629. doi: 10.1155/2017/1621629

Liang, H., Paxinos, G., and Watson, C. (2011). Projections from the brain to the spinal cord in the mouse. *Brain Struct. Funct.* 215, 159–186. doi: 10.1007/s00429-010-0281-x

Lin, S., Li, Y., Lucas-Osma, A. M., Hari, K., Stephens, M. J., Singla, R., et al. (2019). Locomotor-related V3 interneurons initiate and coordinate muscles spasms after spinal cord injury. *J. Neurophysiol.* 121, 1352–1367. doi: 10.1152/jn.00776.2018

Ljunggren, E. E., Haupt, S., Ausborn, J., Ampatzis, K., and El Manira, A. (2014). Optogenetic activation of excitatory premotor interneurons is sufficient to generate coordinated locomotor activity in larval zebrafish. *J. Neurosci.* 34, 134–139. doi: 10.1523/JNEUROSCI.4087-13.2014

Loy, K., and Bareyre, F. M. (2019). Rehabilitation following spinal cord injury: how animal models can help our understanding of exercise-induced neuroplasticity. *Neural Regen. Res.* 14:405. doi: 10.4103/1673-5374.245951

Lu, D. C., Niu, T., and Alaynick, W. A. (2015). Molecular and cellular development of spinal cord locomotor circuitry. *Front. Mol. Neurosci.* 8:25. doi: 10.3389/fnmol.2015.00025

Lundfald, L., Restrepo, C. E., Butt, S. J. B., Peng, C.-Y., Droho, S., Endo, T., et al. (2007). Phenotype of V2-derived interneurons and their relationship to the axon guidance molecule EphA4 in the developing mouse spinal cord. *Eur. J. Neurosci.* 26, 2989–3002. doi: 10.1111/j.1460-9568.2007.05906.x

MacLellan, M. J., Ivanenko, Y. P., Catavitello, G., La Scaleia, V., and Lacquaniti, F. (2013). Coupling of upper and lower limb pattern generators during human crawling at different arm/leg speed combinations. *Exp. Brain Res.* 225, 217–225. doi: 10.1007/s00221-012-3364-5

Mantziaris, C., Bockemühl, T., Holmes, P., Borgmann, A., Daun, S., and Büschges, A. (2017). Intra- and intersegmental influences among central pattern generating networks in the walking system of the stick insect. *J. Neurophysiol.* 118, 2296–2310. doi: 10.1152/jn.00321.2017

Martinez, M., Delivet-Mongrain, H., Leblond, H., and Rossignol, S. (2012). Incomplete spinal cord injury promotes durable functional changes within the spinal locomotor circuitry. *J. Neurophysiol.* 108, 124–134. doi: 10.1152/jn.00073.2012

Matsushita, M., Ikeda, M., and Hosoya, Y. (1979). The location of spinal neurons with long descending axons (long descending propriospinal tract neurons) in the cat: a study with the horseradish peroxidase technique. *J. Comp. Neurol.* 184, 63–79. doi: 10.1002/cne.901840105

Matsuyama, K., Kobayashi, S., and Aoki, M. (2006). Projection patterns of lamina VIII commissural neurons in the lumbar spinal cord of the adult cat: an anterograde neural tracing study. *Neuroscience* 140, 203–218. doi: 10.1016/j.neuroscience.2006.02.005

Matsuyama, K., Nakajima, K., Mori, F., Aoki, M., and Mori, S. (2004). Lumbar commissural interneurons with reticulospinal inputs in the cat: morphology and discharge patterns during fictive locomotion. *J. Comp. Neurol.* 474, 546–561. doi: 10.1002/cne.20131

May, Z., Fenrich, K. K., Dahlby, J., Batty, N. J., Torres-Espín, A., and Fouad, K. (2017). Following spinal cord injury transected reticulospinal tract axons develop new collateral inputs to spinal interneurons in parallel with locomotor recovery. *Neural Plast.* 2017:1932875. doi: 10.1155/2017/1932875

Menétrey, D., De Pommery, J., and Roudier, F. (1985). Propriospinal fibers reaching the lumbar enlargement in the rat. *Neurosci. Lett.* 58, 257–261. doi: 10.1016/0304-3940(85)90174-6

Miller, S., Reitsma, D. J., and Van Der Meché, F. G. A. (1973). Functional organization of long ascending propriospinal pathways linking lumbo-sacral and cervical segments in the cat. *Brain Res.* 62, 169–188. doi: 10.1016/0006-8993(73)90626-4

Mitchell, E. J., McCallum, S., Dewar, D., and Maxwell, D. J. (2016). Corticospinal and reticulospinal contacts on cervical commissural and long descending propriospinal neurons in the adult rat spinal cord evidence for powerful reticulospinal connections. *PLoS One* 11:e0152094. doi: 10.1371/journal.pone.0152094

Molenaar, I., and Kuypers, H. G. (1978). Cells of origin of propriospinal fibers and of fibers ascending to supraspinal levels. A HRP study in cat and rhesus monkey. *Brain Res.* 152, 429–450. doi: 10.1016/0006-8993(78)91102-2

Mondello, S. E., Sunshine, M. D., Fischedick, A. E., Dreyer, S. J., Horwitz, G. D., Anikeeva, P., et al. (2018). Optogenetic surface stimulation of the rat cervical spinal cord. *J. Neurophysiol.* 120, 795–811. doi: 10.1152/jn.00461.2017

Moran-Rivard, L., Kagawa, T., Saueressig, H., Gross, M. K., Burrill, J., and Goulding, M. (2001). Evx1 is a postmitotic determinant of v0 interneuron identity in the spinal cord. *Neuron* 29, 385–399. doi: 10.1016/S0896-6273(01)00213-6

Moraud, E. M., Capogrosso, M., Formento, E., Wenger, N., DiGiovanna, J., Courtine, G., et al. (2016). Mechanisms underlying the neuromodulation of spinal circuits for correcting gait and balance deficits after spinal cord injury. *Neuron* 89, 814–828. doi: 10.1016/j.neuron.2016.01.009

Nathan, P. W., Smith, M., and Deacon, P. (1996). Vestibulospinal, reticulospinal and descending propriospinal nerve fibres in man. *Brain* 119, 1809–1833. doi: 10.1093/brain/119.6.1809

Ni, Y., Nawabi, H., Liu, X., Yang, L., Miyamichi, K., Tedeschi, A., et al. (2014). Characterization of long descending premotor propriospinal neurons in the spinal cord. *J. Neurosci.* 34, 9404–9417. doi: 10.1523/JNEUROSCI.1771-14.2014

Oueghlani, Z., Simonnet, C., Cardoit, L., Courtand, G., Cazalets, J.-R., Morin, D., et al. (2018). Brainstem steering of locomotor activity in the newborn rat. *J. Neurosci.* 38, 7725–7740. doi: 10.1523/JNEUROSCI.1074-18.2018

Pearcey, G. E. P., and Zehr, E. P. (2019). We are upright-walking cats: human limbs as sensory antennae during locomotion. *Physiol. Bethesda MD* 34, 354–364. doi: 10.1152/physiol.00008.2019

Pocratsky, A. M., Burke, D. A., Morehouse, J. R., Beare, J. E., Riegler, A. S., Tsoulfas, P., et al. (2017). Reversible silencing of lumbar spinal interneurons unmasks a task-specific network for securing hindlimb alternation. *Nat. Commun.* 8:1963. doi: 10.1038/s41467-017-02033-x

Quinlan, K. A., and Kiehn, O. (2007). Segmental, synaptic actions of commissural interneurons in the mouse spinal cord. *J. Neurosci.* 27, 6521–6530. doi: 10.1523/JNEUROSCI.1618-07.2007

Reed, W. R., Shum-Siu, A., Onifer, S. M., and Magnuson, D. S. K. (2006). Inter-enlargement pathways in the ventrolateral funiculus of the adult rat spinal cord. *Neuroscience* 142, 1195–1207. doi: 10.1016/j.neuroscience.2006.07.017

Robinson, G. A., and Goldberger, M. E. (1986). The development and recovery of motor function in spinal cats. II. Pharmacological enhancement of recovery. *Exp. Brain Res.* 62, 387–400. doi: 10.1007/bf00238858

Rose, P. K., and Richmond, F. J. (1981). White-matter dendrites in the upper cervical spinal cord of the adult cat: a light and electron microscopic study. *J. Comp. Neurol.* 199, 191–203. doi: 10.1002/cne.901990204

Rosenzweig, E. S., Brock, J. H., Lu, P., Kumamaru, H., Salegio, E. A., Kadoya, K., et al. (2018). Restorative effects of human neural stem cell grafts on the primate spinal cord. *Nat. Med.* 24, 484–490. doi: 10.1038/nm.4502

Rossignol, S., and Frigon, A. (2011). Recovery of locomotion after spinal cord injury: some facts and mechanisms. *Annu. Rev. Neurosci.* 34, 413–440. doi: 10.1146/annurev-neuro-061010-113746

Ruder, L., Takeoka, A., and Arber, S. (2016). Long-distance descending spinal neurons ensure quadrupedal locomotor stability. *Neuron* 92, 1063–1078. doi: 10.1016/j.neuron.2016.10.032

Shah, P. K., Garcia-Alias, G., Choe, J., Gad, P., Gerasimenko, Y., Tillakaratne, N., et al. (2013). Use of quadrupedal step training to re-engage spinal interneuronal networks and improve locomotor function after spinal cord injury. *Brain* 136, 3362–3377. doi: 10.1093/brain/awt265

Sivertsen, M. S., Perreault, M.-C., and Glover, J. C. (2016). Pontine reticulospinal projections in the neonatal mouse: internal organization and axon trajectories. *J. Comp. Neurol.* 524, 1270–1291. doi: 10.1002/cne.23904

Skinner, R. D., Adams, R. J., and Remmel, R. S. (1980). Responses of long descending propriospinal neurons to natural and electrical types of stimuli in cat. *Brain Res.* 196, 387–403. doi: 10.1016/0006-8993(80)90403-5

Skup, M., Gajewska-Wozniak, O., Grygielewicz, P., Mankovskaya, T., and Czarkowska-Bauch, J. (2012). Different effects of spinalization and locomotor training of spinal animals on cholinergic innervation of the soleus and tibialis anterior motoneurons. *Eur. J. Neurosci.* 36, 2679–2688. doi: 10.1111/j.1460-9568.2012.08182.x

Sławińska, U., Majczyński, H., Dai, Y., and Jordan, L. M. (2012). The upright posture improves plantar stepping and alters responses to serotonergic drugs in spinal rats. *J. Physiol.* 590, 1721–1736. doi: 10.1113/jphysiol.2011.224931

Stelzner, D. J., and Cullen, J. M. (1991). Do propriospinal projections contribute to hindlimb recovery when all long tracts are cut in neonatal or weanling rats? *Exp. Neurol.* 114, 193–205. doi: 10.1016/0014-4886(91)90036-c

Stepien, A. E., Tripodi, M., and Arber, S. (2010). Monosynaptic rabies virus reveals premotor network organization and synaptic specificity of cholinergic partition cells. *Neuron* 68, 456–472. doi: 10.1016/j.neuron.2010.10.019

Stokke, M. F., Nissen, U. V., Glover, J. C., and Kiehn, O. (2002). Projection patterns of commissural interneurons in the lumbar spinal cord of the neonatal rat. *J. Comp. Neurol.* 446, 349–359. doi: 10.1002/cne.10211

Swieck, K., Conta-Steencken, A., Middleton, F. A., Siebert, J. R., Osterhout, D. J., and Stelzner, D. J. (2019). Effect of lesion proximity on the regenerative response of long descending propriospinal neurons after spinal transection injury. *BMC Neurosci.* 20:10. doi: 10.1186/s12868-019-0491-y

Taccola, G., Sayenko, D., Gad, P., Gerasimenko, Y., and Edgerton, V. R. (2018). And yet it moves: recovery of volitional control after spinal cord injury. *Prog. Neurobiol.* 160, 64–81. doi: 10.1016/j.pneurobio.2017.10.004

Takeoka, A., and Arber, S. (2019). Functional local proprioceptive feedback circuits initiate and maintain locomotor recovery after spinal cord injury. *Cell Rep.* 27, 71–85.e3. doi: 10.1016/j.celrep.2019.03.010

Takeoka, A., Vollenweider, I., Courtine, G., and Arber, S. (2014). Muscle spindle feedback directs locomotor recovery and circuit reorganization after spinal cord injury. *Cell* 159, 1626–1639. doi: 10.1016/j.cell.2014.11.019

Talpalar, A. E., Bouvier, J., Borgius, L., Fortin, G., Pierani, A., and Kiehn, O. (2013). Dual-mode operation of neuronal networks involved in left-right alternation. *Nature* 500, 85–88. doi: 10.1038/nature12286

Theisen, C. C., Sachdeva, R., Austin, S., Kulich, D., Kranz, V., and Houle, J. D. (2017). Exercise and peripheral nerve grafts as a strategy to promote regeneration after acute or chronic spinal cord injury. *J. Neurotrauma* 34, 1909–1914. doi: 10.1089/neu.2016.4640

Tom, V. J., Sandrow-Feinberg, H. R., Miller, K., Santi, L., Connors, T., Lemay, M. A., et al. (2009). Combining peripheral nerve grafts and chondroitinase promotes functional axonal regeneration in the chronically injured spinal cord. *J. Neurosci. Off. J. Soc. Neurosci.* 29, 14881–14890. doi: 10.1523/JNEUROSCI.3641-09.2009

Torres-Espín, A., Beaudry, E., Fenrich, K., and Fouad, K. (2018). Rehabilitative training in animal models of spinal cord injury. *J. Neurotrauma* 35, 1970–1985. doi: 10.1089/neu.2018.5906

Tosolini, A. P., and Morris, R. (2016). Targeting motor end plates for delivery of adenoviruses: an approach to maximize uptake and transduction of spinal cord motor neurons. *Sci. Rep.* 6:33058. doi: 10.1038/srep33058

Tuszynski, M. H., and Steward, O. (2012). Concepts and methods for the study of axonal regeneration in the CNS. *Neuron* 74, 777–791. doi: 10.1016/j.neuron.2012.05.006

van den Brand, R., Heutschi, J., Barraud, Q., DiGiovanna, J., Bartholdi, K., Huerlimann, M., et al. (2012). Restoring voluntary control of locomotion after paralyzing spinal cord injury. *Science* 336, 1182–1185. doi: 10.1126/science.1217416

Vavrek, R., Girgis, J., Tetzlaff, W., Hiebert, G. W., and Fouad, K. (2006). BDNF promotes connections of corticospinal neurons onto spared descending interneurons in spinal cord injured rats. *Brain J. Neurol.* 129, 1534–1545. doi: 10.1093/brain/awl087

Wagner, F. B., Mignardot, J.-B., Le Goff-Mignardot, C. G., Demesmaeker, R., Komi, S., Capogrosso, M., et al. (2018). Targeted neurotechnology restores walking in humans with spinal cord injury. *Nature* 563, 65–71. doi: 10.1038/s41586-018-0649-2

Wang, Y., Wu, W., Wu, X., Sun, Y., Zhang, Y. P., Deng, L.-X., et al. (2018). Remodeling of lumbar motor circuitry remote to a thoracic spinal cord injury promotes locomotor recovery. *eLife* 7. doi: 10.7554/eLife.39016

Wannier, T., Bastiaanse, C., Colombo, G., and Dietz, V. (2001). Arm to leg coordination in humans during walking, creeping and swimming activities. *Exp. Brain Res.* 141, 375–379. doi: 10.1007/s002210100875

Whelan, P., Bonnot, A., and O'Donovan, M. J. (2000). Properties of rhythmic activity generated by the isolated spinal cord of the neonatal mouse. *J. Neurophysiol.* 84, 2821–2833. doi: 10.1152/jn.2000.84.6.2821

Wiggin, T. D., Anderson, T. M., Eian, J., Peck, J. H., and Masino, M. A. (2012). Episodic swimming in the larval zebrafish is generated by a spatially distributed spinal network with modular functional organization. *J. Neurophysiol.* 108, 925–934. doi: 10.1152/jn.00233.2012

Ying, Z., Roy, R. R., Edgerton, V. R., and Gómez-Pinilla, F. (2005). Exercise restores levels of neurotrophins and synaptic plasticity following spinal cord injury. *Exp. Neurol.* 193, 411–419. doi: 10.1016/j.expneurol.2005.01.015

Yokota, K., Kobayakawa, K., Kubota, K., Miyawaki, A., Okano, H., Ohkawa, Y., et al. (2015). Engrafted neural stem/progenitor cells promote functional recovery through synapse reorganization with spared host neurons after spinal cord injury. *Stem Cell Rep.* 5, 264–277. doi: 10.1016/j.stemcr.2015.06.004

Zagoraiou, L., Akay, T., Martin, J. F., Brownstone, R. M., Jessell, T. M., and Miles, G. B. (2009). A cluster of cholinergic premotor interneurons modulates mouse locomotor activity. *Neuron* 64, 645–662. doi: 10.1016/j.neuron.2009.10.017

Zaporozhets, E., Cowley, K. C., and Schmidt, B. J. (2006). Propriospinal neurons contribute to bulbospinal transmission of the locomotor command signal in the neonatal rat spinal cord. *J. Physiol.* 572, 443–458. doi: 10.1113/jphysiol.2005.102376

Zaporozhets, E., Cowley, K. C., and Schmidt, B. J. (2011). Neurochemical excitation of propriospinal neurons facilitates locomotor command signal transmission in the lesioned spinal cord. *J. Neurophysiol.* 105, 2818–2829. doi: 10.1152/jn.00917.2010

Zehr, E. P., Barss, T. S., Dragert, K., Frigon, A., Vasudevan, E. V., Haridas, C., et al. (2016). Neuromechanical interactions between the limbs during human locomotion: an evolutionary perspective with translation to rehabilitation. *Exp. Brain Res.* 234, 3059–3081. doi: 10.1007/s00221-016-4715-4

Zehr, E. P., Hundza, S. R., and Vasudevan, E. V. (2009). The quadrupedal nature of human bipedal locomotion. *Exerc. Sport Sci. Rev.* 37, 102–108. doi: 10.1097/JES.0b013e31819c2ed6

Zhang, J., Lanuza, G. M., Britz, O., Wang, Z., Siembab, V. C., Zhang, Y., et al. (2014). V1 and v2b interneurons secure the alternating flexor-extensor motor activity mice require for limbed locomotion. *Neuron* 82, 138–150. doi: 10.1016/j.neuron.2014.02.013

Zhang, Y., Narayan, S., Geiman, E., Lanuza, G. M., Velasquez, T., Shanks, B., et al. (2008). V3 spinal neurons establish a robust and balanced locomotor rhythm during walking. *Neuron* 60, 84–96. doi: 10.1016/j.neuron.2008.09.027

Ziemlińska, E., Kügler, S., Schachner, M., Wewiór, I., Czarkowska-Bauch, J., and Skup, M. (2014). Overexpression of BDNF increases excitability of the lumbar spinal network and leads to robust early locomotor recovery in completely spinalized rats. *PLoS One* 9:e88833. doi: 10.1371/journal.pone.0088833

Conflict of Interest: The authors declare that the research was conducted in the absence of any commercial or financial relationships that could be construed as a potential conflict of interest.

frontiers in Cellular Neuroscience

ORIGINAL RESEARCH
published: 20 November 2019
doi: 10.3389/fncel.2019.00516

Spinal V3 Interneurons and Left–Right Coordination in Mammalian Locomotion

Simon M. Danner[1†], Han Zhang[2†], Natalia A. Shevtsova[1†], Joanna Borowska-Fielding[2], Dylan Deska-Gauthier[2], Ilya A. Rybak[1] and Ying Zhang[2*]*

[1] Department of Neurobiology and Anatomy, College of Medicine, Drexel University, Philadelphia, PA, United States,
[2] Department of Medical Neuroscience, Brain Repair Centre, Faculty of Medicine, Dalhousie University, Halifax, NS, Canada

OPEN ACCESS

Edited by:
Kristine C. Cowley,
University of Manitoba, Canada

Reviewed by:
Donald C. Bolser,
University of Florida, United States
Dirk Bucher,
New Jersey Institute of Technology, United States
Klas Kullander,
Uppsala University, Sweden

***Correspondence:**
Ilya A. Rybak
rybak@drexel.edu
Ying Zhang
Ying.Zhang@dal.ca

† These authors have contributed equally to this work

Specialty section:
This article was submitted to Cellular Neurophysiology, a section of the journal Frontiers in Cellular Neuroscience

Received: *17 June 2019*
Accepted: *04 November 2019*
Published: *20 November 2019*

Citation:
Danner SM, Zhang H, Shevtsova NA, Borowska-Fielding J, Deska-Gauthier D, Rybak IA and Zhang Y (2019) Spinal V3 Interneurons and Left–Right Coordination in Mammalian Locomotion. Front. Cell. Neurosci. 13:516. doi: 10.3389/fncel.2019.00516

Commissural interneurons (CINs) mediate interactions between rhythm-generating locomotor circuits located on each side of the spinal cord and are necessary for left-right limb coordination during locomotion. While glutamatergic V3 CINs have been implicated in left-right coordination, their functional connectivity remains elusive. Here, we addressed this issue by combining experimental and modeling approaches. We employed $Sim1^{Cre/+}$; Ai32 mice, in which light-activated Channelrhodopsin-2 was selectively expressed in V3 interneurons. Fictive locomotor activity was evoked by NMDA and 5-HT in the isolated neonatal lumbar spinal cord. Flexor and extensor activities were recorded from left and right L2 and L5 ventral roots, respectively. Bilateral photoactivation of V3 interneurons increased the duration of extensor bursts resulting in a slowed down on-going rhythm. At high light intensities, extensor activity could become sustained. When light stimulation was shifted toward one side of the cord, the duration of extensor bursts still increased on both sides, but these changes were more pronounced on the contralateral side than on the ipsilateral side. Additional bursts appeared on the ipsilateral side not seen on the contralateral side. Further increase of the stimulation could suppress the contralateral oscillations by switching to a sustained extensor activity, while the ipsilateral rhythmic activity remained. To delineate the function of V3 interneurons and their connectivity, we developed a computational model of the spinal circuits consisting of two (left and right) rhythm generators (RGs) interacting via $V0_V$, $V0_D$, and V3 CINs. Both types of V0 CINs provided mutual inhibition between the left and right flexor RG centers and promoted left-right alternation. V3 CINs mediated mutual excitation between the left and right extensor RG centers. These interactions allowed the model to reproduce our current experimental data, while being consistent with previous data concerning the role of $V0_V$ and $V0_D$ CINs in securing left–right alternation and the changes in left–right coordination following their selective removal. We suggest that V3 CINs provide mutual excitation between the spinal neurons involved in the control of left and right extensor activity, which may promote left-right synchronization during locomotion.

Keywords: spinal cord, central pattern generator, locomotion, commissural neurons, V3, optogenetic stimulation, computational modeling

INTRODUCTION

The rhythmic activities controlling locomotor movements in mammals are generated by neural circuits within the spinal cord, representing so-called central pattern generators (CPGs; Graham Brown, 1911; Grillner, 1981, 2006; Kiehn, 2006, 2011; Rossignol et al., 2006). It is commonly accepted that each limb is controlled by a separate spinal CPG and that CPGs controlling fore and hind limbs are located in the left and right sides of cervical and lumbar enlargements, respectively. These CPGs are connected by spinal commissural interneurons (CINs) that coordinate their activities, hence defining locomotor gaits. CINs project axons across the spinal cord midline and affect interneurons and motoneurons located on the contralateral side of the cord (Kjaerulff and Kiehn, 1997; Butt and Kiehn, 2003; Quinlan and Kiehn, 2007; Jankowska, 2008).

Several classes of spinal CINs, including two subtypes of V0 CINs (excitatory $V0_V$ and inhibitory $V0_D$) and the excitatory V3 CIN, have been identified based on their transcription factor profiles (Lanuza et al., 2004; Goulding, 2009; Gosgnach, 2011). Both subtypes of V0 CINs promote left–right alternation, and their functional ablation results in aberrant left–right synchronization. *In vitro*, selective ablation of $V0_D$ CINs disrupted left-right alternation at low locomotor frequencies while ablation of $V0_V$ CINs disrupted left-right alternation at higher locomotor frequencies (Talpalar et al., 2013). Thus, V0 CINs are necessary for securing left-right alternation.

In vivo, an increase of locomotor speed in rodents is accompanied by a transition from left–right alternating gaits (walk and trot) to left-right synchronized gaits (like gallop and bound). Yet, the CIN networks promoting left–right synchronization at higher locomotor speeds, or during V0 ablation, are poorly understood. Our previous modeling studies suggested that left-right synchronization could be performed by V3 CINs providing mutual excitation between the left and right rhythm-generating circuits (Rybak et al., 2013, 2015; Shevtsova et al., 2015; Danner et al., 2016, 2017; Shevtsova and Rybak, 2016). Although this suggestion allowed our previous models to reproduce the results of the above experimental studies, including the effects of V0 CIN ablation *in vitro* and *in vivo*, the role and connectivity of V3 neurons suggested by these models have not been tested experimentally and remained hypothetical.

V3 interneurons, defined by their post-mitotic expression of the transcription factor single-minded homolog 1 (Sim1), are excitatory, and the majority of them project to the contralateral side of the spinal cord (Zhang et al., 2008). Genetic deletion of V3 interneurons did not affect left-right alternation, but caused unstable gaits in walking mice, and generated imbalanced and less robust rhythmic fictive locomotion in isolated neonatal spinal cords (Zhang et al., 2008). While these experimental data strongly suggest that V3 interneurons are involved in the control of locomotion, their exact function and commissural connectivity remain mainly unknown.

To address V3's functional connectivity between left-right spinal circuits, we used *in vitro* preparations of isolated spinal cords from neonatal mice, in which fictive locomotion was induced by neuroactive drugs. This preparation allows studying functional connectivity between genetically identified spinal interneurons, involved in CPG operation and left-right coordination. We took advantage of an optogenetic approach, which enabled us to specifically regulate the activity of V3 interneurons on each side of the isolated spinal cord during fictive locomotion. We then designed an updated computational model of spinal circuits that incorporated the connectivity of V3 CINs suggested from our experimental studies. Together our experimental and modeling results provide convincing evidence that V3 interneurons contribute to synchronization of the left-right locomotor activity (under appropriate conditions) by providing mutual excitation between the extensor centers of the left and right CPGs.

RESULTS

Optical Activation of Lumbar V3 Interneurons Increases the Intensity of Extensor Motor Activity and Slows Oscillation Frequency of Drug-Evoked Fictive Locomotion

To assess the function of V3 interneurons in the spinal locomotor network, we used an optogenetic approach that allowed us to selectively activate V3 interneurons in different regions of the isolated spinal cords from *Sim1*$^{Cre/+}$; *Rosa26 ChR2-EYFP* (Sim1cre-Ai32) mice, which express channelrhodopsin2 (ChR2) and enhanced yellow fluorescent protein (EYFP) in Sim1 positive cells.

To verify the expression of ChR2-EYFP in Sim1 positive V3 interneurons, we crossed Sim1cre-Ai32 with *Rosa26tdTom (Ai14)* to generate Sim1$^{Cre/+}$; tdTom; Ai32 mice. Sim1$^{Cre/+}$; tdTom has been well characterized and widely used in our previous studies (Borowska et al., 2013, 2015; Blacklaws et al., 2015). In Sim1$^{Cre/+}$; tdTom; Ai32 spinal cords, ChR2-EYFP fusion protein could be specifically detected around all tdTom positive cells (**Figure 1A**), which demonstrated the co-expression of ChR2-EYFP and tdTom in Sim1+V3 interneurons. Using whole-cell patch-clamp recordings, we confirmed that the blue fluorescent light (488 nm) could produce membrane depolarization and evoke persistent spiking only in EYFP expressing cells (22/22) from the slices of Sim1cre-Ai32 or Sim1$^{Cre/+}$; tdTom; Ai32 mice at postnatal day (P) 2–3 (**Figures 1B1–B3**). None of EYFP negative cells (10/10) showed any direct response to the light (**Figure 1B1**). The evoked spiking activity continued within a 20-s period with or without glutamatergic receptor blockers (CNQX and AP-5; **Figures 1B2,B3**). These results confirmed that V3 interneurons in the isolated spinal cords of Sim1cre-Ai32 mouse could be selectively activated by the blue fluorescent light.

To investigate the role of V3 interneurons and their interactions with CPG circuits, we shined fluorescent light onto the ventral spinal cord of neonatal Sim1cre-Ai32 mice during fictive locomotion evoked by a 5-HT/NMDA mixture (5-HT 8 μM, NMDA 7–8 μM) and analyzed the effects of light stimulation on the ongoing rhythmic activity (**Figure 2**). Flexor and extensor activities on each side of the cord were evaluated based on the recordings from L2 and L5

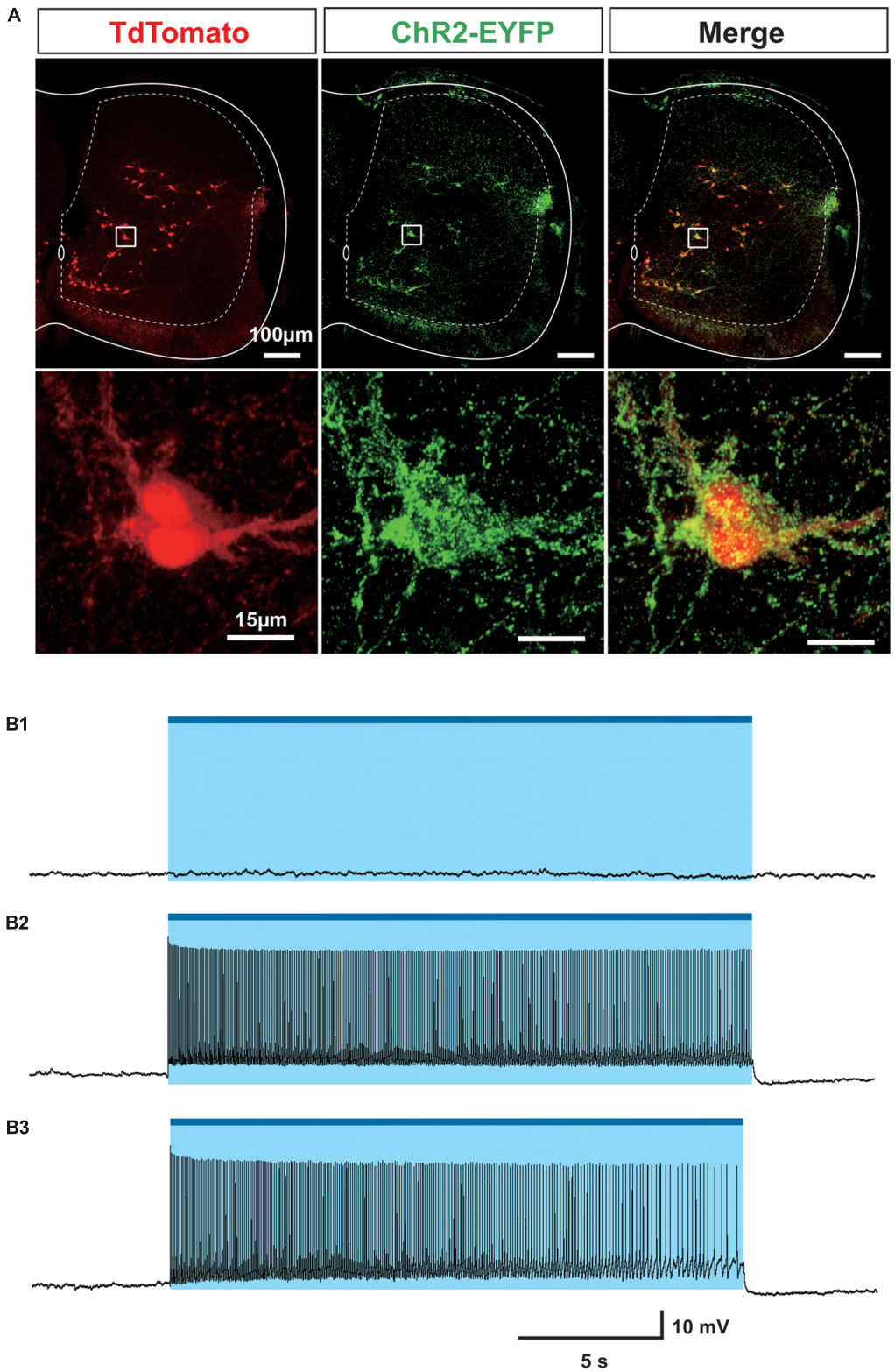

FIGURE 1 | Investigation of Sim1 cell in Sim1$^{Cre/+}$; Ai32 mouse. **(A)** ChR2-EYFP (Green) and tdTom (red) co-express in Sim1 + V3 interneurons in the spinal cord of Sim1$^{Cre/+}$; tdTom; Ai32 mice. Upper: representative image of a cross section of a spinal cord from Sim1$^{Cre/+}$; tdTom; Ai32 mouse. Lower: enlarged image of the insets. **(B1)** Light did not activate EYFP negative cell. **(B2)** Patch clamp recordings of Sim1$^{Cre/+}$; Ai32 cell with optical activation. **(B3)** Patch clamp recording of Sim1$^{Cre/+}$; Ai32 cell with optical activation with fast synaptic transmission blocker. Blue bar and shaded blue area represent the optical activation (light-on) period.

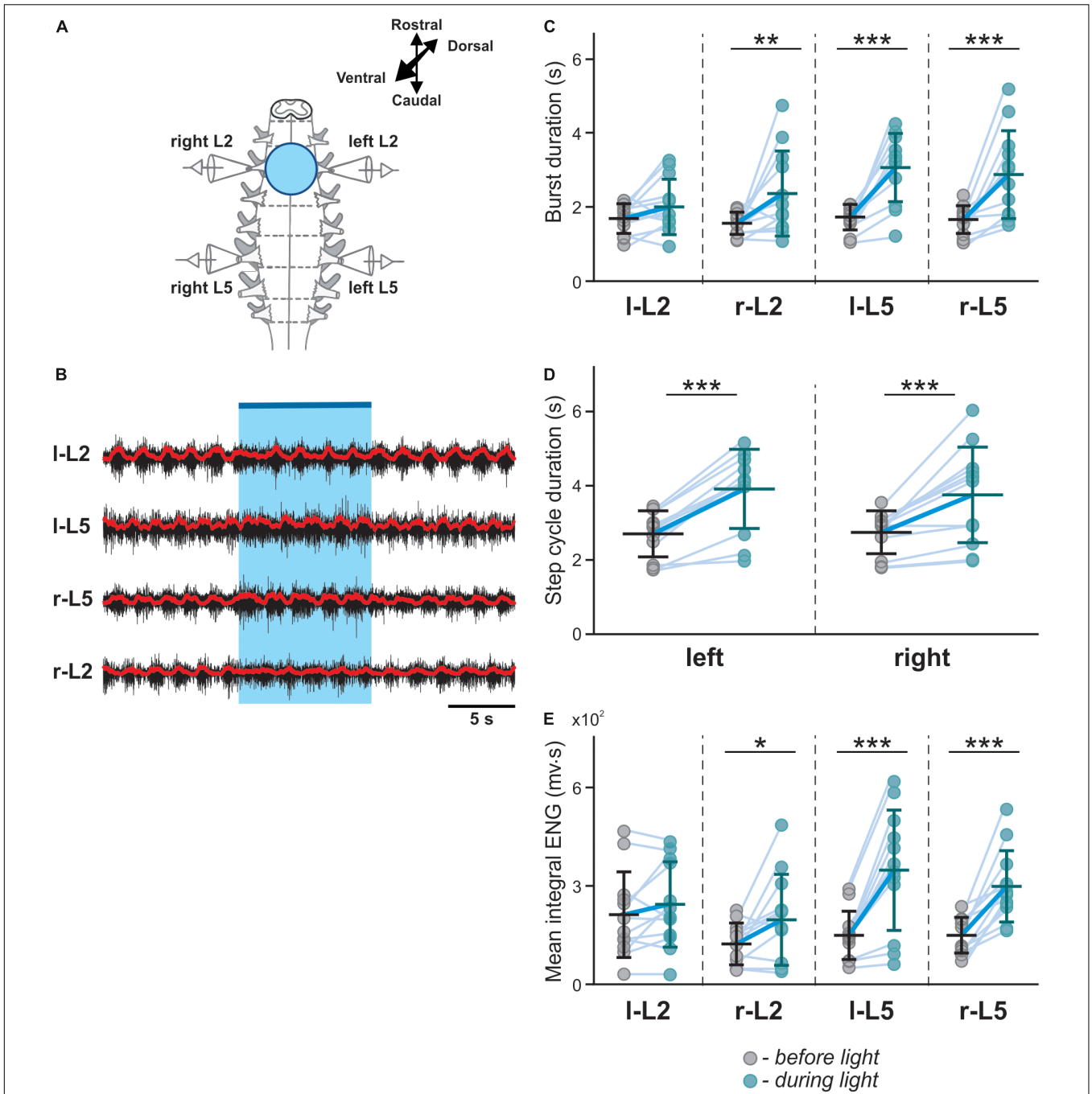

FIGURE 2 | Symmetric optical activation of both sides of V3 interneurons in L2 ventral region during drug-evoked fictive locomotion and changes in ENG characteristics. **(A)** Experimental setup. **(B)** Optical activation of lumbar V3 interneurons increases the intensity of extensor motor output and slows oscillation frequency of drug-evoked fictive locomotion. Fictive locomotion was induced by drug cocktail (5-HT 8 μM, NMDA 8 μM) in Sim1cre-Ai32 cord. The blue bar on the top and shaded blue area represent the optical stimulation period. Red lines are rectified and smoothed traces of the original ENG recordings (black). **(C–E)** Burst duration, step cycle duration, and mean integral ENG during drug-induced locomotor-like activity (n = 12) before (gray circles) and during (blue circles) optical activation. Each circle represents the average value of estimated parameter for one trace. Light blue lines connecting two circles represent parameter increase in one cord. Thick, dark blue line represent the average of increase. * indicates $P < 0.05$, ** indicates $0.01 < P < 0.05$, *** indicates $0.0001 < P < 0.001$.

ventral roots, respectively. Optogenetic stimulation with blue fluorescent light applied on the whole L2 ventral spinal cord (**Figure 2A**) slowed down the ongoing rhythmic activity, as evident by an increased locomotor cycle period (**Figures 2B,D**; n = 12, left L5 P = 0.0005, right L5 P = 0.0010). The increased cycle duration was mainly attributed to an increase

in the L5-burst durations, while L2-burst durations did not significantly change in response to the applied stimulation (**Figures 2B,C**). Furthermore, the optogenetic stimulation caused an increase in the amplitude of integral ENG bursts in L5, but not in L2 ventral roots (**Figures 2B,E**). These results suggest that lumbar V3 neurons interact with locomotor CPGs and provide activation of extensor circuits, either directly or transynaptically.

Biased Optical Activation of V3 Interneurons in Spinal Segment L2 Leads to Asymmetrical Left–Right Motor Activity

Since most V3 neurons are commissural interneurons, activation of V3s on one side of the spinal cord should more strongly impact the contralateral circuits. To test this hypothesis, we used a 20x, 1.0 numerical aperture (NA) objective to deliver the light onto a small area on one side of the spinal cord (**Figure 3A**). We then selected the illuminated region by manually adjusting the field diaphragm to have the activation zone between approximately one-third to a half of the spinal cord (**Figure 3B**) and the intensity of the light-emitting diode (LED) light to regulate the number of V3 neurons being activated.

Under these experimental conditions, we found that optical activation of V3 interneurons on one side of the cord significantly prolonged L5 burst durations and step cycles on both sides (**Figures 3C,D2,E**; $P < 0.0001$), while L2 burst durations were not significantly affected (**Figure 3D1**). However, the contralateral L5 burst durations were influenced more strongly than those of ipsilateral L5 (**Figure 3F**). Consequently, the step-cycle period also changed more strongly on the contralateral side than the ipsilateral side (**Figure 3E**), which led to a left-right asymmetric activity with more bursts on the ipsilateral than on the contralateral side. Emergence of additional bursts in an integer relationship is a fundamental property of (weakly-) coupled oscillators, with asymmetric drive (Pikovsky et al., 2001; Pikovsky and Rosenblum, 2003; Rubin et al., 2011), suggesting that tonically activated V3 neurons mainly affect (and slow down) the contralateral CPG.

We also noticed a dose-response relationship between stimulation intensity and the prolongation of the contralateral cycle period and L5 burst duration (**Figures 4A–C**). At the highest applied light intensity, the rhythm of the contralateral cord can be suppressed, resulting in almost sustained extensor activity (**Figure 4C**). To further evaluate the relation between the asymmetric changes of the fictive locomotor activity in two sides of the spinal cord and the imbalanced activation intensity of V3 neurons, we systematically manipulated the focal size and light intensity to study the response to three levels of stimulation (low, medium and high intensity; see methods). Interestingly, the L5 burst duration on the contralateral side to the light stimulation showed a positive linear correlation to the optical stimulation intensity (**Figures 4D1,D2**; $R^2 = 0.5081$, $P < 0.0001$), but not the ipsilateral L5 ($R^2 = 0.007813$) or both L2s ($R^2 = 0.003418$, $R^2 = 0.1186$ for ipsilateral and contralateral sides, respectively). In turn, the changes of step cycle of contralateral locomotor activities also showed a positive linear correlation with the optical stimulation intensity (**Figure 4E**; $R^2 = 0.4842$, $P < 0.0001$). This result indicates that the asymmetric response is dependent on the activation of V3 neurons on one side of the spinal cord.

Together, our experiments showed that the activation of V3 neurons increased extensor activity, and prolonged burst and step cycle duration predominantly on the contralateral side with a smaller effect on the ipsilateral side. These resulted in left-right asymmetric rhythmic activity with lower-frequency bursting on the contralateral than on the ipsilateral side, suggesting that V3 neurons mainly affect the extensor activity of the contralateral CPG.

Modeling Left–Right Interactions Between Rhythm Generators

To further delineate the function and connectivity of the spinal V3 interneurons involved in left–right coordination, we developed a computational model of the lumbar locomotor circuitry. We built upon our previous model (Shevtsova et al., 2015) with the assumption that V3 neurons slow down the contralateral rhythm by exciting the extensor centers of the contralateral rhythm generators and transsynaptically inhibiting the flexor centers. Our goal was to update the model so that it could reproduce the effect of bilateral and unilateral stimulation of V3 neurons revealed in the above experiments without disrupting its ability to reproduce previous experimental findings concerning the effects of ablation of $V0_V$, $V0_D$ and all V0 CINs on the left-right coordination (Talpalar et al., 2013).

Model Schematic

The updated model consisted of two rhythm generating networks (RGs), one for each side of the spinal cord (**Figure 5**). Each RG included two excitatory populations, representing flexor (F) and extensor (E) RG centers that mutually inhibited each other through populations of inhibitory interneurons (InF and InE). Similar to our previous model (Shevtsova et al., 2015), all neurons in both RG centers included a persistent (slowly inactivating) sodium current, allowing them to intrinsically generate rhythmic bursting. Because of the mutual excitation between the neurons within each center, which synchronized their activity, each center could intrinsically generate a population rhythmic bursting activity. However, according to the setup of initial neuronal excitability, under normal conditions, the extensor centers, if uncoupled, expressed sustained activation and the rhythmic activity of each RG were defined by the activity of flexor centers, which then provided rhythmic inhibition of the corresponding extensor centers via the InF populations (see **Figure 5** and Zhong et al., 2012; Rybak et al., 2015; Shevtsova et al., 2015; Shevtsova and Rybak, 2016). Interactions between F and E centers of the left and right RGs were mediated by populations of V3, $V0_V$ and $V0_D$ CINs (**Figure 5**). Drug-induced fictive locomotion was modeled by an unspecific increase of the excitability of all neurons in the network through a depolarization of the leakage reversal

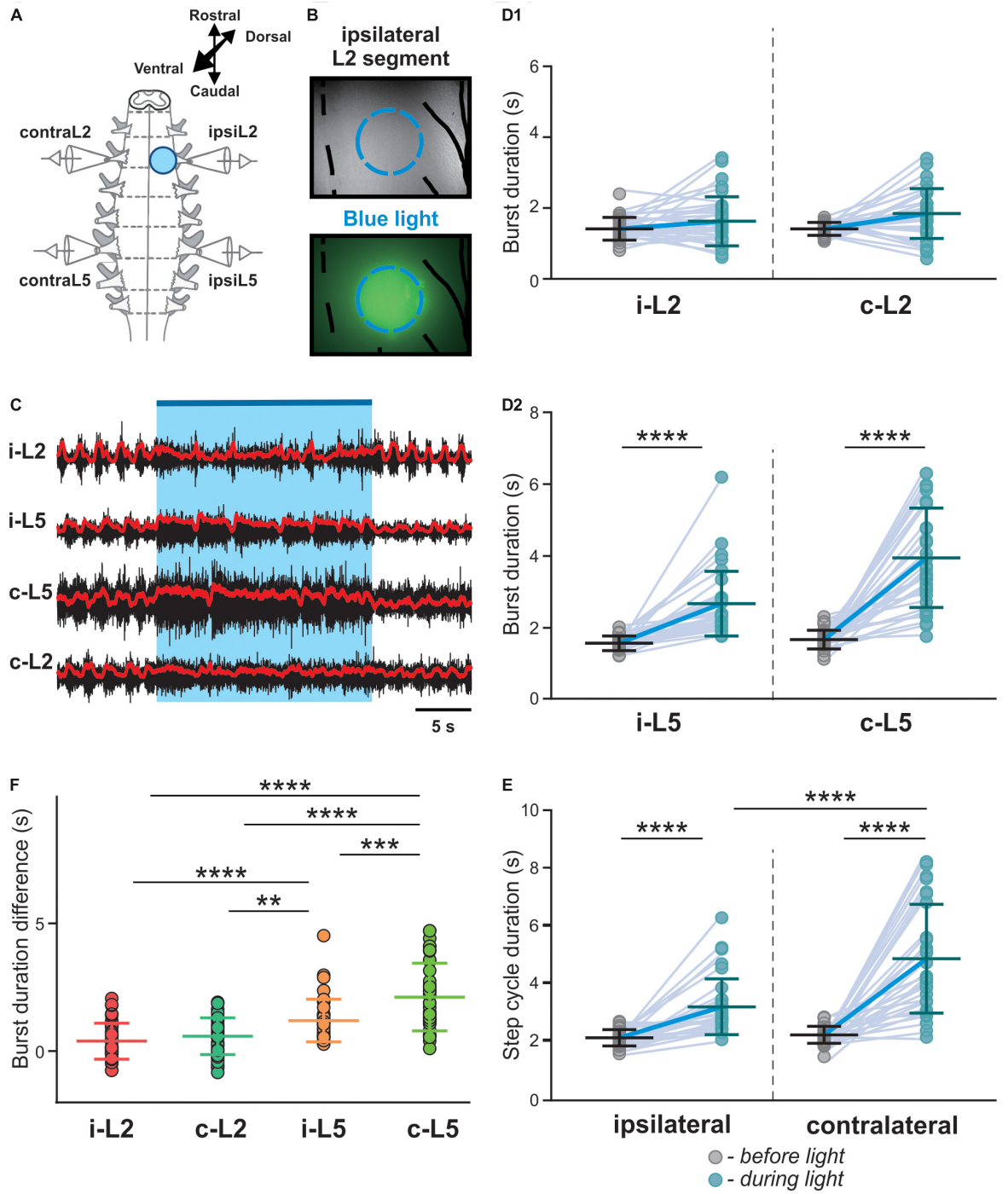

FIGURE 3 | Biased optical activation of V3 interneurons in spinal segment L2 and corresponding changes in ENG characteristics in spinal segment L2 and L5 during drug-induced locomotor-like activity. **(A)** Illustration of experimental setup for recording motor activity evoked by optical stimulation on the left spinal segment L2 from ventral side during drug-evoked fictive locomotion. **(B)** Image of the optical stimulation area. Black dashed line represents the midline of spinal cord. Blue dashed circle illustrates the light illuminated region. Black line on the right shows the frame of Nerve L2 and lateral edge of the spinal cord. **(C)** Recording trace during optical stimulation. Biased optical activation of V3 interneurons in spinal segment L2 leads to asymmetrical left-right extensor motor activity. Blue bar and area indicate the stimulation period. Red lines are rectified and smoothed traces of the original ENG recordings (black). **(D1,D2)** Average of burst duration of L2 **(D1)** and L5 **(D2)** during drug-induced locomotor-like activity (n = 33) before (gray circles) and during (blue circles) optical stimulation in ipsilateral and contralateral cord. **(E)** The average of step cycle duration of ipsilateral and contralateral L5 activities during drug-induced locomotor-like activity (n = 33) before (gray circles) and during (blue circles) optical stimulation. Light blue lines connecting two circles represent change in one cord. Thick, dark blue line represent the average of change. **** indicates $P < 0.0001$. **(F)** Average of locomotor burst duration difference between before and during biased optical stimulation. ** indicates $0.001 < P < 0.01$, *** indicates $0.0001 < P < 0.001$, **** indicates $P < 0.0001$; n = 33.

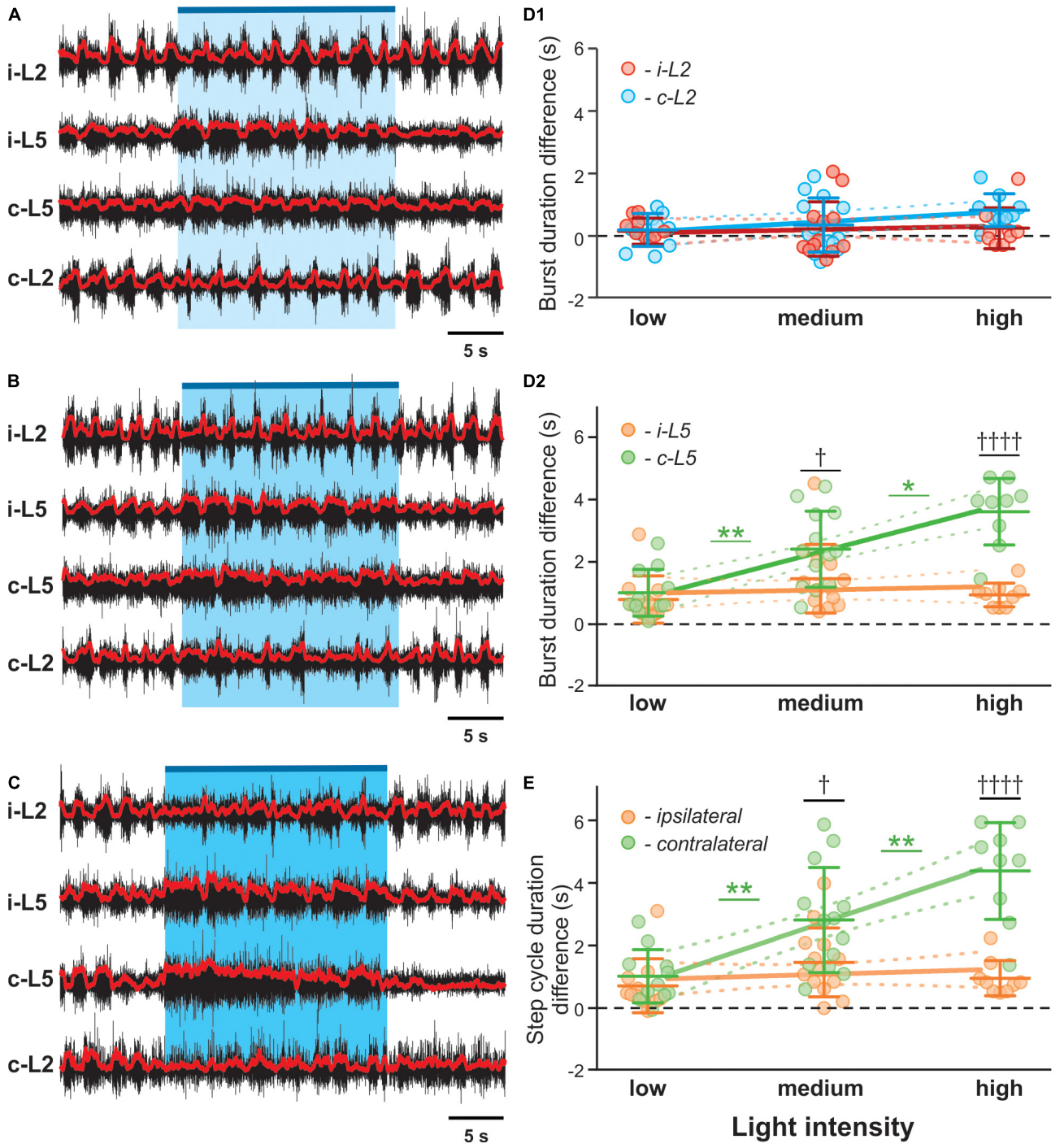

FIGURE 4 | V3 activated contralateral extensor motor activity is correlated with optical stimulation intensity. Representative traces of locomotor activity induced by drug (5-HT 8 μM, NMDA 8 μM) in $Sim1^{Cre/+}$; Ai32 cord at low **(A)**, medium **(B)**, and high **(C)** light intensity. Blue bar on the top of each trace and shaded blue area represent the optical stimulation period. The brightness of blue shaded area indicates light intensity. **(D1,D2,E)** Dependence of ENG characteristics on light intensity during biased optical stimulation. Average of burst duration difference of L2 **(D1)** and L5 **(D2)** between before and during optical stimulation under low, medium and high stimulation intensity during drug-induced locomotor-like activity (low $n = 11$, medium $n = 13$, high $n = 9$). * Indicates $0.01 < P < 0.05$, ** indicates $0.001 < P < 0.01$. † indicates $0.01 < P < 0.05$, †††† indicates $P < 0.0001$. Linear regression slope is orange for ipsilateral L5 and light green for contralateral L5 and red for ipsilateral L2 and blue for contralateral L2. **(E)** Step cycle period difference between ipsilateral and contralateral L5 under low, medium and high stimulation intensity during drug-induced locomotor-like activity (low $n = 11$, medium $n = 13$, high $n = 9$). †††† indicates $P < 0.0001$, ** indicates $0.001 < P < 0.01$. Slope of contralateral L5 burst duration and step cycle difference are significantly non-zero.

potentials in each neuron. The drug concentration was defined by the parameter α (see section Materials and Methods).

In the present model, the organization of interactions between left and right RGs mediated by $V0_V$ and $V0_D$ populations of CINs followed that of our previous models (Shevtsova et al., 2015; Danner et al., 2016, 2017; Shevtsova and Rybak, 2016; Ausborn et al., 2019). Specifically (see **Figure 5**), the populations of inhibitory $V0_D$ CINs provided direct mutual inhibition between the left and right flexor centers of the RGs, while the populations of excitatory $V0_V$ CINs mediated mutual inhibition between the same flexor centers through oligosynaptic pathways (each $V0_V$ population received excitation from the ipsilateral flexor center through a local population of V2a neurons and inhibited the flexor center of the contralateral RG through a population of local inhibitory neurons, Ini). Both $V0_V$ and $V0_D$ pathways ensured left-right alternation.

The organization of V3 CIN pathways in the present model differed from the previous models and was constructed to fit our experimental results. Based on these results we suggested that V3 populations mediate mutual excitation between the extensor centers of the left and right RGs (**Figure 5**) and promoted inhibition of the contralateral flexor centers.

Each population of neurons in our model (**Figure 5**) consisted of 50–200 neurons (**Table 1**). All neurons were modeled in the Hodgkin-Huxley style (for details see Materials and Methods, section Computational Modeling and **Table 1**). Heterogeneity within the populations was ensured by randomizing the baseline value for leakage reversal potential and initial conditions for the values of membrane potential and channel kinetics variables. Connections between the populations were modeled as sparse random synaptic connections. Model equations and simulation procedures are listed in Section "Materials and Methods." Population specific parameters are listed in **Table 1** and connection weights and probabilities are specified in **Table 2**.

The Model Exhibits Characteristic Features of Drug-Induced Fictive Locomotion and Frequency-Dependent Changes of Left–Right Coordination Following Removal of V0 Commissural Interneurons

First, we characterized the model performance under normal conditions by simulating drug-induced fictive locomotion (**Figure 6**). The model exhibited alternation between the rhythmic activities of the flexor and extensor RG centers on each side as well as alternation between the activities of the left and right RGs. By increasing α (simulating an increase in the drug concentration) the burst frequency increased (**Figures 6A–C**). The frequency increase was accompanied by

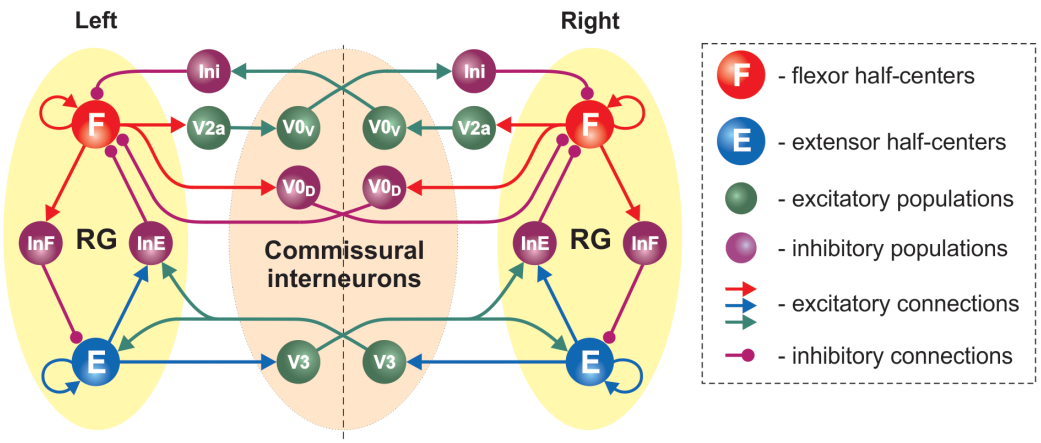

FIGURE 5 | Model schematic of the bilateral spinal circuits consisting of two interconnected rhythm generators. Spheres represent neural populations and lines the synaptic connections between them. The rhythm generator (RG) in each side includes flexor and extensor centers (F and E, respectively) interacting via the inhibitory InF and InE populations. The left and right RGs interact via commissural interneurons ($V0_D$, $V0_V$, and V3).

TABLE 1 | Number of neurons and neuron parameters in different populations.

Neuron type	N, number of neurons	$\bar{g}_{Na}$, mS/cm^2	$\bar{g}_{NaP}$, mS/cm^2	$\bar{g}_K$, mS/cm^2	g_L, mS/cm^2	$\bar{E}_{LO}$, mV
F	200	25	0.75(±0.00375)	2	0.07	−67(±0.67)
E	100	25	0.75(±0.00375)	2	0.07	−60(±0.6)
InF	100	10		5	0.1	−67(±1.34)
InE	100	10		5	0.1	−72(±1.44)
V0D	50	10		5	0.1	−68(±2.04)
V2a	50	40		5	0.8	−60.5(±1.21)
V0V	50	10		5	0.1	−62(±1.24)
Ini	50	10		5	0.1	−64(±1.28)
V3	100	10		5	0.1	−68(±2.04)

TABLE 2 | Average weights $\bar{w}_{ji}$ and probabilities (p) of synaptic connections.

Source population	Target populations ($\bar{w}_{ji}$, probability of connection p)
i-F	i-F(0.009, p = 0.1);
	i-InF(0.01, p = 0.1);
	i-V2a(0.01, p = 0.1);
	i-V0$_D$(0.06, p = 0.1)
i-E	i-E(0.018, p = 0.1);
	i-InE(0.12, p = 0.1);
	i-V3(0.2, p = 0.05)
i-InF	i-E(−0.15, p = 0.1)
i-InE	i-F(−0.3, p = 0.1)
i-Ini	i-F(−0.5, p = 0.1)
i-V2a	i-V0$_V$(1.5, p = 0.1)
i-V0$_V$	c-Ini(1.5, p = 0.1)
i-V0$_D$	c-F (−0.18, p = 0.1)
i-V3	c-E(0.05, p = 0.05);
	c-inE(1, p = 0.05)

Prefixes i- and c- indicate ipsi- and contralateral populations.

an asymmetric decrease of the burst durations: extensor burst durations decreased more than flexor burst durations. At all frequencies, left–right alternation was maintained. Thus, the model reproduced the main characteristics of drug-induced fictive locomotion in mice.

To test whether the model is still consistent with the frequency-dependent changes in left–right coordination following the removal of V0 CINs (Talpalar et al., 2013), we simulated the selective removal of V0$_V$, V0$_D$ or both V0 CIN populations by setting all connection weights from the selected types of neurons to 0. Removal of V0$_V$ CIN populations did not change left-right alternation at low locomotor frequencies (**Figure 7A1**), but demonstrated left-right synchronized activity at high oscillation frequencies (**Figure 7A2**). Removal of V0$_D$ CINs had the opposite effect: left-right synchronization occurred at low frequencies (**Figure 7B1**), while left-right alternation was maintained at high frequencies (**Figure 7B2**). Finally, removal of both types of V0 CIN populations led to left-right synchronization at all frequencies (**Figures 7C1,C2**). Thus, similar to the previous model (Shevtsova et al., 2015) the present model was able to reproduce the experimental results on the speed-dependent role of V0$_V$ and V0$_D$ in support of left-right alternation (Talpalar et al., 2013).

The Model Reproduces Deceleration of the Rhythm by Tonic Stimulation of V3 Neurons

To simulate bilateral optogenetic stimulation of V3 CINs (see Section Optical Activation of Lumbar V3 Interneurons Increases the Intensity of Extensor Motor Activity and Slows Oscillation Frequency of Drug-Evoked Fictive Locomotion), we incorporated a channelrhodopsin ionic current, I_{ChR}, in V3 neurons (see Materials and Methods, Section Simulations of Changes in the Locomotor Frequency by Neuroactive Drugs and Application of Photostimulation), which was activated in all V3 neurons for 15 s during ongoing locomotor activity.

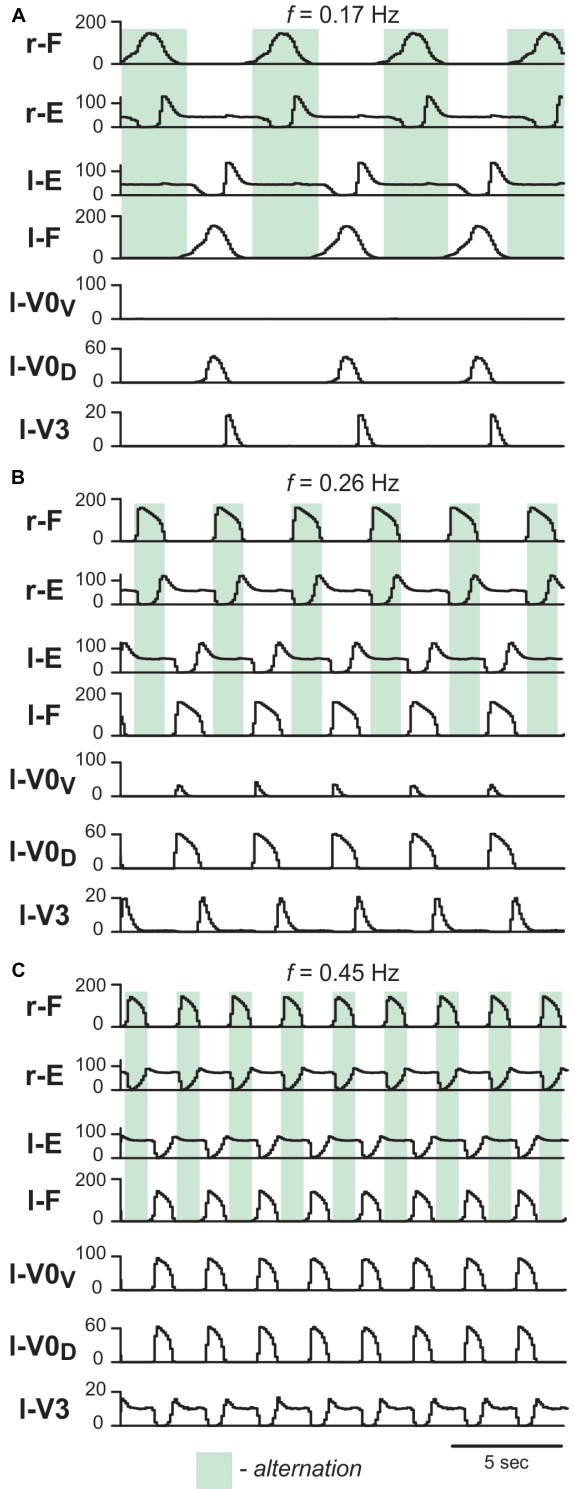

FIGURE 6 | Model performance under normal conditions. Integrated population activities of flexor (F) and extensor (E) rhythm generator centers and left commissural interneurons are shown at low (**A**; α = 0.01), medium (**B**; α = 0.03), and high excitation levels (**C**; α = 0.09). Activities of populations in this and following figures are shown as average histograms of neuron activity [spikes/(N × s), where N is a number of neurons in population; bin = 100 ms]. Shaded green areas show intervals of right flexor activities. r-: right; l-: left.

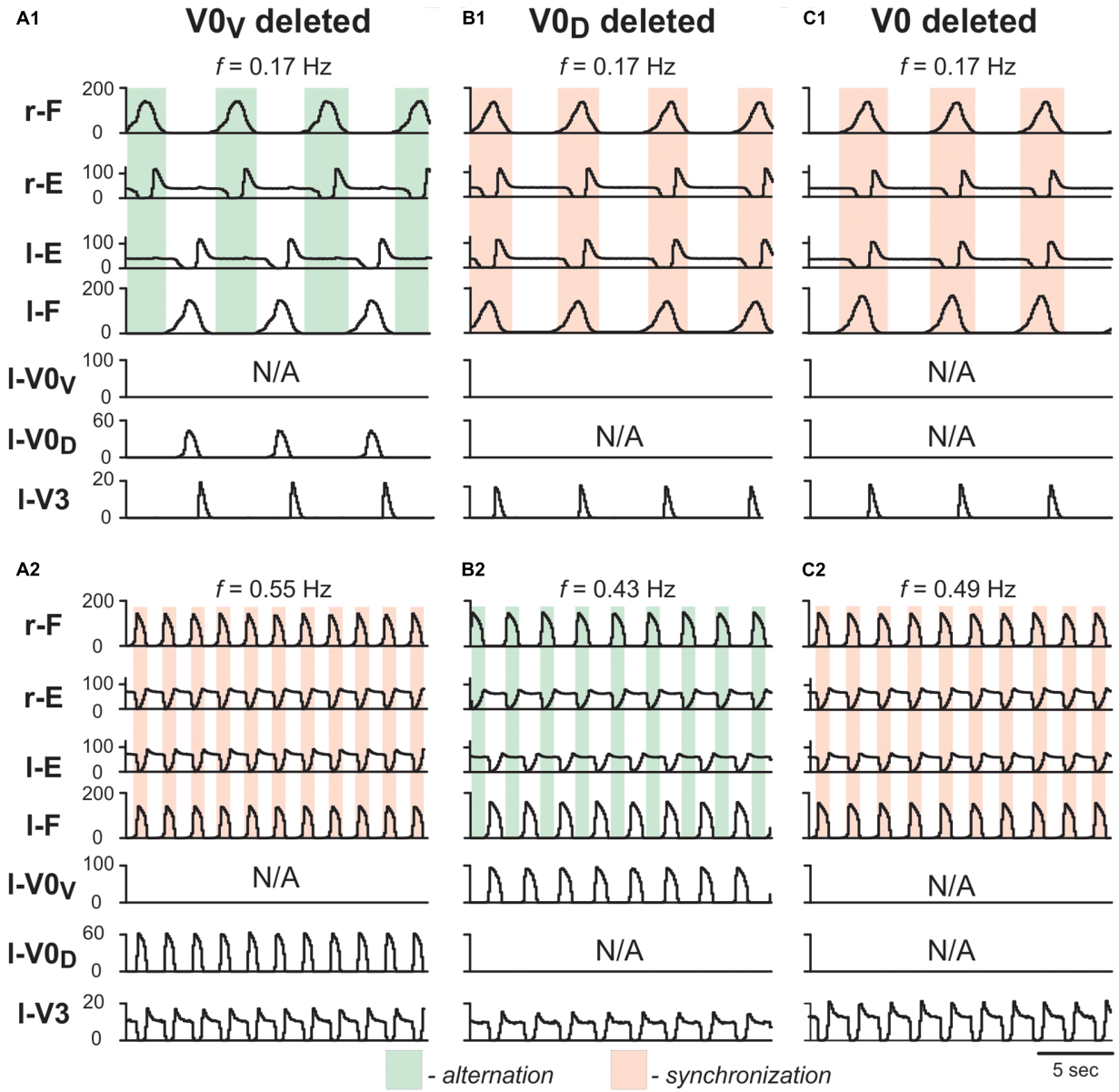

FIGURE 7 | Model performance after removal of $V0_V$, $V0_D$ and all V0 commissural interneurons. Integrated population activities of flexor and extensor rhythm generator centers (F and E, respectively) and left commissural interneurons are shown after removal of $V0_V$ **(A1,A2)**, $V0_D$ **(B1,B2)**, and all V0 **(C1,C2)**, at a low (**A1,B1,C1**; $\alpha = 0.01$) and a high (**A2,B2,C2**; $\alpha = 0.08$) excitation level and oscillation frequency. Shaded areas show intervals of right flexor activities. Green indicates left–right alternation and pink left–right synchronization. r-: right; l-: left.

The results of these simulations with progressively increased stimulation intensity are shown in **Figures 8**, **9**. At any value, the applied stimulation increased the firing rate of active V3 neurons and recruited new neurons that were silent before stimulation (**Figures 8A2–C2,A3–C3**). Immediately with its onset, V3-stimulation increased the cycle period and reduced the burst frequency of both RGs (**Figures 8A1,B1**). The frequency reduction was mainly caused by a prolongation of the extensor burst duration. Flexor-extensor and left–right alternation were preserved during this stimulation. With increasing value of stimulation, the frequency was progressively decreased (**Figures 8A1,B1**). At high stimulation values, the rhythm could be stopped, resulting in sustained activation of both extensor centers and suppression of both flexor centers (**Figure 8C1**). Once the stimulation was stopped, the model exhibited a short transitional period (one or two cycles) and then returned to the same burst frequency and pattern that were expressed before stimulation.

To study the effect of bilateral stimulation intensity on model behavior in more detail, we performed a simulation when the value of g_{ChR} (conductance of the channelrhodopsin ionic current, I_{ChR}, that characterizes the intensity of photostimulation

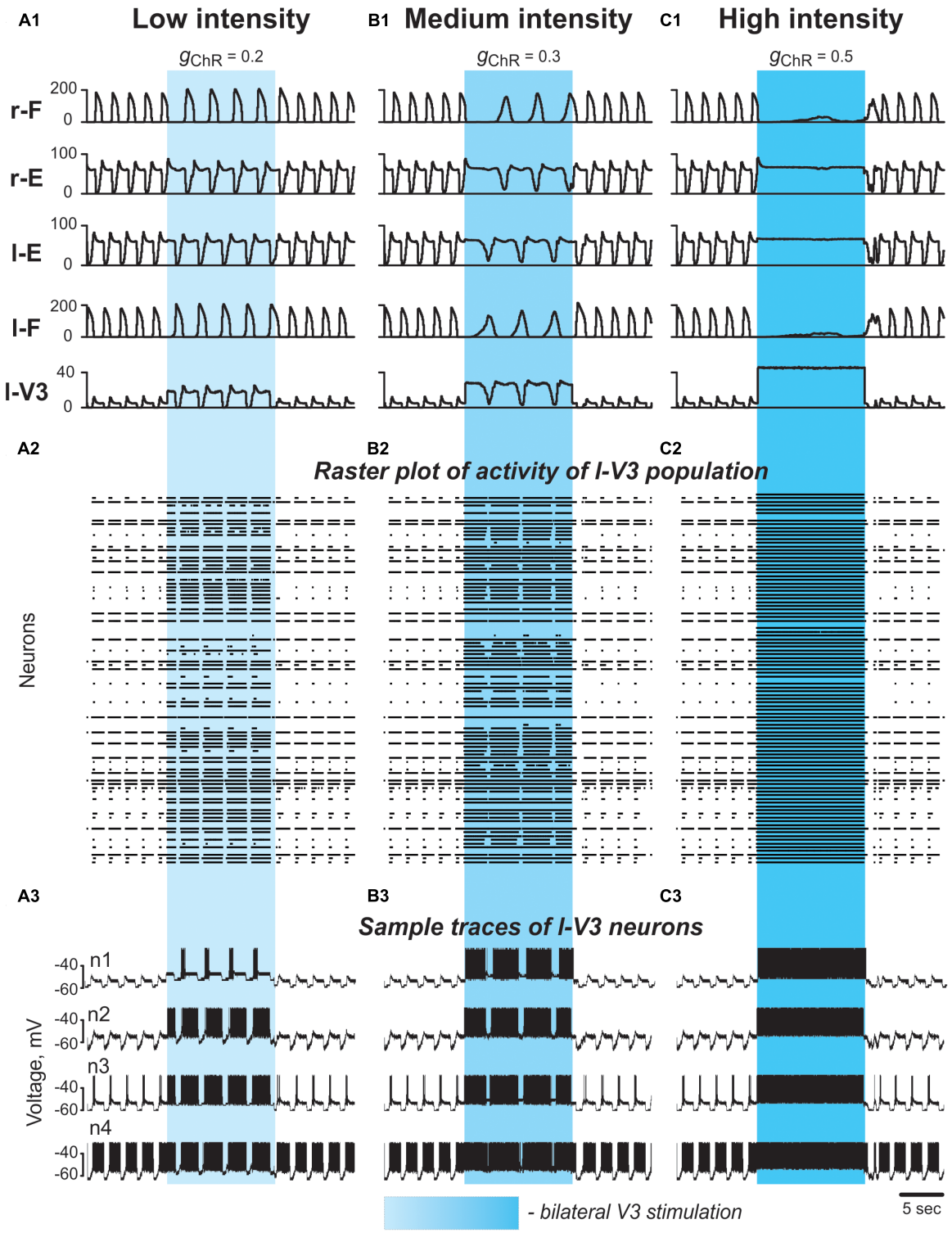

FIGURE 8 | Effect of bilateral stimulation of V3 commissural interneurons during fictive locomotion in the model. **(A1–A3)** Low V3-stimulation intensity (g_{ChR} = 0.2). **(B1–B3)** Medium V3-stimulation intensity (g_{ChR} = 0.3). **(C1–C3)** High V3-stimulation intensity (g_{ChR} = 0.5). Stimulation was applied to all V3 neurons (on both sides of the cord). For all stimulations fictive locomotion was evoked at α = 0.06. **(A1,B1,C1)** Integrated population activities of the flexor and extensor rhythm generator centers and the left V3 population. **(A2,B2,C2)** Raster plots of spikes elicited by neurons in the left V3 population. **(A3,B3,C3)** Traces of the membrane potential of sample neurons in the left V3 population with different excitability. Shaded blue areas show the interval when V3 stimulation was applied. r-: right; l-: left.

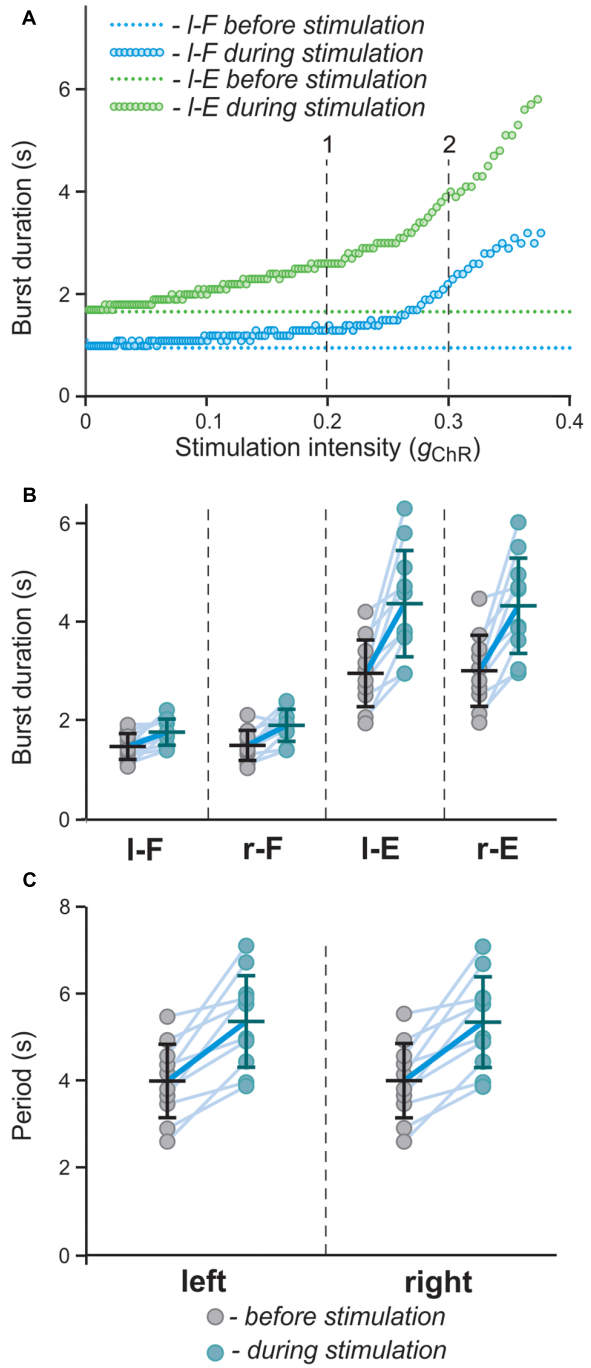

FIGURE 9 | Effect of bilateral stimulation of V3 interneurons on flexor and extensor burst duration s and oscillation period in the model. **(A)** Dependence of flexor and extensor burst duration on stimulation intensity (g_{ChR}; shown for the left side only). Intensity of stimulation was gradually changed from 0 to 0.4. The vertical lines (1 and 2) correspond to simulations shown in **Figures 8A1,A2**, respectively. **(B,C)** Flexor and extensor burst duration and period of oscillations in a series of model experiments (n = 12) with randomly chosen parameters α and g_{ChR} before (gray circles) and during (blue circles) bilateral stimulation of V3 populations. Each circle represents the average value of estimated parameter for one simulation. Light blue lines connecting two circles represent parameter increase in one simulation Thick, dark blue line represent the average of increase.

in the model) was slowly changed from 0 to 0.4 (see section Materials and Methods). The results of this simulation (**Figure 9A**) show that both flexor and extensor phases increase with increasing intensity of stimulation and the slope of this increase is higher for larger values of g_{ChR}. To simulate experimental variability, in a series of simulations parameters α (defining the average level of neuron excitation in the model) and g_{ChR} were randomly chosen from a uniform distribution in intervals [0.01; 0.06] and [0.18; 0.4], respectively. For each pair (α, g_{ChR}) a simulation was run in which average flexor and extensor burst durations and period of oscillations were calculated and compared to the control condition (g_{ChR} = 0; see **Figures 9B,C**). These results qualitatively reproduce the experimental results shown in **Figures 2D,E**.

Altogether our results show that the model closely reproduces our experimental findings of bilateral optogenetic stimulation of V3 neurons during drug-induced fictive locomotion when stimulation was applied at the midline and equally affected left and right V3 neurons (see section Optical Activation of Lumbar V3 Interneurons Increases the Intensity of Extensor Motor Activity and Slows Oscillation Frequency of Drug-Evoked Fictive Locomotion).

The reduction of the oscillation frequency when V3 neurons were stimulated occurred because both (left and right) extensor centers were activated by V3 neurons and they both provided an additional inhibition to the corresponding flexor centers through the corresponding inhibitory populations (InE), which reduced the average excitation of the flexor centers (**Figure 5**). In addition, activated V3 neurons provided direct excitation of the contralateral InE populations inhibiting the corresponding flexor centers. Note that the frequency of persistent sodium current-dependent oscillations positively correlates with the average excitation of a population of neurons with this current and mutually excitatory interconnection (Butera et al., 1999; Rybak et al., 2004, 2015). Since the rhythm in our model was generated by flexor centers, the reduction of their excitation during V3 neuron activation led to the reduction of oscillation frequency generated in both RGs. Furthermore, the reciprocal excitation of the extensor centers through V3 CINs created a positive feedback loop that amplified the firing rates of its constituent neurons and consequently the net inhibition exerted on the flexor centers.

The Model Reproduces Asymmetric Changes of the Locomotor Rhythm by Unilateral Stimulation of V3 Neurons

To simulate the effects of unilateral activation of V3 neurons during locomotor activity (see section Biased Optical Activation of V3 Interneurons in Spinal Segment L2 Leads to Asymmetrical Left–Right Motor Activity), we activated I_{ChR} in all V3 neurons located on one side of the cord. At a low value of unilateral activation of ipsilateral V3 population (**Figure 10A**), the extensor burst durations and the cycle periods increased on both sides, while the flexor-extensor and left-right alternation remained unchanged, which was similar to the effect of bilateral stimulation. With increasing value of stimulation (**Figures 10B,C**), the rhythm of the contralateral circuits was progressively slowed down, and additional bursts appeared

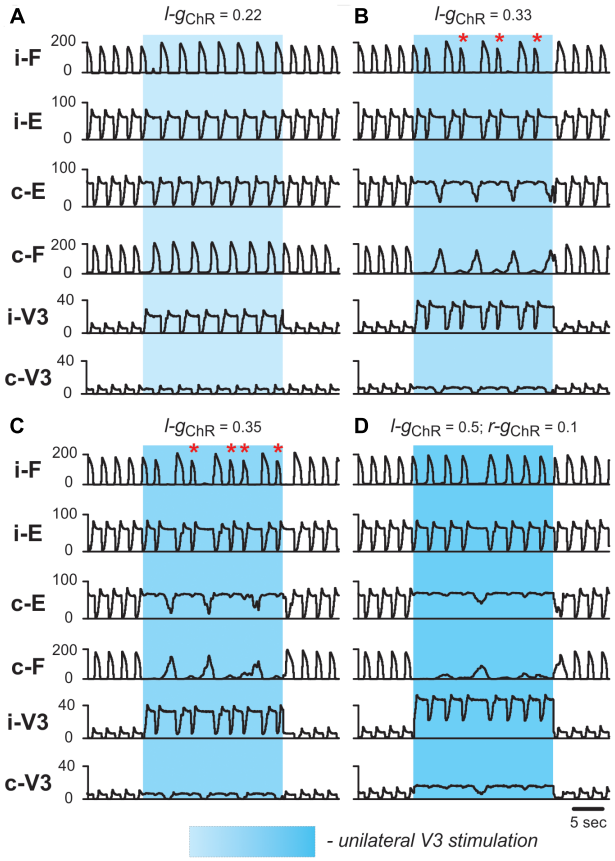

FIGURE 10 | Effect of unilateral stimulation of V3 commissural interneurons during fictive locomotion in the model. Fictive locomotion was evoked at α = 0.065. All panels show integrated population activities of the flexor (F) and extensor (E) rhythm generator centers and the V3 populations ipsi- and contralateral to the stimulation. Shaded blue areas show the interval when V3-stimulation was applied. Four different stimulation intensities are shown: **(A)** g_{ChR} = 0.22; **(B)** g_{ChR} = 0.33; **(C)** g_{ChR} = 0.35; **(D)** g_{ChR} = 0.5 in ipsilateral and g_{ChR} = 0.1 in contralateral V3 population. Red asterisks mark additional flexor bursts on ipsilateral side. i-: ipsilateral; c-: contralateral.

ipsilateral to the stimulation. **Figure 10B** shows a stable 2-to-1 relationship between the number of burst ipsilateral and contralateral to the stimulation. In **Figure 10C** one can see both 2-to-1 and 3-to-1 relationships. In all cases, reciprocity between the flexor centers maintained. Our simulations shown in **Figures 10B,C** qualitatively reproduced the experimental results concerning the response of the fictive locomotor pattern to the weak and medium unilateral optical stimulation of V3 neurons (**Figures 4A,B**) where one can also see an unequal number of flexor bursts on ipsi- and contralateral sides (marked by asterisks in **Figures 10B,C**).

This effect is even more obvious on the bifurcation diagrams in **Figures 11A1,A2** that show flexor and extensor phase durations plotted against parameter g_{ChR}, which has been gradually increased from 0 to 0.4. At lower values of g_{ChR}, both flexor and extensor phases progressively increase with an increase of parameter g_{ChR}. At a critical value of g_{ChR}, the curves characterizing dependence of flexor and extensor phase durations on g_{ChR} bifurcate into two and then three branches. The bifurcation diagram in **Figure 11B1** demonstrates that the stable regime at lower g_{ChR} values is characterized by a 1:1 ratio between the numbers of bursts in the contra- and ipsilateral flexor centers and then with increasing g_{ChR} the model starts to exhibit also 1:2 and 1:3 burst ratios with multiple bursts of the ipsilateral flexor center during one period of contralateral oscillations. In the diagrams in **Figures 11A1,B1** the bifurcations (transitions between regimes) can be seen as discontinuities. Transitions between stable regimes of 1:1, 1:2, and 1:3 ratios happen through intermediate quasiperiodic regimes where 1:1 and 1:2 or 1:2 and 1:3 ratios between the numbers of contra- and ipsilateral bursts occur and alternate with different integer intervals. To assess transition between regimes in more detail, in a series of simulations we fixed parameter g_{ChR} at some values (marked by red circles and vertical dashed lines in **Figure 11B1**) and estimated the timing of burst onsets in ipsi- and contralateral flexor centers for 40 s of simulated time. The results of these simulations are shown as the diagrams of ipsi- and contralateral flexor burst onsets in **Figure 11B2**. These diagrams demonstrate how the 1:1 regime at lower values of g_{ChR} transitions to the 1:2 regime through an intermediate quasiperiodic {1:1; 1:2} regime as g_{ChR} increases, and then to the 1:3 regime though another quasiperiodic {1:2; 1:3} regime.

The 1:2, 1:3 and intermediate quasiperiodic regimes are characterized by increased variability of burst durations during a single recording (see **Figures 11A1,A2**). Such behavior obviously affects the estimated average phase duration and period in particular experiments. Indeed, in experimental results shown in **Figures 3D1**, **4D1**, in individual recordings the flexor burst duration decreases during photostimulation as compared to the control condition, while on average there is either an increase (**Figure 3D1**) or no change (**Figure 4D1**). This is reproduced in our simulations (**Figures 12A1,B**), in which the results are shown for a series of computer experiments when parameters α and g_{ChR} were randomly chosen in intervals [0.01; 0.06] and [0.18; 0.4], respectively, and for each pair (α, g_{ChR}) a single simulation was performed to estimate average values for burst duration and oscillation period and compare with the control condition. These simulation results closely reproduce the experimental results shown in **Figures 3D1,E**. Interestingly, when the results of these simulations were conditionally separated according to the value of parameter g_{ChR} and the differences in flexor and extensor burst durations and period of oscillation in stimulated vs. control conditions were plotted against stimulation strength (similar to what was done in experiment in the spinal cord *in vitro*, see **Figures 4D1,E**), these results strikingly resembled the experimental results in **Figures 4D1,E** and demonstrated asymmetric response in the ipsi- and contralateral RG centers. Altogether, our modeling results strongly support the hypothesis that activation of V3 interneurons on one side of the spinal cord more strongly impacts the contralateral circuits.

To simulate the effects of high intensity and larger focal area unilateral stimulation, an additional weak stimulation of the contralateral V3 neuron population was applied (**Figure 10D**). In this case, the rhythmic activity on the ipsilateral side slowed down

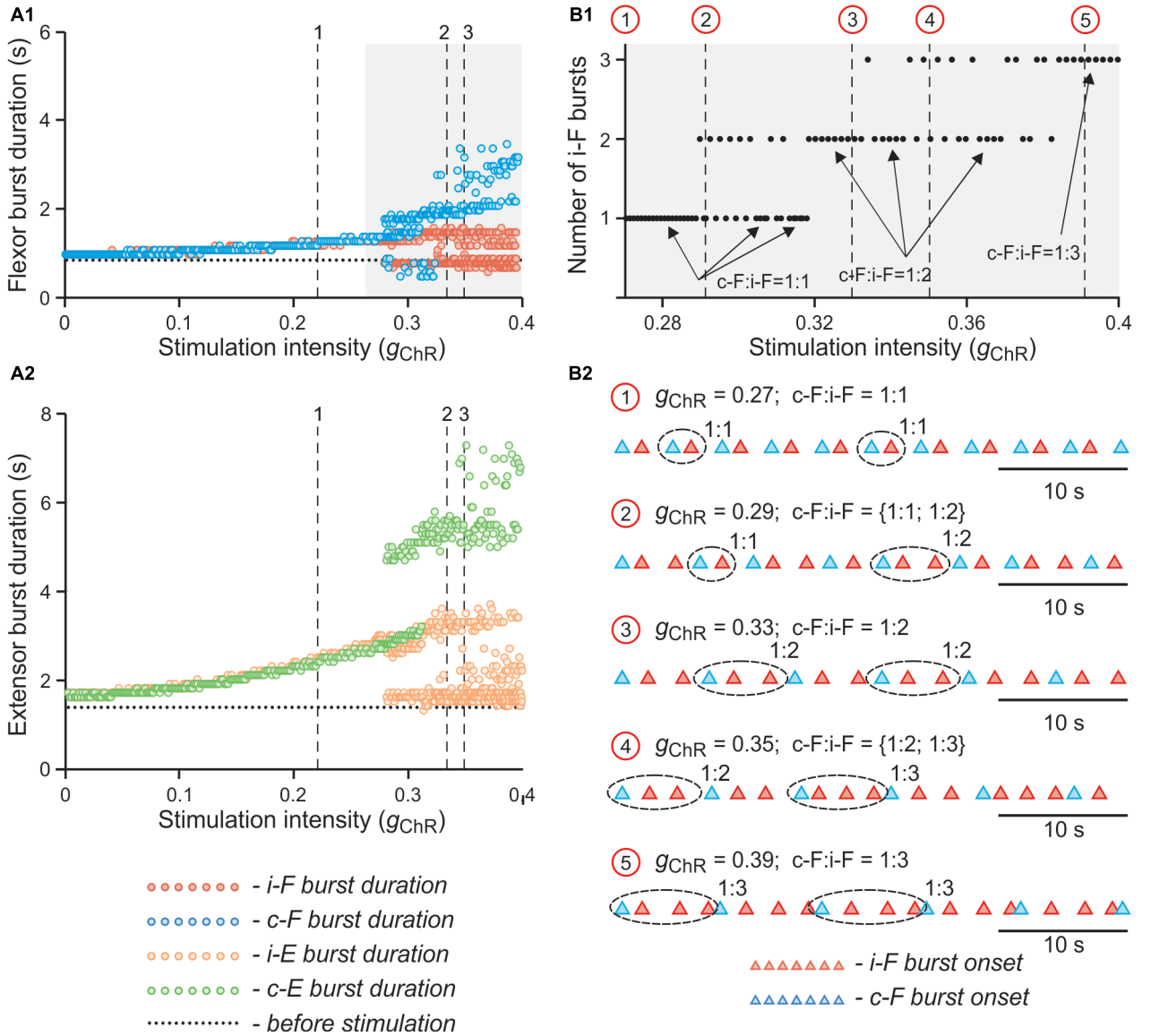

FIGURE 11 | Effect of unilateral stimulation intensity of V3 interneurons on flexor and extensor burst durations and oscillation period in the model. **(A1,A2)** Dependence of flexor **(A1)** and extensor **(A2)** burst durations on intensity of stimulation (g_{ChR}) when stimulation was applied to the left V3 population. Intensity of stimulation was gradually changed from 0 to 0.4. The vertical lines (1, 2 and 3) correspond to simulations shown in **Figures 10A–C**, respectively. **(B1,B2)** Dependence of number of additional ipsilateral flexor bursts during single contralateral period on parameter g_{ChR} at higher values of stimulation intensity In **(B1)**, g_{ChR} was gradually changed from 0.27 to 0.4. Arrows indicate 1:1, 1:2, and 1:3 ratios between the number of ipsi- and contralateral flexor bursts. Red circles and vertical lines indicate selected values of g_{ChR} for which additional simulations were run when g_{ChR} was fixed. In **(B2)**, the timing of flexor burst onsets for these simulations are shown. The corresponding values of g_{ChR} for each simulation are indicated above each trace. Traces are shown for 40 s of simulated time. i-: ipsilateral; c-: contralateral; F - flexor rhythm generator center.

during the stimulation and the contralateral extensor centers became constantly active, while irregular low-amplitude activity of the contralateral flexor centers occurred. This behavior of the model was similar to the results of experimental studies at a high intensity unilateral stimulation when the rhythm of the contralateral cord was suppressed, resulting in almost sustained extensor activity (**Figure 4C**). Based on our simulation results, we suggest that at high stimulation intensities the stimulation partly affected V3 neurons on the side contralateral to stimulation.

DISCUSSION

In the current study, we combined experimental studies with computational modeling to investigate the potential roles that V3 interneurons play in the spinal locomotor network. In our experiments, we used the *in vitro* preparations of isolated spinal cords from neonatal (P2-P3) mice in which fictive locomotion was induced by a mixture of neuroactive drugs (NMDA and 5-HT). Although the isolated neonatal spinal cords

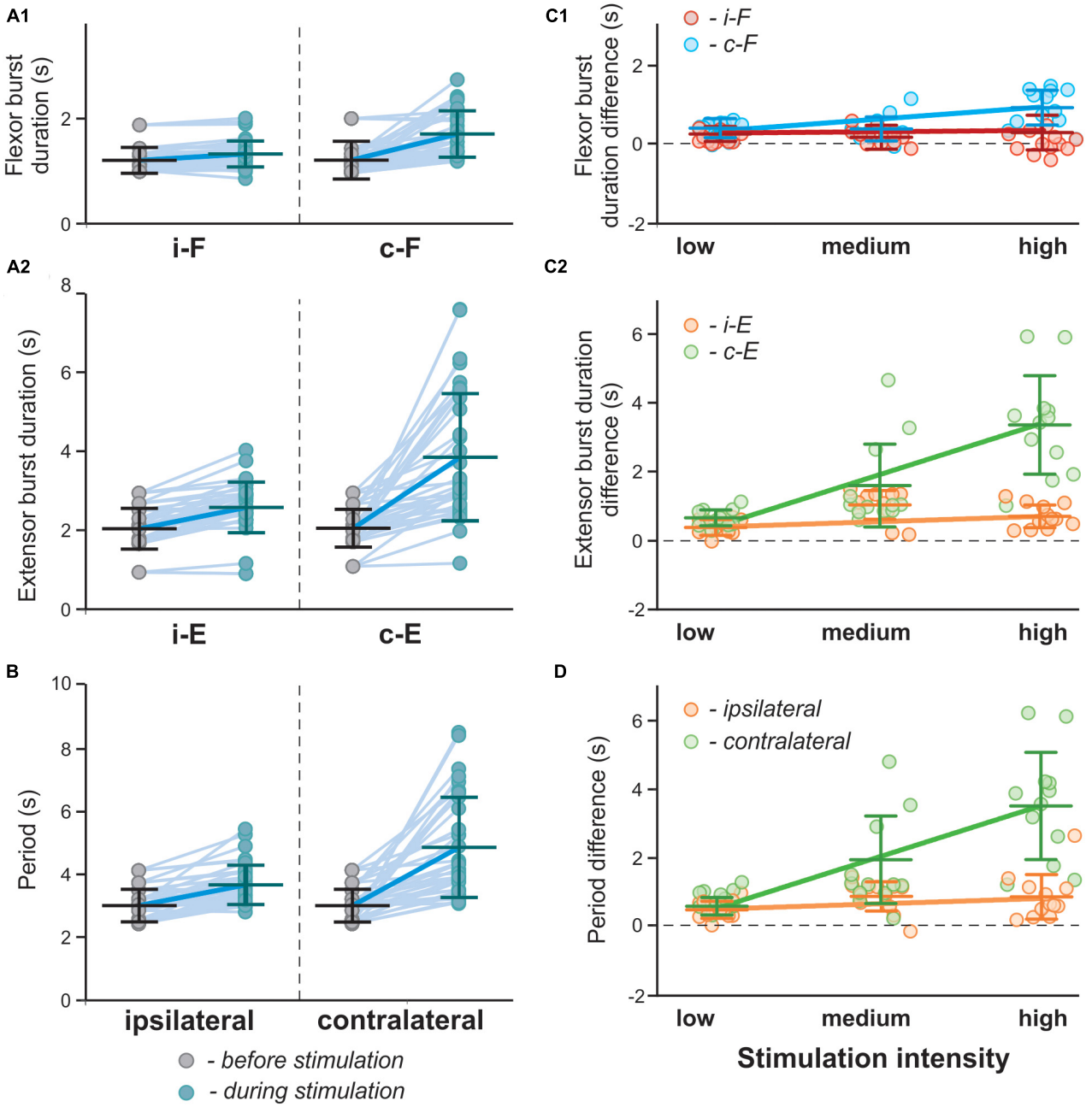

FIGURE 12 | Effect of unilateral stimulation of V3 interneurons on flexor and extensor burst durations and oscillation period in the model. **(A1,A2,B)** Flexor **(A1)** and extensor **(A2)** burst duration and period of oscillations **(B)** in a series of model experiments with randomly chosen parameters α and g_{ChR} before (gray circles) and during (blue circles) stimulation of the left V3 populations. Each circle represents the average value of estimated parameter for one simulation. Light blue lines connecting two circles represent parameter change in one simulation Thick, dark blue line represent the average of change. **(C1,C2,D)** Differences in flexor **(C1)** and extensor **(C2)** burst duration and period of oscillations **(D)** for the above modeling experiments estimated according to stimulation intensity. Low stimulation intensity corresponds to $g_{ChR} \in [0.18, 0.25]$, medium, $g_{ChR} \in [0.26, 0.33]$, in stimulations with high intensity $g_{ChR} \in [0.33, 0.4]$. Linear regression slopes are orange for ipsilateral and green for contralateral extensor centers and red for ipsilateral and blue for contralateral flexor extensor centers. i-: ipsilateral; c-: contralateral.

are characterized by a lack of supra-spinal and sensory inputs and are from young animals whose weight bearing ability is not fully developed, this preparation allows studying basic CPG circuits and functional interactions between genetically identified spinal interneurons (Kjaerulff and Kiehn, 1997; Lanuza et al., 2004; Gosgnach et al., 2006; Zhang et al., 2008). Using optogenetic approaches, we were able to selectively activate V3 interneurons at different regions of the spinal cord during drug-evoked fictive locomotion. Our computational model of locomotor circuits was able to qualitatively reproduce the experimental results. Our

study revealed that lumbar V3 interneurons strongly enhance the contralateral extensor activity and regulate the frequency of the locomotor oscillations. We suggest that spinal V3 CINs mediate mutual excitation between the extensor centers of the left and right rhythm generators in the lumbar spinal cord, which might support the synchronization of left-right activity under certain conditions during locomotion. In addition, we show that unilateral activation of V3 CINs can produce left-right asymmetrical rhythmic outputs, which provides a potential mechanism for the separate regulation of left–right limb movements as required for changing direction or during split-belt locomotion (Kiehn, 2016).

Optogenetic Activation of V3 Interneurons

Mapping the functional connectivity among neurons in the central nervous system is vital to understand circuit mechanisms underlying behavior. This is especially true within the spinal cord, which generates the rhythmic and patterned motor outputs necessary for coordinated movement (Grillner, 2006; Kiehn, 2006, 2011; Danner et al., 2015). However, uncovering the functional circuitry within the spinal cord has proven difficult due to a lack of clear anatomical organization compared to other brain regions. In the current study, novel optogenetic tools (Dougherty et al., 2013; Hägglund et al., 2013; Levine et al., 2014) have enabled us to specifically, reversibly, and acutely regulate the activity of a molecularly identified group of spinal neurons. By using Sim1cre-Ai32 mice (Chopek et al., 2018), we were able to target V3 interneurons on both or just one side of the isolated spinal cord, allowing us to start dissecting the function of V3 CINs in spinal locomotor circuits.

Using whole-cell patch-clamp recordings, we could verify that all ChR2-EYFP-expressing cells in the lumbar spinal slices could be exclusively depolarized by blue fluorescent light and elicit spikes during periods of the light pulses (10–20 s). During our functional study, however, we had to keep the whole lumbar cord intact and deliver the LED light on the ventral surface of the isolated spinal cord. Thus, we expect to have activated V3 neurons that had cell bodies and terminals located or neurites passing the illuminated region that is relatively close to the ventral surface. Although we were not able to specify the particular group of V3s, which we might be activating, we kept the light intensity, size and position consistent to limit variability across experiments.

The V3 CINs Provide Excitation to the Contralateral CPG Extensor Center

The identification of genetically defined interneuron populations has enabled us to characterize their specific functions in locomotor behaviors (Goulding, 2009; Gosgnach et al., 2017; Deska-Gauthier and Zhang, 2019). Until now, however, most experimental data were obtained by genetically eliminating certain classes of spinal interneurons without clear understanding of connectivity among the spinal interneurons (Lanuza et al., 2004; Gosgnach et al., 2006; Crone et al., 2008; Zhang et al., 2008; Talpalar et al., 2013; Bellardita and Kiehn, 2015; Haque and Gosgnach, 2019). In the case of V3 interneurons, genetic deletion of entire V3 population reduced the general robustness of the rhythmicity of the *in vivo* and *in vitro* locomotor activity and led to unstable gaits (Zhang et al., 2008). Our previous anatomical studies were only able to show that V3 cells had broad projections to contralateral motor neurons and other ventral spinal interneurons along the lumbar spinal cord, but we still do not know their precise anatomical position and their role in the CPG network (Zhang et al., 2008; Blacklaws et al., 2015). The current spatially controlled activation of V3 neurons was the first step to overcome this limitation to decipher their functional role in the spinal cord.

We found that the bilateral photoactivation of V3 neurons in the isolated spinal cord during fictive locomotion increased the intensity and duration of L5 bursts and prolonged the step cycles in all recorded lumbar roots whereas the duration of bursts in L2 roots was not significantly affected. These results suggested that, under our experimental condition, the photoactivated V3 interneurons predominantly excited the circuits responsible for extensor activities, which in turn reduced the frequency of fictive locomotion oscillations. This conclusion became more evident when we activated V3 interneurons only on one-side of the cord with varied light intensities. With such stimulations, we found that only the increase of burst duration of contralateral L5 were positively correlated to the intensity of the illuminating light, and at high intensity of unilateral photostimulation the contralateral L5 activity could express a sustained activity. More interestingly, such uneven regulation of contralateral extensor excitability by V3 CINs significantly decreased the bursting frequency of the contralateral ventral root output, which led to asymmetrical oscillation of the motor outputs on the two sides of the spinal cord. Thus, our experimental results support the conclusion that the lumbar V3 interneurons, or at least a sub-group of them, strongly regulate the extensor activity and step cycle duration on the contralateral side of the cord.

Similar to other genetically defined types of spinal interneuron populations (Bikoff et al., 2016; Gosgnach et al., 2017; Deska-Gauthier and Zhang, 2019), the V3 population is heterogeneous and consists of sub-populations with different anatomical, physiological and molecular profiles (Borowska et al., 2013, 2015). In the present study, however, we did not consider different subtype of V3 neurons. When we delivered the LED fluorescent light on the ventral surface of the spinal cord, we most likely activated a mixed group of different V3 neuron types in the illuminated region. Nonetheless, this discovery has provided direct evidence that some subtypes of V3 neurons can regulate the rhythm and pattern of the locomotor output through manipulating the contralateral extensor circuits.

Model Prediction: V3 Interneurons Project to Local Contralateral Inhibitory V1 Neurons

To reproduce the experimental results, it was necessary to model connections from the V3 CINs to the local contralateral inhibitory populations that inhibit the contralateral flexor centers

(InE; **Figure 5**). The main function of these connections in the present model was to allow for the reduction in frequency with V3 stimulation. In our previous models (Danner et al., 2016, 2017), we had introduced hypothetical inhibitory commissural interneuron populations mediating inhibition from the extensor centers to the contralateral flexor centers. These connections allowed for perfect alternation (0.5 normalized phase difference) between the left and right RGs. In the present model, the V3 connection to the local contralateral inhibitory neurons achieved the same function while no additional populations were needed.

The classes of V1 and V2b inhibitory neurons have been implicated in mediating flexor-extensor alternation (Zhang et al., 2014). Specifically, V1 neurons were suggested to provide inhibition from the extensor to the flexor RGs (Zhang et al., 2014; Shevtsova and Rybak, 2016): the same connection pattern as the InE populations in our model (**Figure 5**). Thus, our model predicts that V3 CINs project to contralateral V1 neurons that inhibit the flexor center. This prediction awaits experimental verification.

Coordination of Left–Right Activities by V3 Interneurons During Locomotion

Until now, several types of CINs, including V0, V3, and dI6, have been identified in the ventral spinal cord (Lanuza et al., 2004; Zhang et al., 2008; Andersson et al., 2012; Talpalar et al., 2013; Bellardita and Kiehn, 2015; Haque et al., 2018). When each of these CIN types, except V3, was genetically deleted, the left–right hind-limb alternation was affected. Particularly, $V0_V$ and $V0_D$ CINs were shown to secure the speed-dependent left-right alternation at walking and trotting gaits without effects on hind-limb synchronization observed during gallop and bound (Talpalar et al., 2013; Bellardita and Kiehn, 2015). On the other hand, deletion of V3 CINs did not affect the left-right alternation of the limb movement during walk and trot (Zhang et al., 2008). We had suggested that V3 represent the CIN populations that mediate left–right synchronization in certain conditions (e.g., when some or all V0 CINs are genetically removed) and during gallop and bound. In our previous computational models (Rybak et al., 2013; Shevtsova et al., 2015; Danner et al., 2016, 2017; Shevtsova and Rybak, 2016), to perform this function the V3 CINs were assigned to explicitly mediate mutual excitation between the flexor centers of the left and right rhythm generators. However, our current experimental outcome contradicts this assumption, suggesting functional connections of V3 CINs to the contralateral extensor centers instead of the flexor centers. To match our experimental findings, we changed the connection of simulated V3 populations from the activation of contralateral flexor centers to the activation of contralateral extensor centers. With this change in the V3 connectivity we were able to qualitatively reproduce all our current and previous experimental results, including speed-dependent left–right alternation mediated by $V0_V$ and $V0_D$.

This unification of the experimental and computational data confirmed that the proposed organization of our current computational model of spinal circuits is plausible, and that V3 interneurons can mediate the synchronization of left-right hind-limb activities through mutual excitation of extensor centers of the left and right spinal rhythm generators.

Excitatory commissural neurons (such as the V3 CINs) have been reported to mediate reticulospinal and vestibulospinal input as well as input from ipsilateral somatosensory afferents to contralateral motoneurons (Bruggencate et al., 1969; Bruggencate and Lundberg, 1974; Matsuyama et al., 2004; Cabaj et al., 2006). Kasumacic et al. (2015) further described a population of commissural interneurons that directly receives vestibulospinal input and contributes to contralateral extensor activity. These pathways are thought to be involved in stabilizing posture during locomotion. Based on our results, the V3 class is a likely candidate for mediating and integrating these inputs. Thus, studying interaction and convergence of supraspinal and somatosensory afferent inputs on V3 might lead to a better understanding of the role and function of these pathways during locomotion.

Activation of V3s of one side of the spinal cord resulted in asymmetric modulation of extensor and flexor phase durations between the two sides of the cord. This allows a suggestion that V3 interneurons may play important functional roles in left–right coordination when changing the direction of movement, walking on a curved path (Courtine and Schieppati, 2003a,b), on unequal surfaces or a split-belt treadmill (Forssberg et al., 1980; Yang et al., 2005; Frigon, 2017). Such locomotor behaviors may be controlled by an additional supraspinal or afferent activation/suppression to V3 neuron populations on one side of the cord. In these situations, different speeds for left-right limbs are necessary for maintaining stable locomotion. The precise mechanisms underlying such movements are still unknown, but it has been indicated that the independent but closely coordinated CPG circuits in both sides of the spinal cord are involved (Frigon, 2017). In our current experimental and modeling studies, we could induce asymmetric rhythmic activities with an unequal number of bursts between the two sides of the spinal cord by unilaterally activating V3 neurons. These results closely resemble the findings in split-belt locomotion with a large speed difference for the left and right belts, in which additional steps were observed on the fast side (Forssberg et al., 1980; Yang et al., 2005; Frigon, 2017). Such activity patterns are reminiscent of those of (weakly-)coupled oscillators, with asymmetric drive (Pikovsky et al., 2001; Pikovsky and Rosenblum, 2003; Rubin et al., 2011) and since our data were obtained in an isolated spinal cord preparation, they provide even more convincing evidence of the existence of a CPG on either side of the cord.

In conclusion, our study provides strong evidence that spinal V3 CINs are involved in left-right limb coordination during locomotion presumably by providing mutual excitation between the extensor centers of the left and right rhythm generators and mediating inhibition from the extensor centers to their contralateral flexor centers through an additional inhibitor interneuron population. In addition, we have shown that unilateral activation of V3 CINs can produce left-right asymmetric rhythmic outputs. Which led us to suggest that V3 neurons are involved in changing the direction of movements and/or in control of locomotion through complex environments.

MATERIALS AND METHODS

Animals

The generation and genotyping of Sim1$^{Cre/+}$ mice were described previously by Zhang et al. (2008). Ai32 mice were from the Jackson Laboratory (Stock No. 012569). It contains Rosa26-cytomegalovirus early enhancer element/chicken beta-actin promoter (CAG)-loxP–Stop codons–3x SV40 polyA–loxP (LSL)-channelrhodopsin2 (ChR2)-enhanced yellow fluorescent protein (EYFP)-woodchick hepatitis virus posttranscriptional enhancer (WPRE; RC-ChR2). Sim1cre-Ai32 mice were generated by breeding these two strains expressed ChR2/EYFP fusion-protein in Sim1 expressing cells. TdTomato Ai14 (Jackson Laboratory Stock No. 007908) conditional reporter (referred as tdTom) mice were generated and genotyped as previously described (Blacklaws et al., 2015). Sim1$^{Cre/+}$; tdTom; Ai32 mice were generated by crossing Sim1$^{Cre/+}$; tdTom mice with Ai32 mice. All procedures were performed in accordance with the Canadian Council on Animal Care and approved by the University Committee on Laboratory Animals at Dalhousie University.

Electrophysiology and Immunohistochemistry

Preparation

All experiments were performed using spinal cords from Sim1cre-Ai32 mice (isolated spinal cord recording and whole-cell patch-clamp recording) and Sim1$^{Cre/+}$; tdTom; Ai32 mice (whole-cell patch-clamp recording) at postnatal day (P) P2-P3. The mice were anesthetized, and the spinal cords caudal to thoracic (T) 8 segments were dissected in an ice-cold oxygenated Ringer's solution (111 mm NaCl, 3.08 mm KCl, 11 mm glucose, 25 mm NaHCO3, 1.25 mm MgSO4, 2.52 mm CaCl2, and 1.18 mm KH2PO4, pH 7.4). The spinal cord was then transferred to the recording chamber to recover at room temperature for 1 h before recording in Ringer's solution.

Isolated Whole-Cord Recordings

Electroneurogram (ENG) recordings of the (lumbar) L2 and L5 ventral roots were conducted using differential AC amplifier (A-M system, model 1700) with the band-pass filter between 300 Hz and 1 kHz. Analog signals were transferred and recorded through the Digidata 1400A board (Molecular Devices) under the control of pCLAMP10.3 (Molecular Devices). Fictive locomotor activity was induced by applying 5-hydroxytryptamine (5-HT, 8 μM) and NMDA (7–8 μM) in the Ringer's solution.

Optical Stimulation of V3 Interneurons

To activate ChR2 in V3 interneurons, 488 nm fluorescent light was delivered by Colibri.2 illumination system (Zeiss) through 10x or 20 × 1.0 numerical aperture (NA) objectives mounted on an up-right microscope (Examiner, Zeiss) onto the ventral surface of the isolated spinal cord, a protocol adopted from other studies (Hägglund et al., 2013; Levine et al., 2014). This allowed us to have relative fixed focal areas. In addition, using the Colibri system, we were able to control the LED light intensity accurately. Only when we needed to compare the intensity-dependent changes, we would manually adjust the focal size of the field diaphragm and LED light intensity.

To perform unilateral stimulation, we manually adjusted the field diaphragm and LED light intensity to cover the whole half side of the spinal cord to be the largest illuminated area, and then to reduce the illuminated region between approximately one-third to a half of the spinal cord (**Figure 4B**) to regulate the number of V3 neurons being activated. For each cord, we set the stimuli with largest focal area and 100% light intensity as the high intensity group, then reduced focal area to medium group, and the smallest focal area less than medium group (one of third) and/or reduced light intensity to less than 50% as the low intensity group.

Continuous light stimuli with duration of 10 and 20 s were used. To use such long-lasting stimuli, we needed to make sure that they do not cause any damage of tissue and neuronal behavior. Our special studies did not find any damage produced by such stimulations in our experiments including possible effects on patch-clamp or whole cord recordings. The results of such experiments are shown in **Supplementary Figure 1**. Specifically, under whole cell-patch-clamp configuration, we used three consecutive 20-s light pulses to EYFP or tdTomato positive cell and showed that the firing patterns of cells were the same during each stimulation (**Supplementary Figure 1A1**) and their response to injected current the same before and after optical stimulation (**Supplementary Figure 1A2**; n = 22). In contrast, under the same conditions, the EYFP and tdTomato-negative neurons didn't respond to the light stimulation (**Supplementary Figure 1B1**) but could generate normal spiking activity in response to injected current (**Supplementary Figure 1B2**; n = 10). To further verify that the optical stimulation did not affect neuronal activity, we applied maximum optical stimulation (100% light intensity, 10x objective) on the spinal cord of Cre negative Ai32 mice. The activity of all recorded nerves remained unchanged under and after the 20-s light pulses (**Supplementary Figure 1C**).

Whole-Cell Patch-Clamp Recordings

The experimental procedures were detailed in Borowska et al. (2013). Briefly, 300 μM slices from the spinal cord lumbar region (T13–L3) from P2-3 Sim1cre-Ai32 or Sim1$^{Cre/+}$; tdTom; Ai32 mice were prepared in an ice-cold oxygenated sucrose solution (3.5 mm KCL, 25 mm NaHCO3, 1.2 mm KH2PO4, 1.3 mm MgSO4, 1.2 mm CaCl2, 10 mm glucose, 212.5 mm sucrose, and 2 mm MgCl2, pH 7.4) on a vibratome (Vibratome 300, Vibratome). Slices were incubated in an oxygenated Ringer's solution (111 mm NaCl, 3.08 mm KCl, 11 mm glucose, 25 mm NaHCO3, 1.25 mm MgSO4, 2.52 mm CaCl2, and 1.18 mm KH2PO4, pH 7.4) at room temperature for >30 min for recovery before recording. EYFP fluorescence-positive, tdTom fluorescence-positive and fluorescence-negative cells were visually identified using a 40× water-immersion objective (numerical aperture, 0.8) with the aid of a DAGE-MTI IR-1000 CCD camera.

Conventional whole-cell patch-clamp recordings were made in voltage- and current-clamp modes using a MultiClamp 700B amplifier (Molecular Devices). Analog signals were filtered at 10 kHz with the Digidata 1400A board (Molecular Devices)

under control of pCLAMP10.3 (Molecular Devices). Patch-clamp recording pipettes with a resistance of 5–8 MΩ were filled with solution containing 128 mm K-gluconate, 4 mm NaCl, 0.0001 mm CaCl2, 10 mm HEPES, 1 mm glucose, 5 mm Mg-ATP, and 0.3 mm GTP-Li, pH 7.2 and the fluorescent light was delivered through the 40x objective.

Immunohistochemistry and Confocal Image Capture

Following recording, 300 μM spinal slices from P2-3 $Sim1^{Cre/+}$; tdTom; Ai32 mice were fixed in 4% paraformaldehyde (Electron Microscopy Science) for 10 min. Sections were then rinsed three times in 0.1% Triton X-100 (PBS-T) for 1 h total (20 min each rinse) at room temperature. Sections were then incubated in primary antibody solution for 2 days at 4°C. Primary antibody solutions consisted of 90% PBS, 10% Horse Serum (Invitrogen), and primary antibodies. Primary antibodies used were Rabbit anti DsRed (1:2000, Cat#600-401-379, Rockland) and Chicken anti GFP (1:1000, Cat#GFP-1010, Aves Labs). Following primary antibody incubation, sections were rinsed three times in PBS for 1 h total (20 min each rinse) at room temperature. Sections were then incubated in secondary antibody solution overnight at 4°C. Secondary antibody solutions consisted of 90% PBS, 10% Horse Serum (Invitrogen), Alexa Fluor 647-conjugated streptavidin (Jackson ImmunoResearch Laboratories, Inc.), and secondary antibodies. Secondary antibodies used were Fluorescein-Labelled Goat anti-Chicken IgY (1:500, Cat#F-1005, Aves Labs) and Alexa Fluor® 594-conjugated Donkey Anti-Rabbit IgG (1:500, Cat# 711-585-152, Jackson ImmunoResearch Laboratories, Inc.). Lastly, sections were rinsed in PBS for 1 h total (20 min each rinse) at room temperature. Sections were then mounted on glass slides (Fisherbrand) with Dako fluorescent mounting medium and 1.5 cover slips (VWR). All images were collected on a Zeiss LSM 710 upright confocal microscope.

Data Analysis

All recorded traces were transferred to Spike2 (Version 7.09a, Cambridge Electronic Design). The raw recordings were initially rectified and smoothed (τ = 0.05 s) using Spike2. To measure the durations of flexor and extensor bursts and the step cycle we used the smoothed signals to identify burst onset and offset times. To identify these times in noisy recordings we set a threshold that was equal to 15% of the bust amplitude (difference between maximal and minimal values) and identified intersections of the smoothed signals with the threshold. The duration of each burst was measured as a time interval between burst's onset and offset. The step cycle duration was measured as a time interval between onset times of two consecutive bursts. The average of step cycle durations and burst durations of five consecutive cycles before the light-on and all the cycles during the light were used as a pair of data before and during light, respectively. The steps interrupted at the beginning or the end of light were excluded from the calculation.

Statistical analysis was performed in Prism7 (GraphPad Software, Inc.). Wilcoxon signed-rank test was used to compare the difference between the activity before and after the light. Linear contrasts were used to determine the relationship of the burst duration difference of activities in four nerves and step cycle difference in ipsilateral and contralateral side among three intensities. One-way ANOVA was used to determine the statistical significance among the burst duration of activity in four nerves. An α-error of $P < 0.5$ was regarded as significant. Data in the Results represent the mean ± SD.

Computational Modeling

Neuron Model

All neurons were simulated in the Hodgkin–Huxley style as single-compartment models. The membrane potential, V, in neurons of the left and right flexor and extensor centers was described by the following differential equation

$$C \times \frac{dV}{dt} = -I_{Na} - I_{NaP} - I_K - I_L - I_{SynE} - I_{Synl}, \quad (1)$$

where C is the membrane capacitance and t is time.

In all other populations, the neuronal membrane potential was described as follows:

$$C \times \frac{dV}{dt} = -I_{Na} - I_K - I_L - I_{SynE} - I_{Synl} - I_{ChR}. \quad (2)$$

The ionic currents in Equations (1) and (2) were described as follows:

$$\begin{aligned} I_{NaP} &= \bar{g}_{Na} \times m_{Na}^3 \times h_{Na} \times (V - E_{Na}); \\ I_{NaP} &= \bar{g}_{NaP} \times m_{NaP}^3 \times h_{NaP} \times (V - E_{Na}); \\ I_K &= \bar{g}_K \times m_K^4 \times (V - E_K); \\ I_L &= g_L \times (V - E_L); \\ I_{ChR} &= g_{ChR} \times (V - E_{ChR}), \end{aligned} \quad (3)$$

where I_{Na} is the fast Na^+ current with maximal conductance $\bar{g}_{Na}$; I_{NaP} is the persistent (slowly inactivating) Na^+ current with maximal conductance $\bar{g}_{NaP}$ (present only in RG neurons); I_K is the delayed-rectifier K^+ current with maximal conductance $\bar{g}_K$; I_L is the leakage current with constant conductance g_L; I_{ChR} is the channelrhodopsin current with the conductance g_{ChR} (present only in V3 neurons). E_{Na}, E_K, E_L, and E_{ChR} are the reversal potentials for Na^+, K^+, leakage, and channelrhodopsin currents, respectively; variables m and h with indexes indicating ionic currents are the activation and inactivation variables of the corresponding ionic channels.

Activation m and inactivation h of voltage-dependent ionic channels (e.g., Na, NaP, and K) in Equation (3) were described by the following differential equations:

$$\begin{aligned} \tau_{mi}(V) \times \frac{d}{dt} m_i &= m_{\infty i}(V) - m_i; \\ \tau_{hi}(V) \times \frac{d}{dt} h_i &= h_{\infty i}(V) - h_i, \end{aligned} \quad (4)$$

where $m_{\infty i}(V)$ and $h_{\infty i}(V)$ define the voltage-dependent steady-state activation and inactivation of the channel i, respectively, and $\tau_{mi}(V)$ and $\tau_{hi}(V)$ define the corresponding time constants. Activation of the sodium channels is considered to be

instantaneous. The expressions for channel kinetics in Equation (4) are described as follows:

$$\begin{aligned} m_{\infty Na}(V) &= (1+\exp(-(V+34)/7.8))^{-1}; \\ \tau_{mNa} &= 0; \\ h_{\infty Na}(V) &= (1+\exp((V+55)/7))^{-1}; \\ \tau_{hNa}(V) &= 20/(\exp((V+50)/15)) + \exp(-(V+50)/16); \\ m_{\infty NaP}(V) &= (1+\exp(-(V+47.1)/3.1))^{-1}; \\ \tau_{mNaP} &= 0; \\ h_{\infty NaP}(V) &= (1+\exp((V+60/6.8))^{-1}; \\ \tau_{hNap}(V) &= 8000/\cosh((V+60)/13.6); \\ m_{\infty K}(V) &= (1+\exp(-(V+28)/4))^{-1}; \\ \tau_{mK}(V) &= 3.5/\cosh((V+40)/40); \\ h_K &= 1. \end{aligned} \quad (5)$$

The maximal conductances for ionic currents and the leak reversal potentials, E_L, for different populations are given in **Table 1**.

The synaptic excitatory (I_{SynE} with conductance g_{SynE} and reversal potential E_{SynE}) and inhibitory (I_{SynI} with conductance g_{SynI} and reversal potential E_{SynI}) currents were described as follows:

$$\begin{aligned} I_{SynE} &= g_{SynE} \times (V - E_{SynE}); \\ I_{SynI} &= g_{SynI} \times (V - E_{SynI}). \end{aligned} \quad (6)$$

where g_{SynE} and g_{Synl} are equal to zero at rest and are activated by the excitatory or inhibitory inputs, respectively:

$$\begin{aligned} g_{SynE_i}(t) &= \bar{g}_E \times \sum_j S\{w_{ji}\} \times \sum_{t_{kj}<t} \exp(-(t-t_{kj})/\tau_{SynE}); \\ g_{Synli}(t) &= \bar{g}_I \times \sum_j S\{-w_{ji}\} \times \sum_{t_{kj}<t} \exp(-(t-t_{kj})/\tau_{Synl}), \end{aligned} \quad (7)$$

where $S\{x\} = x$, if $x \geq 0$, and 0 if $x < 0$. Each spike arriving to neuron i in a target population from neuron j in a source population at time t_{kj} increases the excitatory synaptic conductance by $\bar{g}_E \times w_{ji}$ if the synaptic weight $w_{ji} > 0$, or increases the inhibitory synaptic conductance by $-\bar{g}_I \times w_{ji}$ if the synaptic weight $w_{ji} < 0$. $\bar{g}_E$ and $\bar{g}_I$ define an increase in the excitatory or inhibitory synaptic conductance, respectively, produced by one arriving spike at $|w_{ji}| = 1$. τ_{SynE} and τ_{SynI} are the decay time constants for g_{SynE} and g_{SynI}, respectively.

The following general neuronal parameters were assigned: $C = 1\ \mu F \cdot cm^{-2}$; $E_{Na} = 55$ mV; $E_K = -80$ mV; $E_{ChR} = -10$ mV; $E_{SynE} = -10$ mV; $E_{SynI} = -70$ mV; $\bar{g}_E = \bar{g}_I = 0.05$ mS/cm^2; $\tau_{SynE} = \tau_{SynI} = 5$ ms.

Neuron Populations

Each neuron population in the model contained 50–200 neurons. The numbers of neurons in each population are shown in **Table 1**.

Random synaptic connections between the neurons of interacting populations were assigned prior to each simulation based on probability of connection, p, so that, if a population A was assigned to receive an excitatory (or inhibitory) input from a population B, then each neuron in population A would get the corresponding synaptic input from each neuron in population B with the probability $p\{A, B\}$. If $p\{A, B\} < 1$, a random number generator was used to define the existence of each synaptic connection; otherwise [if $p\{A, B\} = 1$] each neuron in population A received synaptic input from each neuron of population B. Values of synaptic weights (w_{ji}) were set using random generator and were based on average values of these weights $\bar{w}$ and variances, which were defined as 5% of $\bar{w}$ for excitatory connections ($\bar{w} > 0$) and 10% of $\bar{w}$ for inhibitory connections ($\bar{w} < 0$). The average weights and probabilities of connections are specified in **Table 2**.

Heterogeneity of neurons within each population was provided by random distributions of the base values of the mean leakage reversal potentials $\bar{E}_{Li0}$ (see mean values ± SD for each i-th population in **Table 1**) and initial conditions for the values of membrane potential and channel kinetics variables. The base values of $\bar{E}_{Li0}$ and all initial conditions were assigned prior to simulations from their defined average values and variances using a random number generator, and a settling period of 10–200 s was allowed in each simulation.

Simulations of Changes in the Locomotor Frequency by Neuroactive Drugs and Application of Photostimulation

In the model, the frequency of rhythmic oscillations depended on the parameter α, that defined the level of average neuronal excitation in each population i (Shevtsova et al., 2015):

$\bar{E}_{Li} = \bar{E}_{Li0} \times (1 - \alpha)$ where $\bar{E}_{Li0}$ represents the base value of mean leakage reversal potential in the population at $\alpha = 0$ (see **Table 1**).

To simulate the effect of photostimulation, we selectively activated the V3 neurons either bi- or unilaterally by increasing the channelrhodopsin current conductance (g_{ChR}), which was set to 0 in control conditions.

To estimate changes in model behavior after increase of the channelrhodopsin current conductance (g_{ChR}), we used two methods. In the first method, simulations were run at the fixed value of g_{ChR} (**Figures 8**, **10**, **11B2**). The values of g_{ChR} for these particular simulations are indicated in the corresponding figure legends. This method was also used to estimate the robustness of the model and simulate variability of experimental condition and individual spinal cords (**Figures 9B,C**, **12**). To do this, we performed a series of simulations for both experimental conditions (bilateral and unilateral activation of V3 neurons) when parameters α, defining the level of average neuronal excitation in each population, and g_{ChR}, characterizing intensity of photostimulation, were randomly chosen in the range [0.01, 0.06] for α and [0.18, 0.4] for g_{ChR}. For each pair (α, g_{ChR}) a simulation was run and average values for flexor and extensor burst durations and oscillation period were calculated and compared with control condition when the model behavior was estimated with the same α and $g_{ChR} = 0$.

In the second method, the integrated population activities were computed continuously during slow-ramp increase of g_{ChR}. This method was used to study the effect of stimulation intensity on model behavior in more detail (see **Figures 9A**, **11A1,B1**). The value of g_{ChR} was slowly increased from 0 to 0.4 (0.01 during 100 s of simulated time). For each locomotor cycle durations of flexion and extension phases or number of ipsilateral flexor bursts were calculated and plotted against the parameter g_{ChR}.

Computer Simulations

All simulations were performed using the custom neural simulation package NSM 2.5.11[1] developed at Drexel University by S. N. Markin, I. A. Rybak, and N. A. Shevtsova. This simulation package was previously used for the development of several spinal cord models (Rybak et al., 2006a,b, 2013; McCrea and Rybak, 2007, 2008; Zhong et al., 2012; Shevtsova et al., 2015; Shevtsova and Rybak, 2016). Differential equations were solved using the exponential Euler integration method with a step size of 0.1 ms. Simulation results were saved as ASCI files containing time moments of spikes for RG populations. Model configuration files to create the simulations presented in the paper are available at https://github.com/RybakLab/nsm/tree/master/models/Danner-2019-V3.

Data Analysis in Computer Simulations

The results of simulations were processed by custom Matlab scripts (The Mathworks, Inc., Matlab 2019a). To assess the model behavior, the averaged integrated activities of flexor and extensor centers (average number of spikes per neuron) were used to calculate the flexor and extensor burst durations and oscillation period. The timing of onsets and offsets of flexor and extensor bursts was determined at a threshold level equal to 10–25% of the average difference between maximal and minimal burst amplitude for particular population in the current simulation. The locomotor period was defined as the duration between two consecutive onsets of the extensor centers. Duration of individual simulations depended on the value of parameter α, and to robustly estimate average value of burst duration and oscillation period in the first method, the first 10–20 transitional cycles were omitted to allow stabilization of model variables, and the values of model parameters were averaged for 10–20 consecutive cycles. In the second method, to validate our results we selectively run additional simulation with a slower ramp increase (0.01 during 500 s of simulated time) or with a fixed value of parameter in proximity of bifurcation points.

[1] https://github.com/RybakLab/nsm

DATA AVAILABILITY STATEMENT

The datasets generated for this study are available on request to the corresponding author. The simulation software (NSM) and model configuration files are publically available at https://github.com/RybakLab/nsm.

ETHICS STATEMENT

The animal study was reviewed and approved by the University Committee on Laboratory Animals at Dalhousie University.

AUTHOR CONTRIBUTIONS

SD, HZ, NS, IR, and YZ: conceptualization, methodology, and writing (original draft preparation, review, and editing). YZ, HZ, JB-F, and DD-G: experiments. SD and NS: modeling. SD, HZ, and NS: formal analysis and software. HZ and SD: data curation. SD, HZ, and NS: visualization. IR and YZ: supervision, project administration, and funding acquisition.

FUNDING

This work was supported by CIHR grant MOP110950 and NSERC grant RGPIN 04880 (YZ) and NIH grants R01 NS090919 (IR), R01 NS095366 (NS), and R01 NS100928 (SD).

ACKNOWLEDGMENTS

The authors thank Mr. Dallas Bennett for managing the transgenic mice for the experiments.

SUPPLEMENTARY MATERIAL

The Supplementary Material for this article can be found online at: https://www.frontiersin.org/articles/10.3389/fncel.2019.00516/full#supplementary-material

FIGURE S1 | Long-pulse photoactivation did not damage cells. Representative traces of whole cell patch-clamp recordings of ChR2-EYFP positive **(A1)** and negative **(B1)** neurons receiving 3 consecutive 20-s 488 fluorescent light-pulses and representative traces of whole cell patch-clamp recordings of ChR2-EYFP positive **(A2)** and negative **(B2)** neurons injected with 1-s 50 pA depolarization current before (left) and after (right) the 3 light stimulations. **(C)** A lack of response of Ai32 cord to the light.

REFERENCES

Andersson, L. S., Larhammar, M., Memic, F., Wootz, H., Schwochow, D., Rubin, C.-J., et al. (2012). Mutations in DMRT3 affect locomotion in horses and spinal circuit function in mice. *Nature* 488, 642–646. doi: 10.1038/nature11399

Ausborn, J., Shevtsova, N. A., Caggiano, V., Danner, S. M., and Rybak, I. A. (2019). Computational modeling of brainstem circuits controlling locomotor frequency and gait. *eLife* 8:e43587. doi: 10.7554/eLife.43587

Bellardita, C., and Kiehn, O. (2015). Phenotypic characterization of speed-associated gait changes in mice reveals modular organization of locomotor networks. *Curr. Biol.* 25, 1426–1436. doi: 10.1016/j.cub.2015.04.005

Bikoff, J. B., Gabitto, M. I., Rivard, A. F., Drobac, E., Machado, T. A., Miri, A., et al. (2016). Spinal inhibitory interneuron diversity delineates variant motor microcircuits. *Cell* 165, 207–219. doi: 10.1016/j.cell.2016.01.027

Blacklaws, J., Deska-Gauthier, D., Jones, C. T., Petracca, Y. L., Liu, M., Zhang, H., et al. (2015). Sim1 is required for the migration and axonal projections

of V3 interneurons in the developing mouse spinal cord: sim1 functions in the developing spinal cord. *Dev. Neurobiol.* 75, 1003–1017. doi: 10.1002/dneu.22266

Borowska, J., Jones, C. T., Deska-Gauthier, D., and Zhang, Y. (2015). V3 interneuron subpopulations in the mouse spinal cord undergo distinctive postnatal maturation processes. *Neuroscience* 295, 221–228. doi: 10.1016/j.neuroscience.2015.03.024

Borowska, J., Jones, C. T., Zhang, H., Blacklaws, J., Goulding, M., and Zhang, Y. (2013). Functional subpopulations of V3 interneurons in the mature mouse spinal cord. *J. Neurosci.* 33, 18553–18565. doi: 10.1523/JNEUROSCI.2005-13.2013

Bruggencate, G. T., Burke, R., Lundberg, A., and Udo, M. (1969). Interaction between the vestibulospinal tract, contralateral flexor reflex afferents and la afferents. *Brain Res.* 14, 529–532.

Bruggencate, G. T., and Lundberg, A. (1974). Facilitatory interaction in transmission to motoneurones from vestibulospinal fibres and contralateral primary afferents. *Exp. Brain Res.* 19, 248–270. doi: 10.1007/BF00233233

Butera, R. J., Rinzel, J., and Smith, J. C. (1999). Models of respiratory rhythm generation in the pre-Bötzinger complex. II. Populations of coupled pacemaker neurons. *J. Neurophysiol.* 82, 398–415. doi: 10.1152/jn.1999.82.1.398

Butt, S. J. B., and Kiehn, O. (2003). Functional identification of interneurons responsible for left-right coordination of hindlimbs in mammals. *Neuron* 38, 953–963.

Cabaj, A., Stecina, K., and Jankowska, E. (2006). Same spinal interneurons mediate reflex actions of group ib and group ii afferents and crossed reticulospinal actions. *J. Neurophysiol.* 95, 3911–3922. doi: 10.1152/jn.01262.2005

Chopek, J. W., Nascimento, F., Beato, M., Brownstone, R. M., and Zhang, Y. (2018). Sub-populations of spinal v3 interneurons form focal modules of layered pre-motor microcircuits. *Cell Rep.* 25, 146–156.e3. doi: 10.1016/j.celrep.2018.08.095

Courtine, G., and Schieppati, M. (2003a). Human walking along a curved path. I. Body trajectory, segment orientation and the effect of vision. *Eur. J. Neurosci.* 18, 177–190. doi: 10.1046/j.1460-9568.2003.02736.x

Courtine, G., and Schieppati, M. (2003b). Human walking along a curved path. II. Gait features and EMG patterns. *Eur. J. Neurosci.* 18, 191–205. doi: 10.1046/j.1460-9568.2003.02737.x

Crone, S. A., Quinlan, K. A., Zagoraiou, L., Droho, S., Restrepo, C. E., Lundfald, L., et al. (2008). Genetic ablation of V2a ipsilateral interneurons disrupts left-right locomotor coordination in mammalian spinal cord. *Neuron* 60, 70–83. doi: 10.1016/j.neuron.2008.08.009

Danner, S. M., Hofstoetter, U. S., Freundl, B., Binder, H., Mayr, W., Rattay, F., et al. (2015). Human spinal locomotor control is based on flexibly organized burst generators. *Brain* 138, 577–588. doi: 10.1093/brain/awu372

Danner, S. M., Shevtsova, N. A., Frigon, A., and Rybak, I. A. (2017). Computational modeling of spinal circuits controlling limb coordination and gaits in quadrupeds. *eLife* 6:e31050. doi: 10.7554/eLife.31050

Danner, S. M., Wilshin, S. D., Shevtsova, N. A., and Rybak, I. A. (2016). Central control of interlimb coordination and speed-dependent gait expression in quadrupeds. *J. Physiol.* 594, 6947–6967. doi: 10.1113/JP272787

Deska-Gauthier, D., and Zhang, Y. (2019). The functional diversity of spinal interneurons and locomotor control. *Curr. Opin. Physiol.* 8, 99–108. doi: 10.1016/j.cophys.2019.01.005

Dougherty, K. J., Zagoraiou, L., Satoh, D., Rozani, I., Doobar, S., Arber, S., et al. (2013). Locomotor rhythm generation linked to the output of spinal shox2 excitatory interneurons. *Neuron* 80, 920–933. doi: 10.1016/j.neuron.2013.08.015

Forssberg, H., Grillner, S., Halbertsma, J., and Rossignol, S. (1980). The locomotion of the low spinal cat. II. Interlimb coordination. *Acta Physiol. Scand.* 108, 283–295. doi: 10.1111/j.1748-1716.1980.tb06534.x

Frigon, A. (2017). The neural control of interlimb coordination during mammalian locomotion. *J. Neurophysiol.* 117, 2224–2241. doi: 10.1152/jn.00978.2016

Gosgnach, S. (2011). The role of genetically-defined interneurons in generating the mammalian locomotor rhythm. *Integr. Comp. Biol.* 51, 903–912. doi: 10.1093/icb/icr022

Gosgnach, S., Bikoff, J. B., Dougherty, K. J., El Manira, A., Lanuza, G. M., and Zhang, Y. (2017). Delineating the diversity of spinal interneurons in locomotor circuits. *J. Neurosci.* 37, 10835–10841. doi: 10.1523/JNEUROSCI.1829-17.2017

Gosgnach, S., Lanuza, G. M., Butt, S. J. B., Saueressig, H., Zhang, Y., Velasquez, T., et al. (2006). V1 spinal neurons regulate the speed of vertebrate locomotor outputs. *Nature* 440, 215–219. doi: 10.1038/nature04545

Goulding, M. (2009). Circuits controlling vertebrate locomotion: moving in a new direction. *Nat. Rev. Neurosci.* 10, 507–518. doi: 10.1038/nrn2608

Graham Brown, T. (1911). The intrinsic factors in the act of progression in the mammal. *Proc. R. Soc. B Biol. Sci.* 84, 308–319. doi: 10.1098/rspb.1911.0077

Grillner, S. (1981). "Control of locomotion in bipeds, tetrapods, and fish," in *Handbook of Physiology, the Nervous System, Motor Control*, eds J. M. Brookhart, and V. B. Mountcastle, (Bethesda, MD: American Physiological Society), 1179–1236.

Grillner, S. (2006). Biological pattern generation: the cellular and computational logic of networks in motion. *Neuron* 52, 751–766. doi: 10.1016/j.neuron.2006.11.008

Hägglund, M., Dougherty, K. J., Borgius, L., Itohara, S., Iwasato, T., and Kiehn, O. (2013). Optogenetic dissection reveals multiple rhythmogenic modules underlying locomotion. *Proc. Natl. Acad. Sci. U.S.A.* 110, 11589–11594. doi: 10.1073/pnas.1304365110

Haque, F., and Gosgnach, S. (2019). Mapping Connectivity Amongst interneuronal components of the locomotor CPG. *Front. Cell Neurosci.* 13:443. doi: 10.3389/fncel.2019.00443

Haque, F., Rancic, V., Zhang, W., Clugston, R., Ballanyi, K., and Gosgnach, S. (2018). WT1-expressing interneurons regulate left-right alternation during mammalian locomotor activity. *J. Neurosci.* 38, 5666–5676. doi: 10.1523/JNEUROSCI.0328-18.2018

Jankowska, E. (2008). Spinal interneuronal networks in the cat: elementary components. *Brain Res. Rev.* 57, 46–55. doi: 10.1016/j.brainresrev.2007.06.022

Kasumacic, N., Lambert, F. M., Coulon, P., Bras, H., Vinay, L., Perreault, M.-C., et al. (2015). Segmental organization of vestibulospinal inputs to spinal interneurons mediating crossed activation of thoracolumbar motoneurons in the neonatal mouse. *J. Neurosci.* 35, 8158–8169. doi: 10.1523/JNEUROSCI.5188-14.2015

Kiehn, O. (2006). Locomotor circuits in the mammalian spinal cord. *Annu. Rev. Neurosci.* 29, 279–306. doi: 10.1146/annurev.neuro.29.051605.112910

Kiehn, O. (2011). Development and functional organization of spinal locomotor circuits. *Curr. Opin. Neurobiol.* 21, 100–109. doi: 10.1016/j.conb.2010.09.004

Kiehn, O. (2016). Decoding the organization of spinal circuits that control locomotion. *Nat. Rev. Neurosci.* 17, 224–238. doi: 10.1038/nrn.2016.9

Kjaerulff, O., and Kiehn, O. (1997). Crossed rhythmic synaptic input to motoneurons during selective activation of the contralateral spinal locomotor network. *J. Neurosci.* 17, 9433–9447. doi: 10.1523/jneurosci.17-24-09433.1997

Lanuza, G. M., Gosgnach, S., Pierani, A., Jessell, T. M., and Goulding, M. (2004). Genetic identification of spinal interneurons that coordinate left-right locomotor activity necessary for walking movements. *Neuron* 42, 375–386.

Levine, A. J., Hinckley, C. A., Hilde, K. L., Driscoll, S. P., Poon, T. H., Montgomery, J. M., et al. (2014). Identification of a cellular node for motor control pathways. *Nat. Neurosci.* 17, 586–593. doi: 10.1038/nn.3675

Matsuyama, K., Mori, F., Nakajima, K., Drew, T., Aoki, M., and Mori, S. (2004). Locomotor role of the corticoreticular – reticulospinal – spinal interneuronal system. *Prog Brain Res.* 143, 239–249.

McCrea, D. A., and Rybak, I. A. (2007). Modeling the mammalian locomotor CPG: insights from mistakes and perturbations. *Prog. Brain Res.* 165, 235–253.

McCrea, D. A., and Rybak, I. A. (2008). Deletions of rhythmic motoneuron activity during fictive locomotion and scratch provide clues to the organization of the mammalian central pattern generator. *Brain Res. Rev.* 57, 134–146. doi: 10.1016/j.brainresrev.2007.08.006

Pikovsky, A., Michael, R., and Kurths, J. (2001). *Synchronization: A Universal Concept in Nonlinear Science*. Cambridge: Cabridge University Press.

Pikovsky, A., and Rosenblum, M. (2003). Synchronization: a general phenomenon in an oscillatory world. *Nova Acta Leopold* 88, 255–268.

Quinlan, K. A., and Kiehn, O. (2007). Segmental, synaptic actions of commissural interneurons in the mouse spinal cord. *J. Neurosci.* 27, 6521–6530. doi: 10.1523/JNEUROSCI.1618-07.2007

Rossignol, S., Dubuc, R., and Gossard, J.-P. (2006). Dynamic sensorimotor interactions in locomotion. *Physiol. Rev.* 86, 89–154. doi: 10.1152/physrev.00028.2005

Rubin, J. E., Bacak, B. J., Molkov, Y. I., Shevtsova, N. A., Smith, J. C., and Rybak, I. A. (2011). Interacting oscillations in neural control of breathing: modeling and qualitative analysis. *J. Comput. Neurosci.* 30, 607–632.

Rybak, I. A., Dougherty, K. J., and Shevtsova, N. A. (2015). Organization of the mammalian locomotor cpg: Review of computational model and circuit architectures based on genetically identified spinal interneurons. *eNeuro* 2:ENEURO.0069-15.2015. doi: 10.1523/ENEURO.0069-15.2015

Rybak, I. A., Shevtsova, N. A., and Kiehn, O. (2013). Modelling genetic reorganization in the mouse spinal cord affecting left-right coordination during locomotion. *J. Physiol.* 591, 5491–5508. doi: 10.1113/jphysiol.2013.261115

Rybak, I. A., Shevtsova, N. A., Lafreniere-Roula, M., and McCrea, D. A. (2006a). Modelling spinal circuitry involved in locomotor pattern generation: insights from deletions during fictive locomotion. *J. Physiol.* 577, 617–639. doi: 10.1113/jphysiol.2006.118703

Rybak, I. A., Stecina, K., Shevtsova, N. A., and McCrea, D. A. (2006b). Modelling spinal circuitry involved in locomotor pattern generation: insights from the effects of afferent stimulation. *J. Physiol.* 577, 641–658. doi: 10.1113/jphysiol.2006.118711

Rybak, I. A., Shevtsova, N. A., Ptak, K., and McCrimmon, D. R. (2004). Intrinsic bursting activity in the pre-Bötyinger complex: role of persistent sodium and potassium currents. *Biol. Cybern.* 90, 59–74. doi: 10.1007/s00422-003-0447-1

Shevtsova, N. A., and Rybak, I. A. (2016). Organization of flexor-extensor interactions in the mammalian spinal cord: insights from computational modelling. *J. Physiol.* 594, 6117–6131. doi: 10.1113/JP272437

Shevtsova, N. A., Talpalar, A. E., Markin, S. N., Harris-Warrick, R. M., Kiehn, O., and Rybak, I. A. (2015). Organization of left-right coordination of neuronal activity in the mammalian spinal cord: insights from computational modelling. *J. Physiol.* 593, 2403–2426. doi: 10.1113/JP270121

Talpalar, A. E., Bouvier, J., Borgius, L., Fortin, G., Pierani, A., and Kiehn, O. (2013). Dual-mode operation of neuronal networks involved in left–right alternation. *Nature* 500, 85–88. doi: 10.1038/nature12286

Yang, J. F., Lamont, E. V., and Pang, M. Y. C. (2005). Split-belt treadmill stepping in infants suggests autonomous pattern generators for the left and right leg in humans. *J. Neurosci.* 25, 6869–6876. doi: 10.1523/JNEUROSCI.1765-05.2005

Zhang, J., Lanuza, G. M., Britz, O., Wang, Z., Siembab, V. C., Zhang, Y., et al. (2014). V1 and V2b interneurons secure the alternating flexor-extensor motor activity mice require for limbed locomotion. *Neuron* 82, 138–150. doi: 10.1016/j.neuron.2014.02.013

Zhang, Y., Narayan, S., Geiman, E., Lanuza, G. M., Velasquez, T., Shanks, B., et al. (2008). V3 spinal neurons establish a robust and balanced locomotor rhythm during walking. *Neuron* 60, 84–96. doi: 10.1016/j.neuron.2008.09.027

Zhong, G., Shevtsova, N. A., Rybak, I. A., and Harris-Warrick, R. M. (2012). Neuronal activity in the isolated mouse spinal cord during spontaneous deletions in fictive locomotion: insights into locomotor central pattern generator organization. *J. Physiol.* 590, 4735–4759. doi: 10.1113/jphysiol.2012.240895

Conflict of Interest: The authors declare that the research was conducted in the absence of any commercial or financial relationships that could be construed as a potential conflict of interest.

frontiers in Systems Neuroscience

ORIGINAL RESEARCH
published: 15 January 2020
doi: 10.3389/fnsys.2019.00082

Novel Activity Detection Algorithm to Characterize Spontaneous Stepping During Multimodal Spinal Neuromodulation After Mid-Thoracic Spinal Cord Injury in Rats

Raymond Chia[1,2], Hui Zhong[3], Bryce Vissel[1,2], V. Reggie Edgerton[1,3,4,5,6,7] and Parag Gad[1,4]**

[1] Faculty of Science, Centre for Neuroscience and Regenerative Medicine, University of Technology Sydney, Sydney, NSW, Australia, [2] St Vincent's Centre for Applied Medical Research, Sydney, NSW, Australia, [3] Department of Integrative Biology and Physiology, University of California, Los Angeles, Los Angeles, CA, United States, [4] Department of Neurobiology, University of California, Los Angeles, Los Angeles, CA, United States, [5] Department of Neurosurgery, University of California, Los Angeles, Los Angeles, CA, United States, [6] Brain Research Institute, University of California, Los Angeles, Los Angeles, CA, United States, [7] Institut Guttmann, Hospital de Neurorehabilitació, Institut Universitari Adscrit a la Universitat Autònoma de Barcelona, Barcelona, Spain

OPEN ACCESS

Edited by:
Michelle Maria Rank,
The University of Melbourne, Australia

Reviewed by:
Marin Manuel,
Université Paris Descartes, France
László Demkó,
Balgrist University Hospital, Switzerland
Andrew C. Smith,
Regis University, United States

***Correspondence:**
V. Reggie Edgerton
vre@ucla.edu
Parag Gad
paraggad@gmail.com

Received: *13 September 2019*
Accepted: *16 December 2019*
Published: *15 January 2020*

Citation:
Chia R, Zhong H, Vissel B, Edgerton VR and Gad P (2020) Novel Activity Detection Algorithm to Characterize Spontaneous Stepping During Multimodal Spinal Neuromodulation After Mid-Thoracic Spinal Cord Injury in Rats. Front. Syst. Neurosci. 13:82. doi: 10.3389/fnsys.2019.00082

A mid-thoracic spinal cord injury (SCI) severely impairs activation of the lower limb sensorimotor spinal networks, leading to paralysis. Various neuromodulatory techniques including electrical and pharmacological activation of the spinal networks have been successful in restoring locomotor function after SCI. We hypothesized that the combination of self-training in a natural environment with epidural stimulation (ES), quipazine (Quip), and strychnine (Strych) would result in greater activity in a cage environment after paralysis compared to either intervention alone. To assess this, we developed a method measuring and characterizing the chronic EMG recordings from tibialis anterior (TA) and soleus (Sol) muscles while rats were freely moving in their home cages. We then assessed the relationship between the change in recorded activity over time and motor-evoked potentials (MEPs) in animals receiving treatments. We found that the combination of ES, Quip, and Strych (sqES) generated the greatest level of recovery followed by ES + Quip (qES) while ES + Strych (sES) and ES alone showed least improvement in recorded activity. Further, we observed an exponential relationship between late response (LR) component of the MEPs and spontaneously generated step-like activity. Our data demonstrate the feasibility and potential importance of quantitatively monitoring mechanistic factors linked to activity-dependence in response to combinatorial interventions compared to individual therapies after SCI.

Keywords: sub-threshold spinal cord stimulation, spinal cord injury, spontaneous cage activity, EMG, muscle coordination, strychnine, quipazine, evoked potentials

INTRODUCTION

Numerous studies of different animal models of spinal cord injury (SCI) have demonstrated that modulating the physiological states of spinal networks, pharmacologically and electrically and in combination with motor training enables improved motor performance (Edgerton et al., 2004; Ichiyama et al., 2005; Gerasimenko et al., 2008; Lavrov et al., 2008; Courtine et al., 2009; Harkema et al., 2011; Rossignol and Frigon, 2011; Gad et al., 2013a,b; Angeli et al., 2014; Gerasimenko Y. et al., 2015; Capogrosso et al., 2016; Formento et al., 2018; Gill et al., 2018). Specific pharmacology methods including the use of quipazine (Quip) (Fong et al., 2005; Ichiyama et al., 2008b; Gad et al., 2015; Taccola et al., 2018) and strychnine (Strych) (de Leon et al., 1999; Gad et al., 2013b, 2015) have been effective in activation in the locomotor spinal neural networks to enable locomotor activity in rodent with severe paralysis. Similar interventional approaches have been observed in humans with a severe spinal injury (Gerasimenko Y. et al., 2015; Gerasimenko Y. P. et al., 2015). Recently, we explored the effects of long-term sub-motor threshold ES in rats with complete mid-thoracic spinal transections (Gad et al., 2013a). These data demonstrated that when rats received sub-motor threshold ES moved around their home cages five times more than when they were not receiving ES, thus demonstrating the possibility to use ES to enable "self-training" in an environment while patients could be performing routine activities of daily living.

The objective of this study was to identify spinal rat's hindlimb stepping like activity based on EMG patterns and to quantify the effects of multi-modal neuromodulation on spontaneous locomotor activity in standard individual housing cages. We hypothesized that multiple neuromodulatory modalities can transform non-functional spinal networks into more excitable physiological states to enable "self-training" in freely moving spinal rats in their home environments. In addition, motor-evoked potentials (MEPs) observed in hindlimb EMG signals could present a functional biomarker of these novel physiological states (Gad et al., 2015). Spinal rats that had previously been trained to step on a treadmill in presence of Strych and Quip were tested in their home cages under five different conditions, i.e., no ES (Pre), ES, ES + Quip (qES), ES + Strych (sES), and ES + Quip + Strych (sqES). To test these hypotheses, we developed a novel Thresholding Offline Kinematic and EMG Data Analysis method (TOKEDA) to characterize motor behaviors to neuromodulatory interventions. TOKEDA has the capability to be scaled up or down with respect to its sensitivity to detect multiple movement and electrophysiological events during spontaneous activity under different environments.

MATERIALS AND METHODS

Animal Preparation and Care

Data were obtained from four adult female Sprague Dawley rats (270–300 g body weight). Pre and post-surgical animal care procedures have been described previously (Roy et al., 1992). The rats were housed individually in cages with food and water provided *ad libitum*. All survival surgical procedures were conducted under aseptic conditions and with the rats deeply anesthetized with isoflurane gas (1.5–2%) administered via facemask. All procedures described below are in accordance with the National Institute of Health Guide for the Care and Use of Laboratory Animals and approved by the Animal Research Committee at UCLA.

Head Connector and Intramuscular EMG Electrode Implantation

A small incision was made at the midline of the skull. The muscles and fascia were retracted laterally, small grooves were made in the skull with a scalpel, and the skull was dried thoroughly. Two amphenol head connectors with Teflon-coated stainless steel wires (AS 632, Cooner Wire, Chatsworth, CA, United States) were securely attached to the skull with screws and dental cement as described previously (Ichiyama et al., 2008a). The tibialis anterior (TA, ankle flexor) and soleus (Sol) (ankle extensor) muscles were implanted bilaterally with intramuscular EMG recording electrodes (Roy et al., 1992). Skin and fascial incisions were made to expose the belly of each muscle. Two wires extending from the skull-mounted connector were routed subcutaneously to each muscle. The wires were inserted into the muscle belly with a 23-gauge needle, and a small notch (0.5–1.0 mm) was removed from the insulation of each wire to expose the conductor and form the recording electrodes. The wires were secured within the belly of each muscle via a suture on the wire at its entrance into and exit from the muscle belly. The proper placement of the electrodes was verified during the surgery by stimulation through the head connector and postmortem via dissection.

Spinal Cord Transection and Electrode Implantation Procedures and Post-surgical Animal Care

A partial laminectomy was performed to expose the T8–T9 spinal cord, and then a complete spinal cord transection to include the dura was performed with microscissors. Two surgeons verified the completeness of the transection by lifting the cut ends of the spinal cord with fine forceps and passing a glass probe through the lesion site. Gel foam was inserted into the gap created by the transection as a coagulant and to separate the cut ends of the spinal cord. For epidural electrode implantation, partial laminectomies were performed to expose the spinal cord levels L2 and S1. Two Teflon-coated stainless steel wires from the head connector were passed under the spinous processes and above the dura mater of the remaining vertebrae between the partial laminectomy sites. After a small portion (∼1-mm notch) of the Teflon coating was removed and the conductor was exposed on the surface facing the spinal cord, the electrodes were sutured to the dura mater at the midline of the spinal cord above and below the electrode sites with 8.0 Ethilon suture (Ethicon, New Brunswick, NJ, United States). Two common ground (indifferent EMG and ES) wires (∼1 cm of the Teflon removed distally) were inserted subcutaneously in the mid-back region on the right side (EMG) and midline (ES) close to the tail. All wires (for both EMG

and ES) were coiled in the back region to provide stress relief. All incision areas were irrigated liberally with warm, sterile saline. All surgical sites were closed in layers with 5.0 Vicryl (Ethicon, New Brunswick, NJ, United States) for all muscle and connective tissue layers and for the skin incisions in the hind-limbs and 5.0 Ethilon for the back skin incision. Buprenex (0.01–0.05 mg/kg s every 8–12 h) was used to provide analgesia. Analgesics were initiated before completion of the surgery and continued for a minimum of 2 days. The rats were allowed to recover fully from anesthesia in an incubator. The rats were housed individually in cages that had ample CareFresh bedding, and the bladders of the spinal rats were expressed manually three times daily for the first 2 weeks after surgery and two times daily thereafter. The hind-limbs of the spinal rats were moved passively through a full range of motion once per day to maintain joint mobility. All of these procedures have been described in detail previously (Courtine et al., 2009).

Training Procedures

All rats were trained for bipedal stepping and standing on a motor driven rodent body weight supporting treadmill for 5 days/week, 20 min/day for 6 weeks starting at 12 days post-injury (dpi), including the days of testing (de Leon et al., 2002). Bipolar ES between L2 and S1 (current flowing from L2 to S1) at frequency of 40 Hz, pulse width 0.2 ms was used in combination with Quip (0.3 mg/kg; de Leon et al., 1999) and Strych (0.5 mg/kg; Gad et al., 2013a) injected intraperitoneally 10 min before each training/testing session. ES was only delivered during the 20 min/day training periods as described previously (Ichiyama et al., 2005). Chronic step training was used to train and reinforce locomotor neural networks that generate spontaneous cage activity (Gad et al., 2013a). At the early stages of training, ES intensity was set at threshold or at super-threshold to invoke locomotive activity. As training continued, the stimulation intensity was gradually reduced, dependent upon the stepping performance of each rat until the stimulation intensity of below threshold.

Stimulation and Testing Procedures

The threshold for eliciting muscle twitch and corresponding time linked EMG response in the Sol was identified. The sub-threshold level was set to 20% below the motor threshold during the recording of spontaneous cage activity. ES was delivered only during the training and testing periods. Each rat prior to testing was injected intraperitoneally 10 min prior to beginning the testing, with the prescribed neuromodulating pharmacology. The spontaneous activity of the spinal rats was determined in their home cage. Spinal rats that had previously been trained to step on a treadmill in presence of Strych and Quip were tested under five different conditions, i.e., no ES (Pre), ES, ES + Quip (qES), ES + Strych (sES), and ES + Quip + Strych (sqES). The head connector was coupled to a set of amplifiers and a stimulator. The swivel arrangement was attached to allow the rats to roam freely in the cage. There was food distributed throughout the cage floor to encourage movement and exploration. IR video data were recorded using a camcorder for select conditions. EMG data were amplified and recorded using custom LabView-based data acquisition software with a sampling frequency of 10 kHz (**Figure 1F**). Data were recorded continuously for 6 h between 8 p.m. and 2 a.m. One out of the 20 experiments ($n = 4$ rats, five experiments/rat) were conducted every night and were randomized with at least 1 day gap between two successive recordings for a rat and all 20 experiments were completed within 3 weeks. Note that the first 20 min EMG recordings for rat #1 in the sqES and all recording channels for rats #2 and #4 for the ES only case were corrupted and unable to be used.

Signal Processing

The raw EMG signal was filtered with a third order Butterworth bandpass filter with cut-off frequencies of 30–1000 Hz (**Figure 1A**). This attenuates DC offset and higher frequency noise. To make the signal more sensitive to change, the bandpass filtered signal was fed into a Teiger Keiser Energy Operator (TKEO) algorithm (Solnik et al., 2010). The output was rectified and smoothened across a 50-Hz cut-off low pass filter (**Figure 1B**).

Thresholding

To determine the threshold of activity across each channel, the 6 h recordings were broken up in to 10 s bins (**Figure 1F**). A threshold sampling method was used to determine periods of rest throughout each bin. To find periods of rest, the data were averaged across 10 ms and the minimum was selected as the first point of interest. A sliding window procedure was implemented to approximate the entire period of rest within the 10 s bin. This was limited by a first differential magnitude of 0.1 mV/s or logarithmic threshold of 300 ln (mV). It was found that during periods of slower, more gradual ramping EMG activity, the first and second differential values were not sufficiently sensitive. To account for slow ramping activity, the logarithmic threshold was implemented. This enables the software to detect both quick and slower adapting changes across the EMG signal.

A double thresholding mechanism was used to detect bursts of EMG. The mean and standard deviation of the detected rest period was calculated and used to determine a threshold for EMG magnitude. Given the circumstance of recording and filtering, a scaling constant (J) of 7 was used. Finally, to complete the double thresholding, a time criterion was implemented for each channel, where the TA channel time threshold was 0.1 s and Sol channel time threshold was 0.3 s. If the signal magnitude was below the time threshold, it was not considered bursting activity. The minimum criteria for an EMG magnitude to remain above the motor threshold as defined by:

$$\text{threshold} = \mu_{\text{rest}} + J^{*}\sigma_{\text{rest}}$$

For an example of a period of an EMG signal which met the magnitude threshold but not the time criteria, see the RSol channel of **Figure 1A**.

Activity Detection

To detect instances of step-like behavior, a dataset was generated using IR video data. A total of 26.7 h of video data was collected. Step-like, standing, and rest events were compiled into a dataset of activity. These data were then synchronized with

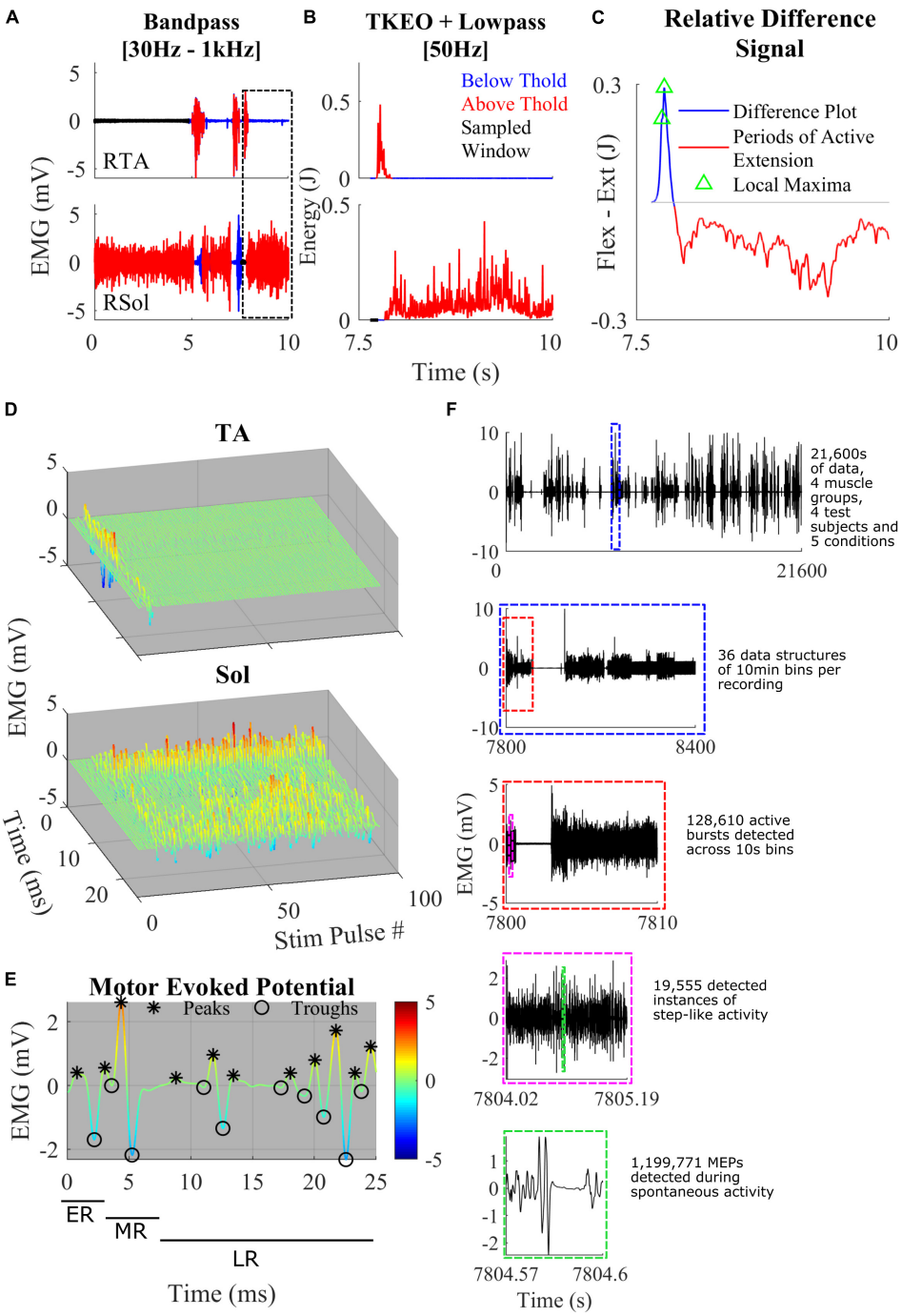

FIGURE 1 | (A) Representative band-pass filtering of TA and Sol. The boxed area shows a close-up example of the thresholding and the normalized difference plot used to characterize step-like activity. Regions of the signal below threshold (blue), above threshold (red), and rest (black) were recorded. **(B)** TKEO signal conditioned, rectified, and smoothed EMG signal from the TA and Sol muscle of a spinal rat during spontaneous cage activity. A representative example of a singular hind-limb step within the first hour of recording spontaneous activity. **(C)** The relative difference between the normalized values of the TA and Sol from graphs **(B)**. The gray line *y*-axis = 0. The blue line is a trace of the relative difference plot and in red is the periods of active extension, identified through thresholding. Green triangles represent points of local maxima during active flexion. These features were used to detect spontaneous hind-limb step-like activity. **(D)** A singular identified step using the TOKEDA method as summarized in graphs **A–C**. This plot illustrates motor evoked potentials (MEPs) over time for the tibialis anterior (TA) and Soleus (Sol), respectively. **(E)** A representative MEP from the TA recording shown in panel **D**. Color scaling reflects amplitude in mV. Note the windows marking the early, middle, and late responses and peaks (*) and troughs (o). **(F)** A breakdown of the volume of data involved within the experiments and the process of data structure and analysis. Out of four possible channels, displayed in the top-most subplot is the full 6 h EMG recording of RSol from a singular treatment. Highlighted within the dashed blue box is a 10-min section in which the total hour was sectioned to give a total of 36 files per 6 h recording. The dashed red line bins the 10-min files for thresholding, burst detection, and step detection. The dashed magenta box represents a singular instance of step-like activity from the beginning of swing to the end of the stance phase. Within the dashed green box is a singular MEP measured within a singular instance of the step-like event.

EMG recordings of the TA and Sol of both left and right hindlimbs to produce 300 EMG samples from a combined total of 217 step-like events and 83 non-functional activity events. While there were several standing events detected throughout the 6 h period, analyses were limited to step-like events only.

A relative difference signal between a normalized TA and Sol recording was calculated to determine instances of spontaneous step-like activity (**Figure 1C**). The TA and Sol signals were normalized to account for missing force-EMG measurements. This signal was used as a representation of coordination between extension and flexion of the ankle. It was assumed that if the signal was positive, the ankle was applying a greater flexion force on the joint compared to extension, vice versa for negative magnitudes. A peak during the positive region of a signal followed by a sharp dip into the negative portion of the signal was associated with the reduction in flexion activity during swing phase and an activation of extensors during the stance phase. Peaks from the relative difference signal were only considered if they were positive in magnitude and during an active TA EMG burst. By using the active burst regions as a "filter," many false positives of locomotion initiation were removed.

For conservative activity detection, a step was only registered when a positive peak was followed by a negative signal during an active extension EMG burst achieved within a threshold of 0.5 s. Only peaks with a magnitude greater than the difference threshold of 0.01, in the relative difference signal and only magnitude differences greater than the difference threshold were considered. The time and magnitude thresholds were characterized from numerous test examples in the given dataset. In order to filter coordination and reflect false positives, a time threshold for active Sol burst was characterized at 0.25 s. Finally, a minimum period between each local maxima of 0.2 s was set. This was to ensure that only the last local maxima within the TA burst was selected.

Accuracy was defined as the ratio between correctly detected events over the total number of sampled events. Precision was defined as the number of true positives out of both true and false positives; thus, an estimate of the number of actual step-like events detected. Recall was defined as the number of true positives out of false negatives and true positives; thus, an estimate for detecting all relevant step-like events within the existing dataset.

For a complete algorithm process illustration, refer to **Figure 2**.

MEP Analysis

For granular electrophysiological analysis, the entire step cycle was defined from the beginning of the swing phase to the end of the stance phase. This was set at the point where the relative difference signal first reaches zero before the detected peak and where the negative signal reaches zero or the extension EMG burst has ended (**Figure 1C**). With these defined windows of step-like activity, MEPs were analyzed to extract electrophysiological features such as the number of positive peaks and integrated EMG for both the middle and late response (LR) (**Figures 1D,E**). The MEPs were extracted from the bandpass-filtered EMG data. Using a recording of the stimulation pulses, the end of each 40 Hz stimulation pulse was used to separate the EMG signal into 25 ms MEPs. The early response (ER), middle response (MR), and LR time windows were defined as 1–4, 4–7, and 7–25 ms, respectively (**Figure 1E**). To successfully detect the peaks and troughs of the MEP signal, a threshold using the second differential was used. Each MEP was interpolated to double the number of points. Using the interpolated signal, the local maxima and local minima with a minimum separation of 0.6 ms and minimum prominence of 0.2 were found. These local maxima and minima were filtered through a second differential threshold of 1.5×10^6 such that only peaks and troughs that met the threshold criteria were accepted (**Figure 1C**). This was used to calculate the area under the curve (IEMG), peak-to-peak, and total number of peaks.

Statistical Analyses

All data reported as means ± standard error (SE). Statistically significant differences were determined using a one-way ANOVA with the Tukey–Kramer *post hoc* test, correlation coefficients were calculated using Pearson's linear coefficient. All statistical difference was set at $P < 0.05$. All results reporting step-like activity were normalized to no intervention (Pre) measurements.

RESULTS

Task Recognition Validity

To test the validity of the task recognition algorithm derived from the relative difference signal, the point of change from flexion phase to extension phase during a "step-like" event was logged (difference signal equals zero). A dataset of IR video and EMG-derived step-like examples were collected to form the human-observation-based dataset. In this dataset, the onset and completion of a step-like or rest event for each limb was logged to a millisecond precision. The human-observation dataset comprised of 300 EMG samples from a combined total of 217 step-like events and 83 non-functional activity events. A validation script checked the algorithm event log against the human-observation dataset. To gather a sense of relevance in detected step-like patterns, accuracy, precision, and recall were calculated from the validation script. The relative difference signal detected step-like activity performed with an accuracy of 83%, precision of 88%, and recall of 89%.

Electropharmacological Treatments Modulate the Functional State of Spinal Circuitry

All interventional conditions increased the number of spontaneous step-like activity compared to baseline (Pre-intervention) (**Figure 3**). Quip or Strych significantly increased the number of recorded step-like activity in all animals tested. A significant level of variability was observed among rats, especially in the qES and sqES experiments. However, sqES treatment generated the highest number of steps recorded when compared to Pre and ES ($P < 0.05$).

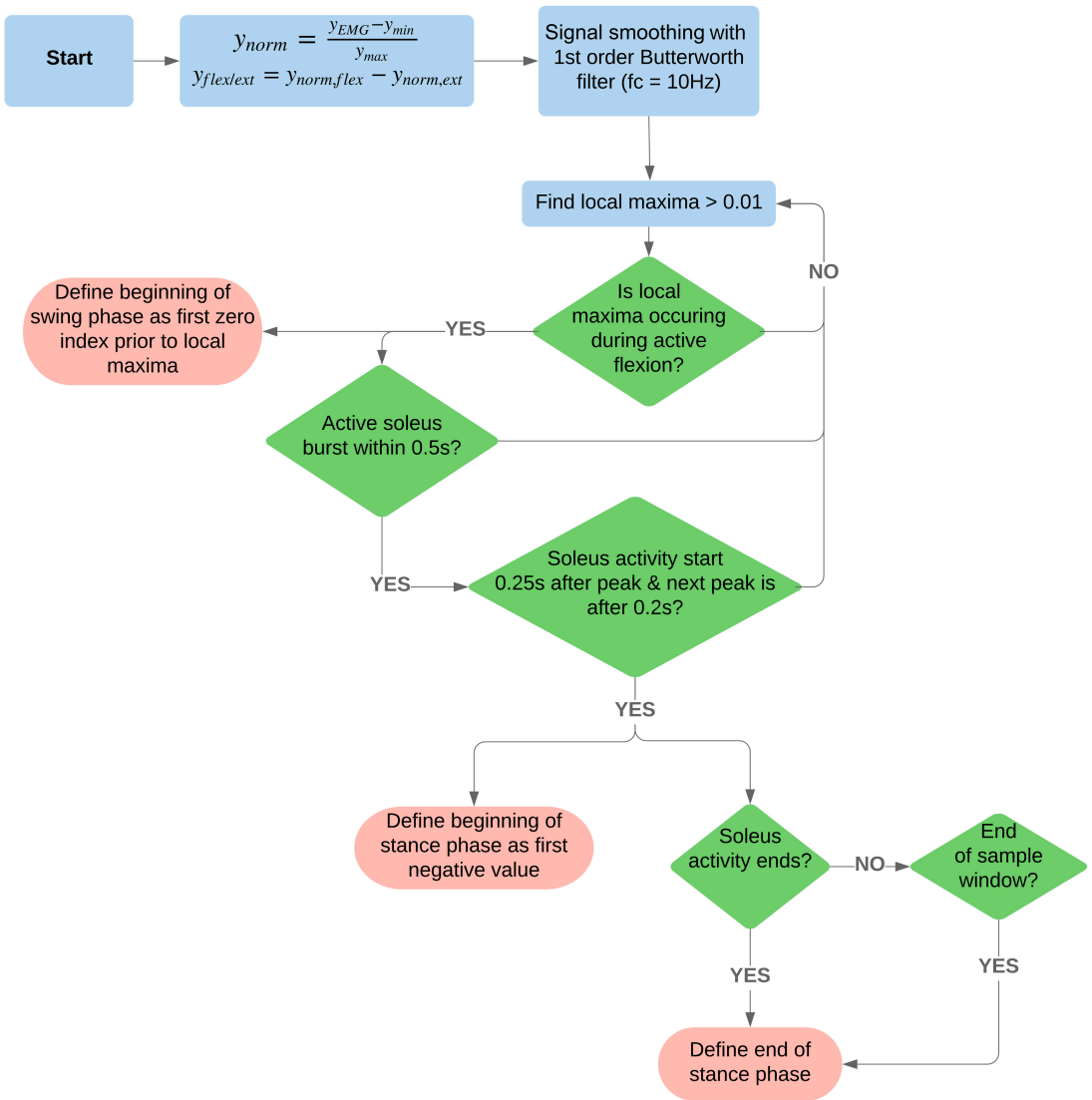

FIGURE 2 | Flowchart of the signal processing and algorithm used to detect beginning and end of swing and stance phases. For access to the code, see the following GitLab repository, https://code.research.uts.edu.au/13035516/tokeda.git.

Since a single bolus dose of a pharmacological treatment was administered at the start of the experiment, we observed a time-dependent phenomenon in the number of steps detected with the greatest level of activity observed in the first 120 min (**Figure 4**). These observations were specific to the rapid registration of step-like activity for sqES and qES treatments (**Figure 5B**). This time-dependent phenomenon was not observed in Pre or ES cases. The stepping activity occurred stochastically throughout the 6 h (**Figures 4**, **5B**). Spontaneous step-like activity during the first 120 min occurred with longer, more consistent step lengths and increased muscle activity during sqES and qES (**Figures 4**, **5A,B**). During continuous stepping activity, an average stance period of ∼2 s was observed (**Figure 4**). Both the step activity and stance period across the population had lower variability during sqES compared to other conditions tested (**Figures 4**, **5B**). A smaller variance was present in the sqES stance period compared to qES within the first 2 h. In addition, during the entire 6-h period, overall left–right symmetry was maintained suggesting a bipedal response (**Figure 4**).

Inclusion of multiple pharmacological agents in the presence of ES resulted in a more consistent and greater IEMG response (**Figure 5A**). While sES reduced the variability across both extensor and flexor muscles in the hindlimbs, the inclusion of Quip significantly increased IEMG magnitude compared to Pre ($P < 0.05$) (**Figures 5A**, **6A**). For the ES and Pre treatments, the IEMG of TA differed in shape compared to Sol with wider error bands while the sES, qES, and sqES relatively coordinated activity in the TA and Sol muscles with narrower error bands were observed (**Figure 5A**). Differences between TA and Sol may be explained by the higher occurrence of

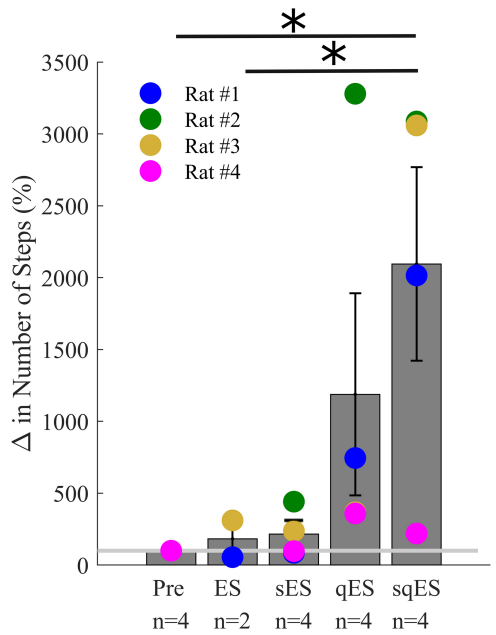

FIGURE 3 | Mean% change in step-like events for each rat over the 6-h period for each treatment (*). The light gray line is set at 100%, normalized to pre-treatment for each rat. Results for sqES were significantly different compared to Pre and ES ($P < 0.05$).

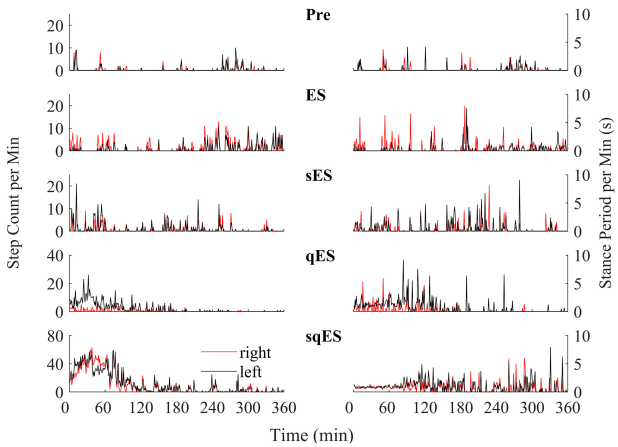

FIGURE 4 | An example of the step-like activity across interventions plotted as number of steps per minute and mean stance periods for the **left** (black) and **right** (red) hind limb for rat #3. For other rat performances, refer to **Supplementary Figures 1–3**.

co-contractions and organized coordinated activity during the pharmacological interventions. The steep gradient was only observed during the first 2 h of sqES and qES and becomes more linear during hours 2–6, possibly indicating the effective half-life of the drug. Significant correlation was observed between the overall muscle activity (IEMG) and the steps registered across both right hind-limb muscles (**Figure 6C**, $P < 0.05$). Both sqES and qES have an exponential relationship between IEMG and step-like activity, while sES, ES, and Pre reflect a linear correlation. sqES intervention had the largest SE across both the *x*- and *y*-axes of **Figure 6C** whereas sES and Pre have minimally discernible spread among the sampled population. Increased baseline tone in Sol during rest correlates ($R = 0.6943$, $P < 0.05$) with the increased step-like activity across all conditions and rats and consistent with the overall summed IEMG across the 6 h (**Figure 6B**). There appears to be a breakaway condition given the logarithmic response in the basal tone in Sol represented (**Figure 6B**).

Evoked Responses Correlate With Spontaneous Step-Like Activity

Motor-evoked potentials were analyzed across the Sol during spontaneous step-like activity as these signals more accurately reflect the state of the neural networks associated with the trained task. The detected peaks in the middle and LRs (MRs and LRs) of the Sol during spontaneous step-like activity in their home cages were exponentially correlated (**Figure 7**). Due to the sub-threshold nature of spinal stimulation, the evoked responses appeared to be non-time linked to the stimulation pulses when compared to suprathreshold stimulation on a treadmill (Gad et al., 2013b). Each of the treatments had linear regression applied to both the LRs and MRs. Both ES and sES display a negative gradient associative with decreasing change in step-like activity when compared with Pre while qES and sqES have a steep positive gradient. The combination of all data points was fitted to an exponential equation where both the LRs and MRs have a similar relationship with step-like activity, the MR trend has a lower first-order coefficient when compared to the LR. As anticipated, the sqES and qES evoked the highest number of LRs and MRs which corresponded to a greater number of detected spontaneous step-like activity.

DISCUSSION

We developed a method for identifying spinal rat's hind-limb stepping like activity based on EMG patterns recorded from the Sol and TA to determine the effects of multi-modal neuromodulation on spontaneous locomotor activity in standard individual housing cages. These results describe the functional and electrophysiological changes in response to activity-specific training in combination with enabling ES and pharmacological interventions. For access to longitudinal functional analyses, refer Gad et al. (2015). This experiment was conducted to determine the feasibility of developing a quantitative electrophysiological assessment tool of spontaneous cage activity of rats as an estimate of neuromuscular activity.

Several strategies have been developed for detecting rat activity within a caged setting using a variety of sensing methods. These include the use of vibration/tilt sensing (Parreno et al., 1985; Megens et al., 1987; Ganea et al., 2007), IR beams (Clarke et al., 1985), IR and non-IR video tracking (Tamborini et al., 1989; Morrel-Samuels and Krauss, 1990; Aragão et al., 2011; Gad et al., 2013a; York et al., 2013), capacitive flooring (Pernold et al., 2019), optical touch sensors (Mendes et al., 2015), RFID (Redfern et al.,

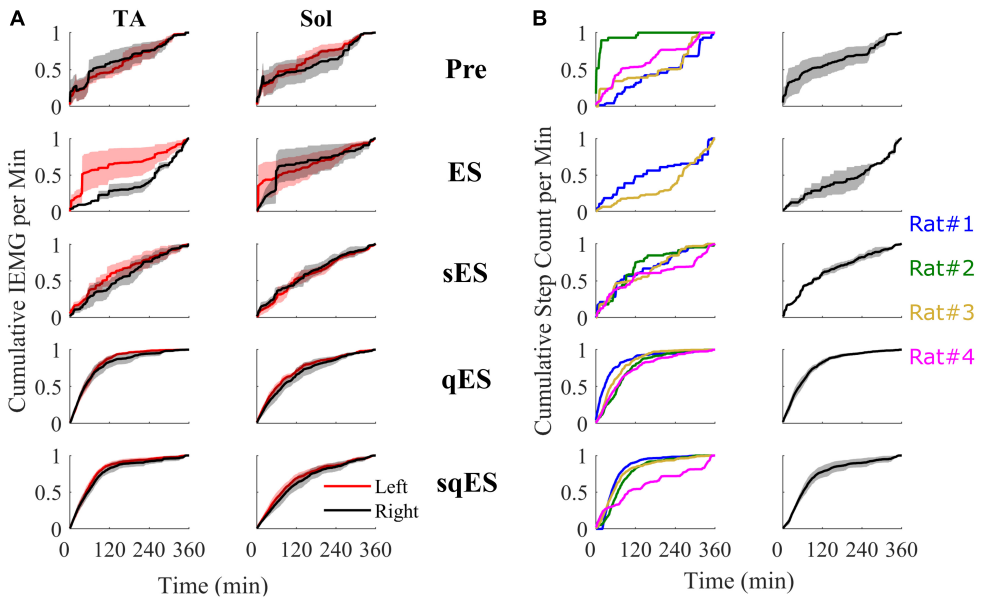

FIGURE 5 | All cumulative sum plots are normalized per animal from 0 to 1. **(A)** Cumulative sum of IEMG in of the left and right TA and Sol. **(B)** On the left is a cumulative sum plot of the step-like events occurring over time for each treatment (blue, red, gold, and magenta represents rat #1, #2, #3, and #4, respectively). On the right is the averaged cumulative sum plot. Shaded is the standard error.

2017), and radar technology (Martin and Unwin, 1980; Rose et al., 1985; Young et al., 1996; Genewsky et al., 2017). Most pattern recognition approaches based on EMG recordings have been used to control prosthetics (Huang et al., 2009, 2010). A more complex approach involves the use of Hidden Markov Models (HMMs) to represent stochastic processes using time series data to predict the probability of model states (Lee, 2008). However, the detection of spontaneous self-recovering movement after paralysis outside of a controlled clinical environment is rarely explored quantitatively due to the limitation associated with securely attaching sensors or markers at specific locations, etc. Use of antennas attached to a rat have been used to track gross body movements through a maze of tubes. It was shown that self-motivated training within a "enriched environment" lead to superior performance in skilled movement compared to restricted task-specific training. This "RatTrack" system allows for testing self-initiated and task-specific training and dose–responses (Starkey et al., 2014). While the mentioned efforts can be extended in the direction of automation, each of these methods lack the ability to have a direct measurement of the neuromotor parameters. TOKEDA relies solely on chronically implanted EMG electrodes for sensing to assess *in vivo* responses to different combinations of electrical and pharmacological neuromodulatory interventions. Having access to neuromuscular activity synchronized with stimulation pulses directly linked to behaviors provides a direct and realistic measurements of reorganizing neural networks throughout a chronic period as the nervous system becomes more functional (Edgerton et al., 2008). As the MEPs and associated behavior are directly linked from an "input–output" relationship, we hypothesize that a biomarker for reorganization may be discernible from the presented data. This notion has been reflected in past research papers (Lavrov et al., 2006, 2008; Gad et al., 2015; Alam et al., 2017). Unfortunately, without the use of kinematic recordings, information such as locomotion speed, step quality, step length, and other kinematic-related metrics remain remarkedly rare given the availability of the appropriate technologies.

Long-term recordings of electrophysiological data in laboratory animals and humans before and after treatment for a dysfunction have been performed previously (Alaimo et al., 1984). The existing hypothesis regarding the possibility of electrophysiological biomarkers is the emergence of MRs and LRs in MEPs during activity-driven training (Lavrov et al., 2006, 2008; Gad et al., 2015). There appear to be underlying neurological mechanisms involved in time-related modulation in MEPs during treadmill activities. In Gad et al. (2015), it was shown that re-emergence in LRs and reduced MRs with changes in modulation of flexor extensor motor pools reflect plasticity of the neural networks. Another study reports a correlation between the MR and LR with changes in the EMG activity level of the corresponding muscle, perhaps, reflecting in part monosynaptic and polysynaptic pathways, respectively, to motor pools (Gerasimenko et al., 2006). In the present paper, we explore the characteristics of the same signals during spontaneous *in vivo* step-like activity within an enriched caged environment. Paralleled between these findings, **Figure 7** presents an exponentially increasing trend between the emergence of LRs and the functional response to hind-limb step training. Notably, while Gad et al. (2015) concludes a reduced reliance on MRs may indicate a change in targeted neural networks and neuro-plastic mechanisms, **Figure 7** illustrates no distinct difference between LRs and MRs beside a

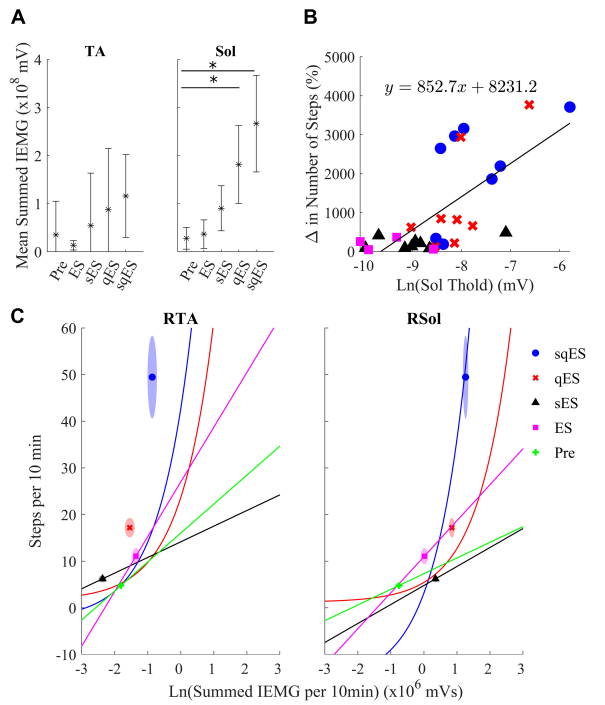

FIGURE 6 | (A) The average sum of IEMG across all the animals in each treatment in the TA and Sol channels for both sides and the 95% confidence interval. The Sol channel for sqES and qES was significantly different from Pre (*$P < 0.05$). There is a trend of increasing mean and standard error in IEMG in both TA and Sol as more interventions are introduced on top of ES. **(B)** The graph depicts the relationship of the calculated EMG amplitude threshold required to determine burst activity of the neural networks in the Sol and the change in step-like activity normalized to pre intervention for all rat subjects in both hindlimbs. The treatments, sqES, qES, sES, and ES are plotted in blue, red, black, and magenta, respectively. A linear regression of the natural logarithm of Sol threshold values against the normalized change in step-like activity results in $R = 0.6943$. Inclusion of pharmacology and ES increases the ln(Sol) threshold, only qES and sqES have drastic change in detected step-like events. **(C)** Ln(Total IEMG/10 min) plotted against step-like events/10 min across 6 h for sqES, qES, sES, ES, and Pre in the right hind-limb. In the corresponding shaded area is the standard error for the *x*- and *y*-axis represented in an ellipse. A Pearson's linear correlation coefficient reveals significant positive correlation in all interventions for both hind-limbs ($P < 0.05$ in all cases). While the sES, ES, and Pre interventions are linearly correlated, the qES and sqES have an exponential relationship between the natural log of the total IEMG/10 min and the step-like events/10 min. Note that sqES, qES, and ES have a distinct *y*-axis error bound while the *x*-axis error bound is less notable. This is especially notable in the RSol graph.

slightly lower exponential coefficient. These contrasting reports may be due to the small sample size or due to difference in experimental environment. While Gad et al. (2015) performed experiments within a weight-supported treadmill setting, the presented experiment was conducted in a weight bearing, free roaming environment. This difference in locomotive setting may introduce disruptions to the reorganization of neural networks due to the loss of highly organized and predictable patterns of sensory input that is normally generated with step training on a treadmill (Edgerton and Roy, 2009; Taccola et al., 2018).

Additionally, note that the highlighted outliers in **Figure 7** were not included in the regression calculations. These data points suggest that at below average low MEP peak counts, high levels of activity can occur. These outliers were measured from the same rat within the same experiment. During analysis of the video data, an unusual frequency of induced, air-stepping was observed (**Supplementary Videos 1, 2**). The fact that some number of these counted step-like events were not enabled but rather induced by ES may result in minimal polysynaptic pathways being activated during air-stepping, i.e., when the proprioceptive and tactile afferents typically associated in over-ground, weight-bearing hind-limb locomotion were not present. A number of possible reasons could provide explanation as to why repetitive, non-weight bearing cycles could readily occur.

The exponential trend visible in **Figure 7** alongside the data in **Figures 6B,C** present the possibility of a "breakaway" point where the minimum level of neuronal activity and polysynaptic mechanisms is required for significant functional improvement. It was only when Quip was introduced where a significant improvement in spontaneous step-like activity was observed. Given the extensive research provided with training under the influence of Strych, one would expect that Strych experiments would provide equal benefit when compared with Quip (de Leon et al., 1999; Gad et al., 2013b, 2015).

Albeit a small sample size, these data extend the hypothesis of the existence of electrophysiological biomarkers and warrant the extension of further investigation into longer term longitudinal studies and the involvement of more robust algorithms and *in vivo* sensing technologies. These observations alongside the previously discussed representation of plastic mechanisms in MEPs agree with our initial hypothesis of multiple neuromodulatory modalities transforming non-functional spinal networks to a more excitable state to enable "self-training."

Presented here is a novel method of simultaneously identifying step-like activity while recording electrophysiological biomarkers of stepping. The value of these types of data can be further improved with the introduction of additional sensors in order to compose a more comprehensive assessment of movements as occurs *in vivo* in a variety of environments. As gait patterns have a state-specific nature, repeating the task recognition exercise using a stochastic probability based method such as HMMs (Byung-Woo et al., 1997; Sy Bor et al., 2006; Naeem and Bigham, 2007; Lee, 2008) or long short-term memory (LSTM) (How et al., 2014; Tsironi et al., 2017) with the existing datasets may improve the overall accuracy of the task recognition. The present data provide an example of a "proof of concept" approach to examine the level of activity dependence that is present when testing the efficacy of an intervention. It is technically becoming more feasible to chronically record EMG from many muscles to detect how the reorganization of neuronal networks that control locomotion can be focused on the patterns of coordination of flexion/extension, abduction/adduction, and non-repetitive tasks such as grip and pinch maneuvers as well as repetitive tasks such as cycling, etc. Moreover, the ability to measure the state of the locomotive neural circuitry to determine the

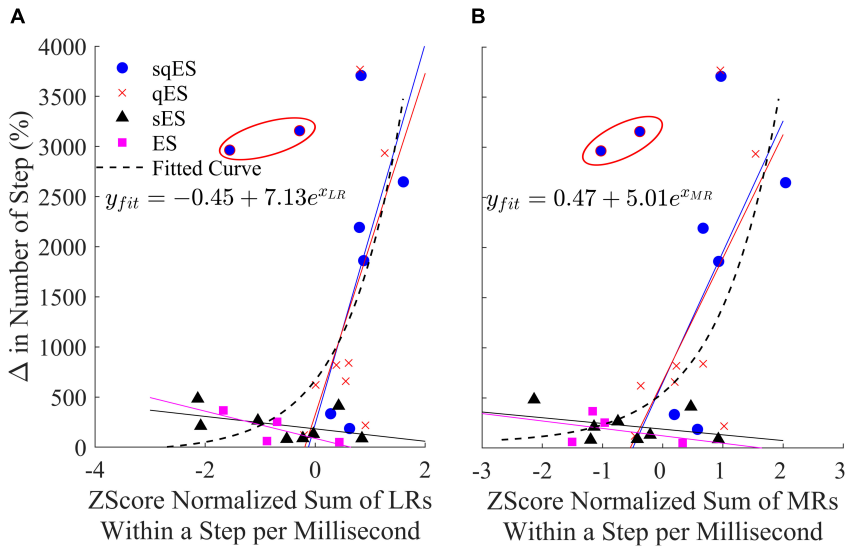

FIGURE 7 | (A) Change in the number of late and **(B)** middle peaks responses (normalized to pre values) for each rat, treatment, and left and right hind-limb of the Sol MEPs. Circled in red are two outliers identified as rat #3 during the sqES treatment. Additionally, linear regressions for each of the respective treatments in their corresponding color are plotted. An exponential curve (dashed line) encompasses all treatments.

direct relationship between the treatment provided and the underlying neuronal mechanics serves as detailed insight as the subject undergoes training, providing the opportunity to adjust treatments in order to maintain an enabling effect, maximizing activity-dependent recovery.

In addition, our algorithm was used to examine the effect of pharmacology in combination with ES by directly comparing the occurrence of step-like activity within a chronic self-training environment. The ability to record chronically for 6 h in a natural environment highlights the functional and electrophysiological changes over time and could represent a functional biomarker of recovery post paralysis. This leads to a potentially critical question in the rehabilitation strategy post paralysis. Can daily periods of sub-threshold electrical neuromodulation of the spinal circuitry enhance the performance of motor skills as well as or even more than when a task-specific rehabilitation paradigm is imposed? If that is the case, then the results will have an immediate impact on how neuromodulation can be used to enhance sensorimotor recovery in individuals with other neural disorders than SCI. Spinal circuits controlling stepping and standing (locomotion and posture) can be improved after a SCI by practicing those tasks, i.e., by increasing the activation of those circuits (Ahissar and Hochstein, 1997; Bayona et al., 2005). The data presented here demonstrate that there is a minimal amount of spontaneous activity in the sensorimotor circuits that control standing and stepping after a mid-thoracic spinal cord transection in adult rats (**Figures 4**, **5**) that can be further enhanced using multimodal neuromodulatory mechanisms. In effect this enhanced level of spontaneous activity can be viewed as a "self-training" phenomenon. Clinically, the presence of a "self-training" effect would have an immediate and significant impact on designing rehabilitation strategies.

While the presented data are based on data derived from spinally injured rats that have had multiple training sessions under the influence of ES and pharmacological agents, longitudinal functional data and analysis can be found in the paper presented previously (Gad et al., 2015). Longitudinal functional analyses were performed at 12, 22, 35, and 49 days past injury with hindlimb joint kinematics tracked with EMG recordings of the TA and Sol under ES, qES, sES, and sqES conditions during standing and step training in a weight supported treadmill. Future work should include continual measurements of functional neurological changes as reported here, but throughout a training period. The present data are largely focused on the acute effects of spontaneous activity after completion of electrical and pharmacological neuromodulation which facilitated self-training (**Figure 4**). A repetition of this experiment with a larger sample size and with a regimented level of a specific motor task would be of significant interest. Adaptation of the existing algorithm with machine-learning algorithms such as HMMs and LSTM could further enhance our understanding of the more critical variables intrinsic to the mechanisms of activity dependent modulation of neuromotor facilitated reorganization.

CONCLUSION

We successfully demonstrated the proof of concept algorithm to detect specific functional hind-limb spontaneous locomotion using minimal biosignals while monitoring biomarkers that represent a polysynaptic neurophysiological system input–output response of the spinal circuitry that controls locomotive activity. In addition, we observed a correlation between these biomarkers and the functional responses to spinally evoked

potentials. By incorporating complex machine-learning methods and measuring kinematic output, the algorithm developed can be readily scaled to detect more complex tasks.

DATA AVAILABILITY STATEMENT

The datasets generated for this study are available on request to the corresponding author.

ETHICS STATEMENT

The animal study was reviewed and approved by the Animal Research Committee at UCLA. All procedures described are in accordance with the National Institute of Health Guide for the Care and Use of Laboratory Animals.

AUTHOR CONTRIBUTIONS

RC developed the algorithm and performed the data analysis. PG performed the experiments and consulted in data analysis. HZ performed the surgeries. RC, PG, and VE interpreted the data. RC, HZ, PG, BV, and VE wrote the manuscript. All authors read and approved the final manuscript.

FUNDING

This study was funded by the Dana & Albert R. Broccoli Charitable Foundation, Nanette and Burt Forester, including matching by PwC LLP and the Australian Department of Education Research Training Program.

ACKNOWLEDGMENTS

The authors thank Valentine Zinchenko for his technical support.

SUPPLEMENTARY MATERIAL

The Supplementary Material for this article can be found online at: https://www.frontiersin.org/articles/10.3389/fnsys.2019.00082/full#supplementary-material

REFERENCES

Ahissar, M., and Hochstein, S. (1997). Task difficulty and the specificity of perceptual learning. *Nature* 387, 401–406. doi: 10.1038/387401a0

Alaimo, M. A., Smith, J. L., Roy, R. R., and Edgerton, V. R. (1984). EMG activity of slow and fast ankle extensors following spinal cord transection. *J. Appl. Physiol. Respir. Environ. Exerc. Physiol.* 56, 1608–1613. doi: 10.1152/jappl.1984.56.6.1608

Alam, M., Garcia-Alias, G., Jin, B., Keyes, J., Zhong, H., Roy, R. R., et al. (2017). Electrical neuromodulation of the cervical spinal cord facilitates forelimb skilled function recovery in spinal cord injured rats. *Exp. Neurol.* 291, 141–150. doi: 10.1016/j.expneurol.2017.02.006

Angeli, C. A., Edgerton, V. R., Gerasimenko, Y. P., and Harkema, S. J. (2014). Altering spinal cord excitability enables voluntary movements after chronic complete paralysis in humans. *Brain* 137(Pt 5), 1394–1409. doi: 10.1093/brain/awu038

Aragão, R. D. S., Rodrigues, M. A. B., de Barros, K. M. F. T., Silva, S. R. F., Toscano, A. E., de Souza, R. E., et al. (2011). Automatic system for analysis of locomotor activity in rodents—A reproducibility study. *J. Neurosci. Methods* 195, 216–221. doi: 10.1016/j.jneumeth.2010.12.016

Bayona, N. A., Bitensky, J., Salter, K., and Teasell, R. (2005). The role of task-specific training in rehabilitation therapies. *Top. Stroke Rehabil.* 12, 58–65. doi: 10.1310/bqm5-6ygb-mvj5-wvcr

Byung-Woo, M., Ho-Sub, Y., Jung, S., Yun-Mo, Y., and Toshiaki, E. (1997). "Hand gesture recognition using hidden Markov models," in *Proceedings of the 1997 IEEE International Conference on Systems, Man, and Cybernetics. Computational Cybernetics and Simulation*. Orlando, IL.

Capogrosso, M., Milekovic, T., Borton, D., Wagner, F., Moraud, E. M., Mignardot, J.-B., et al. (2016). A brain-spine interface alleviating gait deficits after spinal cord injury in primates. *Nature* 539, 284–288. doi: 10.1038/nature20118

Clarke, R. L., Smith, R. F., and Justesen, D. R. (1985). An infrared device for detecting locomotor activity. *Behav. Res. Methods Instr. Comput.* 17, 519–525. doi: 10.3758/bf03207645

Courtine, G., Gerasimenko, Y., van den Brand, R., Yew, A., Musienko, P., Zhong, H., et al. (2009). Transformation of nonfunctional spinal circuits into functional states after the loss of brain input. *Nat. Neurosci.* 12:1333. doi: 10.1038/nn.2401

de Leon, R. D., Reinkensmeyer, D. J., Timoszyk, W. K., London, N. J., Roy, R. R., and Reggie Edgerton, V. (2002). "Chapter 11 Use of robotics in assessing the adaptive capacity of the rat lumbar spinal cord," in *Progress in Brain Research*, eds McKerracher, L. Doucet, G. and Rossignol, S. (Amsterdem: Elsevier) 137, 141–149. doi: 10.1016/s0079-6123(02)37013-4

de Leon, R. D., Tamaki, H., Hodgson, J. A., Roy, R. R., and Edgerton, V. R. (1999). Hindlimb locomotor and postural training modulates glycinergic inhibition in the spinal cord of the adult spinal cat. *J. Neurophysiol.* 82, 359–369. doi: 10.1152/jn.1999.82.1.359

Edgerton, V. R., Courtine, G., Gerasimenko, Y. P., Lavrov, I., Ichiyama, R. M., Fong, A. J., et al. (2008). Training locomotor networks. *Brain Res. Rev.* 57, 241–254.

Edgerton, V. R., and Roy, R. R. (2009). Activity-dependent plasticity of spinal locomotion: implications for sensory processing. *Exerc. Sport Sci. Rev.* 37, 171–178. doi: 10.1097/JES.0b013e3181b7b932

Edgerton, V. R., Tillakaratne, N. J. K., Bigbee, A. J., de Leon, R. D., and Roy, R. R. (2004). Plasticity of the spinal neural circuitry after injury. *Annu. Rev. Neurosci.* 27, 145–167.

Fong, A. J., Cai, L. L., Otoshi, C. K., Reinkensmeyer, D. J., Burdick, J. W., Roy, R. R., et al. (2005). Spinal cord-transected mice learn to step in response to quipazine treatment and robotic training. *J. Neurosci.* 25, 11738–11747. doi: 10.1523/jneurosci.1523-05.2005

Formento, E., Minassian, K., Wagner, F., Mignardot, J. B., Le Goff-Mignardot, C. G., Rowald, A., et al. (2018). Electrical spinal cord stimulation must preserve proprioception to enable locomotion in humans with spinal cord injury. *Nat. Neurosci.* 21, 1728–1741. doi: 10.1038/s41593-018-0262-6

Gad, P., Choe, J., Shah, P., Garcia-Alias, G., Rath, M., Gerasimenko, Y., et al. (2013a). Sub-threshold spinal cord stimulation facilitates spontaneous motor activity in spinal rats. *J. NeuroEng. Rehabil.* 10, 108–108. doi: 10.1186/1743-0003-10-108

Gad, P., Lavrov, I., Shah, P., Zhong, H., Roy, R. R., Edgerton, V. R., et al. (2013b). Neuromodulation of motor-evoked potentials during stepping in spinal rats. *J. Neurophysiol.* 110, 1311–1322. doi: 10.1152/jn.00169.2013

Gad, P., Roy, R. R., Choe, J., Creagmile, J., Zhong, H., Gerasimenko, Y., et al. (2015). Electrophysiological biomarkers of neuromodulatory strategies to recover motor function after spinal cord injury. *J. Neurophysiol.* 113, 3386–3396. doi: 10.1152/jn.00918.2014

Ganea, K., Liebl, C., Sterlemann, V., Müller, M., and Schmidt, M. (2007). Pharmacological validation of a novel home cage activity counter in mice. *J. Neurosci. Methods* 162, 180–186. doi: 10.1016/j.jneumeth.2007.01.008

Genewsky, A., Heinz, D. E., Kaplick, P. M., Kilonzo, K., and Wotjak, C. T. (2017). A simplified microwave-based motion detector for home cage activity monitoring in mice. *J. Biol. Eng.* 11:36. doi: 10.1186/s13036-017-0079-y

Gerasimenko, Y., Gorodnichev, R., Moshonkina, T., Sayenko, D., Gad, P., and Reggie Edgerton, V. (2015). Transcutaneous electrical spinal-cord stimulation in humans. *Ann. Phys. Rehabil. Med.* 58, 225–231. doi: 10.1016/j.rehab.2015.05.003

Gerasimenko, Y., Roy, R. R., and Edgerton, V. R. (2008). Epidural stimulation: comparison of the spinal circuits that generate and control locomotion in rats, cats and humans. *Exp. Neurol.* 209, 417–425. doi: 10.1016/j.expneurol.2007.07.015

Gerasimenko, Y. P. I, Lavrov, A., Courtine, G., Ichiyama, R. M., Dy, C. J., Zhong, H., et al. (2006). Spinal cord reflexes induced by epidural spinal cord stimulation in normal awake rats. *J. Neurosci. Methods* 157, 253–263. doi: 10.1016/j.jneumeth.2006.05.004

Gerasimenko, Y. P., Lu, D. C., Modaber, M., Zdunowski, S., Gad, P., Sayenko, D. G., et al. (2015). Noninvasive reactivation of motor descending control after paralysis. *J. Neurotrauma* 32, 1968–1980. doi: 10.1089/neu.2015.4008

Gill, M. L., Grahn, P. J., Calvert, J. S., Linde, M. B. I, Lavrov, A., Strommen, J. A., et al. (2018). Neuromodulation of lumbosacral spinal networks enables independent stepping after complete paraplegia. *Nat. Med.* 24, 1677–1682. doi: 10.1038/s41591-018-0175-7

Harkema, S., Gerasimenko, Y., Hodes, J., Burdick, J., Angeli, C., Chen, Y., et al. (2011). Effect of epidural stimulation of the lumbosacral spinal cord on voluntary movement, standing, and assisted stepping after motor complete paraplegia: a case study. *Lancet* 377, 1938–1947. doi: 10.1016/S0140-6736(11)60547-3

How, D. N. T., Sahari, K. S. M., Hu, Y., and Loo Chu, K. (2014). "Multiple sequence behavior recognition on humanoid robot using long short-term memory (LSTM)," in *Proceedings of the 2014 IEEE International Symposium on Robotics and Manufacturing Automation (ROMA)*. Ipoh.

Huang, H., Kuiken, T. A., and Lipschutz, R. D. (2009). A strategy for identifying locomotion modes using surface electromyography. *IEEE Trans. Bio-Med. Eng.* 56, 65–73. doi: 10.1109/TBME.2008.2003293

Huang, H., Zhang, F., Sun, Y. L., and He, H. (2010). Design of a robust EMG sensing interface for pattern classification. *J. Neural Eng.* 7, 056005–056005. doi: 10.1088/1741-2560/7/5/056005

Ichiyama, R. M., Courtine, G., Gerasimenko, Y. P., Yang, G. J., van den Brand, R. I, Lavrov, A., et al. (2008a). Step training reinforces specific spinal locomotor circuitry in adult spinal rats. *J. Neurosci.* 28, 7370–7375. doi: 10.1523/JNEUROSCI.1881-08.2008

Ichiyama, R. M., Gerasimenko, Y., Jindrich, D. L., Zhong, H., Roy, R. R., and Edgerton, V. R. (2008b). Dose dependence of the 5-HT agonist quipazine in facilitating spinal stepping in the rat with epidural stimulation. *Neurosci. Lett.* 438, 281–285. doi: 10.1016/j.neulet.2008.04.080

Ichiyama, R. M., Gerasimenko, Y. P., Zhong, H., Roy, R. R., and Edgerton, V. R. (2005). Hindlimb stepping movements in complete spinal rats induced by epidural spinal cord stimulation. *Neurosci. Lett.* 383, 339–344. doi: 10.1016/j.neulet.2005.04.049

Lavrov, I., Dy, C. J., Fong, A. J., Gerasimenko, Y., Courtine, G., Zhong, H., et al. (2008). Epidural stimulation induced modulation of spinal locomotor networks in adult spinal rats. *J. Neurosci.* 28, 6022–6029. doi: 10.1523/jneurosci.0080-08.2008

Lavrov, I., Gerasimenko, Y. P., Ichiyama, R. M., Courtine, G., Zhong, H., Roy, R. R., et al. (2006). Plasticity of spinal cord reflexes after a complete transection in adult rats: relationship to stepping ability. *J. Neurophysiol.* 96, 1699–1710. doi: 10.1152/jn.00325.2006

Lee, K. (2008). EMG-based speech recognition using hidden markov models with global control variables. *IEEE Trans. Biomed. Eng.* 55, 930–940. doi: 10.1109/TBME.2008.915658

Martin, P., and Unwin, D. (1980). A microwave doppler radar activity monitor. *Behav. Res. Methods Instrument.* 12, 517–520. doi: 10.3758/bf03201826

Megens, A., Voeten, J., Rombouts, J., Meert, T. F., and Niemegeers, C. (1987). Behavioural activity of rats measured by a new method based on the piezo-electric principle. *Psychopharmacology* 93, 382–388.

Mendes, C. S., Bartos, I., Márka, Z., Akay, T., Márka, S., and Mann, R. S. (2015). Quantification of gait parameters in freely walking rodents. *BMC Biol.* 13:50–50. doi: 10.1186/s12915-015-0154-0

Morrel-Samuels, P., and Krauss, R. M. (1990). Cartesian analysis: a computer-video interface for measuring motion without physical contact. *Behav. Res. Methods Instr. Computers* 22, 466–470. doi: 10.3758/bf03203196

Naeem, U., and Bigham, J. (2007). "A comparison of two hidden markov approaches to task identification in the home environment," in *Proceedings of the 2007 2nd International Conference on Pervasive Computing and Applications*. Birmingham.

Parreno, A., Saraza, M., and Subero, C. (1985). A new stabilimeter for small laboratory animals. *Physiol. Behav.* 34, 475–478. doi: 10.1016/0031-9384(85)90215-x

Pernold, K., Iannello, F., Low, B. E., Rigamonti, M., Rosati, G., Scavizzi, F., et al. (2019). Towards large scale automated cage monitoring – Diurnal rhythm and impact of interventions on in-cage activity of C57BL/6J mice recorded 24/7 with a non-disrupting capacitive-based technique. *PLoS One* 14:e0211063. doi: 10.1371/journal.pone.0211063

Redfern, W. S., Tse, K., Grant, C., Keerie, A., Simpson, D. J., Pedersen, J. C., et al. (2017). Automated recording of home cage activity and temperature of individual rats housed in social groups: the rodent big brother project. *PLoS One* 12:e0181068. doi: 10.1371/journal.pone.0181068

Rose, F., Dell, P., and Love, S. (1985). Doppler shift radar monitoring of activity of rats in a behavioural test situation. *Physiol. Behav.* 35, 85–87. doi: 10.1016/0031-9384(85)90175-1

Rossignol, S., and Frigon, A. (2011). Recovery of locomotion after spinal cord injury: some facts and mechanisms. *Ann. Rev. Neurosci.* 34, 413–440. doi: 10.1146/annurev-neuro-061010-113746

Roy, R. R., Hodgson, J. A., Lauretz, S. D., Pierotti, D. J., Gayek, R. J., and Edgerton, V. R. (1992). Chronic spinal cord-injured cats: surgical procedures and management. *Lab. Anim. Sci.* 42, 335–343.

Solnik, S., Rider, P., Steinweg, K., DeVita, P., and Hortobágyi, T. (2010). Teager-Kaiser energy operator signal conditioning improves EMG onset detection. *Eur. J Appl. Physiol.* 110, 489–498. doi: 10.1007/s00421-010-1521-8

Starkey, M. L., Bleul, C., Kasper, H., Mosberger, A. C., Zörner, B., Giger, S., et al. (2014). High-impact, self-motivated training within an enriched environment with single animal tracking dose-dependently promotes motor skill acquisition and functional recovery. *Neurorehabil. Neural Repair* 28, 594–605. doi: 10.1177/1545968314520721

Sy Bor, W., Quattoni, A., Morency, L., Demirdjian, D., and Darrell, T. (2006). "Hidden conditional random fields for gesture recognition," in *Proceedings of the2006 IEEE Computer Society Conference on Computer Vision and Pattern Recognition (CVPR'06)*. New York, NY.

Taccola, G., Sayenko, D., Gad, P., Gerasimenko, Y., and Edgerton, V. R. (2018). And yet it moves: recovery of volitional control after spinal cord injury. *Prog. Neurobiol.* 160, 64–81. doi: 10.1016/j.pneurobio.2017.10.004

Tamborini, P., Sigg, H., and Zbinden, G. (1989). Quantitative analysis of rat activity in the home cage by infrared monitoring. Application to the acute toxicity testing of acetanilide and phenylmercuric acetate. *Arch. Toxicol.* 63, 85–96. doi: 10.1007/bf00316429

Tsironi, E., Barros, P., Weber, C., and Wermter, S. (2017). An analysis of convolutional long short-term memory recurrent neural networks for gesture recognition. *Neurocomputing* 268, 76–86. doi: 10.1016/j.neucom.2016.12.088

York, J. M., Blevins, N. A., McNeil, L. K., and Freund, G. G. (2013). Mouse short- and long-term locomotor activity analyzed by video tracking software. *J. Vis. Exp.* 20:50252. doi: 10.3791/50252

Young, C., Young, M., Li, Y., and Lin, M. (1996). A new ultrasonic method for measuring minute motion activities on rats. *J. Neurosci. Methods* 70, 45–49. doi: 10.1016/s0165-0270(96)00102-1

Conflict of Interest: VE holds shareholder interest in NeuroRecovery Technologies and holds certain inventorship rights on intellectual property licensed by The Regents of the University of California to NeuroRecovery Technologies and its subsidiaries. PG and VE hold shareholder interest in SpineX Inc.

The remaining authors declare that the research was conducted in the absence of any commercial or financial relationships that could be construed as a potential conflict of interest.

frontiers in Cellular Neuroscience

ORIGINAL RESEARCH
published: 15 January 2020
doi: 10.3389/fncel.2019.00573

Biphasic Effect of Buspirone on the H-Reflex in Acute Spinal Decerebrated Mice

*Yann Develle and Hugues Leblond**

Department of Anatomy, CogNAC Research Group, Université du Québec à Trois-Rivières, Trois-Rivières, QC, Canada

Pharmacological treatment facilitating locomotor expression will also have some effects on reflex expression through the modulation of spinal circuitry. Buspirone, a partial serotonin receptor agonist (5-HT_{1A}), was recently shown to facilitate and even trigger locomotor movements in mice after complete spinal lesion (Tx). Here, we studied its effect on the H-reflex after acute Tx in adult mice. To avoid possible impacts of anesthetics on H-reflex depression, experiments were performed after decerebration in un-anesthetized mice (N = 20). The H-reflex in plantar muscles of the hind paw was recorded after tibial nerve stimulation 2 h after Tx at the 8th thoracic vertebrae and was compared before and every 10 min after buspirone (8 mg/kg, i.p.) for 60 min (N = 8). Frequency-dependent depression (FDD) of the H-reflex was assessed before and 60 min after buspirone. Before buspirone, a stable H-reflex could be elicited in acute spinal mice and FDD of the H-reflex was observed at 5 and 10 Hz relative to 0.2 Hz, FDD was still present 60 min after buspirone. Early after buspirone, the H-reflex was significantly decreased to 69% of pre-treatment, it then increased significantly 30–60 min after treatment, reaching 170% 60 min after injection. This effect was not observed in a control group (saline, N = 5) and was blocked when a 5-HT_{1A} antagonist (NAD-299) was administered with buspirone (N = 7). Altogether results suggest that the reported pro-locomotor effect of buspirone occurs at a time where there is a 5-HT_{1A} receptors mediated reflex depression followed by a second phase marked by enhancement of reflex excitability.

Keywords: serotonin, 5-HT_{1A} receptor agonist, spinal cord injury, locomotion, sensorimotor

OPEN ACCESS

Edited by:
Katinka Stecina,
University of Manitoba, Canada

Reviewed by:
De-Lai Qiu,
Yanbian University, China
Grzegorz Hess,
Jagiellonian University, Poland
Claire Francesca Meehan,
University of Copenhagen, Denmark

***Correspondence:**
Hugues Leblond
hugues.leblond@uqtr.ca

Specialty section:
This article was submitted to Cellular Neurophysiology, a section of the journal Frontiers in Cellular Neuroscience

Received: *13 June 2019*
Accepted: *12 December 2019*
Published: *15 January 2020*

Citation:
Develle Y and Leblond H (2020) Biphasic Effect of Buspirone on the H-Reflex in Acute Spinal Decerebrated Mice. Front. Cell. Neurosci. 13:573. doi: 10.3389/fncel.2019.00573

INTRODUCTION

During locomotion, afferent inputs from the hind limbs serve to control the excitability of spinal networks. They adjust motor output by direct impact on either motoneurons or interneurons, comprising those of the central pattern generator (CPG) that is responsible for locomotion (Rossignol, 2006). After complete spinal cord injury, sensory feedback becomes the only source of input remaining to the spinal cord, it has the power to re-arrange spinal circuits below the lesion, as shown by the positive outcome of treadmill training in adult cats (Lovely et al., 1986; Barbeau and Rossignol, 1987; Belanger et al., 1996), rats (Edgerton et al., 1997; Ichiyama et al., 2008; Otoshi et al., 2009), and mice (Leblond et al., 2003). The plasticity involved in this recovery of locomotion necessarily entails changes in several reflex pathways (Côté et al., 2003; Côté and Gossard, 2004).

In spinal animals, pharmacological treatments that mimic neurotransmitters from severed, descending fibers also have neuromodulator effects on locomotor networks and can improve recovery of locomotion (Chau et al., 1998a,b). As is the case with locomotor training, drugs that enable functional recovery also regulate spinal reflexes (Côté et al., 2003; Frigon et al., 2012). For example, in cats with complete spinal lesion, the noradrenergic agonist clonidine, which is known to trigger hind limb locomotion (Barbeau and Rossignol, 1987), was also found to modify spinal neuron responses to peripheral inputs (Barbeau and Rossignol, 1987; Chau et al., 1998a; Côté et al., 2003; Frigon et al., 2012). In rodents, serotoninergic (5-HT) drugs are effective in triggering and facilitating locomotion after complete spinal lesion (Schmidt and Jordan, 2000; Slawinska et al., 2014). Recent work in our laboratory has established that treatment with the US Food and Drug Administration-approved 5-HT_{1A} receptor partial agonist buspirone (Loane and Politis, 2012) can initiate locomotion in the hind limbs of adult mice immediately after complete spinal lesion (Jeffrey-Gauthier et al., 2018). As drugs with pro-locomotor properties also modify reflex pathways, buspirone may alter reflex excitability in mice after complete spinal lesion.

The effects of 5-HT_{1A} agonists on spinal reflexes have been tested earlier in different animal models, but there is still no consensus today as to whether the outcome is excitatory or inhibitory. On the one hand, *in vitro* results on isolated brainstem and spinal cord in neonatal rats indicate that buspirone decreases monosynaptic reflex excitability (Yomono et al., 1992). This observation concurs with other studies that have demonstrated 5-HT_{1A} receptor inhibition in reflex pathways (Nagano et al., 1988; Crick et al., 1994; Hasegawa and Ono, 1996a,b; Honda and Ono, 1999). On the other hand, some have reported excitatory effects of 5-HT_{1A} (Clarke et al., 1996), mainly by showing facilitatory effects on motoneuron depolarization (Takahashi and Berger, 1990; Zhang, 1991; Perrier et al., 2003; Grunnet et al., 2004) or monosynaptic reflex enhancement (Honda and Ono, 1999). Is it possible that substances with excitatory effects on locomotion also have inhibitory effects on spinal cord excitability?

The present study was performed with a newly developed model of decerebrated mice and was designed to investigate the modulation of reflex pathways in the absence of pharmacological anesthesia. This was required, since locomotion involves wide re-organization of reflex pathways, as shown mainly in decerebrated cat preparations in which new relays were described in the absence of anesthesia (McCrea, 2001). Some reflex pathways are thus state-dependent, meaning that they occur only when the CPG is driving locomotion or when drugs known to trigger locomotion are given (Gossard et al., 1994; Perreault et al., 1995; Leblond et al., 2000, 2001).

Here, the main objective is to assess the effect of buspirone, at a dose level that is known to trigger locomotion (Jeffrey-Gauthier et al., 2018), on H-reflex amplitude in adult decerebrated mice after acute spinal cord lesion. This reflex, the electrical analog of the tendon tap reflex, is primarily mediated by monosynaptic pathways (Misiaszek, 2003) and regroup both sensori- and motor systems. A second objective was to evaluate if the observed buspirone effect was mediated by 5-HT_{1A} by blocking these receptors with the specific 5-HT_{1A} antagonist NAD-299 (Johansson et al., 1997). The results show a biphasic effect of buspirone on the H-reflex: a significant decrease was first observed followed by an increase of the reflex 30 min later. Since buspirone had no effect if preceded by NAD-299, it is suggested that reflex modulation by buspirone is mediated by 5-HT_{1A} receptors. Some of these results have been presented in abstract form Develle and Leblond (2016).

MATERIALS AND METHODS

Animal Care and Ethics

Experiments were performed on 20 C57 mice, of either sex (Charles River Laboratories, Saint-Constant, QC, Canada), weighing 20–30 g. Their living conditions were strictly controlled by laboratory and facility staff. They were housed in cages with food and water available *ad libitum*. All manipulations and procedures were in accordance with Canadian Council on Animal Care guidelines and were approved by the Université du Québec à Trois-Rivières Animal Care Committee. The mice were randomly assigned to 1 of 3 groups in acute, terminal experiments to evaluate the effect of buspirone on the H-reflex: a group ($N = 8$) exposed to buspirone, a group ($N = 7$) exposed to 5-HT_{1A} antagonist NAD-299 and buspirone, and controls ($N = 5$) treated with saline.

Anesthesia

All surgeries were performed under isoflurane anesthesia (2% mixed with O_2 95% and CO_2 5%, 200 ml/min). General anesthesia was first induced through a mask: then, the animals were tracheotomized to maintain anesthesia and allow artificial ventilation (SAR-830/P Ventilator, CWE, Inc., Ardmore, PA, United States) adjusted to preserve expired CO_2 level between 3 and 4% (CapStar-100 CO_2 monitor, CWE, Inc.). Body temperature was monitored by rectal probe and maintained at $37 \pm 0.5°C$ with heating pad.

Spinalization

The objective was to measure the H-reflex after complete spinal cord section. It was performed early in the surgery to minimize the impact of the decerebration on the spinal circuitry. The paravertebral muscles were cleared from both vertebral laminae after skin incision targeting the 8th thoracic vertebra. Then, double laminectomy exposed the spinal cord at this level. After perforation of the dura mater with a needle, a small piece of lidocaine-soaked cotton (xylocaine 2%) was applied for 1 min to prevent uncontrolled secondary neural damage or lumbar spinal cord excitotoxicity. Then, the spinal cord was transected with micro-scissors and confirmed by visual observation of the gap between the rostral and caudal stumps. Finally, Surgicel® absorbable hemostat (Ethicon, Johnson & Johnson, United States) was inserted between the two parts of the spinal cord before the skin was sutured.

Decerebration

Spinal network activities are traditionally assessed in decerebrate preparations, especially from cats, rats and rabbits, with recent adaptation to mice (Dobson and Harris, 2012; Meehan et al., 2012, 2017). Data were, therefore, acquired in decerebrated, unanesthetized mice to avoid the unwanted effects of anesthesia. The carotid arteries were first ligated to minimize cerebral perfusion while the animals were secured in a stereotaxic frame (Model 980 Small Animal Spinal Unit, Kopf Instruments, Sunland-Tujunga, CA, United States) equipped with a small mouse and neonatal rat adaptor (Stoelting Company, Wood Dale, IL, United States). They were then craniotomized, taking care to leave the superior sagittal sinus intact. Bone wax (Ethicon, Johnson & Johnson, United States) was applied to the skull when necessary to prevent bleeding. The dura mater was removed gently to expose the cortex for transection with a razor blade 1 mm rostral to the lambda. The rostral part of neural tissue and the occipital cortex were removed, by gentle suctioning with an adapted micro-vacuum, corresponding to pre-collicular-pre-mamillar decerebration. The cavity was finally filled with Gelfoam® thin soak hemostat sponge (Pfizer Inc., New York, NY, United States), and the skin was closed with suture.

H-Reflex Recording

After decerebration, the left hind limb was fixed in extension and an incision was made on top of the gastrocnemius muscles to separate and expose the tibial nerve. A pool was formed with skin flaps and filled with mineral oil to avoid nerve desiccation. The tibial nerve was mounted on a home-made bipolar hook electrode for stimulation. One-ms single-pulsed stimulations were delivered by a constant-current stimulator (Model DS4, Digitimer Ltd., Welwyn Garden City, United Kingdom) triggered by a computer-controlled sequencer (Power 1401 acquisition system, Cambridge Electronic Design, Cambridge, United Kingdom).

Paired, fine, multistrained stainless steel wires (AS631Cooner Wire, Chatsworth, CA, United States) were inserted under the skin, between the second and third medial toes, toward the intrinsic foot muscles, for electromyographic (EMG) recording. Signals were amplified 1,000×, bandpass-filtered at 30–3,000 Hz (Grass P55 AC Preamplifier, Natus Neurology, Inc., Pleasanton, CA, United States), and digitized for data acquisition (Spike 2 software, Cambridge Electronic Design, Cambridge, United Kingdom). A ground electrode was inserted in the skin between the stimulating and recording electrodes.

Anesthesia was stopped, followed by 60-min rest, which corresponds to approximately 120–150 min post-spinalization, to avoid undesirable anesthesia-induced effects. Typically, mice can spontaneously move its forelimbs at this time but it should be noted that reflex recording was always made during a quiescent EMG background.

Drug Administration

The H-reflex was compared between the three groups of mice: (1) buspirone only; (2) NAD-299 and buspirone; and (3) control. A catheter was inserted to facilitate i.p., administration without moving the animals. Buspirone (8 mg/kg, i.p.) was given in a volume of 0.1 cc of saline (0.9%) in the first group. This dose of buspirone was chosen since it was shown to trigger locomotion (Jeffrey-Gauthier et al., 2018). The second group received the 5-HT_{1A} antagonist NAD-299 (0.66 mg/kg) (Johansson et al., 1997) 10 min before buspirone treatment. The third group received 0.1cc of saline only (0.9%).

Data Acquisition and Analysis

Stimulus–response curves (e.g., **Figure 1B**) were charted by gradually increasing tibial nerve stimulation intensity to ascertain the maximal H-reflex (4–6 ms latency) concomitant with stable M-wave (1–3 ms latency). At this intensity, which corresponded to approximately 1.8 times the motor threshold, Ia muscle spindle afferents were mainly activated. Responses to tibial nerve stimulation intensity were recorded before and every 10 min after the injection for a total of 60 min. Reflex amplitude was estimated with the H/M ratio which estimate the relative amount of motor neuron activated by the reflex loop as compared to the whole motor pool activated by the stimulation. This standardization allow a better inter-subject comparison of the reflex evolution in time and treatment.

Frequency-dependent depression was tested before and 60 min after injection in the buspirone treated mice by varying stimulation frequency between 4 blocks of 30 stimulations (0.2, 5, 10, and 0.2 Hz; 60 s inter-block interval). The first five responses of each block were discarded to allow H-reflex stabilization. Analyses comprised only recordings with stable M-wave throughout the protocol (<10% variation) to ensure recording stability.

Data were analyzed with Spike2 software (Cambridge Electronic Design) and Excel software (Microsoft Corporation, Redmond, WA, United States). Peak-to-peak amplitudes of the H-reflex and M-wave were measured to establish the H/M ratio so that the results could be compared between animals. Mean ratio at each time point was computed by averaging 30 stimulations at 0.2 Hz. In the frequency-dependent depression (FDD) protocol, mean H/M ratio was averaged from 25 successive responses for each block.

Statistical analysis was conducted with Statistica software (version 13, StatSoft Inc., Tulsa, OK, United States), and the significance threshold was set at $p \leq 0.05$. Distribution's normality was confirmed by the Kolmogorov–Smirnov test for each group separately. To be able to perform a balanced ANOVA, one missing sample at T60 in the group injected with saline, one in the group which receive both NAD-299 and buspirone and two in the buspirone treated group were replaced by the mean of the group for this timepoint. Then, Greenhouse-Geisser-corrected mixed ANOVA ascertained the effects of the intra-subject factor *time* and the inter-subject factor *treatment* on reflex amplitude. Fisher *post hoc* was used to observed periods presenting significant variations in comparison to pre-injection values. In the buspirone group, we further examined the impact of the frequency of stimulation (0.2, 5, and 10 Hz) on H/M ratio before (T = 0 min) and 60 min after (T = 60 min) buspirone injection. A repeated-measure ANOVA was used to verify the effects of frequency and buspirone and possible interaction

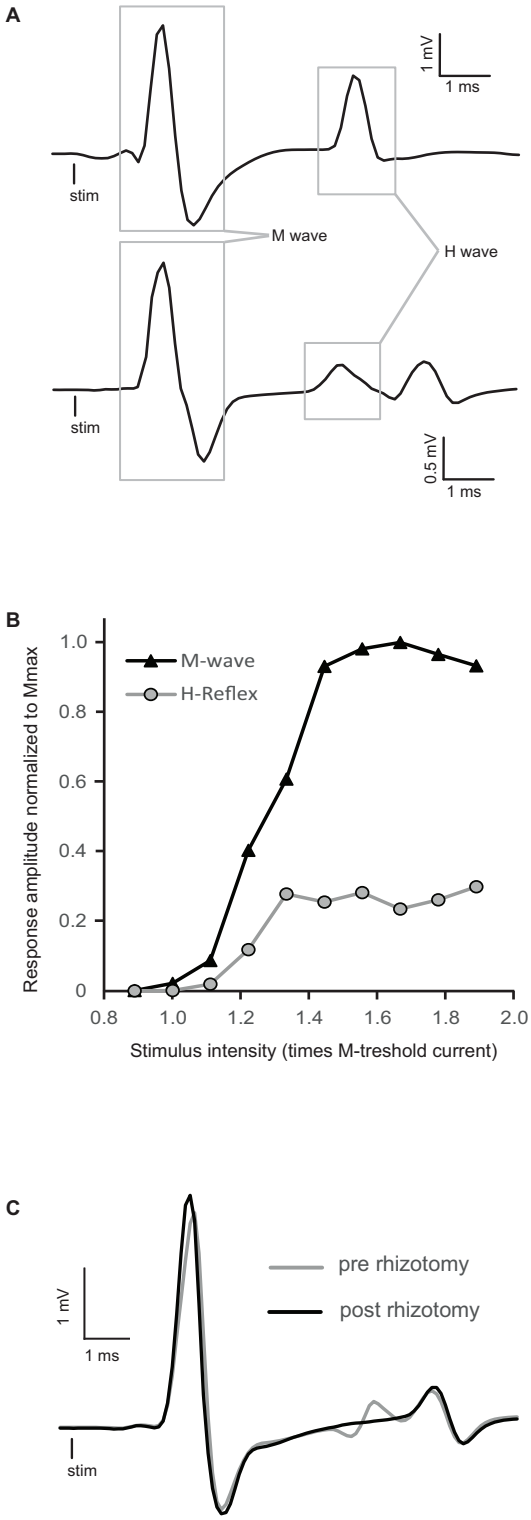

FIGURE 1 | Raw traces of H-reflex and representative recruitment curve. **(A)** Averaged traces of electromyographic (EMG) recording showing typical examples of H-reflexes in decerebrated spinal mice. The M-wave is the depolarization of the whole motoneuron pool activated by stimulation, whereas the H-wave is the motor response induced by primary afferent *(Continued)*

FIGURE 1 | Continued
depolarization. **(B)** Peak-to-peak amplitude of EMG responses recorded in intrinsic foot muscles by progressively increasing tibial nerve stimulation intensity. This stimulus–response curve is tested to find the stimulation intensity that will allow a stable reflex amplitude evaluation. It should be around Hmax, which specifically activates Ia primary afferents, concomitant with a stable M-wave response at the beginning of the M-wave plateau. In this particular example, stimulation around 1.4 times the motor threshold would be chosen. **(C)** Comparison of EMG traces of the H-reflex recorded before (gray trace) and after a complete dorsal rhizotomy (black trace). Sectioning all the dorsal roots at the lumbar enlargement abolished the H-reflex.

(frequency × buspirone) on H/M ratio. When appropriate, effects were adjusted using the Greenhouse–Geisser correction.

RESULTS

H-Reflex in Acute Spinal Decerebrated Mice

Stimulus–response curves were recorded for each mouse to establish at which intensity the H-reflex should be evoked to test the effect of buspirone. Typical examples of the H-reflex and stimulus–response curves are depicted in **Figures 1A,B**, respectively. Stimulation intensity was increased progressively until the whole pool of fibers in the tibial nerve was recruited, as indicated by a plateau being reached in the M-wave in **Figure 1B**. The H-reflex was usually evoked close to the motor threshold, and after an initial rise, it too plateaued and did not manifest a classical decrease in amplitude as it is observed in humans after reaching maximum (Knikou, 2008). This pattern was observed in all animals. Stimulation intensity was selected so that stable M-wave could be evoked as near as possible to beginning of the plateau (1.4T in the example depicted in **Figure 1B**).

As illustrated in **Figure 1A** (bottom trace), some responses included a third deflection with longer latency beginning about 7–8 ms post-stimulation. This late response was poorly depressed, if not depressed at all by stimulation frequency, in contrast to the response localized between 4 and 6 ms. For this reason this third deflection was not taken into account in the measurement of H-reflex. In one mouse, reflex recordings were made after a laminectomy and a complete lumbar dorsal rhizotomy to make sure that the first deflection was indeed the result of the activation of monosynaptic sensory inputs. By comparing the gray trace (pre-rhizotomy) and the black trace (post-rhizotomy) in **Figure 1C**, it is clear that the rhizotomy abolished the early components of the response and not the later responses. This indicates that this later response is not the result of segmental afferent inputs activation, since the dorsal roots are cut, and might be associated with antidromic muscle responses [namely F-wave (Meinck, 1976; Gozariu et al., 1998)].

Buspirone Effect on the H-Reflex

Since buspirone can produce locomotion in chronic spinal mice (Jeffrey-Gauthier et al., 2018), we examined whether this behavioral effect could be related to changes in monosynaptic reflex excitability. **Figure 2A** displays H-reflex raw traces

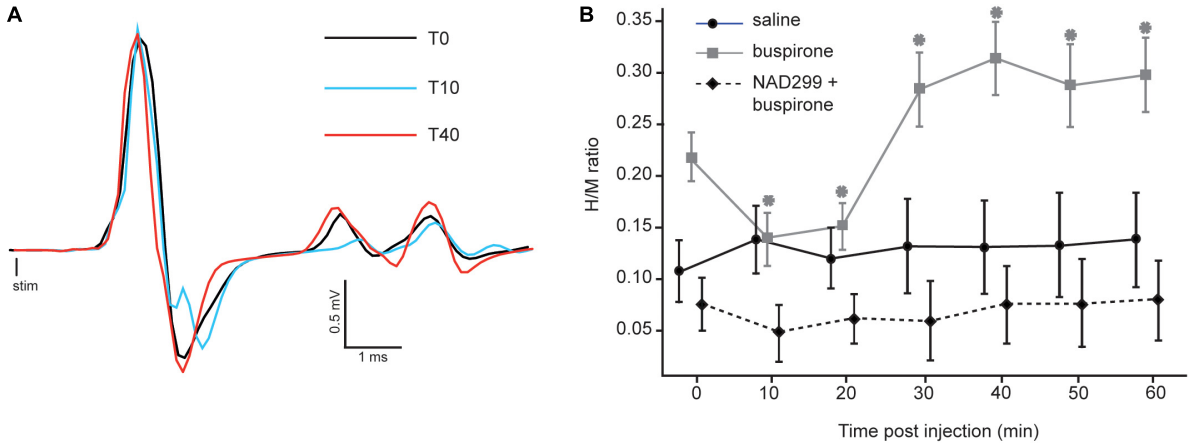

FIGURE 2 | Effect of buspirone on the H-reflex. **(A)** Averaged EMG traces obtained at three critical time points after buspirone administration. The H-reflex amplitude shows an initial decrease 10 min after buspirone administration (blue trace) and an increase 40 min after buspirone (red trace). **(B)** Mean H/M ratios for mice from the three groups. For the buspirone group (gray line), the mean H-reflex is significantly lower than baseline at 10 and 20 min after buspirone whereas it is significantly higher than baseline at 30–40–50 and 60 min (*$p < 0.01$). The amplitude of the mean H-reflex over time is no different than baseline in the saline group (black line) or the NAD-299 + buspirone group (dotted line).

averaged from 30 stimulations recorded from intrinsic foot muscles before (black trace), 10 (blue trace) and 40 min (red trace) after buspirone administration in 1 mouse. Average H-reflex decreased dramatically in this mouse 10 min after buspirone, then increased considerably 40 min later.

TABLE 1 | H/M ratio for each mouse.

Time (min)	0	10	20	30	40	50	60
Buspirone (*N* = 8)							
B1	0.350	0.287	0.302	0.463	0.494	0.460	0.510
B2	0.290	0.091	0.111	0.164	0.245	0.215	0.390
B3	0.272	0.131	0.128	0.365	0.398	0.303	0.365
B4	0.256	0.084	0.129	0.372	0.389	0.306	0.360
B5	0.205	0.281	0.186	0.391	0.257	0.554	0.312
B6	0.206	0.148	0.226	0.232	0.261	0.197	0.142
B7	0.140	0.116	0.142	0.272	0.409	0.216	0.216
B8	0.076	0.050	0.054	0.067	0.091	0.094	0.121
NAD-299 + buspirone (*N* = 7)							
BN1	0.058	0.042	0.064	0.058	0.065	0.079	0.077
BN2	0.037	0.016	0.034	0.026	0.040	0.034	0.038
BN3	0.076	0.050	0.078	0.029	0.103	0.114	0.116
BN4	0.055	0.008	0.009	0.033	0.040	0.041	0.035
BN5	0.039	0.036	0.039	0.050	0.041	0.029	0.039
BN6	0.163	0.120	0.151	0.160	0.169	0.171	0.167
BN7	0.093	0.053	0.046	0.055	0.060	0.063	0.074
Saline (*N* = 5)							
S1	0.124	0.143	0.077	0.104	0.068	0.090	0.110
S2	0.189	0.266	0.229	0.292	0.293	0.294	0.301
S3	0.124	0.127	0.133	0.111	0.120	0.124	0.116
S4	0.081	0.142	0.135	0.162	0.167	0.123	0.135
S5	0.069	0.054	0.071	0.034	0.050	0.077	0.069

Peak to peak amplitude of H- and M-responses are compared using the H/M ratio which are given in this table for each mouse in all groups each 10 min for 60 min.

The H/M ratio was measured for each mouse every 10 min for 60 min in each group (see **Table 1**). It was compared between the three groups using a mixed ANOVA to examine whether buspirone could change monosynaptic reflex excitability and whether this effect could be blocked by NAD-299, an antagonist of 5-HT_{1A} receptors. Results indicate that reflex excitability was different between groups across time points (interaction: $F_{12,102} = 4.4$, $p < 0.001$; $\eta^2_p = 0.34$: see **Figure 2B**). Indeed, the buspirone group showed a biphasic change in monosynaptic reflex excitability with an early inhibition followed by facilitation. This effect was not observed for the saline group and was blocked when buspirone was administered after a treatment with the 5-HT_{1A} antagonist NAD-299. Fisher *post hoc* test revealed that changes in reflex excitability were significant for each time point compared with T0 in the buspirone group (all $p < 0.01$). In contrast, no significant change was observed for any time point compared with baseline for the saline group (all $p > 0.3$) or for the NAD-299 + buspirone group (all $p > 0.2$).

Frequency-Dependent Depression of the H-Reflex

The H-reflex is characterized by frequency-dependent behavior: as stimulation frequency increases from 0.2 to 10 Hz, the reflex amplitude is depressed. **Figure 3A** shows a typical example of FDD of the H-reflex in a mouse before buspirone treatment. In this example, frequency of stimulation at 5 Hz (green trace) or 10 Hz (purple trace) almost completely abolished the H-reflex that was observed at 0.2 Hz (black trace). In order to investigate if the observed late effect of buspirone on the H-reflex could be the result of a disinhibitory mechanism, FDD was thus compared at T0 (**Figure 3B**, black line) and 60 min after treatment (**Figure 3B**, gray line) in the buspirone group. Overall, H/M ratio was altered by the frequency of stimulation (principal effect of frequency: $F_{2,12} = 17.6$, $p = 0.006$, $\eta_p^2 = 0.75$) and by

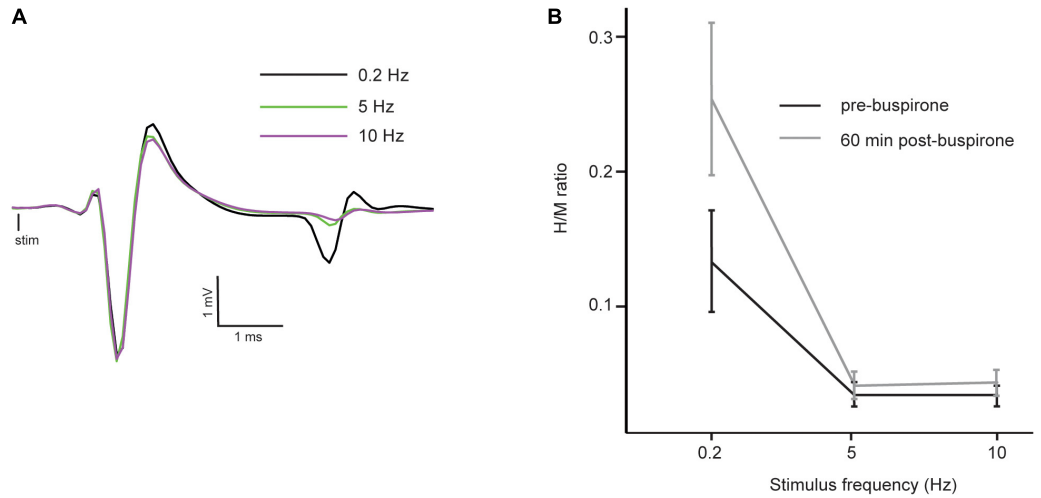

FIGURE 3 | Reflex inhibition at 5 and 10 Hz. **(A)** Averaged EMG traces at 0.2 Hz (black trace), 5 Hz (green trace) and 10 Hz (purple trace) in a mouse before the administration of buspirone showing a typical example of depression of the H-reflex at higher frequency of stimulation (FDD). Consistency in fiber recruitment by stimulation is assessed by stable M-wave between each trial. **(B)** Mean H/M ratios at different stimulation frequencies in the buspirone group before (black line) and 60 min (gray line) after buspirone administration. The frequency significantly depressed the mean H/M ratio both before and after buspirone indicating that FDD is not abolished by the treatment.

buspirone (principal effect of buspirone: $F_{1,12} = 6.8$, $p = 0.04$, $\eta_p{}^2 = 0.53$). The FDD of the H/M ratio differed marginally at T60 compared to T0 (frequency × buspirone interaction: $F_{2,12} = 4.6$, $p = 0.07$, $\eta_p{}^2 = 0.43$). *Post hoc* analysis revealed that the H/M ratio differences between T0 and T60 reached significance at 0.2 Hz ($p = 0.002$), but not at 5 and 10 Hz ($p = 0.83$ and $p = 0.76$, respectively).

DISCUSSION

The use of the adult decerebrated mouse preparation allowed us to study the effect of buspirone on the H-reflex after acute spinal lesion in a system that was not altered by the presence of anesthetic drugs. The main result of this study was that buspirone had a depressive impact on H-reflex amplitude for the first 20 min after drug administration. This depressive outcome was then attenuated and even reversed to an increased effect on the H-reflex which became significant 40 min post-dose. The absence of reflex variations when the buspirone treatment is given after 5-HT_{1A} receptor blocking by NAD-299 suggest a participation of this receptor in this observed buspirone activity. Since there is still an even stronger FDD 60 min after buspirone, the observed reflex enhancement later after buspirone is not likely to involve a loss of inhibitory control.

Buspirone Act as a 5-HT_{1A} Receptor Agonist on the Reflex

Buspirone is not a pure 5-HT_{1A} agonist, it also shows some affinity for dopaminergic and other serotoninergic receptors (Loane and Politis, 2012). By using the selective antagonist NAD-299 we show here that 5-HT_{1A} receptors activation is essential for buspirone induced modulation of H-reflex excitability. Even if this reflex is mainly of monosynaptic nature, it is well known that it remains under the control of several elements (Misiaszek, 2003). The 5-HT_{1A} receptors can be found at numerous locations on these elements including presynaptic, intrasynaptic and even outside the synaptic innervation. This heterogeneity probably explains why 5-HT have such multiple and opposite effects on motor circuits of the spinal cord, as elegantly reviewed in Perrier and Cotel (2015).

The short-term impact of buspirone observed in our experiments, i.e., reflex reduction, concurs with the literature on the effect of 5-HT_{1A} agonists. Indeed, monosynaptic reflex reduction has been shown with the 5-HT_{1A} agonist 8-OH-DPAT in rats with complete spinal lesion under α-chloralose or urethane anesthesia (Nagano et al., 1988; Hasegawa and Ono, 1996a; Honda and Ono, 1999). More recently, buspirone was used as a 5-HT_{1A} agonist and it was shown that systemic administration in awake humans reduces about 30% of F-wave amplitude, indicating direct decrease in motoneuron excitability and output (D'Amico et al., 2017).

Because 5-HT_{1A} receptors are mainly present on dorsal laminae of the spinal cord, it was proposed to be also involved in afferent regulation (Giroux et al., 1999; Noga et al., 2009). Such participation in afferent modulation by 5-HT_{1A} receptors has been confirmed by Crick et al. (1994) in rats (Hasegawa and Ono, 1996b). They showed that monosynaptic reflexes evoked by dorsal root stimulation are depressed by 8-OH-DPAT administration with no change in motoneuronal excitability. This suggests that reflex depression is induced by lowering neurotransmitter release at the presynaptic level. Such afferent regulation could be generated by 5-HT_{1A} receptors on afferent neurons and could be responsible for increased GABA-mediated inhibition (Gharagozloo et al., 1990).

The Absence of Anesthesia and Reversal From Inhibitory to Excitatory Effects of Buspirone

A reversal of the effect buspirone (or any other 5-HT_{1A} agonist) from inhibitory to excitatory later post-treatment has not been reported so far. Such differences with previous experiments could be related to the use of decerebrated preparations and the absence of anesthesia (Meehan et al., 2017) that affect reflex modulation (Ho and Waite, 2002) see also (Schmidt and Jordan, 2000). Indeed, for example, experiments on decerebrated cats disclosed reversal of group I autogenetic inhibition to polysynaptic excitation in extensor motoneurons after exposure to clonidine or L-DOPA, drugs that promote locomotion in spinal cats (Conway et al., 1987; Gossard et al., 1994). Interneurons involved in this reflex reversal are shared with CPGs and supraspinal inputs (Leblond et al., 2000, 2001).

Low threshold stimulation like the one used in the present study might also activate oligosynaptic pathways by some other large-diameter afferent fibers, such as type Ib afferents, that are also in contact with motoneurons. Because such depolarization involves the polysynaptic circuitry, the motor response would have longer delay and may be dissociated from monosynaptic activation (e.g., **Figure 1A**, bottom trace). Still, long-lasting effects on motoneurons by these pathways are not to be excluded and could be implicated in signal amplitude recorded by EMG.

Indeed, the absence of anesthesia most likely allowed otherwise quiescent spinal networks to be active and participate in the modulation of membrane conductance, affecting motoneuronal responsiveness (Harvey et al., 2006a,b; Li et al., 2006; Murray et al., 2010; see also D'Amico et al., 2014). However, slowly activated currents, like persistent inward currents, required long-duration input and could not be fully actuated by brief stimulations like the ones used in our study (Murray et al., 2011).

It is still not fully clear why the H-reflex was enhanced during the second phase of our experiment and this will be discussed in a later section. Nonetheless, to evaluate if this reversal from inhibition to excitation can be explained by a disinhibition, we measured FDD of the H-reflex. The FDD, also named homosynaptic depression or post-activation depression, was used in many animal models to study spinal reflex disinhibition (Thompson et al., 1992; Yates et al., 2008; Cote et al., 2011; Jeffrey-Gauthier et al., 2019). It was shown that this depression can occurs at higher rate of stimulation without any variation of motoneuronal excitability, reflecting a decreased probability of neurotransmitter release by the activated fibers as a consequence of their repeated activation (Hultborn et al., 1996). Our hypothesis was that disinhibition, in other word a lack of FDD 60 min after buspirone, would explain why there is a higher H-reflex at that moment. Our results showed that FDD is still present 60 min post-buspirone, suggesting that disinhibition would not explain the observed increase of reflex amplitude.

Opposite Effect of 5-HT_{1A} According to Receptor Location on the Motoneuron

As mentioned above, 5-HT_{1A} receptors are located at various locations that can get activated simultaneously. On the one hand, at the synaptic level, 5-HT is responsible for modulating fast-activated potassium channels via 5-HT_{1A} receptors (Jackson and White, 1990; Penington and Kelly, 1990). It was shown that 5-HT_{1A} receptors inhibit TASK-1 potassium channels that would contribute to the excitatory effect of 5-HT on spinal motoneurons (Perrier et al., 2003). By lowering outward cation flux, 5-HT_{1A} receptors shortened the refractory period and facilitated motoneuronal depolarization (Grunnet et al., 2004; Santini and Porter, 2010). This mechanism augments motoneuronal excitability and enhances motor responses to synaptic stimulation. On the other hand, there are extrasynaptic 5-HT_{1A} receptors that can be activated by spill-over during high 5-HT release at the synaptic level or background concentration of 5-HT (e.g., in systemic administration) that are known to be inhibitory. Indeed, 5-HT_{1A} receptor stimulation on axon hillocks elicits inhibition of sodium channels that are responsible for initiation of action potentials in motoneurons (Cotel et al., 2013; Perrier et al., 2013; Perrier and Cotel, 2015; Petersen et al., 2016). This inhibition decreases the number of spikes triggered and consequently reduce the amplitude of the EMG.

Thus, when large dose of buspirone is given, as in our experiments, 5-HT_{1A} receptors inhibit motoneuron output and decrease reflex amplitude through activity at the axon hillock sites even if there is an excitation at the synaptic level. This dual effect of 5-HT_{1A} receptors on motoneuronal excitability may be involved in the observed biphasic effect of buspirone over time on reflex amplitude through a switch in dominance of receptor type activity.

Indeed, drug action is concentration-dependent, and buspirone pharmacokinetics undergoes a biphasic elimination cycle (Sethy and Francis, 1988). The first half-life of the drug is reached after 24.8 min, a period that matches the transition phase of reflex amplitude in treated animals. This region relies mainly on the participation of astrocytes that have been demonstrated to be involved in 5-HT re-uptake, especially at the extrasynaptic level (Henn and Hamberger, 1971; Ritchie et al., 1981; Kimelberg and Katz, 1985; De-Miguel et al., 2015). Such region-dependent differences in the 5-HT clearance mechanisms could explain the biphasic effect of buspirone on reflex amplitude over time. Moreover, a desensitization of 5-HT_{1A} receptors after their pharmacological activation have been reported and should be considered as well in that reversal (Seth et al., 1997).

Reflex Inhibition Concomitant With Excitatory Effect on Locomotion

It was shown in another study from our laboratory that buspirone exerts a considerable acute facilitation of spinally mediated locomotion in mice after a complete mid-thoracic section of the spinal cord (Jeffrey-Gauthier et al., 2018). Indeed, by using the same amount of buspirone than in the present experiments, we were able to trigger locomotion right after the injection in previously paralyzed mice as early as 2 days after a complete lesion. Buspirone was also shown to potentiate locomotion when combined with other treatments (Ung et al., 2012; Gerasimenko et al., 2015). Since we find herein that buspirone have an early depressive effect on the H-reflex, it suggest that locomotion can be triggered during depression

of sensorimotor excitability induced by this treatment. This paradox is also observed with the 5-HT_{1A} partial agonist 8-OH-DPAT, which is known to inhibit the monosynaptic reflex (Nagano et al., 1988; Hasegawa and Ono, 1996a; Honda and Ono, 1999) and can facilitate recovery of locomotor function in spinal rats (Antri et al., 2003, 2005). Sensory inputs provided by the treadmill seem sufficient to initiate and maintain locomotor rhythm with buspirone. The same observation was made in cats where clonidine, a noradrenergic agonist that can trigger locomotion on a treadmill after a complete spinal lesion, reduce reflexes evoked by stimulation of the dorsum of the foot (Barbeau and Rossignol, 1987; Chau et al., 1998a).

These observations with adult animals that walk on a treadmill seem to disagree with results obtained during fictive locomotion in neonatal rodents where 5-HT_{1A} was reported to have an inhibitory effect on the spinal rhythmic activity (Beato and Nistri, 1998; Liu and Jordan, 2005; Pearlstein et al., 2005; Dunbar et al., 2010). For example, in the brainstem-spinal cord of neonatal mice, 5-HT release during fictive locomotion was enhanced by citalopram, a selective 5-HT re-uptake inhibitor, and a decreased burst duration and amplitude was observed (Dunbar et al., 2010). Since selective 5-HT_{1A} and 5-HT_{1B} antagonists reversed the inhibitory effect of citalopram, it was concluded that these receptors may rather be involved in rhythm inhibition. A similar conclusion has been drawn with neonatal rats where blocking 5-$HT_{1A/1B}$ receptors during motor activity, produced by brainstem stimulation, induced speed-up of the rhythm (Liu and Jordan, 2005). In both these studies, locomotor speed was impaired by 5-HT_{1A} receptor but the alternate pattern of locomotor rhythm was not blocked.

This discrepancy between results obtained during fictive locomotion or locomotion over a treadmill, when there is some exteroceptive stimulation, suggest that sensorimotor control is fundamental to the pro-locomotor effect of buspirone. Many studies employing different methodologies to induce locomotion have disclosed that reflex modulation is associated with locomotor expression (Grillner and Shik, 1973; McCrea, 2001; Frigon et al., 2012). Similarly, buspirone treatment induces spinal reflex re-organization and promotes locomotor activity.

CONCLUSION

In summary, even if the role of 5-HT on motoneuron excitability has been extensively studied for more than 50 years, our knowledge is still scarce on how this neuromodulator contribute to sensorimotor control. The heterogeneity of 5-HT receptors locations (pre-, intra- or extra-synaptically) make it really difficult to assess the outcome of a treatment with this neuromodulator after a complete spinal cord injury. Reflecting this heterogeneity, buspirone, if given at a dose that can trigger locomotion, was shown to have biphasic consequence on the H-reflex in time after an acute lesion of the spinal cord, starting with an early and acute inhibition, followed by an excitation of the reflex. This effect seems to be mediated by the activation of 5-HT_{1A} receptors.

DATA AVAILABILITY STATEMENT

The datasets generated for this study are available on request to the corresponding author.

ETHICS STATEMENT

The animal study was reviewed and approved by the Comité de bons soins aux animaux.

AUTHOR CONTRIBUTIONS

YD designed the study, conducted the experiments, acquired and analyzed the data, and wrote the manuscript. HL conceived and designed the study, acquired and analyzed the data, wrote the manuscript, and obtained funding for this work. Both authors have approved the final version of the manuscript and agreed to be accountable for all aspects of the work.

FUNDING

This work was funded by the Natural Sciences and Engineering Research Council (NSERC) of Canada (Grant 05403-2014 to HL). YD was supported by studentship from the Université du Québec à Trois-Rivières (Department of Anatomy).

ACKNOWLEDGMENTS

This manuscript has been released as a Pre-Print at BioRxiv (https://doi.org/10.1101/281451).

REFERENCES

Antri, M., Barthe, J. Y., Mouffle, C., and Orsal, D. (2005). Long-lasting recovery of locomotor function in chronic spinal rat following chronic combined pharmacological stimulation of serotonergic receptors with 8-OHDPAT and quipazine. *Neurosci. Lett.* 384, 162–167. doi: 10.1016/j.neulet.2005.04.062

Antri, M., Mouffle, C., Orsal, D., and Barthe, J. (2003). 5-HT 1A receptors are involved in short- and long-term processes responsible for 5-HT-induced locomotor function recovery in chronic spinal rat. *Eur. J. Neurosci.* 18, 1963–1972. doi: 10.1046/j.1460-9568.2003.02916.x

Barbeau, H., and Rossignol, S. (1987). Recovery of locomotion after chronic spinalization in the adult cat. *Brain Res.* 412, 84–95. doi: 10.1016/0006-8993(87)91442-9

Beato, M., and Nistri, A. (1998). Serotonin-induced inhibition of locomotor rhythm of the rat isolated spinal cord is mediated by the 5-HT1 receptor class. *Proc. Biol. Sci.* 265, 2073–2080. doi: 10.1098/rspb.1998.0542

Belanger, M., Drew, T., Provencher, J., and Rossignol, S. (1996). A comparison of treadmill locomotion in adult cats before and after spinal transection. *J. Neurophysiol.* 76, 471–491. doi: 10.1152/jn.1996.76.1.471

Chau, C., Barbeau, H., and Rossignol, S. (1998a). Early locomotor training with clonidine in spinal cats. *J. Neurophysiol.* 79, 392–409. doi: 10.1152/jn.1998.79.1.392

Chau, C., Barbeau, H., and Rossignol, S. (1998b). Effects of intrathecal α1 and α2-noradrenergic agonists and norepinephrine on locomotion in chronic spinal cats. *J. Neurophysiol.* 79, 2941–2963. doi: 10.1152/jn.1998.79.6.2941

Clarke, R. W., Harris, J., and Houghton, A. K. (1996). Spinal 5-HT-receptors and tonic modulation of transmission through a withdrawal reflex pathway in the decerebrated rabbit. *Br. J. Pharmacol.* 119, 1167–1176. doi: 10.1111/j.1476-5381.1996.tb16019.x

Conway, B. A., Hultborn, H., and Kiehn, O. (1987). Proprioceptive input resets central locomotor rhythm in the spinal cat. *Exp. Brain Res.* 68, 643–656.

Côté, M., and Gossard, J. (2004). Step training-dependent plasticity in spinal cutaneous pathways. *J. Neurosci.* 24, 11317–11327. doi: 10.1523/jneurosci.1486-04.2004

Côté, M. A., Ménard, A., and Gossard, J. P. (2003). Spinal cats on the treadmill: changes in load pathways. *J. Neurosci.* 23, 2789–2796. doi: 10.1523/jneurosci.23-07-02789.2003

Cote, M. P., Azzam, G. A., Lemay, M. A., Zhukareva, V., and Houle, J. D. (2011). Activity-dependent increase in neurotrophic factors is associated with an enhanced modulation of spinal reflexes after spinal cord injury. *J. Neurotrauma* 28, 299–309. doi: 10.1089/neu.2010.1594

Cotel, F., Exley, R., Cragg, S. J., and Perrier, J. (2013). Serotonin spillover onto the axon initial segment of motoneurons induces central fatigue by inhibiting action potential initiation. *Proc. Natl. Acad. Sci. U.S.A.* 110, 4774–4779. doi: 10.1073/pnas.1216150110

Crick, H., Manuel, N. A., and Wallis, D. I. (1994). A novel 5-HT receptor or a combination of 5-HT receptor subtypes may mediate depression of a spinal monosynaptic reflex in vitro. *Neuropharmacology* 33, 897–904. doi: 10.1016/0028-3908(94)90188-0

D'Amico, J. M., Butler, A. A., Héroux, M. E., Cotel, F., Perrier, J. F., Butler, J. E., et al. (2017). Human motoneurone excitability is depressed by activation of serotonin 1A receptors with buspirone. *J. Physiol.* 595, 1763–1773. doi: 10.1113/JP273200

D'Amico, J. M., Condliffe, E. G., Martins, K. J. B., Bennett, D. J., and Gorassini, M. A. (2014). Recovery of neuronal and network excitability after spinal cord injury and implications for spasticity. *Front. Integr. Neurosci.* 8:36. doi: 10.3389/fnint.2014.00036

De-Miguel, F. F., Leon-Pinzon, C., Noguez, P., and Mendez, B. (2015). Serotonin release from the neuronal cell body and its long-lasting effects on the nervous system. *Philos. Trans. R. Soc. Lond. B Biol. Sci.* 370, 20140196. doi: 10.1098/rstb.2014.0196

Develle, Y., and Leblond, H. (2016). "Effect buspirone effect on H-reflex in acute decerebrated mice," in *Proceedings of the SFN 46th annual meeting*, San Diego, CA.

Dobson, K. L., and Harris, J. (2012). A detailed surgical method for mechanical decerebration of the rat. *Exp. Physiol.* 97, 693–698. doi: 10.1113/expphysiol.2012.064840

Dunbar, M. J., Tran, M. A., and Whelan, P. J. (2010). Endogenous extracellular serotonin modulates the spinal locomotor network of the neonatal mouse. *J. Physiol.* 588, 139–156. doi: 10.1113/jphysiol.2009.177378

Edgerton, V. R., De Leon, R. D., Tillakaratne, N., Recktenwald, M., Hodqson, J., and Roy, R. R. (1997). Use-dependent plasticity in spinal stepping and standing. *Adv. Neurol.* 72, 233–247.

Frigon, A., Johnson, M. D., and Heckman, C. J. (2012). Differential modulation of crossed and uncrossed reflex pathways by clonidine in adult cats following complete spinal cord injury. *J. Physiol.* 590, 973–989. doi: 10.1113/jphysiol.2011.222208

Gerasimenko, Y., Lu, D., Modaber, M., Zdunowski, S., Gad, P., Sayenko, D., et al. (2015). Noninvasive reactivation of motor descending control after paralysis. *J. Neurotrauma* 32, 1968–1980. doi: 10.1089/neu.2015.4008

Gharagozloo, A., Holohean, A. M., Hackman, J. C., and Davidoff, R. A. (1990). Serotonin and GABA-induced depolarizations of frog primary afferent fibers. *Brain Res.* 532, 19–24. doi: 10.1016/0006-8993(90)91736-z

Giroux, N., Rossignol, S., and Reader, T. A. (1999). Autoradiographic study of α1- and α2-noradrenergic and serotonin 1A receptors in the spinal cord of normal and chronically transected cats. *J. Comp. Neurol.* 406, 402–414. doi: 10.1002/(sici)1096-9861(19990412)406:3<402::aid-cne8>3.0.co;2-f

Gossard, J. P., Brownstone, R. M., Barajon, I., and Hultborn, H. (1994). Transmission in a locomotor-related group Ib pathway from hindlimb extensor muscles in the cat. *Exp. Brain Res.* 98, 213–228.

Gozariu, M., Roth, V., Keime, F., Le Bars, D., and Willer, J. C. (1998). An electrophysiological investigation into the monosynaptic H-reflex in the rat. *Brain Res.* 782, 343–347. doi: 10.1016/s0006-8993(97)01402-9

Grillner, S., and Shik, M. L. (1973). On the descending control of the lumbosacral spinal cord from the "mesencephalic locomotor region". *Acta Physiol. Scand.* 87, 320–333. doi: 10.1111/j.1748-1716.1973.tb05396.x

Grunnet, M., Jespersen, T., and Perrier, J. (2004). 5-HT 1A receptors modulate small-conductance Ca 2+ -activated K + channels. *J. Neurosci. Res.* 78, 845–854. doi: 10.1002/jnr.20318

Harvey, P. J., Li, X., Li, Y., and Bennett, D. J. (2006a). 5-HT2 receptor activation facilitates a persistent sodium current and repetitive firing in spinal motoneurons of rats with and without chronic spinal cord injury. *J. Neurophysiol.* 96, 1158–1170. doi: 10.1152/jn.01088.2005

Harvey, P. J., Li, X., Li, Y., and Bennett, D. J. (2006b). Endogenous monoamine receptor activation is essential for enabling persistent sodium currents and repetitive firing in rat spinal motoneurons. *J. Neurophysiol.* 96, 1171–1186. doi: 10.1152/jn.00341.2006

Hasegawa, Y., and Ono, H. (1996a). Effect of (±)-8-hydroxy-2-(di-n-propylamino)tetralin hydrobromide on spinal motor systems in anesthetized intact and spinalized rats. *Eur. J. Pharmacol.* 295, 211–214. doi: 10.1016/0014-2999(95)00759-8

Hasegawa, Y., and Ono, H. (1996b). Effects of 8-OH-DPAT, a 5-HT1A receptor agonist, and DOI, a 5-HT2A/2C agonist, on monosynaptic transmission in spinalized rats. *Brain Res.* 738, 158–161. doi: 10.1016/0006-8993(96)00991-2

Henn, F. A., and Hamberger, A. (1971). Glial cell function: uptake of transmitter substances. *Proc. Natl. Acad. Sci. U.S.A.* 68, 2686–2690. doi: 10.1073/pnas.68.11.2686

Ho, S. M., and Waite, P. M. (2002). Effects of different anesthetics on the paired-pulse depression of the H reflex in adult rat. *Exp. Neurol.* 177, 494–502. doi: 10.1006/exnr.2002.8013

Honda, M., and Ono, H. (1999). Differential effects of (R)- and (S)-8-hydroxy-2-(di-n-propylamino)tetralin on the monosynaptic spinal reflex in rats. *Eur. J. Pharmacol.* 373, 171–179. doi: 10.1016/s0014-2999(99)00284-8

Hultborn, H., Illert, M., Nielsen, J., Paul, A., Ballegaard, M., and Wiese, H. (1996). On the mechanism of the post-activation depression of the H-reflex in human subjects. *Exp. Brain Res.* 108, 450–462.

Ichiyama, R. M., Courtine, G., Gerasimenko, Y. P., Yang, G. J., van den Brand, R., Lavrov, I. A., et al. (2008). Step training reinforces specific spinal locomotor circuitry in adult spinal rats. *J. Neurosci.* 28, 7370–7375. doi: 10.1523/JNEUROSCI.1881-08.2008

Jackson, D., and White, S. (1990). Receptor subtypes mediating facilitation by serotonin of excitability of spinal motoneurons. *Neuropharmacology* 29, 787–797. doi: 10.1016/0028-3908(90)90151-g

Jeffrey-Gauthier, R., Josset, N., Bretzner, F., and Leblond, H. (2018). Facilitation of locomotor spinal networks activity by buspirone after a complete spinal cord lesion in mice. *J. Neurotrauma* 35, 2208–2221. doi: 10.1089/neu.2017.5476

Jeffrey-Gauthier, R., Piche, M., and Leblond, H. (2019). H-reflex disinhibition by lumbar muscle inflammation in a mouse model of spinal cord injury. *Neurosci. Lett.* 690, 36–41. doi: 10.1016/j.neulet.2018.10.005

Johansson, L., Sohn, D., Thorberg, S. O., Jackson, D. M., Kelder, D., Larsson, L. G., et al. (1997). The pharmacological characterization of a novel selective 5-hydroxytryptamine1A receptor antagonist, NAD-299. *J. Pharmacol. Exp. Ther.* 283, 216–225.

Kimelberg, H. K., and Katz, D. M. (1985). High-affinity uptake of serotonin into immunocytochemically identified astrocytes. *Science* 228, 889–891. doi: 10.1126/science.3890180

Knikou, M. (2008). The H-reflex as a probe: pathways and pitfalls. *J. Neurosci. Methods* 171, 1–12. doi: 10.1016/j.jneumeth.2008.02.012

Leblond, H., Espérance, M., Orsal, D., and Rossignol, S. (2003). Treadmill locomotion in the intact and spinal mouse. *J. Neurosci.* 23, 11411–11419. doi: 10.1523/jneurosci.23-36-11411.2003

Leblond, H., Ménard, A., and Gossard, J. P. (2000). Bulbospinal control of spinal cord pathways generating locomotor extensor activities in the cat. *J. Physiol.* 525, 225–240. doi: 10.1111/j.1469-7793.2000.t01-1-00225.x

Leblond, H., Ménard, A., and Gossard, J. P. (2001). Corticospinal control of locomotor pathways generating extensor activities in the cat. *Exp. Brain Res.* 138, 173–184. doi: 10.1007/s002210100696

Li, X., Murray, K. C., Harvey, P. J., Ballou, E. W., and Bennett, D. J. (2006). Serotonin facilitates a persistent calcium current in motoneurons of rats with and without chronic spinal cord injury. *J. Neurophysiol.* 97, 1236–1246. doi: 10.1152/jn.00995.2006

Liu, J., and Jordan, L. M. (2005). Stimulation of the parapyramidal region of the neonatal rat brain stem produces locomotor-like activity involving spinal 5-HT7 and 5-HT2A receptors. *J. Neurophysiol.* 94, 1392–1404. doi: 10.1152/jn.00136.2005

Loane, C., and Politis, M. (2012). Buspirone: what is it all about? *Brain Res.* 1461, 111–118. doi: 10.1016/j.brainres.2012.04.032

Lovely, R. G., Gregor, R. J., Roy, R. R., and Edgerton, V. R. (1986). Effects of training on the recovery of full-weight-bearing stepping in the adult spinal cat. *Exp. Neurol.* 92, 421–435. doi: 10.1016/0014-4886(86)90094-4

McCrea, D. A. (2001). Spinal circuitry of sensorimotor control of locomotion. *J. Physiol.* 533, 41–50. doi: 10.1111/j.1469-7793.2001.0041b.x

Meehan, C. F., Grondahl, L., Nielsen, J. B., and Hultborn, H. (2012). Fictive locomotion in the adult decerebrate and spinal mouse *in vivo*. *J. Physiol.* 590, 289–300. doi: 10.1113/jphysiol.2011.214643

Meehan, C. F., Mayr, K. A., Manuel, M., Nakanishi, S. T., and Whelan, P. J. (2017). Decerebrate mouse model for studies of the spinal cord circuits. *Nat. Protoc.* 12, 732–747. doi: 10.1038/nprot.2017.001

Meinck, H. M. (1976). Occurrence of the H reflex and the F wave in the rat. *Electroencephalogr. Clin. Neurophysiol.* 41, 530–533. doi: 10.1016/0013-4694(76)90064-x

Misiaszek, J. E. (2003). The H-reflex as a tool in neurophysiology: its limitations and uses in understanding nervous system function. *Muscle Nerve* 28, 144–160. doi: 10.1002/mus.10372

Murray, K. C., Nakae, A., Stephens, M. J., Rank, M., D'Amico, J., Harvey, P. J., et al. (2010). Recovery of motoneuron and locomotor function after spinal cord injury depends on constitutive activity in 5-HT(2C) receptors. *Nat. Med.* 16, 694–700. doi: 10.1038/nm.2160

Murray, K. C., Stephens, M. J., Rank, M., Amico, J., Gorassini, M. A., and Bennett, D. J. (2011). Polysynaptic excitatory postsynaptic potentials that trigger spasms after spinal cord injury in rats are inhibited by 5-HT1B and 5-HT1F receptors. *J. Neurophysiol.* 106, 925–943. doi: 10.1152/jn.01011.2010

Nagano, N., Ono, H., and Fukuda, H. (1988). Functional significance of subtypes of 5-HT receptors in the rat spinal reflex pathway. *Gen. Pharmacol.* 19, 789–793. doi: 10.1016/0306-3623(88)90211-x

Noga, B. R., Johnson, D. M. G., Riesgo, M. I., and Pinzon, A. (2009). Locomotor-activated neurons of the cat. I. serotonergic innervation and co-localization of 5-HT7, 5-HT2a and 5-HT1a receptors in the thoraco-lumbar spinal cord. *J. Neurophysiol.* 102, 1560–1576. doi: 10.1152/jn.91179.2008

Otoshi, C. K., Walwyn, W. M., Tillakaratne, N. J. K., Zhong, H., Roy, R. R., and Edgerton, V. R. (2009). Distribution and localization of 5-HT(1A) receptors in the rat lumbar spinal cord after transection and deafferentation. *J. Neurotrauma* 26, 575–584. doi: 10.1089/neu.2008.0640

Pearlstein, E., Ben Mabrouk, F., Pflieger, J. F., and Vinay, L. (2005). Serotonin refines the locomotor-related alternations in the *in vitro* neonatal rat spinal cord. *Eur. J. Neurosci.* 21, 1338–1346. doi: 10.1111/j.1460-9568.2005.03971.x

Penington, N. J., and Kelly, J. S. (1990). Serotonin receptor activation reduces calcium current in an acutely dissociated adult central neuron. *Neuron* 4, 751–758. doi: 10.1016/0896-6273(90)90201-p

Perreault, M. C., Angel, M. J., Guertin, P., and McCrea, D. A. (1995). Effects of stimulation of hindlimb flexor group II afferents during fictive locomotion in the cat. *J. Physiol.* 487, 211–220. doi: 10.1113/jphysiol.1995.sp020872

Perrier, J., Alaburda, A., and Hounsgaard, J. (2003). 5-HT(1A) receptors increase excitability of spinal motoneurons by inhibiting a TASK-1-like K(+) current in the adult turtle. *J. Physiol.* 548, 485–492. doi: 10.1111/j.1469-7793.2003.00485.x

Perrier, J., and Cotel, F. (2015). Serotonergic modulation of spinal motor control. *Curr. Opin. Neurobiol.* 33, 1–7. doi: 10.1016/j.conb.2014.12.008

Perrier, J., Rasmussen, H., Christensen, R., and Petersen, A. (2013). Modulation of the intrinsic properties of motoneurons by serotonin. *Curr. Pharm. Des.* 19, 4371–4384. doi: 10.2174/1381612811319990341

Petersen, A. V., Cotel, F., and Perrier, J. (2016). Plasticity of the axon initial segment: fast and slow processes with multiple functional roles. *Neuroscientist* 23, 364–373. doi: 10.1177/1073858416648311

Ritchie, T., Glusman, S., and Haber, B. (1981). The filum terminale of the frog spinal cord, a nontransformed glial preparation: II. Uptake of serotonin. *Neurochem Res* 6, 441–452. doi: 10.1007/bf00963859

Rossignol, S. (2006). Plasticity of connections underlying locomotor recovery after central and/or peripheral lesions in the adult mammals. *Philos. Trans. R. Soc. Lond. B Biol. Sci.* 361, 1647–1671. doi: 10.1098/rstb.2006.1889

Santini, E., and Porter, J. T. (2010). M-type potassium channels modulate the intrinsic excitability of infralimbic neurons and regulate fear expression and extinction. *J. Neurosci.* 30, 12379–12386. doi: 10.1523/JNEUROSCI.1295-10.2010

Schmidt, B. J., and Jordan, L. M. (2000). The role of serotonin in reflex modulation and locomotor rhythm production in the mammalian spinal cord. *Brain Res. Bull.* 53, 689–710. doi: 10.1016/s0361-9230(00)00402-0

Seth, P., Gajendiran, M., and Ganguly, D. K. (1997). Desensitization of spinal 5-HT1A receptors to 8-OH-DPAT: an in vivo spinal reflex study. *Neuroreport* 8, 2489–2493. doi: 10.1097/00001756-199707280-00015

Sethy, V., and Francis, J. (1988). Pharmacokinetics of buspirone as determined by ex vivo (3H)-DPAT binding. *Life Sci.* 42, 1045–1048. doi: 10.1016/0024-3205(88)90559-0

Slawinska, U., Miazga, K., and Jordan, L. (2014). The role of serotonin in the control of locomotor movements and strategies for restoring locomotion after spinal cord injury. *Acta Neurobiol. Exp.* 74, 172–187.

Takahashi, T., and Berger, A. J. (1990). Direct excitation of rat spinal motoneurones by serotonin. *J. Physiol.* 423:63. doi: 10.1113/jphysiol.1990.sp018011

Thompson, F. J., Reier, P. J., Lucas, C. C., and Parmer, R. (1992). Altered patterns of reflex excitability subsequent to contusion injury of the rat spinal cord. *J. Neurophysiol.* 68, 1473–1486. doi: 10.1152/jn.1992.68.5.1473

Ung, R.-V., Rouleau, P., and Guertin, P. A. (2012). Functional and physiological effects of treadmill training induced by buspirone, carbidopa, and L-DOPA in clenbuterol-treated paraplegic mice. *Neurorehab. Neural. Repair* 26, 385–394. doi: 10.1177/1545968311427042

Yates, C., Charlesworth, A., Allen, S. R., Reese, N. B., Skinner, R. D., and Garcia-Rill, E. (2008). The onset of hyperreflexia in the rat following complete spinal cord transection. *Spinal Cord* 46, 798–803. doi: 10.1038/sc.2008.49

Yomono, H. S., Suzuki, H., and Yoshioka, K. (1992). Serotonergic fibers induce a long-lasting inhibition of monosynaptic reflex in the neonatal rat spinal cord. *Neuroscience* 47, 521–531. doi: 10.1016/0306-4522(92)90162-u

Zhang, L. (1991). Effects of 5-hydroxytryptamine on cat spinal motoneurons. *Can. J. Physiol. Pharmacol.* 69, 154–163. doi: 10.1139/y91-022

Conflict of Interest: The authors declare that the research was conducted in the absence of any commercial or financial relationships that could be construed as a potential conflict of interest.

frontiers in Systems Neuroscience

REVIEW
published: 17 January 2020
doi: 10.3389/fnsys.2019.00084

Role of Propriospinal Neurons in Control of Respiratory Muscles and Recovery of Breathing Following Injury

Victoria N. Jensen[1], *Warren J. Alilain*[2,3] *and Steven A. Crone*[4,5,6]*

[1]Neuroscience Graduate Program, University of Cincinnati College of Medicine, Cincinnati, OH, United States, [2]Spinal Cord and Brain Injury Research Center, University of Kentucky College of Medicine, Lexington, KY, United States, [3]Department of Neuroscience, University of Kentucky College of Medicine, Lexington, KY, United States, [4]Division of Neurosurgery, Cincinnati Children's Hospital Medical Center, Cincinnati, OH, United States, [5]Division of Developmental Biology, Cincinnati Children's Hospital Medical Center, Cincinnati, OH, United States, [6]Department of Neurosurgery, University of Cincinnati College of Medicine, Cincinnati, OH, United States

Respiratory motor failure is the leading cause of death in spinal cord injury (SCI). Cervical injuries disrupt connections between brainstem neurons that are the primary source of excitatory drive to respiratory motor neurons in the spinal cord and their targets. In addition to direct connections from bulbospinal neurons, respiratory motor neurons also receive excitatory and inhibitory inputs from propriospinal neurons, yet their role in the control of breathing is often overlooked. In this review, we will present evidence that propriospinal neurons play important roles in patterning muscle activity for breathing. These roles likely include shaping the pattern of respiratory motor output, processing and transmitting sensory afferent information, coordinating ventilation with motor activity, and regulating accessory and respiratory muscle activity. In addition, we discuss recent studies that have highlighted the importance of propriospinal neurons for recovery of respiratory muscle function following SCI. We propose that molecular genetic approaches to target specific developmental neuron classes in the spinal cord would help investigators resolve the many roles of propriospinal neurons in the control of breathing. A better understanding of how spinal circuits pattern breathing could lead to new treatments to improve breathing following injury or disease.

Keywords: neuroplasticity, spinal cord injury (SCI), interneurons, breathing, central pattern generation (CPG)

OPEN ACCESS

Edited by:
Michael A. Lane,
Drexel University, United States

Reviewed by:
Michael G. Fehlings,
Toronto Western Hospital, Canada
Carmelo Bellardita,
University of Copenhagen, Denmark
David Fuller,
University of Florida, United States

***Correspondence:**
Steven A. Crone
steven.crone@cchmc.org

Received: *27 August 2019*
Accepted: *16 December 2019*
Published: *17 January 2020*

Citation:
Jensen VN, Alilain WJ and Crone SA (2020) Role of Propriospinal Neurons in Control of Respiratory Muscles and Recovery of Breathing Following Injury. Front. Syst. Neurosci. 13:84. doi: 10.3389/fnsys.2019.00084

INTRODUCTION

Respiratory failure is the leading cause of death in spinal cord injury (SCI) (Berlly and Shem, 2007; Berlowitz et al., 2016). Connections between brainstem respiratory centers and respiratory motor neurons in the spinal cord are disrupted following injury, leading to loss of respiratory drive. Since respiratory motor neurons also receive excitatory and inhibitory inputs from propriospinal neurons, spinal circuits may serve as substrates to improve breathing following injury (Lane, 2011; Lee and Fuller, 2011; Marchenko et al., 2015; Zholudeva et al., 2018b). For the purposes of this review, we refer to propriospinal neurons as neurons whose cell bodies are located in the spinal cord but do not project outside the central nervous system. They may have short segmental projections, long multi-segmental spinal projections, and/or projections

to the brainstem. Propriospinal neurons appear to contribute to patterning respiratory motor output to ensure efficient and appropriate ventilation over a wide range of behaviors and physiological conditions, whereas brainstem neurons are primarily responsible for generating the three phases of respiratory rhythm (inspiration, post-inspiration, and active expiration; Del Negro et al., 2018; Ramirez and Baertsch, 2018). This review will summarize some of the roles of spinal circuits in the control of breathing in healthy animals, as well as their potential roles in adapting to injury to maintain ventilation. We will also discuss how modern tools to label or manipulate specific developmental neuron classes could help investigators further probe the role of propriospinal neurons in the control of breathing.

PROPRIOSPINAL NEURONS PATTERN RESPIRATORY MOTOR ACTIVITY

Breathing requires a complex system of muscles to draw air into the lungs, maintain an open airway, and subsequently expel air out of the lungs. This requires coordination between different inspiratory and expiratory muscles, as well as precise control of the amplitude and timing of respiratory muscle activity. Propriospinal neurons play important roles in patterning this activity. Although more work is needed to better define the functional roles of propriospinal neurons in the control of breathing, there is evidence that these roles include shaping the pattern of respiratory motor output, processing and transmitting sensory afferent information, and coordinating ventilation with motor activity (**Figure 1**).

Propriospinal Neurons Shape the Pattern of Respiratory Motor Output

Intraspinal stimulation studies indicate that a complex propriospinal network located throughout the cervical and thoracic cord can control the activity of inspiratory muscles (Sunshine et al., 2018). Respiratory propriospinal neurons have been described in the spinal cord of the cat, dog, rat, mouse, and human. They are located in cervical, thoracic and lumbar spinal segments and are distributed throughout the ventral horn, intermediate laminae, and dorsal horn (for reviews, see Lane, 2011; Ikeda et al., 2017; Zaki Ghali et al., 2019). These neurons include pre-phrenic neurons in C3–6 (near the phrenic nucleus, whose motor neurons innervate the diaphragm) as well as high cervical spinal cord neurons in C1-2 (Oku et al., 2008; Okada et al., 2009; Jones et al., 2012). Inspiratory and expiratory neurons are also found in the thoracic cord and it has been estimated that they outnumber bulbospinal respiratory neurons by 10 to 1 (Kirkwood et al., 1988). Both excitatory and inhibitory respiratory neurons have been described (Saywell et al., 2011; Iizuka et al., 2016, 2018). Propriospinal neurons that control limb movements, posture, or autonomic functions are also found in the cervical and thoracic cord. Consequently, propriospinal neurons cannot be distinguished based on location alone. In fact, some propriospinal neurons may perform dual functions in respiration and limb movements (Le Gal et al., 2016). In addition, propriospinal neurons may influence respiratory centers *via* ascending projections to the brainstem (Lane et al., 2008; Jones et al., 2012). Thus, respiratory propriospinal neurons include a diverse group of neurons throughout the spinal cord that likely perform many distinct functions.

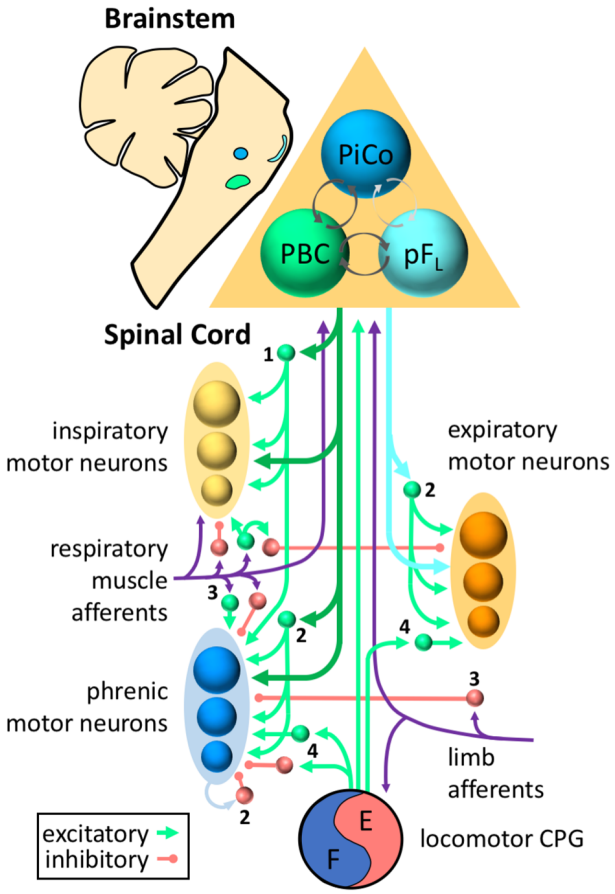

FIGURE 1 | Roles for propriospinal neurons in control of respiratory muscles. Respiratory rhythm is generated by three oscillators located in discrete regions of the brainstem—the pre-Bötzinger complex (PBC, green) for inspiration, the lateral parafacial region (pFL, turquoise) for active expiration, and the post-inspiratory complex (PiCo, blue) for the post-inspiratory phase of breathing. Excitatory and inhibitory interactions (with inhibition typically dominating) between the three oscillators ensure coordination of each phase (dark gray arrows = known connections, light gray arrows = hypothesized connections). The inspiratory drive is transmitted from the brainstem to the spinal cord *via* bulbospinal neurons of the rostral ventral respiratory group (dark green arrows), whereas expiratory drive is transmitted *via* bulbospinal neurons of the caudal ventral respiratory group (turquoise arrows). Bulbospinal pathways can provide drive directly to phrenic motor neurons (blue), other inspiratory motor neurons (yellow, e.g., external intercostal, scalene, etc.), or expiratory motor neurons (orange, e.g., abdominal muscles). In addition, bulbospinal pathways can activate propriospinal neurons (excitatory = green, inhibitory = red) that modulate respiratory motor activity. Sensory afferents (purple) from respiratory muscles or limb muscles can project to propriospinal neurons as well as the brainstem. For clarity, not all neurons/connections are shown. The roles of propriospinal neurons in controlling breathing include: **(1)** coordinating different respiratory motor pools; **(2)** patterning the activity of respiratory motor neurons within the same motor pool; **(3)** processing and transmitting afferent input; and **(4)** coordinating locomotor and respiratory activity.

Propriospinal neurons likely help coordinate activity between different respiratory muscle groups, as upper cervical neurons have been described that control both phrenic and intercostal motor neurons (Lipski and Duffin, 1986). Further, dual tracing studies have described individual cervical neurons connected to both phrenic and intercostal motor neurons (Lane et al., 2008). Although bulbospinal neurons project throughout the spinal cord and can synchronize inspiratory motor neurons across multiple segments, propriospinal neurons appear to synchronize inspiratory motor neurons on a longer time scale and thus may provide an additional level of modulatory control (Kirkwood et al., 1982a,b). Likewise, although separate bulbospinal pathways provide the inspiratory and expiratory drive to respiratory motor neurons, propriospinal networks may provide reciprocal inhibition between inspiratory and expiratory intercostal motorneurons (Aminoff and Sears, 1971). These propriospinal networks may provide an additional level of control for modulation of breathing by sensory afferents or the cerebral cortex.

It has been hypothesized that propriospinal neurons can modify the amplitude of motor output by relaying and/or amplifying central respiratory drive to motor neurons. This is based on observations that at least a subset of propriospinal neurons are innervated by inspiratory rVRG neurons or display inspiratory-related phasic bursting (Hilaire et al., 1983, 1986; Palisses et al., 1989; Duffin and Iscoe, 1996; Hayashi et al., 2003; Lane et al., 2008; Sandhu et al., 2015). Multiunit recordings of spinal neurons and cross-correlation analyses have identified both excitatory and inhibitory pre-phrenic propriospinal neurons in the rat cervical cord (Sandhu et al., 2015; Streeter et al., 2017). Acute intermittent hypoxia (a known driver of respiratory plasticity) enhances functional connectivity between excitatory neurons and pre-phrenic propriospinal neurons, suggesting that changes in propriospinal neuron function can increase motor output (Streeter et al., 2017). In addition, inhibitory neurons help pattern the duration of motor output. Studies of the rat phrenic nucleus have identified inspiratory, expiratory, and tonic firing inhibitory (GABAergic) interneurons (Marchenko et al., 2015; Ghali, 2018). The inspiratory inhibitory neurons include, but are probably not limited to, Renshaw cells that provide recurrent inhibition to phrenic and intercostal motor neurons (Kirkwood et al., 1981; Hilaire et al., 1983, 1986; Lipski et al., 1985; Iizuka et al., 2018). Blocking GABAergic inhibition by spinal neurons alters the shape of the phrenic motor burst and increases activity during expiration (Marchenko et al., 2015). Thus, it is likely that spinal circuits shape the relatively uniform respiratory drive from the brainstem into a pattern of activity-specific for each motor pool, at least under some conditions.

Why do we need muscle-specific patterns of motor activity? One explanation is that propriospinal neurons help ensure that breathing is efficient by making effective use of body biomechanics, which can vary between species and even individuals. The timing, discharge frequency, and patterns of activity vary between inspiratory motor pools during breathing (Butler et al., 2014). It has been proposed that "neuromechanical matching" of the drive to the inspiratory motor neurons ensures the most efficient contraction of inspiratory muscles based on their mechanical advantage (De Troyer et al., 2005; Butler et al., 2014). In humans, for example, rostral intercostal muscles are preferentially recruited for inspiration because they provide a higher mechanical advantage compared to caudal intercostal muscles. This pattern cannot be attributed solely to intrinsic motor neuron properties and does not require afferent input. Moreover, this pattern is mediated by spinal circuits because the same pattern of intercostal muscle activity is seen following high-frequency electrical stimulation of the spinal cord in animals with a C2 spinal section as is observed in spontaneously breathing dogs (DiMarco and Kowalski, 2011). Neuromechanical matching of the inspiratory drive to respiratory muscles is likely mediated by excitatory propriospinal neurons because blocking inhibitory neurotransmission does not alter the rostrocaudal gradient of thoracic inspiratory motor activity in a neonatal rat spinal cord preparation (Oka et al., 2019). Because disease and injury can alter an individual's breathing biomechanics, plasticity within propriospinal circuits is likely critical to maintaining efficient breathing.

Propriospinal Neurons Process and Transmit Sensory Afferent Information

Respiratory muscle afferents influence multiple aspects of respiratory motor output as well as autonomic functions (for review, see Nair et al., 2017b). Phrenic afferents include group Ia (muscle spindle that sense stretch), Ib (Golgi tendon organs that sense tension/load), group III and IV afferents that sense metabolites/fatigue, and pressure-sensitive afferents in the diaphragm that might be Pacinian corpuscles (Nair et al., 2017b). Compared to limb or intercostal muscles, the diaphragm has a relatively low proportion of Ia afferents, but the significance of this difference for respiratory control is not clear (Corda et al., 1965; Road, 1990). It is important to note that proprioceptive reflexes mediated by muscle afferents (that project into the spinal cord) are distinct from the Hering-Breuer reflex mediated by vagal pulmonary stretch receptors that project to the brainstem. Proprioceptive information is used in many ways to control the pattern of breathing through local spinal circuits as well as spino-bulbar-spinal circuits.

Propriospinal neurons likely play a key role in the processing of afferent information and relaying it to the appropriate targets in the spinal cord and brainstem. In support of this hypothesis, phrenic afferents rarely project directly to phrenic motor neurons that control the diaphragm; instead, most project it to the interneurons in the dorsal or intermediate laminae (Nair et al., 2017a). Notably, the propriospinal neurons in the cervical cord that respond to phrenic afferent stimulation appear to be largely distinct from the neurons that receive rhythmic respiratory drive (Cleland and Getting, 1993; Iscoe and Duffin, 1996).

Respiratory afferents mediate both excitatory and inhibitory reflexes *via* spinal and supraspinal circuits (Gill and Kuno, 1963; Marlot et al., 1987; Macron et al., 1988). For example, stimulation of the phrenic nerve in various animal models can cause bilateral inhibition of the diaphragm (the phrenic-to-phrenic reflex; Gill and Kuno, 1963; Marlot et al., 1987; Speck and Revelette, 1987), as well as external intercostal muscles (the phrenic-to-intercostal

reflex; Brichant and De Troyer, 1997; De Troyer, 1998; De Troyer et al., 1999). A spinal transection at C2 abolishes the contralateral phrenic-to-phrenic reflex, but the ipsilateral reflex is maintained (Speck, 1987). This result suggests that spinal circuits mediate ipsilateral inhibition of respiratory muscles but supraspinal circuits are involved in contralateral inhibition. However, it is not known whether the contralateral reflex is mediated by a spino-bulbar-spinal loop or whether supraspinal input is merely required to facilitate a spinal reflex, as has been demonstrated for group Ib and II afferent control of limb muscles (Cabaj et al., 2006). Phrenic afferents can also inhibit the diaphragm, intercostal and scalene muscles in humans and the latency suggests that it might involve brainstem circuits (Butler et al., 2003). The circuitry may involve multiple components as phrenic nerve stimulation can produce a biphasic response in which inhibition is followed by a long latency excitatory response (Marlot et al., 1987; Supinski et al., 1993). Moreover, the impact of afferents can be quite significant as high-intensity stimulation of phrenic group III–IV afferents can stimulate ventilation up to 4–5 times baseline values (Yu and Younes, 1999). Thus, the regulation of breathing by phrenic afferents is complex-involving multiple afferent types (and presumably spinal interneuron types) as well as both spinal and supraspinal circuitry.

Intercostal afferents sense changes in the muscles controlling the chest wall and can influence not only intercostal muscle activity, but also diaphragm and accessory respiratory muscle activity (Butler et al., 2014; McBain et al., 2016). Stimulation of intercostal afferents can either inhibit or facilitate phrenic motor activity and reflexes appear to be mediated by spinal (excitatory and inhibitory) and supraspinal (inhibitory) components (Decima et al., 1967; Decima and von Euler, 1969; Remmers, 1973; Bellingham, 1999). Short-latency intersegmental reflexes have also been described between intercostal and scalene muscles in humans (McBain et al., 2016). The significance of spinal intersegmental reflexes for coordinating respiratory muscle activity may best be illustrated by the observation that proprioceptive afferents can entrain phrenic nerve activity to chest movements driven by a ventilator even in 'spinalized' animals (Persegol et al., 1987).

Identifying the propriospinal and brainstem neurons that mediate the different types of afferent input and investigating how each of them influences respiratory motor activity could advance the development of diaphragm pacing or spinal stimulation devices to retore ventilation following disease or injury.

Propriospinal Neurons Help Coordinate Ventilation and Motor Activity

During exercise, mammals increase ventilation to maintain proper arterial oxygen and carbon dioxide levels despite elevated metabolic activity (Forster et al., 2012; Guyenet and Bayliss, 2015). This is accomplished without directly sensing the rate of gas exchange in muscle or lungs. The mechanisms that lead to exercise hyperpnea are thought to include both a feed-forward central command mechanism (particularly at the onset of exercise) as well as group III/IV afferent feedback from limb muscles (Forster et al., 2012). Although the circuits that mediate these responses to match ventilation to motor activity are not currently known, it is likely that propriospinal neurons play critical roles. In addition to ensuring appropriate overall respiratory activity levels, propriospinal neurons are likely involved in the cycle-by-cycle coordination between locomotor and respiratory periods, which we refer to as entrainment.

There is mounting evidence that spinal respiratory circuits receive input from the locomotor central pattern generator (CPG). For example, activation of fictive locomotion in isolated brainstem/spinal cord preparations can cause an increase in phrenic burst frequency as well as entrainment of locomotor and respiratory periods (Le Gal et al., 2014; Yazawa, 2014). These responses are likely mediated in part by reciprocal connections between spinal and brainstem circuits. However, there are also intersegmental interactions within the spinal cord that link the locomotor and respiratory circuits. For example, phrenic motor neurons can be driven by lumbar spinal circuits when local inhibition is blocked even following a C1 transection (Cregg et al., 2017). In addition, there is entrainment (a 1:1 coupling between successive periods) between locomotor and phrenic motor output in spinalized rabbits (Viala et al., 1987). This entrainment might reflect direct interaction between the locomotor CPG and spinal circuits driving respiration (Viala, 1986). In fact, the division between "locomotor" and "respiratory" circuits might not be as precise as is usually assumed. Bimodal spinal neurons were recently described in a neonatal brainstem spinal cord preparation that were expiratory and also received flexor-related drive *via* propriospinal pathways (Le Gal et al., 2016). Additional research is needed to investigate the potential overlap between locomotor and respiratory neurons in the spinal cord and brainstem as well as their interconnections, particularly in adult animals.

Limb muscle afferents play important roles in matching locomotor and respiratory activity (exercise hyperpnea) as well as coupling the respiratory and locomotor cycles (entrainment; Shevtsova et al., 2019). However, as some afferents have direct projections to the brainstem, the role of propriospinal neurons in mediating these effects needs further investigation. For example, stimulation of limb muscles or nerves can increase phrenic activity *via* brainstem respiratory centers but can also inhibit phrenic activity *via* spinal circuits (Eldridge et al., 1981). *In vitro* preparations have been used to demonstrate that limb afferent stimulation affects the rate of ventilation (i.e., coordinating overall locomotor and respiratory activity levels) through its effects on spinal neurons of the locomotor CPG (Morin and Viala, 2002). On the other hand, entrainment of the locomotor and respiratory periods appears to occur *via* ascending limb afferent projections directly to brainstem respiratory centers (Morin and Viala, 2002; Giraudin et al., 2008, 2012). This is consistent with experiments showing that stimulation of limb muscle afferents and phrenic afferents can increase ventilation in an additive manner, suggesting they act through different mechanisms (Ward et al., 1992). The fact that spinalized rabbits show locomotor-respiratory entrainment after treatment with nialamide and DOPA suggests that multiple mechanisms of entrainment may exist (Viala, 1986). These experiments suggest that limb afferent stimulation and/or limb

motor rehabilitation could improve breathing following disease or injury.

Propriospinal Neurons Regulate Accessory Respiratory Muscle Activity

Accessory respiratory muscles enhance ventilation under conditions of increased oxygen demand. Inspiratory accessory respiratory muscles are used to increase thoracic volume to ensure sufficient ventilation and include the scalene, trapezius, pectoralis, sternocleidomastoid and parasternal muscles (Sieck and Gransee, 2012). Like the diaphragm and external intercostal muscles, accessory respiratory muscles receive rhythmic drive from the ventral respiratory group of the medulla, but additional pathway(s) may also contribute to activating accessory respiratory muscles at the onset of exercise or following disease or injury (De Troyer et al., 2005; Butler, 2007; Johnson and Mitchell, 2013; Butler et al., 2014). Expiratory accessory respiratory muscles include the internal intercostals and abdominal muscles. In healthy humans, accessory respiratory muscles help stabilize the thoracic cavity during eupnea and enhance ventilation during conditions of high oxygen demand, such as exercise (Sieck and Gransee, 2012; Aliverti, 2016). Accessory respiratory muscles are also used to increase ventilation following neuromuscular disease and injury (Johnson and Mitchell, 2013).

Recent studies have implicated propriospinal circuits in the recruitment of accessory respiratory muscles for breathing. Romer et al. (2017) showed that chemogenetic activation of V2a neurons is sufficient to activate scalene and trapezius accessory respiratory muscles and increase ventilation. A subsequent study showed that chemogenetic inhibition of V2a neurons also surprisingly activated scalene and trapezius accessory respiratory muscles (Jensen et al., 2019). Since accessory respiratory muscle activation was not accompanied by impaired diaphragm activity, it was postulated that a subset of V2a neurons (presumably different from the subset that activates inspiratory accessory respiratory muscles) participates in an inhibitory pathway to prevent accessory respiratory muscle activation at rest, when they are not needed. However, these studies did not distinguish whether spinal or brainstem V2a neurons are responsible for activating or inhibiting accessory respiratory muscles. Additional studies are necessary to further elucidate the role of different propriospinal neurons in controlling accessory respiratory muscle activity.

Propriospinal neurons serve important roles in patterning respiratory muscle activity to promote efficient and effective ventilation, even during exercise or following disease and injury. A better understanding of these pathways could aid in the development of therapies to improve breathing when pathways to/from the brainstem are disrupted following SCI.

ROLES OF PROPRIOSPINAL NEURONS IN RECOVERY OF RESPIRATORY MOTOR FUNCTION AFTER INJURY

In the following sections, we describe evidence that propriospinal circuits involved in breathing undergo significant anatomical and functional changes following injury. We provide evidence that these changes significantly contribute to the recovery of respiratory function that can be seen following SCI. Moreover, we suggest that therapies targeting propriospinal neurons may improve the recovery of breathing in patients failing to recover on their own.

Propriospinal Neurons Show Altered Anatomical and Functional Connectivity to Respiratory Motor Neurons Following Injury

Propriospinal neurons show anatomical and functional changes that suggest they contribute to the spontaneous recovery of respiratory function following SCI. For example, despite the presence of inhibitory molecules, cervical spinal commissural interneurons show substantial axonal regeneration across the midline of the cat spinal cord following a midsagittal axotomy without any therapeutic intervention (Fenrich and Rose, 2009). Moreover, these commissural interneurons form functional synapses with motor neurons within 2–3 months, as confirmed by electrophysiology (Fenrich and Rose, 2009). Uninjured propriospinal neurons below the site of an injury may also undergo changes in connectivity. For example, the connectivity between spinal V2a neurons and phrenic motor neurons is increased in rats 2 weeks following a C2 hemisection injury (Zholudeva et al., 2017). Spinal plasticity is not unique to respiratory interneurons, as the emergence of novel intraspinal circuits to enhance motor behavior has been reported across multiple levels of the spinal cord (Bareyre et al., 2004; Courtine et al., 2008; Filli and Schwab, 2015).

Functional changes within propriospinal circuits both above and below a SCI are likely important for recovery from injury. Caudal to a C2 hemisection injury, excitatory connections between propriospinal neurons across the cord show a bias for the contralateral-to-ipsilateral direction, suggesting that changes in spinal circuits may help relay drive to neurons deprived of input following injury (Streeter et al., 2020). Changes in propriospinal circuits also occur above a spinal cord lesion. For example, expiratory bulbospinal neurons make more functional projections to propriospinal neurons (but not motor neurons) in the thoracic cord above an injury (Ford et al., 2016). Taken together, these studies suggest that propriospinal neurons may be important mediators of respiratory plasticity following SCI. However, additional studies are necessary to investigate how the plasticity of respiratory circuits can be leveraged to further improve breathing following injury.

Propriospinal Neurons Modulate Respiratory Motor Output Following Spinal Cord Injury

Spinal stimulation studies have demonstrated the importance, as well as the potential, of spinal circuits to drive breathing following SCI. Studies from dogs and rats completely transected at the cervical level show that high-frequency spinal cord stimulation on the ventral surface at thoracic levels activates both intercostal and diaphragmatic muscles,

as well as enhances inspired volume (DiMarco and Kowalski, 2009, 2011, 2019; Kowalski et al., 2013). This stimulation acts through propriospinal neuron networks rather than descending brainstem input, as it is effective 5 days after a complete trans-section when bulbospinal axons have already degenerated (DiMarco and Kowalski, 2019). Moreover, the specific pattern of respiratory muscle activity is the same after transection as it was prior to the injury, demonstrating the importance of spinal circuits for patterning activity (DiMarco and Kowalski, 2011). High-frequency spinal cord stimulation has also successfully been used to restore cough in patients with SCI (DiMarco et al., 2014). Direct intraspinal stimulation has also been used in rats to activate phrenic motor neurons for breathing, likely *via* propriospinal neurons (Mercier et al., 2017). However, the neural substrates upon which the spinal cord stimulation acts are not currently clear.

Additional evidence that spinal circuits are sufficient to drive and sustain breathing comes from studies using optogenetics to alter activity in cervical neurons (Alilain et al., 2008). Alilain et al. (2008) were able to restore activity to the ipsilateral diaphragm after a C2 hemisection by exciting channel rhodopsin expressing neurons at the level of the phrenic nucleus (which included phrenic motor neurons as well as excitatory and inhibitory propriospinal neurons) with light. In addition to direct activation of phrenic motor activity with light stimulation, they also observed a rhythmic waxing and waning of rhythmic bursting activity even after cessation of photostimulation, which was hypothesized to result from spinal network activity. These results suggest that spinal respiratory networks may exhibit central pattern generator properties, at least under some conditions.

Maintenance of respiratory function following injury is likely dependent on excitatory propriospinal neurons. In a mouse model of non-traumatic SCI, respiratory function is maintained despite substantial damage to spinal tracts and phrenic motor neuron loss, similar to most human patients with cervical myelopathy. However, silencing glutamatergic propriospinal neurons results in impaired breathing in injured, but not healthy mice (Satkunendrarajah et al., 2018). These results indicate that propriospinal neurons normally help sustain breathing following injury. Further, increasing the activity of glutamatergic neurons can also restore function to the diaphragm following an acute C2 hemisection injury (Satkunendrarajah et al., 2018). Thus, increasing the activity of excitatory propriospinal neurons holds promise as a therapy to improve breathing following traumatic or non-traumatic injuries.

Inhibitory propriospinal neurons are also important modulators of respiratory function following SCI. For example, blocking the effects of inhibitory interneurons using a GABA receptor antagonist can restore rhythmic bursting activity to a paralyzed hemidiaphragm below a C2 hemisection injury (Zimmer and Goshgarian, 2007). In addition, Cregg et al. (2017) used an *ex vivo* neonatal spinal cord preparation to show that blocking inhibitory neurons could elicit phrenic motor neuron bursting even after complete C1 transection. Optogenetic stimulation of excitatory neurons could evoke phrenic bursts in their preparation, but only when inhibitory neurotransmission was blocked (Cregg et al., 2017). Thus, phrenic motor neurons appear to be targets of excitatory pathways that are normally latent due to the activity of inhibitory neurons. These results are consistent with studies of locomotor circuits that demonstrate that inhibitory neurons can act as critical obstacles of functional recovery after SCI and that targeting these neurons can improve recovery (Chen et al., 2018).

Several groups have investigated the potential of induced pluripotent stem cell (iPSC) derived propriospinal neurons as a potential therapy to restore respiratory motor function. For example, iPSC derived V2a and V3 neurons have been generated from mouse or human cells (Brown et al., 2014; Xu et al., 2015; Iyer et al., 2016; Butts et al., 2017, 2019; White and Sakiyama-Elbert, 2019). iPSC derived V2a neurons have been transplanted into the spinal cord where they survive and appear to form synapses with host neurons (Butts et al., 2017; Zholudeva et al., 2018a). Moreover, iPSC derived V2a neurons appear to benefit recovery because rats who received a spinal injection of V2a neurons along with neural progenitor cells showed a greater recovery of diaphragm function 1 month after a C2 hemisection than rats who received neural progenitor cells alone (Zholudeva et al., 2018a). Thus, both intrinsic and extrinsic propriospinal neurons may be able to promote recovery of breathing following injury.

USING DEVELOPMENTAL MARKERS TO TARGET PROPRIOSPINAL NEURON CLASSES AND TEST THEIR ROLES IN BREATHING

A better understanding of which propriospinal neurons are important for breathing and how they contribute to the recovery of function will be vital for developing treatments. For example, therapies that target all excitatory and/or all inhibitory neurons in the spinal cord could produce unwanted side effects in SCI patients, including spasticity, chronic pain, and autonomic dysregulation. Here, we provide some evidence that developmental spinal neuron classes play distinct roles in locomotor and respiratory circuits as well as speculate on potential functions of these neurons in cases where a role in breathing is not yet known.

Developmental Neuron Classes Perform Distinct Functions

Molecular genetic approaches to label specific developmental classes of spinal neurons have allowed investigators to begin dissecting the complex circuitry of the spinal cord (Grillner and El Manira, 2015; Lu et al., 2015; Kiehn, 2016; Gosgnach et al., 2017; Ziskind-Conhaim and Hochman, 2017; Dougherty and Ha, 2019). Developmental studies have identified 10 progenitor domains that give rise to six dorsal (dI1–6) and four ventral (V0–V3) classes of propriospinal neurons. Characterization of the progenitors and/or the post-mitotic neurons derived from each domain has identified specific molecular markers (i.e., transcription factors) that distinguish each class of neurons. Each class is found throughout the spinal cord from cervical to sacral segments. A similar pattern of transcription

factor expression is also found during the development of the brainstem, giving rise to comparable broadly defined neuron classes (Gray, 2013). Roles for each neuron class in the control of locomotion have been investigated through experiments in which the development, survival, or function of a specific class of neurons is altered while assessing locomotor function. From these studies, it has become apparent that the different developmental subclasses of propriospinal neurons have different properties (i.e., neurotransmitter identity, projection pattern, presynaptic inputs) and perform different roles in locomotion (Lu et al., 2015; Ziskind-Conhaim and Hochman, 2017).

A summary of the properties and connectivity of the major developmental neuron classes in the ventral part of the spinal cord is shown in **Figure 2.** Most of the data in this figure is based on studies of locomotor circuits in the lumbar spinal cord (Lu et al., 2015; Ziskind-Conhaim and Hochman, 2017). However, it is likely that many of the properties and functions of these neurons are conserved in respiratory circuits, but with some important differences. For example, V2a and V0 neurons work together to ensure that the left and right limbs alternate during locomotion. Efficient breathing, however, requires synchronous inspiration and expiration on the left and right sides. V0 neurons (most likely in the brainstem) are critical for this coordination because disruption of commissural projections of V0 neurons results in left-right desynchronized inspiration (and neonatal lethality; Wu et al., 2017). Thus, similar neural building blocks may be used in different ways in locomotor vs. respiratory circuits.

Importantly, each broad developmental class of neurons can be further subdivided into multiple subtypes that likely play distinct roles in motor behaviors. For example, the V1 class includes Renshaw cells, Ia inhibitory neurons, as well as additional inhibitory neuron classes (Alvarez et al., 2005). In fact, detailed gene expression analyses can divide V1 neurons into over 50 inferred neuron subtypes and V2a neurons into at least 11 subtypes (Bikoff et al., 2016; Gabitto et al., 2016; Hayashi et al., 2018; Sweeney et al., 2018). Once markers of specific subtypes are identified, intersectional genetic tools may be used to elucidate specific roles for different neural subtypes in breathing or other motor functions (Ray et al., 2011; Brust et al., 2014; Hennessy et al., 2017).

Potential Roles for Developmental Neuron Classes in Breathing

Many, if not all, of the cardinal developmental neuron classes, are likely to play a role in the control of breathing. Genetic tools to target subsets of these neurons may help to elucidate the roles of these neurons in respiratory circuits as well as help identify the cellular targets most likely to improve breathing following injury.

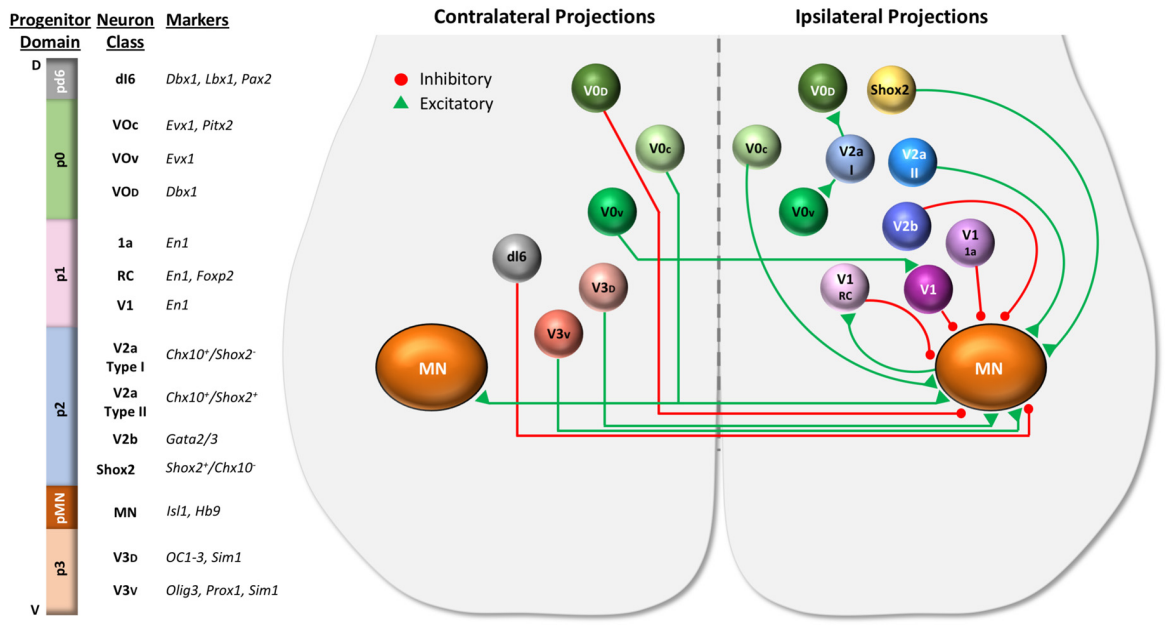

FIGURE 2 | Spinal cord progenitor domains give rise to distinct developmental neuron classes. Distinct progenitor domains organized along the dorsal (D) to ventral (V) axis give rise to distinct classes of neurons. Shown on the left are progenitor domains located in the ventral portion of the spinal cord, including the motor neuron progenitor (pMN) domain, four ventral progenitor domains (p0–p3), and one dorsal progenitor domain (pd6), along with the neuron classes they give rise to and molecular markers used to identify the neuron classes derived from each domain. The dorsal progenitor domains pd1–5 are not shown. The diagram of the ventral spinal cord on the right illustrates some of the properties (excitatory vs. inhibitory, ipsilateral vs. contralateral projections, etc.) as well as the interactions between ventral neuron classes. Commissural propriospinal neurons (shown on the left side of cord) project contralaterally across the midline to contact neurons on the opposite side of the spinal cord. These propriospinal neurons include dI6, V0, and V3 classes. Ipsilaterally projecting propriospinal neuron classes are shown on the right side of the cord. The broad neuronal classes may be further divided into subclasses. For example, the V1 class includes Renshaw cells (V1 RC), Ia inhibitory neurons (V1 1a), and other inhibitory neurons (V1). V2 neurons can be divided into Chx10+ V2a neurons, Gata 2/3+ V2b neurons, and Shox2 (non-Chx10+) neurons. Chx10 expressing V2a neurons can be further divided based on Shox2 expression into type I (V2a I) and type II (V2a II) neurons.

For example, Wu et al. (2017) used a combination of viral tracing and transgenic labeling methods to show that brainstem neurons of the V0 class in the PBC and rVRG are critical components of the circuits driving inspiration. Moreover, they were able to disrupt the development of these neurons to demonstrate the importance of commissural projections for the synchronous activity of the left and right side of the diaphragm.

In locomotor circuits, V1 neurons shape motor bursts to control the duration of stance and swing phases of the step cycle and thus the speed of walking (Gosgnach et al., 2006). Renshaw cells (a subset of V1 neurons) provide recurrent inhibition to phrenic and intercostal motor neurons (Kirkwood et al., 1981; Hilaire et al., 1983, 1986; Lipski et al., 1985; Iizuka et al., 2018), but the role of most V1 neurons in breathing is unknown. One could hypothesize that the GABAergic neurons that shape respiratory motor bursts (Marchenko et al., 2015) are a subset(s) of V1 neurons. Experiments in which V1 neurons are optogenetically activated or silenced could test the significance of inhibitory modulation from V1 neurons on respiratory motor output *in vitro*, or even in healthy or injured animals. In addition, the role of proprioceptive afferents in the control of breathing could be further probed by mapping their targets in the spinal cord and brainstem (Nair et al., 2017a) and manipulating the activity of each of their targets. These targets are likely to include subsets of V1 neurons (e.g., Ia and Ib inhibitory neurons), but may also include additional neuron types.

In locomotor circuits, V2a neurons are important for speed-dependent control of gait (left-right alternation of limbs) as well as the regularity of motor bursts (Crone et al., 2008, 2009). V2a neurons in the brainstem appear to be important for generating regular, frequent breathing in neonatal mice (Crone et al., 2012), but are dispensable for breathing in adult mice at rest (Jensen et al., 2019). In adult mice, V2a neurons appear to be particularly important for the control of accessory respiratory muscles. For example, there appear to be at least two subsets of V2a neurons in the cervical cord, one subset that activates accessory inspiratory muscles at rest (Romer et al., 2017) and another subset that prevents their activation at rest when they are not needed (Jensen et al., 2019; see "Propriospinal Neurons Regulate Accessory Respiratory Muscle Activity" section). These results suggest that a major role for V2a neurons may be in matching recruitment of accessory respiratory muscles to levels of motor activity, but this hypothesis has not yet been directly tested.

The major role of V3 neurons in locomotor circuits is to balance excitation across the left and right sides of the cord (Zhang et al., 2008). Although commissural projections of V0 bulbospinal neurons synchronize the inspiratory drive between the left and right sides (Wu et al., 2017), one could speculate that V3 neurons also play a role in balancing the activity of respiratory circuits across the cord that may be particularly important in the context of injury when damage may be more severe on one side of the cord (e.g., the circuit changes described by Streeter et al., 2020). An additional potential role for V3 neurons in breathing includes transmitting afferent input to respiratory motor neurons or propriospinal neurons. For example, V3 neurons mediate sensory-evoked muscle spasms of tail muscles following SCI (Lin et al., 2019). Additional research is necessary to identify the roles of V3 neurons in respiratory circuits as well as their potential roles in plasticity following injury.

CONCLUSIONS

There is convincing evidence that propriospinal neurons help pattern the activity of respiratory muscles in order to meet the needs of the organism. This is a dynamic process that involves a variety of neurons with unique roles. In SCI, the need to modulate motor function is escalated and the roles of propriospinal neurons in the control of breathing may be amplified. Indeed, there is mounting evidence that spinal circuitry is altered after disease and injury, that spinal network plasticity contributes to recovery, and that propriospinal neurons are an attractive therapeutic target to improve respiratory motor function. Developmental markers that can be used to identify and genetically mark (or manipulate) specific classes of propriospinal neurons have been valuable tools to investigate the function of neurons within circuits. These tools will continue to be useful as we investigate mechanisms of neuroplasticity that promote recovery of function following injury. Overall, a better understanding of the circuitry that controls breathing in uninjured animals and the changes that occur following injury should lead to new therapies to improve breathing.

AUTHOR CONTRIBUTIONS

SC, WA, and VJ wrote the article.

REFERENCES

Alilain, W. J., Li, X., Horn, K. P., Dhingra, R., Dick, T. E., Herlitze, S., et al. (2008). Light-induced rescue of breathing after spinal cord injury. *J. Neurosci.* 28, 11862–11870. doi: 10.1523/JNEUROSCI.3378-08.2008

Aliverti, A. (2016). The respiratory muscles during exercise. *Breathe* 12, 165–168. doi: 10.1183/20734735.008116

Alvarez, F. J., Jonas, P. C., Sapir, T., Hartley, R., Berrocal, M. C., Geiman, E. J., et al. (2005). Postnatal phenotype and localization of spinal cord V1 derived interneurons. *J. Comp. Neurol.* 493, 177–192. doi: 10.1002/cne.20711

Aminoff, M. J., and Sears, T. A. (1971). Spinal integration of segmental, cortical and breathing inputs to thoracic respiratory motoneurones. *J. Physiol.* 215, 557–575. doi: 10.1113/jphysiol.1971.sp009485

Bareyre, F. M., Kerschensteiner, M., Raineteau, O., Mettenleiter, T. C., Weinmann, O., and Schwab, M. E. (2004). The injured spinal cord spontaneously forms a new intraspinal circuit in adult rats. *Nat. Neurosci.* 7, 269–277. doi: 10.1038/nn1195

Bellingham, M. C. (1999). Synaptic inhibition of cat phrenic motoneurons by internal intercostal nerve stimulation. *J. Neurophysiol.* 82, 1224–1232. doi: 10.1152/jn.1999.82.3.1224

Berlly, M., and Shem, K. (2007). Respiratory management during the first five days after spinal cord injury. *J. Spinal Cord Med.* 30, 309–318. doi: 10.1080/10790268.2007.11753946

Berlowitz, D. J., Wadsworth, B., and Ross, J. (2016). Respiratory problems and management in people with spinal cord injury. *Breathe* 12, 328–340. doi: 10.1183/20734735.012616

Bikoff, J. B., Gabitto, M. I., Rivard, A. F., Drobac, E., Machado, T. A., Miri, A., et al. (2016). Spinal inhibitory interneuron diversity delineates variant motor microcircuits. *Cell* 165, 207–219. doi: 10.1016/j.cell.2016.01.027

Brichant, J. F., and De Troyer, A. (1997). On the intercostal muscle compensation for diaphragmatic paralysis in the dog. *J. Physiol.* 500, 245–253. doi: 10.1113/jphysiol.1997.sp022014

Brown, C. R., Butts, J. C., McCreedy, D. A., and Sakiyama-Elbert, S. E. (2014). Generation of v2a interneurons from mouse embryonic stem cells. *Stem Cells Dev.* 23, 1765–1776. doi: 10.1089/scd.2013.0628

Brust, R. D., Corcoran, A. E., Richerson, G. B., Nattie, E., and Dymecki, S. M. (2014). Functional and developmental identification of a molecular subtype of brain serotonergic neuron specialized to regulate breathing dynamics. *Cell Rep.* 9, 2152–2165. doi: 10.1016/j.celrep.2014.11.027

Butler, J. E. (2007). Drive to the human respiratory muscles. *Respir. Physiol. Neurobiol.* 159, 115–126. doi: 10.1016/j.resp.2007.06.006

Butler, J. E., Hudson, A. L., and Gandevia, S. C. (2014). The neural control of human inspiratory muscles. *Prog. Brain Res.* 209, 295–308. doi: 10.1016/B978-0-444-63274-6.00015-1

Butler, J. E., McKenzie, D. K., and Gandevia, S. C. (2003). Reflex inhibition of human inspiratory muscles in response to contralateral phrenic nerve stimulation. *Respir. Physiol. Neurobiol.* 138, 87–96. doi: 10.1016/s1569-9048(03)00161-7

Butts, J. C., Iyer, N., White, N., Thompson, R., Sakiyama-Elbert, S., and McDevitt, T. C. (2019). V2a interneuron differentiation from mouse and human pluripotent stem cells. *Nat. Protoc.* 14, 3033–3058. doi: 10.1038/s41596-019-0203-1

Butts, J. C., McCreedy, D. A., Martinez-Vargas, J. A., Mendoza-Camacho, F. N., Hookway, T. A., Gifford, C. A., et al. (2017). Differentiation of V2a interneurons from human pluripotent stem cells. *Proc. Natl. Acad. Sci. U S A* 114, 4969–4974. doi: 10.1073/pnas.1608254114

Cabaj, A., Stecina, K., and Jankowska, E. (2006). Same spinal interneurons mediate reflex actions of group Ib and group II afferents and crossed reticulospinal actions. *J. Neurophysiol.* 95, 3911–3922. doi: 10.1152/jn.01262.2005

Chen, B., Li, Y., Yu, B., Zhang, Z., Brommer, B., Williams, P. R., et al. (2018). Reactivation of dormant relay pathways in injured spinal cord by KCC2 manipulations. *Cell* 174, 521.e13–535.e13. doi: 10.3410/f.733662739.793550374

Cleland, C. L., and Getting, P. A. (1993). Respiratory-modulated and phrenic afferent-driven neurons in the cervical spinal cord (C4–C6) of the fluorocarbon-perfused guinea pig. *Exp. Brain Res.* 93, 307–311. doi: 10.1007/bf00228399

Corda, M., Voneuler, C., and Lennerstrand, G. (1965). Proprioceptive innervation of the diaphragm. *J. Physiol.* 178, 161–177. doi: 10.1113/jphysiol.1965.sp007621

Courtine, G., Song, B., Roy, R. R., Zhong, H., Herrmann, J. E., Ao, Y., et al. (2008). Recovery of supraspinal control of stepping *via* indirect propriospinal relay connections after spinal cord injury. *Nat. Med.* 14, 69–74. doi: 10.1038/nm1682

Cregg, J. M., Chu, K. A., Hager, L. E., Maggard, R. S. J., Stoltz, D. R., Edmond, M., et al. (2017). A latent propriospinal network can restore diaphragm function after high cervical spinal cord injury. *Cell Rep.* 21, 654–665. doi: 10.1016/j.celrep.2017.09.076

Crone, S. A., Quinlan, K. A., Zagoraiou, L., Droho, S., Restrepo, C. E., Lundfald, L., et al. (2008). Genetic ablation of V2a ipsilateral interneurons disrupts left-right locomotor coordination in mammalian spinal cord. *Neuron* 60, 70–83. doi: 10.1016/j.neuron.2008.08.009

Crone, S. A., Viemari, J. C., Droho, S., Mrejeru, A., Ramirez, J. M., and Sharma, K. (2012). Irregular breathing in mice following genetic ablation of V2a neurons. *J. Neurosci.* 32, 7895–7906. doi: 10.1523/JNEUROSCI.0445-12.2012

Crone, S. A., Zhong, G., Harris-Warrick, R., and Sharma, K. (2009). In mice lacking V2a interneurons, gait depends on speed of locomotion. *J. Neurosci.* 29, 7098–7109. doi: 10.1523/JNEUROSCI.1206-09.2009

De Troyer, A. D. (1998). The canine phrenic-to-intercostal reflex. *J. Physiol.* 508, 919–927. doi: 10.1111/j.1469-7793.1998.919bp.x

De Troyer, A., Brunko, E., Leduc, D., and Jammes, Y. (1999). Reflex inhibition of canine inspiratory intercostals by diaphragmatic tension receptors. *J. Physiol.* 514, 255–263. doi: 10.1111/j.1469-7793.1999.255af.x

De Troyer, A., Kirkwood, P. A., and Wilson, T. A. (2005). Respiratory action of the intercostal muscles. *Physiol. Rev.* 85, 717–756. doi: 10.1152/physrev.00007.2004

Decima, E. E., and von Euler, C. (1969). Intercostal and cerebellar influences on efferent phrenic activity in the decerebrate cat. *Acta Physiol. Scand.* 76, 148–158. doi: 10.1111/j.1748-1716.1969.tb04459.x

Decima, E. E., von Euler, C., and Thoden, U. (1967). Spinal intercostal-phrenic reflexes. *Nature* 214, 312–313. doi: 10.1038/214312a0

Del Negro, C. A., Funk, G. D., and Feldman, J. L. (2018). Breathing matters. *Nat. Rev. Neurosci.* 19, 351–367. doi: 10.1038/s41583-018-0003-6

DiMarco, A. F., and Kowalski, K. E. (2009). High-frequency spinal cord stimulation of inspiratory muscles in dogs: a new method of inspiratory muscle pacing. *J. Appl. Physiol.* 107, 662–669. doi: 10.1152/japplphysiol.00252.2009

DiMarco, A. F., and Kowalski, K. E. (2011). Distribution of electrical activation to the external intercostal muscles during high frequency spinal cord stimulation in dogs. *J. Physiol.* 589, 1383–1395. doi: 10.1113/jphysiol.2010.199679

DiMarco, A. F., and Kowalski, K. E. (2019). High-frequency spinal cord stimulation in a subacute animal model of spinal cord injury. *J. Appl. Physiol.* 127, 98–102. doi: 10.1152/japplphysiol.00006.2019

DiMarco, A. F., Kowalski, K. E., Hromyak, D. R., and Geertman, R. T. (2014). Long-term follow-up of spinal cord stimulation to restore cough in subjects with spinal cord injury. *J. Spinal Cord Med.* 37, 380–388. doi: 10.1179/2045772313y.0000000152

Dougherty, K. J., and Ha, N. T. (2019). The rhythm section: an update on spinal interneurons setting the beat for mammalian locomotion. *Curr. Opin. Physiol.* 8, 84–93. doi: 10.1016/j.cophys.2019.01.004

Duffin, J., and Iscoe, S. (1996). The possible role of C5 segment inspiratory interneurons investigated by cross-correlation with phrenic motoneurons in decerebrate cats. *Exp. Brain Res.* 112, 35–40. doi: 10.1007/bf00227175

Eldridge, F. L., Gill-Kumar, P., Millhorn, D. E., and Waldrop, T. G. (1981). Spinal inhibition of phrenic motoneurones by stimulation of afferents from peripheral muscles. *J. Physiol.* 311, 67–79. doi: 10.1113/jphysiol.1981.sp013573

Fenrich, K. K., and Rose, P. K. (2009). Spinal interneuron axons spontaneously regenerate after spinal cord injury in the adult feline. *J. Neurosci.* 29, 12145–12158. doi: 10.1523/JNEUROSCI.0897-09.2009

Filli, L., and Schwab, M. E. (2015). Structural and functional reorganization of propriospinal connections promotes functional recovery after spinal cord injury. *Neural Regen. Res.* 10, 509–513. doi: 10.4103/1673-5374.155425

Ford, T. W., Anissimova, N. P., Meehan, C. F., and Kirkwood, P. A. (2016). Functional plasticity in the respiratory drive to thoracic motoneurons in the segment above a chronic lateral spinal cord lesion. *J. Neurophysiol.* 115, 554–567. doi: 10.1152/jn.00614.2015

Forster, H. V., Haouzi, P., and Dempsey, J. A. (2012). Control of breathing during exercise. *Compr. Physiol.* 2, 743–777. doi: 10.1002/cphy.c100045

Gabitto, M. I., Pakman, A., Bikoff, J. B., Abbott, L. F., Jessell, T. M., and Paninski, L. (2016). Bayesian sparse regression analysis documents the diversity of spinal inhibitory interneurons. *Cell* 165, 220–233. doi: 10.1016/j.cell.2016.01.026

Ghali, M. G. Z. (2018). Phrenic motoneurons: output elements of a highly organized intraspinal network. *J. Neurophysiol.* 119, 1057–1070. doi: 10.1152/jn.00705.2015

Gill, P. K., and Kuno, M. (1963). Excitatory and inhibitory actions on phrenic motoneurones. *J. Physiol.* 168, 274–289. doi: 10.1113/jphysiol.1963.sp007192

Giraudin, A., Cabirol-Pol, M. J., Simmers, J., and Morin, D. (2008). Intercostal and abdominal respiratory motoneurons in the neonatal rat spinal cord: spatiotemporal organization and responses to limb afferent stimulation. *J. Neurophysiol.* 99, 2626–2640. doi: 10.1152/jn.01298.2007

Giraudin, A., Le Bon-Jégo, M., Cabirol, M. J., Simmers, J., and Morin, D. (2012). Spinal and pontine relay pathways mediating respiratory rhythm entrainment by limb proprioceptive inputs in the neonatal rat. *J. Neurosci.* 32, 11841–11853. doi: 10.1523/JNEUROSCI.0360-12.2012

Gosgnach, S., Bikoff, J. B., Dougherty, K. J., El Manira, A., Lanuza, G. M., and Zhang, Y. (2017). Delineating the diversity of spinal interneurons in locomotor circuits. *J. Neurosci.* 37, 10835–10841. doi: 10.1523/JNEUROSCI.1829-17.2017

Gosgnach, S., Lanuza, G. M., Butt, S. J., Saueressig, H., Zhang, Y., Velasquez, T., et al. (2006). V1 spinal neurons regulate the speed of vertebrate locomotor outputs. *Nature* 440, 215–219. doi: 10.1038/nature04545

Gray, P. A. (2013). Transcription factors define the neuroanatomical organization of the medullary reticular formation. *Front. Neuroanat.* 7:7. doi: 10.3389/fnana.2013.00007

Grillner, S., and El Manira, A. (2015). The intrinsic operation of the networks that make us locomote. *Curr. Opin. Neurobiol.* 31, 244–249. doi: 10.1016/j.conb.2015.01.003

Guyenet, P. G., and Bayliss, D. A. (2015). Neural control of breathing and CO_2 homeostasis. *Neuron* 87, 946–961. doi: 10.1016/j.neuron.2015.08.001

Hayashi, F., Hinrichsen, C. F., and McCrimmon, D. R. (2003). Short-term plasticity of descending synaptic input to phrenic motoneurons in rats. *J. Appl. Physiol.* 94, 1421–1430. doi: 10.1152/japplphysiol.00599.2002

Hayashi, M., Hinckley, C. A., Driscoll, S. P., Moore, N. J., Levine, A. J., Hilde, K. L., et al. (2018). Graded arrays of spinal and supraspinal V2a interneuron subtypes underlie forelimb and hindlimb motor control. *Neuron* 97, 869.e5–884.e5. doi: 10.1016/j.neuron.2018.01.023

Hennessy, M. L., Corcoran, A. E., Brust, R. D., Chang, Y., Nattie, E. E., and Dymecki, S. M. (2017). Activity of *tachykinin1*-expressing *pet1* raphe neurons modulates the respiratory chemoreflex. *J. Neurosci.* 37, 1807–1819. doi: 10.1523/JNEUROSCI.2316-16.2016

Hilaire, G., Khatib, M., and Monteau, R. (1983). Spontaneous respiratory activity of phrenic and intercostal Renshaw cells. *Neurosci. Lett.* 43, 97–101. doi: 10.1016/0304-3940(83)90135-0

Hilaire, G., Khatib, M., and Monteau, R. (1986). Central drive on Renshaw cells coupled with phrenic motoneurons. *Brain Res.* 376, 133–139. doi: 10.1016/0006-8993(86)90907-8

Iizuka, M., Ikeda, K., Onimaru, H., and Izumizaki, M. (2018). Expressions of VGLUT1/2 in the inspiratory interneurons and GAD65/67 in the inspiratory Renshaw cells in the neonatal rat upper thoracic spinal cord. *IBRO Rep.* 5, 24–32. doi: 10.1016/j.ibror.2018.08.001

Iizuka, M., Onimaru, H., and Izumizaki, M. (2016). Distribution of respiration-related neuronal activity in the thoracic spinal cord of the neonatal rat: an optical imaging study. *Neuroscience* 315, 217–227. doi: 10.1016/j.neuroscience.2015.12.015

Ikeda, K., Kawakami, K., Onimaru, H., Okada, Y., Yokota, S., Koshiya, N., et al. (2017). The respiratory control mechanisms in the brainstem and spinal cord: integrative views of the neuroanatomy and neurophysiology. *J. Physiol. Sci.* 67, 45–62. doi: 10.1007/s12576-016-0475-y

Iscoe, S., and Duffin, J. (1996). Effects of stimulation of phrenic afferents on cervical respiratory interneurones and phrenic motoneurones in cats. *J. Physiol.* 497, 803–812. doi: 10.1113/jphysiol.1996.sp021811

Iyer, N. R., Huettner, J. E., Butts, J. C., Brown, C. R., and Sakiyama-Elbert, S. E. (2016). Generation of highly enriched V2a interneurons from mouse embryonic stem cells. *Exp. Neurol.* 277, 305–316. doi: 10.1016/j.expneurol.2016.01.011

Jensen, V. N., Seedle, K., Turner, S. M., Lorenz, J. N., and Crone, S. A. (2019). V2a neurons constrain extradiaphragmatic respiratory muscle activity at rest. *eNeuro* 6:ENEURO.0492-18.2019. doi: 10.1523/eneuro.0492-18.2019

Johnson, R. A., and Mitchell, G. S. (2013). Common mechanisms of compensatory respiratory plasticity in spinal neurological disorders. *Respir. Physiol. Neurobiol.* 189, 419–428. doi: 10.1016/j.resp.2013.05.025

Jones, S. E., Saad, M., Lewis, D. I., Subramanian, H. H., and Dutschmann, M. (2012). The nucleus retroambiguus as possible site for inspiratory rhythm generation caudal to obex. *Respir. Physiol. Neurobiol.* 180, 305–310. doi: 10.1016/j.resp.2011.12.007

Kiehn, O. (2016). Decoding the organization of spinal circuits that control locomotion. *Nat. Rev. Neurosci.* 17, 224–238. doi: 10.1038/nrn.2016.9

Kirkwood, P. A., Munson, J. B., Sears, T. A., and Westgaard, R. H. (1988). Respiratory interneurones in the thoracic spinal cord of the cat. *J. Physiol.* 395, 161–192. doi: 10.1113/jphysiol.1988.sp016913

Kirkwood, P. A., Sears, T. A., Stagg, D., and Westgaard, R. H. (1982a). The spatial distribution of synchronization of intercostal motoneurones in the cat. *J. Physiol.* 327, 137–155. doi: 10.1113/jphysiol.1982.sp014224

Kirkwood, P. A., Sears, T. A., Tuck, D. L., and Westgaard, R. H. (1982b). Variations in the time course of the synchronization of intercostal motoneurones in the cat. *J. Physiol.* 327, 105–135. doi: 10.1113/jphysiol.1982.sp014223

Kirkwood, P. A., Sears, T. A., and Westgaard, R. H. (1981). Recurrent inhibition of intercostal motoneurones in the cat. *J. Physiol.* 319, 111–130. doi: 10.1113/jphysiol.1981.sp013895

Kowalski, K. E., Hsieh, Y. H., Dick, T. E., and DiMarco, A. F. (2013). Diaphragm activation *via* high frequency spinal cord stimulation in a rodent model of spinal cord injury. *Exp. Neurol.* 247, 689–693. doi: 10.1016/j.expneurol.2013.03.006

Lane, M. A. (2011). Spinal respiratory motoneurons and interneurons. *Respir. Physiol. Neurobiol.* 179, 3–13. doi: 10.1016/j.resp.2011.07.004

Lane, M. A., White, T. E., Coutts, M. A., Jones, A. L., Sandhu, M. S., Bloom, D. C., et al. (2008). Cervical prephrenic interneurons in the normal and lesioned spinal cord of the adult rat. *J. Comp. Neurol.* 511, 692–709. doi: 10.1002/cne.21864

Le Gal, J. P., Juvin, L., Cardoit, L., and Morin, D. (2016). Bimodal respiratory-locomotor neurons in the neonatal rat spinal cord. *J. Neurosci.* 36, 926–937. doi: 10.1523/JNEUROSCI.1825-15.2016

Le Gal, J. P., Juvin, L., Cardoit, L., Thoby-Brisson, M., and Morin, D. (2014). Remote control of respiratory neural network by spinal locomotor generators. *PLoS One* 9:e89670. doi: 10.1371/journal.pone.0089670

Lee, K. Z., and Fuller, D. D. (2011). Neural control of phrenic motoneuron discharge. *Respir. Physiol. Neurobiol.* 179, 71–79. doi: 10.1016/j.resp.2011.02.014

Lin, S., Li, Y., Lucas-Osma, A. M., Hari, K., Stephens, M. J., Singla, R., et al. (2019). Locomotor-related V3 interneurons initiate and coordinate muscles spasms after spinal cord injury. *J. Neurophysiol.* 121, 1352–1367. doi: 10.1152/jn.00776.2018

Lipski, J., and Duffin, J. (1986). An electrophysiological investigation of propriospinal inspiratory neurons in the upper cervical cord of the cat. *Exp. Brain Res.* 61, 625–637. doi: 10.1007/bf00237589

Lipski, J., Fyffe, R. E., and Jodkowski, J. (1985). Recurrent inhibition of cat phrenic motoneurons. *J. Neurosci.* 5, 1545–1555. doi: 10.1523/JNEUROSCI.05-06-01545.1985

Lu, D. C., Niu, T., and Alaynick, W. A. (2015). Molecular and cellular development of spinal cord locomotor circuitry. *Front. Mol. Neurosci.* 8:25. doi: 10.3389/fnmol.2015.00025

Macron, J. M., Marlot, D., Wallois, F., and Duron, B. (1988). Phrenic-to-phrenic inhibition and excitation in spinal cats. *Neurosci. Lett.* 91, 24–29. doi: 10.1016/0304-3940(88)90243-1

Marchenko, V., Ghali, M. G., and Rogers, R. F. (2015). The role of spinal GABAergic circuits in the control of phrenic nerve motor output. *Am. J. Physiol. Regul. Integr. Comp. Physiol.* 308, R916–R926. doi: 10.1152/ajpregu.00244.2014

Marlot, D., Macron, J. M., and Duron, B. (1987). Inhibitory and excitatory effects on respiration by phrenic nerve afferent stimulation in cats. *Respir. Physiol.* 69, 321–333. doi: 10.1016/0034-5687(87)90086-7

McBain, R. A., Taylor, J. L., Gorman, R. B., Gandevia, S. C., and Butler, J. E. (2016). Human intersegmental reflexes from intercostal afferents to scalene muscles. *Exp. Physiol.* 101, 1301–1308. doi: 10.1113/ep085907

Mercier, L. M., Gonzalez-Rothi, E. J., Streeter, K. A., Posgai, S. S., Poirier, A. S., Fuller, D. D., et al. (2017). Intraspinal microstimulation and diaphragm activation after cervical spinal cord injury. *J. Neurophysiol.* 117, 767–776. doi: 10.1152/jn.00721.2016

Morin, D., and Viala, D. (2002). Coordinations of locomotor and respiratory rhythms *in vitro* are critically dependent on hindlimb sensory inputs. *J. Neurosci.* 22, 4756–4765. doi: 10.1523/JNEUROSCI.22-11-04756.2002

Nair, J., Bezdudnaya, T., Zholudeva, L. V., Detloff, M. R., Reier, P. J., Lane, M. A., et al. (2017a). Histological identification of phrenic afferent projections to the spinal cord. *Respir. Physiol. Neurobiol.* 236, 57–68. doi: 10.1016/j.resp.2016.11.006

Nair, J., Streeter, K. A., Turner, S. M. F., Sunshine, M. D., Bolser, D. C., Fox, E. J., et al. (2017b). Anatomy and physiology of phrenic afferent neurons. *J. Neurophysiol.* 118, 2975–2990. doi: 10.1152/jn.00484.2017

Oka, A., Iizuka, M., Onimaru, H., and Izumizaki, M. (2019). Inhibitory thoracic interneurons are not essential to generate the rostro-caudal gradient of the thoracic inspiratory motor activity in neonatal rat. *Neuroscience* 397, 1–11. doi: 10.1016/j.neuroscience.2018.11.037

Okada, Y., Yokota, S., Shinozaki, Y., Aoyama, R., Yasui, Y., Ishiguro, M., et al. (2009). Anatomical architecture and responses to acidosis of a novel respiratory neuron group in the high cervical spinal cord (HCRG) of the neonatal rat. *Adv. Exp. Med. Biol.* 648, 387–394. doi: 10.1007/978-90-481-2259-2_44

Oku, Y., Okabe, A., Hayakawa, T., and Okada, Y. (2008). Respiratory neuron group in the high cervical spinal cord discovered by optical imaging. *Neuroreport* 19, 1739–1743. doi: 10.1097/wnr.0b013e328318edb5

Palisses, R., Persegol, L., and Viala, D. (1989). Evidence for respiratory interneurones in the C3–C5 cervical spinal cord in the decorticate rabbit. *Exp. Brain Res.* 78, 624–632. doi: 10.1007/bf00230250

Persegol, L., Palisses, R., and Viala, D. (1987). Different mechanisms involved in supraspinal and spinal reflex regulation of phrenic activity through chest movements. *Neuroscience* 23, 631–640. doi: 10.1016/0306-4522(87)90081-9

Ramirez, J. M., and Baertsch, N. (2018). Defining the rhythmogenic elements of mammalian breathing. *Physiology* 33, 302–316. doi: 10.1152/physiol.00025.2018

Ray, R. S., Corcoran, A. E., Brust, R. D., Kim, J. C., Richerson, G. B., Nattie, E., et al. (2011). Impaired respiratory and body temperature control upon acute serotonergic neuron inhibition. *Science* 333, 637–642. doi: 10.1126/science.1205295

Remmers, J. E. (1973). Extra-segmental reflexes derived from intercostal afferents: phrenic and laryngeal responses. *J. Physiol.* 233, 45–62. doi: 10.1113/jphysiol.1973.sp010296

Road, J. D. (1990). Phrenic afferents and ventilatory control. *Lung* 168, 137–149. doi: 10.1007/bf02719685

Romer, S. H., Seedle, K., Turner, S. M., Li, J., Baccei, M. L., and Crone, S. A. (2017). Accessory respiratory muscles enhance ventilation in ALS model mice and are activated by excitatory V2a neurons. *Exp. Neurol.* 287, 192–204. doi: 10.1016/j.expneurol.2016.05.033

Sandhu, M. S., Baekey, D. M., Maling, N. G., Sanchez, J. C., Reier, P. J., and Fuller, D. D. (2015). Midcervical neuronal discharge patterns during and following hypoxia. *J. Neurophysiol.* 113, 2091–2101. doi: 10.1152/jn.00834.2014

Satkunendrarajah, K., Karadimas, S. K., Laliberte, A. M., Montandon, G., and Fehlings, M. G. (2018). Cervical excitatory neurons sustain breathing after spinal cord injury. *Nature* 562, 419–422. doi: 10.1038/s41586-018-0595-z

Saywell, S. A., Ford, T. W., Meehan, C. F., Todd, A. J., and Kirkwood, P. A. (2011). Electrophysiological and morphological characterization of propriospinal interneurons in the thoracic spinal cord. *J. Neurophysiol.* 105, 806–826. doi: 10.1152/jn.00738.2010

Shevtsova, N. A., Marchenko, V., and Bezdudnaya, T. (2019). Modulation of respiratory system by limb muscle afferents in intact and injured spinal cord. *Front. Neurosci.* 13:289. doi: 10.3389/fnins.2019.00289

Sieck, G. C., and Gransee, H. M. (2012). *Respiratory Muscles: Structure, Function and Regulation.* Lexington, KY: Morgan and Claypool Life Sciences.

Speck, D. F. (1987). Supraspinal involvement in the phrenic-to-phrenic inhibitory reflex. *Brain Res.* 414, 169–172. doi: 10.1016/0006-8993(87)91341-2

Speck, D. F., and Revelette, W. R. (1987). Attenuation of phrenic motor discharge by phrenic nerve afferents. *J. Appl. Physiol.* 62, 941–945. doi: 10.1152/jappl.1987.62.3.941

Streeter, K. A., Sunshine, M. D., Patel, S., Gonzalez-Rothi, E. J., Reier, P. J., Baekey, D. M., et al. (2017). Intermittent hypoxia enhances functional connectivity of midcervical spinal interneurons. *J. Neurosci.* 37, 8349–8362. doi: 10.1523/JNEUROSCI.0992-17.2017

Streeter, K. A., Sunshine, M. D., Patel, S. R., Gonzalez-Rothi, E. J., Reier, P. J., Baekey, D. M., et al. (2020). Mid-cervical interneuron networks following high cervical spinal cord injury. *Respir. Physiol. Neurobiol.* 271:103305. doi: 10.1016/j.resp.2019.103305

Sunshine, M. D., Ganji, C. N., Reier, P. J., Fuller, D. D., and Moritz, C. T. (2018). Intraspinal microstimulation for respiratory muscle activation. *Exp. Neurol.* 302, 93–103. doi: 10.1016/j.expneurol.2017.12.014

Supinski, G. S., Dick, T., Stofan, D., and DiMarco, A. F. (1993). Effects of intraphrenic injection of potassium on diaphragm activation. *J. Appl. Physiol.* 74, 1186–1194. doi: 10.1152/jappl.1993.74.3.1186

Sweeney, L. B., Bikoff, J. B., Gabitto, M. I., Brenner-Morton, S., Baek, M., Yang, J. H., et al. (2018). Origin and segmental diversity of spinal inhibitory interneurons. *Neuron* 97, 341.e3–355.e3. doi: 10.1016/j.neuron.2017.12.029

Viala, D. (1986). Evidence for direct reciprocal interactions between the central rhythm generators for spinal "respiratory" and locomotor activities in the rabbit. *Exp. Brain Res.* 63, 225–232. doi: 10.1007/bf00236841

Viala, D., Persegol, L., and Palisses, R. (1987). Relationship between phrenic and hindlimb extensor activities during fictive locomotion. *Neurosci. Lett.* 74, 49–52. doi: 10.1016/0304-3940(87)90049-8

Ward, M. E., Vanelli, G., Hashefi, M., and Hussain, S. N. (1992). Ventilatory effects of the interaction between phrenic and limb muscle afferents. *Respir. Physiol.* 88, 63–76. doi: 10.1016/0034-5687(92)90029-v

White, N., and Sakiyama-Elbert, S. E. (2019). Derivation of specific neural populations from pluripotent cells for understanding and treatment of spinal cord injury. *Dev. Dyn.* 248, 78–87. doi: 10.1002/dvdy.24680

Wu, J., Capelli, P., Bouvier, J., Goulding, M., Arber, S., and Fortin, G. (2017). A V0 core neuronal circuit for inspiration. *Nat. Commun.* 8:544. doi: 10.1038/s41467-017-00589-2

Xu, H., Iyer, N., Huettner, J. E., and Sakiyama-Elbert, S. E. (2015). A puromycin selectable cell line for the enrichment of mouse embryonic stem cell-derived V3 interneurons. *Stem Cell Res. Ther.* 6:220. doi: 10.1186/s13287-015-0213-z

Yazawa, I. (2014). Reciprocal functional interactions between the brainstem and the lower spinal cord. *Front. Neurosci.* 8:124. doi: 10.3389/fnins.2014.00124

Yu, J., and Younes, M. (1999). Powerful respiratory stimulation by thin muscle afferents. *Respir. Physiol.* 117, 1–12. doi: 10.1016/s0034-5687(99)00056-0

Zaki Ghali, M. G., Britz, G., and Lee, K. Z. (2019). Pre-phrenic interneurons: characterization and role in phrenic pattern formation and respiratory recovery following spinal cord injury. *Respir. Physiol. Neurobiol.* 265, 24–31. doi: 10.1016/j.resp.2018.09.005

Zhang, Y., Narayan, S., Geiman, E., Lanuza, G. M., Velasquez, T., Shanks, B., et al. (2008). V3 spinal neurons establish a robust and balanced locomotor rhythm during walking. *Neuron* 60, 84–96. doi: 10.1016/j.neuron.2008.09.027

Zholudeva, L. V., Iyer, N., Qiang, L., Spruance, V. M., Randelman, M. L., White, N. W., et al. (2018a). Transplantation of neural progenitors and V2a interneurons after spinal cord injury. *J. Neurotrauma* 35, 2883–2903. doi: 10.1089/neu.2017.5439

Zholudeva, L. V., Qiang, L., Marchenko, V., Dougherty, K. J., Sakiyama-Elbert, S. E., and Lane, M. A. (2018b). The neuroplastic and therapeutic potential of spinal interneurons in the injured spinal cord. *Trends Neurosci.* 41, 625–639. doi: 10.1016/j.tins.2018.06.004

Zholudeva, L. V., Karliner, J. S., Dougherty, K. J., and Lane, M. A. (2017). Anatomical recruitment of spinal V2a interneurons into phrenic motor circuitry after high cervical spinal cord injury. *J. Neurotrauma* 34, 3058–3065. doi: 10.1089/neu.2017.5045

Zimmer, M. B., and Goshgarian, H. G. (2007). GABA, not glycine, mediates inhibition of latent respiratory motor pathways after spinal cord injury. *Exp. Neurol.* 203, 493–501. doi: 10.1016/j.expneurol.2006.09.001

Ziskind-Conhaim, L., and Hochman, S. (2017). Diversity of molecularly defined spinal interneurons engaged in mammalian locomotor pattern generation. *J. Neurophysiol.* 118, 2956–2974. doi: 10.1152/jn.00322.2017

Conflict of Interest: The authors declare that the research was conducted in the absence of any commercial or financial relationships that could be construed as a potential conflict of interest.

frontiers in Systems Neuroscience

ORIGINAL RESEARCH
published: 09 April 2020
doi: 10.3389/fnsys.2020.00017

Music Restores Propriospinal Excitation During Stroke Locomotion

*Iseline Peyre[1,2], Berthe Hanna-Boutros[3], Alexandra Lackmy-Vallee[1], Claire Kemlin[4], Eléonore Bayen[4], Pascale Pradat-Diehl[1,4] and Véronique Marchand-Pauvert[1]**

[1] Sorbonne Université, Inserm, CNRS, Laboratoire d'Imagerie Biomédicale, LIB, Paris, France, [2] Sorbonne Université, CNRS, Institut de Recherche et de Coordination en Acoustique Musique (IRCAM), UMR Sciences et Technologies de la Musique et du Son (STMS), Paris, France, [3] Physical Therapy Department, Holy Family University, Batroun, Lebanon, [4] Sorbonne Université, AP-HP, GRC n°24, Handicap Moteur et Cognitif & Réadaptation (HaMCRe), Paris, France

Music-based therapy for rehabilitation induces neuromodulation at the brain level and improves the functional recovery. In line with this, musical rhythmicity improves post-stroke gait. Moreover, an external distractor also helps stroke patients to improve locomotion. We raised the question whether music with irregular tempo (arrhythmic music), and its possible influence on attention would induce neuromodulation and improve the post-stroke gait. We tested music-induced neuromodulation at the level of a propriospinal reflex, known to be particularly involved in the control of stabilized locomotion; after stroke, the reflex is enhanced on the hemiparetic side. The study was conducted in 12 post-stroke patients and 12 controls. Quadriceps EMG was conditioned by electrical stimulation of the common peroneal nerve, which produces a biphasic facilitation on EMG, reflecting the level of activity of the propriospinal reflex between ankle dorsiflexors and quadriceps (CPQ reflex). The CPQ reflex was tested during treadmill locomotion at the preferred speed of each individual, in 3 conditions randomly alternated: without music vs. 2 arrhythmic music tracks, including a pleasant melody and unpleasant aleatory electronic sounds (AES); biomechanical and physiological parameters were also investigated. The CPQ reflex was significantly larger in patients during walking without sound, compared to controls. During walking with music, irrespective of the theme, there was no more difference between groups. In controls, music had no influence on the size of CPQ reflex. In patients, CPQ reflex was significantly larger during walking without sound than when listening to the melody or AES. No significant differences have been revealed concerning the biomechanical and the physiological parameters in both groups. Arrhythmic music listening modulates the spinal excitability during post-stroke walking, restoring the CPQ reflex activity to normality. The plasticity was not accompanied by any clear improvement of gait parameters, but the patients reported to prefer walking with music than without. The role of music as external focus of attention is discussed. This study has shown that music can modulate propriospinal neural network particularly involved in the gait control during the first training session. It is speculated that repetition may help to consolidate plasticity and would contribute to gait recovery after stroke.

Keywords: propriospinal neurons, spinal cord, locomotion, stroke, music therapy

OPEN ACCESS

Edited by:
Katinka Stecina, University of Manitoba, Canada

Reviewed by:
Cheryl M. Glazebrook, University of Manitoba, Canada
Shinya Suzuki, Health Sciences University of Hokkaido, Japan

****Correspondence:***
Véronique Marchand-Pauvert veronique.marchand-pauvert@inserm.fr

Received: *04 October 2019*
Accepted: *10 March 2020*
Published: *09 April 2020*

Citation:
Peyre I, Hanna-Boutros B, Lackmy-Vallee A, Kemlin C, Bayen E, Pradat-Diehl P and Marchand-Pauvert V (2020) Music Restores Propriospinal Excitation During Stroke Locomotion. Front. Syst. Neurosci. 14:17. doi: 10.3389/fnsys.2020.00017

INTRODUCTION

Stroke is the third main cause of disability in the world (World Health Organization, 2014). The after-effects include multiple sensory, cognitive and motor impairments, which limit the autonomy in the daily life activities at different degrees from one individual to another (Cerniauskaite et al., 2012). In particular, the gait recovery represents one of the major emphasis during rehabilitation (Wade et al., 1985). Among the various rehabilitation approaches, programs based on the use of sounds and music are the subject of a growing interest. With the emergence of music therapy profession, several novel sound or music-based methods and interventions for rehabilitation have been developed, including the use of rhythmic auditory stimulation (RAS), music listening, music practice (instrumental or vocal) and, more recently, the use of device-assisted real-time sound-movement coupling (movement sonification). Short-term benefits of RAS on gait parameters, including gait freezing, and on non-motor functions (mood, anxiety) have been reported especially in Parkinson disease, and the preliminary results in other movement disorders are promising (Burt et al., 2019; Devlin et al., 2019). In patients with stroke, several studies on music-supported therapies during rehabilitation of upper limb have reported an improvement of motor functions, together with changes in neural excitability and connectivity at the brain level (Altenmüller et al., 2009; Schneider et al., 2010; Rojo et al., 2011; Amengual et al., 2013; Grau-Sánchez et al., 2013; Ripollés et al., 2016; Ghai, 2018). Regarding the locomotor functions, the approach most commonly tested so far used RAS, which consists in beating a regular tempo with a metronome calibrated on the steps of the patients. The step synchronization with the metronome improves the cadence, the step length and the walking speed (Yoo and Kim, 2016), and a Cochrane review has concluded in favor of the potential benefits of this method to improve gait after stroke (Magee et al., 2017).

Beyond the effects on the locomotor rhythmicity, the patients may pay attention to the sound or to the music they are listening to, which might also influence their walking abilities. In line with this, it has been shown that internal focus of attention during post-stroke gait rehabilitation, e.g., encouraging the patients to be aware of their movements and their performance, may reduce automaticity and hinder learning and retention (Johnson et al., 2013). Inversely, an external focus of attention, e.g., asking the patients to walk on markers on the floor, is useful to improve post-stroke walking (Kim et al., 2019). In healthy subjects, the attention paid to movement modulates the activity in the sensory-motor brain areas, and different subareas in the motor cortex are activated during attended and unattended movements (Binkofski et al., 2002; Johansen-Berg and Matthews, 2002). After stroke, the attention on movement is reinforced, even for stereotyped movement like locomotion. Therefore, there is a possibility that the neural networks for attended and unattended movements are modified after stroke, which would reflect on descending inflow, modulating the subcortical excitability, including the one of spinal cord. Our first objective was to distract the patients and to draw their attention away from their walk, but not too much to limit the risk of falls which is increased when stroke patients are too much disturbed by external cues (external distractors). To test the hypothesis whether music would keep the attention of the patients and would influence post-stroke locomotion independently of the well-known effect of rhythm cues on the locomotor cadence, we tested the effect of music with irregular tempo (arrhythmic music), one pleasant and one unpleasant assuming that both would captivate the patients differentially.

It has been well-established that listening to music and its practice induce remodeling of brain structures, with reorganization of neural networks in both healthy subjects and stroke patients (Altenmüller and Schlaug, 2015; O'Kelly et al., 2016). Regarding the spinal cord, which is particularly involved in the control of locomotion (Grillner and El Manira, 2019), the effect of sound on spinal activity has started to be explored at the beginning of the 20th century. In 1914, Forbes and Sherrington have observed a facilitating effect of sound on the Hoffmann (H) reflex in decerebrate cats (Barnes and Thomas, 1968). Later on, the neuromodulatory effect of sound on spinal reflexes has also been reported in humans (Rossignol and Jones, 1976; Delwaide and Schepens, 1995; Ruscheweyh et al., 2011; Roy et al., 2012). To date, no study has explored the effect of music on spinal excitability during post-stroke walking. Accordingly, in the present study, we have addressed the question whether a pleasant and unpleasant arrhythmic music would modify differentially the spinal cord excitability and gait parameters in stroke patients, compared to healthy subjects. The spinal excitability was evaluated by investigating the propriospinal reflex that is particularly involved in the control of lower limb muscle synergies during posture and locomotion in humans (Pierrot-Deseilligny and Burke, 2012). This reflex constitutes an interesting metric of spinal activity during locomotion for evaluating the neuromodulation. Classically, the propriospinal excitation is investigated by studying the modulation of the biphasic facilitation produced by electrical stimulation of the common peroneal (CP) nerve on quadriceps (Q) electromyogram (EMG), termed as CPQ reflex in the following. Accordingly, we investigated the modulation of the CPQ reflex during post-stroke locomotion, to determine whether the music can modify it, independently from its rhythmic effect, but by its possible influence on attention.

METHODS

Ethical Approval

The study conformed to the latest revision of the Declaration of Helsinki. The procedures were approved by Assistance Publique-Hôpitaux de Paris (AP-HP, clinical research sponsor) and have obtained the authorizations of the national French ethics committees (CPP Ile de France VI—Pitié-Salpêtrière; PHRC 95078, DRCD 070804). All the subjects have provided their written informed consent prior their inclusion in the experimental procedure.

Inclusion Criteria

Twelve patients with a first history of stroke were included in the study (3 females; mean age ± 1 standard deviation, SD:

55.8 ± 13.5; range 29–78 years old). All but 1 had a unilateral lesion (supported by MRI or CT-scan examination): 9 had right hemiparesis, 2 left hemiparesis and the last one had bilateral lesions but predominant hemiparesis on the right side. The cause of stroke was ischemia in 10/12 patients, and hemorrhage in the 2 last remaining patients. At the time of the experiments, the time since stroke ranged from 2 to 17 months (6.3 ± 5.3 months). All the patients had experienced severe gait impairment lasting more than 1 week after stroke, and 5/12 patients did not use walking aid anymore at the time of the experiment; the 7 other patients used a cane, plus an ankle splint in 2 of them. All of them were able to walk at least 20 min on the treadmill, by holding the security bars (laterally or frontally); the body weight support device was not used in this study. Seven patients exhibited cognitive and mood disorders, including attention deficit in 1, depression in 1, partial anosognosia in 1, apraxia in 2, hemineglect in 1, slight cognitive impairments in 2. Only 5 patients receive botulinum toxin therapy but not in the investigated muscles (tibialis anterior—TA—and quadriceps), and only 1 patient had oral antispastic (dantrolene sodium 50 mg/day; see **Table 1**).

Twelve healthy subjects (controls) participated in the experiments (4 females; 52.0 ± 6.5 years old; range 32–67 years old). The inclusion criteria included no history of neurological disorders and no orthopedic trauma in lower limbs.

Recordings

EMG activities were recorded using single-use bipolar surface electrodes (foam electrodes with solid gel; 2-cm apart; FIAB, Florence, Italy) that were secured on the skin, over the muscle belly of TA and vastus lateralis (VL). The electrodes were plugged to wifi connectors that transmitted the signals to an EMG zero wire system (Cometa Srl, Milan, Italy). The signals were amplified and filtered (x 1,000–5,000; 10–500-Hz bandpass) before being digitally stored on a personal computer (2-kHz sampling rate; Power 1,401 controlled by Spike2, CED, Cambridge, UK). A pressure transducer was placed under the foot, to time the ground contact and to determine the beginning of the walking stance phase. The transducer was connected to the EMG zero wire system by wifi, to synchronize the recording of EMG activities and the signal from foot contact (**Figures 1A–D**). The delay for the wifi transmission was 12 ms for both the foot contact and EMG recordings, so we did not need to realign the TTL and EMG signals and the 0-ms latency was centered on the artifact to evaluate the latency of the CPQ reflex (**Figure 2**). In controls, the transducer was placed on the heel of the foot (in the shoe), and in patients, on the forefoot (middle and external aspect of the plantar aspect of the foot; in the shoe, as in controls). Indeed, the patients did not contact the ground with the heel but with forefoot because of foot drop on the paretic side and slow speed (as in Achache et al., 2010). The patients were tested on their hemiparetic side only, because the CPQ reflex was found particularly enhanced on this side, compared to the non-paretic side (Achache et al., 2010); the controls were tested on the right side.

The recordings were performed during stabilized treadmill locomotion (Biodex Medical Systems Inc., Shirley, New York, USA). At the beginning of the experiment, the subjects walked on the treadmill for 5–10 min before recordings, to accustom themselves to treadmill walking, and to determine their comfortable speed: 0.2 ± 0.1 $m.s^{-1}$ (0.1–0.4) in patients vs. 1.0 ± 0.2 $m.s^{-1}$ (range 0.7–1.3) in controls (*t*-test, $p < 0.001$). In patients, the speed for recordings was not their maximum speed, but it was the one at which they felt secure and they were able to walk for 2–3 min (∼ recording duration) without fatigue. The walking speed in each individual was constant throughout the experiment to avoid any change in the CPQ reflex due to speed rate changes (Iglesias et al., 2008b).

Conditionings

Percutaneous electrical stimulations (1-ms duration rectangular pulse; DS7A, Digitimer Ltd, Hertfordshire, UK) were applied to the CP nerve through bipolar surface electrodes (two 2-cm diameter brass half balls covered by wet sponge tissue, spaced by ∼5 cm). The electrodes were placed on each side of the fibula neck, to evoke a motor response first in TA, without activation of the peroneal muscle group at the motor threshold (checked by tendon palpation during quiet standing). The CP nerve stimulation is then more effective for eliciting a biphasic excitation in VL motoneurons (CPQ; Simonetta-Moreau et al., 1999). During walking, the CP nerve stimulations were triggered by a TTL signal generated by the signal from the pressure transducer, at the time of foot contact.

Experimental Procedures

The first acquisition consisted in collecting EMG activities in TA and VL, and the foot contact signals during walking at comfortable speed in each participant, without conditioning, to design the walking pattern (**Figures 1E–H**). According to previous studies (Marchand-Pauvert and Nielsen, 2002; Iglesias et al., 2008b), the trigger delay (after foot contact) for the CP nerve stimulation was determined in each individual, according to their walking pattern so as to deliver the conditioning stimuli at the beginning of the walking stance phase, within the first part of the ascending phase of the VL EMG burst, so as to produce the CPQ reflex within the middle of this phase. Only 1 trigger delay was tested in each individual, and it was kept constant throughout the experiment, to avoid any change in CPQ reflex due to a change in the trigger delay (Marchand-Pauvert and Nielsen, 2002). The mean trigger delay was 32.9 ± 23.5 ms (range 0–65 ms) in controls vs. 52.1 ± 11.8 ms (range 0–120 ms) in patients (Mann-Whitney U test, $p = 0.32$). The maximal amplitude of the direct motor (M) response in TA EMG (Mmax) was measured when the subjects walked at the speed and the delay investigated. The stimulus intensity was then reduced so as to produce a constant M response of ∼80% of Mmax, whose size was monitored throughout the experiment. This response was produced with stimulus intensities around 2–2.5 x the threshold for M response (x MT), i.e., above the threshold for activating group I and group II muscle spindle afferents (Pierrot-Deseilligny and Burke, 2005). At this intensity, the stimulation did not perturb the gait cycle. During a recording session, 100 foot-contacts triggered the computer, which randomly delivered 50 CP nerve stimulations (conditioned EMG) or no stimulation

TABLE 1 | Clinical data and CPQ reflex.

						CPQ			Spasticity			
Patient	**Delay**	**Hemiparesis**	**Origin**	**Walking aid**	**Cognitive impairments**	**No music**	**With melody**	**With AES**	**Medication**	**TA**	**Soleus**	**VL**
1	2	R	Isch.	+	−	145.7	134.3	117.6	−	1	1	1
2	5	R+	Isch.	+	+	224.0	211.5	140.3	BoNT	0	1	0
3	9	R	Hem.	+	+	148.6	133.8	113.2	BoNT	0	4	1
4	2	R	Isch.	−	−	213.2	194.5	176.8	Dandro.	0	1	2
5	17	R	Isch.	+	−	134.5	118.7	106.7	BoNT	3	3	2
6	6	R	Hem.	+	−	148.7	121.6	138.7	BoNT	1	4	3
7	16	L	Isch.	−	+	115.6	121.3	85.2	−	2	2	1
8	3	R	Isch.	+	−	142.8	95.4	125.6	BoNT	0	3	2
9	7	R	Isch.	+	+	142.5	111.5	124.4	−	0	0	0
10	3	R	Isch.	−	+	184.0	143.2	143.2	−	0	0	0
11	2	L	Isch.	−	+	274.0	172.5	167.5	−	0	0	0
12	3	R	Isch.	−	+	130.6	109.5	118.6	−	0	0	0

Patient, Inclusion rank of the patient; Delay, time since stroke in months; Hemiparesis, side of hemiparesis with R for right, R+ for right predominance and L for left; Origin, Isch. for ischemia and Hem. for hemorrhage; Walking aid, patients using canes (+) or not (-); Cognitive impairment, patients with (+) or without cognitive impairments (-); CPQ, size of CPQ reflex (area of conditioned EMG % mean unconditioned EMG), observed during walking without sound, with melody and with AES; Medication, patients with medication for spasticity (Botulinum toxin injection, BoNT, or Dantrolene, Dantro.) or not (-); TA, Soleus; VL, score to rectified Ashworth scale (Spasticity).

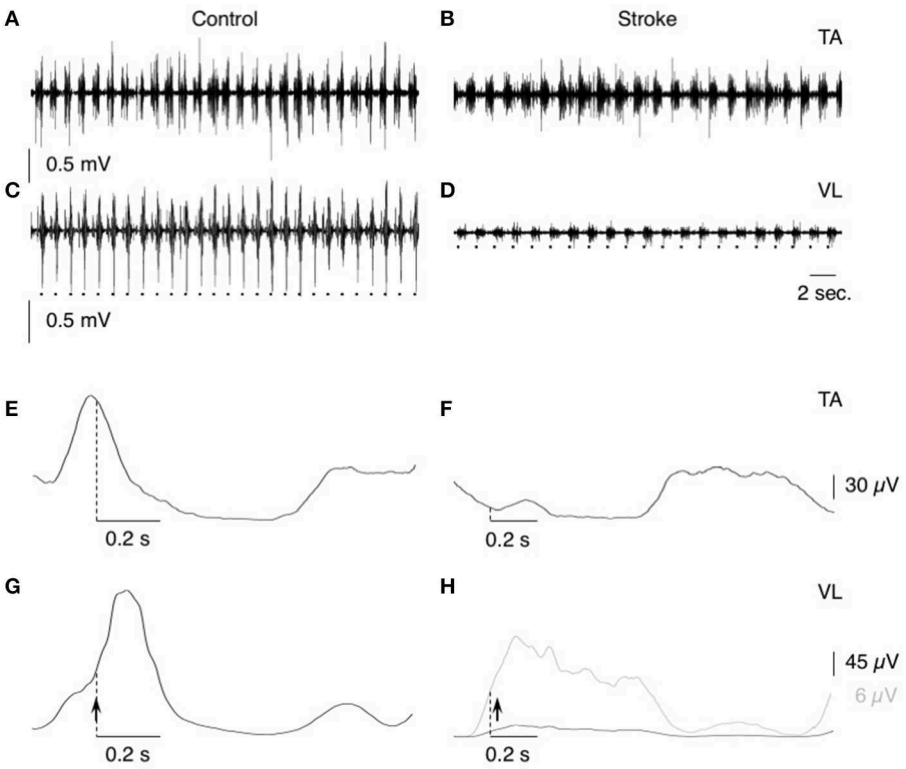

FIGURE 1 | EMG activities during treadmill walking. **(A–D)** Raw EMG activity during treadmill walking in tibialis anterior (TA; **A,B**) and vastus lateralis (VL; **C,D**) in one control (speed 1 m.s^{-1}; **A,C**) and one patient (speed 0.33 m.s^{-1}; **B,D**). The dots at the bottom indicate the time of heel contact. **(E,F)** the raw EMG activities have been rectified and 50-ms smoothed before averaging ($N = 50$ steps) in tibialis anterior (TA; **E,F**) and vastus lateralis (VL; **G,H**) in the same individuals as in **(A–D)**. In **(H)** the gray line represents the mean EMG activity with optimized Y-scale for the patient. Dotted vertical lines indicate the time of heel contact, and vertical arrows, when the conditioning stimuli were delivered during the gait cycle.

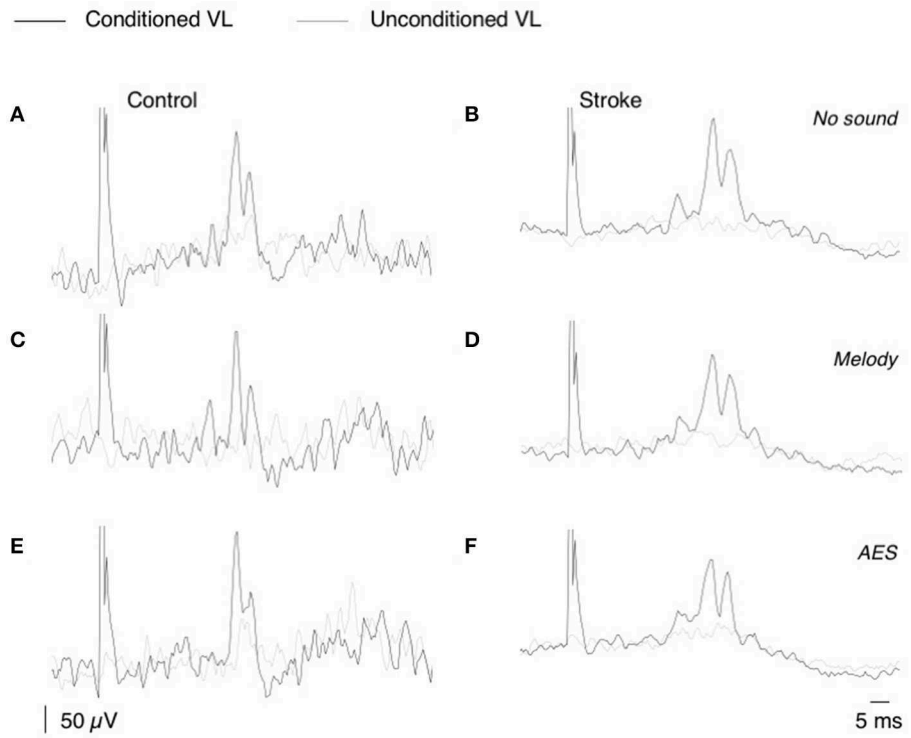

FIGURE 2 | CPQ reflex produced by CP nerve stimuli on VL EMG. **(A,F)** Mean unconditioned (gray line) and mean conditioned (black line) rectified VL EMG in one control subject **(A,C,E)**, and one patient **(B,D,F)**; same subjects as in **Figure 1**. The CP nerve stimulation ($N = 50$, 2–2.5 × MT) was triggered by the heel contact and was delivered with 0-ms delay in the control subject and 40-ms delay in the patient. Unconditioned and conditioned recordings were randomly alternated during the EMG acquisition performed without sound **(A,B)**, with melody **(C,D)**, or AES **(E,F)**.

(unconditioned EMG). Three recording sessions were randomly alternated in each group: 1 without sound, 1 with a melody (Yiruma, 2001), and 1 with aleatory electronic sounds (AES, especially composed for the protocol; **Supplementary Audio**). At the beginning of each recording session, the subjects walked without music, and when the locomotion was stable, we turned on the music (or not in the no-sound condition), and then the computer, to trigger the stimulations and to record the EMG activities. Music sound was not used as a trigger; it was continuously displayed all during the recording session. The volume of the sound was determined at the beginning of the protocol, covering the treadmill noise, and we made sure that it was comfortable for each individual and it did not induce any startle response (especially when we turned the music on). Both the melody and AES had a variable tempo and were similar for each individual. None of the subjects had already heard the 2 musical themes before the experiment. They listened both themes only during the 2 recording sessions with music. At the end of the experiment, each individual indicated what he thought about each musical theme.

Biomechanical and physiological parameters were collected during the recording sessions, at the same time than EMG activities. The sensors below the belt of the treadmill allows to record each step during the gait cycle. The subjects wore a thoracic belt with sensors that allowed to collect by Bluetooth, the heartbeat and the breathing rhythm (Zephyr^{TM} performance system, Medtronic, Boulder, CO, USA; Labchart, ADInstruments Ltd., Thame Oxfordshire, UK).

Analysis

The CP nerve stimulation produced a biphasic facilitation on the rectified VL EMG averages (**Figure 2**), and an area analysis was performed for a quantitative estimate of the corresponding excitation produced in VL motoneurons (CPQ reflex; Marchand-Pauvert and Nielsen, 2002; Achache et al., 2010). For this, the mean conditioned and unconditioned EMG were superimposed to determine the latency and the duration of the CPQ reflex (e.g., 32.5–41.5 ms in the control illustrated in **Figures 2A,C,E**, and 34–46.5 ms in the patient illustrated in **Figures 2B,D,F**); the area of the CPQ reflex was evaluated within the analysis window confined to its latency and duration. Both conditioned and unconditioned EMG were analyzed within the same analysis window, and the area of the conditioned EMG was normalized to the mean area of the unconditioned EMG, giving a quantitative metric of the excitation underlying the CPQ reflex. In each individual, the same window of analysis was used for analyzing the EMG collected during the session without sound and those during the 2 sessions with music.

The ambulation index was automatically calculated by the software of the treadmill. This index is a composite score relative to 100, based on foot-to-foot time distribution ratio and average step cycle. The score 100 indicates that the walking pattern was symmetrical (step length and duration, duration of single and double support phase); the smaller the index the less symmetrical the gait.

Statistics

Statistical analyses were performed with SigmaPlot 13.0 (Systat Software Inc., San Jose, CA, USA). The significance level α was fixed at 0.05 and the results were considered statistically significant only if $p < 0.05$. Mean values are indicated ± 1 standard deviation. Homoscedasticity (Levene median test) and normality (Shapiro-Wilk test) were first verified to allow parametric analyses (unpaired *t*-test, two-ways ANOVA).

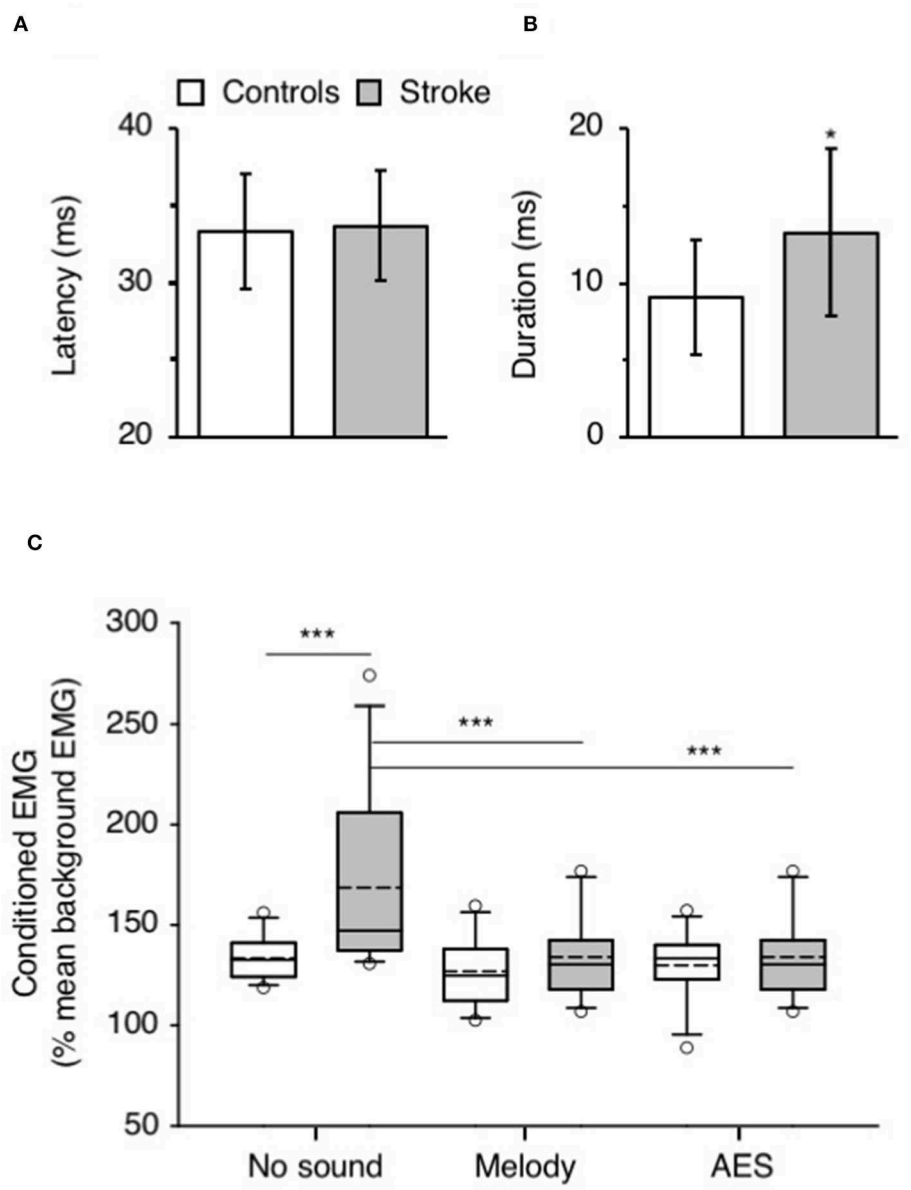

FIGURE 3 | Music-induced modulation of CPQ reflex. **(A)** Mean latency (ms) of CPQ reflex in controls (white column) and in patients with stroke (gray column). The vertical error bars indicate ± 1 × SD. **(B)** Mean duration (ms) of the CPQ reflex in both groups, same legend as in **(A)**. **(C)** Mean CPQ reflex expressed as the area of conditioned EMG (% mean unconditioned EMG) in the group of controls (white box; $N = 12$) and in the group of stroke patients (gray box; $N = 12$). The CPQ reflex was investigated during walking without sound and when listening to melody or AES. The box plot charts illustrate the data distribution in each condition. The boundary of the box closest to 0 indicates the 25th percentile (Q1), the continuous line within the box marks the median and the dotted line, the mean. The boundary farthest from 0 indicates the 75th percentile (Q3). The whiskers (error bars) above and below indicate the 90th and 10th percentiles, respectively. The open circles represent the 5% outliers. $^{*}p < 0.05$, $^{***}p < 0.001$.

Alternatively, non-parametric methods were used (Mann-Whitney U test, ANOVA on ranks), and *post hoc* multiple pairwise comparisons were performed with Student Newman Keuls method. For clarity, the statistical tests and the parameters included in each test are specifically indicated in Results.

RESULTS

Music Induced CPQ Reflex Modulation During Post-stroke Locomotion

Figure 2 shows that CP nerve stimuli produced a biphasic facilitation on the mean rectified VL EMG (CPQ reflex) at a latency about 30–35 ms after the stimulus, in both the control (**Figures 2A,C,E**) and the patient with stroke (**Figures 2B,D,F**). A CPQ reflex was similarly observed in VL EMG in all the participants. **Figure 3A** illustrates the mean latency of the CPQ reflex in controls and patients, which occurred with similar latency in both groups (33.6 ± 3.7 ms in controls vs. 33.7 ± 3.5 in stroke; *t*-test, $p = 0.97$). On the other hand, the duration of the CPQ reflex was significantly longer in patients than in controls (13.2 ± 5.4 vs. 9.0 ± 3.7 ms; *t*-test, $p < 0.05$).

In **Figure 2**, the area of the CPQ reflex was larger in the patient than in the control (compare the difference between black and gray lines). In the control, the CPQ reflex was hardly modified with music while in the patient, both the first and the second peak of the CPQ reflex (early and late component) were smaller with music, compared to no-sound condition. In the group of patients, the 2 components were similarly modified with music. Therefore, and to facilitate the reading, we only present the modulation of the CPQ reflex in both groups, without dissociating the early and late component. The box plots in **Figure 3C** illustrate the size range of the CPQ reflex in the group of controls and the group of patients. ANOVA on ranks was significant ($p < 0.05$), and *post hoc* pairwise comparisons (Student Newman Keuls method) revealed that the CPQ reflex was significantly larger in patients than in controls during walking without sound ($p < 0.001$); during walking with music, irrespective of musical theme, there was no more difference between groups. In the group of controls, the CPQ reflex was similar, whether the subjects listened to music or not ($0.78 < p < 1$). In the group of patients, the CPQ reflex was significantly larger during walking without sound (no sound vs. melody, $p < 0.001$; no sound vs. AES, $p < 0.001$), and it was of similar size, whether the patients listened to the melody or to AES (melody vs. AES, $p = 0.78$). The music-induced changes in the CPQ reflex size were rather homogeneous across the patient group: the CPQ reflex was depressed when listening to music in all patients, except in the patient #7 in whom it was depressed only when listening to AES (**Table 1**).

Walking speed, trigger delay for CP nerve stimuli and background EMG influence the CPQ size during walking (Marchand-Pauvert and Nielsen, 2002; Iglesias et al., 2008b). Both walking speed and trigger delay were kept constant throughout the experiment. Two-ways ANOVA was performed to compare the background EMG, and as could be expected given the lower speed in patients, compared to controls, the mean level of unconditioned EMG was lower in patients than in controls ($p < 0.001$) but it did not change between trials without sound and those with melody or AES ($p = 0.18$; interaction subject group x sound context: $p = 0.14$; **Table 2**). Therefore, the change in CPQ reflex within a group cannot be supported by a change in the level of the background EMG when listening to music or not.

TABLE 2 | Background EMG. Mean unconditioned EMG (mV/ms; ± 1 SD) in controls (1st raw) and patients with stroke (2nd raw) during walking without sound (1st column), when listening to melody (2nd column), or to AES (3rd column).

	No sound	Melody	AES
Controls	0.315 ± 0.171	0.370 ± 0.245	0.333 ± 0.213
Stroke* **	0.079 ± 0.055	0.082 ± 0.057	0.079 ± 0.056

*** $p < 0.001$.

Sound Preferences

At the end of the experiment, the participants gave their impression on the musical themes, whether they preferred one or another. All of them but 1 preferred the melody, compared to AES; 1 control preferred AES. Another control reported that AES were annoying, and another one indicated that he found them very strange. Most of the patients preferred to walk with music than without, and they preferred the melody. Three patients have indicated that they found AES annoying and strange, and were particularly attentive to it. However, they found the melody was more pleasant, rocked by it.

Biomechanical and Physiological Parameters

Figure 4A shows the mean step length on both sides in controls and patients. ANOVA on ranks was significant ($p < 0.001$), and *post hoc* pairwise comparisons (Student Newman Keuls method) revealed significant longer step length in controls than in patients ($P < 0.001$), whatever the audio conditions. In patients, the step length tended to be smaller on the affected side but the difference was not significant ($0.10 < p < 0.93$). Most importantly, the music had no influence of the step length in both groups ($0.35 < p < 0.99$ in controls, $0.10 < p < 0.93$ in stroke patients).

Figure 4B illustrates the mean ambulatory index in both groups. Irrespective of the audio context, the ambulation index was significantly smaller in patients than in controls (ANOVA on ranks $p < 0.001$; Student Newman Keuls $p < 0.001$ for all comparisons controls vs. stroke). In both groups, the ambulation index did not change whether the participants listened to music or not ($0.52 < p < 0.73$ in controls, and $0.56 < p < 0.99$ in patients).

Figure 5 shows the mean heart rate (**Figure 5A**) and the mean breathing rate (**Figure 5B**) in both groups, in each audio context. ANOVA on ranks did not reveal any difference between groups and audio contexts for both physiological parameters ($p = 0.28$ for heart rate and $p = 0.87$ for breathing rate).

DISCUSSION

This study has shown that the CPQ reflex, particularly enhanced on the paretic side of post-stroke patients, was significantly

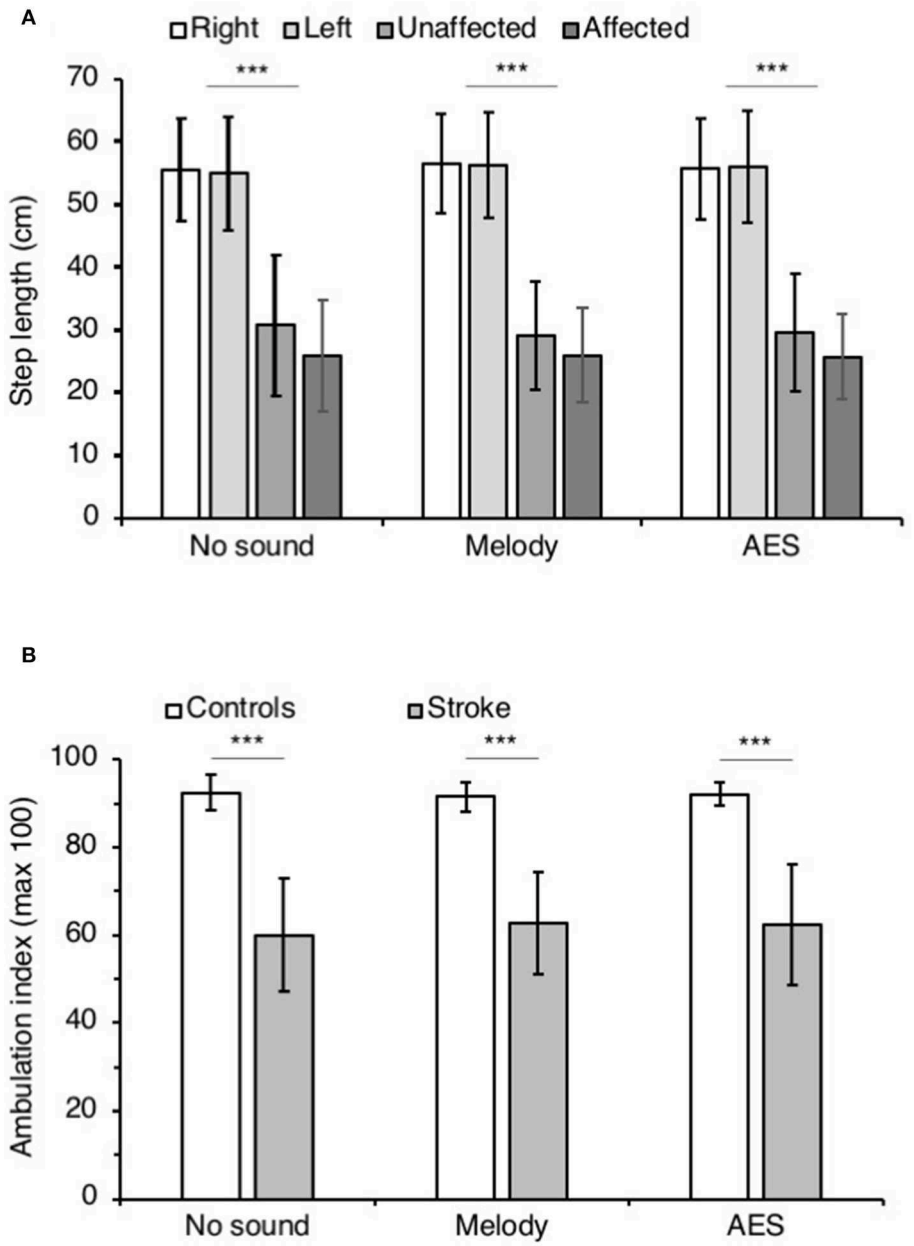

FIGURE 4 | Step parameters. **(A)** Mean step length (cm) in controls on the right (white columns) and the left side (light gray), and in patients with stroke on the affected (middle gray columns) and the unaffected side (dark gray columns). The vertical error bars indicate ± 1 × SD. **(B)** Mean ambulation index in controls (white columns) and in patients with stroke (gray columns). Vertical bars as in **(A)**. The step parameters were collected during walking without sound and when listening to melody or AES. ***$p < 0.001$.

depressed when listening to a music theme, whether a melody or AES, during walking. With music, the CPQ reflex in patients recovered a normal size, as observed in matched controls. On the other hand, music had no influence on the CPQ reflex in controls. Lastly, the music-induced neuromodulation was not accompanied by any change in biomechanical and physiological parameters.

Origin and Role of the CPQ Reflex

The CPQ is mediated by group I and group II muscle spindle afferents from ankle dorsiflexors, which project onto spinal interneurons impinging on motoneurons supplying quadriceps (Forget et al., 1989a,b; Marque et al., 1996; Chaix et al., 1997). Several lines of evidence support that the interneurons transmitting the excitation to quadriceps motoneurons in

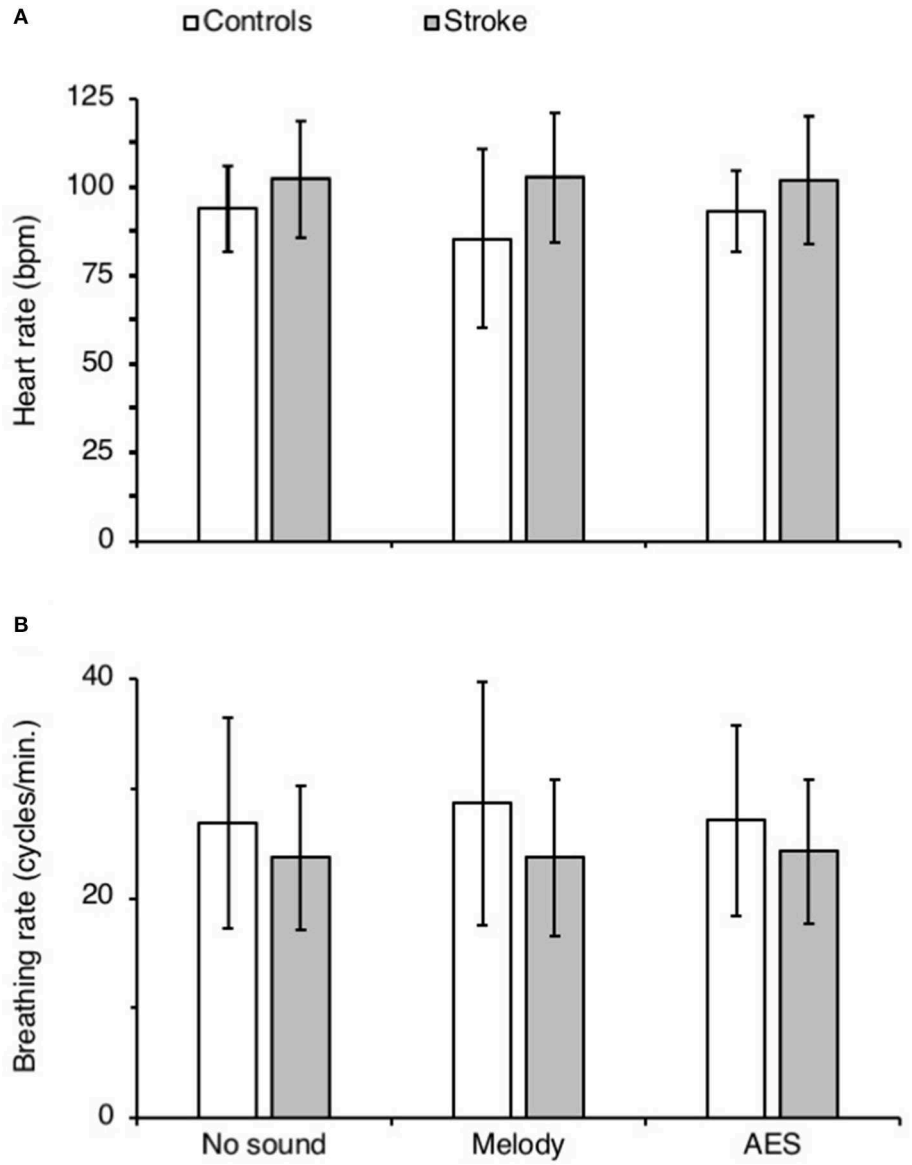

FIGURE 5 | Physiological parameters. **(A,B)** Mean heart (bpm, **A**) and breathing rate (cycles.min.$^{-1}$) in controls (white columns) and in patients with stroke (gray columns), calculated during each recording session with (Melody or AES) and without music (No sound). The vertical error bars indicate ± 1 × SD.

humans, are similar to the L3-L4 mid-lumbar interneurons in cats, also termed as propriospinal neurons or group II interneurons (Jankowska, 1992; Pierrot-Deseilligny and Burke, 2005). These interneurons are part of a complex spinal neural network that constitutes a crossroad between the motor cortex, the midbrain monoaminergic structures, and the peripheral mechanoreceptors. The descending (of pyramidal and extrapyramidal origin) and peripheral inputs (of various origins) are integrated by the lumbar propriospinal system that does not only transmit the motor command to motoneurons passively, but integrates all the converging inputs and diffuses its projections onto lumbar motoneurons (both agonists and antagonists), for a fine control of the lower limb muscle synergies during movement (Chaix et al., 1997; Marchand-Pauvert et al., 1999; Simonetta-Moreau et al., 1999; Rémy-Néris et al., 2003; Maupas et al., 2004; Pierrot-Deseilligny and Burke, 2005). It has been shown that the lumbar propriospinal system is particularly involved in the control of posture and locomotion in humans (Marchand-Pauvert and Nielsen, 2002; Marchand-Pauvert et al., 2005). More importantly, the propriospinal reflex between ankle dorsiflexors and quadriceps, is particularly enhanced during walking at the preferred speed (more automatic than slow or fast speed walking), independently of motor cortex influence, which led the authors to propose that this reflex is likely involved in the

automatic control of posture during locomotion, assisting the contraction of quadriceps during the lengthening contraction of ankle dorsiflexors, at the beginning of stance (Marchand-Pauvert and Nielsen, 2002; Marchand-Pauvert et al., 2005; Iglesias et al., 2008a,b, 2012). After stroke, the propriospinal excitation has been found particularly enhanced on the paretic side of patients, at rest and during walking (Marque et al., 2001; Achache et al., 2010). The late part of the CPQ reflex (mediated by group II afferents) is particularly enhanced during post-stroke walking, whether the patients are compared to controls walking at their preferred speed ($\sim$1.0 m.s^{-1}) or slowly (at $\sim$0.2 m.s^{-1} like stroke patients; Figure 3E in Achache et al., 2010). The CPQ reflex increased with the level of background EMG (Marchand-Pauvert and Nielsen, 2002), which could participate in the difference in reflex size between controls and patients but this is unlikely because (i) the level of background EMG was lower in patients (especially due to slow speed) than in controls, so a smaller CPQ reflex could be expected instead, and (ii) Achache et al. (2010) reported smaller CPQ reflex in controls walking at the same speed and with similar background EMG as in patients. To our knowledge, the propriospinal reflex is the only one that has been found particularly involved in the control of muscle synergies during locomotion (Pierrot-Deseilligny and Burke, 2012), and thus likely constitutes an interesting metric of spinal activity during locomotion in humans, for evaluating the neuromodulation.

In all the subjects, the CP nerve stimulation produced a biphasic facilitation on VL EMG occurring about 30–35 ms after the artifact. Previous studies using the modulations of rectified EMG after CP nerve stimuli reported similar latencies and duration (Marchand-Pauvert and Nielsen, 2002; Iglesias et al., 2008b; Achache et al., 2010). Different methodologies have been used to elucidate the origin of the CPQ reflex, by studying the modulation of averaged EMG, of H reflex amplitude, of the size of motor evoked potential (produced by transcranial magnetic stimulation, TMS), and of single motor unit discharge (Marchand-Pauvert et al., 2005). All the studies converge on the conclusion that the CPQ reflex is mediated by mid-lumbar propriospinal neurons (Pierrot-Deseilligny and Burke, 2012). After stroke, it has been shown that the CPQ reflex is particularly enhanced in patients and might be involved in spasticity (Marque et al., 2001; Maupas et al., 2004), and/or might assist muscle synergies to assist and maintain the upright posture during post-stroke locomotion (Achache et al., 2010). There is no consensus whether the propriospinal hyperactivity after stroke helps or limits the motor recovery after stroke. During walking without sound, the present study also reports an enhanced CPQ reflex in patients, which further supports the spinal hyperexcitability and hyperactivity at the level of the CPQ reflex after stroke. Walking with music, the CPQ reflex returned to normal level in patients, similar to controls. Until then, the CPQ reflex has only been depressed pharmacologically, by antispastics (Rémy-Néris et al., 2003; Maupas et al., 2004). To date, our study is the first one showing that a physiological stimuli (music) can modulate and restore a reflex activity in stroke survivors.

Possible Mechanisms Underlying the Music-Induced Neuromodulation

The spinal excitations mediated by the propriospinal neurons to lumbar motoneurons are strongly controlled by descending inputs. This was evidenced by studies using TMS, or comparing the excitation at rest and during voluntary movements (Forget et al., 1989a; Marchand-Pauvert et al., 1999, 2005). The descending inputs are likely of cortical origin in part, but also might arise from the extrapyramidal system. Indeed, it has been shown that the CPQ reflex, and the group II component in particular, is depressed by monoamines (Rémy-Néris et al., 2003; Maupas et al., 2004; Marchand-Pauvert et al., 2011), as reported in cats regarding the group II spinal reflexes (Jankowska, 1992; Pierrot-Deseilligny and Burke, 2005). Additionally, the high-frequency deep brain stimulation of subthalamic nuclei in patients with Parkinson disease reduces the CPQ reflex to normal values (Marchand-Pauvert et al., 2011). Therefore, the CPQ reflex is particularly sensitive to a change in the corticospinal inputs and in the neuromodulation from midbrain structures. Accordingly, it has been suggested that the alteration of the descending control to spinal neural networks after stroke, likely contributes to the enhanced propriospinal reflex observed in patients at rest and during locomotion (Marque et al., 2001; Rémy-Néris et al., 2003; Maupas et al., 2004; Achache et al., 2010).

In healthy subjects, TMS over the primary motor cortex inhibits the CPQ reflex during locomotion (Iglesias et al., 2008a), and the cortical contribution to quadriceps activity during walking is weak compared to a more volitional movement like an isolated tonic contraction of quadriceps (Iglesias et al., 2012). Thus, it has been suggested that the control of quadriceps during stabilized locomotion is likely subcortical in origin, and the propriospinal system plays a significant role in the transmission of the motor command to motoneurons, in line with the role of midbrain structures in the control of spinal locomotor central pattern generators (CPGs) in vertebrates (Grillner and El Manira, 2019). Alternatively, the role of proprioceptive feedback, especially muscle spindle group II afferents that are particularly active during TA lengthening contraction at the beginning of stance, has been raised (Marchand-Pauvert and Nielsen, 2002). However, given the weakness in ankle dorsiflexors after stroke and the resulting foot drop, this feedback might be less in patients and likely contributes only poorly to the CPQ reflex. Therefore, we assume that the enhanced propriospinal CPQ reflex during post-stroke walking likely results from modification of the subcortical influence on spinal circuitries likely of reticular origin. In line with this, connections from the cerebral cortex to the reticular formation in the brainstem allow motor commands to be sent over the reticulospinal tract to spinal networks, and after stroke, these pathways are likely particularly involved in the functional recovery (Baker et al., 2015; Li, 2017).

Several studies have reported music-induced excitability changes at the brain level and, given the change in reflex activity observed in resting subjects listening to music, a possible change in descending inputs likely influences the spinal excitability

as well (see Introduction). Indeed, it has been proposed that the neuromodulation of spinal reflex as a result of sound exposition, is of reticulospinal origin (startle response; Delwaide and Schepens, 1995). In our study, the music did not produce any startle response and did not influence at all the CPQ reflex in controls; the CPQ reflex was of similar size whether the subjects listened to music or not. Therefore, the possible descending music-induced neuromodulation had only little or no influence on spinal activity during locomotion. One possible explanation would be a saturation of the reticular system during locomotion, but this is unlikely given the possibility of startle during walking. Alternatively, there might be a saturation of the reflex activity under the reticulospinal influence, becoming less sensitive to music-induced additional reticulospinal inputs in controls. Further studies in controls walking at a slower speed (with lower CPQ reflex activity) than their preferred speed (but not as slow as in patients because the CPQ reflex is hardly evoked at $\sim$0.2 m.s^{-1} in controls) would help to determine if music-induced neuromodulation would also occur in controls (Iglesias et al., 2008b; Achache et al., 2010). On the contrary, in stroke patients, the CPQ reflex was depressed by music, reaching normal values as those observed in controls. This might be related to the neuromodulation in the cortico-reticulo-spinal system following stroke, used for motor commands and functional recovery (Baker et al., 2015; Li, 2017). On the other hand, it is not clear whether the reticulospinal hyperexcitability and associated spasticity is a good or maladaptive plasticity (Li, 2017).

Repercussions on Post-stroke Walking

The results in patients indicate that the cortico-reticulo-spinal system might be modulated after stroke, when using music and sounds as distractors. Indeed, all the patients paid attention to the music during the recording sessions, whether they listened to the melody or AES. The music likely functioned as an external focus of attention that is known to improve the post-stroke walking (Kim et al., 2019). However, the change in spinal excitability was not associated to a change in the biomechanical parameters, while RAS has been shown to improve the cadence and the step length during post-stroke walking (Yoo and Kim, 2016; Magee et al., 2017); walking speed is also enhanced with RAS but since we used the same treadmill velocity (to avoid any change in CPQ reflex due to speed; Iglesias et al., 2008b), we cannot conclude on this parameter. One possible explanation for this result is that we used music with irregular tempo, to avoid any step synchronization, and the absence of change in the gait parameters likely supports the necessity of constant rhythm (like RAS), to observe short term benefits on locomotor cadence. However, it is interesting to note that the arhythmical melody and AES we used were able to modulate the spinal excitability without behavioral repercussion. The patients only performed two short walking sessions with music. There is a possibility that more repetitions are needed to consolidate the plasticity and to observe clear improvements of the walking pattern. In addition, our basic biomechanical approach was too limited and likely not sensitive enough for being really conclusive. Furthermore, we did not investigate the change in walking speed because changing the treadmill speed would have altered the CPQ reflex (Iglesias et al., 2008b); something that needs to be taken into account in future studies.

All the patients preferred the melody compared to AES. We selected the melody because we found it more pleasant than AES, and most of the subjects shared our opinion. The emotional states and their changes are difficult to evaluate but heartbeat and respiratory rhythm are sensitive. However, we did not find any change with music and objectively the subjects did not appear particularly affected in one direction or another by the melody or AES. Therefore, we assume the emotional charge was likely not different between the melody and AES, and they likely paid attention equally to both themes during walking (comparable external focus of attention). On the other hand, they preferred to walk when listening a music or sounds, compared to nothing. Therefore, there is a possibility that the change in spinal excitability might be also related to some extent to the influence of music on mood, as reported at the level of the brain (Altenmüller and Schlaug, 2015). In any case, the present study has shown that listening to music or sounds after stroke is efficient to modulate the synaptic activity at the level of the propriospinal reflex that is known to be particularly involved in locomotion. We assume that repetitive training walking sessions with music may help to counteract the post-stroke spinal hyperexcitability, which limits muscle synergies during walking and hinder to some extent the functional recovery.

CONCLUSION

It has been well-established that the rehabilitation with music is more efficient than the one without music (Galinska, 2015). Interestingly, most of the physiotherapists report that a session of rehabilitation is always better with music, the patients performing better than without music but, apparently, they do not know why. On the other hand, our patients reported they preferred walking with music, than without, whatever it was. This study has shown that during only one training session, music and sounds modulate the spinal activity, at the level of the propriospinal network that is known to be particularly involved in stabilized walking. In normal conditions, the CPQ reflex is particularly active when the subjects walk at their preferred speed corresponding to a more automatic locomotion, which does not require too much attention, as compared to slow or fast speed. We discussed the point that music and sounds have likely acted as external focus of attention. Restoring the propriospinal reflex to normal value with music listening might be a sign that the walking control under these conditions was more automatic than without music. This might help recovering locomotor automatisms (with less volitional step control). However, the spinal plasticity was not accompanied by any change of gait parameters, likely because the parameters we tested were not sensitive enough and that more training sessions are required to objectify gait improvement. Future studies using the propriospinal reflex as a biomarker of music-induced plasticity

and patient follow-up would be interesting to further confirm the interest of music with or without regular tempo, to improve post-stroke walking.

DATA AVAILABILITY STATEMENT

All datasets generated for this study are included in the article/**Supplementary Material**.

ETHICS STATEMENT

The studies involving human participants were reviewed and approved by CPP Ile de France VI—Pitié-Salpêtrière; PHRC 95078, DRCD 070804. The patients/participants provided their written informed consent to participate in this study.

AUTHOR CONTRIBUTIONS

IP, CK, PP-D, and VM-P conceptualized the study and has developed the protocol. BH-B, CK, EB, and PP-D have selected the patients and performed the clinical evaluation. VM-P and AL-V have selected the controls. VM-P, BH-B, and AL-V performed the experiments. VM-P and IP analyzed the data and wrote the draft of the manuscript. VM-P performed the statistics. All authors participated in finalizing the manuscript.

FUNDING

This study was supported by a grant from Institut pour la Recherche sur la Moelle Epinière (IRME). IP was supported by a grant from Institut Universitaire d'Ingénierie en Santé (IUIS) of Sorbonne Université.

ACKNOWLEDGMENTS

The authors wish to express their grateful to all the participants and to the staff of the department of rehabilitation of the Pitié-Salpêtrière Hospital. The authors also deeply thank Guillaume Le Borgne who *ex gratia* composed the AES for the protocol.

SUPPLEMENTARY MATERIAL

The Supplementary Material for this article can be found online at: https://www.frontiersin.org/articles/10.3389/fnsys.2020.00017/full#supplementary-material

REFERENCES

Achache, V., Mazevet, D., Iglesias, C., Lackmy, A., Nielsen, J. B., Katz, R., et al. (2010). Enhanced spinal excitation from ankle flexors to knee extensors during walking in stroke patients. *Clin. Neurophysiol.* 121, 930–938. doi: 10.1016/j.clinph.2009.12.037

Altenmüller, E., Marco-Pallares, J., Münte, T. F., and Schneider, S. (2009). Neural reorganization underlies improvement in stroke-induced motor dysfunction by music-supported therapy. *Ann. N. Y. Acad. Sci.* 1169, 395–405. doi: 10.1111/j.1749-6632.2009.04580.x

Altenmüller, E., and Schlaug, G. (2015). Apollo's gift: new aspects of neurologic music therapy. *Prog. Brain Res.* 217, 237–252. doi: 10.1016/bs.pbr.2014.11.029

Amengual, J. L., Rojo, N., Veciana de Las Heras, M., Marco-Pallarés, J., Grau-Sánchez, J., Schneider, S., et al. (2013). Sensorimotor plasticity after music-supported therapy in chronic stroke patients revealed by transcranial magnetic stimulation. *PLoS ONE* 8:e61883. doi: 10.1371/journal.pone.0061883

Baker, S. N., Zaaimi, B., Fisher, K. M., Edgley, S. A., and Soteropoulos, D. S. (2015). Pathways mediating functional recovery. *Prog. Brain Res.* 218, 389–412. doi: 10.1016/bs.pbr.2014.12.010

Barnes, C. D., and Thomas, J. S. (1968). Effects of acoustic stimulation on the spinal cord. *Brain Res.* 7, 303–305. doi: 10.1016/0006-8993(68)90107-8

Binkofski, F., Fink, G. R., Geyer, S., Buccino, G., Gruber, O., Shah, N. J., et al. (2002). Neural activity in human primary motor cortex areas 4a and 4p is modulated differentially by attention to action. *J. Neurophysiol.* 88, 514–519. doi: 10.1152/jn.2002.88.1.514

Burt, J., Ravid, E. N., Bradford, S., Fisher, N. J., Zeng, Y., Chomiak, T., et al. (2019). The effects of music-contingent gait training on cognition and mood in parkinson disease: a feasibility study. *Neurorehabil. Neural Repair* 34, 82–92. doi: 10.1177/1545968319893303

Cerniauskaite, M., Quintas, R., Koutsogeorgou, E., Meucci, P., Sattin, D., Leonardi, M., et al. (2012). Quality-of-life and disability in patients with stroke. *Am. J. Phys. Med. Rehabil.* 91:S393. doi: 10.1097/PHM.0b013e31823d4df7

Chaix, Y., Marque, P., Meunier, S., Pierrot-Deseilligny, E., and Simonetta-Moreau, M. (1997). Further evidence for non-monosynaptic group I excitation of motoneurones in the human lower limb. *Exp. Brain Res.* 115, 35–46. doi: 10.1007/PL00005683

Delwaide, P. J., and Schepens, B. (1995). Auditory startle (audio-spinal) reaction in normal man: EMG responses and H reflex changes in antagonistic lower limb muscles. *Electroencephalogr. Clin. Neurophysiol.* 97, 416–423. doi: 10.1016/0924-980X(95)00136-9

Devlin, K., Alshaikh, J. T., and Pantelyat, A. (2019). Music therapy and music-based interventions for movement disorders. *Curr. Neurol. Neurosci. Rep.* 19:83. doi: 10.1007/s11910-019-1005-0

Forget, R., Hultborn, H., Meunier, S., Pantieri, R., and Pierrot-Deseilligny, E. (1989a). Facilitation of quadriceps motoneurones by group I afferents from pretibial flexors in man. 2. Changes occurring during voluntary contraction. *Exp. Brain Res.* 78, 21–27. doi: 10.1007/BF00230682

Forget, R., Pantieri, R., Pierrot-Deseilligny, E., Shindo, M., and Tanaka, R. (1989b). Facilitation of quadriceps motoneurones by group I afferents from pretibial flexors in man. 1. Possible interneuronal pathway. *Exp. Brain Res.* 78, 10–20. doi: 10.1007/BF00230681

Galinska, E. (2015). Music therapy in neurological rehabilitation settings. *Psychiatr. Pol.* 49, 835–846. doi: 10.12740/PP/25557

Ghai, S. (2018). Effects of real-time (Sonification) and rhythmic auditory stimuli on recovering arm function post stroke: a systematic review and meta-analysis. *Front. Neurol.* 9:488. doi: 10.3389/fneur.2018.00488

Grau-Sánchez, J., Amengual, J. L., Rojo, N., Veciana de Las Heras, M., Montero, J., Rubio, F., et al. (2013). Plasticity in the sensorimotor cortex induced by Music-supported therapy in stroke patients: a TMS study. *Front. Hum. Neurosci.* 7:494. doi: 10.3389/fnhum.2013.00494

Grillner, S., and El Manira, A. (2019). Current principles of motor control, with special reference to vertebrate locomotion. *Physiol. Rev.* 100, 271–320. doi: 10.1152/physrev.00015.2019

Iglesias, C., Lourenco, G., and Marchand-Pauvert, V. (2012). Weak motor cortex contribution to the quadriceps activity during human walking. *Gait Posture* 35, 360–366. doi: 10.1016/j.gaitpost.2011.10.006

Iglesias, C., Nielsen, J. B., and Marchand-Pauvert, V. (2008a). Corticospinal inhibition of transmission in propriospinal-like neurones during human walking. *Eur. J. Neurosci.* 28, 1351–1361. doi: 10.1111/j.1460-9568.2008.06414.x

Iglesias, C., Nielsen, J. B., and Marchand-Pauvert, V. (2008b). Speed-related spinal excitation from ankle dorsiflexors to knee extensors during human walking. *Exp. Brain Res.* 188, 101–110. doi: 10.1007/s00221-008-1344-6

Jankowska, E. (1992). Interneuronal relay in spinal pathways from proprioceptors. *Prog. Neurobiol.* 38, 335–378. doi: 10.1016/0301-0082(92)90024-9

Johansen-Berg, H., and Matthews, P. M. (2002). Attention to movement modulates activity in sensori-motor areas, including primary motor cortex. *Exp. Brain Res.* 142, 13–24. doi: 10.1007/s00221-001-0905-8

Johnson, L., Burridge, J. H., and Demain, S. H. (2013). Internal and external focus of attention during gait re-education: an observational study of physical therapist practice in stroke rehabilitation. *Phys. Ther.* 93, 957–966. doi: 10.2522/ptj.20120300

Kim, S. A., Ryu, Y. U., and Shin, H. K. (2019). The effects of different attentional focus on poststroke gait. *J. Exerc. Rehabil.* 15, 592–596. doi: 10.12965/jer.1938360.180

Li, S. (2017). Spasticity, motor recovery, and neural plasticity after stroke. *Front. Neurol.* 8:120. doi: 10.3389/fneur.2017.00120

Magee, W. L., Clark, I., Tamplin, J., and Bradt, J. (2017). Music interventions for acquired brain injury. *Cochrane Database Syst. Rev.* 1:CD006787. doi: 10.1002/14651858.CD006787.pub3

Marchand-Pauvert, V., Gerdelat-Mas, A., Ory-Magne, F., Calvas, F., Mazevet, D., Meunier, S., et al. (2011). Both L-DOPA and HFS-STN restore the enhanced group II spinal reflex excitation to a normal level in patients with Parkinson's disease. *Clin. Neurophysiol.* 122, 1019–1026. doi: 10.1016/j.clinph.2010.08.015

Marchand-Pauvert, V., Nicolas, G., Marque, P., Iglesias, C., and Pierrot-Deseilligny, E. (2005). Increase in group II excitation from ankle muscles to thigh motoneurones during human standing. *J. Physiol.* 566, 257–271. doi: 10.1113/jphysiol.2005.087817

Marchand-Pauvert, V., and Nielsen, J. B. (2002). Modulation of non-monosynaptic excitation from ankle dorsiflexor afferents to quadriceps motoneurones during human walking. *J. Physiol.* 538, 647–657. doi: 10.1113/jphysiol.2001.012675

Marchand-Pauvert, V., Simonetta-Moreau, M., and Pierrot-Deseilligny, E. (1999). Cortical control of spinal pathways mediating group II excitation to human thigh motoneurones. *J. Physiol.* 517(Pt 1), 301–313. doi: 10.1111/j.1469-7793.1999.0301z.x

Marque, P., Pierrot-Deseilligny, E., and Simonetta-Moreau, M. (1996). Evidence for excitation of the human lower limb motoneurones by group II muscle afferents. *Exp. Brain Res.* 109, 357–360. doi: 10.1007/BF00231793

Marque, P., Simonetta-Moreau, M., Maupas, E., and Roques, C. F. (2001). Facilitation of transmission in heteronymous group II pathways in spastic hemiplegic patients. *J. Neurol. Neurosurg. Psychiatry* 70, 36–42. doi: 10.1136/jnnp.70.1.36

Maupas, E., Marque, P., Roques, C. F., and Simonetta-Moreau, M. (2004). Modulation of the transmission in group II heteronymous pathways by tizanidine in spastic hemiplegic patients. *J. Neurol. Neurosurg. Psychiatry* 75, 130–135.

O'Kelly, J., Fachner, J. C., and Tervaniemi, M. (2016). Editorial: dialogues in music therapy and music neuroscience: collaborative understanding driving clinical advances. *Front. Hum. Neurosci.* 10:585. doi: 10.3389/fnhum.2016.00585

Pierrot-Deseilligny, E., and Burke, D. (2005). *The Circuitry of the Human Spinal Cord. 1st Edn.* New York, NY: Cambridge University Press. doi: 10.1017/CBO9780511545047

Pierrot-Deseilligny, E., and Burke, D. (2012). *The Circuitry of the Human Spinal Cord. 2nd Edn.* New York, NY: Cambridge University Press. doi: 10.1017/CBO9781139026727

Rémy-Néris, O., Denys, P., Daniel, O., Barbeau, H., and Bussel, B. (2003). Effect of intrathecal clonidine on group I and group II oligosynaptic excitation in paraplegics. *Exp. Brain Res.* 148, 509–514. doi: 10.1007/s00221-002-1313-4

Ripollés, P., Rojo, N., Grau-Sánchez, J., Amengual, J. L., Càmara, E., Marco-Pallarés, J., et al. (2016). Music supported therapy promotes motor plasticity in individuals with chronic stroke. *Brain Imaging Behav.* 10, 1289–1307. doi: 10.1007/s11682-015-9498-x

Rojo, N., Amengual, J., Juncadella, M., Rubio, F., Camara, E., Marco-Pallares, J., et al. (2011). Music-supported therapy induces plasticity in the sensorimotor cortex in chronic stroke: a single-case study using multimodal imaging (fMRI-TMS). *Brain Inj.* 25, 787–793. doi: 10.3109/02699052.2011.576305

Rossignol, S., and Jones, G. M. (1976). Audio-spinal influence in man studied by the H-reflex and its possible role on rhythmic movements synchronized to sound. *Electroencephalogr. Clin. Neurophysiol.* 41, 83–92. doi: 10.1016/0013-4694(76)90217-0

Roy, M., Lebuis, A., Hugueville, L., Peretz, I., and Rainville, P. (2012). Spinal modulation of nociception by music. *Eur. J. Pain.* 16, 870–877. doi: 10.1002/j.1532-2149.2011.00030.x

Ruscheweyh, R., Kreusch, A., Albers, C., Sommer, J., and Marziniak, M. (2011). The effect of distraction strategies on pain perception and the nociceptive flexor reflex (RIII reflex). *Pain* 152, 2662–2671. doi: 10.1016/j.pain.2011.08.016

Schneider, S., Müünte, T., Rodriguez-Fornells, A., Sailer, M., and Altenmüüller, E. (2010). Music-supported training is more efficient than functional motor training for recovery of fine motor skills in stroke patients. *Music Percept. Interdiscip. J.* 27, 271–280. doi: 10.1525/mp.2010.27.4.271

Simonetta-Moreau, M., Marque, P., Marchand-Pauvert, V., and Pierrot-Deseilligny, E. (1999). The pattern of excitation of human lower limb motoneurones by probable group II muscle afferents. *J. Physiol.* 517, 287–300. doi: 10.1111/j.1469-7793.1999.0287z.x

Wade, D. T., Langton-Hewer, R., Skilbeck, C. E., and David, R. M. (1985). *Stroke: A Critical Approach to Diagnosis, Treatment, and Management*. Chicago, CA: Year Book Medical Publishers; Open Library; Internet Archives.

World Health Organization (2014). *Global Status Report on Noncommunicable Diseases 2014* (No. WHO/NMH/NVI/15.1). WHO.

Yiruma (2001). *Rivers Flow in You© Extract From First Love (Sound Recording)*. Universal Music.

Yoo, G. E., and Kim, S. J. (2016). Rhythmic auditory cueing in motor rehabilitation for stroke patients: systematic review and meta-analysis. *J. Music Ther.* 53, 149–177. doi: 10.1093/jmt/thw003

Conflict of Interest: The authors declare that the research was conducted in the absence of any commercial or financial relationships that could be construed as a potential conflict of interest.

frontiers in Cellular Neuroscience

ORIGINAL RESEARCH
published: 28 April 2020
doi: 10.3389/fncel.2020.00081

Critical Components for Spontaneous Activity and Rhythm Generation in Spinal Cord Circuits in Culture

*Samuel Buntschu, Anne Tscherter, Martina Heidemann and Jürg Streit**

Department of Physiology, University of Bern, Bern, Switzerland

Neuronal excitability contributes to rhythm generation in central pattern generating networks (CPGs). In spinal cord CPGs, such intrinsic excitability partly relies on persistent sodium currents (I_{NaP}), whereas respiratory CPGs additionally depend on calcium-activated cation currents (I_{CAN}). Here, we investigated the contributions of I_{NaP} and I_{CAN} to spontaneous rhythm generation in neuronal networks of the spinal cord and whether they mainly involve Hb9 neurons. We used cultures of ventral and transverse slices from the E13–14 embryonic rodent lumbar spinal cord on multielectrode arrays (MEAs). All cultures showed spontaneous bursts of network activity. Blocking synaptic excitation with the AMPA receptor antagonist CNQX suppressed spontaneous network bursts and left asynchronous intrinsic activity at about 30% of the electrodes. Such intrinsic activity was completely blocked at all electrodes by both the I_{NaP} blocker riluzole as well as by the I_{CAN} blocker flufenamic acid (FFA) and the more specific TRPM4 channel antagonist 9-phenanthrol. All three antagonists also suppressed spontaneous bursting completely and strongly reduced stimulus-evoked bursts. Also, FFA reduced repetitive spiking that was induced in single neurons by injection of depolarizing current pulses to few spikes. Other antagonists of unspecific cation currents or calcium currents had no suppressing effects on either intrinsic activity (gadolinium chloride) or spontaneous bursting (the TRPC channel antagonists clemizole and ML204 and the T channel antagonist TTA-P2). Combined patch-clamp and MEA recordings showed that Hb9 interneurons were activated by network bursts but could not initiate them. Together these findings suggest that both I_{NaP} through Na^+-channels and I_{CAN} through putative TRPM4 channels contribute to spontaneous intrinsic and repetitive spiking in spinal cord neurons and thereby to the generation of network bursts.

Keywords: rhythm generation, intrinsic spiking, TRP channels, multielectrode arrays, central pattern generator, I_{CAN}, I_{NaP}

OPEN ACCESS

Edited by:
Michelle Maria Rank,
The University of Melbourne, Australia

Reviewed by:
Werner Kilb,
Johannes Gutenberg University Mainz, Germany
Klaus Ballanyi,
University of Alberta, Canada

***Correspondence:**
Jürg Streit
streit@pyl.unibe.ch

Received: *02 December 2019*
Accepted: *19 March 2020*
Published: *28 April 2020*

Citation:
Buntschu S, Tscherter A, Heidemann M and Streit J (2020) Critical Components for Spontaneous Activity and Rhythm Generation in Spinal Cord Circuits in Culture. Front. Cell. Neurosci. 14:81. doi: 10.3389/fncel.2020.00081

INTRODUCTION

Central pattern generator networks (CPGs) provide rhythmic output to muscles to support repetitive movements used in locomotion or breathing (Feldman et al., 2013; Kiehn, 2016). The mechanisms involved in such rhythm generation are still not fully understood. Especially, it is not clear, which types of interneurons contribute to rhythm generation, which circuits they form and which ion channels and receptors contribute to their intrinsic excitability. In the lumbar spinal cord, several types of genetically identified interneurons (Hb9, Shox 2 and V2a) have been proposed to participate in CPG networks (Ziskind-Conhaim et al., 2010; Dougherty et al., 2013; Ljunggren et al., 2014). For Hb9 interneurons, however, a key role for rhythm generation is still under debate (Caldeira et al., 2017).

In the mammalian spinal cord, the persistent sodium current I_{NaP} has been proposed to be involved in rhythm generation. This current is activated at sub-threshold potentials around −60 mV and probably represents a special state of the voltage-dependent Na^+ channel (Urbani and Belluzzi, 2000). It contributes to intrinsic spiking of neurons and rhythm generation in organotypic and dissociated cultures of the spinal cord (Darbon et al., 2004; Yvon et al., 2007; Czarnecki et al., 2009) as well as in the neonatal rat spinal cord (Tazerart et al., 2007, 2008; Ziskind-Conhaim et al., 2008).

In respiratory circuits of the brainstem, two types of ion channels are proposed and debated to contribute to intrinsic firing of pacemaker neurons and thus participate in rhythm and pattern generation (Del Negro et al., 2005, 2018; Pace et al., 2007a,b; Koizumi et al., 2018; Picardo et al., 2019). In the first type of neurons, intrinsic spiking is based on I_{NaP}, in the second type on a cation current that is activated by Ca^{2+} (I_{CAN}). I_{CAN} is believed to be mediated by TRPM and/or TRPC channels (Ben-Mabrouk and Tryba, 2010; Mrejeru et al., 2011). It has been shown to underlie sustained depolarization, persistent activity and rhythm generation in a subset of neurons in the pre-Bötzinger complex (Pace et al., 2007b; Del Negro et al., 2010) and other neuronal circuits (Schiller, 2004; Mrejeru et al., 2011). In the spinal cord there is so far only some evidence for the role of I_{CAN} in intrinsic spiking of dorsal horn neurons but not in motor rhythm generation in the ventral spinal cord (Wang et al., 2006; Li and Baccei, 2011).

Rhythm generation is also a prominent feature in isolated neuronal networks in culture. In organotypic cultures of transverse slices of embryonic rat spinal cord, rhythms consisting of bursting activity with intraburst oscillations have been described previously (Ballerini et al., 1999; Tscherter et al., 2001). We demonstrated that this type of spontaneous rhythmic activity is based on intrinsic firing in a subset of neurons and on glutamatergic excitatory and recurrent GABA-ergic inhibitory connections in the network (Czarnecki et al., 2008). Also, we showed that intrinsic firing depends on I_{NaP} and hyperpolarization-activated cation currents I_h (Darbon et al., 2004).

In the present article, we show that similar rhythms are produced in ventral circuits of the rat spinal cord in longitudinal slices cultured on multielectrode arrays (MEAs) as previously described in cultures from transverse slices. We then investigated the relative contributions of I_{NaP} and I_{CAN} to intrinsic spiking and rhythm generation and we searched for a putative role of HB9 interneurons in the generation of bursting activity.

MATERIALS AND METHODS

Culture Preparation

Cultures were obtained from spinal cords of either 14 days old rat embryos (E14) from Wistar rats purchased from Janvier (Le Genest St Isle, France) or of 13-day old embryos from Hlxb9-GFP mice [B6.CG-TG(Hlxb9-GFP)1Tmj/J] that express a green fluorescent protein (GFP) under the Hlxb9 promoter (obtained from Jackson Laboratory). The embryos were delivered by cesarean section from deeply anesthetized pregnant animals (after an intramuscular injection of 0.4 ml pentobarbital, Streuli Pharma SA, Switzerland), followed by an additional intraperitoneal application of pentobarbital. Deep anesthesia was confirmed before the section using the withdrawal reflex of the hind paw. This procedure guaranteed minimal suffering of animals (grade 0). The number of animals used to prepare the cultures was kept to a minimum. Animal care was under guidelines approved by Swiss local authorities (Amt für Landwirtschaft und Natur des Kantons Bern, Veterinärdienst, Sekretariat Tierversuche, approval Nr. BE 52/11 and BE 35/14). These guidelines are in agreement with the European Community Directive 86/609/EEC. After decapitation of the embryos, the lumbar parts of the backs were cut out and isolated from their limbs and viscera. Then they were cut into four to five 225 μm thick frontal slices with a tissue chopper and kept at 4°C in the slicing medium (Dulbecco's Modified Eagle's Medium with Glutamax, 25 mM Hepes and Antibiotics). Custom-made MEAs (external size 21 × 21 mm, Qwane Biosystems, Lausanne, Switzerland) were coated for 1 h with diluted (1:50) Matrigel® (Falcon/Biocoat, Becton Dickinson AG, Switzerland). After dissecting the spinal cord slices from the surrounding tissue the two most ventral of them were fixed on top of each MEA by using reconstituted chicken plasma coagulated by thrombin (both Sigma–Aldrich, Switzerland). In addition to the cultures of longitudinal slices from rat spinal cord, we also prepared cultures of transverse slices from mouse and rat spinal cord as previously described (Tscherter et al., 2001). The cultures were maintained in sterile plastic tubes containing 3 ml of nutrient medium and incubated in roller drums rotating at 1 r.p.m in a 5% CO_2-containing atmosphere at 36.5°C (Streit et al., 2001). The medium was composed of 79% Dulbecco's modified Eagle's medium with Glutamax, 10% horse serum (both Gibco BRL, Switzerland), 10% H_2O and 5 ng/ml 2.5S nerve growth factor (Sigma–Aldrich, Switzerland). Half of the medium was replaced once to twice per week.

MEA Recording and Analysis

MEAs consisted of 68 platinum-plated electrodes laid out in the form of a rectangle. The electrodes measured 40 μm × 40 μm and were spaced 200 μm apart (center to center, e.g., **Figure 1A**). Recordings were made from cultures of 3–10 weeks *in vitro* age. An MEA with culture was mounted in a recording chamber

on the stage of an upright microscope (Olympus BX 45, Tokyo, Japan) of a patch-clamp setup that was equipped with fluorescence microscopy settings to allow for the visualization of GFP-expressing neurons. The medium was replaced by an extracellular solution containing (in mM): NaCl, 145; KCl, 4; $MgCl_2$, 1; $CaCl_2$, 2, HEPES, 5; Na-pyruvate, 2; glucose, 5; pH 7.4. Recordings were made 5 min after the solution change in the absence of continuous superfusion with a solution change every 10–15 min. All recordings were made at room temperature (RT; 24 ± 4°C). Under these conditions, the cultures showed spontaneous network bursting activity that usually originated from all over the slices and remained stable for several hours.

Electrodes that were covered by the spinal cord slice (usually 40–60) were selected by eye and their recordings digitized at 6 kHz, visualized and stored on the hard disc using custom-made virtual instruments within Labview (National Instruments, Switzerland), as described previously (Streit et al., 2001). Detection of the extracellularly recorded action potentials and further analysis were done offline with the software package IGOR (WaveMetrics, Lake Oswego, OR, USA) as described previously (Tscherter et al., 2001). The detected signals were fast voltage transients (<4 ms), which correspond to single action potentials in neurons (somata or axons, single-unit activity). These transients often appeared in clusters (multi-unit activity) originating from closely timed action potentials of several neurons recorded by one electrode. When they appeared at more than 250 Hz (= upper limit of temporal resolution of the detector), they could not be separated from each other and therefore such activity was set by definition to 333 Hz (Tscherter et al., 2001). No attempt was made to sort the spikes recorded by one electrode. The selectivity of event detection for spiking activity was assessed using recordings obtained in the presence of tetrodotoxin (TTX, 1.5 μM) as a zero reference.

The processed data were displayed as event raster plots, network activity plots, and activity distribution plots (see **Figure 1**). Event raster plots show the time markers of the detected activity of each selected electrode (= channel). Network activity plots show the total activity of all selected channels summed within a sliding window of 10 ms, shifted by 1 ms steps. Activity distribution plots show filled circles whose diameters are proportional to the total activity of the electrodes projected on a picture of the slice culture. Total activity is measured as the mean of the activity per second detected by each electrode during the whole recording period (usually 10 min). From the TTX reference, the selectivity threshold for each channel was set at 0.1 events/s. Channels with an activity above the threshold were defined as active (see **Figure 2**).

We defined clusters of activity that appear at several electrodes as bursts. Bursts were detected by setting a threshold at 50% of maximum activity in network activity plots and by defining the burst start as the time of the first event within this burst after a minimum silent period of 5 ms and the burst end as the time of the last event before a minimum silent period of 200 ms. The frequency of oscillations within the bursts were determined by counting the peaks of network activity plots within the first 1–2 s of a burst. For each burst, we identified the start point as the channel that first showed activity. Burst sources were defined as channels where bursts started more often than expected from the quotient of the number of bursts vs. the number of active channels.

Electrical Stimulation with MEA Electrodes

Electrical stimulation was done with MEA electrodes using monopolar biphasic stimuli with a duration of 0.1 ms and an amplitude of 1–2 V that was delivered from a custom-made stimulator. The stimuli were applied to one electrode. The evoked events were recorded at all other MEA electrodes and quantified as network activity in a time window following the stimuli.

Whole-Cell Patch-Clamp Recording and Analysis

Intracellular voltage measurements were obtained from individual neurons in the slice using the whole-cell patch-clamp technique with an Axopatch 200 amplifier (Molecular Devices Inc., Sunnyvale, CA, USA). For patch-clamp experiments, we used continuous superfusion (1.5 ml/min) at RT. The extracellular solution was the same as for MEA experiments. The patch pipettes were filled with a solution containing (in mM): K-gluconate 120; KCl 10; HEPES, 10; Mg-ATP, 4; Na_2-GTP, 0.3; Na_2-phosphocreatine, 10; pH 7.3 (with KOH). They were connected to the amplifier using a chloride silver wire. The electrodes had a resistance of 3–4 MΩ. No series resistance compensation was applied. Native resting membrane potentials were in the range of –45 to –75 mV. A junction potential of 15 mV was systematically corrected. The recordings were digitized at 6–10 kHz, visualized and stored on a computer using pClamp software (Molecular Devices Inc.). The signals were analyzed offline using custom-made programs in IGOR (WaveMetrics, Lake Oswego, OR, USA) and Clampfit software (Molecular Devices Inc).

Immunohistochemistry

Cultures were fixed with 4% paraformaldehyde in phosphate-buffered saline (PBS, 0.1 M, pH 7.4) for 1–2 h at 4°C and then rinsed three times in PBS (0.1 M, pH 7.4) and stored at 4°C until used. Cultures were incubated in 2% chicken or 2% donkey serum, 0.5% bovine serum albumin (BSA) and 0.5% Triton X-100 in PBS (0.1 M, pH 7.4; blocking solution) for 1 h at RT and subsequently incubated in a humid chamber overnight at 4°C with goat polyclonal antibody to choline acetyltransferase (ChAT; AB144P; Chemicon, 1:100), diluted and mixed in PBS (0.1 M, pH 7.4), Triton X-100 (0.5%), BSA (0.5%). Cultures were then rinsed three times in PBS (0.1 M, pH 7.4) Triton X-100 (0.5%) and incubated with Alexa fluor 488 conjugated chicken polyclonal anti-goat antibody (A-21467; Invitrogen, 1:200) for 2 h at RT. This component was diluted and mixed in PBS (0.1 M, pH 7.4), Triton X-100 (0.5%).

Finally, samples were rinsed three times in PBS (0.1 M, pH 7.4) and then mounted with mowiol (4–88 Fluka from Sigma–Aldrich), which is an anti-fade mounting medium. Labeled neurons were visualized using a confocal microscope (Zeiss SLM 510 Meta).

The specificity of the immunostaining protocols above was tested by incubating cultured slices without the primary antibody. No immunostaining was observed in these slices.

Statistics

Averages are expressed as mean ± SEM. Differences between groups were evaluated for the burst rates and the total activity using the *T*-test and for the number of active channels using the Chi-square test. Significance was accepted when $p < 0.05$.

Chemicals and Drug Application

All chemicals were dissolved in extracellular solution at the final concentration. For drug application, the bath solution was exchanged twice with the drug-containing solution using a syringe, resulting in a final exchange of the bath solution by about 90–95%. For prolonged drug application (>15 min) the bath solution was exchanged with a drug-containing solution several times. The following agents were used: CNQX (6-cyano-7-nitroquinoxaline-2,3-dione), D-APV (D-(2R)-amino-5-phosphonovaleric acid), riluzole (2-amino-6-(trifluoromethoxy)benzothiazole), flufenamic acid (FFA), 9-phenanthrol, gadolinium chloride, clemizole hydrochloride and ML204 (4-Methyl-2-(1piperidinyl)-quinoline; all Sigma); TTA-P2 (3,5-dichloro-N-[1-(2,2-dimethyl-tetrahydropyran-4-ylmethyl)-4-fluoro-piperidin-4-ylmethyl]-benzamide): Alomone Labs; gabazine (2-(3-Carboxypropyl)-3-amino-6-(4methoxyphenyl)pyridazinium bromide: Abcam).

RESULTS

Spontaneous Activity in Longitudinal Slice Cultures

To study circuits from the ventral spinal cord *in vitro* we cultured longitudinal slices of lumbar ventral rat spinal cord (see **Figure 1B**). Similar to what we have described before for transverse slice cultures, all of the longitudinal slice cultures showed spontaneous activity (mean activity: 15.8 ± 14.7 events/s/channel) that was organized in network bursts (see **Figure 1A**). Such bursts consisted of periods with high rates of simultaneous multi-unit activity at many electrodes that were interrupted by periods of low network activity. Bursts appeared at a rate of about 1–20 per minute (mean rate: 5.8 ± 5.6/min, $n = 27$) and lasted for about 100 ms up to several tens of seconds (mean burst duration: 10.4 ± 15.4 s, $n = 27$). Activity during burst was spread over the whole slices with some preference for the edges (see **Figure 1B**). Most of the bursts contained intra-burst oscillations (see **Figure 1A**) with frequencies of 3–20 Hz (mean initial frequency: 12 ± 6.2 Hz, $n = 24$, that usually became slower towards the end of the bursts). Bursts usually started from several preferential sites that we called burst sources (mean number of burst sources per culture: 4.9 ± 2.4, $n = 25$). These sites were randomly spread over the whole area of the slices (see **Figure 1C**).

As in the circuits of transversal slice and of dissociated neurons (Streit et al., 2001; Tscherter et al., 2001), we recorded intrinsic activity in the cultures after synaptic disconnection of the networks in the presence of blockers of excitatory synaptic transmission. When the glutamatergic synaptic transmission was blocked with the AMPA receptor antagonist CNQX (10 μM), the bursts disappeared and were replaced by asynchronous activity at low rates (1.7 ± 1.1 events/s/channel, $n = 13$) in a fraction of channels (in 34.1 ± 21.9% of the active channels, $n = 13$, see **Figures 1D–F**). Again, the sites of the channels with such spontaneous intrinsic activity were spread over the slices in different cultures without obvious preferential sites except a slight preference for the rims of the slices (see **Figure 1E**), similar to the total activity and the burst sources.

Together these findings suggest that the spontaneous activity in cultures of longitudinal ventral horn slices is based on similar mechanisms as previously proposed for spinal cord networks in cultures from transverse slices and dissociated spinal cord neurons (Tscherter et al., 2001; Darbon et al., 2002; Yvon et al., 2005; Czarnecki et al., 2008): irregular spontaneous intrinsic activity in a fraction of neurons cause bursts and oscillations through recurrent excitation in synaptically coupled networks.

Bursting and Intrinsic Activity Are Based on I_{NaP} and I_{CAN}

Using pharmacological ion channel blockers, we next investigated which inward currents may be involved in the spontaneous intrinsic activity. We have previously found that persistent sodium currents (I_{NaP}) are involved in the generation of intrinsic firing and spontaneous bursting in spinal cord networks in culture (Darbon et al., 2004; Czarnecki et al., 2008). We, therefore, tested the effect of the I_{NaP} blocker riluzole at high doses of 20 μM on intrinsic and bursting activity. At such doses, riluzole has been shown to completely block I_{NaP} with minor effects on transient sodium currents and thus on evoked single spikes (Czarnecki et al., 2009).

Riluzole decreased the rate and duration of bursts leading to a complete block of bursting within 15–45 min (see **Figures 2A**, **3A,B**; $p < 0.001$, $n = 7$, *T*-test). In contrast to CNQX, no spontaneous intrinsic activity persisted after cessation of bursting (0/368 active channels in seven cultures vs. 243/710 active channels with CNQX in 13 cultures, see **Figures 2A**, **3C**; $p < 0.001$, Chi-square test). In the presence of CNQX, riluzole decreased the number of active channels from 31 to 6/193 channels in four cultures (see **Figure 3D**; $p < 0.001$, Chi-square test).

Next, we tested the contribution of I_{CAN} to intrinsic activity and spontaneous bursting. To our surprise, we found that the I_{CAN} blocker FFA (100 μM) had practically the same effects on spontaneous activity as riluzole. It reduced burst rate and duration up to a complete cessation of spontaneous bursting (see **Figures 2B**, **3A,B**; $p < 0.001$, $n = 8$, *T*-test) without leaving spontaneous intrinsic activity after 20–30 min (3/670 active channels in 10 cultures, see **Figures 2B**, **3C**; $p < 0.001$, Chi-square test). Also, FFA suppressed intrinsic activity in the presence of CNQX (from 179 to 3/484 active channels in 10 cultures, see **Figure 3D**, $p < 0.001$, Chi-square test).

Since FFA interferes with a variety of ion channels (Guinamard et al., 2013) we tested the more specific I_{CAN} blocker 9-phenanthrol for its effects on spontaneous bursting and intrinsic firing in conventional slice cultures. 9-phenanthrol

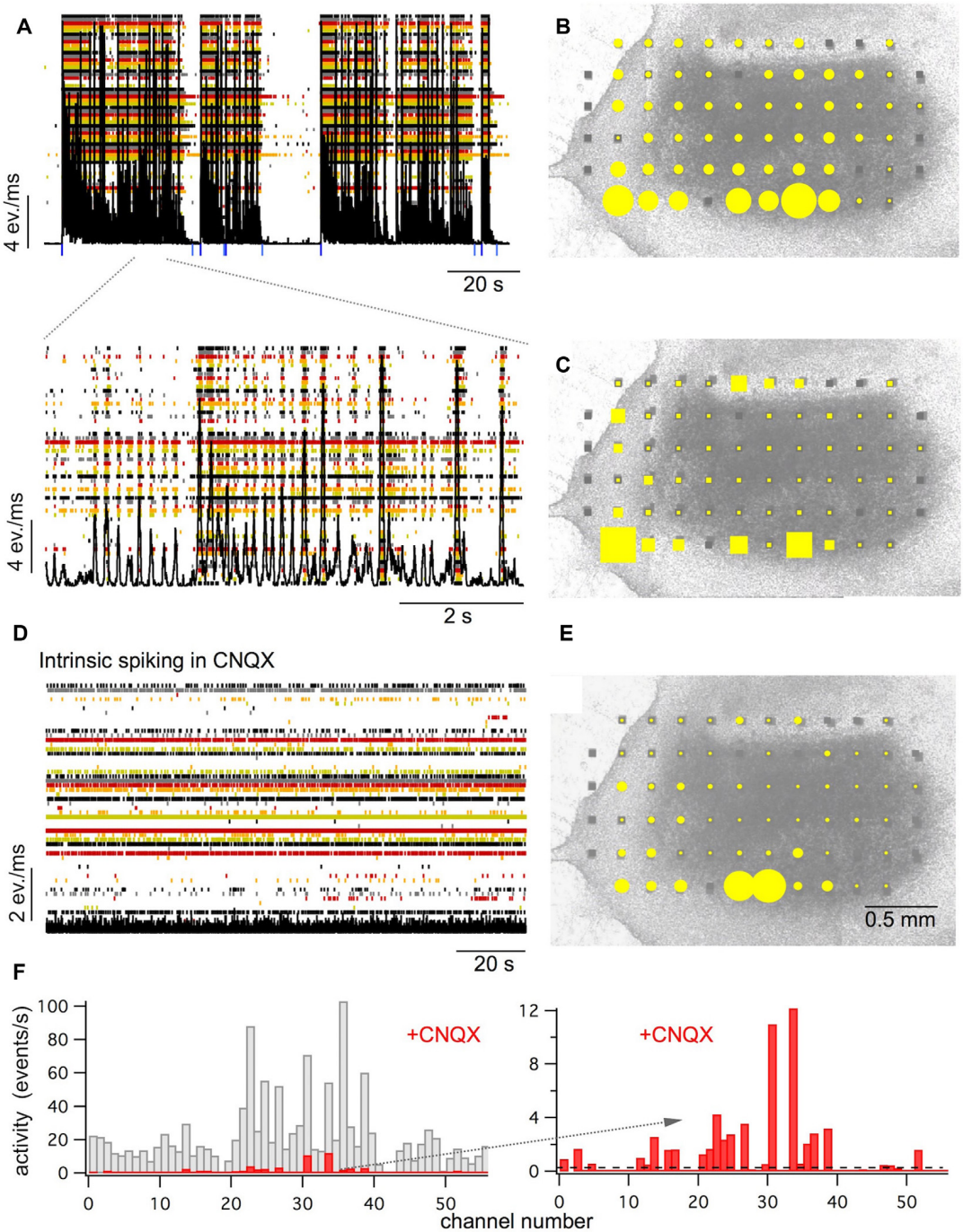

FIGURE 1 | Spontaneous activity in longitudinal spinal cord slice cultures. **(A)** Raster plot of the activity recorded by 61 electrodes (in color) superimposed by the network activity plot (black). Spontaneous activity is composed of network bursts and intraburst oscillations (see lower extract with higher time resolution). Blue marks show the starts and stops of the detected bursts. **(B)** The activity distribution plot (yellow dots) superimposed on a picture of the culture at 30 days *in vitro*. The size of the yellow dots represents the relative amount of multiple unit activity recorded at the electrode within 10 min. **(C)** Sites where bursts start with high probability (burst sources: yellow square size shows the percentage of bursts starting at this electrode) superimposed on a picture of the culture. **(D)** Raster and network activity plot after blockade of the fast glutamatergic synaptic transmission with the AMPA receptor antagonist CNQX (10 μM). Note that network bursts are suppressed and irregular low-level activity (intrinsic spiking) at about 30–40% of the electrodes appears. **(E)** The activity distribution plot for intrinsic activity (yellow dots) recorded after blockade of the fast glutamatergic synaptic transmission with CNQX superimposed on a picture of the culture. **(F)** Channel activity histograms for bursting activity as shown under **(A,B**; gray) and for intrinsic activity in the presence of CNQX as shown under **(D,E**; red). Extract on the right side shows intrinsic activity at higher resolution. The dashed line shows the detection threshold for intrinsic activity set at 0.1 events/s (see also **Figure 2**). All recordings shown under **(A–E)** are from the same slice.

is reported to specifically inhibit the TRPM4 ion channel (Guinamard et al., 2014). Like FFA, 9-phenanthrol (100 μM) completely suppressed spontaneous bursting (see **Figures 2C**, **3A,B**; $n = 8$, $p < 0.001$, *T*-test) and asynchronous activity within 30–60 min (to 2/112 active channels in 13 experiments, see **Figures 2C**, **3C**; $p < 0.001$, Chi-square test). In the presence of CNQX, 9-phenanthrol reduced the active channels from 147 to 1/365 in 10 experiments (see **Figure 3D**; $p < 0.001$, Chi-square test).

To investigate the contribution of other channels that are possibly involved in I_{CAN}, we further tested the effects of gadolinium chloride, an unspecific blocker of I_{CAN} and stretch-activated ion channels (Adding et al., 2001), and of the TRPC blockers clemizole chloride (TRPC5) and ML204 (TRPC4). Gadolinium (30 μM) fully suppressed bursting within 30 min (see **Figures 2D**, **3A,B**; $n = 5$, $p < 0.001$, *T*-test), but did not suppress the asynchronous intrinsic activity compared to CNQX (118/296 active channels in eight experiments, see **Figures 2D**, **3C**, $p = 0.89$, chi-square test). In the presence of CNQX, it slightly reduced the active channels from 96 to 67/163 in four experiments (see **Figure 3D**; $p < 0.005$, chi-square test) but did not fully suppress intrinsic activity. This effect was therefore clearly distinct from the effects of FFA and 9-phenanthrol.

Clemizole (3 μM) and ML204 (10 μM) had no effect on burst rate (see **Figure 3A**; $p = 0.27$ and 0.06, respectively, $n = 5$, *T*-test) and total activity (see **Figure 3B**; $p = 0.56$ and 0.08, respectively, $n = 5$, *T*-test) within 50 min.

Taken together, these results suggest that I_{NaP} through sodium channels and I_{CAN} through TRPM4 channels are the main contributors that control spontaneous intrinsic firing of spinal cord neurons in culture and network bursting based on this intrinsic activity. The finding that blocking one current suppresses intrinsic activity at almost all electrodes in the network excludes the hypothesis, that two different populations of neurons with distinct intrinsic firing mechanisms are present. More likely, spontaneous intrinsic firing is based on the cooperation of I_{NaP} and I_{CAN} in individual neurons. Since I_{NaP} is activated by depolarization in the range of −60 to −30 mV while I_{CAN} is activated by rising intracellular Ca^{2+}, we hypothesized that low-voltage-activated calcium channels (T-type calcium channels) may act as a link for the cooperation of the two currents for spike generation. We, therefore, investigated whether the specific T-type calcium channel blocker TTA-P2 has an effect on bursting and total spontaneous activity in our cultures. We found no effect of 1 μM TTA-P2 on burst rate (see **Figure 3A**; $p = 0.07$, $n = 5$, *T*-test) or total activity (see **Figure 3B**; $p = 0.28$, $n = 5$, *T*-test).

Involvement of I_{CAN} and I_{NaP} in Bursting Activity Induced by Electrical Stimulation

We have previously shown that riluzole at 10–20 μM suppresses repetitive firing during sustained depolarization in individual neurons and the generation of network bursts by extracellular electrical stimulation (Darbon et al., 2004). We, therefore, tested whether FFA has similar effects as riluzole in suppressing bursting activity that is evoked by electrical stimulation. We found that FFA suppressed stimulus-evoked bursts of activity within 20–30 min while leaving few individual responses to the stimuli intact (see **Figure 4A**; $p < 0.001$, $n = 8$; *T*-test), thereby reducing the stimulus-evoked network bursting activity to less than 10% of control values (see **Figure 4B**). Riluzole and 9-phenanthrol also strongly reduced stimulus-induced network bursting activity to about 20% of control (see **Figures 4D,E**; $p < 0.001$, $n = 7$, *T*-test).

To investigate the effect of FFA on the repetitive firing of neurons during sustained depolarization we injected depolarizing and hyperpolarizing current pulses (2 s long, 50–300 pA in 50 pA steps) into four neurons using whole-cell patch-clamp. We found that in all neurons injection of depolarizing current pulses at spiking threshold (100–200 pA) evoked repetitive firing at an average number of 14 ± 3.4 spikes during the 2 s pulses (see **Figure 4C**). FFA (100 μM) caused a progressive suppression of repetitive firing leading to single spikes after 25 min of drug application at threshold currents (100–200 pA; see **Figure 4C**). The rheobase current in these 4 cells increased from 100–150 pA to 150–200 pA (one step) with FFA. During the injection of the strongest current pulses of 200–300 pA, the average number of spikes in the four cells was suppressed from 54 ± 43 to 1.5 ± 0.5 (1–2) per 2 s with FFA. The input resistance did not change with FFA in these four neurons (214 ± 77.2 MΩ in FFA vs. 176 ± 33.5 MΩ, $p = 0.299$, *T*-test).

Together these findings suggest that both I_{CAN} and I_{NaP} also contribute to repetitive firing during sustained depolarization of neurons and thereby to the size and duration of network bursts.

Do Hb9 Interneurons Have a Role in Burst Generation?

It has been proposed and debated whether Hb9 excitatory interneurons have a critical role in the generation of rhythmic activity in spinal cord circuits (Ziskind-Conhaim et al., 2010; Dougherty et al., 2013; Ljunggren et al., 2014; Caldeira et al., 2017) and whether persistent sodium currents play a crucial role in such rhythm generation (Tazerart et al., 2008; Ziskind-Conhaim et al., 2008). We, therefore, investigated whether Hb9 interneurons may have a critical role in the initiation of spontaneous bursts in spinal cord slice cultures. Since our low-density MEA recordings from slice cultures did not allow us to directly assign signals from MEA electrodes to immunohistochemically identified neurons, we combined MEA recordings with single-cell recordings from GFP labeled neurons in transverse slice cultures from the spinal cord of e13 Hb9-GFP mouse embryos. As shown in **Figures 5C,D**, spontaneous bursts of network activity that are similar to those described in cultures from rat slices also appear in cultures of embryonic mouse spinal cord slices (Avossa et al., 2003; Furlan et al., 2007). GFP positive neurons were visualized using fluorescence microscopy (see **Figure 5A**) and single-cell recordings were made using the whole-cell patch-clamp method. To exclude putative motoneurons from this analysis, we stained the cultures for ChAT after the experiments. By comparing the pictures from the recorded cells to the ChAT stainings, of the same cultures on the MEAs we selected 31 GFP-labeled neurons that were not stained positive for ChAT in 14 cultures for this analysis.

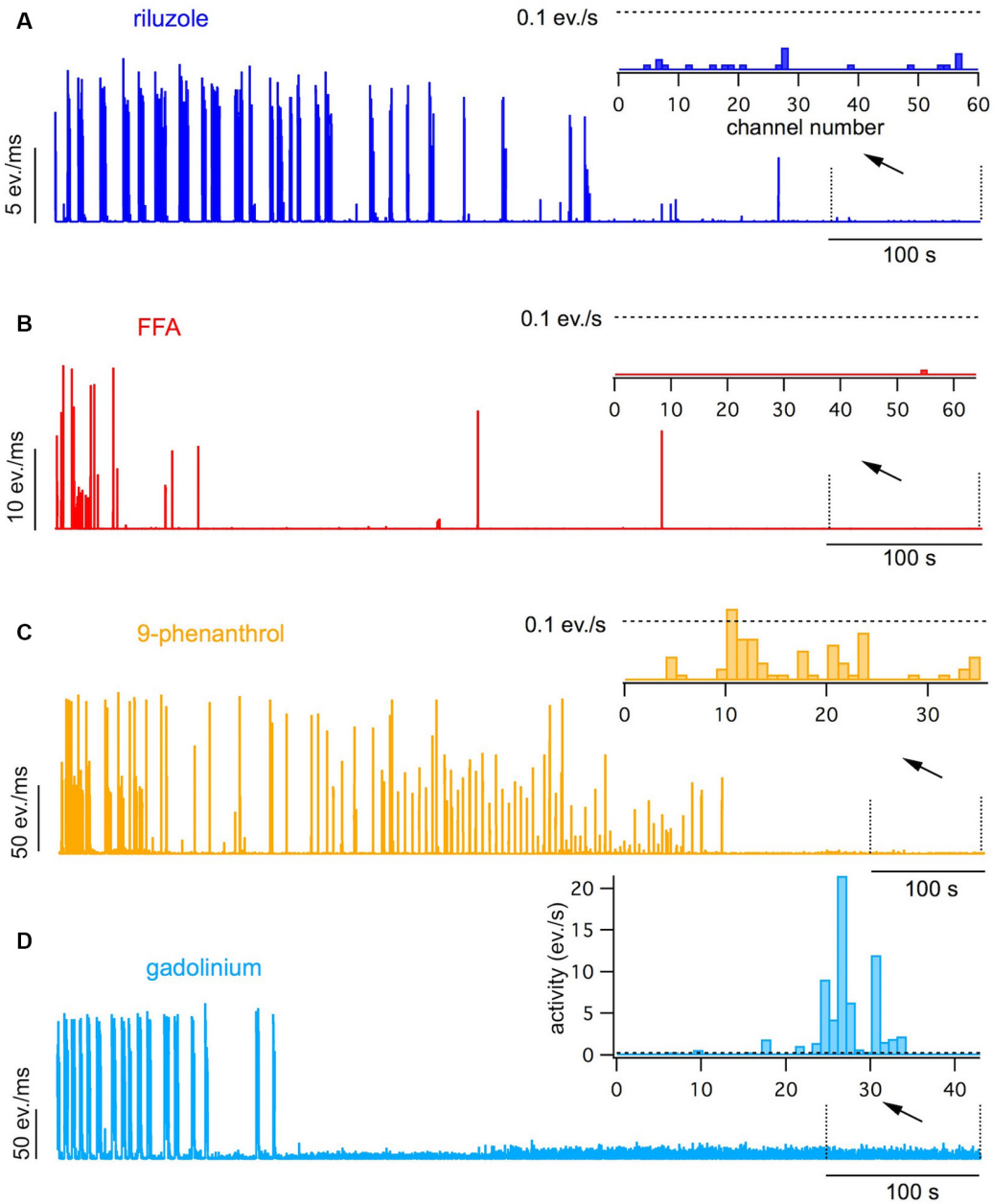

FIGURE 2 | Effects of 20 μM riluzole **(A)**, 100 μM flufenamic acid (FFA; **B**), 100 μM 9-phenanthrol **(C)** and 30 μM gadolinium chloride **(D)** on spontaneous bursting and intrinsic activity. Network activity plots obtained during exposure to the antagonists following a pre-exposition to the antagonist for 15–20 min are shown. Insets show the channel activity histograms obtained in the last 100 s of the exposure. Dotted lines show the detection threshold for intrinsic activity set a 0.1 events/s. Note that all antagonists completely blocked spontaneous bursting, but only riluzole, FFA and 9-phenanthrol completely suppressed intrinsic activity.

These neurons had a mean resting membrane potential of −52.9 ± 5.4 mV (±SD). During the injection of depolarizing current pulses, 28 of 31 showed repetitive firing as shown in **Figure 5B**. All of these neurons showed synaptic potentials that were correlated with the network bursts, but only 18 of them showed spontaneous spiking during network bursts as shown in **Figure 5C**. Neurons with spontaneous spikes were significantly more depolarized than those without spontaneous spikes (−50.3 ± 5.1 vs. −56.4 ± 3.7 mV; $n = 18$ vs.13; $p < 0.001$). The spikes always rode on synaptic potentials with a delayed onset relative to the start of the network burst as shown in **Figure 5C**. Trains of repetitive spikes that were evoked by current injection in individual Hb9 interneurons never evoked network bursts ($n = 28$ neurons, see **Figure 5D**). Spiking activity in these neurons was thus driven by the network bursts but did not initiate them.

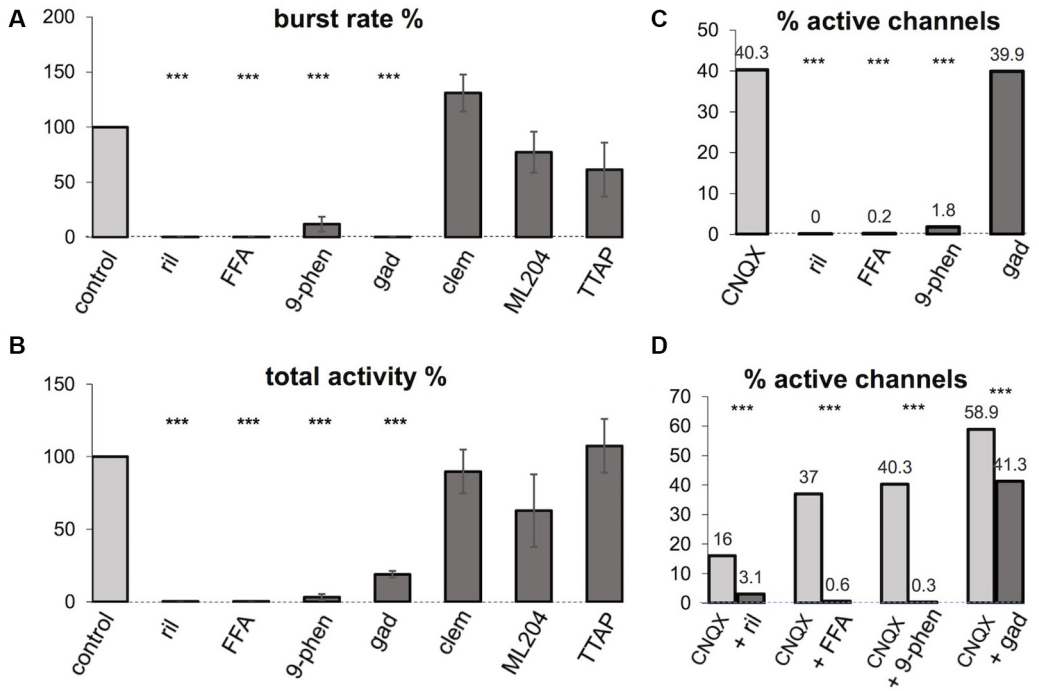

FIGURE 3 | Effects of various ion channel antagonists on spontaneous burst rate and intrinsic activity. ril: 20 μM riluzole; FFA: 100 μM flufenamic acid; 9-phen: 100 μM 9-phenanthrol; gad: 30 μM gadolinium chloride; clem: 3 μM clemizole hydrochloride; ML204: 10 μM ML204; TTAP: 1 μM TTA-P2; CNQX: 10 μM CNQX. **(A,B)** Normalized burst rate and total activity after exposure to the antagonist for 30–60 min in percent of the control value (± SEM). ***Significant difference to control ($p < 0.001$, $n = 5$–21 experiments per antagonist, *T*-test). **(C)** Number of active channels after exposure to the antagonist for 30–60 min in percent of the control values (number of active channels during bursting activity). ***Significant difference to CNQX ($p < 0.001$, $n = 5$–21 experiments per antagonist, Chi-square test). **(D)** Effects of channel antagonists on the number of active channels in the presence of CNQX in percent of the control values during bursting activity. ***Significant difference to CNQX ($p < 0.001$, $n = 4$–10 experiments per antagonist, Chi-square test).

DISCUSSION

The main finding of this study is that the I_{CAN} blockers FFA and 9-phenanthrol, similar to the I_{NaP} blocker riluzole, completely block intrinsic activity and spontaneous bursting in spinal cord networks and strongly reduce stimulus-evoked network responses. The finding that both riluzole and FFA suppress spontaneous intrinsic activity in disconnected networks at almost all electrodes is not compatible with the hypothesis that I_{NaP} and I_{CAN} contribute to the generation of intrinsic spiking in two distinct populations of neurons (Del Negro et al., 2005). More likely it suggests that I_{CAN} and I_{NaP} cooperate in individual neurons to support intrinsic and repetitive firing.

Mechanisms of Spontaneous Network Bursting in Spinal Cord Circuits in Culture

In the present experiments, we found spontaneous bursts of activity, often with intraburst oscillations in cultures of longitudinal ventral slices of the lumbar spinal cord of E14 rat embryos cut in the frontal plane. As in transverse slices, we found both short and long bursts with synchronous oscillations in the whole slice. These patterns of activity are similar to those previously reported in cultures of transverse spinal cord slices (Ballerini et al., 1999; Tscherter et al., 2001; Czarnecki et al., 2008) and also resemble the patterns called superbursts that appear in some cultures of dissociated cortical neurons (Wagenaar et al., 2006). The neuronal circuits in spinal cord cultures from both transverse and ventral longitudinal slices are therefore capable to generate synchronous bursting activity while lacking other aspects of organotypic pattern generation in isolated spinal cord preparations or *in vivo* like alternating patterns between the left and the right side of the spinal cord (Kiehn, 2016). As previously reported for networks in transverse slices (Czarnecki et al., 2008), such spontaneous bursting patterns involve recurrent network excitation through glutamatergic synaptic circuits since the block of glutamatergic transmission suppressed the bursting and left irregular asynchronous spontaneous activity in roughly 30% of the channels (see **Figure 1D**). We have previously shown in cultures of dissociated spinal neurons and transverse slices that such asynchronous activity represents spontaneous intrinsic spiking in part of the neurons (Darbon et al., 2002). Such intrinsic activity can be blocked by riluzole and thus depends on I_{NaP} (Darbon et al., 2004; Czarnecki et al., 2008).

I_{NaP} has also been shown to be involved in the generation of intrinsic spiking and in pacemaker activities in CPG networks of the spinal cord (Tazerart et al., 2007, 2008; Ziskind-Conhaim et al., 2010), the brainstem (Pace et al., 2007b) and the cortex (Le Bon-Jego and Yuste, 2007).

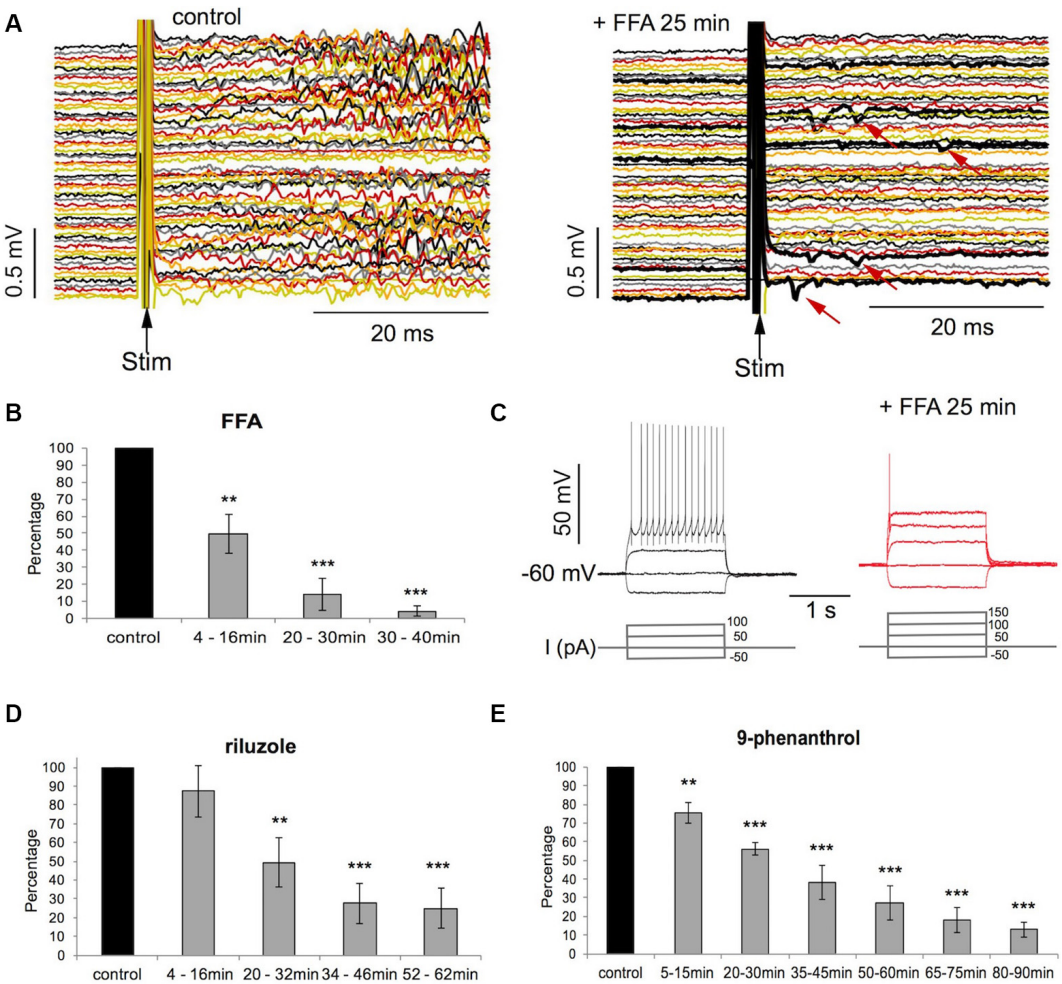

FIGURE 4 | Evoked activity is suppressed by FFA, riluzole, and 9-phenanthrol. **(A)** MEA recordings of activity in 60 channels evoked by electrical stimulation before and after exposure to FFA (100 μM). Note the few spikes (arrows) evoked by stimulation in FFA. **(B)** Decrease of evoked activity (in % of control) with time of FFA exposure ($n = 8$, $^{**}p < 0.01$; $^{***}p < 0.001$, T-test). **(C)** Intracellular patch-clamp recordings from one neuron during current injection. Note that FFA evoked repetitive firing is reduced to a single spike and activation threshold is increased by one current step (50 pA). **(D,E)** Decrease of evoked activity (in % of control) with time of exposure to riluzole ($n = 7$, $^{**}p < 0.01$; $^{***}p < 0.001$, T-test) and 9-phenanthrol ($n = 7$, $^{**}p < 0.01$; $^{***}p < 0.001$, T-test).

Contributions of I_{NaP} and I_{CAN} in Circuits of the Ventral Spinal Cord

In the pre-Bötzinger nucleus of the brain stem, inspiratory pattern generators were proposed to operate with two types of pacemaker neurons with different mechanisms that drive intrinsic firing. One is based on I_{NaP}, the other on I_{CAN} (Del Negro et al., 2005). However, it is not clear to what extent I_{CAN} activates cells from resting potential or whether it needs additional currents for depolarization since I_{CAN} is known to be involved in the generation of plateau potentials in motoneurons and neocortical neurons (Schiller, 2004; Del Negro et al., 2010). In the spinal cord, there is so far no evidence for the involvement of I_{CAN} in pattern generator networks. In the lamprey, some effects of FFA are reported but attributed as rather unspecific effects than being indicative of a contribution of I_{CAN} (Wang et al., 2006). Only in pain circuits of the dorsal spinal cord, pacemaker neurons are reported to potentially depend both on I_{NaP} and I_{CAN} (Li and Baccei, 2011). Our finding that the I_{CAN} blockers FFA and 9-phenanthrol completely suppress spontaneous bursting and intrinsic firing in cultures of longitudinal slices from ventral spinal cord show, that I_{CAN} also critically contributes to intrinsic firing and spontaneous rhythm generation in circuits of the ventral mammalian spinal cord. Furthermore, since blockers of I_{NaP} and I_{CAN} both completely block intrinsic firing at all electrodes, a distinct population of neurons with different mechanisms of intrinsic spiking are unlikely. Instead, these findings are more compatible with the hypothesis that both I_{CAN} and I_{NaP} contribute to intrinsic spiking in individual neurons and thus to rhythm generation in the network. This view is similar to the concept of a group pacemaker that was recently proposed for rhythm generation in the pre-Bötzinger complex (Del Negro et al., 2018).

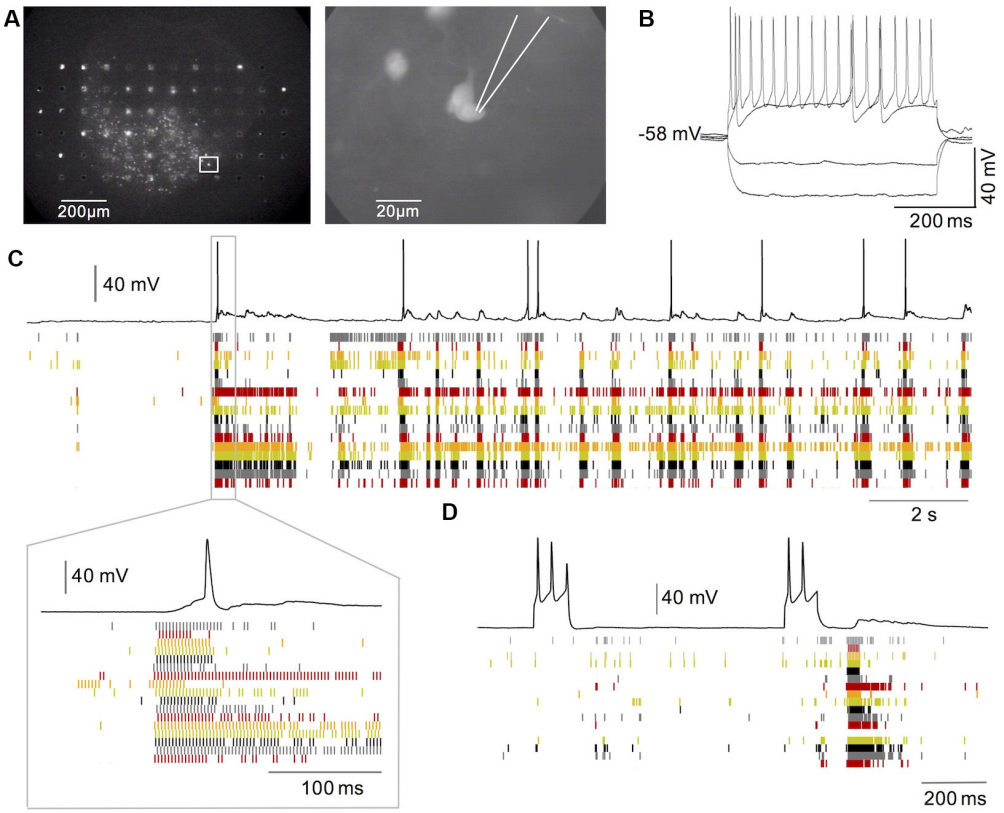

FIGURE 5 | Network-driven activity in GFP-labelled HB9 interneurons. **(A)** GFP labeled neurons in a spinal cord slice culture from HB9-GFP mice on MEA. **(B)** Repetitive firing induced in such a neuron by current injection. **(C)** Intracellular recording from one GFP neuron (black trace) in combination with MEA recordings (raster plot). Note that synaptic and spiking activity in the neuron is correlated to the network activity and follows network bursts with a delay. **(D)** Combined single neuron and network recording during activation of the neuron through current injection. Note that repetitive firing in the neuron cannot evoke network bursts.

We have previously shown that at the concentration used for this study (20 μM), riluzole suppresses repetitive spiking during current injection but leaves the initial spike intact (Darbon et al., 2004), showing that the suppression of intrinsic spiking is not simply due to the suppression of spike generation in general. Here, we show the same effects for the I_{CAN} blocker FFA: repetitive firing in individual neurons during injection of depolarizing current pulses is suppressed and reduced to one or two spikes by FFA. Also, both FFA and 9-phenanthrol reduce stimulus-induced network bursts to about 20% of control. Together these results suggest that I_{CAN} and I_{NaP} contribute to both intrinsic firing and repetitive firing during sustained depolarization.

The identity of intrinsically firing neurons in culture is not clear. Among others, excitatory Hb9 interneurons have been discussed as pacemaker neurons in rodent CPGs (Ziskind-Conhaim et al., 2008). In line with this hypothesis, we found a spontaneous activity that is correlated to network bursts in the majority of HB9 interneurons in HB9 GFP mice. However, for none of these neurons could activation of the neuron evoke network bursts. These findings argue against a prominent role of HB9 interneurons as intrinsically active cells that can initiate spontaneous network bursts in spinal cord cultures. It does however not exclude that these neurons may represent an important pacemaker under *in vivo* conditions or in more acute preparations (Ziskind-Conhaim et al., 2010; Caldeira et al., 2017).

Possible Involvement of TRPM4 Channels

Our conclusion critically depends on the assumption that the effects of FFA are due to the block of I_{CAN}. In neurons, the effective dose of FFA to block I_{CAN} is reported to be around 100 μM (Pace et al., 2007a; Li and Baccei, 2011; Guinamard et al., 2013; Tsuruyama et al., 2013). At such doses, however, it is highly unspecific and has many other effects in addition to blocking I_{CAN}. FFA was initially developed as a non-steroidal anti-inflammatory drug that inhibits the cyclo-oxygenases. This compound turned out to have a variety of effects on receptors and ion channels of the central nervous system (for review see Guinamard et al., 2013). At the concentration used in this study, it blocks several types of TRP channels (mainly belonging to the families of TRPC, TRPM and TRPV), chloride channels (including GABA A channels), Connexins, L-type Ca^{2+} channels, NMDA channels and nicotinic channels. Furthermore, at higher doses than used in this study (200 μM), FFA can interfere with sodium channel inactivation and thereby contribute to the suppression of repetitive firing (Yau et al., 2010) and it can

even activate some channels like TRPA and nicotinic channels. Nevertheless, we believe that the effects reported here are mainly due to a block of TRPM4 channels since 9-phenanthrol, a specific blocker of the TRPM4 channel (Guinamard et al., 2014), could fully reproduce the effects of FFA on intrinsic activity and on spontaneous and evoked bursting. However, also 9-phenanthrol at doses used in this study (100 μM) can have unspecific effects (Guinamard et al., 2014). Therefore, we tested other inhibitors of unspecific cation currents in terms of their effectiveness to block intrinsic activity and network bursting. In contrast to 9-phenanthrol, these blockers only reproduced some of the effects of FFA on rhythmic activity like gadolinium chloride, an unspecific blocker of I_{CAN} that had its major effects on stretch-activated ion channels (Adding et al., 2001), or they had no effects like the TRPC4 antagonist ML204 (Miller et al., 2011) or the TRPC5 antagonist clemizole (Richter et al., 2014). TRPC4/5 channels are reported to contribute to seizure generation in hippocampal circuits (Phelan et al., 2013; Zheng, 2017). We have previously shown that block of connexins or nicotinic channels in transverse slice cultures reduces spontaneous activity, but never completely blocked spontaneous bursting and intrinsic activity (Magloire and Streit, 2009). Also, the NMDA blocker APV and the GABA A blockers bicuculline and picrotoxin increased spontaneous activity in spinal cord slice cultures (Czarnecki et al., 2008). In summary, TRPM4 channels are the most likely structures underlying I_{CAN} in our experiments. TRPM4 channels are expressed in neurons and axons of mouse and human spinal cord (Schattling et al., 2012) and are involved in the output of the breathing CPG in mice (Koizumi et al., 2018; Picardo et al., 2019). Nevertheless, we cannot exclude the involvement of other unspecific cation channels of the TRPM, TRPC or TRPV families that are inhibited by FFA. Some of these channels like TRPC3/7 (Ben-Mabrouk and Tryba, 2010; Koizumi et al., 2018; Picardo et al., 2019), TRPM2/4 (Mrejeru et al., 2011) or TRPV2 (Bouhadfane et al., 2013) have been shown to play a role in rhythm or pattern generation in mammalian neuronal circuits.

The mechanisms involved in the block of the TRPM4 channels by FFA and 9-phenanthrol are unknown. It, therefore, remains an open question why these effects develop so slowly. The effects of CNQX rapidly occurred within seconds. Therefore, the slow establishment of effects cannot be attributed to the mode of application that was the same for all drugs. Both FFA and 9-phenanthrol, as well as riluzole, are lipophilic substances (Guinamard et al., 2013, 2014). It has been shown for several lipophilic anesthetics like propofol (Gredell et al., 2004) as well as etomidate and thiopental (Voss et al., 2013) that they show slow diffusion into mammalian cortical slices causing equilibrium times for drug distribution and effectiveness in the range of hours. Although the diffusion coefficients of FFA, 9-phenanthrol or riluzole are not known, they may be low enough to cause slow diffusion and thus the slow establishment of effects even in the relatively thin slices present in the spinal cord cultures.

We can only speculate about the mechanism of cooperation between TRPM4 and sodium channels at the resting membrane potential to intrinsically activate the neurons. A possible link would be T-type calcium channels that are activated at voltages between the resting membrane and the threshold potential and could thus be opened by depolarization through I_{NaP} and activate I_{CAN} by increasing intracellular Ca^2. T-type calcium channels have been proposed to be implicated in rhythm generation in mouse spinal cord (Anderson et al., 2012). However, in the present study, the specific T-type blocker TTA-P2 (Choe et al., 2011) did not affect spontaneous bursting and intrinsic spiking. This finding excludes a critical role of T-type calcium channels in the cooperation between I_{CAN} and I_{NaP}. Another possibility is that the neurons are depolarized into the activation range of I_{NaP} through TRPM4-induced fluctuations in membrane potential induced by intracellular calcium. Spontaneous intracellular calcium fluctuations have indeed been reported in spinal cord slice cultures (Fabbro et al., 2007). This hypothesis needs further investigation in future experiments.

In summary, we propose that I_{NaP} through sodium channels and I_{CAN} through putative TRPM4 channels jointly contribute to the generation of intrinsic and repetitive firing in intrinsically active neurons and thus to the generation of network bursting in the spinal cord circuits in culture.

DATA AVAILABILITY STATEMENT

The raw data supporting the conclusions of this article will be made available by the authors, without undue reservation, to any qualified researcher.

ETHICS STATEMENT

The use of animals for the preparation of slice cultures for this study was reviewed and approved by Swiss local authorities: Amt für Landwirtschaft und Natur des Kantons Bern, Veterinärdienst, Sekretariat Tierversuche, approval Nr. BE 52/11 and BE 35/14.

AUTHOR CONTRIBUTIONS

JS designed and coordinated the research. SB, AT, MH and JS performed research and analyzed data. JS wrote a first draft of the manuscript. All authors contributed to and approved the final manuscript.

FUNDING

This work was supported by the Swiss National Science Foundation (Schweizerischer Nationalfonds zur Förderung der Wissenschaftlichen Forschung; Grant No. 31003A_140754 to JS).

ACKNOWLEDGMENTS

We thank Cornelia Bichsel and Ruth Rubli for excellent preparation and maintenance of the cultures, Denis de Limoges, Christian Dellenbach, Stefan von Känel, Hans Ruchti and Jürg Burkhalter for technical support and Hans-Peter Clamann for critically reading the manuscript.

REFERENCES

Adding, L. C., Bannenberg, G. L., and Gustafsson, L. E. (2001). Basic experimental studies and clinical aspects of gadolinium salts and chelates. *Cardiovasc. Drug Rev.* 19, 41–56. doi: 10.1111/j.1527-3466.2001.tb00182.x

Anderson, T. M., Abbinanti, M. D., Peck, J. H., Gilmour, M., Brownstone, R. M., and Masino, M. A. (2012). Low-threshold calcium currents contribute to locomotor-like activity in neonatal mice. *J. Neurophysiol.* 107, 103–113. doi: 10.1152/jn.00583.2011

Avossa, D., Rosato Siri, M., Mazzarol, F., and Ballerini, L. (2003). Spinal circuits formation: a study of developmentally regulated markers in organotypic cultures of embryonic mouse spinal cord. *Neuroscience* 122, 391–405. doi: 10.1016/j.neuroscience.2003.07.006

Ballerini, L., Galante, M., Grandolfo, M., and Nistri, A. (1999). Generation of rhythmic patterns of activity by ventral interneurones in rat organotypic spinal slice culture. *J. Physiol.* 517, 459–475. doi: 10.1111/j.1469-7793.1999.0459t.x

Ben-Mabrouk, F., and Tryba, A. K. (2010). Substance P modulation of TRPC3/7 channels improves respiratory rhythm regularity and I_{CAN}-dependent pacemaker activity. *Eur. J. Neurosci.* 31, 1219–1232. doi: 10.1111/j.1460-9568.2010.07156.x

Bouhadfane, M., Tazerart, S., Moqrich, A., Vinay, L., and Brocard, F. (2013). Sodium-mediated plateau potentials in lumbar motoneurons of neonatal rats. *J. Neurosci.* 33, 15626–15641. doi: 10.1523/JNEUROSCI.1483-13.2013

Caldeira, V., Dougherty, K. J., Borgius, L., and Kiehn, O. (2017). Spinal Hb9::Cre-derived excitatory interneurons contribute to rhythm generation in the mouse. *Sci. Rep.* 7:41369. doi: 10.1038/srep41369

Choe, W., Messinger, R. B., Leach, E., Eckle, V. S., Obradovic, A., Salajegheh, R., et al. (2011). TTA-P2 is a potent and selective blocker of T-type calcium channels in rat sensory neurons and a novel antinociceptive agent. *Mol. Pharmacol.* 80, 900–910. doi: 10.1124/mol.111.073205

Czarnecki, A., Magloire, V., and Streit, J. (2008). Local oscillations of spiking activity in organotypic spinal cord slice cultures. *Eur. J. Neurosci.* 27, 2076–2088. doi: 10.1111/j.1460-9568.2008.06171.x

Czarnecki, A., Magloire, V., and Streit, J. (2009). Modulation of intrinsic spiking in spinal cord neurons. *J. Neurophysiol.* 102, 2441–2452. doi: 10.1152/jn.00244.2009

Darbon, P., Scicluna, L., Tscherter, A., and Streit, J. (2002). Mechanisms controlling bursting activity induced by disinhibition in spinal cord networks. *Eur. J. Neurosci.* 15, 671–683. doi: 10.1046/j.1460-9568.2002.01904.x

Darbon, P., Yvon, C., Legrand, J. C., and Streit, J. (2004). I-NaP underlies intrinsic spiking and rhythm generation in networks of cultured rat spinal cord neurons. *Eur. J. Neurosci.* 20, 976–988. doi: 10.1111/j.1460-9568.2004.03565.x

Del Negro, C. A., Funk, G. D., and Feldman, J. L. (2018). Breathing matters. *Nat. Rev. Neurosci.* 19, 351–367. doi: 10.1038/s41583-018-0003-6

Del Negro, C. A., Hayes, J. A., Pace, R. W., Brush, B. R., Teruyama, R., and Feldman, J. L. (2010). Synaptically activated burst-generating conductances may underlie a group-pacemaker mechanism for respiratory rhythm generation in mammals. *Prog Brain Res* 187, 111–136. doi: 10.1016/b978-0-444-53613-6.00008-3

Del Negro, C. A., Morgado-Valle, C., Hayes, J. A., Mackay, D. D., Pace, R. W., Crowder, E. A., et al. (2005). Sodium and calcium current-mediated pacemaker neurons and respiratory rhythm generation. *J. Neurosci.* 25, 446–453. doi: 10.1523/JNEUROSCI.2237-04.2005

Dougherty, K. J., Zagoraiou, L., Satoh, D., Rozani, I., Doobar, S., Arber, S., et al. (2013). Locomotor rhythm generation linked to the output of spinal Shox2 excitatory interneurons. *Neuron* 80, 920–933. doi: 10.1016/j.neuron.2013.08.015

Fabbro, A., Pastore, B., Nistri, A., and Ballerini, L. (2007). Activity-independent intracellular Ca^{2+} oscillations are spontaneously generated by ventral spinal neurons during development *in vitro*. *Cell Calcium* 41, 317–329. doi: 10.1016/j.ceca.2006.07.006

Feldman, J. L., Del Negro, C. A., and Gray, P. A. (2013). Understanding the rhythm of breathing: so near, yet so far. *Ann. Rev. Physiol.* 75, 423–452. doi: 10.1146/annurev-physiol-040510-130049

Furlan, F., Taccola, G., Grandolfo, M., Guasti, L., Arcangeli, A., Nistri, A., et al. (2007). ERG conductance expression modulates the excitability of ventral horn GABAergic interneurons that control rhythmic oscillations in the developing mouse spinal cord. *J. Neurosci.* 27, 919–928. doi: 10.1523/JNEUROSCI.4035-06.2007

Gredell, J. A., Turnquist, P. A., MacIver, M. B., and Pearce, R. A. (2004). Determination of diffusion and partition coefficients of propofol in rat brain tissue: implications for studies of drug action *in vitro*. *Br. J. Anaesth.* 93, 810–817. doi: 10.1093/bja/aeh272

Guinamard, R., Hof, T., and Del Negro, C. A. (2014). The TRPM4 channel inhibitor 9-phenanthrol. *Br. J. Pharmacol.* 171, 1600–1613. doi: 10.1111/bph.12582

Guinamard, R., Simard, C., and Del Negro, C. (2013). Flufenamic acid as an ion channel modulator. *Pharmacol. Ther.* 138, 272–284. doi: 10.1016/j.pharmthera.2013.01.012

Kiehn, O. (2016). Locomotor circuits in the mammalian spinal cord. *Nat. Rev. Neurosci.* 17, 224–238. doi: 10.1038/nrn.2016.9

Koizumi, H., John, T. T., Chia, J. X., Tariq, M. F., Phillips, R. S., Mosher, B., et al. (2018). Transient receptor potential channels TRPM4 and TRPC3 critically contribute to respiratory motor pattern formation but no rhythmogenesis in rodent brainstem ciruits. *eNeuro* 5:ENEURO.0332-17.2018. doi: 10.1523/eneuro.0332-17.2018

Le Bon-Jego, M., and Yuste, R. (2007). Persistently active, pacemaker-like neurons in neocortex. *Front. Neurosci.* 1, 123–129. doi: 10.3389/neuro.01.1.1.009.2007

Li, J., and Baccei, M. L. (2011). Pacemaker neurons within newborn spinal pain circuits. *J. Neurosci.* 31, 9010–9022. doi: 10.1523/JNEUROSCI.6555-10.2011

Ljunggren, E. E., Haupt, S., Ausborn, J., Ampatzis, K., and El Manira, A. (2014). Optogenetic activation of excitatory premotor interneurons is sufficient to generate coordinated locomotor activity in larval zebrafish. *J. Neurosci.* 34, 134–139. doi: 10.1523/JNEUROSCI.4087-13.2014

Magloire, V., and Streit, J. (2009). Intrinsic activity and positive feedback in motor circuits in organotypic spinal cord slice cultures. *Eur. J. Neurosci.* 30, 1487–1497. doi: 10.1111/j.1460-9568.2009.06978.x

Miller, M., Shi, J., Zhu, Y., Kustov, M., Tian, J. B., Stevens, A., et al. (2011). Identification of ML204, a novel potent antagonist that selectively modulates native TRPC4/C5 ion channels. *J. Biol. Chem.* 286, 33436–33446. doi: 10.1074/jbc.M111.274167

Mrejeru, A., Wei, A., and Ramirez, J. M. (2011). Calcium-activated non-selective cation currents are involved in generation of tonic and bursting activity in dopamine neurons of the substantia nigra pars compacta. *J. Physiol.* 589, 2497–2514. doi: 10.1113/jphysiol.2011.206631

Pace, R. W., Mackay, D. D., Feldman, J. L., and Del Negro, C. A. (2007a). Role of persistent sodium current in mouse preBotzinger Complex neurons and respiratory rhythm generation. *J. Physiol.* 580, 485–496. doi: 10.1113/jphysiol.2006.124602

Pace, R. W., Mackay, D. D., Feldman, J. L., and Del Negro, C. A. (2007b). Inspiratory bursts in the preBotzinger complex depend on a calcium-activated non-specific cation current linked to glutamate receptors in neonatal mice. *J. Physiol.* 582, 113–125. doi: 10.1113/jphysiol.2007.133660

Phelan, K. D., Shwe, U. T., Abramowitz, J., Wu, H., Rhee, S. W., Howell, M. D., et al. (2013). Canonical transient receptor channel 5 (TRPC5) and TRPC1/4 contribute to seizure and excitotoxicity by distinct cellular mechanisms. *Mol. Pharmacol.* 83, 429–438. doi: 10.1124/mol.112.082271

Picardo, M. C. D., Sugimura, Y. K., Dorst, K. D., Kallurkar, P. S., Akins, V. T., Ma, X., et al. (2019). Trpm4 ion channels in pre-Bötzinger complex interneurons are essential for breathing motor pattern but not rhythm. *PLoS Biol.* 17:e2006094. doi: 10.1371/journal.pbio.2006094

Richter, J. M., Schaefer, M., and Hill, K. (2014). Clemizole hydrochloride is a novel and potent inhibitor of transient receptor potential channel TRPC5. *Mol. Pharmacol.* 86, 514–521. doi: 10.1124/mol.114.093229

Schattling, B., Steinbach, K., Thies, E., Kruse, M., Menigoz, A., Ufer, F., et al. (2012). TRPM4 cation channel mediates axonal and neuronal degeneration in experimental autoimmune encephalomyelitis and multiple sclerosis. *Nat. Med.* 18, 1805–1811. doi: 10.1038/nm.3015

Schiller, Y. (2004). Role of a calcium-activated cation current during epileptiform discharges and its possible role in sustaining seizure-like events in neocortical slices. *J. Neurophysiol.* 92, 862–872. doi: 10.1152/jn.00972.2003

Streit, J., Tscherter, A., Heuschkel, M. O., and Renaud, P. (2001). The generation of rhythmic activity in dissociated cultures of rat spinal cord. *Eur. J. Neurosci.* 14, 191–202. doi: 10.1046/j.0953-816x.2001.01636.x

Tazerart, S., Viemari, J.-C., Darbon, P., Vinay, L., and Brocard, F. (2007). Contribution of persistent sodium current to locomotor pattern generation in neonatal rats. *J. Neurophysiol.* 98, 613–628. doi: 10.1152/jn.00316.2007

Tazerart, S., Vinay, L., and Brocard, F. (2008). The persistent sodium current generates pacemaker activities in the central pattern generator for locomotion and regulates the locomotor rhythm. *J. Neurosci.* 28, 8577–8589. doi: 10.1523/JNEUROSCI.1437-08.2008

Tscherter, A., Heuschkel, M. O., Renaud, P., and Streit, J. (2001). Spatiotemporal characterization of rhythmic activity in rat spinal cord slice cultures. *Eur. J. Neurosci.* 14, 179–190. doi: 10.1046/j.0953-816x.2001.01635.x

Tsuruyama, K., Hsiao, C.-F., and Chandler, S. H. (2013). Participation of persistent sodium current and calcium-activated nonspecific cationic current to burst generation in trigeminal principal sensory neurons. *J Neurophysiol* 110, 1903–1914. doi: 10.1152/jn.00410.2013

Urbani, A., and Belluzzi, O. (2000). Riluzole inhibits the persistent sodium current in mammalian CNS neurons. *Eur. J. Neurosci.* 12, 3567–3574. doi: 10.1046/j.1460-9568.2000.00242.x

Voss, L. J., van Kahn, C., and Sleigh, J. W. (2013). Quantification of neocortical slice diffusion characteristics using pharmacokinetic and pharmacodynamic modelling. *ISRN Neurosci.* 2013:759640. doi: 10.1155/2013/759640

Wagenaar, D. A., Pine, J., and Potter, S. M. (2006). An extremely rich repertoire of bursting patterns during the development of cortical cultures. *BMC Neurosci.* 7:11. doi: 10.1186/1471-2202-7-11

Wang, D., Grillner, S., and Wallen, P. (2006). Effects of flufenamic acid on fictive locomotion, plateau potentials, calcium channels and NMDA receptors in the lamprey spinal cord. *Neuropharmacology* 51, 1038–1046. doi: 10.1016/j.neuropharm.2006.06.012

Yau, H.-J., Baranauskas, G., and Martina, M. (2010). Flufenamic acid decreases neuronal excitability through modulation of voltage-gated sodium channel gating. *J. Physiol.* 588, 3869–3882. doi: 10.1113/jphysiol.2010.193037

Yvon, C., Czarnecki, A., and Streit, J. (2007). Riluzole-induced oscillations in spinal networks. *J. Neurophysiol.* 97, 3607–3620. doi: 10.1152/jn.00924.2006

Yvon, C., Rubli, R., and Streit, J. (2005). Patterns of spontaneous activity in unstructured and minimally structured spinal networks in culture. *Exp. Brain Res.* 165, 139–151. doi: 10.1007/s00221-005-2286-x

Zheng, F. (2017). TRPC channels and epilepsy. *Adv. Exp. Med. Biol.* 976, 123–135. doi: 10.1007/978-94-024-1088-4_11

Ziskind-Conhaim, L., Mentis, G. Z., Wiesner, E. R., and Titus, D. J. (2010). Synaptic integration of rhythmogenic neurons in the locomotor circuitry: the case of Hb9 interneurons. *Ann. N Y Acad. Sci.* 1198, 72–84. doi: 10.1111/j.1749-6632.2010.05533.x

Ziskind-Conhaim, L., Wu, L., and Wiesner, E. P. (2008). Persistent sodium current contributes to induced voltage oscillations in locomotor-related Hb9 interneurons in the mouse spinal cord. *J. Neurophysiol.* 100, 2254–2264. doi: 10.1152/jn.90437.2008

Conflict of Interest: The authors declare that the research was conducted in the absence of any commercial or financial relationships that could be construed as a potential conflict of interest.

Advantages of publishing in Frontiers

OPEN ACCESS
Articles are free to read for greatest visibility and readership

FAST PUBLICATION
Around 90 days from submission to decision

HIGH QUALITY PEER-REVIEW
Rigorous, collaborative, and constructive peer-review

TRANSPARENT PEER-REVIEW
Editors and reviewers acknowledged by name on published articles

Frontiers
Avenue du Tribunal-Fédéral 34
1005 Lausanne | Switzerland

Visit us: www.frontiersin.org
Contact us: frontiersin.org/about/contact

REPRODUCIBILITY OF RESEARCH
Support open data and methods to enhance research reproducibility

DIGITAL PUBLISHING
Articles designed for optimal readership across devices

FOLLOW US
@frontiersin

IMPACT METRICS
Advanced article metrics track visibility across digital media

EXTENSIVE PROMOTION
Marketing and promotion of impactful research

LOOP RESEARCH NETWORK
Our network increases your article's readership